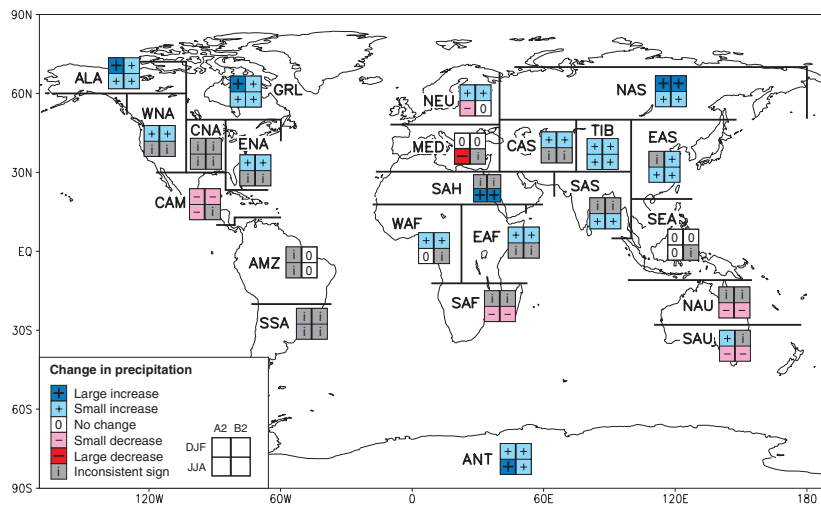


SRES versus IS92a

- In broad terms, the temperature results from SRES are similar to the IS92a results. In each of the two SRES and IS92a cases, warming is in excess of 40% above the global average in Alaska, northern Canada, Greenland, northern Asia, and Tibet (ALA, GRL, NAS and TIB) in DJF and in central Asia and Tibet (CAS and TIB) in JJA. All four cases also show warming less than the global average in South and Southeast Asia, and southern South America (SAS, SEA and SSA) in JJA.
- The main difference in the results is that there are substantially more instances for the SRES cases where there is disagreement on the magnitude of the relative regional warming. This difference is mainly evident in tropical and Southern Hemisphere regions.
- The precipitation results from SRES are also broadly similar to the corresponding IS92a results. There are many regions where the direction of precipitation change (although not necessarily the magnitude of this change) is consistent across all four cases. In DJF this is true for increase in northern mid- to high latitude regions, Antarctica and tropical Africa (ALA, GRL, WNA, ENA, NEU, NAS, TIB, CAS, WAF, EAF and ANT) and decrease in Central America (CAM). In JJA it is true for increase in high latitude regions (ALA, GRL, NAS and ANT) and for decrease in southern and northern Australia (SAU and NAU). Little change in Southeast Asia in DJF and little change or increase over South Asia in JJA are also consistent results.
- Although there are no cases where the SRES and IS92a results indicate precipitation changes of opposite direction, there are some notable differences. In the Sahara and in East Asia (SAH and EAS) in JJA, the results for both SRES scenarios show consistent increase whereas this was not true in either of the IS92a cases. On the other hand, in central North America and northern Australia (CNA and NAU) in DJF, and in East Africa (EAF) in JJA, the results for both SRES scenarios show model disagreement whereas the IS92a scenarios showed a consistent direction of change (increase in CNA, and decrease in EAF and NAU). It is also notable that the consistent decrease in JJA precipitation over the Mediterranean basin (MED) seen for both IS92a cases is present for SRES only for the A2 scenario (for which the decrease is large).



Box 10.1, Figure 2: Analysis of inter-model consistency in regional precipitation change. Regions are classified as showing either agreement on increase with an average change of greater than 20% ('Large increase'), agreement on increase with an average change between 5 and 20% ('Small increase'), agreement on a change between -5 and +5% or agreement with an average change between -5 and 5% ('No change'), agreement on decrease with an average change between -5 and -20% ('Small decrease'), agreement on decrease with an average change of less than -20% ('Large decrease'), or disagreement ('Inconsistent sign'). A consistent result from at least seven of the nine models is deemed necessary for agreement.

Uncertainty

The above comparisons concern the quantification of two different sources of uncertainty represented in the cascade of uncertainty described in Chapter 13, Section 13.5.1 (Figure 13.2). These include uncertainties in future emissions (IS92a GG and GS; SRES A2 and B2), and uncertainties in modelling the response of the climate system to a given forcing (samples of up to nine AOGCMs). Agreement across the different scenarios and climate models suggests, relatively speaking, less uncertainty about the nature of regional climate change than where there is disagreement. For example, the agreement for northern latitude winter precipitation extends across all emission scenarios and all models, whereas there is considerable disagreement (greater uncertainty) for tropical areas in JJA. Note that these measures of uncertainty are qualitative and applied on a relatively coarse spatial scale. It should also be noted that the range of uncertainty covered by the four emissions scenarios does not encompass the entire envelope of uncertainty of emissions (see Chapter 9, Section 9.2.2.4, and Chapter 13, Section 13.5.1). The range of models (representing the uncertainties in modelling the response to a given forcing) is somewhat more complete than in earlier analyses, but also limited.

strong tendency for precipitation to increase, particularly in the north-west of the continent. This tendency was replaced in the first coupled AOGCMs by one of little change or precipitation decrease, which has remained when the most recent coupled models are considered. Whetton *et al.* (1996a) partly attributed the contrast in the regional precipitation response of the two types of experiments to contrasts in their hemispheric patterns of warming.

Lal *et al.* (1998b) surveyed the results for the Indian subcontinent of seventeen climate change experiments including both equilibrium $2\times\text{CO}_2$ and transient AOGCM simulations with and without sulphate aerosol forcing. In the simulations forced only by GHG increases, most models show wet season (JJA) rainfall increases over the region of less than 5% per degree of global warming. A minority of experiments show rainfall decreases. The experiments which included scenarios of increasing sulphate forcing all showed reduced rainfall increases, or stronger rainfall decreases, than their corresponding GHG-only experiments.

For the central plains of North America, IPCC (1990) noted a good deal of similarity in the response of equilibrium $2\times\text{CO}_2$ experiments, with precipitation decreases prevailing in the summer and increases in the winter of less than 10%. In the second group of experiments (nine transient runs with AOGCMs) a wider range of responses was found (in the SAR). In winter, changes in precipitation ranged from about -12 to +20% for the time of CO_2 doubling, and most of the models (six out of nine) exhibited increases. In summer, the range of change was narrower, within $\pm 10\%$, but there was no clear majority response towards increases or decreases. Doherty and Mearns (1999) found that the CGCM1 and HadCM2 models simulated opposite changes in precipitation in both seasons over North America. While overall there is a tendency for more decreases to be simulated in the summer and more increases in the winter, there does not seem to be a reduction in the uncertainty for this region through the progression of climate models.

Many studies have considered GCM-simulated patterns of climate change in the European region (e.g., Barrow *et al.*, 1996; Hulme and Brown, 1998; Osborn and Hulme, 1998; Räisänen, 1998; Benestad *et al.* 1999; Osborn *et al.*, 1999). Hulme *et al.* (2000) provide an overview of simulated changes in the region by considering the results of twenty-three climate change simulations (forced by GHG change only) produced between the years 1983 and 1998 and including mixed-layer $1\times$ and $2\times\text{CO}_2$ equilibrium experiments as well as transient experiments. Figure 10.7 shows their results for simulated change in annual precipitation, averaged by latitude and normalised to percentage change per degree of global warming. It may be seen that the consensus amongst current models for drying in southern Europe and wetter conditions in northern Europe represents a continuation of a pattern established amongst the earlier simulations. The effect of model development has primarily been to intensify this pattern of response.

Variations across simulations in the regional enhanced GHG results of AOGCMs, which are particularly evident for precipitation, represent a major uncertainty in any assessment of regional climate change. Such variation may arise due to differences in forcing, systematic model-to-model differences in the regional

response to a given forcing or differences due to natural decadal to inter-decadal scale variability in the models. Giorgi and Francisco (2000a,b) analysed AOGCM simulations including different models, forcing scenarios and ensembles of simulations, and found that the greatest source of uncertainty in regional climate change simulation was due to inter-model differences, with intra-ensemble and inter-scenario differences being less important (see Figures 10.3 and 10.5). However, it should be noted that Giorgi and Francisco (2000a,b) used long (thirty year) means and large (sub-continental scale) regions and that the uncertainty due to simulated natural variability would be larger when shorter averaging periods, or smaller regions, are used. The results of Hulme *et al.* (1999) also suggest that low-frequency natural climatic variability is important at the sub-regional scale in Europe and can mask the enhanced GHG signal.

Regional changes in the mean pattern of atmospheric circulation have been noted in various studies, although typically the changes are not marked (e.g., Huth, 1997; Schubert, 1998). Indeed, the work of Conway (1998) and Wilby *et al.* (1998b) suggests that the contribution of changes in synoptic circulation to regional climate change may be relatively small compared to that of sub-synoptic processes.

10.3.2.2 Climate variability and extreme events

Gregory and Mitchell (1995) identified in an equilibrium $2\times\text{CO}_2$ simulation with the Hadley Centre model a tendency for daily temperature variability over Europe to increase in JJA and to decrease in DJF. Subsequent work on temperature variability at daily to monthly and seasonal time-scales has tended to confirm this pattern, as found by Buishand and Beersma (1996) over Europe, Beersma and Buishand (1999) over southern Europe, northern Europe and central North America and Boer *et al.* (2000b) throughout the northern mid-latitudes. This tendency can also be seen in the results of Giorgi and Francisco (2000a) for a set of transient HadCM2 simulations over different regions of the globe.

Daily high temperature extremes are likely to increase in frequency as a function of the increase in mean temperature, but this increase is modified by changes in daily variability of temperature. There is a corresponding decrease in the frequency of daily low temperature extremes. Kharin and Zwiers (2000) and Zwiers and Kharin (1997) found that in all regions of the globe the CGCM1 model simulated substantial increases in the magnitude of extreme daily maximum and minimum temperatures, with an average frequency of occurrence of once per twenty years. Delworth *et al.* (1999) considered simulated changes of a ‘heat index’ (a measure which combines the effect temperature and moisture) in the GFDL R15a model. Their results indicated that seasonally warm and humid areas such as the south-eastern United States, India, Southeast Asia and northern Australia can experience increases in the heat index substantially greater than that expected due to warming alone.

There is a strong correlation between precipitation inter-annual variability and mean precipitation. Increases in mean precipitation are likely to be associated with increases in variability, and precipitation variability is likely to decrease in areas of reduced mean precipitation. In general, where simulated

changes in regional precipitation variability have been examined, increases are more commonly noted. Giorgi and Francisco (2000a) found a tendency for regional interannual variability of seasonal mean precipitation to increase in HadCM2 simulations in many of the regions they considered. Increases in interannual variability also predominated in the CGCM1 simulation (Boer *et al.*, 2000b) although there were areas of decrease, particularly in areas where mean rainfall decreased. Beersma and Buishand (1999) mostly found increases in monthly precipitation variance over southern Europe, northern Europe and central North America. A number of studies have reported a tendency for interannual rainfall variability to increase over South Asia (SAR; Lal *et al.*, 2000). McGuffie *et al.* (1999) identified a tendency for increased daily rainfall variability in two models over the Sahel, North America, South Asia, southern Europe and Australia. It should also be noted that in many regions interannual climatic variability is strongly related to ENSO, and thus will be affected by changes in ENSO behaviour (see Chapter 9).

The tendency for increased rainfall variability in enhanced GHG simulations is reflected in a tendency for increases in the intensity and frequency of extreme heavy rainfall events. Such increases have been documented in regionally focused studies for Europe, North America, South Asia, the Sahel, southern Africa, Australia and the South Pacific (Hennessy *et al.*, 1997; Bhaskaran and Mitchell, 1998; McGuffie *et al.* 1999; Jones, R.N. *et al.*, 2000) as well as in the global studies of Kharin and Zwiers (2000) and Zwiers and Kharin (1998). For example, Hennessy *et al.* (1997) found that under $2\times\text{CO}_2$ conditions the one-year return period events in Europe, Australia, India and the USA increased in intensity by 10 to 25% in two models.

Changes in the occurrence of dry spells or droughts have been assessed for some regions using recent model results. Joubert *et al.* (1996) examined drought occurrence over southern Africa in an equilibrium $2\times\text{CO}_2$ CSIRO simulation and noted areas of both substantial increase and decrease. Gregory *et al.* (1997) looked at drought occurrence over Europe and North America in a transient simulation using both rainfall-based and soil moisture-based measures of drought. In all cases, marked increases were obtained. This was attributed primarily to a reduction in the number of rainfall events rather than a reduction in mean rainfall. Marked increases in the frequency and intensity of drought were found also by Kothavala (1997) over Australia using the Palmer drought severity index.

Fewer studies have considered changes in variability and extremes of synoptic circulation under enhanced GHG conditions. Huth (1997) noted little change in synoptic circulation variability under equilibrium $2\times\text{CO}_2$ conditions over North America and Europe. Katzfey and McInnes (1996) found that the intense cut-off lows off the Australian east coast became less common under equilibrium $2\times\text{CO}_2$ conditions in the CSIRO model, although they had limited confidence in this result.

10.3.3 Summary and Recommendations

Analysis of transient simulations with AOGCMs indicates that average climatic features are generally well simulated at the planetary and continental scale. At the regional scale, area-average

biases in the simulation of present day climate are highly variable from region to region and across models. Seasonal temperature biases are typically within the range of $\pm 4^\circ\text{C}$ but exceed $\pm 5^\circ\text{C}$ in some regions, particularly in DJF. Precipitation biases are mostly between -40 and $+80\%$, but exceed 100% in some regions. These regional biases are, in general terms, smaller than those of a similar analysis presented in the SAR. When it has been assessed, many aspects of model variability have compared well against observations, although significant model-dependent biases have been noted. Model performance was poorer at the finer scales, particularly in areas of strong topographical variation. This highlights the need for finer resolution regionalisation techniques.

Simulated changes in mean climatic conditions for the last decades of the 21st century (compared to present day climate) vary substantially among models and among regions. All land regions undergo warming in all seasons, with the warming being generally more pronounced over cold climate regions and seasons. Average precipitation increases over most regions, especially in the cold season, due to an intensified hydrological cycle. However, some exceptions occur in which most models concur in simulating decreases in precipitation. The magnitude of regional precipitation change varies considerably among models with the typical range being around 0 to 50%, where the direction of change is strongly indicated, and around -30 to $+30\%$ where it is not. There is strong tendency for models to simulate regional increases in precipitation variability with associated increases in the frequency of extreme rainfall events. Increased interannual precipitation variability is also commonly simulated and, in some regions, increases in drought or dry-spell occurrence have been noted. Daily to interannual variability of temperature is simulated to decrease in winter and increase in summer in mid-latitude Northern Hemisphere land areas.

10.4 GCMs with Variable and Increased Horizontal Resolution

This section deals with the relatively new idea of deriving regional climate information from AGCMs with variable and increased horizontal resolution. Although the basic methodology is suggested in the work of Bengtsson *et al.* (1995), where a high resolution GCM was used to simulate changes in tropical cyclones in a warmer climate, it is only in the last few years that such models have been used more widely to predict regional aspects of climate change. Even so, only a limited number of experiments have been conducted to date (see Table 10.1) and hence what follows is not a definitive evaluation of the technique but an initial exploration of its potential.

10.4.1 Simulations of Current Climate

Analysis of current climate simulations has considered both deviations from the observed climate and effects of changes in resolution on the model's climatology. Most studies have considered just the mean climate and some measures of variability, either globally or for a particular region of interest. The only extreme behaviour studied in any detail was the simulation of tropical cyclones. Even for mean climate, no comprehensive assessment

Table 10.1: Enhanced and variable resolution GCM control and anomaly simulations. Resolution is given as either the spectral truncation or grid-point spacing depending on the model's formulation (and with a range for variable resolution models). The equivalent grid-point resolution of spectral truncation T42 is $2.8^\circ \times 2.8^\circ$ (scaling linearly).

Institution	Model	Horizontal Resolution	Control Forcing	Anomaly Forcing	Region of interest
MPI	ECHAM3	T42	ECHAM/LSG	ECHAM/LSG	Euro/Global
MPI	ECHAM3/4	T106	Obs	ECHAM/OPYC	Euro/Global
UKMO	HadAM2b	$0.83^\circ \times 1.25^\circ$	Obs		Global
UKMO	HadAM3a	$0.83^\circ \times 1.25^\circ$	Obs	HadCM3	Euro/Global
MRI	JMA	T106	Obs	MRI/GFDL/+2°C	Tropics
CNRM	ARPEGE	T213–T21, T106	Obs/HadCM2	HadCM2	Euro/Global
LGGE	LMDZ	100 to 700km	Obs	CLIMAP	Polar regions

of the surface climatology of variable or high resolution models has been attempted. Europe has been the most common area of study to date, although southern Asia and the polar regions have also received attention

10.4.1.1 Mean climate

The mean circulation is generally well simulated by AGCMs, though relatively large regional-scale biases can still be present. Many features of the large-scale climate of AGCMs are retained at higher resolution (Dèquè and Piedelievre, 1995; Stendel and Roeckner, 1998; May, 1999; Stratton, 1999a). A common change is a poleward shift of the extra-tropical storm track regions. It has been suggested that this is linked to a general deepening of cyclones, noted as a common feature in high-resolution atmospheric models (Machenhauer *et al.*, 1996; Stratton 1999a). More intense activity is also seen at higher resolution in the tropics. For example, a stronger Hadley circulation was observed in ECHAM4 and HadAM3a that worsened agreement with observations (Stendel and Roeckner, 1998; Stratton, 1999b).

The repositioning of the storm tracks generally improves the simulations in the Northern Hemisphere, as it reduces a positive polar surface pressure bias which is present in the models at standard resolution. In the case of HadAM3a, this leads to substantial improvements in Northern Hemisphere low level flow in winter (Figure 10.8). In the Southern Hemisphere, the impact on the circumpolar flow is not consistently positive across models (Figure 10.8; Krinner *et al.*, 1997). In ECHAM4 and HadAM3a, increased resolution has little impact on the negative surface pressure bias over the tropics but improves the low-level South Asian monsoon flow (Lal *et al.*, 1997; Stratton, 1999b).

The existence of these common responses to increased resolution suggests that they result from improved representation of the resolved variables. In contrast, an increase in the intensity of subtropical anticyclones observed in ECHAM4 results from a tropospheric warming promoted by excessive cirrus clouds attributed to a scale-dependent response in the relevant parametrization (Stendel and Roeckner, 1998).

The aim of increasing resolution in AGCMs is generally to improve the simulation of surface climatology compared to coarser resolution models (Cubash *et al.*, 1995). Early experience shows a much more mixed response. ECHAM3 at T42 improved the seasonal cycle of surface temperature in seven regions, compared

to the driving AOGCM, but overall surface temperature was too high (by 2 to 5°C). Increasing the resolution to T106 did not improve winter temperatures and, in summer, the spatial patterns were better but the regional biases worse (Cubasch *et al.*, 1996). For precipitation, spatial patterns were improved in summer but degraded in winter. The summer warming was due to excessive insolation from reduced cloud cover and overly transparent clear skies (Wild *et al.*, 1995). Improved physics in ECHAM4 reduced some of the radiation errors but the precipitation and temperature biases remained (Wild *et al.*, 1996; Stendel and Roeckner, 1998). In simulations of European climate with ARPEGE (Dèquè and Piedelievre, 1995) and HadAM2b/3a (Jones, 1999; Stratton, 1999a), improved flow at higher resolution generally led to better surface temperatures and precipitation. However, over south-eastern Europe, precipitation biases increased in both models, as did the warm temperature bias in HadAM3a.

The increased summer temperatures in Europe in HadAM3a were caused by reduced cloud cover at higher resolution (Jones 1999) and warming and drying, in summer, was seen over all extra-tropical continents (Stratton, 1999b). This clearly demonstrates a potential drawback of increasing the resolution of a model without comprehensively retuning the physics. Krinner *et al.* (1997) showed that, to obtain a reasonable simulation of the surface climatology of the Antarctic with the LMD variable resolution AGCM, many modifications to the model physics were required. The model was then able to simulate surface temperatures to within 2 to 4°C of observations and to provide a good simulation of the ice mass balance (snow accumulation), with both aspects being better than at standard resolution.

10.4.1.2 Climate variability and extreme events

Enhanced resolution improves many aspects of the AGCMs' intra-seasonal variability of circulation at low and intermediate frequencies (Stendel and Roeckner, 1998). However, in some cases values underestimated at standard resolution are overestimated at enhanced resolution (Dèquè and Piedelievre, 1995; Stratton, 1999a,b). Martin (1999) found little sensitivity to resolution in either the interannual or intra-seasonal variability of circulation and precipitation of the South Asian monsoon in HadAM3a. Extreme events have not been studied, with the exception of tropical cyclones. This subject cuts across various sections and chapters and thus is dealt with in Box 10.2.

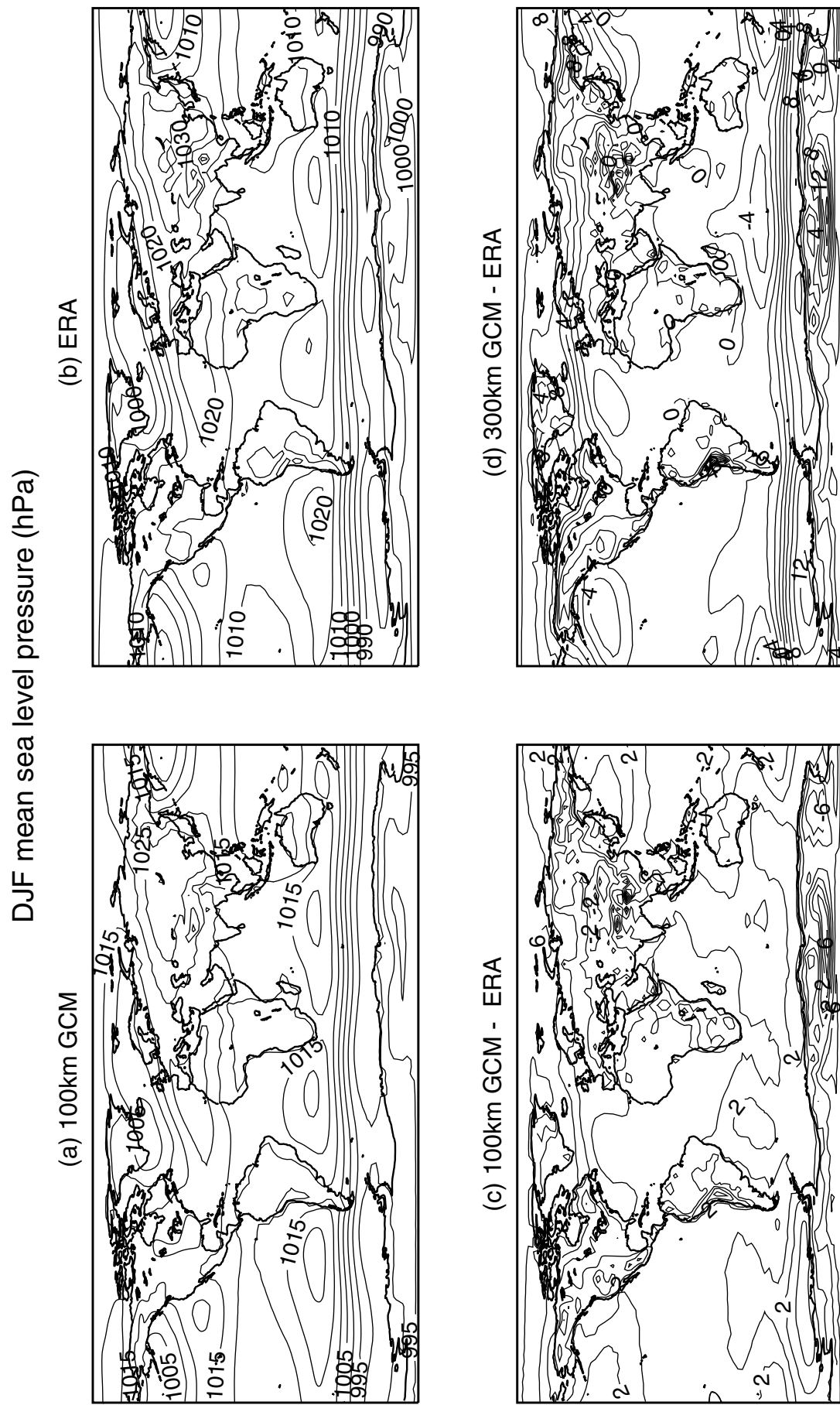


Figure 10.8: Mean sea level pressure for DJF in: (a) HadAM3a at high resolution (100 km), (b) ECMWF reanalysis (ERA), (c) HadAM3a high resolution minus ERA, (d) HadAM3a at standard resolution (300 km) minus ERA. Adapted from Stratton (1999b).

Box 10.2: Tropical cyclones in current and future climates

Simulating a climatology of tropical cyclones

Tropical cyclones can have devastating human and economic impacts (e.g., Pielke and Landsea, 1998) and therefore accurate estimates of future changes in their frequency, intensity and location would be of great value. However, because of their relatively small extent (in global modelling terms) and intense nature, detailed simulation of tropical cyclones for this purpose is difficult. Atmospheric GCMs can simulate tropical cyclone-like disturbances which increase in realism at higher resolution though the intense central core is not resolved (e.g., Bengtsson *et al.*, 1995; McDonald, 1999). Further increases of resolution, by the use of RCMs, provide greater realism (e.g., Walsh and Watterson, 1997) with a very high resolution regional hurricane prediction model giving a reasonable simulation of the magnitude and location of maximum surface wind intensities for the north-west Pacific basin (Knutson *et al.*, 1998). GCMs generally provide realistic simulation of the location and frequency of tropical cyclones (e.g., Tsutsui and Kasahara, 1996; Yoshimura *et al.*, 1999). See also Chapter 8 for more details on tropical cyclones in GCMs.

Tropical cyclones in a warmer climate

Much effort has gone into obtaining and analysing good statistics on tropical cyclones in the recent past. The main conclusion is that there is large decadal variability in the frequency and no significant trend during the last century. One study looking at the century time-scale has shown an increase in the frequency of North Atlantic cyclones from 1851 to 1890 and 1951 to 1990 (Fernandez-Partagas and Diaz, 1996). See Chapter 2 for more details on observed tropical cyclones.

Most assessments of changes in tropical cyclone behaviour in a future climate have been derived from GCM or RCM studies of the climate response to anthropogenically-derived atmospheric forcings (e.g., Bengtsson *et al.*, 1996, 1997; Walsh and Katzfey, 2000). Recently, more focused approaches have been used: nesting a hurricane prediction model in a GCM climate change simulation (Knutson *et al.*, 1998); inserting idealised tropical cyclones into an RCM climate change simulation (Walsh and Ryan, 2000).

In an early use of a high-resolution AGCM, a T106 ECHAM3 experiment simulated a decrease in tropical cyclones in the Northern Hemisphere and a reduction of 50% in the Southern Hemisphere (Bengtsson *et al.*, 1996, 1997). However, the different hemispheric responses raised questions about the model's ability to properly represent tropical cyclones and methodological concerns about the experimental design were raised (Landsea, 1997). In a similar experiment, the JMA model also simulated fewer tropical cyclone-like vortices in both hemispheres (Yoshimura *et al.*, 1999). Other GCM studies have shown consistent basin-dependent changes in tropical cyclone formation under $2\times\text{CO}_2$ conditions (Royer *et al.*, 1998; Tsutsui *et al.*, 1999). Frequencies increased in the north-west Pacific, decreased in the North Atlantic, and changed little in the south-west Pacific. A high resolution HadAM3a simulation reproduced the latter changes, giving changes in timing in the north-west Pacific and increases in frequency in the north-east Pacific and the north Indian basin (McDonald, 1999). Some GCM studies show increases in tropical storm intensity in a warmer climate (Krishnamurti *et al.*, 1998) though these results can probably not be extrapolated to tropical cyclones as the horizontal resolution of these models is insufficient to resolve the cyclone eye. The likely mean response of tropical Pacific sea surface warming having an El Niño-like structure suggests that the pattern of tropical cyclone frequency may become more like that observed in El Niño years (see Chapter 9).

An indication of the likely changes in maximum intensity of cyclones will be better provided by models able to simulate realistic tropical cyclone intensities. A sample of GCM-generated tropical cyclone cases nested in a hurricane prediction model gave increases in maximum intensity (of wind speed) of 5 to 11% in strong cyclones over the north-west Pacific for a 2.2°C SST warming (Knutson and Tuleya, 1999). The RCM study of idealised tropical cyclones (in the South Pacific) showed a small, but not statistically significant, increase in maximum intensity (Walsh and Ryan, 2000). These results are supported by the theory of the maximum potential intensity (MPI) of hurricanes (Emanuel, 1987). A calculation using the MPI framework of Holland (1997) suggested increases of 10 to 20% for a $2\times\text{CO}_2$ climate (Henderson-Sellers *et al.*, 1998). This study also acknowledges physical omissions that would reduce this estimate though Emanuel (2000) suggests there is a linear relationship between MPI and the wind speed of real events. Published modelling studies to date neglect the possible feedback of sea surface cooling induced by the cyclone. However, a recently submitted study using a hurricane model with ocean coupling indicates that the increased maximum intensity by CO_2 warming would still occur even when the sea surface cooling feedback is included (Knutson *et al.*, 2000).

The extreme precipitation associated with tropical cyclones can also be very damaging. The very high resolution studies discussed above suggest that increases in the intensity of tropical cyclones will be accompanied by increases in mean and maximum precipitation rates. In the cases studied, precipitation in the vicinity of the storm centre increased by 20% whereas peak rates increased by 30%. Part of these increases may be due to the increased moisture-holding capacity of a warmer atmosphere but nevertheless point to substantially increasing destructive capacity of tropical cyclones in a warmer climate.

In conclusion, there is some evidence that regional frequencies of tropical cyclones may change but none that their locations will change. There is also evidence that the peak intensity may increase by 5% to 10% and precipitation rates may increase by 20% to 30%. There is a need for much more work in this area to provide more robust results.

10.4.2 Simulations of Climate Change

10.4.2.1 Mean climate

Climate change simulations using ECHAM3 at T42 and T106 resolutions predicted substantially different responses for southern Europe (Cubash *et al.*, 1996). For example, surface temperature response of less than +2°C in summer at T42 increased by over 4°C for much of the region at T106 and winter precipitation increased more at T106 than at T42. An important factor in generating the different responses was the substantial difference in the control simulations. Wild *et al.* (1997) showed a large positive summer surface temperature bias in the T106 control derived from a positive feedback between excessive surface insolation and summer dryness. This mechanism provided a large increase in the insolation, and thus the surface temperature, in the anomaly experiment. As this process was handled poorly in the control simulation, little confidence can be placed in the warming amplification simulated at T106.

A variable grid AGCM climate change experiment using the ARPEGE model and sea surface forcing from HadCM2 predicted moderate warmings over Europe, 1.5°C (northern) to 2.5°C (southern) in winter and 1°C to 3.5°C in summer (Dèquè *et al.*, 1998). In contrast, HadCM2 predicted greater warming and a larger north-south gradient in winter (Figure 10.9). These differences result mainly from the ARPEGE large-scale flow being too zonal and too strong over mainland Europe, which enhances the moderating influence of the SSTs. The precipitation responses are more similar, especially in summer, when both models predict a decrease over most of Europe, maximum -30% in the south. Differences in the control simulations suggest that little confidence should be placed in this result.

In a similar experiment, HadAM3a at $1.25^\circ \times 0.83^\circ$ resolution used observed sea surface forcing and anomalies from a HadCM3 GHG simulation and produced a response at the largest scales in the annual mean similar to the AOGCM (Johns, 1999). However, regionally or seasonally, many differences were evident in the two models, notably in land sea contrasts, monsoon precipitation and some circulation features. Over Europe, large-scale responses in surface temperature and precipitation were similar except for a larger winter surface warming in northern Europe in HadCM3. This was due to a greater melting back of Arctic sea ice which was too extensive in the HadCM3 control (Jones, 1999). In a 30-year ECHAM4 T106 experiment driven by ECHAM4/OPYC simulations for 1970 to 1999 and 2060 to 2089, the simulations of future climate were more similar to each other than those for the present day (May, 1999). This implies that the differences in the control simulations would determine a proportion of the difference in the responses. In these cases better control simulations at high resolution increase the confidence in their responses.

10.4.2.2 Climate variability and extreme events

Due to the limited number and length of simulations and a lack of comprehensive analyses, this subject has been almost completely ignored. The only response in variability or extremes that has received any attention is that of tropical cyclones (Box 10.2).

10.4.3 Summary and Recommendations

Since the SAR, several variable and high-resolution GCMs have been used to provide high-resolution simulations of climate change. Clearly the technique is still in its infancy with only a few modelling studies carried out and for only a limited number of regions. Also, there is little in-depth analysis of the performance of the models and only preliminary conclusions can be drawn.

Many aspects of the models' dynamics and large-scale flow are improved at higher resolution, though this is not uniformly so geographically or across models. Some models also demonstrate improvements in their surface climatologies at higher resolution. However, substantial underlying errors are often still present in high-resolution versions of current AGCMs. In addition, the direct use of high-resolution versions of current AGCMs, without some allowance of the dependence of models physical parameterizations on resolution, leads to some deterioration in the performance of the models.

Regional responses currently appear more sensitive to the AGCM than the SST forcing used. This result is partially due to some of the model responses being dependent on their control simulations and systematic errors within them. These factors and the small number of studies carried out imply that little confidence can be attached to any of the regional projections provided by high and variable resolution AGCM simulations. The improvements seen with this technique are encouraging, but more effort should be put in analysing, and possibly improving the performance of current models at high resolution. This is particularly important in view of the fact that future AOGCMs will likely use models approaching the resolution considered here in the next 5 to 10 years.

10.5 Regional Climate Models

Since the SAR, much insight has been provided into fundamental issues concerning the nested regional modelling technique.

Multi-year to multi-decadal simulations must be used for climate change studies to provide meaningful climate statistics, to identify significant systematic model errors and climate changes relative to internal model and observed climate variability, and to allow the atmospheric model to equilibrate with the land surface conditions (e.g., Jones *et al.*, 1997; Machenhauer *et al.*, 1998; Christensen 1999; McGregor *et al.*, 1999; Kato *et al.*, 2001).

The choice of an appropriate domain is not trivial. The influence of the boundary forcing can reduce as region size increases (Jones *et al.*, 1995; Jacob and Podzun, 1997) and may be dominated by the internal model physics for certain variables and seasons (Noguer *et al.*, 1998). This can lead to the RCM solution significantly departing from the driving data, which can make the interpretation of down-scaled regional climate changes more difficult (Jones *et al.*, 1997). The domain size has to be large enough so that relevant local forcings and effects of enhanced resolution are not damped or contaminated by the application of the boundary conditions (Warner *et al.*, 1997). The exact location of the lateral boundaries can influence the sensitivity to internal parameters (Seth and Giorgi, 1998) or may

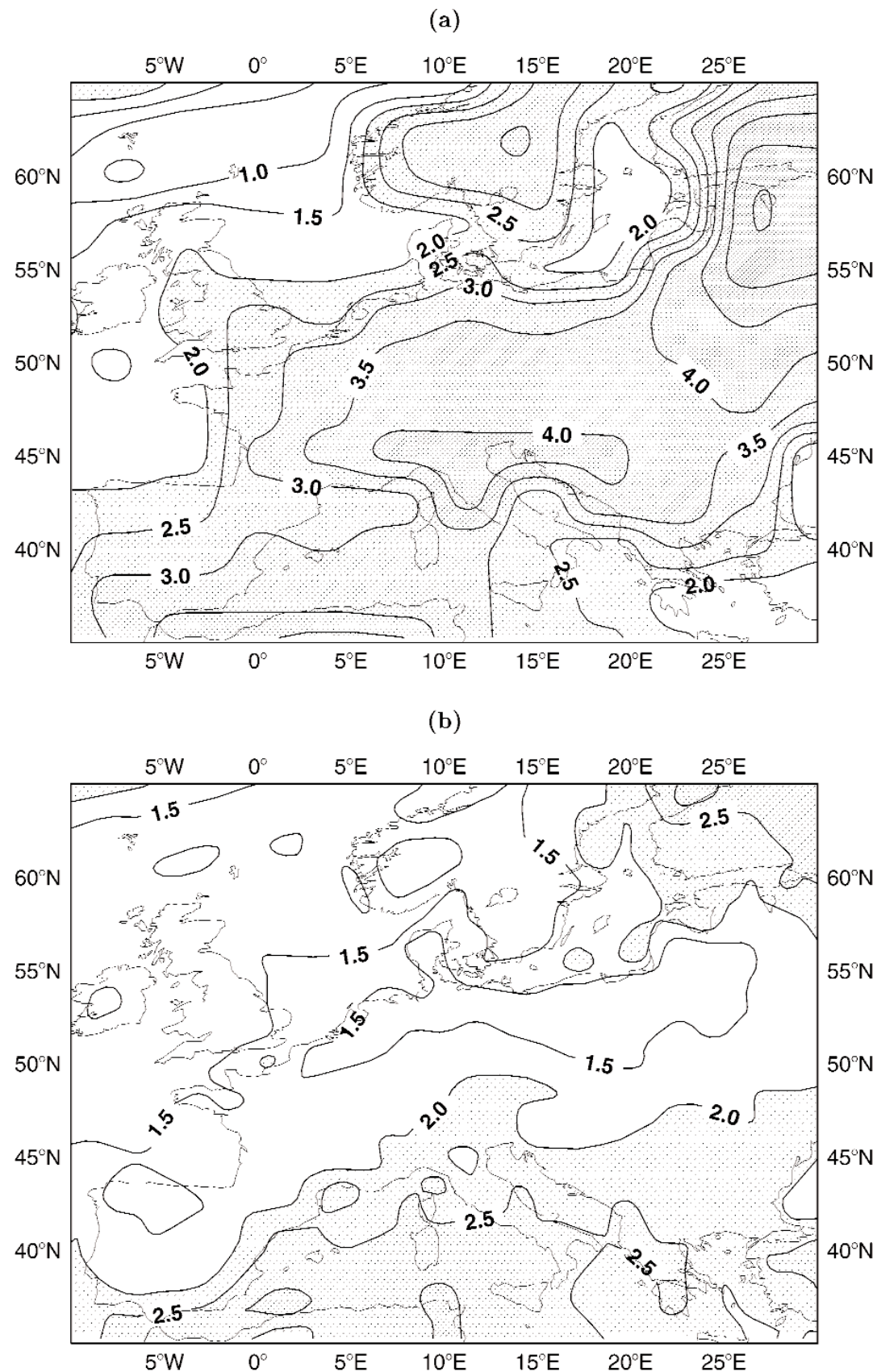


Figure 10.9: Winter surface air temperature change ($^{\circ}\text{C}$) over Europe at the time of CO₂ doubling in (a) a transient climate change experiment with the AOGCM HadCM2 and (b) the stretched grid AGCM ARPEGE driven by SSTs and sea-ice from the HadCM2 integration. From Dèquè *et al.* (1998).

have no significant impact (Bhaskaran *et al.*, 1996). Finally, location of boundaries over areas with significant topography may lead to inconsistencies and noise generation (e.g., Hong and Juang, 1998).

Surface forcing due to land, ocean and sea ice greatly affects regional climate simulation (e.g., Giorgi *et al.*, 1996; Seth and Giorgi, 1998; Wei and Fu, 1998; Christensen, 1999; Pan *et al.*, 1999; Pielke *et al.*, 1999; Rinke and Dethloff, 1999; Chase *et al.*, 2000; Maslanik *et al.*, 2000; Rummukainen *et al.*, 2000). In particular, RCM experiments do not start with equilibrium conditions and therefore the initialisation of surface variables, such as soil moisture and temperature, is important. For example, to reach equilibrium it can require a few seasons for the rooting zone (about 1 m depth) and years for the deep soils (Christensen, 1999).

The choice of RCM resolution can modulate the effects of physical forcings and parametrizations (Giorgi and Marinucci, 1996a; Laprise *et al.*, 1998). The description of the hydrologic cycle generally improves with increasing resolution due to the better topographical representation (Christensen *et al.*, 1998; Leung and Ghan, 1998). Resolving more of the spectrum of atmospheric motions at high resolution improves the representation of cyclonic systems and vertical velocities, but can sometimes worsen aspects of the model climatology (Machenhauer *et al.*, 1998; Kato *et al.*, 1999). Different resolutions may be required to capture relevant forcings in different sub-regions, which can be achieved via multiple one-way nesting (Christensen *et al.*, 1998; McGregor *et al.*, 1999), two-way nesting (Liston *et al.*, 1999) or smoothly varying horizontal grids (Qian and Giorgi, 1999). Only limited studies of the effects of changing vertical resolution have been published (Kato *et al.*, 1999).

RCM model physics configurations are derived either from a pre-existing (and well tested) limited area model system with modifications suitable for climate application (Pielke *et al.*, 1992; Giorgi *et al.*, 1993b,c; Leung and Ghan, 1995, 1998; Copeland *et al.*, 1996; Miller and Kim, 1997; Liston and Pielke 2000; Rummukainen *et al.*, 2000) or are implemented directly from a GCM (McGregor and Walsh, 1993; Jones *et al.*, 1995; Christensen *et al.*, 1996; Laprise *et al.*, 1998). In the first approach, each set of parametrizations is developed and optimised for the respective model resolutions. However, this makes interpreting differences between nested model and driving GCM more difficult, as these will not result only from changes in resolution. Also, the different model physics schemes may result in inconsistencies near the boundaries (Machenhauer *et al.*, 1998; Rummukainen *et al.*, 2000). The second approach maximises compatibility between the models. However, physics schemes developed for coarse resolution GCMs may not be adequate for the high resolutions used in nested regional models and may, at least, require recalibration (Giorgi and Marinucci, 1996a; Laprise *et al.*, 1998; see also Section 10.4). Overall, both strategies have shown performance of similar quality (e.g., IPCC, 1996), and either one may be preferable (Giorgi and Mearns, 1999). In the context of climate change simulations, if there is no resolution dependence, the second approach may be preferable to maximise consistency between RCM and GCM responses to the radiative forcing.

Ocean RCMs have been developed during the last decades for a broad variety of applications. To date, the specific use of these models, in a context similar to the use of nested atmospheric RCMs for climate change studies, is very limited (Kauker, 1998). Although the performance of ocean RCMs has yet to be assessed, it is known that a very high resolution, few tens of kilometres or less, is needed for accurate ocean simulations.

The construction of coupled RCMs is a very recent development. They comprise atmospheric RCMs coupled to other models of climate system components, such as lake, ocean/sea ice, chemistry/aerosol, and land biosphere/hydrology models (Hostetler *et al.*, 1994; Lynch *et al.*, 1995, 1997a,b, 1998; Leung *et al.*, 1996; Bailey *et al.*, 1997; Kim *et al.*, 1998; Qian and Giorgi 1999; Small *et al.*, 1999a,b; Bailey and Lynch, 2000a,b; Mabuchi *et al.*, 2000; Maslanik *et al.*, 2000; Rummukainen *et al.*, 2000; Tsvetsinskaya *et al.*, 2000; Weisse *et al.*, 2000). This promises the development of coupled “regional climate system models”.

10.5.1 Simulations of Current Climate

Simulations of current climate conditions serve to evaluate the performance of RCMs. Since the SAR, a vast number of such simulations have been conducted (McGregor, 1997; Appendices 10.1 to 10.3). These fall into two categories, RCMs driven by observed (or “perfect”) boundary conditions and RCMs driven by GCM boundary conditions. Observed boundary conditions are derived from Numerical Weather Prediction (NWP) analyses (e.g., European Centre for Medium Range Weather Forecast (ECMWF) reanalysis, Gibson *et al.* 1997; or National Center for Environmental Prediction (NCEP) reanalysis, Kalnay *et al.*, 1996). Over most regions they give accurate representation of the large-scale flow and tropospheric temperature structure (Gibson *et al.*, 1997), although errors are still present due to poor data coverage and to observational uncertainty. The analyses may be used to drive RCM simulations for short periods, for comparison with individual episodes, or over long periods to allow statistical evaluation of the model climatology. Comparison with climatologies is the only available evaluation tool for RCMs driven by GCM fields, with the caveats applied to GCM validation concerning the influence of sample size and decadal variability (see Sections 10.2, 10.3, and 10.4). Despite these, relatively short simulations (several years) can identify major systematic RCM biases if they yield departures from observations significantly greater than the observed natural variability (Machenhauer *et al.*, 1996, 1998; Christensen *et al.*, 1997; Jones *et al.*, 1999).

Often a serious problem in RCM evaluation is the lack of good quality high-resolution observed data. In many regions, observations are extremely sparse or not readily available. In addition, only little work has been carried out on how to use point measurements to evaluate the grid-box mean values from a climate model, especially when using sparse station networks or stations in complex topographical terrain (e.g., Osborn and Hulme, 1997). Most of the observational data available at typical RCM resolution (order of 50 km) is for precipitation and daily minimum and maximum temperature. While these fields have been shown to be useful for evaluating model performance, they

are also the end product of a series of complex processes, so that the evaluation of individual model dynamical and physical processes is necessarily limited. Additional fields need to be examined in model evaluation to broaden the perspective on model performance and to help delineate sources of model error. Examples are the surface energy and water fluxes.

Despite these problems, the situation is steadily improving in terms of grid-cell climatologies (Daly *et al.*, 1994; New *et al.*, 1999, 2000; Widman and Bretherton, 2000), with various groups developing high-resolution regional climatologies (e.g., Christensen *et al.*, 1998; Frei and Schär, 1998). In addition, regional programs such as the Global Energy and Water Cycle Experiment (GEWEX) Continental-Scale International Program (GCIP) have been designed with the purpose of developing sets of observation databases at the regional scale for model evaluation (GCIP, 1998).

10.5.1.1 Mean climate: Simulations using analyses of observations
Ideally, experiments using analyses of observations to drive the RCMs should precede any attempt to simulate climate change. The model behaviour, with realistic forcing, should be as close as possible to that of the real atmosphere and experiments driven by analyses of observations can reveal systematic model biases primarily due to the internal model dynamics and physics.

A list of published RCM simulations driven by analyses of observations is given in Appendix 10.1. Many of these studies present regional differences (or biases) of seasonally or monthly-averaged surface air temperature and precipitation from observed values. They indicate that current RCMs can reproduce average observations over regions of size 10^5 to 10^6 km 2 with errors generally below 2°C and within 5 to 50% of observed precipitation, respectively (Giorgi and Shields, 1999; Small *et al.*, 1999a,b; van Lipzig, 1999; Pan *et al.*, 2000). Uncertainties in the analysis fields, used to drive the models, and, in the observed station data sets, should be considered in the interpretation of these biases.

Various RCM intercomparison studies have been carried out to identify different or common model strengths and weaknesses, over Europe by Christensen *et al.* (1997), over the USA by Takle *et al.* (1999), and over East Asia by Leung *et al.* (1999a). For Europe a wide range of performance was reported, with the better models exhibiting a good simulation of surface air temperature (sub-regional monthly bias in the range $\pm 2^\circ\text{C}$), except over south-eastern Europe during summer. For the USA, a major finding was that the model ability to simulate precipitation episodes varied depending on the scale of the relevant dynamical forcing. Organised synoptic-scale precipitation systems were well simulated deterministically, while episodes of mesoscale and convective precipitation were represented in a more stochastic sense, with less degree of agreement with the observed events and among models. Over East Asia, a major factor in determining the model performance was found to be the simulation of cloud radiative processes.

10.5.1.2 Mean climate: Simulations using GCM boundary conditions

Since the SAR, evaluation of RCMs driven by GCM simulations of current climate has gained much attention (Appendix 10.2), as

this is the context in which many RCMs are used (e.g., for climate change experiments). Errors introduced by the GCM representation of large-scale circulations are transmitted to the RCM as, for example, clearly shown by Noguer *et al.* (1998). However, since the SAR, regional biases of seasonal surface air temperature and precipitation have been reduced and are mostly within 2°C, and 50 to 60% of observations (with exceptions in all seasons), respectively (Giorgi and Marinucci, 1996b; Noguer *et al.*, 1998; Jones *et al.*, 1999 for Europe; Giorgi *et al.*, 1998 for the continental USA; McGregor *et al.*, 1998 for Southeast Asia; Kato *et al.*, 2001 for East Asia). The reduction of biases is due to both better large-scale boundary condition fields and improved aspects of internal physics and dynamics in the RCMs.

The regionally averaged biases in the nested RCMs are not necessarily smaller than those in the driving GCMs. However, all the experiments mentioned above, along with those of Leung *et al.* (1999a,b), Laprise *et al.* (1998), Christensen *et al.* (1998) and Machenhauer *et al.* (1998) clearly show that the spatial patterns produced by the nested RCMs are in better agreement with observations because of the better representation of high-resolution topographical forcings and improved land/sea contrasts. For example, in simulations over Europe and central USA, Giorgi and Marinucci (1996a) and Giorgi *et al.* (1998) find correlation coefficients between simulated and observed seasonally averaged precipitation in the range of +0.53 to +0.87 in a nested RCM and -0.69 to +0.85 in the corresponding driving GCM.

The role of the high-resolution forcing was clearly demonstrated in the study of Noguer *et al.* (1998), which showed that the skill in simulating the mesoscale component of the climate signal (Giorgi *et al.*, 1994; Jones *et al.*, 1995) was little sensitive to the quality of the driving data (Noguer *et al.*, 1998). On the other hand, interactions between the large-scale driving data and high resolution RCM forcings can have negative effects. In simulations over the European region of Machenhauer *et al.* (1998), the increased shelter due to the better-resolved mountains in the RCMs caused an intensification of the GCM-simulated excessively dry and warm summer conditions over south-eastern Europe.

Horizontal resolution is especially important for the simulation of the hydrologic cycle. Christensen *et al.* (1998) showed that only at a very high resolution do the mountain chains in Norway and Sweden become sufficiently well resolved to yield a realistic simulation of the surface hydrology (Figure 10.10). An alternative strategy is to utilise a sub-grid scale scheme capable of resolving complex topographical features (Leung *et al.*, 1999a).

10.5.1.3 Climate variability and extreme events

A number of studies have investigated the interannual variability in RCM simulations driven by analyses of observations over different regions (e.g., Lüthi *et al.*, 1996 for Europe; Giorgi *et al.*, 1996 and Giorgi and Shields 1999 for the continental USA; Sun *et al.*, 1999 for East Africa; Small *et al.*, 1999a for central Asia; Rinke *et al.*, 1999 for the Arctic; van Lipzig, 1999 for Antarctica). These show that RCMs can reproduce well interannual anomalies of precipitation and surface air temperature, both in sign and magnitude, over sub-regions varying in size from a few hundred kilometres to about 1,000 km (Figure 10.11).

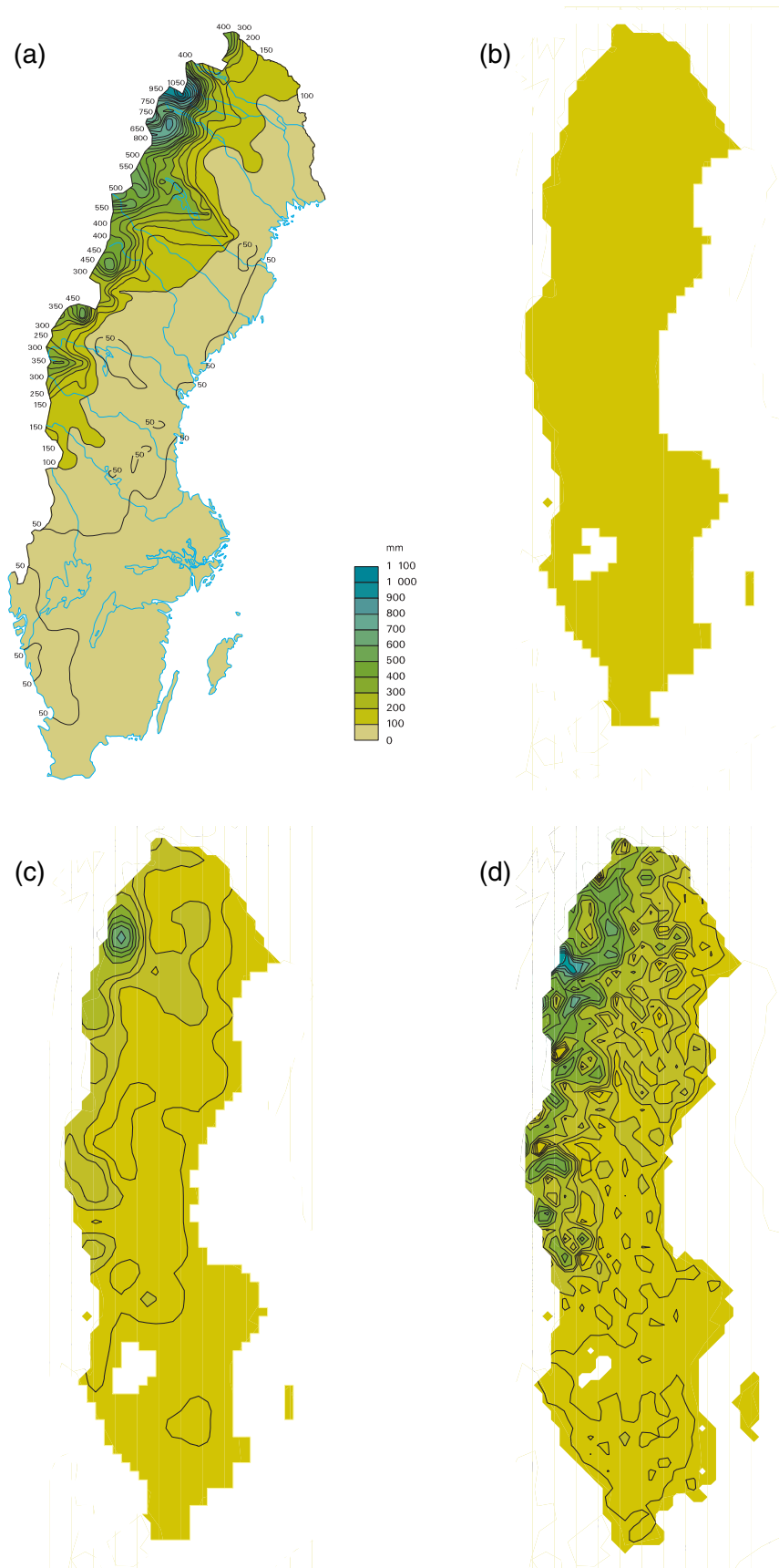


Figure 10.10: Summer (JJA) runoff for Sweden. (a) calculated with a calibrated hydrological model, using daily meteorological station observations and stream gauging stations (Raab and Vedin, 1995); (b) GCM simulation; (c) 55 km RCM simulation; (d) 18 km resolution RCM. Units are mm (from Christensen *et al.*, 1998).

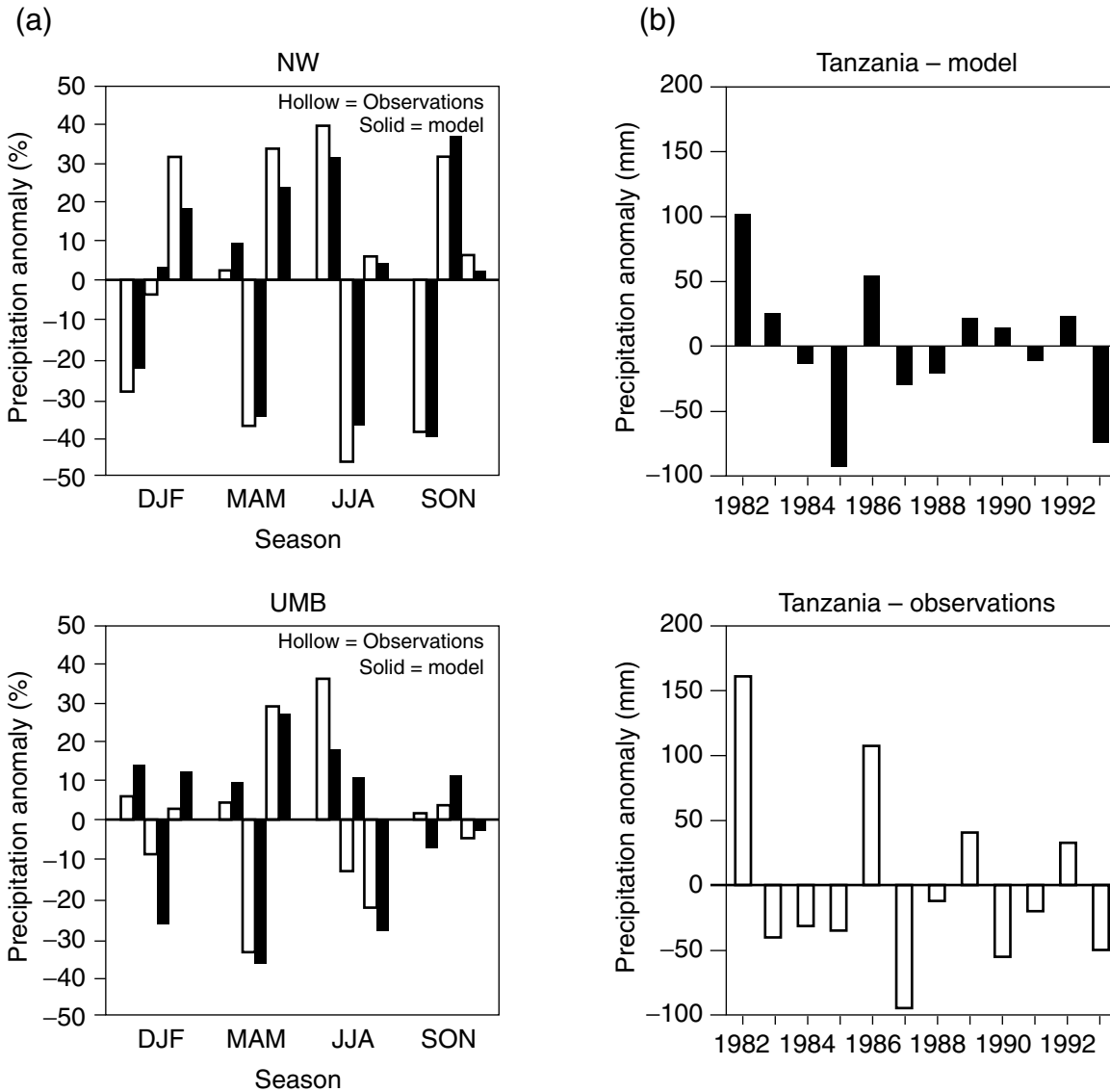


Figure 10.11: Examples of seasonal precipitation anomalies simulated with RCMs driven by analyses of observations over different regions. In all cases the anomalies are calculated as the difference between the precipitation of an individual season and the average for the seasonal value for the entire simulation. (a) (top) Northwestern USA (NW), and (bottom) Upper Mississippi Basin (UMB) for a three year simulation (1993 to 1996) over the continental USA. The three pairs of observed (hollow bars) and simulated (solid bars) anomalies for each season are grouped in sequential order from 1993 to 1996. Units are percentage of the three-year seasonal average (from Giorgi and Shields, 1999, Figure 9). (b) Precipitation anomalies for twelve short-rains periods over Tanzania for the October-December season: (top) model simulation, and (bottom) observations. Units are mm. (From Sun *et al.*, 1999).

At the intra-seasonal scale, the timing and positioning of regional climatological features such as the East Asia rain belt and the Baiu front can be reproduced with a high degree of realism with an RCM (Fu *et al.*, 1998). A good simulation of the intra-seasonal evolution of precipitation during the short rain season of East Africa has also been documented (Sun *et al.*, 1999). However, at shorter time-scales, Dai *et al.* (1999) found that, despite a good simulation of average precipitation, significant problems were exhibited by an RCM simulation of the observed diurnal cycle of precipitation over different regions of the USA.

Only a few examples are available of analysis of variability in RCMs driven by GCMs. At the intra-seasonal scale, Bhaskaran

et al. (1998) showed that the leading mode of sub-seasonal variability of the South Asia monsoon, a 30 to 50 day oscillation of circulation and precipitation anomalies, was more realistically captured by an RCM than the driving GCM. Hassell and Jones (1999) then showed that a nested RCM captured observed precipitation anomalies in the active break phases of the South Asia monsoon (5 to 10 periods of anomalous circulations and precipitation) that were absent from the driving GCM (Figure 10.12).

At the daily time-scale, some studies have shown that nested RCMs tend to simulate too many light precipitation events compared with station data (Christensen *et al.* 1998; Kato *et al.*, 2001). However, RCMs produce more realistic statistics of heavy precipitation events than the driving GCMs, sometimes capturing

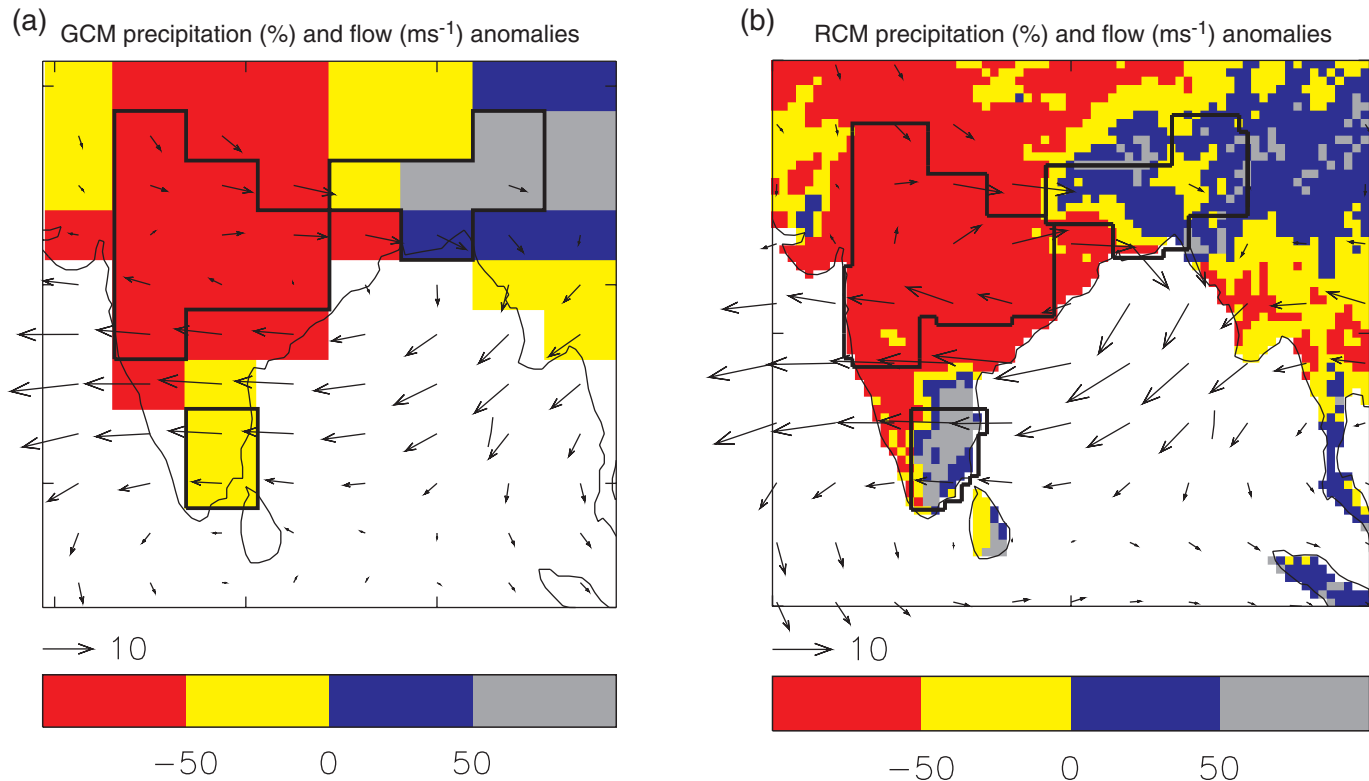


Figure 10.12: Relative characteristics of break and active precipitation composites of the Indian monsoon as simulated by (a) GCM and (b) RCM. Each field is the difference in the break and active composite precipitation as a percentage of the full mean. Overlaid are the 850 hPa wind anomalies (break composite minus active composite, units ms^{-1}). Regions marked where observed ratios are <-50% (central India) and >+50% (Tamil Nadu and north-eastern India) according to Hamilton (1977). From Hassell and Jones (1999).

extreme events entirely absent in the GCMs (Christensen *et al.*, 1998; Jones, 1999). Part of this is due to the inherent disaggregation of grid-box mean values resulting from the RCM's higher horizontal resolution. However, in one study, even when aggregated to the GCM grid scale, the RCM was closer to observations than the driving GCM (Durman *et al.*, 2001).

10.5.2 Simulations of Climate Change

Since the SAR, several multi-year RCM simulations of anthropogenic climate change, either from equilibrium experiments or for time slices of transient simulations, have become available (Appendix 10.3).

10.5.2.1 Mean climate

An important issue when analysing RCM simulations of climate change is the significance of the modelled responses. To date RCM simulations have been mostly aimed at evaluating models and processes rather than producing projections and, as such, they have been relatively short (10 years or less). At short time-scales, natural climate variability may mask all but the largest responses. For example, in an analysis of 10-year RCM simulations over Europe, Machenhauer *et al.* (1998) concluded that generally only the full area averaged seasonal mean surface temperature responses were statistically significant, and in only a few cases were sub-domain deviations from the mean response

significant. The changes in precipitation were highly variable in space, and, in each season, they were only significant in those few sub-areas having the largest changes. Similar results were documented by Pan *et al.* (2000) and Kato *et al.* (2001) for the USA and East Asia, respectively. Hence, 30-year samples may be required to confidently assess the mesoscale response of a RCM (Jones *et al.*, 1997). Partly to improve signal to noise definition, a transient RCM simulation of 140 years duration was recently conducted (Hennessy *et al.*, 1998; McGregor *et al.*, 1999).

Despite the limitations in simulation length, most RCM experiments clearly indicate that, while the large-scale patterns of surface climate change in the nested and driving models are similar, the mesoscale details of the simulated changes can be quite different. For example, significantly different patterns of temperature and rainfall changes were found in a regional climate change simulation for Australia (Whetton *et al.*, 2001). This was most clearly seen in mountainous areas (Figure 10.13). Winter rainfall in southern Victoria increased in the RCM simulation, but decreased in the driving GCM. High resolution topographical modification of the regional precipitation change signal in nested RCM simulations has been documented in other studies (Jones *et al.*, 1997; Giorgi *et al.*, 1998; Machenhauer *et al.*, 1998; Kato *et al.*, 2001).

The response in an RCM can also be modified by changes in regional feedbacks. In a 20 year nested climate change experiment for the Indian monsoon region, Hassell and Jones (1999)

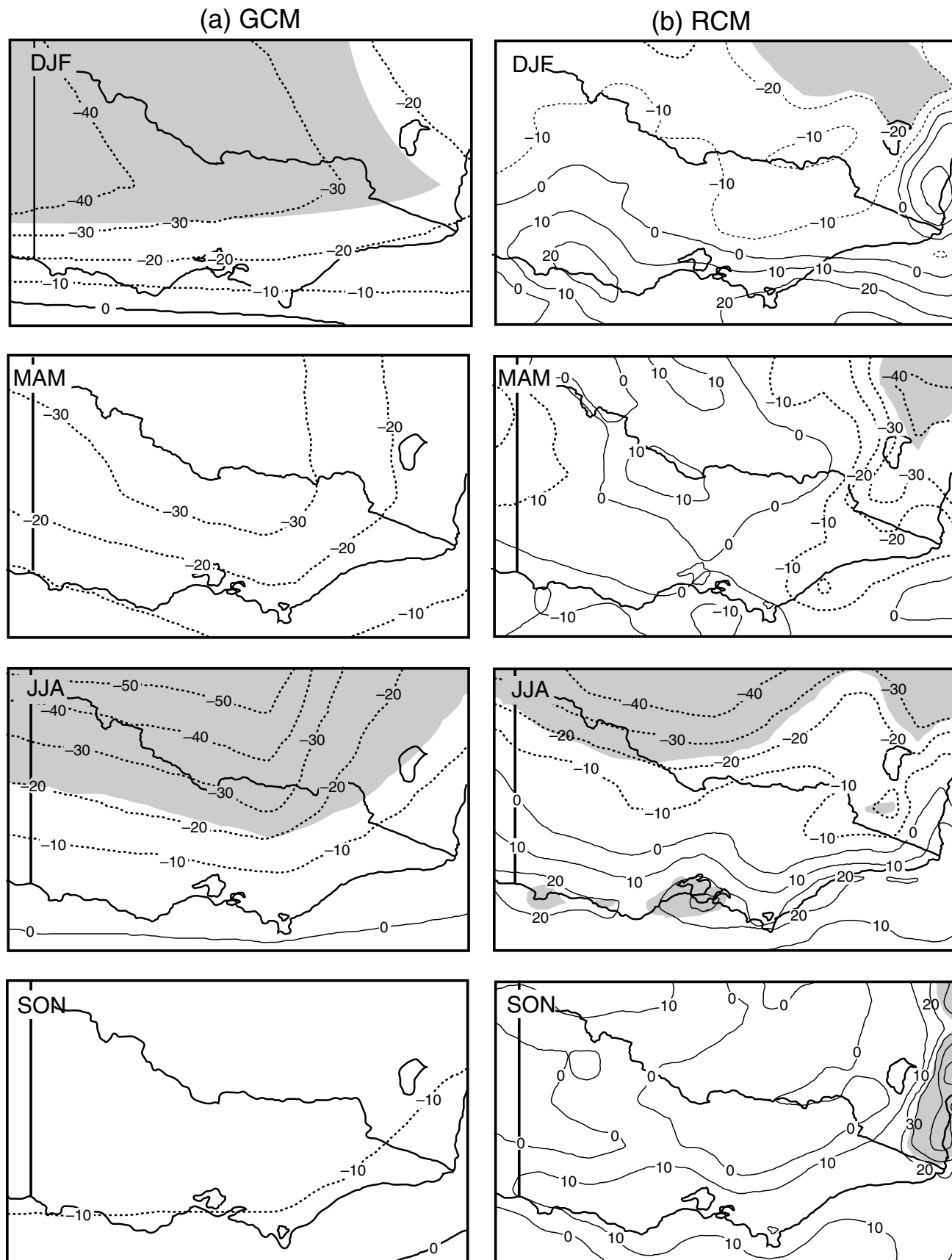


Figure 10.13: Percentage change in mean seasonal rainfall under 2×CO₂ conditions as simulated by a GCM (a) and a RCM (b) for a region around Victoria, Australia. Areas of change statistically significant at the 5% confidence level are shaded. Whetton *et al.* (2001).

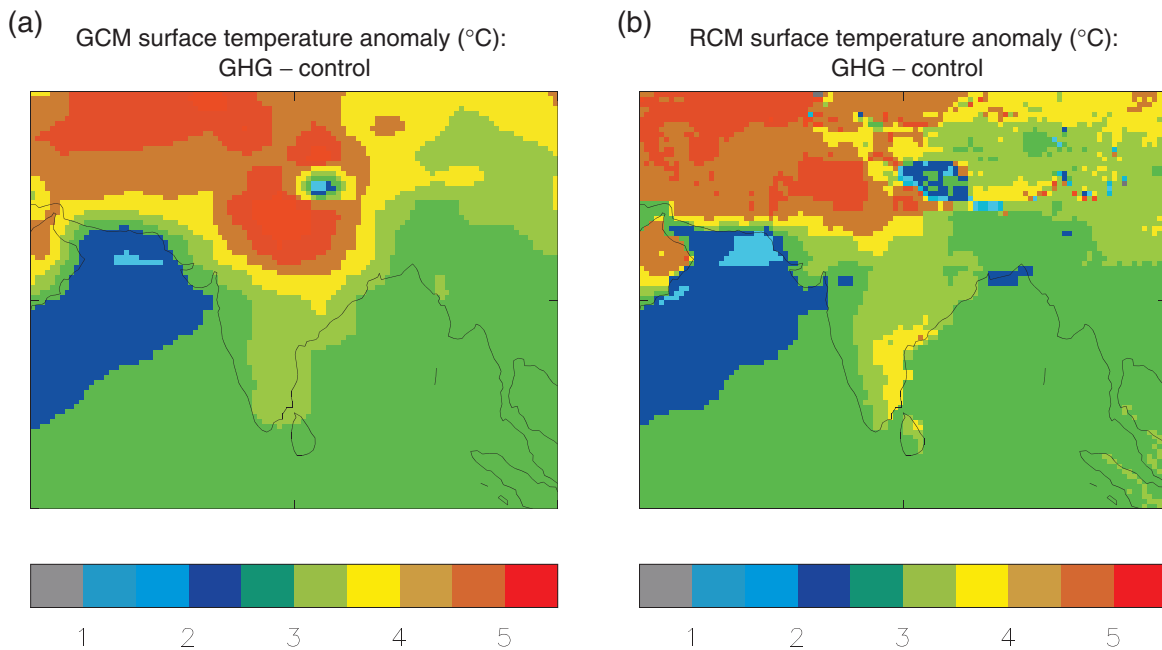


Figure 10.14: Simulated surface air temperature anomaly ($^{\circ}\text{C}$) for JJA, Indian monsoon region. GHG (2040 to 2060) minus control 20 year average for (a) GCM and (b) RCM. From Hassel and Jones (1999).

showed that a maximum anomaly of 5°C seen in central northern India in the GCM simulation was reduced and moved to the north-west in the nested RCM, with a secondary maximum appearing to the south-east (Figure 10.14). The shift of the main maximum was attributed to deficiencies in the GCM control climate that promoted excessive drying of the soil in North-west India. The secondary maximum was attributed to a complex response involving the RCM's better representation of the flow patterns in southern India resulting from an improved representation of the Western Ghats mountains. In this instance, it was argued that the improved realism of the RCM's control simulation increases confidence in its response.

The high resolution representation of mountainous areas in an RCM has made it possible to show that the simulated surface air temperature change signal due to $2\times\text{CO}_2$ concentration could have a marked elevation dependency, resulting in more pronounced warming at high elevations than low elevations as shown in Figure 10.15 (Giorgi *et al.*, 1997). This is primarily caused by a depletion of the snow pack in enhanced GHG conditions and the associated snow albedo feedback mechanism, and it is consistent with observed temperature trends for anomalous warm winters over the alpine region. A similar elevation modulation of the climate change signal has been confirmed in later studies utilising both RCMs and GCMs (e.g., Leung and Ghan, 1999b; Fyfe and Flato, 1999).

The impact of land-use changes on regional climate has been addressed in RCM simulations (e.g., Wei and Fu, 1998; Pan *et al.*, 1999; Pielke *et al.*, 1999; Chase *et al.*, 2000). Land-use changes due to human activities could induce climate modifications, at the regional and local scale, of magnitude similar to the observed climatic changes during the last century (Pielke *et al.*, 1999; Chase *et al.*, 2000). The issue of regional climate modification by

land-use change has been little explored within the context of the global change debate and, because of its potential importance, is in need of further examination.

10.5.2.2 Climate variability and extreme events

Changes in climate variability between control and $2\times\text{CO}_2$ simulations with a nested RCM for the Great Plains of the USA have been reported (Mearns, 1999; Mearns *et al.*, 1999). There is indication of significant decreases in daily temperature variability in winter and increases in temperature variability in summer. These changes are very similar to those of the driving GCM, while changes in variability of precipitation are quite different in the nested and driving models, particularly in summer, with increases being more pronounced in the RCM. Similar results have been documented over the Iberian Peninsula (Gallardo *et al.*, 1999).

Different studies have analysed changes in the frequency of heavy precipitation events in enhanced GHG climate conditions over the European region (Schär *et al.*, 1996; Frei *et al.*, 1998; Durman *et al.*, 2001). They all indicate an increase of up to several tens of percentage points in the frequency of occurrence of precipitation events exceeding 30 mm/day, with these increases being less than those simulated by the driving GCMs (see also Jones *et al.*, 1997). In a transient RCM simulation for 1961 to 2100 over south-eastern Australia, substantial increases were found in the frequency of extreme daily rainfall and days of extreme high maximum temperature (Hennessy *et al.*, 1998). In this long simulation, changes in the frequency of long-duration extreme events (such as droughts) were identified. Finally, increases in the number of typhoons reaching mainland China and in the number of heavy rain days were reported for enhanced GHG conditions in RCM simulations over East Asia (Gao *et al.*, 2001).

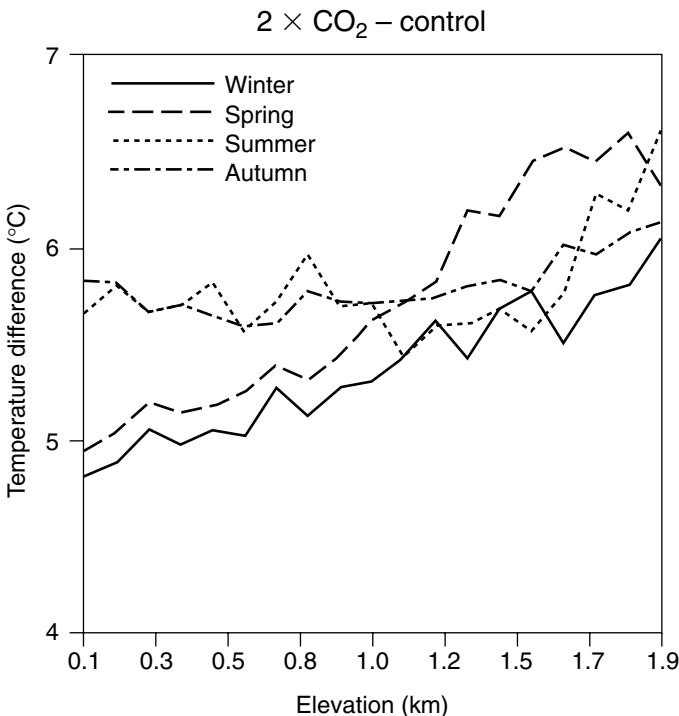


Figure 10.15: Difference between $2 \times \text{CO}_2$ and control run surface air temperature as a function of elevation over the Alpine sub-region for the four seasons. Units are $^{\circ}\text{C}$. From Giorgi *et al.* (1997).

10.5.3 Summary and Recommendations

Since the SAR, significant improvements have been achieved in the areas of development and understanding of the nested regional climate modelling technique. These include many new RCM systems, multiple nesting, coupling with different components of the climate system and research into the effects of domain size, resolution, boundary forcing and internal model variability. As a result, a number of RCM systems are currently available with the capability of high-resolution, multi-decadal simulations in a variety of regional settings. Nested RCMs have shown marked improvements in their ability to reproduce present day average climate, with some of this improvement due to better quality driving fields provided by GCMs. Seasonal temperature and precipitation biases in state-of-the-art RCMs are generally less than 1 to 2°C and a few percent to 50 to 60 % of observed precipitation, respectively, over regions of size 10^5 to 10^6 km^2 . However, it is imperative for the effective use of RCMs in climate change work that the quality of GCM large-scale driving fields continues to improve. Research aiming at reducing systematic errors in both GCMs and RCMs should be carried out. With significantly improved model systems the evidence, so far, indicates that improved regional climate change simulations can be produced in the near future.

The analysis of RCM simulations has extended beyond simple averages to include higher-order climate statistics, and has indicated that RCMs can effectively reproduce interannual variability when driven by good quality forcing fields. However, more analysis and improvements are needed of the model

performance in simulating climate variability at short time-scales (daily to sub-daily).

A serious problem concerning RCM evaluation is a general lack of good quality high-resolution observed data. In many areas, observations are extremely sparse due to complex geography or remoteness of settings. In addition, only a little work has been carried out on how to use point measurements to evaluate the grid-box mean values from a climate model, especially when using sparse station networks. This limits the ability to assess model skill in complex terrain and remote regions. It is essential for the advancement of regional climate understanding and modelling, that more research aiming at improving the quality of data for model evaluation is performed.

Overall, the evidence is strong that regional models consistently improve the spatial detail of simulated climate compared to GCMs because of their better representation of sub-GCM grid scale forcings, especially in regard to the surface hydrologic budget. This is not necessarily the case for region-averaged climate. The increased resolution of RCMs also allows the simulation of a broader spectrum of weather events, in particular concerning higher order climate statistics such as daily precipitation intensity distributions. Analysis of some RCM experiments indicate that this is in the direction of increased agreement with observations.

Several RCM studies have been important for understanding climate change processes, such as the elevation signature of the climate change signal or the effect of climate change at the river catchment level. However, a consistent set of RCM simulations of climate change for different regions which can be used as climate change scenarios for impact work is still not available. Most RCM climate change simulations have been sensitivity and process studies aimed at specific goals. The need is there to co-ordinate RCM simulation efforts and to extend studies to more regions so that ensemble simulations with different models and scenarios can be developed to provide useful information for impact assessments. This will need to be achieved under the auspices of international or large national programmes. Within this context, an important issue is to provide RCM simulations of increasing length to minimise limitations due to sampling problems.

10.6 Empirical/Statistical and Statistical/Dynamical Methods

10.6.1 Introduction

As with the dynamical downscaling of RCMs, the methods described in this section rely on the concept that regional climates are largely a function of the large-scale atmospheric state. In empirical downscaling the cross-scale relationship is expressed as a stochastic and/or deterministic function between a set of large-scale atmospheric variables (predictors) and local/regional climate variables (predictands). Predictor and predictand can be the same variables on different spatial scales (e.g., Bürger, 1997; Wilks, 1999b; Widmann and Bretherton, 2000), but more commonly are different.

When using downscaling for assessing regional climate change, three implicit assumptions are made:

- The predictors are variables of relevance to the local climate variable being derived, and are realistically modelled by the GCM. Tropospheric quantities such as temperature or geopotential height are more skilfully represented than derived variables such as precipitation at the regional or grid scale (e.g., Osborn and Hulme, 1997; Trigo and Palutikof, 1999). Furthermore, there is no theoretical level of spatial aggregation at which GCMs can be considered skilful, though there is evidence that this is several grid lengths (Widmann and Bretherton, 2000).
- The transfer function is valid under altered climatic conditions (see Section 10.6.2.2). This cannot be proven in advance, as it would require the observational record to span all possible future realisations of the predictors. However, it could be evaluated with nested AOGCM/RCM simulations of present and future climate, using the simulation of present climate to determine the downscaling function and testing the function against the future time slice.
- The predictors fully represent the climate change signal. Most downscaling approaches to date have relied entirely on circulation-based predictors and, therefore, can only capture this component of the climate change. More recently other important predictors, e.g., atmospheric humidity, have been considered (e.g., Charles *et al.*, 1999b; Hewitson, 1999).

A diverse range of downscaling methods has been developed, but, in principle, these models are based on three techniques:

- Weather generators, which are random number generators of realistic looking sequences of local climate variables, and may be conditioned upon the large-scale atmospheric state (Section 10.6.2.1);
- Transfer functions, where a direct quantitative relationship is derived through, for example, regression (Section 10.6.2.2);
- Weather typing schemes based on the more traditional synoptic climatology concept (including analogues and phase space partitioning) and which relate a particular atmospheric state to a set of local climate variables (Section 10.6.2.3).

Each of these approaches has relative strengths and weaknesses in representing the range of temporal variance of the local climate predictand. Consequently, the above approaches are often used in conjunction with one another in order to compensate for the relative deficiencies in one method.

Most downscaling applications have dealt with temperature and precipitation. However, a diverse array of studies exists in which other variables have been investigated. Appendix 10.4 provides a non-exhaustive list of past studies indicating predictands, geographical domain, and technique category. In light of the diversity in the literature, we concentrate on references to applications since 1995 and based on recent global climate change projections.

10.6.2 Methodological Options

10.6.2.1 Weather generators

Weather generators are statistical models of observed sequences of weather variables (Wilks and Wilby, 1999). Most of them focus on the daily time-scale, as required by many impact models, but sub-daily models are also available (e.g., Katz and Parlange, 1995). Various types of daily weather generators are available, based on the approach to modelling daily precipitation occurrence, and usually these rely on stochastic processes. Two of the more common are the Markov chain approach (e.g., Richardson, 1981; Hughes *et al.*, 1993; Lettenmaier, 1995; Hughes *et al.*, 1999; Bellone *et al.*, 2000) and the spell length approach (Roldan and Woolhiser, 1982; Racksko *et al.*, 1991; Wilks, 1999a). The adequacy of the stochastic models analysed in these studies varied with the climate characteristics of the locations. For example, Wilks (1999a) found the first-order Markov model to be adequate for the central and eastern USA, but that spell length models performed better in the western USA. An alternative approach would include stochastic mechanisms of storm arrivals able to produce the clustering found in observed sequences (e.g., Smith and Karr, 1985; Foufoula-Georgiou and Lettenmeier, 1986; Gupta and Waymire, 1991; Cowpertwait and O'Connell, 1997; O'Connell, 1999).

In addition to statistical models of precipitation frequency and intensity, weather generators usually produce time-series of other variables, most commonly maximum and minimum temperature, and solar radiation. Others also include additional variables such as relative humidity and wind speed (Wallis and Griffiths, 1997; Parlange and Katz, 2000.) The most common means of including variables other than precipitation is to condition them on the occurrence of precipitation (Richardson, 1981), most often via a multiple variable first-order autoregressive process (Perica and Foufoula-Georgiou, 1996a,b; Wilks, 1999b). The parameters of the weather generator can be conditioned upon a large-scale state (see Katz and Parlange, 1996; Wilby, 1998; Charles *et al.*, 1999a), or relationships between large-scale parameter sets and local-scale parameters can be developed (Wilks, 1999b).

10.6.2.2 Transfer functions

The more common transfer functions are derived from regression-like techniques or piecewise linear or non-linear interpolations. The simplest approach is to build multiple regression models with free atmosphere grid-cell values as predictors for surface variables such as local temperatures (e.g., Sailor and Li, 1999). Other regression models have used fields of spatially distributed variables (e.g., D. Chen *et al.*, 1999), principal components of geopotential height fields (e.g., Hewitson and Crane, 1992), Canonical Correlation Analysis (CCA) and a variant termed redundancy analysis (WASA, 1998) and Singular Value Decomposition (e.g., von Storch and Zwiers, 1999).

Most applications have dealt with monthly or seasonal rainfall (e.g., Busuioc and von Storch, 1996; Dehn and Buma, 1999); local pressure tendencies (a proxy for local storminess; Kaas *et al.*, 1996); climate impact variables such as salinity and oxygen (Heyen and Dippner, 1998; Zorita and Laine, 1999); sea

level (e.g., Cui *et al.*, 1996); and ecological variables such as abundance of species (e.g., Kröncke *et al.*, 1998). In addition statistics of extreme events such as storm surge levels (e.g., von Storch and Reichardt, 1997) and ocean wave heights (WASA, 1998) have been simulated.

An alternative to linear regression is piecewise linear or non-linear interpolation (Brandsma and Buishand, 1997; Buishand and Brandsma, 1999), for example, the “kriging” tools from geostatistics (Biau *et al.*, 1999). One application of this approach is a non-linear model of snow cover duration in Austria derived from European mean temperature and altitude (Hantel *et al.*, 1999). An alternative approach is based on Artificial Neural Networks (ANNs) that allow the fit of a more general class of statistical model (Hewitson and Crane, 1996; Trigo and Palutikof, 1999). For example, Crane and Hewitson (1998) apply ANN downscaling to GCM data in a climate change application over the west coast of the USA using atmospheric circulation and humidity as predictors to represent the climate change signal. The approach was shown to accurately capture the local climate as a function of atmospheric forcing. In application to GCM data, the regional results revealed significant differences from the co-located GCM grid cell, e.g., a significant summer increase in precipitation in the downscaled data (Figure 10.16).

10.6.2.3 Weather typing

This synoptic downscaling approach relates “weather classes” to local and regional climate variations. The weather classes may be defined synoptically or fitted specifically for downscaling purposes by constructing indices of airflow (Conway *et al.*, 1996). The frequency distributions of local or regional climate are then derived by weighting the local climate states with the relative frequencies of the weather classes. Climate change is then estimated by

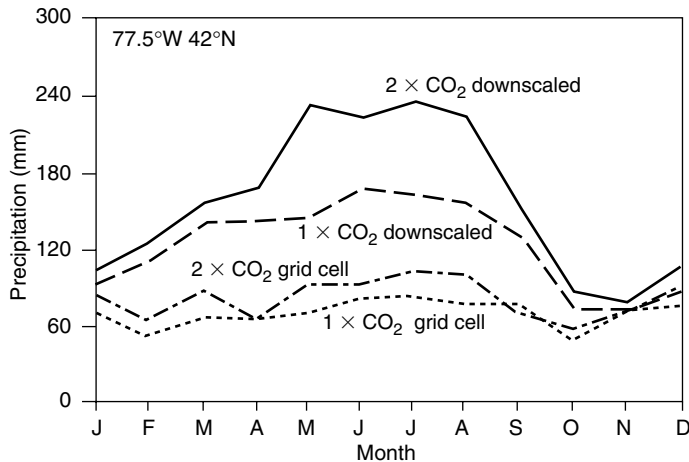


Figure 10.16: Climate change scenario of monthly mean precipitation (mm) over the Susquehanna river basin, USA. Monthly means derived using daily down-scaled precipitation generated with an Artificial Neural Network (ANN) and atmospheric predictors from $1\times\text{CO}_2$ and $2\times\text{CO}_2$ GCM simulations. Also shown are the GCM grid cell precipitation values from the co-located grid cell. From Crane and Hewitson (1998).

determining the change of the frequency of weather classes. However, typing procedures contain a potentially critical weakness in assuming that the characteristics of the weather classes do not change.

In many cases, the local and regional climate states are derived by sampling the observational record. For example, Wanner *et al.* (1997) and Widmann and Schär (1997) used changing global to continental scale synoptic structures to understand and reconstruct Alpine climate variations. The technique was applied similarly for New Zealand (Kidson and Watterson, 1995) and to a study of changing air pollution mechanisms (Jones and Davies, 2000).

An extreme form of weather typing is the analogue method (Zorita *et al.*, 1995). A similar concept, although mathematically more demanding, is Classification And Tree Analysis (CART) which uses a randomised design for picking regional distributions (Hughes *et al.*, 1993; Lettenmaier, 1995). Both analogue and CART approaches return approximately the right level of variance and correct spatial correlation structures.

Weather typing is also used in statistical-dynamical downscaling (SDD), a hybrid approach with dynamical elements (Frey-Buness *et al.*, 1995 and see references in Appendix 10.4). GCM results of a multi-year climate period are disaggregated into non-overlapping multi-day episodes of quasi-stationary large-scale flow patterns. Similar episodes are then grouped in classes of different weather types, and, members of these classes are simulated with an RCM. The RCM results are statistically evaluated, and the frequency of occurrence of the respective classes determines their statistical weight. An advantage of the SDD technique over other empirical downscaling techniques is that it specifies a complete three-dimensional climate state. The advantage over continuous RCM simulations is the reduction in computing time, as demonstrated in Figure 10.17.

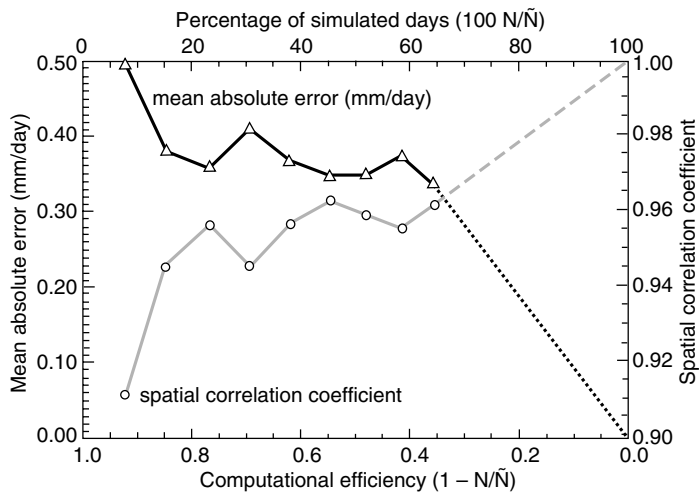


Figure 10.17: Similarity of time mean precipitation distributions obtained in a continuous RCM simulation and through statistical-dynamical downscaling (SDD) for different levels of disaggregation. Black line: mean absolute error (mm/day), grey line: spatial correlation coefficient. Horizontal axis: computational load of SDD. N is the number of days simulated in SDD, \tilde{N} the number of days simulated with the continuous RCM simulation.

10.6.3 Issues in Statistical Downscaling

10.6.3.1 Temporal variance

Transfer function approaches and some weather typing methods suffer from an under prediction of temporal variability, as this is related only in part to the large-scale climate variations (see Katz and Parlange, 1996). Two approaches have been used to restore the level of variability: inflation and randomisation. In the inflation approach the variation is increased by the multiplication of a suitable factor (Karl *et al.*, 1990). A more sophisticated version is “expanded downscaling”, a variant of Canonical Correlation Analysis that ensures the right level of variability (Bürger, 1996; Huth, 1999; Dehn *et al.*, 2000). In the randomisation approaches, the unrepresented variability is added as noise, possibly conditioned on synoptic state (Buma and Dehn, 1998; Dehn and Buma 1999; Hewitson, 1999; von Storch, 1999b).

Often weather generators have difficulty in representing low frequency variance, and conditioning the generator parameters on the large-scale state may alleviate this problem (see Katz and Parlange, 1996; Wilby, 1998; Charles *et al.*, 1999a). For example, Katz and Parlange (1993, 1996) modelled daily time-series of precipitation as a chain-dependent process, conditioned on a discrete circulation index. The results demonstrated that the mean and standard deviation of intensity and the probability of precipitation varied significantly with the circulation, and reproduced the precipitation variance statistics of the observations better than the unconditioned model. The method describes the mean precipitation as a linear function of the circulation state, and the standard deviation as a non-linear function (Figure 10.18).

10.6.3.2 Evaluation

The evaluation of downscaling techniques is essential but problematic. It requires that the validity of the downscaling functions under future climates be demonstrated, and that the

predictors represent the climate change signal. It is not possible to achieve this rigorously as the empirical knowledge available is insufficient. The analysis of historical developments, e.g., by comparing downscaling models between recent and historical periods (Jacobbeit *et al.*, 1998), as well as simulations with GCMs can provide support for these assumptions. However, the success of a statistical downscaling technique for representing present day conditions does not necessarily imply that it would give skilful results under changed climate conditions, and may need independent confirmation from climate model simulations (Charles *et al.*, 1999b).

The classical validation approach is to specify the downscaling technique from a segment of available observational evidence and then assess the performance of the empirical model by comparing its predictions with independent observed values. This approach is particularly valuable when the observational record is long and documents significant changes (greater than 50 years in some cases; Hanssen-Bauer and Førland (1998, 2000)). An example is the analysis of absolute pressure tendencies in the North Atlantic (Kaas *et al.*, 1996). As another example, Wilks (1999b) developed a downscaling function on dry years and found it functioned well in wet years.

An alternative approach is to use a series of comparisons between models and transfer functions (e.g., González-Rouco *et al.*, 1999, 2000). For instance, empirically derived links were shown to be incorporated in a GCM (Busuioc *et al.*, 1999) and a RCM (Charles *et al.*, 1999b). Then a climatic change due to doubling of CO₂ was estimated through the empirical link and compared with the result of the dynamical models. In both cases, the dynamical response was found consistent for the winter season, indicating the validity of the empirical approach, although less robust results were noted in the other seasons.

10.6.3.3 Choice of predictors

There is little systematic work explicitly evaluating the relative skill of different atmospheric predictors (Winkler *et al.*, 1997). This is despite the availability of disparate studies that evaluate a broad range of predictors, predictands and techniques (see Appendix 10.4). Useful summaries of downscaling techniques and the predictors used are also presented in Rummukainen (1997), Wilby (1998), and Wilby and Wigley (2000).

The choice of the predictor variables is of utmost importance. For example, Hewitson and Crane (1996) and Hewitson (1999) have demonstrated how the down-scaled projection of future change in mean precipitation and extreme events may alter significantly depending on whether or not humidity is included as a predictor. The downscaled results can also depend on whether absolute or relative humidity is used as a predictor (Charles *et al.*, 1999b). The implication here is that while a predictor may or may not appear as the most significant when developing the downscaling function under present climates, the changes in that predictor under a future climate may be critical for determining the climate change. Some estimation procedures, for example stepwise regression, are not able to recognise this and exclude variables that may be vital for climate change.

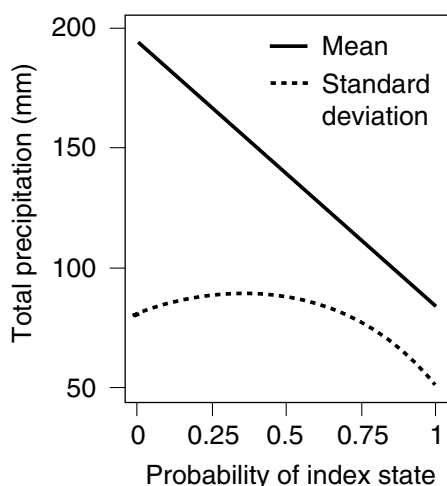


Figure 10.18: Hypothetical changes in mean and standard deviation of January total precipitation at Chico, California, as a function of changing probability that January mean sea level pressure is above normal.

A similar issue exists with respect to downscaling temperature. Werner and von Storch (1993), Hanssen-Bauer and Førland (2000) and Mietus (1999) noted that low-frequency changes in local temperature during the 20th century could only partly be related to changes in circulation. Schubert (1998) makes a vital point in noting that changes of local temperature under doubled atmospheric CO₂ may be dominated by changes in the radiative properties of the atmosphere rather than circulation changes. These can be accounted for by incorporating the large-scale temperature field from the GCM as a surrogate indicator of the changed radiative properties of the atmosphere (Dehn and Buma, 1999) or by using several large-scale predictors, such as gridded temperature and circulation fields (e.g., Gyalistras *et al.*, 1998; Huth, 1999).

With the recent availability of global reanalyses (Kalnay *et al.*, 1996; Gibson *et al.*, 1997), the number of candidate predictor fields has been greatly enhanced (Solman and Nuñez, 1999). Prior to this the empirical evidence about the co-variability of regional/local predictands and large-scale predictors was limited mostly to gridded near surface temperature and/or air pressure. These “new” data sets allow significant improvements in the design of empirical downscaling techniques, in particular by incorporating knowledge about detailed meteorological processes. Taking advantage of these new data sets have allowed systematic evaluation of a broad range of possible predictors for daily precipitation. It has been found that indicators of mid-tropospheric circulation and humidity to be the most critical predictors, with surface flow and humidity information being important under orographic rainfall.

10.6.4 Intercomparison of Statistical Downscaling Methodologies

An increasing number of studies comparing different downscaling studies have emerged since the SAR. However, there is a paucity of systematic studies that use common data sets applied to different procedures and over the same geographic region. A number of articles discussing different empirical and dynamical downscaling approaches present summaries of the relative merits and shortcomings of different procedures (Giorgi and Mearns, 1991; Hewitson and Crane, 1996; Rummukainen, 1997; Wilby and Wigley, 1997; Gyalistras *et al.*, 1998; Kidson and Thompson, 1998; Biau *et al.*, 1999; Murphy, 1999; ; von Storch, 1999b; Zorita and von Storch, 1999; Murphy, 2000). However, these inter-comparisons vary widely with respect to predictors, predictands and measures of skill. Consequently, a systematic, internationally co-ordinated inter-comparison project would be particularly helpful in addressing this issue.

The most systematic and comprehensive study so far compared empirical transfer functions, weather generators, and circulation classification schemes over the same geographical region using climate change simulations and observational data (Wilby and Wigley, 1997; Wilby, 1998). This considered a demanding task to downscale daily precipitation for six locations over North America, spanning arid, moist tropical, maritime, mid-latitude, and continental climate regimes. Fourteen measures of skill were used, strongly emphasising daily statistics, and included

wet and dry spell length, 95th percentile values, wet-wet day probabilities, and several measures of standard deviation. Downscaling procedures in the study included two different weather generators, two variants of an ANN-based technique, and two stochastic/circulation classification schemes based on vorticity classes.

The results require careful evaluation as they indicate relative merits and shortcoming of the different procedures rather than recommending one over another. Overall, the weather generators captured the wet-day occurrence and the amount distributions in the data well, but were less successful at capturing the interannual variability, while the opposite results was found for the ANN procedures. The stochastic/circulation typing schemes, as something of a combination of the principles underlying the other methods, were a better all-round performer.

A factor not yet fully evaluated in any comparative study is that of the temporal evolution of daily events which may be critical for some applications, e.g., hydrological modelling. While a downscaling procedure may correctly represent, for example, the number of rain days, the temporal sequencing of these may be as important. Zorita *et al.* (1995) and Zorita and von Storch (1997) compared a CART technique, a CCA and an ANN technique with the analogue technique, and found the simpler analogue technique performed as well as the more complicated methods.

A number of analyses have dealt with the relative merits of non-linear and linear approaches. For example, the relationships between daily precipitation and circulation indicators are often non-linear (Conway *et al.*, 1996; Brandsma and Buishand, 1997). Similarly, Corte-Real *et al.* (1995) applied multivariate adaptive regression splines (MARS) to approximate the non-linear relationships between large-scale circulation and monthly mean precipitation. In a comparison of kriging and analogues, Biau *et al.* (1999) and von Storch (1999c) show that kriging resulted in better specifications of averaged quantities but too low variance, whereas analogues returned the right variance but lower correlation. In general, it appears that downscaling of the short-term climate variance benefits from the use of non-linear models.

Most of the comparative studies mentioned above come to the conclusion that techniques differ in their success of specifying regional climate, and the relative merits and shortcomings emerge differently in different studies and regions. This is not surprising, as there is considerable flexibility in setting up a downscaling procedure, and the suitability of a technique and the adaptation to the problem at hand varies. This flexibility is a distinct advantage of empirical methods.

10.6.5 Summary and Recommendations

A broad range of statistical downscaling techniques has been developed in the past few years. Users of GCM-based climate information may choose from a large variety of methods conditional upon their needs. Weather generators provide realistic sequences of high temporal resolution events. With transfer functions, statistics of regional and local climate, such as conditional means or quantiles, may consistently be derived from GCM generated data. Techniques based on weather typing serve both purposes, but are less adapted to specific applications.

Downscaling means post-processing GCM data; it cannot account for insufficiencies in the driving GCM. As statistical techniques combine the existing empirical knowledge, statistical downscaling can describe only those links that have been observed in the past. Thus, it is based on the assumption that presently found links will prevail under different climate conditions. It may be, in particular, that under present conditions some predictors appear less relevant, but become significant in describing climate change. It is recommended to test statistical downscaling methods by comparing their estimates with high resolution dynamical model simulations. The advent of decades-long atmospheric reanalyses has offered the community many more atmospheric large-scale variables to incorporate as predictors.

Statistical downscaling requires the availability of long and homogeneous data series spanning the range of observed variance, while the computational resources needed are small. Therefore, statistical downscaling techniques are suitable tools for scientific communities without access to supercomputers and with little experience in process-based climate modelling. Furthermore, statistical techniques may relate directly GCM-derived data to impact relevant variables, such as ecological variables or ocean wave heights, which are not simulated by contemporary climate models.

It is concluded that statistical downscaling techniques are a viable complement to process-based dynamical modelling in many cases, and will remain so in the future.

10.7 Intercomparison of Methods

Few formal comparative studies of different regionalisation techniques have been carried out. To date, published work has mostly focused on the comparison between RCMs and statistical downscaling techniques. Early applications of RCMs for climate change simulations (Giorgi and Mearns, 1991; Giorgi *et al.*, 1994) compared the models against observations or against the driving GCMs, but not against statistical/empirical techniques.

Kidson and Thompson (1998) compared the RAMS (Regional Atmospheric Modelling System) dynamical model and a statistical regression-based technique. Both approaches were applied to downscale reanalysis data (ECMWF) over New Zealand to a grid resolution of 50 km. The statistical downscaling used a screening regression technique to predict local minimum and maximum temperature and daily precipitation, at both monthly and daily time-scales. The regression technique limits each regression equation to five predictors (selected from Empirical Orthogonal Functions (EOFs) of atmospheric fields). Both monthly and daily results indicated little difference in skill between the two techniques, and Kidson and Thompson (1998) suggested that, subject to the assumption of statistical relationships remaining viable under a future climate, the computational requirements do not favour the use of the dynamical model. They also noted, however, that the dynamical model performed better with the convective components of precipitation.

Bates *et al.* (1998) compared a south-western Australia simulation using the DARLAM (CSIRO Division of Atmospheric Research Limited Area Model) model with a down-scaled DARLAM simulation where the downscaling model had

been fitted independently to observational data. The downscaling reproduced observed precipitation probabilities and wet and dry spell frequencies while the DARLAM simulation underestimated the frequency of dry spells and over estimated the probability of precipitation and the frequency of wet spells. In a climate change follow-on experiment, again using both methods, Charles *et al.* (1999b) found a small decrease in probability of precipitation under future climate conditions.

Murphy (1999) evaluated the UK Meteorological Office Unified Model (UM) RCM over Europe against a statistical downscaling model based on regression. Monthly mean surface temperature and precipitation anomalies were down-scaled using predictor sets chosen from a range of candidate variables similar to those used by Kidson and Thompson (1998) (EOFs of atmospheric fields). The results showed similar levels of skill for the dynamical and statistical methods, in line with the Kidson and Thompson (1998) study. The statistical method was nominally better for summertime estimates of temperature, while the dynamical model gave better estimates of wintertime precipitation. Again, the conclusion was drawn that the sophistication of the dynamical model shows little advantage over statistical techniques, at least for present day climates.

Murphy (2000) continued the comparative study by deriving climate change projections for 2080 to 2100 from a simulation with the HadCM2 AOGCM. The dynamical and statistical downscaling techniques were the same regional and statistical models as used by Murphy (1999). The statistical and dynamical techniques produced significantly different predictions of climate change, despite exhibiting similar skill when validated against present day observations. The study identifies two main sources of divergence between the dynamical and statistical techniques: firstly, differences between the strength of the observed and simulated predictor/predictand relationships, and secondly, omission from the regression equations of variables which represent climate change feedbacks, but are weak predictors of natural variability. In particular, the exclusion of specific humidity led to differences between the dynamical and statistical simulations of precipitation change. This point would seem to confirm the humidity issue raised in Section 10.6.3 (Hewitson and Crane 1996, Crane and Hewitson, 1998, Charles *et al.*, 1999b; Hewitson 1999).

Mearns *et al.* (1999) compared RCM simulations and statistical downscaling using a regional model and a semi-empirical technique based on stochastic procedures conditioned on weather types which were classified from circulation fields (700hPa geopotential heights). While Mearns *et al.* suggest that the semi-empirical approach incorporates more physical meaning into the relationships than a pure statistical approach does, this approach does impose the assumption that the circulation patterns are robust into a future climate in addition to the normal assumption that the cross-scale relationships are stationary in time. For both techniques, the driving fields were from the CSIRO AOGCM (Watterson *et al.*, 1995). The variables of interest were maximum and minimum daily temperature and precipitation over central-northern USA (Nebraska). As with the preceding studies, the validation under present climate conditions indicated similar skill levels for the dynamical and statistical approaches, with some advantage by the statistical technique.

In line with the Murphy (2000) study, larger differences were also noted by Mearns *et al.* (1999) when climate change projections were produced. Notably for temperature, the statistical technique produced an amplified seasonal cycle compared to both the RCM and CSIRO data, although similar changes in daily temperature variances were found in both the RCM and the statistical technique (with the statistical approach producing mostly decreases). The spatial patterns of change showed greater variability in the RCM compared with the statistical technique. Mearns *et al.* (1999) suggested that some of the differences found in the results were due to the climate change simulation exceeding the range of data used to develop the statistical model, while the decreases in variance were likely to be a true reflection of changes in the circulation controls. The precipitation results from Mearns *et al.* (1999) are different from earlier studies with the same RCM (e.g., Giorgi *et al.*, 1998) that produced few statistically significant changes.

Extending the comparison beyond simple methodological performance, Wilby *et al.* (2000) compared hydrological responses using data from dynamically and statistically down-scaled climate model output for the Animas River basin in Colorado, USA. While not a climate change projection, the use of output from an RCM and a statistical downscaling approach to drive a distributed hydrological model exemplify the objective of the downscaling. The results indicate that both the statistical and dynamical methods had greater skill (in terms of modelling hydrology) than the coarse resolution reanalysis output used to drive the downscaling. The statistical method had the advantage of requiring very few parameters, an attribute making the procedure attractive for many hydrological applications. The dynamical model output, once elevation-corrected, provided better water balance estimates than raw or elevation-corrected reanalysis output.

Overall, the above comparative studies indicate that for present climate both techniques have similar skill. Since statistical models are based on observed relationships between predictands and predictors, this result may represent a further validation of the performance of RCMs. Under future climate conditions more differences are found between the techniques, and the question arises as to which is “more correct”. While the dynamical model should clearly provide a better physical basis for change, it is still unclear whether different regional models generate similar downscaled changes. With regard to statistical/empirical techniques, it would seem that careful attention must be given to the choice of predictors, and that methodologies which internally select predictors based on explanatory power under present climates may exclude predictors important for determining change under future climate modes.

10.8 Summary Assessment

Today different modelling tools are available to provide climate change information at the regional scale. Coupled AOGCMs are the fundamental models used to simulate the climatic response to anthropogenic forcings and, to date, results from AOGCM simulations have provided the climate information for the vast majority of impact studies. On the other hand, resolution limita-

tions pose severe constraints on the usefulness of AOGCM information, especially in regions characterised by complex physiographic settings. Three classes of regionalisation techniques have been developed to enhance the regional information of coupled AOGCMs: high resolution and variable resolution time-slice AGCM experiments, regional climate modelling, and empirical/statistical and statistical/dynamical approaches.

Since the SAR, substantial progress has been achieved in all regionalisation methods, including better understanding of the techniques, development of a wide variety of modelling systems and methods, application of the techniques to a wide range of studies and regional settings, and reduction of model biases. Modelling work has indicated that regionalisation techniques enhance some aspects of AOGCM regional information, such as the high resolution spatial detail of precipitation and temperature, and the statistics of daily precipitation events. It is important to stress that AOGCM information is the starting point for the application of all regionalisation techniques, so that a foremost requirement in the simulation of regional climate change is that the AOGCMs simulate well the circulation features that affect regional climates. In this respect, indications are that the performance of current AOGCMs is generally improving.

Analysis of AOGCM simulations for broad (sub-continental scale) regions indicates that biases in the simulation of present day regionally and seasonally averaged surface climate variables, although highly variable across regions and models, are generally improved compared with the previous generation models. This implies increased confidence in simulated climatic changes. The performance of models in reproducing observed interannual variability varies across regions and models.

Regional analysis of AOGCM transient simulations extending to 2100, for different scenarios of GHG increase and sulphate aerosol effects, and with a number of modelling systems (some simulations include ensembles of realisations) indicate that the average climatic changes for the late decades of the 21st century compared to present day climate vary substantially across regions and models. The primary source of uncertainty in the simulated changes is associated with inter-model range of changes, with inter-scenario and intra-ensemble range of simulated changes being less pronounced. Despite the range of inter-model results, some common patterns of sub-continental scale climatic changes are emerging, and thus providing increased confidence in the simulation of these changes.

Work performed with all regionalisation techniques indicates that sub-GCM grid scale structure in the regional climate change signal can occur in response to regional and local forcings, although more work is needed to assess the statistical significance of the sub-GCM grid scale signal. In particular, modelling evidence clearly indicates that topography, land use and the surface hydrologic cycle strongly affect the surface climate change signal at the regional to local scale. This implies that the use of AOGCM information for impact studies needs to be taken cautiously, especially in regions characterised by pronounced sub-GCM grid scale variability in forcings, and that suitable regionalisation techniques should be used to enhance the AOGCM results over these regions.

Considerations of various types may enter the choice of the regionalisation technique, as different techniques may be most suitable for different applications and different working environments. High resolution AGCMs offer the primary advantage of global coverage and two-way interactions between regional and global climate. However, due to their computational cost, the resolution increase that can be expected from these models is limited. Variable resolution and RCMs yield a greater increase in resolution, with current RCMs reaching resolutions as fine as a few tens of kilometres or less. RCMs can capture physical processes and feedbacks occurring at the regional scale, but they are affected by the errors of the AOGCM driving fields, and they do not represent regional-to-global climate feedbacks. The effects of regional-to-global feedback processes depend on the specific problem and in many cases may not be important. Two-way GCM-RCM nesting would allow the description of such effects, and some research efforts in that direction are currently under way. Statistical downscaling techniques offer the advantages of being computationally inexpensive, of providing local information which is needed in many impact applications, and of offering the possibility of being tailored to specific applica-

tions. However, these techniques have limitations inherent in their empirical nature.

The combined use of different techniques may provide the most suitable approach in many instances. For example, a high-resolution AGCM simulation could represent an important intermediate step between AOGCM information and RCM or statistical downscaling models. The convergence of results from different approaches applied to the same problem can increase the confidence in the results and differences between approaches can help to understand the behaviour of the models.

Despite recent improvements and developments, regionalisation research is still a maturing process and the related uncertainties are still rather poorly known. One of the reasons for this is that most regionalisation research activities have been carried out independently of each other and aimed at specific objectives. Therefore a coherent picture of regional climate change via available regionalisation techniques cannot yet be drawn. More co-ordinated efforts are thus necessary to improve the integrated hierarchy of models, evaluate the different methodologies, intercompare methods and models and apply these methods to climate change research in a comprehensive strategy.

Appendix 10.1:

List of regional climate model simulations of duration longer than 3 months nested within analyses; also including oceanic RCMs (O-RCM).

References	Grid size	Duration	Region
<i>a) Individual January/July present-day simulations</i>			
Walsh and McGregor (1996)	125 km	7 × 1 month	Antarctica
Rinke <i>et al.</i> (1999)	55 km	11 × 1 month	Arctic
Takle <i>et al.</i> (1999)	50 km	7 × 2 months	USA
Katzfey (1999)	125 km	8 × 1 month	Australia
<i>b) Seasonally-varying present-day simulations</i>			
Giorgi <i>et al.</i> (1993a)	60 km	2 years	USA
Christensen <i>et al.</i> (1995)	56 km	20 months	Europe
Leung and Ghan (1995)	30 and 90 km	1 year	North-west USA
Kim (1997)	20 km	6 months	Western USA
Christensen <i>et al.</i> (1997)	26 to 57 km	11 months to 10 years	Europe
Jenkins (1997)	110 km	2 × 4 months	West Africa
Kidson and Thompson (1998)	50 km	5 years	New Zealand
McGregor <i>et al.</i> (1998)	44 km	1 year	Southeast Asia
Noguer <i>et al.</i> (1998)	50 km	10 years	Europe
Ruti <i>et al.</i> (1998)	30 km	19 months	Europe
Seth and Giorgi (1998)	60 km	2 × 4 months	USA
Leung and Ghan (1998)	90 km	3 years	North-west USA
Kauker (1998)	15 km	15 years	North Sea (O-RCM)
Christensen (1999)	55 km	7 × 1 year	Mediterranean area
Giorgi and Shields (1999)	60 km	3 years	USA
Giorgi <i>et al.</i> (1999)	60 km	13 month	East Asia
Small <i>et al.</i> (1999a)	60 km	5.5 years	Central Asia
van Lipzig (1999)	55 km	10 years	Antarctica
Liston and Pielke (1999)	50 km	1 year	USA
Hong and Leetmaa (1999)	50 km	4 × 3 months	USA
Christensen and Kuhry (2000)	16 km	15 years	Arctic Russia
Pan <i>et al.</i> (2000)	55 km	2 × 10 years	USA
Mabuchi <i>et al.</i> (2000)	30 km	6.5 years	Japanese Islands
Jacob and Podzun (2000)	55 km	10 years	Northern Europe
<i>c) Seasonal tropical or monsoon simulations</i>			
Bhaskaran <i>et al.</i> (1996)	50 km	4 months	Indian monsoon
Ji and Vernekar (1997)	80 km	3 × 5.5 months	Indian monsoon
Wei <i>et al.</i> (1998)	60 km	4 months	Temperate East Asia
Sun <i>et al.</i> (1999)	60 km	10 × 3 month	East Africa
Leung <i>et al.</i> (1999a)	60 km	3 × 3 month	East Asia
Chen and Fu (2000)	60 km	3 years	East Asia

[1995, 1] Third International Conference on Modelling of Global Climate Change and Variability, Hamburg, Germany, 4 to 8 September 1995.

[2000, 2] Submitted to Research Activities in Atmospheric and Oceanic Modelling. (CAS/JSC Working Group on Numerical Experimentation Report) [Geneva]: WMO.

[2000, 3] 80th AMS Annual Meeting, Long Beach, California, 9 to 14 January 2000.

Appendix 10.2:

List of regional climate model simulations of duration longer than 3 months nested within a GCM present day simulation; also including oceanic RCMs (O-RCM) and variable resolution GCMs (var.res.GCM).

References	Grid size	Duration	Region
<i>a) Perpetual January simulation</i>			
McGregor and Walsh (1993)	250 km	10 months	Australia
<i>b) Individual January/July simulations</i>			
Giorgi (1990)	60 km	6 × 1 month	USA
Marinucci and Giorgi (1992)	70 km	5 × 1 month	Europe
McGregor and Walsh (1994)	125 km/60 km	10 × 1 month	Tasmania
Marinucci <i>et al.</i> (1995)	20 km	5 × 1 month	Europe (Alps)
Walsh and McGregor (1995)	125 km	10 × 1 month	Australasia
Podzun <i>et al.</i> (1995)	55 km	5 × 1 month	Europe
Rotach <i>et al.</i> (1997)	20 km	5 × 1 month	Europe (Alps)
Joubert <i>et al.</i> (1999)	125 km	20 × 1 month	South Africa
<i>c) Seasonally-varying simulations</i>			
Giorgi <i>et al.</i> (1994)	60 km	3.5 years	USA
Dèquè and Piedelievre (1995)	T21-T200	10 years	Europe (var.res.GCM)
Hirakuchi and Giorgi (1995)	50 km	5 years	East Asia
Jones <i>et al.</i> (1995)	50 km	10 years	Europe
McGregor <i>et al.</i> (1995)	125 km	10 years	Australasia
Giorgi and Marinucci (1996b)	50 km	5 years	Europe
Giorgi <i>et al.</i> (1997)	50 km	5 years	Europe
Krinner <i>et al.</i> (1997)	~100 km	5 years	Antarctica (var.res.GCM)
Jenkins and Barron (1997)	108 km	7 months	USA – AMIP
Jacob and Podzun (1997)	55 km	4 years	Europe
Walsh and McGregor (1997)	125 km	5 × 18 months	Australasia – AMIP
Christensen <i>et al.</i> (1998)	57 and 19 km	9 years	Scandinavia
Krinner and Genthon (1998)	~100 km	3 years	Greenland (var.res.GCM)
Dèquè <i>et al.</i> (1998)	~60 km	10 years	Europe
Giorgi <i>et al.</i> (1998)	50 km	5 years	USA
Katzfey <i>et al.</i> (1998)	60 and 125 km	20 years	Australia
Laprise <i>et al.</i> (1998)	45 km	5 years	West Canada
Machenauer <i>et al.</i> (1998)	19 to 70 km	5 to 30 years	Europe
McGregor <i>et al.</i> (1998)	44 km	10 years	Southeast Asia
Noguer <i>et al.</i> (1998)	50 km	10 years	Europe
Renwick <i>et al.</i> (1998)	50 km	10 years	New Zealand
Böhm <i>et al.</i> (1998)	55 km	13 month	Northern South America
Kauker (1998)	15 km	5 years	North Sea (O-RCM)
Leung and Ghan (1999a)	90 km	7 years	North-west USA
Gallardo <i>et al.</i> (1999)	50 km	10 years	Iberian Peninsula
Leung <i>et al.</i> (1999b)	90 km	2 years	North-west USA
Haugen <i>et al.</i> (1999)	55 km	20 years	North-west Europe
Jacob and Podzun (2000)	55 km	10 years	Northern Europe
Pan <i>et al.</i> (2000)	55 km	2 × 10 years	USA
Rummukainen <i>et al.</i> (2000)	44 km	10 years	Europe
Kato <i>et al.</i> (2001)	50 km	10 years	East Asia
Gao <i>et al.</i> (2000)	60 km	5 year	China
Chen and Fu (2000)	60 km	3 years	East Asia
<i>c) Seasonal tropical or monsoon simulations</i>			
Jacob <i>et al.</i> (1995)	55 km	6 months	Indian monsoon
Bhaskaran <i>et al.</i> (1998)	50 km	10 years	India – AMIP
Hassel and Jones (1999)	50 km	20 years	Indian monsoon

[1995, 1] Third International Conference on Modelling of Global Climate Change and Variability, Hamburg, Germany, 4 to 8 September 1995.

[1998, 2] International Conference on The Role of Topography in Modelling Weather and Climate. International Centre for Theoretical Physics, Trieste, Italy, 22 to 26 June 1998.

[2000, 3] Submitted to Research Activities in Atmospheric and Oceanic Modelling. (CAS/JSC Working Group on Numerical Experimentation Report) [Geneva]: WMO.

Appendix 10.3:

List of regional climate model simulations of duration longer than 3 months nested within a GCM climate change simulation; also including oceanic RCMs (O-RCM) and variable resolution GCMs (var.res.GCM).

References	Grid size	Duration	Region
<i>a) Individual January/July 2×CO₂ simulations</i>			
Giorgi <i>et al.</i> (1992)	70 km	5 × 1 month	Europe
McGregor and Walsh (1994)	60 km	10 × 1 month	Tasmania
Rotach <i>et al.</i> (1997)	20 km	5 × 1 month	Europe (Alps)
<i>b) Seasonally-varying 2×CO₂ time-slice simulations</i>			
Giorgi <i>et al.</i> (1994)	60 km	3.5 years	USA
Hirakuchi and Giorgi (1995)	50 km	5 years	East Asia
McGregor <i>et al.</i> (1995)	125 km	10 years	Australasia
Giorgi <i>et al.</i> (1997)	50 km	3 years	Europe
Jones <i>et al.</i> (1997)	50 km	10 years	Europe
Dèqué <i>et al.</i> (1998)	About 60 km	10 years	Europe (var.res.GCM)
Giorgi <i>et al.</i> (1998)	50 km	5 years	USA
Joubert <i>et al.</i> (1998)	125 km	10 years	Southern Africa
Laprise <i>et al.</i> (1998)	45 km	5 years	West Canada
Machenauer <i>et al.</i> (1998)	19 to 70 km	5 to 30 years	Europe
McGregor <i>et al.</i> (1998)	44 km	10 years	South-east Asia
Renwick <i>et al.</i> (1998)	50 km	10 years	New Zealand
Kauker (1998)	15 km	5 years	North Sea (O-RCM)
Räisänen <i>et al.</i> (1999)	44 km	10 years	Europe
Hassel and Jones (1999)	50 km	20 years	Indian monsoon
Gallardo <i>et al.</i> (1999)	50 km	10 years	Iberian Peninsula
Haugen <i>et al.</i> (1999)	55 km	20 years	North-west Europe
Leung and Ghan (1999b)	90 km	8 years	North-west USA
Pan <i>et al.</i> (2000)	55 km	2 × 10 years	USA
Kato <i>et al.</i> (2001)	50 km	10 years	East Asia
Gao <i>et al.</i> (2000)	60 km	5 year	China
<i>c) Seasonally-varying fully transient CO₂ simulations</i>			
McGregor <i>et al.</i> (1999)	125 km	140 years	Australasia
McGregor <i>et al.</i> (1999)	60 km	140 years	South-east Australia

[1995, 1] Third International Conference on Modelling of Global Climate Change and Variability, Hamburg, Germany, 4 to 8 September 1995.

[1998, 2] International Conference on The Role of Topography in Modelling Weather and Climate. International Centre for Theoretical Physics, Trieste, Italy, 22 to 26 June 1998.

Appendix 10.4: Examples of downscaling studies.

Technique (utilised in the above categories):

- WG = weather generators (e.g.: Markov-type procedures, conditional probability).
- TF = transfer functions (e.g.: Regression, canonical correlation analysis, and artificial neural networks).
- WT = weather typing (e.g.: cluster analysis, self-organising map, and extreme value distribution).

Predictor variables: C = circulation based (e.g.: sea level pressure fields and geopotential height fields).

T = temperature (at surface or on one or more atmospheric levels). TH = thickness between pressure levels.

VOR = vorticity. W = wind related. Q = specific humidity (at surface or on one or more atmospheric levels).

RH = relative humidity (at surface or on one or more atmospheric levels). Cld = cloud cover.

ZG = spatial gradients of the predictors. O = other.

Predictands: T (temperature); Tmax (maximum temperature); Tmin (minimum temperature); P (precipitation).

Region is the geographic domain.

Time is the time-scale of the predictor and predictand: H (hourly), D (daily), M (monthly), S (seasonal), and A (annual).

Region	Technique	Predictor	Predictand	Time	Author (s)
Africa					
South Africa	TF	C	P	D	Hewitson and Crane, 1996
America					
USA	WT	T	Tmax, Tmin	D	Brown and Katz, 1995
USA	WG	C	P	D	Zorita <i>et al.</i> , 1995
USA	WG, TF	C, T, VOR	P	D	Wilby and Wigley, 1997
USA	TF	C, Q	P	D	Crane and Hewitson, 1998
USA	WG, TF	C, T, VOR	T, P	D	Wilby <i>et al.</i> , 1998a, b
USA	WG, WT	C	T, P	D	Mearns <i>et al.</i> , 1999
USA	TF	C, T, RH, W	T	D	Sailor and Li, 1999
USA	WG		P	D	Bellone <i>et al.</i> , 1999
Mexico and USA	TF	C, TH, O	P	D	Cavazos, 1997
Mexico and USA	TF, WT	C, TH, Q	P	D	Cavazos, 1999
Central Argentina	TF	C, W	T, Tmax, Tmin	M	Solman and Nuñez, 1999
Asia					
Japanese coast	TF	C	Sea level	M	Cui <i>et al.</i> , 1995, 1996
Chinese coast	TF		Sea level variability	M	Cui and Zorita, 1998
Oceania					
New Zealand	WT	C	Tmax, Tmin, P	D	Kidson and Watterson, 1995
New Zealand	TF	C, TH, VOR, W	T, P	D	Kidson and Thompson, 1998
Australia	TF	C	Tmax, Tmin	D	Schubert and Henderson-Sellers, 1997
Australia	TF	C	Tmax, Tmin	D	Schubert, 1998
Australia	WT	C, T	P		Timbal and McAvaney, 1999
Australia	WT				Schnur and Lettenmaier, 1999
Europe					
Europe	WG	VOR, W			Conoway <i>et al.</i> , 1996
Europe	WG, TF	C, P, Tmax, Tmin, O	T, P	D	Semenov and Barrow, 1996
Europe	TF	C, W, VOR, T, Q, O	T, P	M	Murphy, 1998a, b
Europe	TF	C	T, P, vapour pressure	D	Weichert and Bürger, 1998
Germany	TF	T	Phenological event		Maak and van Storch, 1997
Germany	TF	C	Storm surge	M	Von Storch and Reichardt, 1997
Germany	TF		Salinity		Heyen and Dippner, 1998
Germany	WT		Thunderstorms	D	Sept, 1998

Region	Technique	Predictor	Predictand	Time	Author (s)
Germany	TF		Ecological variables		Krönke <i>et al.</i> , 1998
Iberian Peninsula	WG	C	P	D	Cubash <i>et al.</i> , 1996
Iberian Peninsula	TF	C	Tmax, Tmin	D	Trigo and Palutikof, 1998
Iberian Peninsula	TF		T, P		Boren <i>et al.</i> , 1999
Iberian Peninsula	TF		T, P		Ribalaygua <i>et al.</i> , 1999
Spain (and USA)	TF	C	Tmax, Tmin	D	Palutikof <i>et al.</i> , 1997
Spain (and USA)	TF	C	Tmax, Tmin	D	Winkler <i>et al.</i> , 1997
Spain	WT			D	Goodess and Palutikof, 1998
Portugal	TF	C	P	M	Corte-Real <i>et al.</i> , 1995
Portugal	WT	C		D	Corte-Real <i>et al.</i> , 1999
The Netherlands	WT	C, VOR, W	T, P	D,M	Buishand and Brandsma, 1997
Norway	TF	C, O	T, P and others	M	Benestad, 1999a, b
Norway (glaciers)	TF	C, O	Local weather	D	Reichert <i>et al.</i> , 1999
Romania	TF	C	P	M	Busuioc and von Storch, 1996
Romania	TF	C	P	M	Busuioc <i>et al.</i> , 1999
Switzerland	TF		P		Buishand and Klein Tank, 1996
Switzerland	TF		P		Brandsma and Buishand, 1997
Switzerland	TF			D	Widmann and Schär, 1997
Switzerland	WG	C	Local Weather	H	Gyalistras <i>et al.</i> , 1997
Switzerland	TF		P		Buishand and Brandsma, 1999
Poland	TF	C	T, sea level, wave height, salinity, wind, run-off	D,M	Mietus, 1999
Alps	WT				Fuentes and Heimann, 1996
Alps	TF	C, T	T, P	M	Fischlin and Gyalistras, 1997
Alps	WT	C	Snow		Martin <i>et al.</i> , 1997
Alps	WT				Fuentes <i>et al.</i> , 1998
Alps	TF	C, T	T, P,		Gyalistras <i>et al.</i> , 1998
Alps,	TF	C, T	Snow cover		Hantel <i>et al.</i> , 1998
Alps	WT	C, T	Landslide activity		Dehn, 1999a, b
Alps	WT		T, P	D	Heimann and Sept, 1999
Alps	WT		P	D	Fuentes and Heimann, 1999
Alps	TF, WG	C, T	Weather statistics	M	Riedo <i>et al.</i> , 1999
Alps	TF	C	P	M	Burkhardt, 1999
Mediterranean	TF	C, P	T		Palutikof and Wigley, 1995
Mediterranean	TF	C	P	S	Jacobeit, 1996
North Atlantic	TF	C	Pressure tendencies	M	Kaas <i>et al.</i> , 1996
North Atlantic	TF	C	Wave height	M	WASA, 1998
North Sea	TF		Ecological variables		Dippner, 1997a, b
North Sea coast	TF	C	Sea level	M	Langenberg <i>et al.</i> , 1999
Baltic Sea	TF	SLP	Sea level	M	Heyen <i>et al.</i> , 1996
Region not specified					
	WT				Frey-Buness <i>et al.</i> , 1995
	WT	C			Matyasovszky and Bogardi, 1996
	WT				Enke and Spekat, 1997
	TF	C, VOR, W			Kilsby <i>et al.</i> , 1998
	TF		Ecological variables		Heyen <i>et al.</i> , 1998
	TF		P		Biau <i>et al.</i> , 1999
	WG	P	P	D	Wilks, 1999
	WT		P	D	Zorita and von Storch, 1999

References

- Appenzeller**, C., T.F. Stocker and M. Anklin, 1998: North Atlantic Oscillation dynamics recorded in Greenland ice cores. *Science*, **282**, 446–449.
- Arritt**, R., D.C. Goering and C.J. Anderson, 2000: The North American monsoon system in the Hadley Centre coupled ocean-atmosphere GCM. *Geophys. Res. Lett.*, **27**, 565–568.
- Bailey**, D.A., A.H. Lynch and K.S. Hedström, 1997: The impact of ocean circulation on regional polar simulations using the Arctic regional climate system model. *Ann. Glaciol.*, **25**, 203–207.
- Bailey**, D.A. and A.H. Lynch, 2000a: Development of an Antarctic regional climate system model: Part I: Sea ice and large-scale circulation, *J. Climate*, **13**, 1337–1350.
- Bailey**, D.A. and A.H. Lynch, 2000b: Development of an Antarctic regional climate system model: Part II Station validation and surface energy ballance, *J. Climate*, **13**, 1351–1361.
- Barrow**, E., M. Hulme and M. Semenov, 1996: Effect of using difference methods in the construction of climate change scenarios: examples from Europe. *Clim. Res.*, **7**, 195–211.
- Bates**, B., S.P. Charles and J.P. Hughes, 1998: Stochastic downscaling of numerical climate model simulations. *Env. Modelling and Software*, **13**, 325–331.
- Baur**, F., P. Hess and H. Nagel, 1944: Kalender der Grosswetterlagen Europas 1881–1939. Bad Homburg, 35 pp.
- Beersma**, J.J. and T.A. Buishand, 1999: A simple test for equality of variances in monthly climate data. *J. Climate*, **12**, 1770–1779.
- Bellone**, E., J.P. Hughes and P. Gutrop, 2000: A hidden Markov model for downscaling synoptic atmospheric patterns to precipitation amounts. *Clim. Res.*, **15**, 1–12.
- Benestad**, R.E., 1999: Pilot Studies on Enhanced Greenhouse Gas Scenarios for Norwegian Temperature and Precipitation from Empirical Downscaling, DNMI-Klima report 18/99, Norwegian Met. Inst., PO Box 43 Blindern, N0313 Oslo, Norway.
- Benestad**, R.E., I. Hanssen-Bauer, E.J. Førland, K.A. Iden and O.E. Tveito, 1999: Evaluation of monthly mean data fields from the ECHAM4/OPYC3 control integration, DNMI-Klima report 14/99, Norwegian Met. Inst., P.O. Box 43 Blindern, N0313 Oslo, Norway.
- Bengtsson**, L., M. Botzet and M. Esch, 1995: Hurricane-type vortices in a general circulation model. *Tellus*, **47A**, 175–196.
- Bengtsson**, L., M. Botzet and M. Esch, 1997: Numerical simulation of intense tropical storms. *Hurricanes: Climate and Socioeconomics Impacts*, Springer, 67–92.
- Bengtsson**, L., M. Botzet and M. Esch, 1996: Will greenhouse gas induced warming over the next 50 years lead to higher frequency and greater intensity of hurricanes? *Tellus*, **48A**, 57–73.
- Bhaskaran**, B., R.G. Jones, J.M. Murphy and M. Noguer, 1996: Simulations of the Indian summer monsoon using a nested regional climate model: Domain size experiments. *Clim. Dyn.*, **12**, 573–587.
- Bhaskaran**, B. and J.F.B. Mitchell, 1998: Simulated changes in southeast Asian monsoon precipitation resulting from anthropogenic emissions. *Int. J. Climatology*, **18**, 1455–1462.
- Bhaskaran**, B., J.M. Murphy and R.G. Jones, 1998: Intraseasonal Oscillation in the Indian Summer Monsoon Simulated by Global and nested Regional Climate Models. *Mon. Wea. Rev.*, **126**, 3124–3134.
- Biau**, G., E. Zorita, H. von Storch and H. Wackernagel, 1999: Estimation of precipitation by kriging in EOF space. *J. Climate*, **12**, 1070–1085.
- Boer**, G.J., G. Flato and D. Ramsden, 2000b: A transient climate change simulation with greenhouse gas and aerosol forcing: projected climate for the 21st century. *Clim. Dyn.*, **16**, 427–450.
- Boer**, G.J., G. Flato, M.C. Reader and D. Ramsden, 2000a: A transient climate change simulation with greenhouse gas and aerosol forcing: experimental design and comparison with the instrumental record for the 20th century. *Clim. Dyn.*, **16**, 405–426.
- Böhm**, U., R. Podzun and D. Jacob, 1998: Surface Water Balance Estimation for a Semi-Arid Region using a Regional Climate Model and Comparison of Water Balance Components with Global Circulation Model Output and Analysis Data. *Phys. Chem. Earth*, **23**, 405–411.
- Brandsma**, T. and T. A. Buishand, 1997: Statistical linkage of daily precipitation in Switzerland to atmospheric circulation and temperature. *J. Hydrology*, **198**, 98–123.
- Brown**, B. G. and R. W. Katz, 1995: Regional analysis of temperature extremes: Spatial analog for climate change? *J. Climate*, **8**, 108–119.
- Buishand**, T.A. and J.J. Beersma, 1996: Statistical tests for comparison of daily variability in observed and simulated climates. *J. Climate*, **10**, 2538–2550.
- Buishand**, T.A. and A.M.G. Klein Tank, 1996: Regression model for generating time series of daily precipitation amounts for climate change impact studies. *Stochastic Hydrology and Hydraulics*, **10**, 87–106.
- Buishand**, T.A. and T. Brandsma, 1997: Comparison of circulation classification schemes for predicting temperature and precipitation in the Netherlands, *Int. J. Climatol.*, **17**, 875–889.
- Buishand**, T.A. and T. Brandsma, 1999: The dependence of precipitation on temperature at Florence and Livorno. *Clim. Res.*, **12**, 53–63.
- Buma**, J. and M. Dehn, 1998: A method for predicting the impact of climate change on slope stability. *Environmental Geology*, **35**, 190–196.
- Buma**, J. and M. Dehn, 2000: The impact of climate change on a landslide in South East France, simulated using different GCM-scenarios and downscaling methods for local precipitation. *Clim. Res.*, **15**, 69–81.
- Bürger**, G., 1996: Expanded downscaling for generating local weather scenarios *Clim. Res.*, **7**, 111–128.
- Bürger**, G., 1997: On the disaggregation of climatological means and anomalies. *Clim. Res.*, **8**, 183–194.
- Burkhardt**, U., 1999: Alpine precipitation in a tripled CO₂ climate. *Tellus*, **51A**, 289–303.
- Busuioc**, A. and H. von Storch, 1996: Changes in the winter precipitation in Romania and its relation to the large scale circulation. *Tellus*, **48A**, 538–552.
- Busuioc**, A., H. von Storch and R. Schnur, 1999: Verification of GCM generated regional precipitation and of statistical downscaling estimates. *J. Climate*, **12**, 258–272.
- Carril**, A., F.C.G. Menéndez and M.N. Nuñez, 1997: Climate Change Scenarios over the South American Region: An Intercomparison of Coupled General Atmosphere-Ocean Circulation Models. *Int. J. Climatol.*, **17**, 1613–1633.
- Cavazos**, T., 1997: Downscaling large-scale circulation to local rainfall in North-Eastern Mexico. *Int. J. Climatology*, **17**, 1069–1082.
- Cavazos**, T., 1999: Large-Scale Circulation Anomalies Conducive to Extreme Precipitation Events and Derivation of Daily Rainfall in Northeastern Mexico and Southeastern Texas. *J. Climate*, **12**, 1506–1523.
- Charles**, S.P., B.C. Bates, and J.P. Hughes, 1999a: A spatio-temporal model for downscaling precipitation occurrence and amounts. *J. Geophys. Res.*, **104**, 31657–31669.
- Charles**, S.P., B.C. Bates, P.H. Whetton and J.P. Hughes, 1999b: Validation of downscaling models for changed climate conditions: Case study of southwestern Australia. *Clim. Res.*, **12**, 1–14.
- Chase** T.N., R.A. Pielke, T.G.F. Kittel, R.R. Nemani and S.W. Running, 2000: Simulated impacts of historical land cover changes on global climate in northern winter. *Clim. Dyn.*, **16**, 93–106.
- Chen**, D. C. Hellstroem and Y. Chen, 1999: Preliminary analysis and statistical downscaling of monthly temperature in Sweden. Department of Physical Geography, Göteborg, C 16 1999, 76 pp.
- Chen**, M., and C. Fu, 2000: A nest procedure between regional and global climate models and its application in long term regional climate simulation. *Chinese J. Atmos. Sci.*, **24**, 233–262.

- Christensen**, J.H., O.B. Christensen and B. Machenhauer, 1995: On the performance of the HIRHAM limited area regional climate model over Europe, Third Int. Conference on Modelling of Global Climate Change and Variability, Hamburg, Germany, 4-8 September 1995.
- Christensen** J.H., O.B. Christensen, P. Lopez, E. van Meijgaard and M. Botzet, 1996: The HIRHAM4 Regional Atmospheric Climate Model. *DMI Sci. Rep.*, 96-4., 51pp. DMI, Copenhagen.
- Christensen** J.H., B. Machenhauer, R.G. Jones, C. Schär, P.M. Ruti, M. Castro and G. Visconti, 1997: Validation of present-day regional climate simulations over Europe: LAM simulations with observed boundary conditions. *Clim. Dyn.*, **13**, 489–506.
- Christensen** O.B., J.H. Christensen, B. Machenhauer and M. Botzet, 1998: Very high-resolution regional climate simulations over Scandinavia – Present climate. *J. Climate*, **11**, 3204-3229.
- Christensen** O.B., 1999: Relaxation of soil variables in a regional climate model. *Tellus*, **51A**, 674-685.
- Christensen** J.H. and P. Kuhry, 2000: High resolution regional climate model validation and permafrost simulation for the East-European Russian Arctic. *J. Geophys. Res.*, **105**, 29647-29658.
- Cocke**, S.D. and T.E. LaRow, 2000: Seasonal Prediction using a Regional Spectral Model embedded within a Coupled Ocean-Atmosphere Model. *Mon. Wea. Rev.*, **128**, 689-708.
- Conway**, D., 1998: Recent climate variability and future climate change scenarios for the British Isles. *Prog. Phys. Geog.*, **22**, 350-374.
- Conway**, D., R.L. Wilby and P.D. Jones, 1996: Precipitation and air flow indices over the British Isles, *Clim. Res.*, **7**, 169–183.
- Copeland**, J.H., R.A. Pielke and T.G.F. Kittel, 1996: Potential climatic impacts of vegetation change: A regional modeling study. *J. Geophys. Res.*, **101**, 7409–7418.
- Corte-Real**, J., H. Xu and B. Qian, 1999: A weather generator for obtaining daily precipitation scenarios based on circulation patterns. *Clim. Res.*, **12**, 61–75.
- Corte-Real**, J., X. Zhang and X. Wang, 1995: Downscaling GCM information to regional scales: a non-parametric multivariate regression approach, *Clim. Dyn.*, **11**, 413–424.
- Cowpertwait**, P.S.P. and P.E. O'Connel, 1997: A regionalized Neymann-Scott model of rainfall with convective and stratiform cells, *Hydrology and Earth Sciences*, **1**, 71–80.
- Crane**, R.G. and B.C. Hewitson, 1998: Doubled CO₂ climate change scenarios for the Susquehanna Basin: Precipitation. *Int. J. Climatology*, **18**, 65–76.
- Cubasch**, U., H. von Storch, J. Waszkewitz and E. Zorita, 1996: Estimates of climate change in southern Europe using different downscaling techniques. *Clim. Res.*, **7**, 129–149.
- Cubasch**, U., J. Waszkewitz, G. Hegerl and J. Perlwitz, 1995: Regional climate changes as simulated in time-slice experiments. *Clim. Change*, **31**, 273–304.
- Cui**, M. and E. Zorita, 1998: Analysis of the sea-level variability along the Chinese coast and estimation of the impact of a CO₂-perturbed atmospheric circulation. *Tellus*, **50A**, 333–347.
- Cui**, M., H. von Storch and E. Zorita, 1995: Coastal sea level and the large-scale climate state: A downscaling exercise for the Japanese Islands. *Tellus*, **47A**, 132–144.
- Cui**, M., H. von Storch and E. Zorita, 1996: Coast sea level and the large-scale climate state: a downscaling exercise for the Japanese Islands. *Studia Marina Sinica* **36**, 13–32 (in Chinese).
- Dai**, A., F. Giorgi and K. Trenberth, 1999: Observed and model simulated precipitation diurnal cycles over the continental United States. *J. Geophys. Res.*, **104**, 6377–6402.
- Daly**, C., R.P. Neilson and D.L. Phillips, 1994: A statistical-topographic model for mapping climatological precipitation over mountainous terrain. *J. Appl. Met.*, **33**, 140-158.
- Dehn**, M., 1999a: Szenarien der klimatischen Auslösung alpiner Hangrutschungen. Simulation durch Downscaling allgemeiner Zirkulationsmodelle der Atmosphäre. PhD thesis, Bonn. Bonner Geographische Abhandlungen, 99. Bonn, 99pp.
- Dehn**, M., 1999b: Application of an analog downscaling technique for assessment of future landslide activity - a case study in the Italian Alps. *Clim. Res.*, **13**, 103-113.
- Dehn**, M., and J. Buma, 1999: Modelling future landslide activity based on general circulation models. *Geomorphology*, **30**, 175-187.
- Dehn**, M., G. Bürger, J. Buma and P. Gasparotto, 2000: Impact of climate change on slope stability using expanded downscaling. *Engineering Geology*, **55**, 193-204.
- Delworth**, T.L., J.D. Mahlman and T.R. Knutson, 1999: Changes in heat index associated with CO₂-induced global warming. *Clim. Change*, **43**, 369-386.
- Déqué**, M. and J.P. Piedelievre, 1995: High resolution climate simulation over Europe. *Clim. Dyn.*, **11**, 321–339.
- Déqué**, M., P. Marquet and R. G. Jones, 1998: Simulation of climate change over Europe using a global variable resolution general circulation model. *Clim. Dyn.*, **14**, 173-189.
- Dickinson** R.E., R.M. Errico, F. Giorgi and G.T. Bates, 1989: A regional climate model for western United States. *Clim. Change*, **15**, 383–422.
- Dippner**, J. W., 1997a: Recruitment success of different fish stocks in the North Sea in relation to climate variability. *Dtsche Hydrogr. Z.*, **49**, 277-293
- Dippner**, J.W., 1997b: SST anomalies in the North Sea in relation to the North Atlantic Oscillation and the influence on the theoretical spawning time of fish. *Dtsche Hydrogr. Z.*, **49**, 267-275.
- Doherty**, R. and Mearns, L.O., 1999: A Comparison of Simulations of Current Climate from Two Coupled Atmosphere - Ocean GCMs Against Observations and Evaluation of Their Future Climates. Report to the NIGEC National Office. National Center for Atmospheric Research, Boulder, Colorado, 47pp.
- Durman**, C.F., J.M. Gregory, D.H. Hassell and R.G. Jones, 2001. The comparison of extreme European daily precipitation simulated by a global and a regional climate model for present and future climates. *Quart. J. R. Met. Soc.*, (in press).
- Emanuel**, K.A., 1987: The dependence of hurricane intensity on climate. *Nature*, **326**, 483-485.
- Emanuel**, K., 2000: A statistical analysis of tropical cyclone intensity. *Mon. Wea. Rev.*, **128**, 1139-1152.
- Enke**, W and A. Spekat, 1997: Downscaling climate model outputs into local and regional weather elements by classification and regression. *Clim. Res.*, **8**, 195–207.
- Fernandez-Partagas**, J. and H.F. Diaz, 1996: Atlantic hurricanes in the second half of the 19th Century. *Bull. Am. Met. Soc.*, **77**, 2899-2906.
- Fischlin**, A. and D. Gyalistras, 1997: Assessing impacts of climate change on forests in the Alps. *Glob. Ecol. Biogeogr. Lett.*, **6**, 19–37.
- Flato**, G.M., Boer, G.J., Lee, W.G., McFarlane, N.A., Ramsden, D., Reader, M.C. and Weaver, A.J., 2000: The Canadian Centre for Climate Modelling and Analysis global coupled model and its climate. *Clim. Dyn.*, **16**, 451-467.
- Foufoula-Georgiou**, E., and D.P. Lattenmaier, 1987: A Markov renewal model for rainfall occurrences. *Water. Resour. Res.*, **23**, 875-884.
- Frei** C., C. Schär, D. Lüthi and H.C. Davies, 1998: Heavy precipitation processes in a warmer climate. *Geophys. Res. Lett.*, **25**, 1431–1434.
- Frei**, C. and C. Schär, 1998: A precipitation climatology for the Alps from high resolution rain gauge observations. *Int. J. Climatol.*, **18**, 873–900.
- Frey-Bunness**, F., D. Heimann and R. Sausen, 1995: A statistical-dynamical downscaling procedure for global climate simulations. *Theor. Appl. Climatol.*, **50**, 117–131.
- Fu**, C.B., H.L.Wei, M.Chen, B.K.Su, M.Zhao and W.Z. Zheng, 1998: Simulation of the evolution of summer monsoon rainbelts over Eastern China from a regional climate model, *Scientia Atmospherica Sinica*, **22**, 522–534.
- Fuentes**, U. and D. Heimann, 1996: Verification of statistical-dynamical downscaling in the Alpine region. *Clim. Res.*, **7**, 151–186.

- Fuentes**, U., and D. Heimann, 1999: An improved statistical-dynamical downscaling scheme and its application to the Alpine precipitation climatology. *Theor. Appl. Climatol.*, **65**, 119–135.
- Fyfe**, J.C., 1999: On climate simulations of African Easterly waves. *J. Climate*, **12**, 6, 1747–1769.
- Fyfe**, J.C. and G.M. Flato, 1999: Enhanced Climate Change and its Detection over the Rocky Mountains. *J. Climate*, **12**, 230–243.
- Gallardo**, C., M.A. Gártner, J.A. Prego and M. Castro, 1999: Multi-year simulations with a high resolution Regional Climate Model over the Iberian Peninsula: Current climate and $2\times\text{CO}_2$ scenario. Internal Report, Dept. Geofísica y Meteorología, 45 pp. (Available in English on request from: Facultad de Física, Universidad Complutense, 28040 Madrid, Spain).
- Gao**, X., Z. Zhao Y. Ding, R. Huang and F. Giorgi, 2001: Climate change due to greenhouse effects in China as simulated by a regional climate model. *Acta Meteorologica Sinica*, in press.
- GCIP**, 1998: Global Energy and Water Cycle Experiment (GEWEX) Continental-Scale International Project. A Review of Progress and Opportunities. National Academy Press, Washington, D. C., 99 pp.
- Gibson** J. K., P. Källberg, S. Uppala, A. Hernández, A Nomura and E. Serrano, 1997, ERA description. ECMWF Reanalysis Project Report Series 1, ECMWF, Reading, 66 pp.
- Giorgi** F., 1990: Simulation of regional climate using a limited area model nested in a general circulation model. *J. Climate*, **3**, 941–963.
- Giorgi**, F., G.T. Bates and S.J. Nieman, 1993a: The multiyear surface climatology of a regional atmospheric model over the western United States. *J. Climate*, **6**, 75–95.
- Giorgi**, F., C.S. Brodeur and G.T. Bates, 1994: Regional climate change scenarios over the United States produced with a nested regional climate model. *J. Climate*, **7**, 375–399.
- Giorgi**, F. and R. Francisco, 2000a: Uncertainties in regional climate change predictions. A regional analysis of ensemble simulations with the HadCM2 GCM. *Clim. Dyn.*, **16**, 169–182.
- Giorgi**, F. and R. Francisco, 2000b: Evaluating uncertainties in the prediction of regional climate change. *Geophys. Res. Lett.*, **27**, 1295–1298.
- Giorgi**, F., J.W. Hurrell, M.R. Marinucci and M. Beniston, 1997: Elevation signal in surface climate change: A model study. *J. Climate*, **10**, 288–296.
- Giorgi**, F., Y. Huang, K. Nishizawa and C. Fu, 1999: A seasonal cycle simulation over eastern Asia and its sensitivity to radiative transfer and surface processes. *J. Geophys. Res.*, **104**, 6403–6424.
- Giorgi**, F. and M.R. Marinucci, 1996a: An investigation of the sensitivity of simulated precipitation to model resolution and its implications for climate studies. *Mon. Wea. Rev.*, **124**, 148–166.
- Giorgi**, F. and M.R. Marinucci, 1996b: Improvements in the simulation of surface climatology over the European region with a nested modeling system. *Geophys. Res. Lett.*, **23**, 273–276.
- Giorgi**, F., M.R. Marinucci, G.T. Bates and G. DeCanio, 1993b: Development of a second-generation regional climate model (RegCM2). Part II: Convective processes and assimilation of lateral boundary conditions. *Mon. Wea. Rev.*, **121**, 2814–2832.
- Giorgi**, F., M.R. Marinucci, G.T. Bates, 1993c: Development of a second-generation regional climate model (RegCM2). Part I: Boundary-layer and radiative transfer processes. *Mon. Weath. Rev.*, **121**, 2794–2813.
- Giorgi**, F., M.R. Marinucci and G. Visconti, 1992: A $2\times\text{CO}_2$ climate change scenario over Europe generated using a limited area model nested in a general circulation model. 2. Climate change scenario. *J. Geophys. Res.*, **97**, 10011–10028.
- Giorgi**, F. and L.O. Mearns, 1991: Approaches to the simulation of regional climate change: a review. *Rev. Geophys.*, **29**, 191–216.
- Giorgi**, F. and L.O. Mearns, 1999: Regional climate modeling revisited. An introduction to the special issue. *J. Geophys. Res.*, **104**, 6335–6352.
- Giorgi**, F., L.O. Mearns, C. Shields and L. Meyer, 1996: A regional model study of the importance of local vs. remote controls in maintaining the drought 1988 and flood 1993 conditions in the central U.S. *J. Climate*, **9**, 1150–1162.
- Giorgi**, F., L.O. Mearns, C. Shields and L. McDaniel, 1998: Regional nested model simulations of present day and $2\times\text{CO}_2$ climate over the Central Plains of the U.S. *Clim. Change*, **40**, 457–493.
- Giorgi**, F. and C. Shields, 1999: Tests of precipitation parameterizations available in the latest version of the NCAR regional climate model (RegCM) over the continental U.S. *J. Geophys. Res.*, **104**, 6353–6376.
- Goodess**, C. and J. Palutikof, 1998: Development of daily rainfall scenarios for southeast Spain using a circulation-type approach to downscaling. *Int. J. Climatol.*, **18**, 1051–1083.
- Gregory**, J.M. and J.F.B. Mitchell, 1995: Simulation of daily variability of surface temperature and precipitation over Europe in the current and $2\times\text{CO}_2$ climates using the UKMO climate model. *Quart. J. R. Met. Soc.*, **121**, 1451–1476.
- Gregory**, J.M., J.F.B. Mitchell and A.J. Brady, 1997: Summer drought in northern midlatitudes in a time-dependent CO_2 climate experiment. *J. Climate*, **10**, 662–686.
- González-Rouco**, F., H. Heyen, E. Zorita and F. Valero, 1999: Testing the validity of a statistical downscaling method in simulations with global climate models. GKSS Report 99/E/29, GKSS Research Centre, Geesthacht, Germany.
- González-Rouco**, F., H. Heyen, E. Zorita and F. Valero, 2000: Agreement between observed rainfall trends and climate change simulations in the southwest of Europe. *J. Climate*, **13**, 3057–3065.
- Gupta**, V.K. and E. Waymire, 1991: On lognormality and scaling in spatial rainfall averages? *Non-linear variability in geophysics*, 175–183.
- Gyalistras**, D., A. Fischlin and M. Riedo, 1997: Herleitung stündlicher Wetterszenarien unter zukünftigen Klimabedingungen. In: Fuhrer, J. (ed), Klimaänderungen und Grünland - eine Modellstudie über die Auswirkungen zukünftiger Klimaveränderungen auf das Dauergrünland in der Schweiz. vdf, Hochschulverlag AG an der ETH Zürich, 207–276.
- Gyalistras**, D., C. Schär, H.C. Davies and H. Wanner, 1998: Future Alpine climate. In: Cebon, P., U. Dahinden, H.C. Davies, D. Imboden, and C.C. Jaeger (eds) Views from the Alps. Regional Perspectives on Climate Change. Cambridge, Massachusetts: MIT Press, 171–223.
- Hanssen-Bauer**, I. and E.J. Førland 1998: Long-term trends in precipitation and temperature in the Norwegian Arctic: can they be explained by changes in atmospheric circulation patterns? *Clim. Res.*, **10**, 143–153.
- Hanssen-Bauer** I. and E.J. Førland 2000: Temperature and precipitation variations in Norway and their links to atmospheric circulation. *Int. J. Climatology*, **20**, 1693–1708.
- Hantel**, M., M. Ehrendorfer and A. Haslinger, 1999: Climate sensitivity of snow cover duration in Austria. *Int. J. Climatology*, **20**, 615–640.
- Hassell**, D. and R.G. Jones, 1999: Simulating climatic change of the southern Asian monsoon using a nested regional climate model (HadRM2), HCTN 8, Hadley Centre for Climate Prediction and Research, London Road, Bracknell, UK.
- Haugen**, J.E., D. Bjørge and T.E. Nordeng, 1999: A 20-year climate change experiment with HIRHAM, using MPI boundary data. RegClim Techn. Rep. No. 3, 37–44. Available from NILU, P.O. Box 100, N-2007 Kjeller, Norway.
- Heimann**, D. and V. Sept, 2000: Climatic change of summer temperature and precipitation in the Alpine region - a statistical-dynamical assessment. *Theor. Appl. Climatol.*, **66**, 1–12.
- Henderson-Sellers** A., H. Zhang, G. Berz, K. Emanuel, W. Gray, C. Landsea, G. Holland, J. Lighthill, S.-L. Shieh, P. Webster and K. McGuffie, 1998: Tropical cyclones and global climate change: a

- post-IPCC assessment. *Bull. Am. Met. Soc.*, **79**, 19–38.
- Hennessy**, K.J., J.M. Gregory and J.F.B. Mitchell, 1997: Changes in daily precipitation under enhanced greenhouse conditions. *Clim. Dyn.*, **13**, 667–680.
- Hennessy**, K.J., P.H. Whetton, J.J. Katzfey, J.L. McGregor, R.N. Jones, C.M. Page and K.C. Nguyen, 1998: Fine-resolution climate change scenarios for New South Wales. Annual report 1997–1998, research undertaken for the New South Wales Environmental Protection Authority. Chatswood, N.S.W., NSW Environment protection Authority, 48 pp.
- Hewitson**, B.C., 1999: Deriving regional precipitation scenarios from general circulation models, Report K751/1/99, Water Research Commission, Pretoria, South Africa.
- Hewitson**, B.C., and Crane, R.G., 1992: Large-scale atmospheric controls on local precipitation in tropical Mexico. *Geophys. Res. Lett.*, **19**(18), 1835–1838.
- Hewitson**, B.C., and Crane, R.G., 1996: Climate downscaling: Techniques and application, *Clim. Res.*, **7**, 85–95.
- Heyen**, H., and J. W. Dippner, 1998: Salinity in the southern German Bight estimated from large-scale climate data. *Tellus*, **50A**, 545–556.
- Heyen**, H., E. Zorita and H. von Storch, 1996: Statistical downscaling of monthly mean North Atlantic air-pressure to sea-level anomalies in the Baltic Sea. *Tellus*, **48A**, 312–323.
- Heyen**, H., H. Fock and W. Greve, 1998: Detecting relationships between the interannual variability in ecological time series and climate using a multivariate statistical approach - a case study on Helgoland Roads zooplankton. *Clim. Res.*, **10**, 179–191.
- Hirakuchi**, H., Giorgi, F., 1995: Multiyear present-day and $2\times\text{CO}_2$ simulations of monsoon climate over eastern Asia and Japan with a regional climate model nested in a general circulation model. *J. Geophys. Res.*, **100**, 21105–21125.
- HIRETYCS**, 1998. Final report of the HIRETYCS project, European Commission Climate and Environment Programme, Brussels.
- Holland**, G.J., 1997: The maximum potential intensity of tropical cyclones. *J. Atmos. Sci.*, **54**, 2519–2541.
- Hong**, S.-Y., and H. - M. H. Juang, 1998: Orography blending in the lateral boundary of a regional model, *Mon. Wea. Rev.*, **126**, 1714–1718.
- Hong**, S.Y. and A. Leetmaa, 1999: An evaluation of the NCEP RCM for Regional Climate Modeling. *J. Climate*, **12**, 592–609.
- Hostetler**, S.W., F. Giorgi, G.T. Bates and P.J. Bartlein, 1994: Lake-atmosphere feedbacks associated with paleolakes Bonneville and Lahontan. *Science*, **263**, 665–668.
- Hostetler**, S.W., P.J. Bartlein, P.U. Clark, E.E. Small and A.M. Solomon, 2000: Simulated influence of Lake Agassiz on the climate of Central North America 11,000 years ago. *Nature*, **405**, 334–337.
- Hughes**, J. P., D.P. Lettenmaier, and P. Guttorp, 1993: A stochastic approach for assessing the effect of changes in synoptic circulation patterns on gauge precipitation. *Water Resour. Res.*, **29** (10), 3303–3315.
- Hughes**, J.P., P. Guttorp and S.P. Charles, 1999: A non-homogeneous hidden Markov model for precipitation occurrence. *Appl. Statist.*, **48**, 15–30.
- Hulme**, M. and O. Brown, 1998: Portraying climate scenario uncertainties in relation to tolerable regional climate change. *Clim. Res.*, **10**, 1–14.
- Hulme**, M., E.M. Barrow, N. Arnell, P.A. Harrison, T.E. Downing and T.C. Johns, 1999: Relative impacts of human-induced climate change and natural climate variability. *Nature*, **397**, 688–691.
- Hulme**, M., J. Crossley, D. Lister, K.R. Briffa and P.D. Jones, 2000: Climate observations and GCM validation Interim Annual Report to the Department of the Environment, Transport and the Regions, April 1999 to March 2000, CRU, Norwich, UK.
- Huth**, R., 1997: Continental-scale circulation in the UKHI GCM. *J. Climate*, **10**, 1545–1561.
- Huth**, R., 1999: Statistical downscaling in central Europe: Evaluation of methods and potential predictors. *Clim. Res.*, **13**, 91–101.
- IPCC**, 1990: Climate Change: The IPCC Scientific Assessment. [J.T. Houghton , G.J. Jenkins and J.J. Ephraums, (Eds.)], Cambridge University Press, Cambridge, 365 pp.
- IPCC**, 1996: Climate change 1995: The Science of Climate Change. Contribution of Working Group I to the Second Assessment Report of the Intergovernmental Panel on Climate Change [J.T. Houghton, L.G. Meira Filho, B.A. Callander, N. Harris, A. Kattenberg and K. Maskell (eds.)], Cambridge University Press, Cambridge, 572 pp.
- Jacob**, D. and R. Podzun, 1997: Sensitivity study with the Regional Climate Model REMO, *Meteorol. Atmos. Phys.*, **63**, 119–129.
- Jacob**, D. and R. Podzun, 2000: In: Research Activities in Atmospheric and Oceanic Modelling. (CAS/JSC Working Group on Numerical Experimentation Report) [Geneva]: WMO, February 2000, **30**, 7.10–7.11
- Jacob**, D., R. Podzun, M. Lal and U. Cubasch, 1995: Summer monsoon climatology as simulated in a regional climate model nested in a general circulation model, Third Int. Conference on Modelling of Global Climate Change and Variability, Hamburg, Germany, 4–8 September 1995.
- Jacobeit**, J., 1996: Atmospheric circulation changes due to increased greenhouse warming and its impact on seasonal rainfall in the Mediterranean area. In: Climate Variability and Climate Change - Vulnerability and Adaptation, I. Nemesová (Ed.), Proceedings, Prague, Czech Republic, September 11–15, 1995, 71–80.
- Jacobeit**, J. C. Beck and A. Philipp, 1998 : Annual to decadal variability in climate in Europe - objectives and results of the German contribution to the European climate research project ADVICE. - Würzburger Geographische Manuskripte 43, 163 pp.
- Jenkins**, G. S., 1997: The 1988 and 1990 summer season simulations for West Africa. *J. Climate*, **10**, 51255–1272.
- Jenkins**, G. S. and E.J. Barron, 1997: Global climate model and coupled regional climate model. *Global Planet. Change*, **15**, 3–32.
- Ji**, Y. and A.D. Vernekar, 1997: Simulation of the Asian summer monsoons of 1987 and 1988 with a regional model nested in a global GCM. *J. Climate*, **10**, 1965–1979.
- Jóhannesson**, T., T. Jónsson, E. Källén and E. Kaas, 1995: Climate change scenarios for the Nordic countries. *Clim. Res.*, **5**: 181–195.
- Johns**, T.C. , 1999: Initial assessment of global response to greenhouse gas increases in a high resolution atmospheric timeslice experiment compared to the HadCM3 coupled model. DETR report, March 1999, Hadley Centre for Climate Prediction and Research, London Road, Bracknell, UK.
- Jones**, J.M. and T.D. Davies, 2000: Investigation of the climatic influence of air and precipitation chemistry over Europe, and applications to a downscaling methodology to assess future acidic deposition. *Clim. Res.*, **14**, 7–24.
- Jones**, R.G., 1999: The response of European climate to increased greenhouse gases simulated by standard and high resolution GCMs. DETR report, March 1999, Hadley Centre for Climate Prediction and Research, London Road, Bracknell, UK.
- Jones**, R.G., D. Hassel and K. Ward, 1999: First results from the Hadley Centre's new regional climate model including effects of enhanced resolution. DETR report, March 1999, Hadley Centre for Climate Prediction and Research, London Road, Bracknell, UK.
- Jones**, R.G., J.M. Murphy and M. Noguer, 1995: Simulations of climate change over Europe using a nested regional climate model. I: Assessment of control climate, including sensitivity to location of lateral boundaries. *Quart. J. R. Met. Soc.*, **121**, 1413–1449.
- Jones**, R.G., J.M. Murphy, M. Noguer and A.B. Keen, 1997: Simulation of climate change over Europe using a nested regional climate model. II: Comparison of driving and regional model responses to a doubling of carbon dioxide. *Quart. J. R. Met. Soc.*, **123**, 265–292.
- Jones**, R.N., K.J. Hennessy, C.M. Page, A.B. Pittock, R. Suppiah, K.J.E.

- Walsh and P.H. Whetton, 2000: An analysis of the effects of the Kyoto protocol on Pacific Island countries, part Two: Regional climate change scenarios and risk assessment methods. CSIRO/SPREP, in press.
- Joubert**, A.M. and P.D. Tyson, 1996: Equilibrium and fully coupled GCM simulations of future Southern African climates. *South African Journal of Science*, **92**, 471–484.
- Joubert**, A.M., S.J. Mason and J.S. Galpin, 1996: Droughts over southern Africa in a doubled-CO₂ climate. *Int. J. Climatology*, **16**, 1149–1156.
- Joubert**, A., J.J. Katzfey and J. McGregor, 1998: Int. Conference on The Role of Topography in Modelling Weather and Climate. Int. Centre for Theoretical Physics, Trieste, Italy, 22–26 June 1998.
- Joubert**, A.M., J.J. Katzfey, J.L. McGregor, and K.C. Nguyen, 1999: Simulating mid-summer climate over Southern Africa using a nested regional climate model. *J. Geophys. Res.*, **104**, 19015–19025.
- Kaas**, E., T.-S. Li and T. Schmitt, 1996: Statistical hindcast of wind climatology in the North Atlantic and Northwestern European region. *Clim. Res.*, **7**, 97–110.
- Kalnay**, E., M. Kanamitsu, R. Kistler, W. Collins, D. Deaven, L. Gandin, M. Iredell, S. Saha, G. White, J. Woollen, Y. Zhu, M. Chelliah, W. Ebisuzaki, W. Higgins, J. Janowiak, K.C. Mo, C. Ropelewski, J. Wang, A. Leetmaa, R. Reynolds, R. Jenne and D. Joseph, 1996: The NCEP/NCAR 40-Year Reanalysis Project. *Bull. Am. Met. Soc.*, **77**, 437–471.
- Karl**, T.R., W.C. Wang, M.E. Schlesinger, R.W. Knight, D. Portman, 1990: A method of relating general circulation model simulated climate to observed local climate. Part I: Seasonal statistics. *J. Climate*, **3**, 1053–1079.
- Kattenberg**, A., F. Giorgi, H. Grassl, G. A. Meehl, J. F. B. Mitchell, R. J. Stouffer, T. Tokioka, A. J. Weaver, T. M. L. Wigley, 1996: Climate Models – Projections of Future Climate. In : *Climate Change 1995: The Science of Climate Change. Contribution of Working Group I to the Second Assessment Report of the IPCC*. [Houghton, J.T., Meira Filho, L.G., Callander, B.A., Harris, N., Kattenberg, A. and Varney, S. K. (eds.)]. Cambridge University Press, Cambridge, 285–357.
- Kato**, H., H. Hirakuchi, K. Nishizawa, and F. Giorgi, 1999: Performance of the NCAR RegCM in the simulations of June and January climates over eastern Asia and the high-resolution effect of the model. *J. Geophys. Res.*, **104**, 6455–6476.
- Kato**, H., K. Nishizawa, H. Hirakuchi, S. Kadokura, N. Oshima and F. Giorgi. 2001: Performance of the RegCM2.5/NCAR-CSM nested system for the simulation of climate change in East Asia caused by global warming. *J. Met. Soc. Japan* (in press).
- Katz**, R. W. and M. B. Parlange, 1993: Effects of an index of atmospheric circulation on stochastic properties of precipitation. *Water Resour. Res.*, **29**, 2335–2344.
- Katz**, R.W. and M.B. Parlange, 1995: Generalizations of chain-dependent processes: Application to hourly precipitation. *Water Resour. Res.*, **31**, 1331–1341.
- Katz**, R.W. and M. B. Parlange, 1996: Mixtures of stochastic processes: applications to statistical downscaling. *Clim. Res.*, **7**, 185–193.
- Katzfey**, J.J., 1999: Storm tracks in regional climate simulations: Verification and changes with doubled CO₂. *Tellus*, **51A**, 803–814.
- Katzfey**, J.J. and K.L. McInnes, 1996: GCM simulations of eastern Australian cutoff lows. *J. Climate*, **9**, 2337–2355.
- Katzfey**, J.J., J. McGregor and P.H. Whetton, 1998: Int. Conference on The Role of Topography in Modelling Weather and Climate. Int. Centre for Theoretical Physics, Trieste, Italy, 22–26 June 1998.
- Kauker**, F., 1998: Regionalization of climate model results for the North sea. PhD thesis University of Hamburg, 109 pp.
- Kharin**, V.V. and F.W. Zwiers, 2000: Changes in the extremes in an ensemble of transient climate simulations with a coupled atmosphere-ocean GCM. *J. Climate*, **13**, 3760–3788.
- Kida**, H., T. Koide, H. Sasaki and M. Chiba, 1991: A new approach to coupling a limited area model with a GCM for regional climate simulations. *J. Met. Soc. Japan*, **69**, 723–728.
- Kidson**, J. W. and I.G. Watterson, 1995: A synoptic climatological evaluation of the changes in the CSIRO nine-level model with doubled CO₂ in the New Zealand region. *Int. J. Climatology*, **15**, 1179–1194.
- Kidson**, J.W. and C.S. Thompson, 1998: Comparison of statistical and model-based downscaling techniques for estimating local climate variations. *J. Climate*, **11**, 735–753.
- Kilsby**, C.G., P.S.P. Cowpertwait, P.E. O'Connell and P.D. Jones, 1998: Predicting rainfall statistics in England and Wales using atmospheric circulation variables. *Int. J. Climatology*, **18**, 523–539.
- Kim**, J., 1997: Precipitation and snow budget over the southwestern United States during the 1994–1995 winter season in a mesoscale model simulation. *Water. Resour. Res.*, **33**, 2831–2839.
- Kim**, J., N.L. Miller, A.K. Guetter and K.P. Georgakakos, 1998: River flow response to precipitation and snow budget in California during the 1994–95 winter. *J. Climate*, **11**, 2376–2386.
- Kittel**, T.G.F., F. Giorgi and G.A. Meehl, 1998: Intercomparison of regional biases and doubled CO₂-sensitivity of coupled atmospheric-ocean general circulation model experiments. *Clim. Dyn.*, **14**, 1–15.
- Klein**, W.H. and H.R. Glahn, 1974: Forecasting local weather by means of model output statistics. *Bull. Amer. Met. Soc.*, **55**, 1217–1227.
- Knutson**, T.R. and R.E. Tuleya, 1999: Increased hurricane intensities with CO₂-induced warmings as simulated using the GFDL hurricane prediction system. *Clim. Dyn.*, **15**, 503–519.
- Knutson**, T.R., R.E. Tuleya and Y. Kurihara, 1998: Simulated increase of hurricane intensities in a CO₂-warmed world. *Science*, **279**, 1018–1020.
- Knutson**, T.R., R.E. Tuleya, W. Shen and I. Ginis, 2000: Impact of CO₂-induced warming on hurricane intensities as simulated in a hurricane model with ocean coupling. *J. Climate*, **14**, 2458–2468.
- Kothavala**, Z., 1997: Extreme precipitation events and the applicability of global climate models to study floods and droughts. *Math. and Comp. in Simulation*, **43**, 261–268.
- Krinner** G., C. Genton, Z.-X. Li and P. Le Van, 1997: Studies of the Antarctic climate with a stretched grid GCM, *J. Geophys. Res.*, **102**, 13731–13745.
- Krinner** G. and C. Genton, 1998: GCM simulations of the Last Glacial Maximum surface climate of Greenland and Antarctica, *Clim. Dyn.*, **14**, 741–758.
- Krishnamurti**, T.N., R. Correa-Torres, M. Latif and G. Daughenbaugh, 1998: The impact of current and possibly future sea surface temperature anomalies on the frequency of Atlantic hurricanes. *Tellus*, **50A**, 186–210.
- Kröncke**, I., J.W. Dippner, H. Heyen and B. Zeiss, 1998: Long-term changes in macrofauna communities off Norderney (East Frisia, Germany) in relation to climate variability. *Mar. Ecol. Prog. Series*, **167**, 25–36.
- Labraga**, L.C. and M. Lopez, 1997: A comparison of the climate response to increased carbon dioxide simulated by general circulation models with mixed-layer and dynamic ocean representations in the region of South America. *Int. J. Climatology*, **17**, 1635–1650.
- Lal**, M., U. Cubasch, J. Perlitz and J. Waszkewitz, 1997: Simulation of the Indian monsoon climatology in ECHAM3 climate model: sensitivity to horizontal resolution. *Int. J. Climatology*, **17**, 847–858.
- Lal**, M., G.A. Meehl and J.M. Arblaster, 2000: Simulation of Indian summer monsoon rainfall and its intraseasonal variability in the NCAR climate system model. *J. Climate*, in press.
- Lal**, M., P.H. Whetton, A.B. Pittock, and B. Chakraborty, 1998a: Simulation of present-day climate over the Indian subcontinent by general circulation models. *Terrestrial Atmospheric and Oceanic Sciences*, **9**, 69–96.
- Lal**, M., P.H. Whetton, A.B. Pittock, and B. Chakraborty, 1998b: The greenhouse gas-induced climate change over the Indian subcontinent

- as projected by general circulation model experiments. *Terrestrial Atmospheric and Oceanic Sciences*, **9**, 673–690.
- Lamb**, H.H., 1972: British Isles weather types and a register of daily sequence of circulation patterns, 1861–1971. Geophysical Memoir 116, HMSO, London, 85 pp.
- Landsea**, C.W., 1997: Comments on “Will greenhouse gas induced warming over the next 50 years lead to higher frequency and greater intensity of hurricanes?”, *Tellus*, **49A**, 622–623.
- Langenberg**, H. A. Pfizemayer, H. von Storch and J. Sndermann, 1999: Storm related sea level variations along the North Sea coast: natural variability and anthropogenic change. *Cont. Shelf Res.*, **19**, 821–842.
- Laprise** R., D. Caya, M. Giguère, G. Bergeron, H. Côte, J.-P. Blanchet, G.J. Boer and N.A. McFarlane, 1998: Climate and climate change in western Canada as simulated by the Canadian regional climate model. *Atmosphere-Ocean*, **36**, 119–167.
- Lettenmaier**, D., 1995: Stochastic Modeling of precipitation with applications to climate model downscaling. In: H. von Storch and A. Navarra (eds) “Analysis of Climate Variability: Applications of Statistical Techniques”, Springer Verlag, 197–212 (ISBN 3-540-58918-X).
- Leung**, L.R. and S.J. Ghan, 1995: A subgrid parameterization of orographic precipitation. *Theor. Appl. Climatol.*, **52**, 95–118.
- Leung**, L.R. and S.J. Ghan, 1998: Parameterizing subgrid orographic precipitation and surface cover in climate models. *Mon. Wea. Rev.*, **126**, 3271–3291.
- Leung**, L.R. and S.J. Ghan, 1999a: Pacific Northwest climate sensitivity simulated by a regional climate model driven by a GCM. Part I: control simulations. *J. Climate*, **12**, 2010–2030.
- Leung**, L.R. and S.J. Ghan, 1999b: Pacific Northwest climate sensitivity simulated by a regional climate model driven by a GCM. Part II: $2\times\text{CO}_2$ simulations. *J. Climate*, **12**, 2031–2053.
- Leung**, L.R., Wigmosta, M. S., Ghan, S.J., Epstein, D.J., Vail, L.W., 1996: Application of a subgrid orographic precipitation/surface hydrology scheme to a mountain watershed. *J. Geophys. Res.*, **101**, 12803–12817.
- Leung**, L.R., S.J. Ghan, Z.C. Zhao, Y. Luo, W.-C. Wang, and H.-L. Wei, 1999a: Intercomparison of regional climate simulations of the 1991 summer monsoon in eastern Asia. *J. Geophys. Res.*, **104**, 6425–6454.
- Leung**, L.R., A.F. Hamlet, D.P. Lettenmaier and A. Kumar, 1999b: Simulations of the ENSO hydroclimate signals in the Pacific Northwest Columbia River Basin. *Bull. Am. Met. Soc.*, **80**(11), 2313–2329.
- Liston**, G.E. and R.A. Pielke, 2000: A climate version of the regional atmospheric modeling system. *Theor. Appl. Climatol.*, **66**, 29–47..
- Liston**, G.E., R.A. Pielke, Sr., and E.M. Greene, 1999: Improving first-order snow-related deficiencies in a regional climate model. *J. Geophysical Res.*, **104** (D16), 19559–19567.
- Luterbacher**, J., C. Schmutz, D. Gyalistras, E. Xoplaki and H. Wanner, 1999: Reconstruction of monthly NAO and EU indices back to AD 1675. *Geophys. Res. Lett.*, **26**, 2745–2748.
- Lüthi**, D., A. Cress, H.C. Davies, C. Frei and C. Schär, 1996: Interannual variability and regional climate simulations. *Theor. Appl. Climatol.*, **53**, 185–209.
- Lynch**, A. H., W.L. Chapman, J.E. Walsh. and G. Weller, 1995: Development of a regional climate model of the western Arctic. *J. Climate*, **8**, 1555–1570.
- Lynch**, A.H., M.F. Glück, W.L. Chapman, D.A. Bailey,= and J.E. Walsh, 1997a: Remote sensing and climate modeling of the St. Lawrence Is. Polynya, *Tellus*, **49A**, 277–297.
- Lynch**, A.H., D.L. McGinnis, W.L. Chapman and J.S. Tilley, 1997b: A Multivariate comparison of two land surface models integrated into an Arctic regional climate system model. *Ann. Glaciol.*, **25**, 127–131.
- Lynch**, A.H., D.L. McGinnis, and D.A. Bailey, 1998: Snow-albedo feedback and the spring transition in a regional climate system model: Influence of land surface model, *J. Geophys. Res.*, **103**, 29037–29049.
- Maak**, K. and H. von Storch, 1997: Statistical downscaling of monthly mean temperature to the beginning of flowering of Galanthus nivalis L. in Northern Germany. *Int. J. Biometeor.*, **41**, 5–12.
- Mabuchi**, K., Y. Sato and H. Kida, 2000: Numerical study of the relationships between climate and the carbon dioxide cycle on a regional scale. *J. Met. Soc. Japan*, **78**, 25–46.
- Machenhauer**, B., M. Windelband, M. Botzet, R. Jones and M. Déqué, 1996: Validation of present-day regional climate simulations over Europe: Nested LAM and variable resolution global model simulations with observed or mixed layer ocean boundary conditions. MPI Reprot No. 191, MPI, Hamburg, Germany.
- Machenhauer**, B., M. Windelband, M. Botzet, J.H. Christensen, M. Deque, R. Jones, P.M. Rutledge and G. Visconti, 1998: Validation and analysis of regional present-day climate and climate change simulations over Europe. MPI Report No.275, MPI, Hamburg, Germany.
- Marinucci**, M. R. and F. Giorgi, 1992: A $2\times\text{CO}_2$ climate change scenario over Europe generated using a limited area model nested in a general circulation model 1. Present-day seasonal climate simulation. *J. Geophys. Res.*, **97**, 9989–10009.
- Marinucci**, M. R., F. Giorgi, M. Beniston, M. Wild, P. Tschuck, A. Ohmura and A. Bernasconi, 1995: High resolution simulations of January and July climate over the western alpine region with a nested regional modeling system. *Theor. Appl. Climatol.*, **51**, 119–138.
- Martin**, E., B. Timbal and E. Brun, 1997: Downscaling of general circulation model outputs: simulation of the snow climatology of the French Alps and sensitivity to climate change. *Clim. Dyn.*, **13**, 45–56.
- Martin**, G.M., 1999: The simulation of the Asian summer monsoon, and its sensitivity to horizontal resolution, in the UK Meteorological Office Unified Model. *Quart. J. R. Met. Soc.*, **125**, 1499–1525.
- Maslanik**, J.A., A.H. Lynch and M. Serreze, 2000: A case study simulation of Arctic regional climate in a coupled model. *J. Climate*. **13**, 383–401.
- May**, W., 1999: A time-slice experiment with the ECHAM4 AGCM at high resolution: The experimental design and the assessment of climate change as compared to a greenhouse gas experiment with ECHAM4/OPYC at low resolution, DMI Scientific Report 99-2, DMI, Copenhagen.
- May**, W. and E. Roeckner, 2001: A time-slice experiment with the ECHAM4 AGCM at high resolution: The impact of resolution on the assessment of anthropogenic climate change, *Clim. Dyn.*, (in press).
- McDonald**, R. 1999: Changes in tropical cyclones as greenhouse gases are increased. PMSR report, March 1999, Hadley Centre for Climate Prediction and Research, London Road, Bracknell, UK.
- McGregor**, J.L., 1997: Regional climate modelling. *Meteorology and Atmospheric Physics*, **63**, 105–117.
- McGregor**, J.L., J.J. Katzfey and K.C. Nguyen, 1995: Seasonally-varying nested climate simulations over the Australian region, Third Int. Conference on Modelling of Global Climate Change and Variability, Hamburg, Germany, 4–8 September 1995.
- McGregor**, J.L., J.J. Katzfey and K.C. Nguyen, 1998: Fine resolution simulations of climate change for southeast Asia. Final report for a Research Project commissioned by Southeast Asian Regional Committee for START (SARCS), Aspendale, Vic.: CSIRO Atmospheric Research. VI, 15, 35pp.
- McGregor**, J.L., J.J. Katzfey and K.C. Nguyen, 1999: Recent regional climate modelling experiments at CSIRO. In: Research Activities in Atmospheric and Oceanic Modelling. H. Ritchie (ed). (CAS/JSC Working Group on Numerical Experimentation Report; 28; WMO/TD – no. 942) [Geneva]: WMO. P. 7.37–7.38.
- McGregor**, J.L., K. Walsh, 1993: Nested simulations of perpetual January climate over the Australian region. *J. Geophys. Res.*, **98**, 23283–23290.
- McGregor**, J. L., K. Walsh, 1994: Climate change simulations of Tasmanian precipitation using multiple nesting. *J. Geophys. Res.*, **99**,

- 20889–20905.
- McGuffie**, K., A. Henderson-Sellers, N. Holbrook, Z. Kothaval, O. Balachova and J. Hoekstra, 1999: Assessing simulations of daily temperature and precipitation variability with global climate models for present and enhanced greenhouse conditions, *Int. J. Climatol.* **19**, 1–26.
- Mearns**, L.O., I. Bogardi, F. Giorgi, I. Mataysovsky and M. Palecki, 1999: Comparison of climate change scenarios generated daily temperature and precipitation from regional climate model experiments and statistical downscaling, *J. Geophys. Res.*, **104**, 6603–6621.
- Mearns**, L. O., 1999: The effect of spatial and temporal resolution of climate change scenarios on changes in frequencies of temperature and precipitation extremes. In: S. Hassol and J. Katzenberger, Elements of Change 1998, Session 2: Climate Extremes: Changes, Impacts, and Projections. Aspen: Aspen Global Change Institute, 316–323.
- Mietus** M., 1999. The role of regional atmospheric circulation over Europe and North Atlantic in formation of climatic and oceanographic condition in the Polish coastal zone, Research Materials of Institute of Meteorology and Water Management, Meteorological Series, 29, 147pp (in Polish with English summary).
- Miller**, N.L. and J. Kim, 1997: The Regional Climate System Model. In: 'Mission Earth: Modeling and simulation for a sustainable global system', M.G. Clymer and C.R. Mechoso (eds.), Society for Computer Simulation International, 55–60.
- Murphy**, J.M., 1999: An evaluation of statistical and dynamical techniques for downscaling local climate. *J. Climate*, **12**, 2256–2284.
- Murphy**, J.M., 2000: Predictions of climate change over Europe using statistical and dynamical downscaling techniques. *Int. J. Climatology*, **20**, 489–501.
- New**, M., M. Hulme, and P. Jones, 1999: Representing Twentieth-century space-time climate variability. Part 1: development of a 1961–1990 mean monthly terrestrial climatology. *J. Climate*, **12**, 829–856.
- New**, M., M. Hulme, and P. Jones, 2000: Representing Twentieth-century space-time climate variability. Part 2: development of a 1901–1996 mean monthly terrestrial climatology. *J. Climate*, **13**, 2217–2238.
- Noguer**, M., 1994: Using statistical techniques to deduce local climate distributions. An application for model validation. *Met. Apps.*, **1**, 277–287.
- Noguer** M., R.G. Jones and J.M. Murphy, 1998: Sources of systematic errors in the climatology of a nested regional climate model (RCM) over Europe. *Clim. Dyn.*, **14**, 691–712.
- O'Connell**, P. E. 1999: Producing rainfall scenarios for hydrologic impact modelling. In: G. Kiely et al., (editors). Abstract Volume from the EU Environmental and Climate Programme Advanced Study Course on European Water Resources and Climate Change Processes, 53pp.
- Osborn**, T.J. and M. Hulme, 1997: Development of a relationship between station and grid-box rain-day frequencies for climate model evaluation. *J. Climate*, **10**, 1885–1908.
- Osborn**, T.J. and M. Hulme, 1998: Evaluation of the European daily precipitation characteristics from the Atmospheric Model Intercomparison Project, *Int. J. Climatology*, **18**, 505–522.
- Osborn**, T.J., D. Conway, M. Hulme, J.M. Gregory and P.D. Jones, 1999: Air flow influences on local climate: observed and simulated mean relationships for the UK. *Clim. Res.*, **13**, 173–191.
- Palutikof**, J.P., J.A. Winkler, C.M. Goodess and J.A. Andresen, 1997: The simulation of daily temperature time series from GCM output. Part 1: Comparison of model data with observations, *J. Climate*, **10**, 2497–2513.
- Pan**, Z., E. S. Takle, M. Segal and R. Arritt, 1999: Simulation of potential impacts of man-made land use changes on U.S. summer climate under various synoptic regimes, *J. Geophys. Res.*, **104**, 6515–6528.
- Pan**, Z., J.H. Christensen, R.W. Arritt., W.J. Gutowski, E.S. Takle and F. Otieno, 2000: Evaluation of uncertainties in regional climate change simulations. *J. Geophys. Res.*, in press.
- Parlange**, M.B. and R.W. Katz, 2000: An extended version of the Richardson model for simulating daily weather variables. *J. Appl. Meteorol.*, **39**, 610–622.
- Perica**, S. and E. Foufoula-Georgiou, 1996a: Linkage of scaling and thermodynamic parameters of rainfall: Results from midlatitude mesoscale convective systems, *J. Geophys. Res.*, **101**, 7431–7448.
- Perica**, S. and E. Foufoula-Georgiou, 1996b: Model for multiscale disaggregation of spatial rainfall based on coupling meteorological and scaling descriptions, *J. Geophys. Res.*, **101(D21)**, 26347–26361.
- Pielke**, R.A., Jr., and C.W. Landsea, 1998: Normalized hurricane damages in the United States: 1925–95. *Weath. Forecast.*, **13**, 621–631.
- Pielke**, R.A., Sr., W.R. Cotton, R.L. Walko, C.J. Tremback, W.A. Lyons, L.D. Grasso, M.E. Nicholls, M.D. Moran, D.A. Wesley, T.J. Lee and J.H. Copeland, 1992: A comprehensive meteorological modeling system—RAMS, *Meteor. Atmos. Phys.*, **49**, 69–91.
- Pielke**, R.A., Sr., R.L. Walko, L. Steyaert, P.L. Vidale, G.E. Liston and W.A. Lyons, 1999: The influence of anthropogenic landscape changes on weather in south Florida. *Mon. Wea. Rev.*, **127**, 1663–1673.
- Pittock**, A.B., M.R. Dix, K.J. Hennessy, D.R. Jackett, J.J. Katzfey, T.J. McDougall, K.L. McInnes, S.P. O'Farrell, I.N. Smith, R. Suppiah, K.J.E. Walsh, P.H. Whetton and S.G. Wilson, 1995: Progress towards climate change scenario and impact studies for the southwest Pacific. In: The science and impacts of climate change in the Pacific islands, Apia, Western Samoa. Apia, Western Samoa: Conference on the Science and Impacts of Climate Change in the Pacific Islands. 15–2, 21–46.
- Podzun**, R., A. Cress, D. Majewski and V. Renner, 1995: Simulation of European climate with a limited area model. Part II: AGCM boundary conditions. *Contrib. Atmos. Phys.*, **68**, 205–225.
- Qian**, Y. and F. Giorgi, 1999: Interactive coupling of regional climate and sulfate aerosol models over East Asia. *J. Geophys. Res.*, **104**, 6501–6514.
- Raab**, B. and H. Vedin (Eds.), 1995: Climate, Lakes and Rivers: National Atlas for Sweden. SNA Publishing, 176pp and 198 plates.
- Racksko**, P., L. Szeidl and M. Semenov, 1991: A serial approach to local stochastic weather models. *Ecological Modeling*, **57**, 27–41.
- Räisänen**, J., 1998: Intercomparison studies of general circulation model simulations of anthropogenic climate change. Academic dissertation presented at the Faculty of Science, Department of Meterorology, Report 57, University of Helsinki, 50pp.
- Räisänen**, J., M. Rummukainen, A. Ullerstig, B. Bringfelt, U. Hansson and U. Willén, 1999: The first Rossby Centre regional climate scenario - dynamical downscaling of CO₂-induced climate change in the HadCM2 GCM. SMHI Reports Meteorology and Climatology No. 85, 56 pp. Swedish Meteorological and Hydrological Institute, SE-601 76 Norrköping, Sweden.
- Reichert**, B.K., L. Bengtsson and Ove Åkesson, 1999: A statistical modeling approach for the simulation of local paleoclimatic proxy records using GCM output. *J. Geophys. Res.*, **104(D16)**, 19071–19083.
- Renwick**, J. A., J.J. Katzfey, K.C. Nguyen and J.L. McGregor, 1998: Regional model simulations of New Zealand climate. *J. Geophys. Res.*, **103**, 5973–5982.
- Richardson**, C.W., 1981: Stochastic simulation of daily precipitation, temperature, and solar radiation. *Water Resour. Res.*, **17**(1), 182–190.
- Riedo**, M., D. Gyalistras, A. Fischlin and J. Fuhrer, 1999: Using an ecosystem model linked to GCM derived local weather scenarios to analyse effects of climate change and elevated CO₂ on dry matter production and partitioning, and water use in temperate managed grasslands. *Global Change Biol.*, **5**, 213–223.
- Rinke** A. and K. Dethloff, 1999: Sensitivity studies concerning initial and boundary conditions in a regional climate model of the Arctic, *Clim.*

- Res.*, **14**, 101–113.
- Rinke**, A., K. Dethloff and J.H. Christensen, 1999: Arctic winter climate and its interannual variations simulated by a regional climate model. *J. Geophys. Res.*, **104**, 19027–19038.
- Risbey**, J. and P. Stone, 1996: A case study of the adequacy of GCM simulations for input to regional climate change assessments. *J. Climate*, **9**, 1441–1467.
- Roebber**, P.J. and L.F. Bosart, 1998: The sensitivity of precipitation to circulation details. Part I: An analysis of regional analogs. *Mon. Wea. Rev.*, **126**, 437–455.
- Roldan**, J. and D.A. Woolhiser, 1982: Stochastic daily precipitation models. 1. A comparison of occurrence processes. *Water Resour. Res.*, **18**, 1451–1459.
- Rotach**, M.W., M.R.M. Marinucci, M. Wild, P. Tschuck, A. Ohmura, M. Beniston, 1997: Nested regional simulation of climate change over the Alps for the scenario of doubled greenhouse forcing. *Theor. Appl. Climatol.*, **57**, 209–227.
- Royer**, J.-F., F. Chauvin, B. Timbal, P. Araspin and D. Grimal, 1998: A GCM study of the impact of greenhouse gas increase on the frequency of occurrence of tropical cyclones. *Clim. Change*, **38**, 307–343.
- Rummukainen**, M., 1997: Methods for statistical downscaling of GCM simulations, RMK No 80, Swedish Meteorological and Hydrological Institute, Norrköping, Sweden.
- Rummukainen**, M., J. Räisänen, B. Bringfelt, A. Ullerstig, A. Omstedt, U. Willen, U. Hansson and C. Jones, 2000: RCA1 Regional Climate Model for the Nordic Region – Model Description and Results from the Control Run Downscaling of Two GCMs. *Clim. Dyn.*, (in press).
- Ruti** P.M., C. Cacciamani, T. Paccagnella, A. Bargagli and C. Cassardo, 1998: LAM multi-seasonal numerical integrations: performance analysis with different surface schemes. *Contrib. Atmos. Phys.*, **71**, 321–346.
- SAR**, see IPCC (1996a).
- Sailor**, D.J. and X. Li, 1999: A semiempirical downscaling approach for predicting regional temperature impacts associated with climatic change. *J. Climate*, **12**, 103–114.
- Schär** C., C. Frei, D. Lüthi and H.C. Davies, 1996: Surrogate climate change scenarios for regional climate models. *Geophys. Res. Lett.*, **23**, 669–672.
- Schnur**, R. and D. Lettenmaier, 1998: A case study of statistical downscaling in Australia using weather classification by recursive partitioning. *J. Hydrol.*, **212**–123, 362–379.
- Schubert**, S. 1998: Downscaling local extreme temperature changes in south-eastern Australia from the CSIRO Mark2 GCM. *Int. J. Climatol.*, **18**, 1419–1438.
- Schubert**, S. and A. Henderson-Sellers, 1997: A statistical model to downscale local daily temperature extremes from synoptic-scale atmospheric circulation patterns in the Australian region. *Clim. Dyn.*, **13**, 223–234.
- Semenov**, M.A. and E.M. Barrow, 1997: Use of a stochastic weather generator in the development of climate change scenarios. *Clim. Change*, **35**, 397–414.
- Sept**, V., 1998: Untersuchungen der Gewitteraktivität im Süddeutschland Raum mittels statistisch-dynamischer Regionalisierung. Deutsches Zentrum für Luft- und Raumfahrt e.V., Forschungsbericht 98–27, 113 pp.
- Seth**, A. and F. Giorgi, 1998: The effects of domain choice on summer precipitation simulation and sensitivity in a regional climate model, *J. Climate*, **11**, 2698–2712.
- Small**, E.E., F. Giorgi and L.C. Sloan, 1999a: Regional climate model simulation of precipitation in central Asia: Mean and interannual variability. *J. Geophys. Res.*, **104**, 6563–6582.
- Small**, E.E., L.C. Sloan, S. Hostetler and F. Giorgi, 1999b: Simulating the water balance of the Aral Sea with a coupled regional climate-lake model. *J. Geophys. Res.*, **104**, 6583–6602.
- Smith**, J. A. and A. F. Karr, 1985: Statistical inference for point process models of rainfall. *Water Resour. Res.*, **21**(1), 73–80.
- Solman**, S.A. and M.N. Nuñez, 1999: Local estimates of global change: a statistical downscaling approach. *Int. J. Climatology*, **19**, 835–861.
- Starr**, V.P., 1942: Basic principles of weather forecasting. Harper Brothers Publishers, New York, London, 299pp.
- Stendel**, M. and E. Röckner 1998: Impacts of horizontal resolution on simulated climate statistics in ECHAM4. MPI report 253, MPI, Hamburg, Germany.
- Stratton**, R.A. 1999a: A high resolution AMIP integration using the Hadley Centre model HadAM2b. *Clim. Dyn.*, **15**, 9–28.
- Stratton**, R.A. 1999b: The impact of increasing resolution on the HadAM3 climate simulation. HCTN 13, Hadley Centre, The Met. Office, Bracknell, UK.
- Sun**, L., F.H.M. Semazzi, F. Giorgi and L. Ogallo, 1999: Application of the NCAR regional climate model to eastern Africa. 2. Simulations of interannual variability of short rains. *J. Geophys. Res.*, **104**, 6549–6562.
- Takle**, E.S., W.J. Gutowski, R.W. Arritt, Z. Pan, C.J. Anderson, R.S. da Silva, D. Caya, S.-C. Chen, F. Giorgi, J.H. Christensen, S.-Y. Hong, H.-M. H. Juang, J. Katzfey, W.M. Lapenta, R. Laprise, P. Lopez, G.E. Liston, J. McGregor, A. Pielke and J.O. Roads, 1999: Project to intercompare regional climate simulation (PIRCS): Description and initial results. *J. Geophys. Res.*, **104**, 19443–19461.
- Tett**, S.F.B., T.C. Johns and J.F.B. Mitchell, 1997: Global and Regional Variability in a coupled AOGCM. *Clim. Dyn.*, **13**, 303–323.
- Timbal**, B. and B.J. McAvaney, 1999: A downscaling procedure for Australia. BMRC scientific report 74.
- Trigo**, R.M. and J.P. Palutikof, 1999: Simulation of daily temperatures for climate change scenarios over Portugal: a neural network model approach. *Clim. Res.*, **13**, 61–75.
- Tsutsui**, J., A. Kasahara and H. Hirakuchi, 1999: The impacts of global warming on tropical cyclones - a numerical experiment with the T42 version of NCAR CCM2. Proceedings of the 23rd Conference on Hurricanes and tropical meteorology, 10–15 January 1999, Dallas, American Meteorological Society, 1077–1080.
- Tsutsui**, J.-I. and A. Kasahara, 1996: Simulated tropical cyclones using the National Center for Atmospheric Research community climate model. *J. Geophys. Res.*, **101**, 15013–15032.
- Tsvetsinskaya**, E., L.O. Mearns and W.E. Easterling, 2000: Investigating the effect of seasonal plant growth and development in 3-dimensional atmospheric simulations. *J. Climate*, in press.
- van Lipzig**, 1999: The surface mass balance of the Antarctic ice sheet, a study with a regional atmospheric model, Ph. D. thesis, Utrecht University, 154 pp.
- von Storch**, H., 1995: Inconsistencies at the interface of climate impact studies and global climate research. *Meteorol. Zeitschrift* 4 NF, 72–80.
- von Storch**, H., 1999a: The global and regional climate system. In: H. von Storch and G. Flöser: Anthropogenic Climate Change, Springer Verlag, ISBN 3-540-65033-4, 3–36.
- von Storch**, H., 1999b: Representation of conditional random distributions as a problem of “spatial” interpolation. In: J. Gómez-Hernández, A. Soares and R. Froidevaux (Eds.): geoENV II - Geostatistics for Environmental Applications. Kluwer Academic Publishers, Dordrecht, Boston, London, ISBN 0-7923-5783-3, 13–23.
- von Storch**, H., 1999c: On the use of “inflation” in downscaling. *J. Climate*, **12**, 3505–3506.
- von Storch**, H., H. Langenberg and F. Feser, 2000: A spectral nudging technique for dynamical downscaling purposes, *Mon. Wea. Rev.*, **128**, 3664–3673.
- von Storch**, H. and H. Reichardt, 1997: A scenario of storm surge statistics for the German Bight at the expected time of doubled atmospheric carbon dioxide concentration. *J. Climate*, **10**,

- 2653–2662.
- von Storch**, H., E. Zorita and U. Cubasch, 1993: Downscaling of global climate change estimates to regional scales: An application to Iberian rainfall in wintertime. *J. Climate*, **6**, 1161–1171.
- von Storch**, H., and F.W. Zwiers, 1999: Statistical Analysis in Climate Research, Cambridge University Press, ISBN 0 521 45071 3, 494 pp.
- Wallis**, T.W.R. and J.F. Griffiths, 1997: Simulated meteorological input for agricultural models. *Agricultural and Forest Meteorology*, **88**, 241–258.
- Walsh**, K. and J.L McGregor, 1995: January and July climate simulations over the Australian region using a limited area model. *J. Climate*, **8**, 2387–2403.
- Walsh**, K. and J.L McGregor, 1996: Simulations of Antarctic climate using a limited area model. *J. Geophys. Res.*, **101**, 19093–19108.
- Walsh**, K. and J.L. McGregor, 1997: An assessment of simulations of climate variability over Australia with a limited area model. *Int. J. Climatology*, **17**, 201–233.
- Walsh** J.E and J.J. Katzfey, 2000: The impact of climate change on the poleward movement of tropical cyclone-like vortices in a regional model. *J. Climate*, in press.
- Walsh** J.E. and B.F. Ryan, 2000: Tropical cyclone intensity increase near Australia as a result of climate change. *J. Climate*, **13**, 3029–3036.
- Walsh**, K. and I.G. Watterson, 1997: Tropical cyclone-like vortices in a limited area model: comparison with observed climatology. *J. Climate*, **10**, 2240–2259.
- Wanner**, H., R. Rickli, E. Salvisberg, C. Schmutz and M. Schepp, 1997: Global climate change and variability and its influence on Alpine climate - concepts and observations. *Theor. Appl. Climatol.*, **58**, 221–243.
- Warner**, T. T., R.A. Peterson and R.E. Treadon, 1997: A tutorial on lateral conditions as a basic and potentially serious limitation to regional numerical weather prediction. *Bull. Am. Met. Soc.*, **78**, 2599–2617.
- WASA**, 1998: Changing waves and storms in the Northeast Atlantic? *Bull. Am. Met. Soc.*, **79**, 741–760.
- Watterson**, I.G., M.R. Dix, H.B. Gordon and J.L McGregor, 1995: The CSIRO nine-level atmospheric general circulation model and its equilibrium present and doubled CO₂ climate, *Australian Meteorological Magazine*, **44**, 111–125.
- Wei**, H. and C. Fu, 1998: Study of the sensitivity of a regional model in response to land cover change over Northern China. *Hydrological processes*, **12**, 2249–2265.
- Wei**, H., Fu, C., Wang, W.-C., 1998: The effect of lateral boundary treatment of regional climate model on the East Asian summer monsoon rainfall simulation. *Chinese J. Atmos. Sci.*, **22**, 231–243.
- Weichert**, A. and G. Bürger, 1998: Linear versus nonlinear techniques in downscaling. *Clim. Res.*, **10**, 83–93.
- Weisse**, R., H. Heyen and H. von Storch, 2000: Sensitivity of a regional atmospheric model to a state dependent roughness and the need of ensemble calculations. *Mon. Wea. Rev.*, **128**, 3631–3642.
- Werner**, P.C. and F.-W. Gerstengarbe, 1997: A proposal for the development of climate scenarios. *Clim. Res.*, **8**, 171–182.
- Werner**, P.C. and H. von Storch, 1993: Interannual variability of Central European mean temperature in January/February and its relation to the large-scale circulation. *Clim. Res.*, **3**, 195–207.
- Whetton**, P.H., M.H. England, S.P. O'Farrell, I.G. Watterson and A.B. Pittock, 1996a: Global comparison of the regional rainfall results of enhanced greenhouse coupled and mixed layer ocean experiments: implications for climate change scenario development. *Clim. Change*, **33**, 497–519.
- Whetton** P.H., J.J. Katzfey, K.J. Hennessey, X. Wu, J.L. McGregor and K. Nguyen, 2001: Using regional climate models to develop fine resolution scenarios of climate change: An example for Victoria, Australia. *Clim. Res.*, **16**, 181–201.
- Whetton**, P. H., A.B. Pittock, J.C. Labraga, A.B. Mullan and A.M. Joubert, 1996b: Southern Hemisphere climate: comparing models with reality. In: Climate change: developing southern hemisphere perspectives. T. W. Giambelluca, and A. Henderson-Sellers (Eds.). (Research and Developments in Climate and Climatology) Chichester: Wiley, 89–130.
- Widmann**, M. and C. Schär, 1997: A principal component and long-term trend analysis of daily precipitation in Switzerland. *Int. J. Climatology*, **17**, 1333–1356.
- Widmann**, M. and C.S. Bretherton, 2000: Validation of mesoscale precipitation in the NCEP reanalysis using a new gridcell dataset for the northwestern United States. *J. Climate*, **13**, 1936–1950.
- Wilby**, R.L., 1998: Statistical downscaling of daily precipitation using daily airflow and seasonal teleconnection indices. *Clim. Res.* **10**:163–178.
- Wilby**, R.L., H. Hassan and K. Hanaki, 1998a: Statistical downscaling of hydrometeorological variables using general circulation model output. *J. Hydrology*, **205**, 1–19.
- Wilby**, R.L., T.M.L. Wigley, D. Conway, P.D. Jones, B.C. Hewitson, J. Main and D.S. Wilks, 1998b: Statistical downscaling of general circulation model output: A comparison of methods, *Water Resou. Res.*, **34**, 2995–3008.
- Wilby**, R.L. and T.M.L. Wigley, 1997: Downscaling general circulation model output: a review of methods and limitations. *Prog. Phys. Geography*, **21**, 530–548.
- Wilby**, R.L. and Wigley, T.M.L., 2000: Precipitation predictors for downscaling: observed and General Circulation Model relationships. *Int. J. Climatology*, **20**, No. 6, 641–661.
- Wilby**, R.L., L.E. Hay, W.J. Gutowski, R.W. Arritt, E.S. Takle, Z. Pan, G.H. Leavesley and M.P. Clark, 2000: Hydrological responses to dynamically and statistically downscaled climate model output. *Geophys. Res. Lett.*, **27**, No. 8, p1199.
- Wild**, M., A. Ohmura, H. Gilgen and E. Roeckner, 1995: Regional climate simulation with a high resolution GCM: surface radiative fluxes. *Clim. Dyn.*, **11**, 469–486.
- Wild**, M., L. Dümenil, and J.P. Schulz, 1996: Regional climate simulation with a high resolution GCM: surface hydrology. *Climate Dynamics*, **12**, 755–774.
- Wild** M., A. Ohmura and U. Cubasch, 1997: GCM simulated surface energy fluxes in climate change experiments. *J. Climate*, **10**, 3093–3110.
- Wilks**, D. S., 1999a: Interannual variability and extreme-value characteristics of several stochastic daily precipitation models. *Agric. For. Meteorol.*, **93**, 153–169.
- Wilks**, D., 1999b: Multisite downscaling of daily precipitation with a stochastic weather generator. *Clim. Res.*, **11**, 125–136.
- Wilks**, D. S. and R. L. Wilby, 1999: The weather generator game: A review of stochastic weather models. *Prog. Phys. Geography*, **23**, 329–358.
- Williamson**, D.L., 1999: Convergence of atmospheric simulations with increasing horizontal resolution and fixed forcing scales. *Tellus*, **51A**, 663–673.
- Winkler**, J.A., J.P. Palutikof, J.A. Andresen and C.M. Goodess, 1997: The simulation of daily temperature time series from GCM output: Part II: Sensitivity analysis of an empirical transfer function methodology. *J. Climate*, **10**, 2514–2535.
- Yoshimura**, J., M. Sugi and A. Noda, 1999: Influence of greenhouse warming on tropical cyclone frequency simulated by a high-resolution AGCM. Proceedings of the 23rd Conference on Hurricanes and tropical meteorology, 10–15 January 1999, Dallas, American Meteorological Society, 1081–1084.
- Zorita**, E., J. Hughes, D. Lettenmaier, and H. von Storch, 1995: Stochastic characterisation of regional circulation patterns for climate model diagnosis and estimation of local precipitation. *J.*

- Climate*, **8**, 1023–1042.
- Zorita**, E., and A. Laine, 1999: Dependence of salinity and oxygen concentrations in the Baltic Sea on the large-scale atmospheric circulation. *Clim. Res.*, **14**, 25-34.
- Zorita**, E. and H. von Storch, 1997: A survey of statistical downscaling techniques. GKSS report 97/E/20.
- Zorita**, E. and H. von Storch, 1999: The analog method - a simple statistical downscaling technique: comparison with more complicated methods. *J. Climate*, **12**, 2474-2489.
- Zwiers**, F.W. and V.V. Kharin, 1997: Changes in the extremes of climate simulated by CCC GCM2 under CO₂ doubling. *J. Climate*, **11**, 2200-2222.

11

Changes in Sea Level

Co-ordinating Lead Authors

J.A. Church, J.M. Gregory

Lead Authors

P. Huybrechts, M. Kuhn, K. Lambeck, M.T. Nhuan, D. Qin, P.L. Woodworth

Contributing Authors

O.A. Anisimov, F.O. Bryan, A. Cazenave, K.W. Dixon, B.B. Fitzharris, G.M. Flato, A. Ganopolski, V. Gornitz, J.A. Lowe, A. Noda, J.M. Oberhuber, S.P. O'Farrell, A. Ohmura, M. Oppenheimer, W.R. Peltier, S.C.B. Raper, C. Ritz, G.L. Russell, E. Schlosser, C.K. Shum, T.F. Stocker, R.J. Stouffer, R.S.W. van de Wal, R. Voss, E.C. Wiebe, M. Wild, D.J. Wingham, H.J. Zwally

Review Editors

B.C. Douglas, A. Ramirez

Contents

Executive Summary	641	11.3.2.3 Mean sea level change from satellite altimeter observations	663
11.1 Introduction	643	11.3.3 Changes in Extreme Sea Levels: Storm Surges and Waves	664
11.2 Factors Contributing to Sea Level Change	644	11.4 Can 20th Century Sea Level Changes be Explained?	664
11.2.1 Ocean Processes	644	11.5 Future Sea Level Changes	666
11.2.1.1 Observational estimates of ocean warming and ocean thermal expansion	644	11.5.1 Global Average Sea Level Change 1990 to 2100	666
11.2.1.2 Models of thermal expansion	646	11.5.1.1 Projections for a single scenario based on a range of AOGCMs	666
11.2.2 Glaciers and Ice Caps	647	11.5.1.2 Projections for SRES scenarios	670
11.2.2.1 Mass balance studies	647	11.5.2 Regional Sea Level Change	673
11.2.2.2 Sensitivity to temperature change	647	11.5.3 Implications for Coastal Regions	674
11.2.2.3 Sensitivity to precipitation change	649	11.5.3.1 Mean sea level	674
11.2.2.4 Evolution of area	650	11.5.3.2 Extremes of sea level: storm-surges and waves	675
11.2.3 Greenland and Antarctic Ice Sheets	650	11.5.4 Longer Term Changes	675
11.2.3.1 Mass balance studies	650	11.5.4.1 Thermal expansion	675
11.2.3.2 Direct monitoring of surface elevation changes	652	11.5.4.2 Glaciers and ice caps	677
11.2.3.3 Numerical modelling	652	11.5.4.3 Greenland and Antarctic ice sheets	677
11.2.3.4 Sensitivity to climatic change	653		
11.2.4 Interaction of Ice Sheets, Sea Level and the Solid Earth	654	11.6 Reducing the Uncertainties in Future Estimates of Sea Level Change	679
11.2.4.1 Eustasy, isostasy and glacial-interglacial cycles	654	11.6.1 Observations of Current Rates of Global-averaged and Regional Sea Level Change	679
11.2.4.2 Earth rotation constraints on recent sea level rise	656	11.6.2 Ocean Processes	680
11.2.5 Surface and Ground Water Storage and Permafrost	657	11.6.3 Glaciers and Ice Caps	680
11.2.6 Tectonic Land Movements	658	11.6.4 Greenland and Antarctic Ice Sheets	680
11.2.7 Atmospheric Pressure	659	11.6.5 Surface and Ground Water Storage	680
		11.6.6 Summary	681
11.3 Past Sea Level Changes	659	Appendix 11.1: Methods for Projections of Global-average Sea Level Rise	682
11.3.1 Global Average Sea Level over the Last 6,000 Years	659	References	684
11.3.2 Mean Sea Level Changes over the Past 100 to 200 Years	661		
11.3.2.1 Mean sea level trends	661		
11.3.2.2 Long-term mean sea level accelerations	663		

Executive Summary

This chapter assesses the current state of knowledge of the rate of change of global average and regional sea level in relation to climate change. We focus on the 20th and 21st centuries. However, because of the slow response to past conditions of the oceans and ice sheets and the consequent land movements, we consider changes in sea level prior to the historical record, and we also look over a thousand years into the future.

Past changes in sea level

From recent analyses, our conclusions are as follows:

- Since the Last Glacial Maximum about 20,000 years ago, sea level has risen by over 120 m at locations far from present and former ice sheets, as a result of loss of mass from these ice sheets. There was a rapid rise between 15,000 and 6,000 years ago at an average rate of 10 mm/yr.
- Based on geological data, global average sea level may have risen at an average rate of about 0.5 mm/yr over the last 6,000 years and at an average rate of 0.1 to 0.2 mm/yr over the last 3,000 years.
- Vertical land movements are still occurring today as a result of these large transfers of mass from the ice sheets to the ocean.
- During the last 6,000 years, global average sea level variations on time-scales of a few hundred years and longer are likely to have been less than 0.3 to 0.5 m.
- Based on tide gauge data, the rate of global average sea level rise during the 20th century is in the range 1.0 to 2.0 mm/yr, with a central value of 1.5 mm/yr (as with other ranges of uncertainty, it is not implied that the central value is the best estimate).
- Based on the few very long tide gauge records, the average rate of sea level rise has been larger during the 20th century than the 19th century.
- No significant acceleration in the rate of sea level rise during the 20th century has been detected.
- There is decadal variability in extreme sea levels but no evidence of widespread increases in extremes other than that associated with a change in the mean.

Factors affecting present day sea level change

Global average sea level is affected by many factors. Our assessment of the most important is as follows.

- Ocean thermal expansion leads to an increase in ocean volume at constant mass. Observational estimates of about 1 mm/yr over recent decades are similar to values of 0.7 to 1.1 mm/yr obtained from Atmosphere-Ocean General Circulation Models (AOGCMs) over a comparable period. Averaged over the 20th

century, AOGCM simulations result in rates of thermal expansion of 0.3 to 0.7 mm/yr.

- The mass of the ocean, and thus sea level, changes as water is exchanged with glaciers and ice caps. Observational and modelling studies of glaciers and ice caps indicate a contribution to sea level rise of 0.2 to 0.4 mm/yr averaged over the 20th century.
- Climate changes during the 20th century are estimated from modelling studies to have led to contributions of between -0.2 and 0.0 mm/yr from Antarctica (the results of increasing precipitation) and 0.0 to 0.1 mm/yr from Greenland (from changes in both precipitation and runoff).
- Greenland and Antarctica have contributed 0.0 to 0.5 mm/yr over the 20th century as a result of long-term adjustment to past climate changes.
- Changes in terrestrial storage of water over the period 1910 to 1990 are estimated to have contributed from -1.1 to +0.4 mm/yr of sea level rise.

The sum of these components indicates a rate of eustatic sea level rise (corresponding to a change in ocean volume) from 1910 to 1990 ranging from -0.8 to 2.2 mm/yr, with a central value of 0.7 mm/yr. The upper bound is close to the observational upper bound (2.0 mm/yr), but the central value is less than the observational lower bound (1.0 mm/yr), i.e., the sum of components is biased low compared to the observational estimates. The sum of components indicates an acceleration of only 0.2 mm/yr/century, with a range from -1.1 to +0.7 mm/yr/century, consistent with observational finding of no acceleration in sea level rise during the 20th century. The estimated rate of sea level rise from anthropogenic climate change from 1910 to 1990 (from modelling studies of thermal expansion, glaciers and ice sheets) ranges from 0.3 to 0.8 mm/yr. It is very likely that 20th century warming has contributed significantly to the observed sea level rise, through thermal expansion of sea water and widespread loss of land ice.

Projected sea level changes from 1990 to 2100

Projections of components contributing to sea level change from 1990 to 2100 (this period is chosen for consistency with the IPCC Second Assessment Report), using a range of AOGCMs following the IS92a scenario (including the direct effect of sulphate aerosol emissions) give:

- thermal expansion of 0.11 to 0.43 m, accelerating through the 21st century;
- a glacier contribution of 0.01 to 0.23 m;
- a Greenland contribution of -0.02 to 0.09 m;
- an Antarctic contribution of -0.17 to 0.02 m.

Including thawing of permafrost, deposition of sediment, and the ongoing contributions from ice sheets as a result of climate change since the Last Glacial Maximum, we obtain a range of

global-average sea level rise from 0.11 to 0.77 m. This range reflects systematic uncertainties in modelling.

For the 35 SRES scenarios, we project a sea level rise of 0.09 to 0.88 m for 1990 to 2100, with a central value of 0.48 m. The central value gives an average rate of 2.2 to 4.4 times the rate over the 20th century. If terrestrial storage continued at its present rates, the projections could be changed by -0.21 to +0.11 m. For an average AOGCM, the SRES scenarios give results which differ by 0.02 m or less for the first half of the 21st century. By 2100, they vary over a range amounting to about 50% of the central value. Beyond the 21st century, sea level rise will depend strongly on the emissions scenario.

The West Antarctic ice sheet (WAIS) has attracted special attention because it contains enough ice to raise sea level by 6 m and because of suggestions that instabilities associated with its being grounded below sea level may result in rapid ice discharge when the surrounding ice shelves are weakened. The range of projections given above makes no allowance for ice-dynamic instability of the WAIS. It is now widely agreed that major loss of grounded ice and accelerated sea level rise are very unlikely during the 21st century.

Our confidence in the regional distribution of sea level change from AOGCMs is low because there is little similarity between models. However, models agree on the qualitative conclusion that the range of regional variation is substantial compared with the global average sea level rise. Nearly all models project greater than average rise in the Arctic Ocean and less than average rise in the Southern Ocean.

Land movements, both isostatic and tectonic, will continue through the 21st century at rates which are unaffected by climate change. It can be expected that by 2100 many regions currently experiencing relative sea level fall will instead have a rising relative sea level.

Extreme high water levels will occur with increasing frequency (i.e. with reducing return period) as a result of mean sea level rise. Their frequency may be further increased if storms become more frequent or severe as a result of climate change.

Longer term changes

If greenhouse gas concentrations were stabilised, sea level would nonetheless continue to rise for hundreds of years. After 500 years, sea level rise from thermal expansion may have reached only half of its eventual level, which models suggest may lie within ranges of 0.5 to 2.0 m and 1 to 4 m for CO₂ levels of twice and four times pre-industrial, respectively.

Glacier retreat will continue and the loss of a substantial fraction of the total glacier mass is likely. Areas that are currently marginally glaciated are most likely to become ice-free.

Ice sheets will continue to react to climate change during the next several thousand years even if the climate is stabilised. Models project that a local annual-average warming of larger than 3°C sustained for millennia would lead to virtually a complete melting of the Greenland ice sheet. For a warming over Greenland of 5.5°C, consistent with mid-range stabilisation scenarios, the Greenland ice sheet contributes about 3 m in 1,000 years. For a warming of 8°C, the contribution is about 6 m, the ice sheet being largely eliminated. For smaller warmings, the decay of the ice sheet would be substantially slower.

Current ice dynamic models project that the WAIS will contribute no more than 3 mm/yr to sea level rise over the next thousand years, even if significant changes were to occur in the ice shelves. However, we note that its dynamics are still inadequately understood to make firm projections, especially on the longer time-scales.

Apart from the possibility of an internal ice dynamic instability, surface melting will affect the long-term viability of the Antarctic ice sheet. For warmings of more than 10°C, simple runoff models predict that a zone of net mass loss would develop on the ice sheet surface. Irreversible disintegration of the WAIS would result because the WAIS cannot retreat to higher ground once its margins are subjected to surface melting and begin to recede. Such a disintegration would take at least a few millennia. Thresholds for total disintegration of the East Antarctic Ice Sheet by surface melting involve warmings above 20°C, a situation that has not occurred for at least 15 million years and which is far more than predicted by any scenario of climate change currently under consideration.

11.1 Introduction

Sea level change is an important consequence of climate change, both for societies and for the environment. In this chapter, we deal with the measurement and physical causes of sea level change, and with predictions for global-average and regional changes over the next century and further into the future. We reach qualitatively similar conclusions to those of Warrick *et al.* (1996) in the IPCC WGI Second Assessment Report (IPCC, 1996) (hereafter SAR). However, improved measurements and advances in modelling have given more detailed information and greater confidence in several areas. The impacts of sea level change on the populations and ecosystems of coastal zones are discussed in the IPCC WGII TAR (IPCC, 2001).

The level of the sea varies as a result of processes operating on a great range of time-scales, from seconds to millions of years. Our concern in this report is with climate-related processes that have an effect on the time-scale of decades to centuries. In order to establish whether there is a significant anthropogenic influence on sea level, the longer-term and non-climate-related processes have to be evaluated as well.

“Mean sea level” at the coast is defined as the height of the sea with respect to a local land benchmark, averaged over a period of time, such as a month or a year, long enough that fluctuations caused by waves and tides are largely removed. Changes in mean sea level as measured by coastal tide gauges are called “relative sea level changes”, because they can come about either by movement of the land on which the tide gauge is situated or by changes in the height of the adjacent sea surface (both considered with respect to the centre of the Earth as a fixed reference). These two terms can have similar rates (several mm/yr) on time-scales greater than decades. To infer sea level changes arising from changes in the ocean, the movement of the land needs to be subtracted from the records of tide gauges and geological indicators of past sea level. Widespread land movements are caused by the isostatic adjustment resulting from the slow viscous response of the mantle to the melting of large ice sheets and the addition of their mass to the oceans since the end of the most recent glacial period (“Ice Age”) (Section 11.2.4.1). Tectonic land movements, both rapid displacements (earthquakes) and slow movements (associated with mantle convection and sediment transport), can also have an important effect on local sea level (Section 11.2.6).

We estimate that global average eustatic sea level change over the last hundred years is within the range 0.10 to 0.20 m (Section 11.3.2). (“Eustatic” change is that which is caused by an alteration to the volume of water in the world ocean.) These values are somewhat higher than the sum of the predictions of the contributions to sea level rise (Section 11.4). The discrepancy reflects the imperfect state of current scientific knowledge. In an attempt to quantify the processes and their associated rates of sea level change, we have critically evaluated the error estimates (Box 11.1). However, the uncertainties remain substantial, although some have narrowed since the SAR on account of improved observations and modelling.

Box 11.1: Accuracy

For indicating the uncertainty of data (measurements or model results), two options have been used in this chapter.

1. For data fulfilling the usual statistical requirements, the uncertainty is indicated as ± 1 standard deviation ($\pm 1\sigma$).
2. For limited data sets or model results, the full range is shown by quoting either all available data or the two extremes. In these cases, outliers may be included in the data set and the use of an arithmetic mean or central value might be misleading.

To combine uncertainties when adding quantities, we used the following procedures:

- Following the usual practice for independent uncertainties, the variances were added (i.e. the standard deviations were combined in quadrature).
- Ranges were combined by adding their extreme values, because in these cases the true value is very likely to lie within the overall range.
- To combine a standard deviation with a range, the standard deviation was first used to derive a range by taking ± 2 standard deviations about the mean, and then the ranges were combined.

Eustatic sea level change results from changes to the density or to the total mass of water. Both of these relate to climate. Density is reduced by thermal expansion occurring as the ocean warms. Observational estimates of interior temperature changes in the ocean reported by Warrick *et al.* (1996) were limited, and estimates of thermal expansion were made from simple ocean models. Since the SAR, more observational analyses have been made and estimates from several Atmosphere-Ocean General Circulation Models (AOGCMs) have become available (Section 11.2.1). Thermal expansion is expected to contribute the largest component to sea level rise over the next hundred years (Section 11.5.1.1). Because of the large heat capacity of the ocean, thermal expansion would continue for many centuries after climate had been stabilised (Section 11.5.4.1).

Exchanges with water stored on land will alter the mass of the ocean. (Note that sea level would be unaffected by the melting of sea ice, whose weight is already supported by the ocean.) Groundwater extraction and impounding water in reservoirs result in a direct influence on sea level (Section 11.2.5). Climate change is projected to reduce the amount of water frozen in glaciers and ice caps (Sections 11.2.2, 11.5.1.1) because of increased melting and evaporation. Greater melting and evaporation on the Greenland and Antarctic ice sheets (Sections 11.2.3, 11.5.1.1) is also projected, but might be outweighed by increased precipitation. Increased discharge of ice from the ice sheets into the ocean is also possible. The ice sheets react to climate change by adjusting their shape and size on time-scales of up to millennia, so they could still be gaining or losing mass as a result of climate variations over a history extending as far back as the last glacial period, and they would continue to change for thousands of years after climate had been stabilised (Section 11.5.4.3).

Sea level change is not expected to be geographically uniform (Section 11.5.2), so information about its distribution is needed to inform assessments of the impacts on coastal regions. Since the SAR, such information has been calculated from several AOGCMs. The pattern depends on ocean surface fluxes, interior conditions and circulation. The most serious impacts are caused not only by changes in mean sea level but by changes to extreme sea levels (Section 11.5.3.2), especially storm surges and exceptionally high waves, which are forced by meteorological conditions. Climate-related changes in these therefore also have to be considered.

11.2 Factors Contributing to Sea Level Change

11.2.1 Ocean Processes

The pattern of sea level in ocean basins is maintained by atmospheric pressure and air-sea fluxes of momentum (surface wind stress), heat and fresh water (precipitation, evaporation, and fresh-water runoff from the land). The ocean is strongly density stratified with motion preferentially along density surfaces (e.g. Ledwell *et al.*, 1993, 1998). This allows properties of water masses, set by interaction with the atmosphere or sea ice, to be carried thousands of kilometres into the ocean interior and thus provides a pathway for warming of surface waters to enter the ocean interior.

As the ocean warms, the density decreases and thus even at constant mass the volume of the ocean increases. This thermal expansion (or steric sea level rise) occurs at all ocean temperatures and is one of the major contributors to sea level changes during the 20th and 21st centuries. Water at higher temperature or under greater pressure (i.e., at greater depth) expands more for a given heat input, so the global average expansion is affected by the distribution of heat within the ocean. Salinity changes within the ocean also have a significant impact on the local density and thus local sea level, but have little effect on global average sea level change.

The rate of climate change depends strongly on the rate at which heat is removed from the ocean surface layers into the ocean interior; if heat is taken up more readily, climate change is retarded but sea level rises more rapidly. Climate change simulation requires a model which represents the sequestration of heat in the ocean and the evolution of temperature as a function of depth.

The large heat capacity of the ocean means that there will be considerable delay before the full effects of surface warming are felt throughout the depth of the ocean. As a result, the ocean will not be in equilibrium and global average sea level will continue to rise for centuries after atmospheric greenhouse gas concentrations have stabilised.

The geographical distribution of sea level change is principally determined by alterations to the ocean density structure, with consequent effects on ocean circulation, caused by the modified surface momentum, heat and water fluxes. Hsieh and Bryan (1996) have demonstrated how the first signals of sea level rise are propagated rapidly from a source region (for instance, a region of heat input) but that full adjustment takes place more

slowly. As a result, the geographical distribution of sea level change may take many decades to centuries to arrive at its final state.

11.2.1.1 Observational estimates of ocean warming and ocean thermal expansion

Previous IPCC sea level change assessments (Warrick and Oerlemans, 1990; Warrick *et al.*, 1996) noted that there were a number of time-series which indicate warming of the ocean and a resultant thermal expansion (i.e. a steric sea level rise) but there was limited geographical coverage. Comparison of recent ocean temperature data sets (particularly those collected during the World Ocean Circulation Experiment) with historical data is beginning to reveal large-scale changes in the ocean interior. (Section 2.2.2.5 includes additional material on ocean warming, including studies for which there are no estimates of ocean thermal expansion.) However, the absence of comprehensive long ocean time-series data makes detection of trends difficult and prone to contamination by decadal and interannual variability. While there has been some work on interannual variability in the North Atlantic (e.g. Levitus, 1989a,b, 1990) and North Pacific (e.g. Yasuda and Hanawa, 1997; Zhang and Levitus, 1997), few studies have focused on long-term trends.

The most convincing evidence of ocean warming is for the North Atlantic. An almost constant rate of interior warming, with implied steric sea level rise, is found over 73 years at Ocean Station S (south-east of Bermuda). Comparisons of trans-ocean sections show that these changes are widespread (Table 11.1). On decadal time-scales, variations in surface steric height from station S compare well with sea level at Bermuda (Roemmich, 1990) and appear to be driven by changes in the wind stress curl (Sturges and Hong, 1995; Sturges *et al.*, 1998). Variability in the western North Atlantic (Curry *et al.*, 1998) is related to changes in convective activity in the Labrador Sea (Dickson *et al.*, 1996). Over the 20 years up to the early 1990s there has been a cooling of the Labrador Sea Water (as in the Irminger Sea, Read and Gould, 1992), and more recently in the western North Atlantic (Koltermann *et al.*, 1999). For the South Atlantic, changes are more uncertain, particularly those early in the 20th century.

A warming of the Atlantic layer in the Arctic Ocean is deduced by comparison of modern oceanographic sections collected on board ice-breakers (e.g., Quadfasel *et al.*, 1991; Carmack *et al.*, 1997; Swift *et al.*, 1997) and submarines (e.g. Morison *et al.*, 1998; Steele and Boyd, 1998) with Russian Arctic Ocean atlases compiled from decades of earlier data (Treshnikov, 1977; Gorshkov, 1983). It is not yet clear whether these changes result from a climate trend or, as argued by Grotefendt *et al.* (1998), from decadal variability. The published studies do not report estimates of steric sea level changes; we note that a warming of 1°C over the central 200 m of the Atlantic layer would result in a local rise of steric sea level of 10 to 20 mm.

Observations from the Pacific and Indian Oceans cover a relatively short period, so any changes seen may be a result of decadal variability. Wong (1999), Wong *et al.* (1999), Bindoff and McDougall (1994) and Johnson and Orsi (1997) studied changes in the South Pacific. Bindoff and McDougall (2000) studied changes in the southern Indian Ocean. These authors

Table 11.1: Summary of observations of interior ocean temperature changes and steric sea level rise during the 20th century.

Reference	Dates of data	Location, section or region	Depth range (m)	Temperature change ($^{\circ}\text{C}/\text{century}$)	Steric rise (mm/yr) (and heat uptake)	
North Atlantic Ocean						
Read and Gould (1992)	1962–1991	55°N, 40°–10°W	50–3000	-0.3		
Joyce and Robbins (1996)	1922–1995	Ocean Station S 32.17°N, 64.50°W	1500–2500	0.5	0.9 (0.7 W/m^{-2})	
Joyce <i>et al.</i> (1999)	1958, 1985, 1997	20°N–35°N 52°W and 66°W		0.57	1.0	
Parrilla <i>et al.</i> (1994), Bryden <i>et al.</i> (1996)	1957, 1981, 1992	24°N	800–2500	Peak of 1 at 1100 m	0.9 (1 W/m^{-2})	
Roemmich and Wunsch (1984)	1959, 1981	36°N	700–3000	Peak of 0.8 at 1500 m	0.9	
Arhan <i>et al.</i> (1998)	1957, 1993	8°N	1000–2500	Peak of 0.45 at 1700 m	0.6	
Antonov (1993)	1957–1981	45°N–70°N	0–500 800–2500	Cooling 0.4		
South Atlantic Ocean						
Dickson <i>et al.</i> (2001), Arbic and Owens (2001)	1926, 1957	8°S, 33.5°W–12.5°W	1000–2000 (Steric expansion for 100 m to bottom is shown in the right-hand half of the last column)	0.30	-0.1	0.0
	1926, 1957	8°S, 12°W–10.5°E		0.23	0.2	0.2
	1983, 1994	11°S, 34°W–13°W		0.30	1.1	4.4
	1983, 1994	11°S, 12.5°W–12°E		0.08	0.3	2.2
	1926, 1957	16°S, 37°W–14°W		0.10	-0.8	-2.5
	1926, 1957	16°S, 13.5°W–10.5°E		0.05	-0.2	-0.7
	1958, 1983	24°S, 40.5°W–14°W		0.41	0.1	1.0
	1958, 1983	24°S, 13.5°W–12.5°E		0.46	0.6	1.0
	1925, 1959	32°S, 48.5°W–14°W		0.13	-0.4	-0.2
Arctic Ocean						
See text			200–1500	Peak of >1 at 300 m		
North Pacific Ocean						
Thomson and Tabata (1989)	1956–1986	Ocean station Papa 50°N, 145°W			1.1	
Roemmich (1992)	1950–1991	32°N (off the coast of California)	0–300		0.9 ± 0.2	
Wong (1999), Wong <i>et al.</i> (1999, 2001)	1970s, 1990s	3.5°S–60°N			1.4	
		31.5°S–60°N			0.85	
Antonov (1993)	1957–1981	North of 30°N	0–500	Cooling		
South Pacific Ocean						
Holbrook and Bindoff (1997)	1955–1988	S. Tasman Sea	0–100		0.3	
Ridgway and Godfrey (1996), Holbrook and Bindoff (1997)	1955, mid- 1970s	Coral and Tasman Seas	0–100	Warming		
	Since mid- 1970s		0–450	Cooling		
Bindoff and Church (1992)	1967, 1989–1990	Australia– 170°E	43°S 28°S		0.9	
					1.4	
Shaffer <i>et al.</i> (2000)	1967–1995	Eastern S Pacific	43°S 28°S		0.5	
					1.1	
Indian Ocean						
Bindoff and McDougall (1999)	1959–1966, 1987	30°S–35°S	0–900		1.6	
Atlantic, Pacific and Indian Oceans						
Levitus <i>et al.</i> (2000), Antonov <i>et al.</i> (2000)	1955–1995	Global average	0–300	0.7	(0.3 W/m^{-2})	
			0–3000		0.55 mm/yr (0.5 W/m^{-2})	

found changes in temperature and salinity in the upper hundreds of metres of the ocean which are consistent with a model of surface warming and freshening in the formation regions of the water masses and their subsequent subduction into the upper ocean. Such basin-scale changes are not merely a result of vertical thermocline heave, as might result from variability in surface winds.

In the only global analysis to date, Levitus *et al.* (2000) finds the ocean has stored 20×10^{22} J of heat between 1955 and 1995 (an average of 0.5 Wm^{-2}), with over half of this occurring in the upper 300 m for a rate of warming of $0.7^\circ\text{C}/\text{century}$. The steric sea level rise equivalent is 0.55 mm/yr, with maxima in the sub-tropical gyre of the North Atlantic and the tropical eastern Pacific.

In summary, while the evidence is still incomplete, there are widespread indications of thermal expansion, particularly in the sub-tropical gyres, of the order 1 mm/yr (Table 11.1). The evidence is most convincing for the North Atlantic but it also extends into the Pacific and Indian Oceans. The only area where cooling has been observed is in the sub-polar gyre of the North Atlantic and perhaps the North Pacific sub-polar gyre.

11.2.1.2 Models of thermal expansion

A variety of ocean models have been employed for estimates of ocean thermal expansion. The simplest and most frequently

quoted is the one-dimensional (depth) upwelling-diffusion (UD) model (Hoffert *et al.*, 1980; Wigley and Raper, 1987, 1992, 1993; Schlesinger and Jiang, 1990; Raper *et al.*, 1996), which represents the variation of temperature with depth. Kattenberg *et al.* (1996) demonstrated that results from the GFDL AOGCM could be reproduced by the UD model of Raper *et al.* (1996). Using this model, the best estimate of thermal expansion from 1880 to 1990 was 43 mm (with a range of 31 to 57 mm) (Warrick *et al.*, 1996). Raper and Cubasch (1996) and Raper *et al.* (2001) discuss ways in which the UD model requires modification to reproduce the results of other AOGCMs. The latter work shows that a UD model of the type used in the SAR may be inadequate to represent heat uptake into the deep ocean on the time-scale of centuries. De Wolde *et al.* (1995, 1997) developed a two dimensional (latitude-depth, zonally averaged) ocean model, with similar physics to the UD model. Their best estimate of ocean thermal expansion in a model forced by observed sea surface temperatures over the last 100 years was 35 mm (with a range of 22 to 51 mm). Church *et al.* (1991) developed a subduction model in which heat is carried into the ocean interior through an advective process, which they argued better represented the oceans with movement of water along density surfaces and little vertical mixing. Jackett *et al.* (2000) developed this model further and tuned it

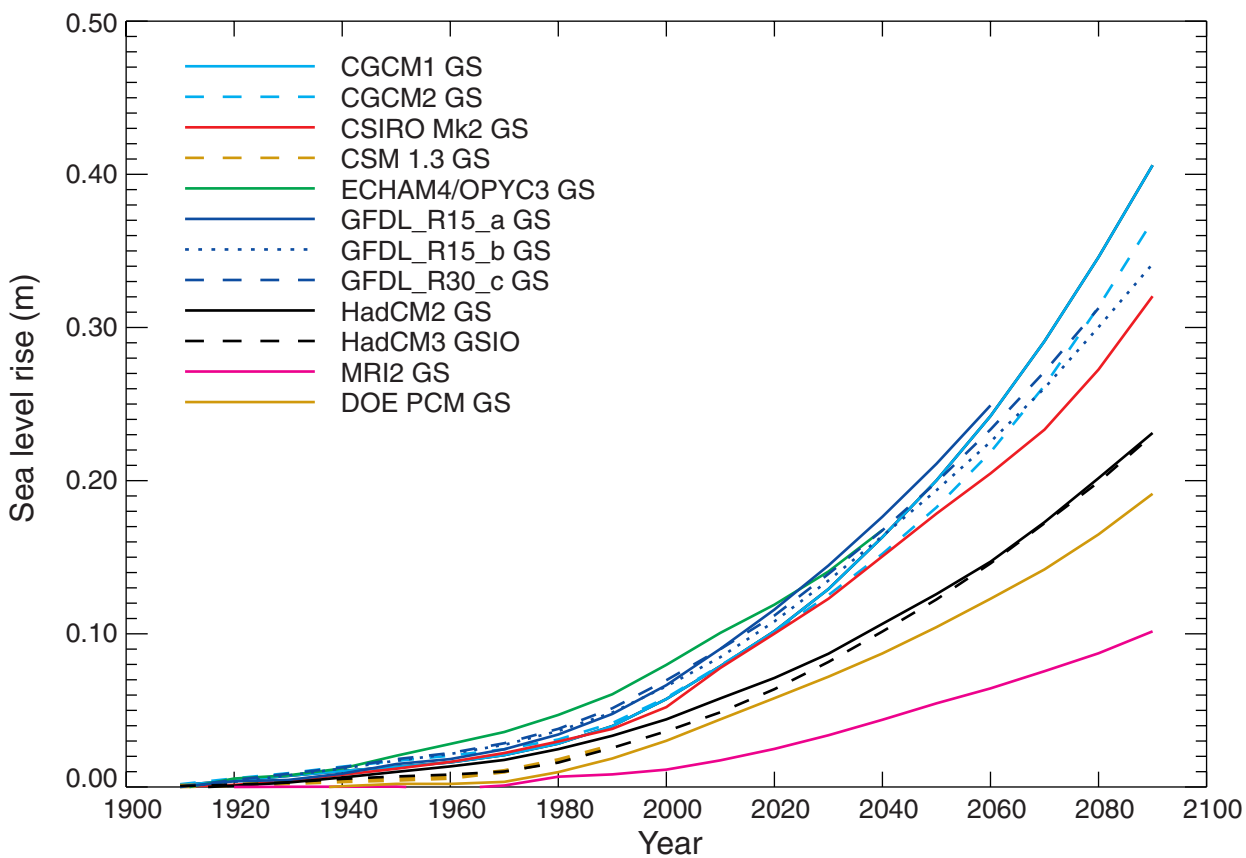


Figure 11.1: Global average sea level changes from thermal expansion simulated in AOGCM experiments with historical concentrations of greenhouse gases in the 20th century, then following the IS92a scenario for the 21st century, including the direct effect of sulphate aerosols. See Tables 8.1 and 9.1 for further details of models and experiments.

by comparison with an AOGCM, obtaining an estimate of 50 mm of thermal expansion over the last 100 years.

The advantage of these simple models is that they require less computing power than AOGCMs and so the sensitivity of results to a range of uncertainties can easily be examined. However, the simplifications imply that important processes controlling the penetration of heat from the surface into the ocean interior are not reproduced and they cannot provide information on the regional distribution of sea level rise. The most satisfactory way of estimating ocean thermal expansion is through the use of AOGCMs (Chapter 8, Section 8.3) (Gregory, 1993; Cubasch *et al.*, 1994; Bryan, 1996; Jaccott *et al.*, 2000; Russell *et al.*, 2000; Gregory and Lowe, 2000). Improvements over the last decade relate particularly to the representation of the effect on mixing by processes which operate on scales too small to be resolved in global models, but which may have an important influence on heat uptake (see Section 8.5.2.2.4). The geographical distribution of sea level change due to density and circulation changes can be obtained from AOGCM results (various methods are used; see Gregory *et al.*, 2001). The ability of AOGCMs to simulate decadal variability in the ocean interior has not yet been demonstrated adequately, partly because of the scarcity of observations of decadal variability in the ocean for testing these models. This is not only an issue of evaluation of model performance; it is also relevant for deciding whether observed trends in

sea level and interior ocean temperatures represent a change which is significantly larger than the natural internal variability of the climate system.

A number of model simulations of the 20th century (Table 9.1) have recently been completed using realistic greenhouse gas and aerosol forcings. Results for global average thermal expansion over periods during the 20th century are given in Figure 11.1 and Table 11.2. They suggest that over the last hundred years the average rate of sea level rise due to thermal expansion was of the order of 0.3 to 0.7 mm/yr, a range which encompasses the simple model estimates, rising to 0.6 to 1.1 mm/yr in recent decades, similar to the observational estimates (Section 11.2.1.1).

11.2.2 Glaciers and Ice Caps

Box 11.2: Mass balance terms for glaciers, ice caps and ice sheets

A glacier, ice cap or ice sheet gains mass by accumulation of snow (snowfall and deposition by wind-drift), which is gradually transformed to ice, and loses mass (ablation) mainly by melting at the surface or base with subsequent runoff or evaporation of the melt water. Some melt water may refreeze within the snow instead of being lost, and some snow may sublimate or be blown off the surface. Ice may also be removed by discharge into a floating ice shelf or glacier tongue, from which it is lost by basal melting and calving of icebergs. Net accumulation occurs at higher altitude, net ablation at lower altitude; to compensate for net accumulation and ablation, ice flows downhill by internal deformation of the ice and sliding and bed deformation at the base. The rate at which this occurs is mainly controlled by the surface slope, the ice thickness, the effective ice viscosity, and basal thermal and physical conditions. The mass balance for an individual body of ice is usually expressed as the rate of change of the equivalent volume of liquid water, in m³/yr; the mass balance is zero for a steady state. Mass balances are computed for both the whole year and individual seasons; the winter mass balance mostly measures accumulation, the summer, surface melting. The specific mass balance is the mass balance averaged over the surface area, in m/yr. A mass balance sensitivity is the derivative of the specific mass balance with respect to a climate parameter which affects it. For instance, a mass balance sensitivity to temperature is in m/yr/°C.

Table 11.2: Rate and acceleration of global-average sea level rise due to thermal expansion during the 20th century from AOGCM experiments with historical concentrations of greenhouse gases, including the direct effect of sulphate aerosols. See Tables 8.1 and 9.1 for further details of models and experiments. The rates are means over the periods indicated, while a quadratic fit is used to obtain the acceleration, assumed constant. Under this assumption, the rates apply to the midpoints (1950 and 1975) of the periods. Since the midpoints are 25 years apart, the difference between the rates is 25 times the acceleration. This relation is not exact because of interannual variability and non-constant acceleration.

	Rate of sea level rise (mm/yr)		Acceleration (mm/yr/century)
	1910 ^a to 1990 ^b	1960 to 1990 ^b	
CGCM1 GS	0.48	0.79	0.7 ± 0.2
CGCM2 GS	0.50	0.71	0.5 ± 0.3
CSIRO Mk2 GS	0.47	0.72	1.1 ± 0.2
CSM 1.3 GS	0.34	0.70	1.2 ± 0.3
ECHAM4/OPYC3 GS	0.75	1.09	1.0 ± 0.5
GFDL_R15_a GS	0.59	0.97	1.4 ± 0.4
GFDL_R15_b GS	0.60	0.88	1.1 ± 0.3
GFDL_R30_c GS	0.64	0.97	1.2 ± 0.3
HadCM2 GS	0.42	0.60	0.8 ± 0.2
HadCM3 GSIO	0.32	0.64	1.3 ± 0.4
DOE PCM GS	0.25	0.63	0.8 ± 0.4

^a The choice of 1910 (rather than 1900) is made to accommodate the start date of some of the model integrations.

^b The choice of 1990 (rather than 2000) is made because observational estimates referred to here do not generally include much data from the 1990s.

11.2.2.1 Mass balance studies

The water contained in glaciers and ice caps (excluding the ice sheets of Antarctica and Greenland) is equivalent to about 0.5 m of global sea level (Table 11.3). Glaciers and ice caps are rather sensitive to climate change; rapid changes in their mass are possible, and are capable of producing an important contribution to the rate of sea level rise. To evaluate this contribution, we need to know the rate of change of total glacier mass. Unfortunately sufficient measurements exist to determine the mass balance (see Box 11.2 for definition) for only a small minority of the world's 10⁵ glaciers.

Table 11.3: Some physical characteristics of ice on Earth.

	Glaciers	Ice caps	Glaciers and ice caps ^a	Greenland ice sheet ^b	Antarctic ice sheet ^b
Number	>160 000	70			
Area (10^6 km^2)	0.43	0.24	0.68	1.71	12.37
Volume (10^6 km^3)	0.08	0.10	0.18 ± 0.04	2.85	25.71
Sea-level rise equivalent ^d	0.24	0.27	0.50 ± 0.10	7.2 ^c	61.1 ^c
Accumulation (sea-level equivalent, mm/yr) ^d			1.9 ± 0.3	1.4 ± 0.1	5.1 ± 0.2

Data sources: Meier and Bahr (1996), Warrick *et al.* (1996), Reeh *et al.* (1999), Huybrechts *et al.* (2000), Tables 11.5 and 11.6.

^a Including glaciers and ice caps on the margins of Greenland and the Antarctic Peninsula, which have a total area of $0.14 \times 10^6 \text{ km}^2$ (Weideck and Morris, 1996). The total area of glaciers and ice-caps outside Greenland and Antarctica is $0.54 \times 10^6 \text{ km}^2$ (Dyurgerov and Meier, 1997a). The glaciers and ice caps of Greenland and Antarctica are included again in the next two columns.

^b Grounded ice only, including glaciers and small ice caps.

^c For the ice sheets, sea level rise equivalent is calculated with allowance for isostatic rebound and sea water replacing grounded ice, and this therefore is less than the sea level equivalent of the ice volume.

^d Assuming an oceanic area of $3.62 \times 10^8 \text{ km}^2$.

A possible approximate approach to this problem is to group glaciers into climatic regions, assuming glaciers in the same region to have a similar specific mass balance. With this method, we need to know only the specific mass balance for a typical glacier in each region (Kuhn *et al.*, 1999) and the total glacier area of the region. Multiplying these together gives the rate of change of glacier mass in the region. We then sum over all regions.

In the past decade, estimates of the regional totals of area and volume have been improved by the application of high resolution remote sensing and, to a lesser extent, by radio-echo-sounding. New glacier inventories have been published for central Asia and the former Soviet Union (Dolgushin and Osipova, 1989; Liu *et al.*, 1992; Kuzmichenok, 1993; Shi *et al.*, 1994; Liu and Xie, 2000; Qin *et al.*, 2000), New Zealand (Chinn, 1991), India (Kaul, 1999) South America (Casassa, 1995; Hastenrath and Ames, 1995; Skvarca *et al.*, Aniya *et al.*, 1997; Kaser, 1999; 1995; Kaser *et al.*, 1996; Rott *et al.*, 1998), and new estimates made for glaciers in Antarctica and Greenland apart from the ice sheets (Weidick and Morris, 1996).

By contrast, specific mass balance is poorly known. Continuous mass balance records longer than 20 years exist for about forty glaciers worldwide, and about 100 have records of more than five years (Dyurgerov and Meier, 1997a). Very few have both winter and summer balances; these data are critical to relating glacier change to climatic elements (Dyurgerov and Meier, 1999). Although mass balance is being monitored on several dozen glaciers worldwide, these are mostly small ($<20 \text{ km}^2$) and not representative of the size class that contains the majority of the mass ($>100 \text{ km}^2$). The geographical coverage is also seriously deficient; in particular, we are lacking information on the most important maritime glacier areas. Specific mass balance exhibits wide variation geographically and over time (Figure 11.2). While glaciers in most parts of the world have had negative mass balance in the

past 20 years, glaciers in New Zealand (Chinn, 1999; Lamont *et al.*, 1999) and southern Scandinavia (Tvede and Laumann, 1997) have been advancing, presumably following changes in the regional climate.

Estimates of the historical global glacier contribution to sea level rise are shown in Table 11.4. Dyurgerov and Meier (1997a) obtained their estimate by dividing a large sample of measured glaciers into seven major regions and finding the mass balance for each region, including the glaciers around the ice sheets. Their area-weighted average for 1961 to 1990 was equivalent to $0.25 \pm 0.10 \text{ mm/yr}$ of sea level rise. Cogley and Adams (1998) estimated a lower rate for 1961 to 1990. However, their results may not be representative of the global average because they do not make a correction for the regional biases in the sample of well investigated glaciers (Oerlemans, 1999). When evaluating data based on observed mass balance, one should note a worldwide glacier retreat

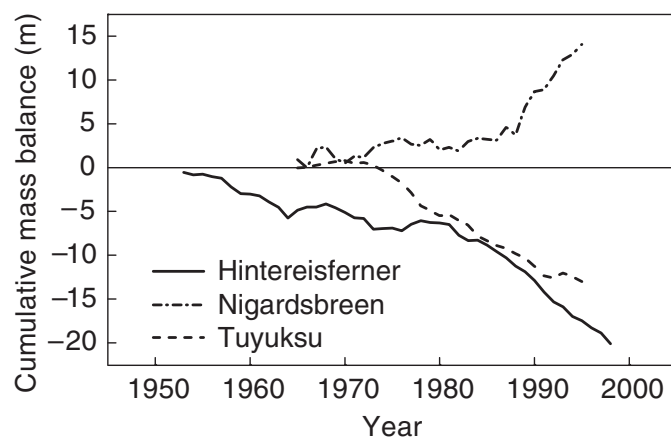


Figure 11.2: Cumulative mass balance for 1952–1998 for three glaciers in different climatic regimes: Hintereisferner (Austrian Alps), Nigardsbreen (Norway), Tuyuksu (Tien Shan, Kazakhstan).

Table 11.4: Estimates of historical contribution of glaciers to global average sea level rise.

Reference	Period	Rate of sea-level rise (mm/yr)	Remarks
Meier (1984)	1900 to 1961	0.46 ± 0.26	
Trupin <i>et al.</i> (1992)	1965 to 1984	0.18	
Meier (1993)	1900 to 1961	0.40	
Zuo and Oerlemans (1997), Oerlemans (1999)	1865 to 1990	0.22 ± 0.07^a	Observed temperature changes with mass balance sensitivities estimated from precipitation in 100 regions
	1961 to 1990	0.3 ^a	
Dyurgerov and Meier (1997b)	1961 to 1990	0.25 ± 0.10	Area-weighted mean of observed mass balance for seven regions
Dowdeswell <i>et al.</i> (1997)	1945 to 1995 approx.	0.13	Observed mass balance, Arctic only
Gregory and Oerlemans (1998)	1860 to 1990	0.15 ^a	General Circulation Model (GCM) temperature changes with mass balance sensitivities from Zuo and Oerlemans (1997)
	1960 to 1990	0.26 ^a	

^a These papers give the change in sea level over the period indicated, from which we have calculated the rate of sea level rise.

following the high stand of the middle 19th century and subsequent small regional readvances around 1920 and 1980.

11.2.2.2 Sensitivity to temperature change

A method of dealing with the lack of mass balance measurements is to estimate the changes in mass balance as a function of climate, using mass balance sensitivities (see Box 11.2 for definition) and observed or modelled climate change for glacier covered regions. Mass-balance modelling of all glaciers individually is not practical because no detailed description exists for the great majority of them, and because local climate data are not available; even regional climate models do not have sufficient resolution, while downscaling methods cannot generally be used because local climate measurements have not been made (see Section 10.7). A number of authors have estimated past glacier net mass loss using past temperature change with present day glacier covered areas and mass balance sensitivities (Table 11.4). In this report, we project future mass balance changes using regional mass balance sensitivities which take account of regional and seasonal climatic information, instead of using the heuristic model of Wigley and Raper (1995) employed by Warrick *et al.* (1996).

Meier (1984) intuitively scaled specific mass balance according to mass balance amplitude (half the difference between winter and summer specific mass balance). Braithwaite and Zhang (1999) demonstrated a dependence of mass balance sensitivity on mass balance amplitude. Oerlemans and Fortuin (1992) derived an empirical relationship between the mass balance sensitivity of a glacier to temperature change and the local average precipitation, which is the principal factor determining its mass turnover rate. Zuo and Oerlemans (1997) extended this idea by distinguishing the effects of temperature changes in summer and outside summer; the former have a stronger influence on mass loss, in general. They made a calculation of glacier net mass loss since 1865. For 1961 to 1990, they obtained a rate of 0.3 mm/yr of sea level rise (i.e., a total of 8 mm, Oerlemans, 1999), very similar to the result of Dyurgerov and

Meier (1997b). Gregory and Oerlemans (1998) applied local seasonal temperature changes over 1860 to 1990 calculated by the HadCM2 AOGCM forced by changing greenhouse gases and aerosols (HadCM2 GS in Table 9.1) to the glacier model of Zuo and Oerlemans.

Zuo and Oerlemans (1997), Gregory and Oerlemans (1998) and Van de Wal and Wild (2001) all stress that the global average glacier mass balance depends markedly on the regional and seasonal distribution of temperature change. For instance, Gregory and Oerlemans (1998) find that projected future glacier net mass loss is 20% greater if local seasonal variation is neglected, and 20% less if regional variation is not included. The first difference arises because annual average temperature change is greater than summer temperature change at high latitudes, but the mass balance sensitivity is greater to summer change. The second is because the global average temperature change is less than the change at high latitudes, where most glaciers are found (Section 9.3.2).

Both the observations of mass balance and the estimates based on temperature changes (Table 11.4) indicate a reduction of mass of glaciers and ice caps in the recent past, giving a contribution to global-average sea level of 0.2 to 0.4 mm/yr over the last hundred years.

11.2.2.3 Sensitivity to precipitation change

Precipitation and accumulation changes also influence glacier mass balance, and may sometimes be dominant (e.g. Raper *et al.*, 1996). Generally, glaciers in maritime climates are more sensitive to winter accumulation than to summer conditions (Kuhn, 1984). AOGCM experiments suggest that global-average annual mean precipitation will increase on average by 1 to 3%/°C under the enhanced greenhouse effect (Figure 9.18). Glacier mass balance modelling indicates that to compensate for the increased ablation from a temperature rise of 1°C a precipitation increase of 20% (Oerlemans, 1981) or 35% (Raper *et al.*, 2000) would be required. Van de Wal and Wild (2001) find that the effect of

precipitation changes on calculated global-average glacier mass changes in the 21st century is only 5% of the temperature effect. Such results suggest that the evolution of the global glacier mass is controlled principally by temperature changes rather than precipitation changes. Precipitation changes might be significant in particular localities, especially where precipitation is affected by atmospheric circulation changes, as seems recently to have been the case with southern Scandinavian glaciers (Oerlemans, 1999).

11.2.2.4 Evolution of area

The above calculations all neglect the change of area that will accompany loss of volume. Hence they are inaccurate because reduction of area will restrict the rate of melting. A detailed computation of transient response with dynamic adjustment to decreasing glacier sizes is not feasible at present, since the required information is not available for most glaciers. Oerlemans *et al.* (1998) undertook such detailed modelling of twelve individual glaciers and ice caps with an assumed rate of temperature change for the next hundred years. They found that neglecting the contraction of glacier area could lead to an overestimate of net mass loss of about 25% by 2100.

Dynamic adjustment of glaciers to a new climate occurs over tens to hundreds of years (Jóhannesson *et al.*, 1989), the time-scale being proportional to the mean glacier thickness divided by the specific mass balance at the terminus. Since both quantities are related to the size of the glacier, the time-scale is not necessarily longer for larger glaciers (Raper *et al.*, 1996; Bahr *et al.*, 1998), but it tends to be longer for glaciers in continental climates with low mass turnover (Jóhannesson *et al.*, 1989; Raper *et al.*, 2000).

Meier and Bahr (1996) and Bahr *et al.* (1997), following previous workers, proposed that for a glacier or an ice sheet in a steady state there may exist scaling relationships of the form $V \propto A^c$ between the volume V and area A, where c is a constant. Such relationships seem well supported by the increasing sample of glacier volumes measured by radio-echo-sounding and other techniques, despite the fact that climate change may be occurring on time-scales similar to those of dynamic adjustment. If one assumes that the volume-area relationship always holds, one can use it to deduce the area as the volume decreases. This idea can be extended to a glacier covered region if one knows the distribution of total glacier area among individual glaciers, which can be estimated using empirical functions (Meier and Bahr, 1996; Bahr, 1997). Using these methods, Van de Wal and Wild (2001) found that contraction of area reduces the estimated glacier net mass loss over the next 70 years by 15 to 20% (see also Section 11.5.1.1).

11.2.3 Greenland and Antarctic Ice Sheets

Together, the present Greenland and Antarctic ice sheets contain enough water to raise sea level by almost 70 m (Table 11.3), so that only a small fractional change in their volume would have a significant effect. The average annual solid precipitation falling onto the ice sheets is equivalent to 6.5 mm of sea level, this input being approximately balanced by loss from melting and iceberg

calving. The balance of these processes is not the same for the two ice sheets, on account of their different climatic regimes. Antarctic temperatures are so low that there is virtually no surface runoff; the ice sheet mainly loses mass by ice discharge into floating ice shelves, which experience melting and freezing at their underside and eventually break up to form icebergs. On the other hand, summer temperatures on the Greenland ice sheet are high enough to cause widespread melting, which accounts for about half of the ice loss, the remainder being discharged as icebergs or into small ice-shelves.

Changes in ice discharge generally involve response times of the order of 10^2 to 10^4 years. The time-scales are determined by isostasy, the ratio of ice thickness to yearly mass turnover, processes affecting ice viscosity, and physical and thermal processes at the bed. Hence it is likely that the ice sheets are still adjusting to their past history, in particular the transition to interglacial conditions. Their future contribution to sea level change therefore has a component resulting from past climate changes as well as one relating to present and future climate changes.

For the 21st century, we expect that surface mass balance changes will dominate the volume response of both ice sheets. A key question is whether ice-dynamical mechanisms could operate which would enhance ice discharge sufficiently to have an appreciable additional effect on sea level rise.

11.2.3.1 Mass balance studies

Traditionally, the state of balance of the polar ice sheets has been assessed by estimating the individual mass balance terms, and making the budget. Only the mass balance of the ice sheet resting on bedrock (the grounded ice sheet) needs to be considered, because changes in the ice shelves do not affect sea level as they are already afloat. Recent mass balance estimates for Greenland and Antarctica are shown in Tables 11.5 and 11.6. Most progress since the SAR has been made in the assessment of accumulation, where the major obstacle is poor coverage by *in situ* measurements. New methods have made use of atmospheric moisture convergence analysis based on meteorological data, remotely sensed brightness temperatures of dry snow, and GCMs (see references in the tables). Recent accumulation estimates display a tendency for convergence towards a common value, suggesting a remaining error of less than 10% for both ice sheets.

For Greenland (Table 11.5), runoff is an important term but net ablation has only been measured directly at a few locations and therefore has to be calculated from models, which have considerable sensitivity to the surface elevation data set and the parameters of the melt and refreezing methods used (Reeh and Starzer, 1996; Van de Wal, 1996; Van de Wal and Ekhholm, 1996; Janssens and Huybrechts, 2000). Summing best estimates of the various mass balance components for Greenland gives a balance of $-8.5 \pm 10.2\%$ of the input, or $+0.12 \pm 0.15$ mm/yr of global sea level change, not significantly different from zero.

During the last five years, some mass balance estimates have been made for individual Greenland sectors. A detailed comparison of the ice flux across the 2,000 m contour with total accumulation revealed most of the accumulation zone to be near to equilibrium, albeit with somewhat larger positive and negative local imbalances (Thomas *et al.*, 1998, 2000). These results are

Table 11.5: Current state of balance of the Greenland ice sheet (10^{12} kg/yr).

Source and remarks	A Accumulation	B Runoff	C Net accumulation	D Iceberg production	E Bottom melting	F Balance
Benson (1962)	500	272	228	215		+13
Bauer (1968)	500	330	170	280		-110
Weidick (1984)	500	295	205	205		± 0
Ohmura and Reeh (1991): New accumulation map	535					
Huybrechts <i>et al.</i> (1991): Degree-day model on 20 km grid	539	256	283			
Robasky and Bromwich (1994): Atmospheric moisture budget analysis from radiosonde data, 1963-1989	545					
Giovinetto and Zwally (1995a): Passive microwave data of dry snow	461 ^a					
Van de Wal (1996): Energy-Balance model on 20 km grid	539	316	223			
Jung-Rothenhäusler (1998): Updated accumulation map	510					
Reeh <i>et al.</i> (1999)	547	276	271	239	32	± 0
Ohmura <i>et al.</i> (1999): Updated accumulation map with GCM data; runoff from ablation-summer temperature parametrization	516	347	169			
Janssens and Huybrechts (2000): recalibrated degree-day model on 5 km grid; updated precipitation and surface elevation maps	542	281	261			
Zwally and Giovinetto (2000): Updated calculation on 50 km grid			216 ^b			
Mean and standard deviation	520 \pm 26	297 \pm 32	225 \pm 41	235 \pm 33	32 \pm 3 ^c	-44 \pm 53 ^d

^a Normalised to ice sheet area of 1.676×10^6 km² (Ohmura and Reeh, 1991).^b Difference between net accumulation above the equilibrium line and net ablation below the equilibrium line.^c Melting below the fringing ice shelves in north and northeast Greenland (Rignot *et al.*, 1997).^d Including the ice shelves, but nearly identical to the grounded ice sheet balance because the absolute magnitudes of the other ice-shelf balance terms (accumulation, runoff, ice-dynamic imbalance) are very small compared to those of the ice sheet ($F=A-B-D-E$).**Table 11.6:** Current state of balance of the Antarctic ice sheet (10^{12} kg/yr).

Source and remarks	A Accumulation over grounded ice	B Accumulation over all ice sheet	C Ice shelf melting	D Runoff	E Iceberg production	F Flux across grounding line
Kotlyakov <i>et al.</i> (1978)		2000	320	60	2400	
Budd and Smith (1985)	1800	2000			1800	1620
Jacobs <i>et al.</i> (1992). Ice shelf melting from observations of melt water outflow, glaciological field studies and ocean modelling.	1528	2144	544	53	2016	
Giovinetto and Zwally (1995a). Passive microwave data of dry snow.	1752 ^a	2279 ^a				
Budd <i>et al.</i> (1995). Atmospheric moisture budget analysis from GASP data, 1989 to 1992.		2190 ^b				
Jacobs <i>et al.</i> (1996). Updated ice-shelf melting assessment.			756			
Bromwich <i>et al.</i> (1998). Atmospheric moisture budget analysis from ECMWF reanalysis and evaporation/ sublimation forecasts, 1985 to 1993.		2190 ^b				
Turner <i>et al.</i> (1999). Atmospheric moisture budget analysis from ECMWF reanalysis, 1979 to 1993.		2106				
Vaughan <i>et al.</i> (1999). 1800 <i>in situ</i> measurements interpolated using passive microwave control field.	1811	2288				
Huybrechts <i>et al.</i> (2000). Updated accumulation map.	1924	2344				
Giovinetto and Zwally (2000). Updated map on 50 km grid.	1883 ^c	2326 ^c				
Mean and standard deviation.	1843 \pm 76 ^d	2246 \pm 86 ^d	540 \pm 218	10 \pm 10 ^e	2072 \pm 304	

^a Normalised to include the Antarctic Peninsula.^b Specific net accumulation multiplied by total area of 13.95×10^6 km² (Fox and Cooper, 1994).^c Normalised to include the Antarctic Peninsula, and without applying a combined deflation and ablation adjustment.^d Mean and standard deviation based only on accumulation studies published since 1995.^e Estimate by the authors.The mass balance of the ice sheet including ice shelves can be estimated as $B-C-D-E=-376 \pm 384 \times 10^{12}$ kg/yr, which is $-16.7 \pm 17.1\%$ of the total input B .Assuming the ice shelves are in balance (and noting that the runoff derives from the grounded ice, not the ice shelves) would imply that $0=F+(B-A)-C-E$, in which case the flux across the grounding line would be $F=A-B+C+E=2209 \pm 391 \times 10^{12}$ kg/yr.

likely to be only little influenced by short-term variations, because in the ice sheet interior, quantities that determine ice flow show little variation on a century time-scale. Recent studies have suggested a loss of mass in the ablation zone (Rignot *et al.*, 1997; Ohmura *et al.*, 1999), and have brought to light the important role played by bottom melting below floating glaciers (Reeh *et al.*, 1997, 1999; Rignot *et al.*, 1997); neglect of this term led to erroneous results in earlier analyses.

For Antarctica (Table 11.6), the ice discharge dominates the uncertainty in the mass balance of the grounded ice sheet, because of the difficulty of determining the position and thickness of ice at the grounding line and the need for assumptions about the vertical distribution of velocity. The figure of Budd and Smith (1985) of $1,620 \times 10^{12}$ kg/yr is the only available estimate. Comparing this with an average value of recent accumulation estimates for the grounded ice sheet would suggest a positive mass balance of around +10% of the total input, equivalent to -0.5 mm/yr of sea level. Alternatively, the flux across the grounding line can be obtained by assuming the ice shelves to be in balance and using estimates of the calving rate (production of icebergs), the rate of melting on the (submerged) underside of the ice shelves, and accumulation on the ice shelves. This results in a flux of $2,209 \pm 391 \times 10^{12}$ kg/yr across the grounding line and a mass balance for the grounded ice equivalent to $+1.04 \pm 1.06$ mm/yr of sea level (Table 11.6). However, the ice shelves may not be in balance, so that the error estimate probably understates the true uncertainty.

11.2.3.2 Direct monitoring of surface elevation changes

Provided that changes in ice and snow density and bedrock elevation are small or can be determined, elevation changes can be used to estimate changes of mass of the ice sheets. Using satellite altimetry, Davis *et al.* (1998) reported a small average thickening between 1978 and 1988 of 15 ± 20 mm/yr of the Greenland ice sheet above 2,000 m at latitudes up to 72°N . Krabill *et al.* (1999) observed a similar pattern above 2,000 m from 1993 to 1998 using satellite referenced, repeat aircraft laser altimetry. Together, these results indicate that this area of the Greenland ice sheet has been nearly in balance for two decades, in agreement with the mass budget studies mentioned above (Thomas *et al.*, 2000). Krabill *et al.* (1999) observed markedly different behaviour at lower altitudes, with thinning rates in excess of 2 m/yr in the south and east, which they attributed in part to excess flow, although a series of warmer-than-average summers may also have had an influence. In a recent update, Krabill *et al.* (2000) find the total ice sheet balance to be -46×10^{12} kg/yr or 0.13 mm/yr of sea level rise between 1993 and 1999, but could not provide an error bar. Incidentally, this value is very close to the century time-scale imbalance derived from the mass budget studies (Table 11.5), although the time periods are different and the laser altimetry results do not allow us to distinguish between accumulation, ablation, and discharge.

Small changes of ± 11 mm/yr were reported by Lingle and Covey (1998) in a region of East Antarctica between 20° and 160°E for the period 1978 to 1988. Wingham *et al.* (1998) examined the Antarctic ice sheet north of 82°S from 1992 to 1996, excluding the marginal zone. They observed no change in

East Antarctica to within ± 5 mm/yr, but reported a negative trend in West Antarctica of -53 ± 9 mm/yr, largely located in the Pine Island and Thwaites Glacier basins. They estimated a century-scale mass imbalance of $-6\% \pm 8\%$ of accumulation for 63% of the Antarctic ice sheet, concluding that the thinning in West Antarctica is likely to result from a recent accumulation deficit. However, the measurements of Rignot (1998a), showing a 1.2 ± 0.3 km/yr retreat of the grounding line of Pine Island Glacier between 1992 and 1996, suggest an ice-dynamic explanation for the observed thinning. Altimetry records are at present too short to confidently distinguish between a short-term surface mass-balance variation and the longer-term ice-sheet dynamic imbalance. Van der Veen and Bolzan (1999) suggest that at least five years of data are needed on the central Greenland ice sheet.

11.2.3.3 Numerical modelling

Modelling of the past history of the ice sheets and their underlying beds over a glacial cycle is a way to obtain an estimate of the present ice-dynamic evolution unaffected by short-term (annual to decadal) mass-balance effects. The simulation requires time-dependent boundary conditions (surface mass balance, surface temperature, and sea level, the latter being needed to model grounding-line changes). Current glaciological models employ grids of 20 to 40 km horizontal spacing with 10 to 30 vertical layers and include ice shelves, basal sliding and bedrock adjustment.

Huybrechts and De Wolde (1999) and Huybrechts and Le Meur (1999) carried out long integrations over two glacial cycles using 3-D models of Greenland and Antarctica, with forcing derived from the Vostok (Antarctica) and Greenland Ice Core Project (GRIP) ice cores. The retreat history of the ice sheet along a transect in central west Greenland in particular was found to be in good agreement with a succession of dated moraines (Van Tatenhove *et al.*, 1995), but similar validation elsewhere is limited by the availability of well-dated material. Similar experiments were conducted as part of the European Ice Sheet Modelling Initiative (EISMINT) intercomparison exercise (Huybrechts *et al.*, 1998). These model simulations suggest that the average Greenland contribution to global sea level rise has been between -0.1 and 0.0 mm/yr in the last 500 years, while the Antarctic contribution has been positive. Four different Antarctic models yield a sea level contribution of between $+0.1$ and $+0.5$ mm/yr averaged over the last 500 years, mainly due to incomplete grounding-line retreat of the West Antarctic ice sheet (WAIS) since the Last Glacial Maximum (LGM) (Figure 11.3). However, substantial uncertainties remain, especially for the WAIS, where small phase shifts in the input sea level time-series and inadequate representation of ice-stream dynamics may have a significant effect on the model outcome. Glacio-isostatic modelling of the solid earth beneath the Antarctic ice sheet with prescribed ice sheet evolution (James and Ivins, 1998) gave similar uplift rates as those presented in Huybrechts and Le Meur (1999), indicating that the underlying ice sheet scenarios and bedrock models were similar, but observations are lacking to validate the generated uplift rates. By contrast, Budd *et al.* (1998) find that Antarctic ice volume is currently increasing at a rate of about 0.08 mm/yr of sea level lowering because in their modelling the Antarctic ice sheet was actually smaller during the LGM than today (for which there

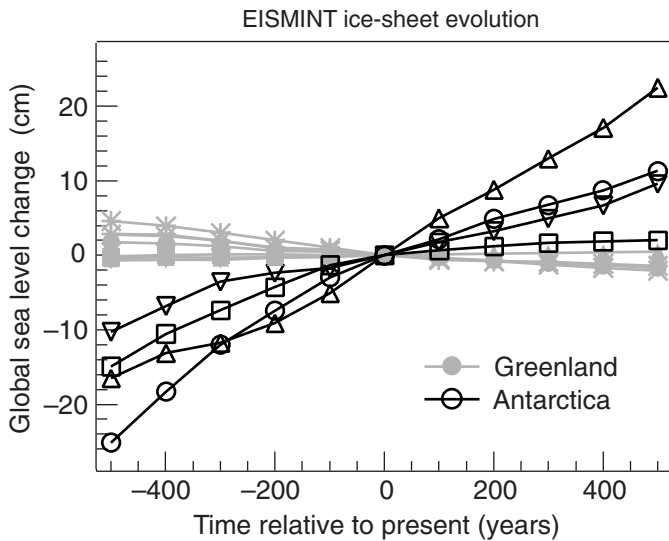


Figure 11.3: Modelled evolution of ice sheet volume (represented as sea level equivalent) centred at the present time resulting from ongoing adjustment to climate changes over the last glacial cycle. Data are from all Antarctic and Greenland models that participated in the EISMINT intercomparison exercise (From Huybrechts *et al.*, 1998).

is, however, little independent evidence) and the effect of the higher accumulation rates during the Holocene dominates over the effects of grounding line changes.

Model simulations of this kind have not included the possible effects of changes in climate during the 20th century. The simulations described later (Section 11.5.1.1), in which an ice sheet model is integrated using changes in temperature and precipitation derived from AOGCM simulations, suggest that anthropogenic climate change could have produced an additional contribution of between -0.2 to 0.0 mm/yr of sea level from increased accumulation in Antarctica over the last 100 years, and between 0.0 and 0.1 mm/yr from Greenland, from both increased accumulation and ablation. The model results for Greenland exhibit substantial interannual variability. Furthermore, because of rising temperatures during the 20th century, the contribution for recent decades is larger than the average for the century. These points must be borne in mind when comparing with results of the direct observation methods for short periods in recent decades (Sections 11.2.3.1 and 11.2.3.2). Note also that the observational results include the ongoing response to past climate change as well as the effect of 20th century climate change.

11.2.3.4 Sensitivity to climatic change

The sensitivity of the ice sheet's surface mass balance has been studied with multiple regression analyses, simple meteorological models, and GCMs (Table 11.7). Most progress since the SAR has been made with several coupled AOGCMs, especially in the “time-slice” mode in which a high-resolution AGCM (Atmospheric General Circulation Model) is driven by output from a low-resolution transient AOGCM experiment for a limited duration of time. Model resolution of typically 100 km allows for a more realistic topography crucial to better

resolving temperature gradients and orographic forcing of precipitation along the steep margins of the polar ice sheets. Even then, GCMs do not yet perform well in reproducing melting directly from the surface energy fluxes. The ablation zone around the Greenland ice sheet is mostly narrower than 100 km, and the important role played by topography therefore requires the use of downscaling techniques to transfer information to local and even finer grids (Glover, 1999). An additional complication is that not all melt water runs off to the ocean and can be partly retained on or in the ice sheet (Pfeffer *et al.*, 1991; Janssens and Huybrechts, 2000).

For Greenland, estimates of the sensitivity to a 1°C local warming over the ice sheet are close to 0.3 mm/yr (with a total range of $+0.1$ to $+0.4$ mm/yr) of global sea level equivalent. This range mainly reflects differences in the predicted precipitation changes and the yearly distribution of the temperature increase, which is predicted to be larger in winter than in summer in the GCMs, but is assumed uniform in the studies of Van de Wal (1996) and Janssens and Huybrechts (2000). Another difference amongst the GCM results concerns the time window over which the sensitivities are assessed. The CSIRO9/T63 sensitivities are estimated from high-resolution runs forced with observed SSTs for the recent past (Smith *et al.*, 1998; Smith, 1999), whereas the ECHAM data are given as specific mass balance changes for doubled minus present atmospheric CO_2 . Thompson and Pollard (1997) report similar results to the ECHAM studies but the corresponding sensitivity value could not be calculated because the associated temperature information is not provided. Some palaeoclimatic data from central Greenland ice cores indicate that variations in precipitation during the Holocene are related to changes in atmospheric circulation rather than directly to local temperature (Kapsner *et al.*, 1995; Cuffey and Clow, 1997), such that precipitation might not increase with temperature (in contrast with Clausen *et al.*, 1988). For glacial-interglacial transitions, the ice cores do exhibit a strong positive correlation between temperature and precipitation (Dansgaard *et al.*, 1993; Dahl-Jensen *et al.*, 1993; Kapsner *et al.*, 1995; Cuffey and Marshall, 2000), as simulated by AOGCMs for anthropogenic warming. Although other changes took place at the glacial-interglacial transition, this large climate shift could be argued to be a better analogue for anthropogenic climate change than the smaller fluctuations of the Holocene. To allow for changes in circulation patterns and associated temperature and precipitation patterns, we have used time-dependent AOGCM experiments to calculate the Greenland contribution (Section 11.5.1).

For Antarctica, mass-balance sensitivities for a 1°C local warming are close to -0.4 mm/yr (with one outlier of -0.8 mm/yr) of global sea level equivalent. A common feature of all methods is the insignificant role of melting, even for summer temperature increases of a few degrees, so that only accumulation changes need to be considered. The sensitivity for the case that the change in accumulation is set proportional to the relative change in saturation vapour pressure is at the lower end of the sensitivity range, suggesting that in a warmer climate changes in atmospheric circulation and increased moisture advection can become equally important, in particular close to the ice sheet margin (Bromwich, 1995; Steig, 1997). Both ECHAM3 and

Table 11.7: Mass balance sensitivity of the Greenland and Antarctic ice sheets to a 1°C local climatic warming.

Source	dB/dT (mm/yr/°C)	Method
Greenland ice sheet		
Van de Wal (1996)	+0.31 ^a	Energy balance model calculation on 20 km grid
Ohmura <i>et al.</i> (1996)	+0.41 ^c [+0.04] ^{cd}	ECHAM3/T106 time slice [2×CO ₂ – 1×CO ₂]
Smith (1999)	[−0.306] ^d	CSIRO9/T63 GCM forced with SSTs 1950–1999
Janssens and Huybrechts (2000)	+0.35 ^a [+0.26] ^b	Recalibrated degree-day model on 5 km grid with new precipitation and surface elevation maps
Wild and Ohmura (2000)	+0.09 ^c [−0.13] ^{cd}	ECHAM4-OPYC3/T106 GCM time slice [2×CO ₂ – 1×CO ₂]
Antarctic ice sheet		
Huybrechts and Oerlemans (1990)	−0.36	Change in accumulation proportional to saturation vapour pressure
Giovinetto and Zwally (1995b)	−0.80 ^e	Multiple regression of accumulation to sea-ice extent and temperature
Ohmura <i>et al.</i> (1996)	−0.41 ^c	ECHAM3/T106 time slice [2×CO ₂ – 1×CO ₂]
Smith <i>et al.</i> (1998)	−0.40	CSIRO9/T63 GCM forced with SSTs 1950–1999
Wild and Ohmura (2000)	−0.48 ^c	ECHAM4-OPYC3/T106 time slice [2×CO ₂ – 1×CO ₂]

dB/dT Mass balance sensitivity to local temperature change expressed as sea level equivalent. Note that this is not a sensitivity to global average temperature change.

^a Constant precipitation.

^b Including 5% increase in precipitation.

^c Estimated from published data and the original time slice results.

^d Accumulation changes only.

^e Assuming sea-ice edge retreat of 150 km per °C.

ECHAM4/OPYC3 give a similar specific balance change over the ice sheet for doubled versus present atmospheric CO₂ to that found by Thompson and Pollard (1997).

In summary, the static sensitivity values suggest a larger role for Antarctica than for Greenland for an identical local temperature increase, meaning that the polar ice sheets combined would produce a sea level lowering, but the spread of the individual estimates includes the possibility that both ice sheets may also balance one another for doubled atmospheric CO₂ conditions (Ohmura *et al.*, 1996; Thompson and Pollard, 1997). For CO₂ increasing according to the IS92a scenario (without aerosol), studies by Van de Wal and Oerlemans (1997) and Huybrechts and De Wolde (1999) calculated sea level contributions for 1990 to 2100 of +80 to +100 mm from the Greenland ice sheet and about −80 mm from the Antarctic ice sheet. On this hundred year time-scale, ice-dynamics on the Greenland ice sheet was found to counteract the mass-balance-only effect by between 10 and 20%. Changes in both the area-elevation distribution and iceberg discharge played a role, although the physics controlling the latter are poorly known and therefore not well represented in the models. Because of its longer response time-scales, the Antarctic ice sheet hardly exhibits any dynamic response on a century time-scale, except when melting rates below the ice shelves were prescribed to rise by in excess of 1 m/yr (O'Farrell *et al.*, 1997; Warner and Budd, 1998; Huybrechts and De Wolde, 1999; see also Section 11.5.4.3).

11.2.4 Interaction of Ice Sheets, Sea Level and the Solid Earth

11.2.4.1 Eustasy, isostasy and glacial-interglacial cycles

On time-scales of 10³ to 10⁵ years, the most important processes affecting sea level are those associated with the growth and decay of the ice sheets through glacial-interglacial cycles. These contributions include the effect of changes in ocean volume and the response of the earth to these changes. The latter are the glacio-hydro-isostatic effects: the vertical land movements induced by varying surface loads of ice and water and by the concomitant redistribution of mass within the Earth and oceans. While major melting of the ice sheets ceased by about 6,000 years ago, the isostatic movements remain and will continue into the future because the Earth's viscous response to the load has a time-constant of thousands of years. Observational evidence indicates a complex spatial and temporal pattern of the resulting isostatic sea level change for the past 20,000 years. As the geological record is incomplete for most parts of the world, models (constrained by the reliable sea level observations) are required to describe and predict the vertical land movements and changes in ocean area and volume. Relative sea level changes caused by lithospheric processes, associated for example with tectonics and mantle convection, are discussed in Section 11.2.6.

Figure 11.4 illustrates global-average sea level change over the last 140,000 years. This is a composite record based on oxygen isotope data from Shackleton (1987) and Linsley

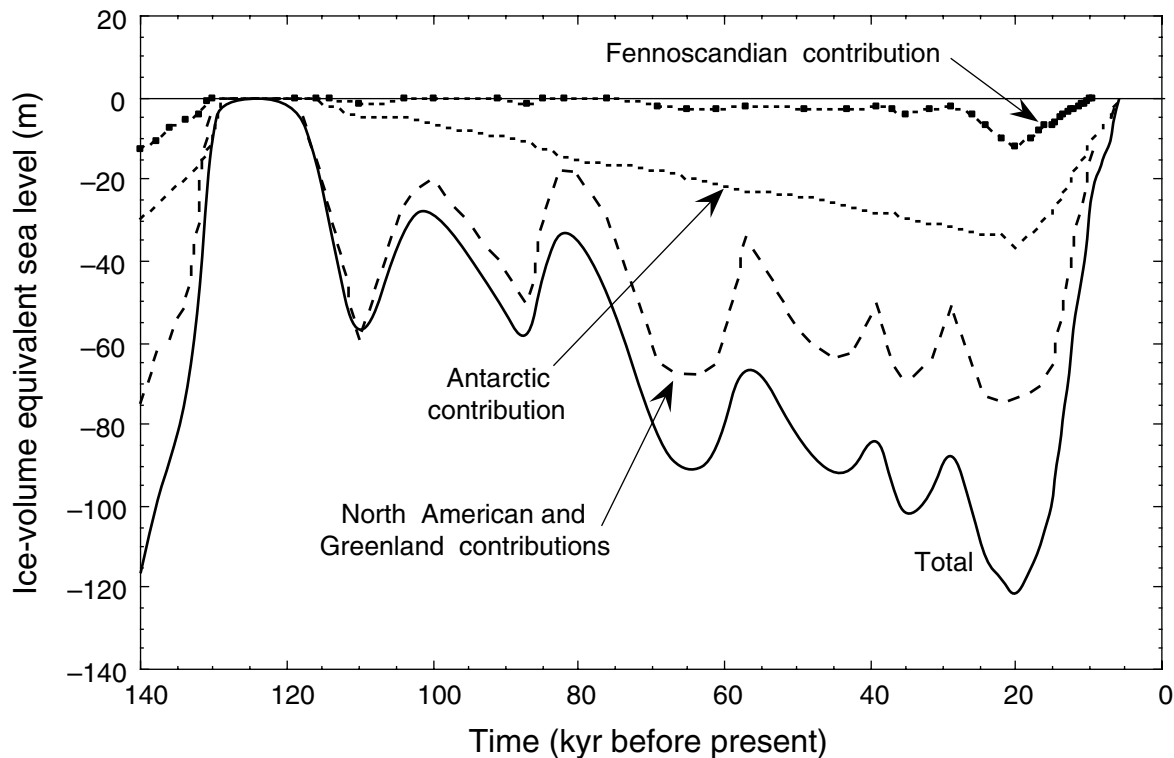


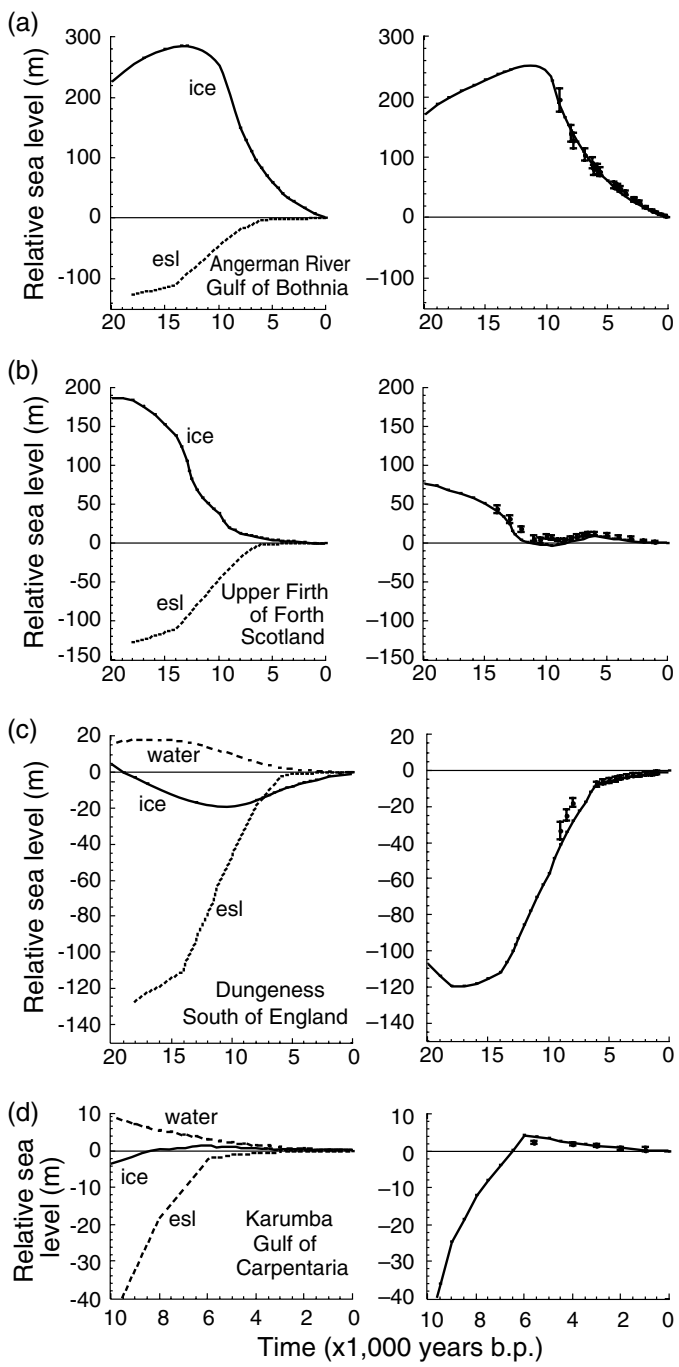
Figure 11.4: Estimates of global sea level change over the last 140,000 years (continuous line) and contributions to this change from the major ice sheets: (i) North America, including Laurentia, Cordilleran ice, and Greenland, (ii) Northern Europe (Fennoscandia), including the Barents region, (iii) Antarctica. (From Lambeck, 1999.)

(1996), constrained by the Huon terrace age-height relationships of Chappell *et al.* (1996a), the estimate of the LGM sea level by Yokoyama *et al.* (2000), the late-glacial eustatic sea level function of Fleming *et al.* (1998), and the timing of the Last Interglacial by Stirling *et al.* (1998). These fluctuations demonstrate the occurrence of sea level oscillations during a glacial-interglacial cycle that exceed 100 m in magnitude at average rates of up to 10 mm/year and more during periods of decay of the ice sheets and sometimes reaching rates as high as 40 mm/year (Bard *et al.*, 1996) for periods of very rapid ice sheet decay. Current best estimates indicate that the total LGM land-based ice volume exceeded present ice volume by 50 to $53 \times 10^6 \text{ km}^3$ (Yokoyama *et al.*, 2000).

Local sea level changes can depart significantly from this average signal because of the isostatic effects. Figure 11.5 illustrates typical observational results for sea level change since the LGM in regions with no significant land movements other than of a glacio-hydro-isostatic nature. Also shown are model predictions for these localities, illustrating the importance of the isostatic effects. Geophysical models of these isostatic effects are well developed (see reviews by Lambeck and Johnston, 1998; Peltier, 1998). Recent modelling advances have been the development of high-resolution models of the spatial variability of the change including the detailed description of ice loads and of the melt-water load distribution (Mitrovica and Peltier, 1991; Johnston, 1993) and the examination of different assumptions about the physics of the earth (Peltier and Jiang, 1996; Johnston *et al.*, 1997; Kaufmann and Wolf, 1999; Tromp and Mitrovica, 1999).

Information about the changes in ice sheets come from field observations, glaciological modelling, and from the sea level observations themselves. Much of the emphasis of recent work on glacial rebound has focused on improved calculations of ice sheet parameters from sea level data (Peltier, 1998; Johnston and Lambeck, 2000; see also Section 11.3.1) but discrepancies between glaciologically-based ice sheet models and models inferred from rebound data remain, particularly for the time of, and before, the LGM. The majority of ice at this time was contained in the ice sheets of Laurentia and Fennoscandia but their combined estimated volume inferred from the rebound data for these regions (e.g., Nakada and Lambeck, 1988; Tushingham and Peltier, 1991, 1992; Lambeck *et al.*, 1998) is less than the total volume required to explain the sea level change of about 120 to 125 m recorded at low latitude sites (Fairbanks, 1989; Yokoyama *et al.*, 2000). It is currently uncertain how the remainder of the ice was distributed. For instance, estimates of the contribution of Antarctic ice to sea level rise since the time of the LGM range from as much as 37 m (Nakada and Lambeck, 1988) to 6 to 13 m (Bentley, 1999; Huybrechts and Le Meur, 1999). Rebound evidence from the coast of Antarctica indicates that ice volumes have changed substantially since the LGM (Zwartz *et al.*, 1997; Bentley, 1999) but these observations, mostly extending back only to 8,000 years ago, do not provide good constraints on the LGM volumes. New evidence from exposure age dating of moraines and rock surfaces is beginning to provide new constraints on ice thickness in Antarctica (e.g., Stone *et al.*, 1998) but the evidence is not yet sufficient to constrain past volumes of the entire ice sheet.

Figure 11.5: Examples of observed relative sea level change (with error bars, right-hand side) and model predictions for four different locations. The model predictions (left-hand side) are for the glacio-hydro-eustatic contributions to the total change (solid line, right hand side). (a) Angermann River, Sweden, near the centre of the former ice sheet over Scandinavia. The principal contribution to the sea level change is the crustal rebound from the ice unloading (curve marked ice, left-hand side) and from the change in ocean volume due to the melting of all Late Pleistocene ice sheets (curve marked esl). The combined predicted effect, including a small water loading term (not shown), is shown by the solid line (right-hand side), together with the observed values. (b) A location near Stirling, Scotland. Here the ice and esl contributions are of comparable magnitude but opposite sign (left-hand side) such that the rate of change of the total contribution changes sign (right-hand side). This result is typical for locations near former ice margins or from near the centres of small ice sheets. (c) The south of England where the isostatic contributions from the water (curve marked water) and ice loads are of similar amplitude but opposite sign. The dominant contribution to sea level change is now the eustatic contribution. This behaviour is characteristic of localities that lie well beyond the ice margins where a peripheral bulge created by the ice load is subsiding as mantle material flows towards the region formerly beneath the ice. (d) A location in Australia where the melt-water load is the dominant cause of isostatic adjustment. Here sea level has been falling for the past 6,000 years. This result is characteristic of continental margin sites far from the former areas of glaciation. (From Lambeck, 1996.)



11.2.4.2 Earth rotation constraints on recent sea level rise

Changes in the Earth's ice sheets introduce a time-dependency in the Earth's inertia tensor whose consequences are observed both in the planet's rotation (as an acceleration in its rotation rate and as a shift in the position of the rotation axis) and in the acceleration of the rotation of satellite orbits about the Earth (Wu and Peltier, 1984; Lambeck, 1988). Model estimates of these changes are functions of mass shifts within and on the Earth and are dependent, therefore, on the past ice sheet geometries, on the Earth's rheology, and on the recent past and present rates of melting of the residual ice sheets. Other geophysical processes also contribute to the time-dependence

of the rotational and dynamical parameters (e.g. Steinberger and O'Connell, 1997). Hence, unique estimates of recent melting cannot be inferred from the observations.

Some constraints on the present rates of change of the ice sheets have, nevertheless, been obtained, in particular through a combination of the rotational observations with geological and tide gauge estimates of sea level change (Wahr *et al.*, 1993; Mitrovica and Milne, 1998; Peltier, 1998; Johnston and Lambeck, 1999). Results obtained so far are preliminary because observational records of the change in satellite orbits are relatively short (Nerem and Klosko, 1996; Cheng *et al.*, 1997) but they will become important as the length of the record increases. Peltier

(1998) has argued that if the polar ice sheets contributed, for example, 0.5 mm/yr to the global sea level rise, then the rotational constraints would require that most of this melting derived from Greenland. Johnston and Lambeck (1999) concluded that a solution consistent with geological evidence, including constraints on sea level for the past 6,000 years (Section 11.3.1), is for a non-steric sea level rise (i.e., not resulting from ocean density changes) of 1.0 ± 0.5 mm/yr for the past 100 years, with 5 to 30% originating from Greenland melting. However, all such estimates are based on a number of still uncertain assumptions such that the inferences are more indicative of the potential of the methodology than of actual quantitative conclusions.

11.2.5 Surface and Ground Water Storage and Permafrost

An important contribution to present day sea level rise could result from changes in the amount of water stored in the ground, on the surface in lakes and reservoirs, and by modifications to surface characteristics affecting runoff or evapotranspiration rates. Changing practices in the use of land and water could make these terms larger in future. However, very little quantitative information is available. For some of the components of the terrestrial water budget, Gornitz *et al.* (1997), updated by Gornitz (2000), give net results which differ substantially from those of Sahagian (2000) and Vörösmarty and Sahagian (2000), and also from those of Sahagian *et al.* (1994) used by Warrick *et al.* (1996). The largest positive contribution to sea level probably comes from ground water mining, which means the extraction of ground water from storage in aquifers in excess of the rate of natural recharge. Gornitz *et al.* (1997) estimate that ground water is mined at a rate that has been increasing in time, currently equivalent to 0.2 to 1.0 mm/yr of sea level, but they assume that much of this infiltrates back into aquifers so the contribution to sea level rise is only 0.1 to 0.4 mm/yr. Sahagian (2000) considers fewer aquifers; consequently he obtains a smaller total of 0.17 mm/yr from mining, but assumes that all of this water eventually reaches the ocean through the atmosphere or runoff. If Sahagian's assumption were applied to the inventory of Gornitz *et al.* it would imply a sea level contribution of 0.2 to 1.0 mm/yr.

Volumes of many of the world's large lakes have been reduced in recent decades through increased irrigation and other water use. Sahagian *et al.* (1994) and Sahagian (2000) estimate that the reduced volumes of the Caspian and Aral Seas (and associated ground water) contribute 0.03 and 0.18 mm/year to sea level rise, on the assumption that the extracted water reaches the world ocean by evapotranspiration. Recent *in situ* records and satellite altimetry data indicate that substantial fluctuations in the level of the Caspian Sea can occur on decadal time-scales (Cazenave *et al.*, 1997) which suggests that short records may not give a good indication of the long-term average. The reduction of lake volumes in China may contribute a further 0.005 mm/yr (Shi and Zhou, 1992). Assuming there are no other large sources, we take 0.2 mm/yr as the upper limit of the present contribution to sea level from lakes. Gornitz *et al.* (1997) do not include a term from lake volume changes, because they assume the water extracted for irrigation largely enters the ground water rather than the world ocean, so we take zero as the lower limit.

Gornitz *et al.* (1997) estimate there is 13.6 mm of sea level equivalent impounded in reservoirs. Most of this capacity was created, at roughly a constant rate, from 1950 to 1990. This rate of storage represents a reduction in sea level of 0.34 mm/yr. They assume that annually $5 \pm 0.5\%$ of the water impounded seeps into deep aquifers, giving a 1990 rate of seepage of 0.61 to 0.75 mm/yr, and a total volume of 15 mm sea level equivalent. We consider that this represents an upper bound, because it is likely that the rate of seepage from any reservoir will decrease with time as the surrounding water table rises, as assumed by Sahagian (2000). On the basis of a typical porosity and area affected, he estimates that the volume trapped as ground water surrounding reservoirs is 1.2 times the volume impounded in reservoirs. His estimate of the storage in reservoirs is 14 to 28 mm sea level equivalent; hence the ground water storage is an additional 17 to 34 mm sea level equivalent. Lack of global inventories means that these estimates of storage may well be too small because of the many small reservoirs not taken into account (rice paddies, ponds, etc., provided they impound water above the water table) (Vörösmarty and Sahagian, 2000). The total stored could be up to 50% larger (Sahagian, 2000).

Gornitz *et al.* (1997) estimate that evapotranspiration of water from irrigated land leads to an increase in atmospheric water content and hence a fall in sea level of 0.14 to 0.15 mm/yr. We consider this to be an overestimate, because it implies a 20th century increase in global tropospheric water content which substantially exceeds observations (Section 2.5.3.2). They further suggest that irrigation water derived from surface sources may infiltrate into aquifers, removing 0.40 to 0.48 mm/yr of sea level equivalent, based on the same assumption as for seepage from reservoirs. Urbanisation leads to reduced infiltration and increased surface runoff, which Gornitz *et al.* (1997) estimate may contribute 0.35 to 0.41 mm/yr of sea level rise. We consider these two terms to be upper bounds because, as with infiltration from reservoirs, a new steady state will be achieved after a period of years, with no further change in storage.

Estimates of the water contributed by deforestation are 0.1 mm/yr (Gornitz *et al.*, 1997) and 0.14 mm/yr (Sahagian, 2000) of sea level rise. Water released by oxidation of fossil fuels, vegetation and wetlands loss is negligible (Gornitz *et al.*, 1997).

Gornitz *et al.* (1997) estimate the total contribution to the 1990 rate of sea level change as -1.2 to -0.5 mm/yr. Integrating their estimates over 1910 to 1990 gives between -32 and -11 mm of sea level rise. In contrast, the estimate of Vörösmarty and Sahagian (2000) for the rate of sea level change from terrestrial storage is 0.06 mm/yr, equivalent to 5.4 mm over 80 years. The estimate of Sahagian *et al.* (1994), quoted by Warrick *et al.* (1996), was 12 mm during the 20th century. These discrepancies emphasise again the unsatisfactory knowledge of these contributions to sea level change.

Table 11.8 shows the ranges we have adopted for the various terms, based on the foregoing discussion. We integrate these terms over 1910 to 1990. (We use the time profiles of Gornitz *et al.* (1997) except that the infiltration from reservoirs is based on the approach of Sahagian (2000), and the rate of

Table 11.8: Estimates of terrestrial storage terms. The values given are those of Gornitz *et al.* (1997) and Sahagian (2000). The estimates used in this report are the maximum and minimum values from these two studies. The average rates over the period 1910 to 1990 are obtained by integrating the decadal averages using the time history of contributions estimated by Gornitz *et al.* (1997).

	Rate of sea level rise for 1990 (mm/yr)						Average rate	
	Gornitz <i>et al.</i> (1997)		Sahagian (2000)		This assessment		1910 to 1990 (mm/yr)	
	min	max	min	max	min	max	min	max
Groundwater mining	+0.1	+0.4	+0.17	+0.17	+0.1	+1.0	0.0	0.5
Lakes	0.0	0.0	+0.2	+0.2	0.0	+0.2	0.0	0.1
Impoundment in reservoirs	-0.38	-0.30	-0.70	-0.35	-0.7	-0.3	-0.4	-0.2
Infiltration from reservoirs	-0.75	-0.61	-0.84	-0.42	-0.8	-0.4	-0.5	-0.2
Evapotranspiration	-0.15	-0.14	0.0	0.0	-0.1	0.0	-0.1	0.0
Infiltration from irrigation	-0.48	-0.40	0.0	0.0	-0.5	0.0	-0.2	0.0
Runoff from urbanisation	+0.35	+0.41	0.0	0.0	+0.4	0.0	0.0	0.1
Deforestation	+0.1	+0.1	+0.14	+0.14	+0.1	0.14	0.1	0.1
Total					-1.9	+1.0	-1.1	0.4

withdrawal from lakes is assumed constant over the last five decades.) This gives a range of -83 to +30 mm of sea level equivalent, or -1.1 to +0.4 mm/yr averaged over the period. However note that the rate of each of the terms increases during the 20th century.

This discussion suggests three important conclusions: (i) the effect of changes in terrestrial water storage on sea level may be considerable; (ii) the net effect on sea level could be of either sign, and (iii) the rate has increased over the last few decades (in the assessment of Gornitz *et al.* (1997) from near zero at the start of the century to -0.8 mm/yr in 1990).

Estimates of ice volume in northern hemisphere permafrost range from 1.1 to $3.7 \times 10^{13} \text{ m}^3$ (Zhang *et al.*, 1999), equivalent to 0.03 to 0.10 m of global-average sea level. It occupies 25% of land area in the northern hemisphere. The major effects of global warming in presently unglaciated cold regions will be changes in the area of permafrost and a thickening of the active layer (the layer of seasonally thawed ground above permafrost). Both of these factors result in conversion of ground ice to liquid water, and hence in principle could contribute to the sea level change. Anisimov and Nelson (1997) estimated that a 10 to 20% reduction of area could occur by 2050 under a moderate climate-change scenario. In the absence of information about the vertical distribution of the ice, we make the assumption that the volume change is proportional to the area change. By 2100, the upper limit for the conversion of permafrost to soil water is thus about 50% of the total, or 50 mm sea level equivalent.

A thickening active layer will result in additional water storage capacity in the soil and thawing of ground ice will not necessarily make water available for runoff. What water is released could be mainly captured in ponds, thermokarst lakes, and marshes, rather than running off. Since the soil moisture in permafrost regions in the warm period is already very high, evaporation would not necessarily increase. We know of no quantitative estimates for these storage terms. We assume that the fraction which runs off lies within 0 and 50% of the available water. Hence we estimate the contribution of

permafrost to sea level 1990 to 2100 as 0 to 25 mm (0 to 0.23 mm/yr). For the 20th century, during which the temperature change has been about five times less than assumed by Anisimov and Nelson for the next hundred years, our estimate is 0 to 5 mm (0 to 0.05 mm/yr).

11.2.6 Tectonic Land Movements

We define tectonic land movement as that part of the vertical displacement of the crust that is of non-glacio-hydro-isostatic origin. It includes rapid displacements associated with earthquake events and also slow movements within (e.g., mantle convection) and on (e.g., sediment transport) the Earth. Large parts of the earth are subject to active tectonics which continue to shape the planet's surface. Where the tectonics occur in coastal areas, one of its consequences is the changing relationship between the land and sea surfaces as shorelines retreat or advance in response to the vertical land movements. Examples include the Huon Peninsula of Papua New Guinea (Chappell *et al.*, 1996b), parts of the Mediterranean (e.g. Pirazzoli *et al.*, 1994; Antonioli and Oliverio, 1996), Japan (Ota *et al.*, 1992) and New Zealand (Ota *et al.*, 1995). The Huon Peninsula provides a particularly good example (Figure 11.6) with 125,000 year old coral terraces at up to 400 m above present sea level. The intermediate terraces illustrated in Figure 11.6 formed at times when the tectonic uplift rates and sea level rise were about equal. Detailed analyses of these reef sequences have indicated that long-term average uplift rates vary between about 2 and 4 mm/yr, but that large episodic (and unpredictable) displacements of 1 m or more occur at repeat times of about 1,000 years (Chappell *et al.*, 1996b). Comparable average rates and episodic displacements have been inferred from Greek shoreline evidence (Stiros *et al.*, 1994). With major tectonic activity occurring at the plate boundaries, which in many instances are also continental or island margins, many of the world's tide gauge records are likely to contain both tectonic and eustatic signals. One value of the geological data is that it permits evaluations to be made of tectonic stability of the tide gauge locality.



Figure 11.6: The raised 125,000 year old coral terraces of the Huon Peninsula of Papua New Guinea up to 400 m above present sea level (Chappell *et al.*, 1996b).

Over very long time-scales (greater than 10^6 years), mantle dynamic processes lead to changes in the shape and volume of the ocean basins, while deposition of sediment reduces basin volume. These affect sea level but at very low rates (less than 0.01 mm/yr and 0.05 mm/yr, respectively; e.g., Open University, 1989; Harrison, 1990).

Coastal subsidence in river delta regions can be an important contributing factor to sea level change, with a typical magnitude of 10 mm/yr, although the phenomenon will usually be of a local character. Regions of documented subsidence include the Mediterranean deltas (Stanley, 1997), the Mississippi delta (Day *et al.*, 1993) and the Asian deltas. In the South China Sea, for example, the LGM shoreline is reported to occur at a depth of about 165 m below present level (Wang *et al.*, 1990), suggesting that some 40 m of subsidence may have occurred in 20,000 years at an average rate of about 2 mm/yr. Changes in relative sea level also arise through accretion and erosion along the coast; again, such effects may be locally significant.

11.2.7 Atmospheric Pressure

Through the inverse barometer effect, a local increase in surface air pressure over the ocean produces a depression in the sea surface of 1 cm per hPa (1 hPa = 1 mbar). Since water is practically incompressible, this cannot lead to a global-average sea level rise, but a long-term trend in surface air pressure patterns could influence observed local sea level trends. This has been investigated using two data sets: (i) monthly mean values of surface air pressure on a $10^\circ \times 5^\circ$ grid for the period 1873 to 1995 for the Northern Hemisphere north of 15°N obtained from the University of East Anglia Climatic Research Unit, and (ii) monthly mean values on a global $5^\circ \times 5^\circ$ grid for the period 1871 to 1994 obtained from the UK Met Office (see Basnett and Parker, 1997, for a discussion of the various data sets). The two data sets present similar spatial patterns of trends for their geographical and temporal overlaps. Both yield small trends of the order 0.02 hPa/yr; values of -0.03 hPa/yr occur in limited

regions of the high Arctic and equatorial Pacific. As found by Woodworth (1987), trends are only of the order of 0.01 hPa/yr in northern Europe, where most of the longest historical tide gauges are located. We conclude that long-term sea level trends could have been modified to the extent of ± 0.2 mm/yr, considerably less than the average eustatic rate of rise. Over a shorter period larger trends can be found. For example, Schönwiese *et al.* (1994) and Schönwiese and Rapp (1997) report changes in surface pressure for the period 1960 to 1990 that could have modified sea level trends in the Mediterranean and around Scandinavia by -0.05 and +0.04 mm/yr respectively.

11.3 Past Sea Level Changes

11.3.1 Global Average Sea Level over the Last 6,000 Years

The geological evidence for the past 10,000 to 20,000 years indicates that major temporal and spatial variation occurs in relative sea level change (e.g., Pirazzoli, 1991) on time-scales of the order of a few thousand years (Figure 11.5). The change observed at locations near the former centres of glaciation is primarily the result of the glacio-isostatic effect, whereas the change observed at tectonically stable localities far from the former ice sheets approximate the global average sea level change (for geologically recent times this is primarily eustatic change relating to changes in land-based ice volume). Glacio-hydro-isostatic effects (the Earth's response to the past changes in ice and water loads) remain important and result in a spatial variability in sea level over the past 6,000 years for localities far from the former ice margins. Analysis of data from such sites indicate that the ocean volume may have increased to add 2.5 to 3.5 m to global average sea level over the past 6,000 years (e.g., Fleming *et al.*, 1998), with a decreasing contribution in the last few thousand years. If this occurred uniformly over the past 6,000 years it would raise sea level by 0.4 to 0.6 mm/year. However, a few high resolution sea level records from the French Mediterranean coast indicate that much of this increase occurred between about 6,000 and 3,000 years ago and that the rate over the past 3,000 years was only about 0.1 to 0.2 mm/yr (Lambeck and Bard, 2000). These inferences do not constrain the source of the added water but likely sources are the Antarctic and Greenland ice sheets with possible contributions from glaciers and thermal expansion.

In these analyses of Late Holocene observations, the relative sea level change is attributed to both a contribution from any change in ocean volume and a contribution from the glacio-hydro-isostatic effect, where the former is a function of time only and the latter is a function of both time and position. It is possible to use the record of sea level changes to estimate parameters for a model of isostatic rebound. In doing this, the spatial variability of sea level change determines the mantle rheology, whereas the time dependence determines any correction that may be required to the assumed history of volume change. Solutions from different geographic regions may lead to variations in the rheology due to lateral variations in mantle temperature, for example, but the eustatic term should be the same, within observational and model uncertainties, in each case (Nakada and Lambeck, 1988). If it is assumed that no eustatic change has occurred in the past 6,000

years or so, but in fact eustatic change actually has occurred, the solution for Earth-model parameters will require a somewhat stiffer mantle than a solution in which eustatic change is included. The two solutions may, however, be equally satisfactory for interpolating between observations. For example, both approaches lead to mid-Holocene highstands at island and continental margin sites far from the former ice sheets of amplitudes 1 to 3 m. The occurrence of such sea level maxima places an upper limit on the magnitude of glacial melt in recent millennia (e.g., Peltier, 2000), but it would be inconsistent to combine estimates of ongoing glacial melt with results of calculations of isostatic rebound in which the rheological parameters have been inferred assuming there is no ongoing melt.

The geological indicators of past sea level are usually not sufficiently precise to enable fluctuations of sub-metre amplitude to be observed. In some circumstances high quality records do exist. These are from tectonically stable areas where the tidal range is small and has remained little changed through time, where no barriers or other shoreline features formed to change the local conditions, and where there are biological indicators that bear a precise and consistent relationship to sea level. Such areas include the micro-atoll coral formations of Queensland, Australia (Chappell, 1982; Woodroffe and McLean, 1990); the coralline algae and gastropod vermetid data of the Mediterranean (Laborel *et al.*, 1994; Morhange *et*

al., 1996), and the fresh-to-marine transitions in the Baltic Sea (Eronen *et al.*, 1995; Hyvarinen, 1999). These results all indicate that for the past 3,000 to 5,000 years oscillations in global sea level on time-scales of 100 to 1,000 years are unlikely to have exceeded 0.3 to 0.5 m. Archaeological evidence for this interval places similar constraints on sea level oscillations (Flemming and Webb, 1986). Some detailed local studies have indicated that fluctuations of the order of 1 m can occur (e.g., Van de Plassche *et al.*, 1998) but no globally consistent pattern has yet emerged, suggesting that these may be local rather than global variations.

Estimates of current ice sheet mass balance (Section 11.2.3.1) have improved since the SAR. However, these results indicate only that the ice sheets are not far from balance. Earth rotational constraints (Section 11.2.4.2) and ice sheet altimetry (Section 11.2.3.2) offer the prospect of resolving the ice sheet mass balance in the future, but at present the most accurate estimates of the long-term imbalance (period of several hundred years) follows from the comparison of the geological sea level data with the ice sheet modelling results (Section 11.2.3.3). The above geological estimates of the recent sea level rates may include a component from thermal expansion and glacier mass changes which, from the long-term temperature record in Chapter 2 (Section 2.3.2), could contribute to a sea level lowering by as much as 0.1 mm/yr. These results

Table 11.9: Recent estimates of sea level rise from tide gauges. The standard error for these estimates is also given along with the method used to correct for vertical land movement (VLM).

	Region	VLM ^a	Rate ± s.e. ^b (mm/yr)
Gornitz and Lebedeff (1987)	Global	Geological	1.2 ± 0.3
Peltier and Tushingham (1989, 1991)	Global	ICE-3G/M1	2.4 ± 0.9 ^c
Trupin and Wahr (1990)	Global	ICE-3G/M1	1.7 ± 0.13
Nakiboglu and Lambeck (1991)	Global	Spatial decomposition	1.2 ± 0.4
Douglas (1991)	Global	ICE-3G/M1	1.8 ± 0.1
Shennan and Woodworth (1992)	NW Europe	Geological	1.0 ± 0.15
Gornitz (1995) ^d	N America E Coast	Geological	1.5 ± 0.7 ^c
Mitrovica and Davis (1995), Davis and Mitrovica (1996)	Global far field (far from former ice sheets)	PGR Model	1.4 ± 0.4 ^c
Davis and Mitrovica (1996)	N America E Coast	PGR Model	1.5 ± 0.3 ^c
Peltier (1996)	N America E Coast	ICE-4G/M2	1.9 ± 0.6 ^c
Peltier and Jiang (1997)	N America E Coast	Geological	2.0 ± 0.6 ^c
Peltier and Jiang (1997)	Global	ICE-4G/M2	1.8 ± 0.6 ^c
Douglas (1997) ^d	Global	ICE-3G/M1	1.8 ± 0.1
Lambeck <i>et al.</i> (1998)	Fennoscandia	PGR Model	1.1 ± 0.2
Woodworth <i>et al.</i> (1999)	British Isles	Geological	1.0

^a This column shows the method used to correct for vertical land motion. ICE-3G/M1 is the Post Glacial Rebound (PGR) model of Tushingham and Peltier (1991). ICE-4G/M2 is a more recent PGR model based on the deglaciation history of Peltier (1994) and the mantle viscosity model of Peltier and Jiang (1996). Nakiboglu and Lambeck (1991) performed a spherical harmonic decomposition of the tide-gauge trends and took the zero-degree term as the global-average rate. They indicated that a PGR signal would make little contribution to this term. The use of geological data is discussed in the text.

^b The uncertainty is the standard error of the estimate of the global average rate.

^c This uncertainty is the standard deviation of the rates at individual sites.

^d See references in these papers for estimates of sea level rise for various other regions.

suggest that the combined long-term ice sheet imbalance lies within the range 0.1 to 0.3 mm/yr. Results from ice sheet models for the last 500 years indicate an ongoing adjustment to the glacial-interglacial transition of Greenland and Antarctica together of 0.0 to 0.5 mm/yr. These ranges are consistent. We therefore take the ongoing contribution of the ice sheets to sea level rise in the 20th and 21st centuries in response to earlier climate change as 0.0 to 0.5 mm/yr. This is additional to the effect of 20th century and future climate change.

11.3.2 Mean Sea Level Changes over the Past 100 to 200 Years

11.3.2.1 Mean sea level trends

The primary source of information on secular trends in global sea level during the past century is the tide gauge data set of the Permanent Service for Mean Sea Level (PSMSL) (Spencer and Woodworth, 1993). The tide gauge measurement is of the level of the sea surface relative to that of the land upon which the gauge is located and contains information on both the displacement of the land and on changes in ocean volume (eustatic changes). The land displacement may be of two types: that caused by active tectonics and that caused by glacial rebound. Corrections for these effects are required if the change in ocean volume is to be extracted from the tide gauge record. Both corrections are imperfectly known and are based on sea level observations themselves, usually from long geological records. Different strategies have been developed for dealing with these corrections but differences remain that are not inconsequential (see Table 11.9).

The sea level records contain significant interannual and decadal variability and long records are required in order to estimate reliable secular rates that will be representative of the last century. In addition, sea level change is spatially variable because of land movements and of changes in the ocean circulation. Therefore, a good geographic distribution of observations is required. Neither requirement is satisfied with the current tide gauge network and different strategies have been developed to take these differences into consideration. Warrick *et al.* (1996), Douglas (1995) and Smith *et al.* (2000) give recent reviews of the subject, including discussions of the Northern Hemisphere geographical bias in the historical data set.

In the absence of independent measurements of vertical land movements by advanced geodetic techniques (Section 11.6.1), corrections for movements are based on either geological data or geophysical modelling. The former method uses geological evidence from locations adjacent to the gauges to estimate the long-term relative sea level change which is assumed to be caused primarily by land movements, from whatever cause. This is subtracted from the gauge records to estimate the eustatic change for the past century. However, this procedure may underestimate the real current eustatic change because the observed geological data may themselves contain a long-term component of eustatic sea level rise (Section 11.3.1). The latter method, glacial rebound modelling, is also constrained by geological observations to estimate earth response functions or ice load parameters, which may therefore themselves contain a component of long-term eustatic sea level

change unless this component is specifically solved for (Section 11.3.1).

A further underestimate of the rate of sea level rise from the geological approach, compared to that from glacial rebound models, will pertain in forebulge areas, and especially the North American east coast, where the linear extrapolation of geological data could result in an underestimate of the corrected rate of sea level change for the past century typically by 0.3 mm/yr because the glacial rebound signal is diminishing with time (Peltier, 2000). However, in areas remote from the former ice sheets this bias will be considerably smaller.

Also, in adding recent mass into the oceans, most studies have assumed that it is distributed uniformly and have neglected the Earth's elastic and gravitational response to the changed water loading (analogous to glacio-hydro-isostatic effect). This will have the effect of reducing the observed rise at continental margin sites from ongoing mass contributions by as much as 30% (cf. Nakiboglu and Lambeck, 1991).

Table 11.9 summarises estimates of the corrected sea level trends for the past century. Estimates cover a wide range as a result of different assumptions and methods for calculating the rate of vertical land movement, of different selections of gauge records for analysis, and of different requirements for minimum record length.

There have been several more studies since the SAR of trends observed in particular regions. Woodworth *et al.* (1999) provided a partial update to Shennan and Woodworth (1992), suggesting that sea level change in the North Sea region has been about 1 mm/yr during the past century. Lambeck *et al.* (1998) combined coastal tide gauge data from Fennoscandinavia together with lake level records and postglacial rebound models to estimate an average regional rise for the past century of 1.1 ± 0.2 mm/yr. Studies of the North American east coast have been particularly concerned with the spatial dependence of trends associated with the Laurentian forebulge. Peltier (1996) concluded a current rate of order 1.9 ± 0.6 mm/yr, larger than the 1.5 mm/yr obtained by Gornitz (1995), who used the geological data approach, and Mitrovica and Davis (1995), who employed Post Glacial Rebound (PGR) modelling. Note that the observations of thermal expansion (Section 11.2.1.1) indicate a higher rate of sea level rise over recent decades in the sub-tropical gyres of the North Atlantic (i.e., off the North American east coast) than the higher latitude sub-polar gyre. Thus the differences between three lower European values compared with the higher North American values may reflect a real regional difference (with spatial variations in regional sea level change being perhaps several tenths of a millimetre per year – see also Section 11.5.2). In China, relative sea level is rising at about 2 mm/yr in the south but less than 0.5 mm/yr in the north (National Bureau of Marine Management, 1992), with an estimated average of the whole coastline of 1.6 mm/yr (Zhen and Wu, 1993) and with attempts to remove the spatially dependent component of vertical land movement yielding an average of 2.0 mm/yr (Shi, 1996). The two longest records from Australia (both in excess of 80 years in length and not included in Douglas, 1997) are from Sydney and Fremantle, on opposite sides of the continent. They show observed rates of relative sea level rise of 0.86 ± 0.12 mm/yr

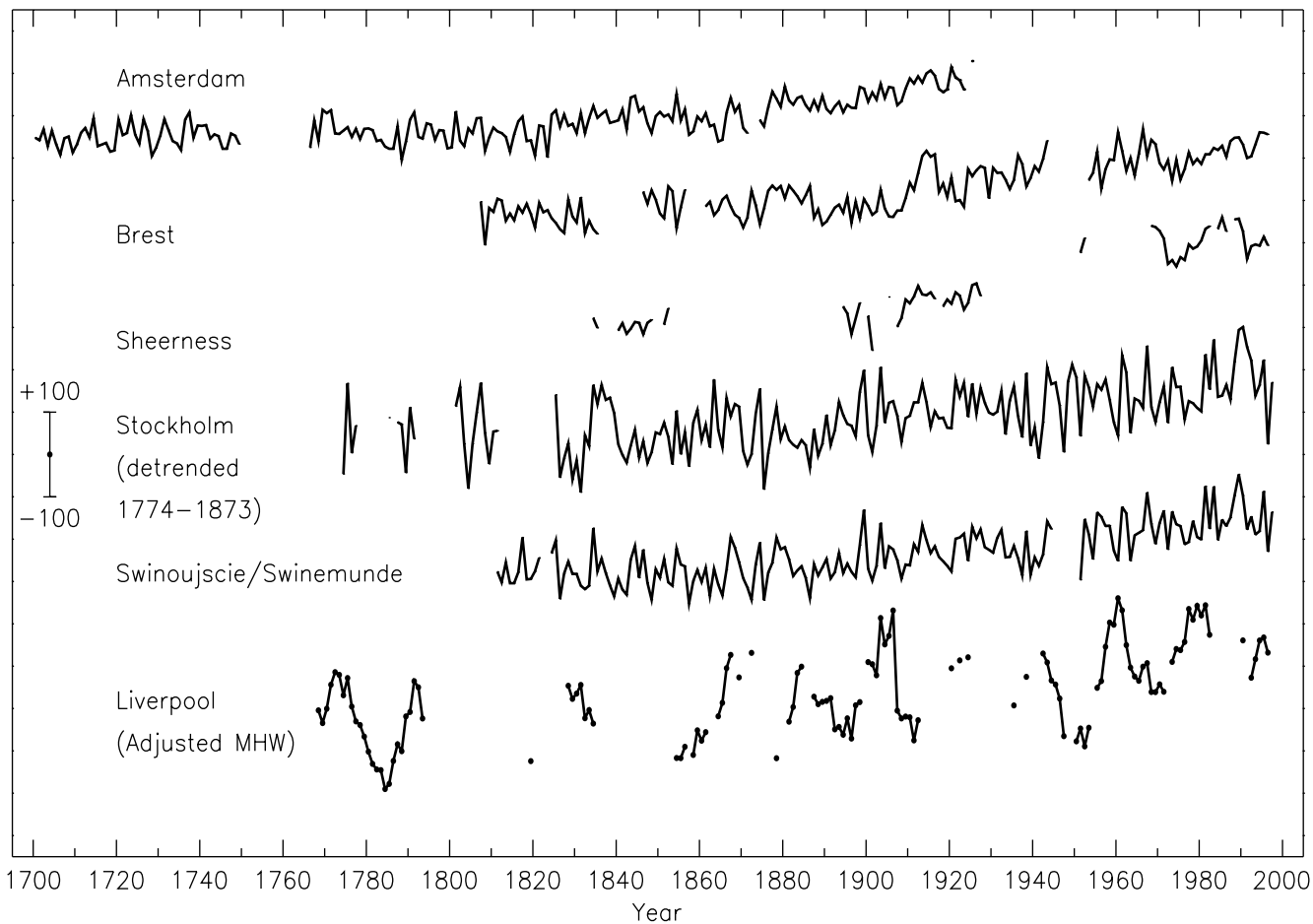


Figure 11.7: Time-series of relative sea level for the past 300 years from Northern Europe: Amsterdam, Netherlands; Brest, France; Sheerness, UK; Stockholm, Sweden (detrended over the period 1774 to 1873 to remove the contribution of postglacial rebound); Swinoujscie, Poland (formerly Swinemunde, Germany); and Liverpool, UK. Data for the latter are of “Adjusted Mean High Water” rather than Mean Sea Level and include a nodal (18.6 year) term. The scale bar indicates ± 100 mm. (Adapted from Woodworth, 1999a.)

and 1.38 ± 0.18 mm/yr over the periods 1915 to 1998 and 1897 to 1998 (Mitchell *et al.*, 2000), corresponding to approximately 1.26 mm/yr and 1.73 mm/yr after glacial rebound correction using the Peltier ICE-4G/M2 model, or 1.07 mm/yr and 1.55 mm/yr using the corrections of Lambeck and Nakada (1990).

There have been only two analyses of global sea level change based on the PSMSL data set published since the SAR. Douglas (1997) provided an update to Douglas (1991) and applied the PGR model of Tushingham and Peltier (1991) to a selected set of twenty-four long tide gauge records, grouped into nine geographical areas, with minimum record length 60 years and average length 83 years. However, the only Southern Hemisphere sites included in this solution were from Argentina and New Zealand. The overall global average of 1.8 ± 0.1 mm/yr agreed with the 1991 analysis, with considerable consistency between area-average trends. The standard error of the global rate was derived from the standard deviation of regional trends, assuming that temporal and spatial variability is uncorrelated between regions. Peltier and Jiang (1997) used essentially the same set of stations as Douglas and a new model for postglacial rebound.

From Table 11.9 one can see that there are six global estimates determined with the use of PGR corrections derived from global models of isostatic adjustment, spanning a range from 1.4 mm/yr (Mitrovica and Davis, 1995; Davis and Mitrovica, 1996) to 2.4 mm/yr (Peltier and Tushingham, 1989, 1991). We consider that these five are consistent within the systematic uncertainty of the PGR models, which may have a range of uncertainty of 0.5 mm/yr depending on earth structure parametrization employed (Mitrovica and Davis, 1995). The average rate of the five estimates is 1.8 mm/yr. There are two other global analyses, of Gornitz and Lebedeff (1987) and Nakiboglu and Lambeck (1991), which yield estimates of 1.2 mm/yr, lower than the first group. Because of the issues raised above with regard to the geological data method for land movement correction, the value of Gornitz and Lebedeff may be underestimated by up to a few tenths of a millimetre per year, although such considerations do not affect the method of Nakiboglu and Lambeck. The differences between the former five and latter two analyses reflect the analysis methods, in particular the differences in corrections for land movements and in selections of tide gauges used, including the effect of any spatial variation in thermal expansion. However, all the discrepancies which could

arise as a consequence of different analysis methods remain to be more thoroughly investigated. On the basis of the published literature, we therefore cannot rule out an average rate of sea level rise of as little as 1.0 mm/yr during the 20th century. For the upper bound, we adopt a limit of 2.0 mm/yr, which includes all recent global estimates with some allowance for systematic uncertainty. As with other ranges (see Box 11.1), we do not imply that the central value is the best estimate.

11.3.2.2 Long-term mean sea level accelerations

Comparison of the rate of sea level rise over the last 100 years (1.0 to 2.0 mm/yr) with the geological rate over the last two millennia (0.1 to 0.2 mm/yr; Section 11.3.1) implies a comparatively recent acceleration in the rate of sea level rise. The few very long tide gauge records are especially important in the search for “accelerations” in sea level rise. Using four of the longest (about two centuries) records from north-west Europe (Amsterdam, Brest, Sheerness, Stockholm), Woodworth (1990) found long-term accelerations of 0.4 to 0.9 mm/yr/century (Figure 11.7). Woodworth (1999a) found an acceleration of order 0.3 mm/yr/century in the very long quasi-mean sea level (or ‘Adjusted Mean High Water’) record from Liverpool. From these records, one can infer that the onset of the acceleration occurred during the 19th century, a suggestion consistent with separate analysis of the long Stockholm record (Ekman, 1988, 1999; see also Mörner, 1973). It is also consistent with some geological evidence from north-west Europe (e.g., Allen and Rae, 1988). In North America, the longest records are from Key West, Florida, which commenced in 1846 and which suggest an acceleration of order 0.4 mm/year/century (Maul and Martin, 1993), and from New York which commenced in 1856 and which has a similar acceleration. Coastal evolution evidence from parts of eastern North America suggest an increased rate of rise between one and two centuries before the 20th century (Kearney and Stevenson, 1991; Varekamp *et al.*, 1992; Kearney, 1996; Van de Plassche *et al.*, 1998; Varekamp and Thomas, 1998; Shaw and Ceman, 2000).

There is no evidence for any acceleration of sea level rise in data from the 20th century data alone (Woodworth, 1990; Gornitz and Solow, 1991; Douglas, 1992). Mediterranean records show decelerations, and even decreases in sea level in the latter part of the 20th century, which may be caused by increases in the density of Mediterranean Deep Water and air pressure changes connected to the North Atlantic Oscillation (NAO) (Tsimplis and Baker, 2000), suggesting the Mediterranean might not be the best area for monitoring secular trends. Models of ocean thermal expansion indicate an acceleration through the 20th century but when the model is subsampled at the locations of the tide gauges no significant acceleration can be detected because of the greater level of variability (Gregory *et al.*, 2001). Thus the absence of an acceleration in the observations is not necessarily inconsistent with the model results.

11.3.2.3 Mean sea level change from satellite altimeter observations

In contrast to the sparse network of coastal and mid-ocean island tide gauges, measurements of sea level from space by satellite

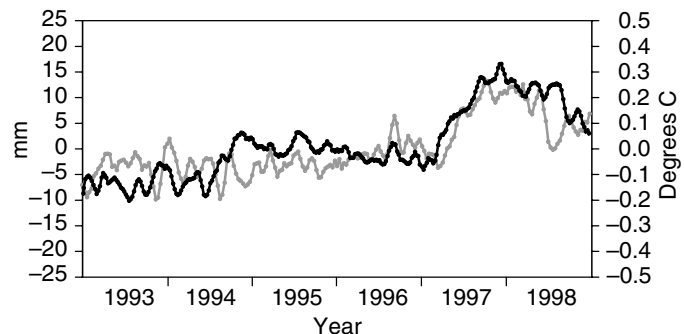


Figure 11.8: Global mean sea level variations (light line) computed from the TOPEX/POSEIDON satellite altimeter data compared with the global averaged sea surface temperature variations (dark line) for 1993 to 1998 (Cazenave *et al.*, 1998, updated). The seasonal components have been removed from both time-series.

radar altimetry provide near global and homogenous coverage of the world’s oceans, thereby allowing the determination of regional sea level change. Satellite altimeters also measure sea level with respect to the centre of the earth. While the results must be corrected for isostatic adjustment (Peltier, 1998), satellite altimetry avoids other vertical land movements (tectonic motions, subsidence) that affect local determinations of sea level trends measured by tide gauges. However, achieving the required sub-millimetre accuracy is demanding and requires satellite orbit information, geophysical and environmental corrections and altimeter range measurements of the highest accuracy. It also requires continuous satellite operations over many years and careful control of biases.

To date, the TOPEX/POSEIDON satellite-altimeter mission, with its (near) global coverage from 66°N to 66°S (almost all of the ice-free oceans) from late 1992 to the present, has proved to be of most value to direct estimates of sea level change. The current accuracy of TOPEX/POSEIDON data allows global average sea level to be estimated to a precision of several millimetres every 10 days, with the absolute accuracy limited by systematic errors.

Careful comparison of TOPEX/POSEIDON data with tide gauge data reveals a difference in the rate of change of local sea level of -2.3 ± 1.2 mm/yr (Mitchum, 1998) or -2 ± 1.5 mm/yr (Cazenave *et al.*, 1999). This discrepancy is caused by a combination of instrumental drift, especially in the TOPEX Microwave Radiometer (TMR) (Haines and Bar-Sever, 1998), and vertical land motions which have not been allowed for in the tide gauge data. The most recent estimates of global average sea level rise from the six years of TOPEX/POSEIDON data (using corrections from tide gauge comparisons) are 2.1 ± 1.2 mm/yr (Nerem *et al.*, 1997), 1.4 ± 0.2 mm/yr (Cazenave *et al.*, 1998; Figure 11.8), 3.1 ± 1.3 mm/yr (Nerem, 1999) and 2.5 ± 1.3 mm/yr (Nerem, 1999), of which the last assumes that all instrumental drift can be attributed to the TMR. When Cazenave *et al.* allow for the TMR drift, they compute a sea level rise of 2.6 mm/yr. Their uncertainty of

± 0.2 mm/yr does not include allowance for uncertainty in instrumental drift, but only reflects the variations in measured global sea level. Such variations correlate with global average sea surface temperature, perhaps indicating the importance of steric effects through ocean heat storage. Cazenave *et al.* (1998) and Nerem *et al.* (1999) argue that ENSO events cause a rise and a subsequent fall in global averaged sea level of about 20 mm (Figure 11.8). These findings indicate that the major 1997/98 El Niño-Southern Oscillation (ENSO) event could bias the above estimates of sea level rise and also indicate the difficulty of separating long-term trends from climatic variability.

After upgrading many of the geophysical corrections on the original European Remote Sensing (ERS) data stream, Cazenave *et al.* (1998) find little evidence of sea level rise over the period April 1992 to May 1996. However, over the time span of overlap between the ERS-1 and TOPEX/POSEIDON data, similar rates of sea level change (about 0.5 mm/yr) are calculated. For the period April 1992 to April 1995, Anzenhofer and Gruber (1998) find a sea level rise of 2.2 ± 1.6 mm/yr.

In summary, analysis of TOPEX/POSEIDON data suggest a rate of sea level rise during the 1990s greater than the mean rate of rise for much of the 20th century. It is not yet clear whether this is the result of a recent acceleration, of systematic differences between the two measurement techniques, or of the shortness of the record (6 years).

11.3.3 Changes in Extreme Sea Levels: Storm Surges and Waves

Lack of adequate data sets means we can not ascertain whether there have been changes in the magnitude and/or frequency of storm surges (aperiodic changes associated with major meteorological disturbances resulting in sea level changes of up to several metres and lasting a few hours to days) in many regions of the world. Zhang *et al.* (1997, 2000) performed a comprehensive analysis of hourly tide gauge data from the east coast of North America, and concluded that there had been no discernible secular trend in storm activity or severity during the past century. European analyses include that of Woodworth (1999b), who found no significant increase in extreme high water level distributions from Liverpool from 1768 to 1993 to those from later epochs, other than what can be explained in terms of changes in local tidal amplitudes, mean sea level and vertical land movement. Vassie (reported in Pugh and Maul, 1999) and Bijl *et al.* (1999) concluded that there was no discernible trend over the last century in the statistics of non-tidal sea level variability around the UK and the eastern North Sea (Denmark, Germany and the Netherlands), above the considerable natural sea level variability on decadal time-scales. In South America, D'Onofrio *et al.* (1999) observed a trend of extreme levels at Buenos Aires of 2.8 mm/yr over 1905 to 1993. On the basis of available statistics, the South American result is consistent with the local mean sea level trend.

Variations in surge statistics can also be inferred from analysis of meteorological data. Kass *et al.* (1996) and the WASA Group (1998) showed that there are no significant overall trends in windiness and cyclonic activity over the North Atlantic

and north-west Europe during the past century, although major variations on decadal times-scales exist. An increase in storminess in the north-east Atlantic in the last few decades (Schmitt *et al.*, 1998) and a recent trend towards higher storm surge levels on the German and Danish coasts (Langenberg *et al.*, 1999) is consistent with natural variability evident over the last 150 years. Pirazzoli (2000) detected evidence for a slight decrease in the main factors contributing to surge development on the French Atlantic coast in the last 50 years. Correlation between the frequency of Atlantic storms and ENSO was demonstrated by Van der Vink *et al.* (1998).

Increases in wave heights of approximately 2 to 3 m over the period 1962 to 1985 off Land's End, south-west England (Carter and Draper, 1988), increases in wave height over a neighbouring area at about 2%/yr since 1950 (Bacon and Carter, 1991, 1993) and wave height variations simulated by the Wave Action Model (WAM) (Günther *et al.*, 1998) are all consistent with decadal variations over most of the north-east Atlantic and North Sea. This variability could be related to the NAO (Chapter 2, Section 2.6.5).

11.4 Can 20th Century Sea Level Changes be Explained?

In order to have confidence in our ability to predict future changes in sea level, we need to confirm that the relevant processes (Section 11.2) have been correctly identified and evaluated. We attempt this by seeing how well we can account for the current rate of change (Section 11.3). We note that:

- some processes affecting sea level have long (centuries and longer) time-scales, so that current sea level change is also related to past climate change,
- some relevant processes are not determined solely by climate,
- fairly long records (at least 50 years according to Douglas, 1992) are needed to detect a significant trend in local sea level, because of the influence of natural variability in the climate system, and
- the network of tide gauges with records of this length gives only a limited coverage of the world's continental coastline and almost no coverage of the mid-ocean.

The estimated contributions from the various components of sea level rise during the 20th century (Table 11.10, Figure 11.9) were constructed using the results from Section 11.2. The sum of these contributions for the 20th century ranges from -0.8 mm/yr to 2.2 mm/yr, with a central value of 0.7 mm/yr. The upper bound is close to the observational upper bound (2.0 mm/yr), but the central value is less than the observational lower bound (1.0 mm/yr), and the lower bound is negative i.e. the sum of components is biased low compared to the observational estimates. Nonetheless, the range is narrower than the range given by Warrick *et al.* (1996), as a result of greater constraints on all the contributions, with the exception of the terrestrial storage terms. In particular, the long-term contribution from the

Table 11.10: Estimated rates of sea level rise components from observations and models (mm/yr) averaged over the period 1910 to 1990. (Note that the model uncertainties may be underestimates because of possible systematic errors in the models.) The 20th century terms for Greenland and Antarctica are derived from ice sheet models because observations cannot distinguish between 20th century and long-term effects. See Section 11.2.3.3.

	Minimum (mm/yr)	Central value (mm/yr)	Maximum (mm/yr)
Thermal expansion	0.3	0.5	0.7
Glaciers and ice caps	0.2	0.3	0.4
Greenland – 20th century effects	0.0	0.05	0.1
Antarctica – 20th century effects	-0.2	-0.1	0.0
Ice sheets – adjustment since LGM	0.0	0.25	0.5
Permafrost	0.00	0.025	0.05
Sediment deposition	0.00	0.025	0.05
Terrestrial storage (not directly from climate change)	-1.1	-0.35	0.4
Total	-0.8	0.7	2.2
Estimated from observations	1.0	1.5	2.0

ice sheets has been narrowed substantially from those given in Warrick *et al.* (1996) by the use of additional constraints (geological data and models of the ice sheets) (Section 11.3.1).

The reason for the remaining discrepancy is not clear. However, the largest uncertainty (by a factor of more than two) is in the terrestrial storage terms. Several of the components of the terrestrial storage term are poorly determined and the quoted limits require several of the contributions simultaneously to lie at the extremes of their ranges. This coincidence is improbable unless the systematic errors affecting the estimates are correlated. Furthermore, while coupled models have improved considerably in recent years, and there is general agreement between the observed and modelled thermal expansion contribution, the models' ability to quantitatively simulate decadal changes in ocean temperatures and thus thermal expansion has not been adequately tested. Given the poor global coverage of high quality tide gauge records and the uncertainty in the corrections for land motions, the observationally based rate of sea level rise this century should also be questioned.

In the models, at least a third of 20th century anthropogenic eustatic sea level rise is caused by thermal expansion, which has a geographically non-uniform signal in sea level change. AOGCMs do not agree in detail about the patterns of geographical variation (see Section 11.5.2). They all give a geographical spread of 20th century trends at individual grid points which is characterised by a standard deviation of 0.2 to 0.5 mm/yr (Gregory *et al.*, 2001). This spread is a result of a combination of spatial non-uniformity of trends and the uncertainty in local trend estimates arising from temporal variability. As yet no published study has revealed a stable pattern of observed non-uniform sea level change. Such a pattern would provide a critical test of models. If there is significant non-uniformity, a trend from a single location would be an inaccurate estimate of the global average. For example, Douglas (1997) averaged nine regions and found a standard deviation of about 0.3 mm/yr (quoted by Douglas as a standard error), similar to the range expected from AOGCMs.

A common perception is that the rate of sea level rise should have accelerated during the latter half of the 20th century. The tide gauge data for the 20th century show no significant acceleration (e.g., Douglas, 1992). We have obtained estimates based on AOGCMs for the terms directly related to anthropogenic climate change in the 20th century, i.e., thermal expansion (Section 11.2.1.2), ice sheets (Section 11.2.3.3), glaciers and ice caps (Section 11.5.1.1) (Figure 11.10a). The estimated rate of sea level rise from anthropogenic climate change ranges from 0.3 to 0.8 mm/yr (Figure 11.10b). These terms do show an acceleration through the 20th century (Figure 11.10a,b). If the terrestrial storage terms have a negative sum (Section 11.2.5), they may offset some of the acceleration in recent decades. The total computed rise (Figure 11.10c) indicates an acceleration of only 0.2 mm/yr/century, with a range from -1.1 to +0.7 mm/yr/century,

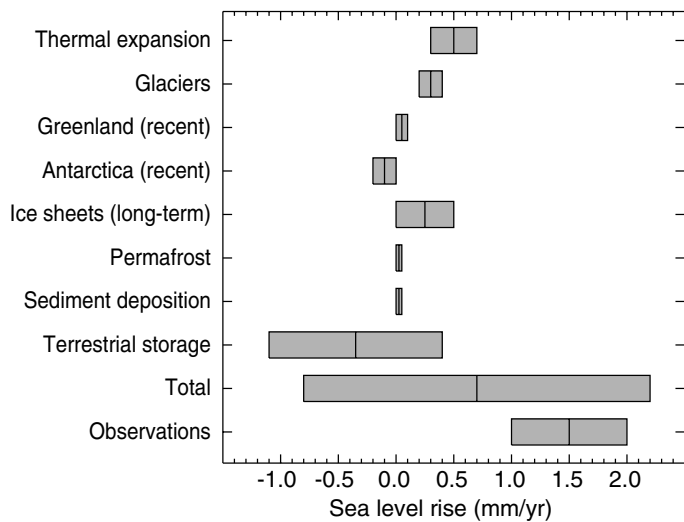


Figure 11.9: Ranges of uncertainty for the average rate of sea level rise from 1910 to 1990 and the estimated contributions from different processes.

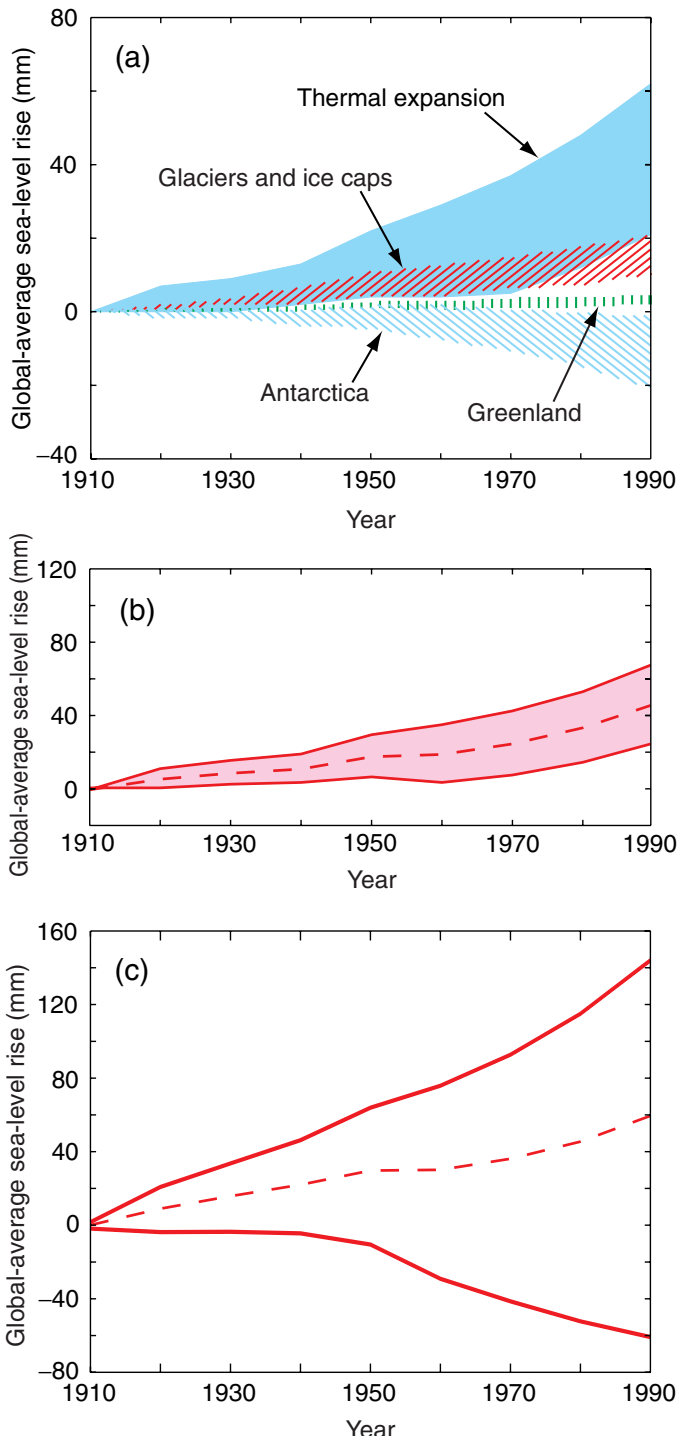


Figure 11.10: Estimated sea level rise from 1910 to 1990. (a) The thermal expansion, glacier and ice cap, Greenland and Antarctic contributions resulting from climate change in the 20th century calculated from a range of AOGCMs. Note that uncertainties in land ice calculations have not been included. (b) The mid-range and upper and lower bounds for the computed response of sea level to climate change (the sum of the terms in (a) plus the contribution from permafrost). These curves represent our estimate of the impact of anthropogenic climate change on sea level during the 20th century. (c) The mid-range and upper and lower bounds for the computed sea level change (the sum of all terms in (a) with the addition of changes in permafrost, the effect of sediment deposition, the long-term adjustment of the ice-sheets to past climate change and the terrestrial storage terms).

consistent with observational finding of no acceleration in sea level rise during the 20th century (Section 11.3.2.2). The sum of terms not related to recent climate change is -1.1 to $+0.9$ mm/yr (i.e., excluding thermal expansion, glaciers and ice caps, and changes in the ice sheets due to 20th century climate change). This range is less than the observational lower bound of sea level rise. Hence it is very likely that these terms alone are an insufficient explanation, implying that 20th century climate change has made a contribution to 20th century sea level rise.

Recent studies (see Sections 2.3.3, 2.3.4) suggest that the 19th century was unusually cold on the global average, and that an increase in solar output may have had a moderate influence on warming in the early 20th century (Section 12.4.3.3). This warming might have produced some thermal expansion and could have been responsible for the onset of glacier recession in the early 20th century (e.g., Dowdeswell *et al.*, 1997), thus providing a possible explanation of an acceleration in sea level rise commencing before major industrialisation.

11.5 Future Sea Level Changes

11.5.1 Global Average Sea Level Change 1990 to 2100

Warrick *et al.* (1996) made projections of thermal expansion and of loss of mass from glaciers and ice-sheets for the 21st century for the IS92 scenarios using two alternative simple climate models. Since the SAR, time-dependent experiments have been run with several AOGCMs (Chapter 9.1.2, Table 9.1) following the IS92a scenario (Leggett *et al.*, 1992) for future concentrations of greenhouse gases, including the direct effect of sulphate aerosols. In Section 11.5.1.1, we use the AOGCM IS92a results to derive estimates of thermal expansion and land ice melt, employing methods from the literature as described in Section 11.2, and we add contributions from thawing of permafrost, sediment deposition, and the continuing adjustment of the ice sheets to climate changes since the LGM. The choice of scenario is not the principal consideration; the main point is that the AOGCMs all follow the same scenario, so the range of results reflects the systematic uncertainty inherent in the modelling of sea level changes. The use of IS92a also facilitates comparison with the result of Warrick *et al.* (1996).

To quantify the uncertainty resulting from the uncertainty in future emissions, and to obtain results consistent with the global-average temperature change projections of Section 9.3.3, in Section 11.5.1.2 we derive projections for thermal expansion and land ice melt for the scenarios of the IPCC Special Report on Emissions Scenarios (SRES) (Nakićenović *et al.*, 2000) (see also Box 9.1 in Chapter 9, Section 9.1). The results are given as sea level change relative to 1990 in order to facilitate comparison with previous IPCC reports, which used 1990 as their base date.

11.5.1.1 Projections for a single scenario based on a range of AOGCMs

Thermal expansion

Over the hundred years 1990 to 2090, the AOGCM experiments for IS92a including sulphate aerosols (GS experiments – see Chapter 9, Table 9.1) show global-average sea level rise from

Table 11.11: Sea level rise from thermal expansion from AOGCM experiments following the IS92a scenario for the 21st century, including the direct effect of sulphate aerosols. See Chapter 8, Table 8.1 and Chapter 9, Table 9.1 for further details of models and experiments. See Table 11.2 for thermal expansion from AOGCM experiments for the 20th century.

Experiment	ΔT_g (°C)	Sea level rise (m)		
		1990 to 2090 ^a	1990 to 2040	1990 to 2090 ^a
CGCM1 GS	3.7	0.12	0.37	
CGCM2 GS	3.6	0.11	0.33	
CSIRO Mk2 GS	2.7	0.11	0.28	
ECHAM4/OPYC3 GS ^b	—	0.11	—	
GFDL_R15_a GS ^c	—	0.13	—	
GFDL_R15_b GS	3.2	0.12	0.29	
GFDL_R30_c GS	2.8	0.12	0.31	
HadCM2 GS	2.5	0.07	0.20	
HadCM3 GSIO	2.8	0.07	0.20	
MRI2 GS	1.5	0.04	0.09	
DOE PCM GS	1.9	0.07	0.17	

^a An end date of 2090, rather than 2100, is chosen to match the last available date in some of the experiments.

^b This experiment ends at 2050.

^c This experiment ends at 2065.

ΔT_g Global average surface air temperature change.

thermal expansion in the range 0.09 to 0.37 m (Figure 11.1, Table 11.11). There is an acceleration through the 21st century; expansion for 2040 to 2090 is greater than for 1990 to 2040 by a factor of 1.4 to 2.1. Since the models experience the same forcing, the differences in the thermal expansion derive from differences in the physical behaviour of the models. Broadly speaking, the range of results reflects the systematic uncertainty of modelling in three factors: the size of the surface warming, the effectiveness of heat uptake by the ocean for a given warming (Gregory and Mitchell, 1997) and the expansion resulting from a given heat uptake (Russell *et al.*, 2000). The separation of the first two factors parallels the distinction made in Section 9.3.4.2 between the effects of climate feedback and heat uptake on the rate of climate change. Since models differ in regard to the second and third factors, experiments with a similar temperature change do not necessarily have a similar thermal expansion, as the results demonstrate.

Glaciers and ice caps

To make projections for future loss of mass from glaciers and ice caps, we have applied the methods of Gregory and Oerlemans (1998) and Van de Wal and Wild (2001) (Sections 11.2.2.2, 11.2.2.4) to the seasonally and geographically dependent temperature changes given by a range of AOGCM IS92a experiments including sulphate aerosols (Table 11.12). We adjust the results to be consistent with the assumption that the climate of 1865 to 1895 was 0.15 K warmer than the steady state for glaciers, following Zuo and Oerlemans (1997) (see also Section 11.4). Precipitation changes are not included, as they are not expected to have a strong influence on the global average (Section 11.2.2.3).

Table 11.12: Calculations of glacier melt from AOGCM experiments following the IS92a scenario for the 21st century, including the direct effect of sulphate aerosols. See Tables 8.1 and 9.1 for further details of models and experiments.

Experiment	B (mm/yr) 1990	ΔT_g (°C) 1990 to 2090	Sea level rise (m) 1990 to 2090		$\partial B / \partial T_g$ (mm/yr/°C)
			Constant area	Changing area	
CGCM1 GS	0.43	3.7	0.15	0.11	0.65
CSIRO Mk2 GS	0.52	2.7	0.15	0.11	0.73
CSM 1.3 GS	0.45	1.8	0.10	0.07	0.61
ECHAM4/OPYC3 GS ^a	0.56	—	—	—	0.64
GFDL_R15_a GS ^b	0.42	—	—	—	0.58
GFDL_R15_b GS	0.44	3.2	0.13	0.09	0.54
GFDL_R30_c GS	0.33	2.8	0.12	0.08	0.53
HadCM2 GS ^c	0.44	2.5	0.11	0.08	0.61
HadCM3 GSIO	0.31	2.8	0.11	0.08	0.62
MRI2 GS	0.22	1.5	0.06	0.05	0.60
DOE PCM GS	0.42	1.9	0.09	0.06	0.59

^a This experiment ends at 2050.

^b This experiment ends at 2065.

^c Similar results for constant area were obtained for an ensemble of HadCM2 GS experiments by Gregory and Oerlemans (1998).

B Global glacier mass balance for constant glacier area, expressed as sea level equivalent.

$\partial B / \partial T_g$ Sensitivity of global glacier mass balance for constant glacier area, expressed as sea level equivalent, to global average surface air temperature change.

ΔT_g Global average surface air temperature change.

Table 11.13: Calculations of ice sheet mass changes using temperature and precipitation changes from AOGCM experiments following the IS92a scenario for the 21st century, including the direct effect of sulphate aerosols, to derive boundary conditions for an ice sheet model. See Tables 8.1 and 9.1 for further details of models and experiments.

Experiment	Greenland					Antarctica				
	Sea level rise (m) 1990 to 2090	Sensitivity (mm/yr/°C)		$\Delta T/\Delta T_g$	1/P dP/dT (%/°C)	Sea level rise (m) 1990 to 2090	Sensitivity (mm/yr/°C)		$\Delta T/\Delta T_g$	
		dB/dT_g	dB/dT				dB/dT_g	dB/dT		
CGCM1 GS	0.03	0.13	0.10	1.3	2.7	-0.02	-0.12	-0.11	1.1	
CSIRO Mk2 GS	0.02	0.16	0.08	2.0	5.9	-0.07	-0.37	-0.33	1.1	
CSM 1.3 GS	0.02	0.15	0.05	3.1	7.8	-0.04	-0.31	-0.27	1.1	
ECHAM4/OPYC3 GS ^a	-	0.03	0.03	1.2	6.5	-	-0.48	-0.32	1.5	
GFDL_R15_a GS ^b	-	0.12	0.06	1.9	4.1	-	-0.18	-0.22	0.8	
HadCM2 GS	0.02	0.10	0.07	1.4	4.0	-0.04	-0.21	-0.17	1.2	
HadCM3 GSIO	0.02	0.09	0.06	1.4	4.5	-0.07	-0.35	-0.28	1.3	
MRI2 GS	0.01	0.08	0.05	1.6	4.4	-0.01	-0.14	-0.12	1.2	
DOE PCM GS	0.02	0.14	0.06	2.2	5.6	-0.07	-0.48	-0.30	1.6	

^a This experiment ends at 2050.

^b This experiment ends at 2065.

dB/dT_g Ice-sheet mass balance sensitivity to global-average surface air temperature change, expressed as sea level equivalent.

dB/dT Ice-sheet mass balance sensitivity to surface air temperature change averaged over the ice sheet, expressed as sea level equivalent.

$\Delta T/\Delta T_g$ Slope of the regression of surface air temperature change averaged over the ice sheet against global-average change.

1/P dP/dT Fractional change in ice-sheet average precipitation as a function of temperature change.

For constant glacier area, from the AOGCM IS92a experiments including sulphate aerosol, predicted sea level rise from glacier melt over the hundred years 1990 to 2090 lies in the range 0.06 to 0.15 m. The variation is due to three factors. First, the global average temperature change varies between models. A larger temperature rise tends to give more melting, but they are not linearly related, since the total melt depends on the time-integrated temperature change. Second, the global mass balance sensitivity to temperature change varies among AOGCMs because of their different seasonal and regional distribution of temperature change. Third, the glaciers are already adjusting to climate change during the 20th century, and any such imbalance will persist during the 21st century, in addition to the further imbalance due to future climate change. The global average temperature change and glacier mass balance sensitivity may not be independent factors, since both are affected by regional climate feedbacks. The sensitivity and the present imbalance are related factors, because a larger sensitivity implies a greater present imbalance.

With glacier area contracting as the volume reduces, the estimated sea level rise contribution is in the range 0.05 to 0.11 m, about 25% less than if constant area is assumed, similar to the findings of Oerlemans *et al.* (1998) and Van de Wal and Wild (2001). The time-dependence of glacier area means the results can no longer be represented by a global glacier mass balance sensitivity.

Glaciers and ice caps on the margins of the Greenland and Antarctic ice sheets are omitted from these calculations, because they are included in the ice sheet projections below. These ice masses have a large area (Table 11.3), but experience little ablation on account of being in very cold climates. Van de Wal

and Wild (2001) find that the Greenland marginal glaciers contribute an additional 6% to glacier melt in a scenario of CO₂ doubling over 70 years. Similar calculations using the AOGCM IS92a results give a maximum contribution of 14 mm for 1990 to 2100. For the Antarctic marginal glaciers, the ambient temperatures are too low for there to be any significant surface runoff. Increasing temperatures will increase the runoff and enlarge the area experiencing ablation, but their contribution is very likely to remain small. For instance, Drewry and Morris (1992) calculate a contribution of 0.012 mm/yr/°C to the global glacier mass balance sensitivity from the glacier area of 20,000 km² which currently experiences some melting on the Antarctic Peninsula.

Lack of information concerning glacier areas and precipitation over glaciers, together with uncertainty over the projected changes in glacier area, lead to uncertainty in the results. This is assessed as ± 40%, matching the uncertainty of the observed mass balance estimate of Dyurgerov and Meier (1997b).

Greenland and Antarctic ice sheets

To make projections of Greenland and Antarctic ice sheet mass changes consistent with the IS92a AOGCM experiments including sulphate aerosols, we have integrated the ice-sheet model of Huybrechts and De Wolde (1999) using boundary conditions of temperature and precipitation derived by perturbing present day climatology according to the geographically and seasonally dependent pattern changes predicted by the T106 ECHAM4 model (Wild and Ohmura, 2000) for a doubling of CO₂. To generate time-dependent boundary conditions, these patterns were scaled with the area average changes over the ice sheets as a function of time for each AOGCM experiment using a method similar to that described by Huybrechts *et al.* (1999).

Table 11.14: Sea level rise 1990 to 2100 due to climate change derived from AOGCM experiments following the IS92a scenario, including the direct effect of sulphate aerosols. See Tables 8.1 and 9.1 for further details of models and experiments. Results were extrapolated to 2100 for experiments ending at earlier dates. The uncertainties shown in the land ice terms are those discussed in this section. For comparison the projection of Warrick *et al.* (1996) (in the SAR) is also included. Note that the minimum of the sum of the components is not identical with the sum of the minima because the smallest values of the components do not all come from the same AOGCM, and because for each model the land ice uncertainties have been combined in quadrature; similarly for the maxima, which also include non-zero contributions from smaller terms.

Experiment	Sea level rise (m) 1990 to 2100									
	Expansion		Glaciers		Greenland		Antarctica ^a		Sum ^b	
	min	max	min	max	min	max	min	max	min	max
CGCM1 GS	0.43	0.03	0.23	0.00	0.07	-0.07	0.02	0.45	0.77	
CSIRO Mk2 GS	0.33	0.02	0.22	-0.01	0.08	-0.12	-0.04	0.29	0.60	
ECHAM4/OPYC3 GS	0.30	0.02	0.18	-0.02	0.03	-0.17	-0.06	0.19	0.48	
GFDL_R15_a GS	0.38	0.02	0.19	-0.01	0.09	-0.09	-0.01	0.37	0.67	
HadCM2 GS	0.23	0.02	0.17	-0.01	0.05	-0.09	0.00	0.21	0.48	
HadCM3 GSIO	0.24	0.02	0.18	0.00	0.05	-0.13	-0.03	0.18	0.46	
MRI2 GS	0.11	0.01	0.11	0.00	0.03	-0.04	0.00	0.11	0.31	
DOE PCM GS	0.19	0.01	0.13	-0.01	0.06	-0.13	-0.04	0.12	0.37	
Range	0.11	0.43	0.01	0.23	-0.02	0.09	-0.17	0.02	0.11	0.77
Central value	0.27		0.12		+0.04		-0.08		0.44	
SAR	Best estimate	0.28		0.16		+0.06		-0.01		0.49
7.5.2.4		Range						0.20		0.86

^a Note that this range does not allow for uncertainty relating to ice-dynamical changes in the West Antarctic ice sheet. See Section 11.5.4.3 for a full discussion.

^b Including contributions from permafrost, sedimentation, and adjustment of ice sheets to past climate change.

The marginal glaciers and ice caps on Greenland and Antarctica were included in the ice sheet area. The calculated contributions from these small ice masses have some uncertainty resulting from the limited spatial resolution of the ice sheet model.

For 1990 to 2090 in the AOGCM GS experiments, Greenland contributes 0.01 to 0.03 m and Antarctica -0.07 to -0.01 m to global average sea level (Table 11.13). Note that these sea level contributions result solely from recent and projected future climate change; they do not include the response to past climate change (discussed in Sections 11.2.3.3 and 11.3.1).

Mass balance sensitivities are derived by regressing rate of change of mass against global or local temperature change (note that they include the effect of precipitation changes) (Table 11.13). The Greenland local sensitivities are smaller than some of the values reported previously from other methods (Section 11.2.3.4 and Table 11.7) and by Warrick *et al.* (1996) because of the larger precipitation increases and the seasonality of temperature changes (less increase in summer) predicted by AOGCMs, and the smaller temperature rise in the ablation zone (as compared to the ice-sheet average) projected by the T106 ECHAM4 time slice results. The Antarctic sensitivities are less negative than those in Table 11.7 because the AOGCMs predict smaller precipitation increases.

The use of a range of AOGCMs represents the uncertainty in modelling changing circulation patterns, which lead to both changes in temperature and precipitation, as noted by Kapsner *et al.* (1995) and Cuffey and Clow (1997) from the results from Greenland ice cores. The range of AOGCM thermodynamic and circulation responses gives a range of 4 to 8%/°C for Greenland precipitation increases, generally less than indicated by ice-cores

for the glacial-interglacial transition, but more than for Holocene variability (Section 11.2.3.4). If precipitation did not increase at all with greenhouse warming, Greenland local sensitivities would be larger, by 0.05 to 0.1 mm/yr/°C (see also Table 11.7). Given that all AOGCMs agree on an increase, but differ on the strength of the relationship, we include an uncertainty of ±0.02 mm/yr/°C in Table 11.13 on the Greenland local sensitivities, being the product of the standard deviation of precipitation increase (1.5%/°C) and the current Greenland accumulation (1.4 mm/yr sea level equivalent, Table 11.5).

Estimates of Greenland runoff (Table 11.5) have a standard error of about ± 10%. This reflects uncertainty in the degree-day method (Braithwaite, 1995) and refreezing parametrization (Janssens and Huybrechts, 2000) used to calculate Greenland ablation. Given that a typical size of the sensitivity of ablation to temperature change is 0.3 mm/yr/°C (Table 11.7), we adopt an additional uncertainty of ± 0.03 mm/yr/°C for the local Greenland sensitivities in Table 11.13. We include a separate uncertainty of the same size to reflect the possible sensitivity to use of different high-resolution geographical patterns of temperature and precipitation change (the T106 ECHAM4 pattern was the only one available). As an estimate of the uncertainty related to changes in iceberg discharge and area-elevation distribution, we ascribe an uncertainty of ± 10% to the net mass change, on the basis of the magnitude of the dynamic response for Greenland described in Section 11.2.3.4.

For Antarctica, uncertainty introduced by ablation model parameters need not be considered because melting remains very small for the temperature scenarios considered for the 21st century. Ice-dynamical uncertainties are much more difficult to

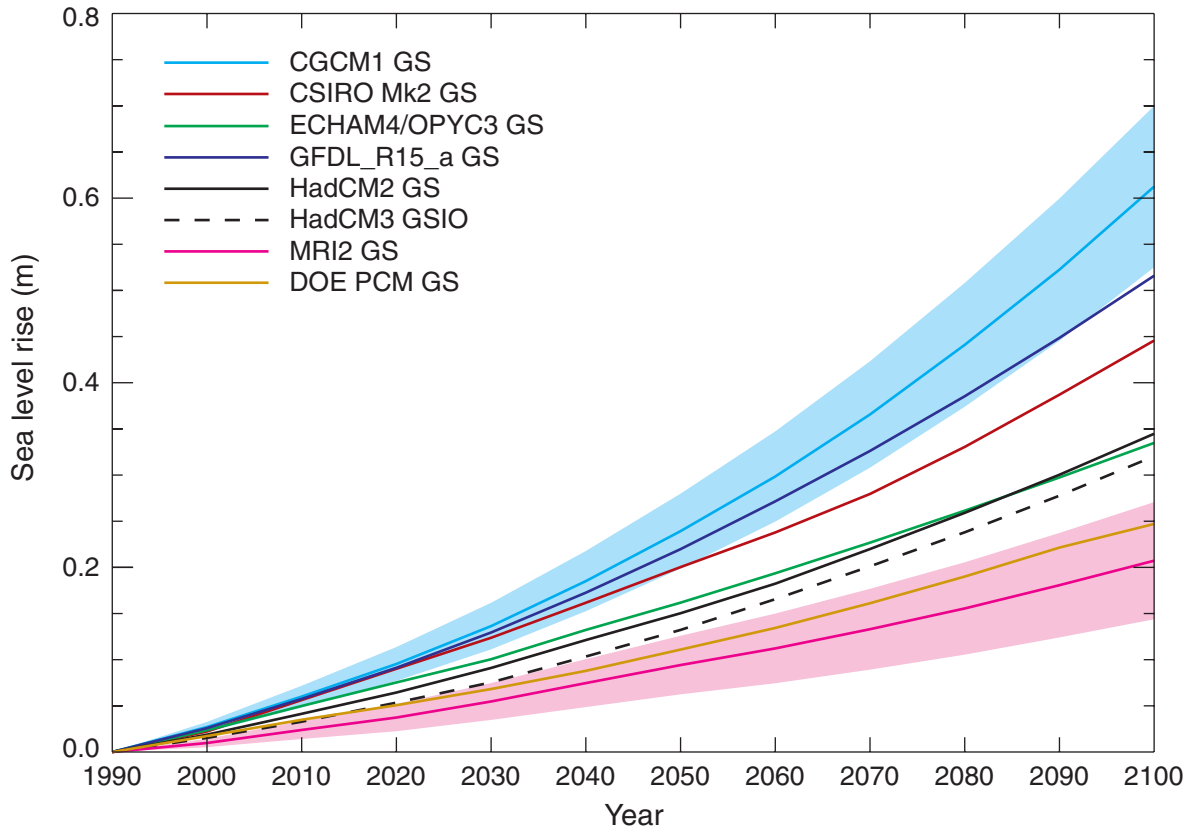


Figure 11.11: Global average sea level rise 1990 to 2100 for the IS92a scenario, including the direct effect of sulphate aerosols. Thermal expansion and land ice changes were calculated from AOGCM experiments, and contributions from changes in permafrost, the effect of sediment deposition and the long-term adjustment of the ice sheets to past climate change were added. For the models that project the largest (CGCM1) and the smallest (MRI2) sea level change, the shaded region shows the bounds of uncertainty associated with land ice changes, permafrost changes and sediment deposition. Uncertainties are not shown for the other models, but can be found in Table 11.14. The outermost limits of the shaded regions indicate our range of uncertainty in projecting sea level change for the IS92a scenario.

determine. See Section 11.5.4.3 for a detailed discussion. We include an uncertainty of 0.08 mm/yr/ $^{\circ}\text{C}$ on the local sensitivity, which is its inter-model standard deviation, to reflect the spread of precipitation changes as a function of temperature.

Total

To obtain predictions of global average sea level rise for 1990–2100 for the IS92a scenario with sulphate aerosols, we calculate the sum of the contributions from thermal expansion, glaciers and ice sheets for each AOGCM, and add the 0 to 0.5 mm/yr from the continuing evolution of the ice sheets in response to past climate change (Section 11.2.3.1) and smaller terms from thawing of permafrost (Section 11.2.5) and the effect of sedimentation (Section 11.2.6). The range of our results is 0.11 to 0.77 m (Table 11.14, Figure 11.11), which should be compared with the range of 0.20 to 0.86 m given by Warrick *et al.* (1996) (SAR Section 7.5.2.4, Figure 7.7) for the same scenario. The AOGCMs have a range of effective climate sensitivities from 1.4 to 4.2 $^{\circ}\text{C}$ (Table 9.1), similar to the range of 1.5 to 4.5 $^{\circ}\text{C}$ used by Warrick *et al.* The AOGCM thermal expansion values are generally larger than those of Warrick *et al.* (SAR Section 7.5.2.4, Figure 7.8), but the other terms are mostly smaller (i.e., more negative in the case of Antarctica).

Warrick *et al.* included a positive term to allow for the possible instability of the WAIS. We have omitted this because it is now widely agreed that major loss of grounded ice and accelerated sea level rise are very unlikely during the 21st century (Section 11.5.4.3). The size of our range is an indication of the systematic uncertainty in modelling radiative forcing, climate and sea level changes. Uncertainties in modelling the carbon cycle and atmospheric chemistry are not covered by this range, because the AOGCMs are all given similar atmospheric concentrations as input.

11.5.1.2 Projections for SRES scenarios

Few AOGCM experiments have been done with any of the SRES emissions scenarios. Therefore to establish the range of sea level rise resulting from the choice of different SRES scenarios, we use results for thermal expansion and global-average temperature change from a simple climate model based on that of Raper *et al.* (1996) and calibrated individually for seven AOGCMs (CSIRO Mk2, CSM 1.3, ECHAM4/OPYC3, GFDL_R15_a, HadCM2, HadCM3, DOE PCM). The calibration is discussed in Chapter 9, Section 9.3.3 and the Appendix to Chapter 9. The AOGCMs used have a range of effective climate sensitivity of 1.7 to 4.2 $^{\circ}\text{C}$ (Table 9.1). We

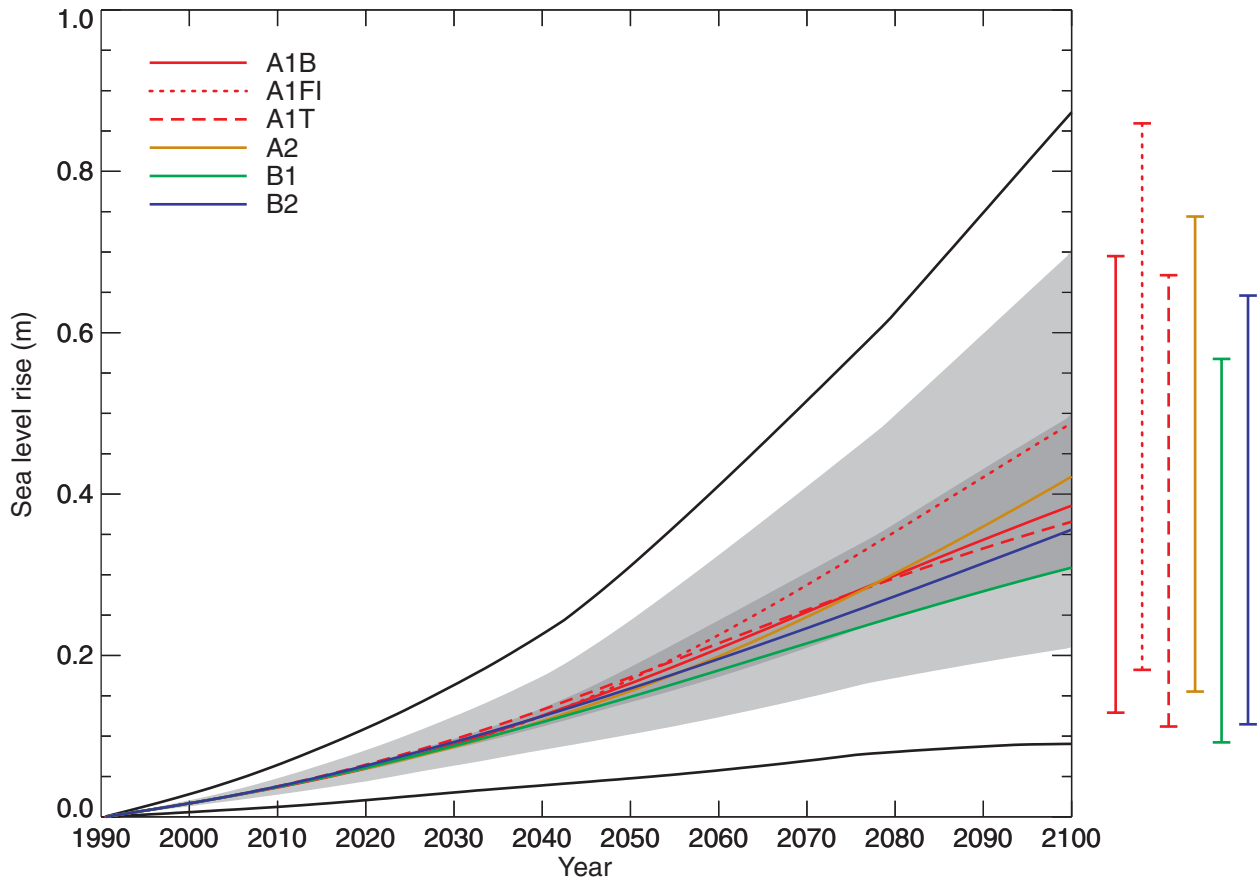


Figure 11.12: Global average sea level rise 1990 to 2100 for the SRES scenarios. Thermal expansion and land ice changes were calculated using a simple climate model calibrated separately for each of seven AOGCMs, and contributions from changes in permafrost, the effect of sediment deposition and the long-term adjustment of the ice sheets to past climate change were added. Each of the six lines appearing in the key is the average of AOGCMs for one of the six illustrative scenarios. The region in dark shading shows the range of the average of AOGCMs for all 35 SRES scenarios. The region in light shading shows the range of all AOGCMs for all 35 scenarios. The region delimited by the outermost lines shows the range of all AOGCMs and scenarios including uncertainty in land-ice changes, permafrost changes and sedimentation. Note that this range does not allow for uncertainty relating to ice-dynamical changes in the West Antarctic ice sheet. See 11.5.4.3 for a full discussion. The bars show the range in 2100 of all AOGCMs for the six illustrative scenarios.

calculate land-ice changes using the global average temperature change from the simple model and the global average mass balance sensitivities estimated from the AOGCM IS92a experiments in Section 11.5.1.1 (Tables 11.12 and 11.13). We add contributions from the continuing evolution of the ice sheets in response to past climate change, thawing of permafrost, and the effect of sedimentation (the same as in Section 11.5.1.1). The methods used to make the sea level projections are documented in detail in the Appendix to this chapter.

For the complete range of AOGCMs and SRES scenarios and including uncertainties in land-ice changes, permafrost changes and sediment deposition, global average sea level is projected to rise by 0.09 to 0.88 m over 1990 to 2100, with a central value of 0.48 m (Figure 11.12). The central value gives an average rate of 2.2 to 4.4 times the rate over the 20th century.

The corresponding range reported by Warrick *et al.* (1996) (representing scenario uncertainty by using all the IS92 scenarios with time-dependent sulphate aerosol) was 0.13 to 0.94 m, obtained using a simple model with climate sensitivities

of 1.5 to 4.5°C. Their upper bound is larger than ours. Ice sheet mass balance sensitivities derived from AOGCMs (see Section 11.5.1.1) are smaller (less positive or more negative) than those used by Warrick *et al.*, while the method we have employed for calculating glacier mass loss (Sections 11.2.2 and 11.5.1.1) gives a smaller sea level contribution for similar scenarios than the heuristic model of Wigley and Raper (1995) employed by Warrick *et al.*

In addition, Warrick *et al.* included an allowance for ice-dynamical changes in the WAIS. The range we have given does not include such changes. The contribution of the WAIS is potentially important on the longer term, but it is now widely agreed that major loss of grounded ice from the WAIS and consequent accelerated sea-level rise are very unlikely during the 21st century. Allowing for the possible effects of processes not adequately represented in present models, two risk assessment studies involving panels of experts concluded that there was a 5% chance that by 2100 the WAIS could make a substantial contribution to sea level rise, of 0.16 m (Titus and

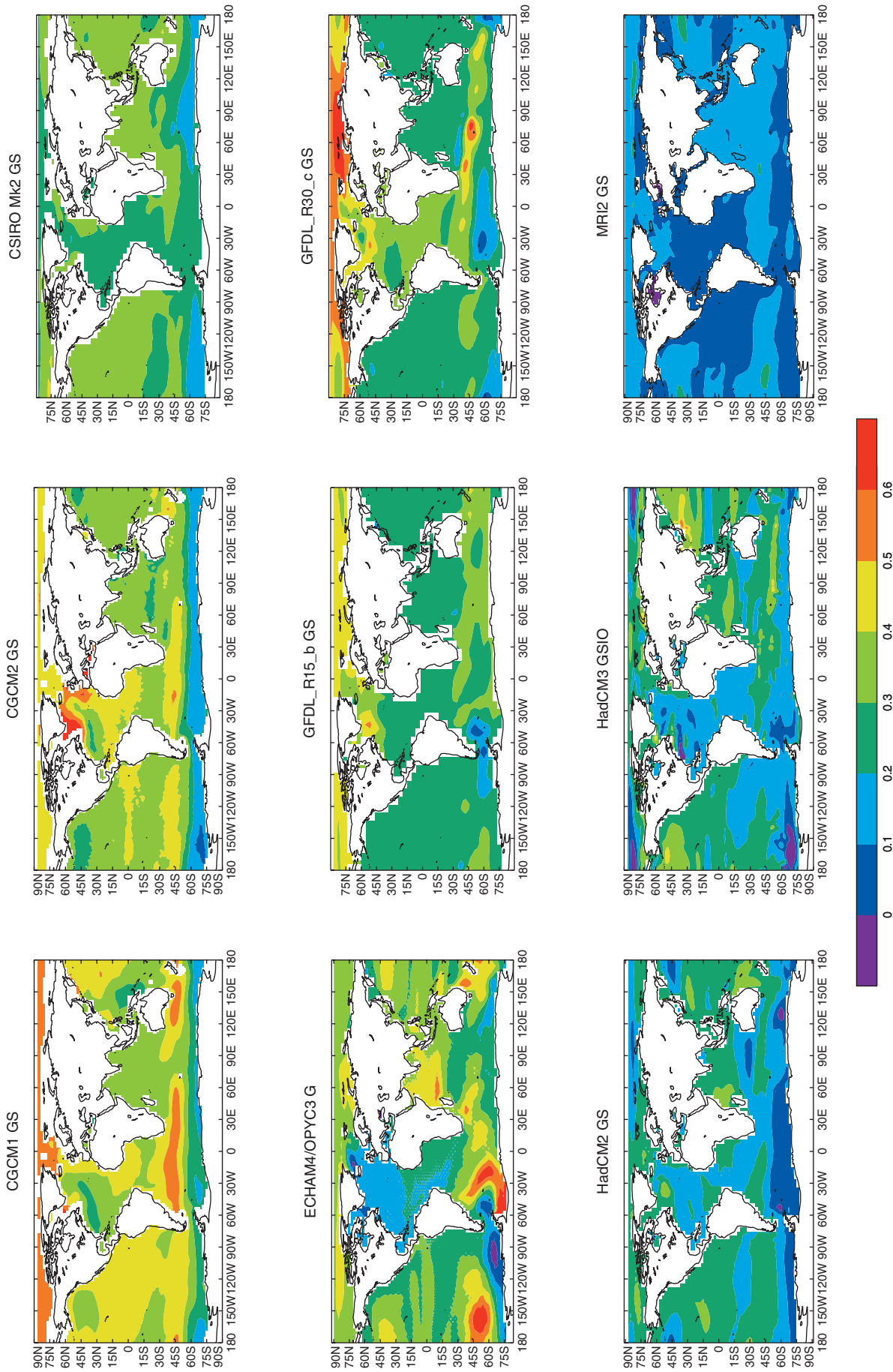


Figure 11.13: Sea level change in metres over the 21st century resulting from thermal expansion and ocean circulation changes calculated from AOGCM experiments following the IS92a scenario and including the direct effect of sulphate aerosol (except that ECHAM4/OPYC3 G is shown instead of GS, because GS ends in 2050). Each field is the difference in sea level change between the last decade of the experiment and the decade 100 years earlier. See Tables 8.1 and 9.1 for further details of models and experiments.

Table 11.15: Spatial standard deviation, local minimum and local maximum of sea level change during the 21st century due to ocean processes, from AOGCM experiments following the IS92a scenario for greenhouse gases, including the direct effect of sulphate aerosols. See Tables 8.1 and 9.1 for further details of models and experiments. Sea level change was calculated as the difference between the final decade of each experiment and the decade 100 years earlier. Sea level changes due to land ice and water storage are not included.

Experiment	Std deviation (m)	Divided by global average		
		Std deviation	Minimum	Maximum
CGCM1 GS	0.07	0.19	0.3	1.6
CGCM2 GS	0.08	0.23	0.2	2.2
CSIRO Mk2 GS	0.05	0.15	0.5	1.3
ECHAM4/OPYC3 G ^a	0.10	0.34	-1.2	2.3
GFDL_R15_b GS	0.05	0.18	0.3	1.8
GFDL_R30_c GS	0.07	0.25	0.2	2.5
HadCM2 GS	0.06	0.29	-0.1	1.7
HadCM3 GSIO	0.07	0.32	-0.5	2.2
MRI2 GS	0.04	0.35	-1.2	2.2

^aThis experiment does not include sulphate aerosols. The ECHAM4/OPYC3 experiment including sulphates extends only to 2050.

Narayanan, 1996) or 0.5 m (Vaughan and Spouge, 2001). These studies also noted a 5% chance of WAIS contributing a sea level fall of 0.18 m or 0.4 m respectively. (See Section 11.5.4.3 for a full discussion.)

The range we have given also does not take account of uncertainty in modelling of radiative forcing, the carbon cycle, atmospheric chemistry, or storage of water in the terrestrial environment. The recent publications by Gornitz *et al.* (1997) and Sahagian (2000) indicate that this last term could be significant (Section 11.2.5). Future changes in terrestrial storage depend on societal decisions on the use of ground water, the building of reservoirs and other factors. We are not currently in a position to make projections incorporating future changes in these factors, although we note that the assumptions behind the construction of the SRES scenarios imply increasing water consumption, which may entail both more ground water extraction and more reservoir capacity. Continued anthropogenic water storage on land at its current rate could change the projected sea level rise 1990 to 2100 by between -0.21 and +0.11 m. We emphasise that estimates of the relevant factors are highly uncertain (see Sections 11.2.5 and 11.4).

The evolution of sea level rise for the average of the seven AOGCMs for each of the six illustrative SRES scenarios is shown in Figure 11.12, and the shading shows the range for all 35 SRES scenarios. It is apparent that the variation due to the choice of scenario alone is relatively small over the next few decades. The range spanned by the SRES scenarios by 2040 is only 0.02 m or less. By 2100, the scenario range has increased to 0.18 m, about 50% of the central value. All the AOGCMs have a similar range at 2100 expressed as a fraction of their central value. Of the six illustrative scenarios, A1FI gives the largest sea level rise and B1 the smallest.

The average-AOGCM range for all 35 scenarios (dark shading in Figure 11.12) covers about one third of the all-AOGCM range (light shading). That is, for sea level rise 1990 to 2100, the uncertainty in climate sensitivity and heat uptake, represented by the spread of AOGCMs, is more important than the uncertainty from choice of emissions scenario. This is

different for three reasons from the case of global average temperature change (Section 9.3.2.1), where the scenario and modelling uncertainties are comparable. First, the compensation between climate sensitivity and heat uptake does not apply to thermal expansion. Second, models with large climate sensitivity and temperature change consequently have a large land-ice melt contribution to sea level. Third, both thermal expansion and land-ice melt depend on past climate change, being approximately proportional to the time-integral of temperature change; the SRES scenarios differ by less in respect of the time-integral of temperature change over the interval 1990 to 2100 than they do in respect of the temperature change at 2100.

11.5.2 Regional Sea Level Change

The geographical distribution of sea level change caused by ocean processes can be calculated from AOGCM results (see Gregory *et al.*, 2001, for methods). This was not possible with the simple climate models used by Warrick *et al.* (1996). Results for sea level change from ocean processes in the 21st century are shown in Figure 11.13 for AOGCM experiments used in Section 11.5.1.1. Some regions show a sea level rise substantially more than the global average (in many cases of more than twice the average), and others a sea level fall (Table 11.15) (note that these figures do not include sea level rise due to land ice changes). The standard deviation of sea level change is 15 to 35% of the global average sea level rise from thermal expansion.

In each of these experiments, a non-uniform pattern of sea level rise emerges above the background of temporal variability in the latter part of the 21st century. However, the patterns given by the different models (Figure 11.13) are not similar in detail. The largest correlations are between models which are similar in formulation: 0.65 between CGCM1 and CGCM2, 0.63 between GFDL_R15_b and GFDL_R30_c. The largest correlations between models from different centres are 0.60 between CSIRO Mk2 and HadCM2, 0.58 between CGCM2 and GFDL_R30_c. The majority of correlations are less than 0.4, indicating no

significant similarity (Gregory *et al.*, 2001). The disagreement between models is partly a reflection of the differences in ocean model formulation that are also responsible for the spread in the global average heat uptake and thermal expansion (Sections 11.2.1.2, 11.5.1.1). In addition, the models predict different changes in surface windstress, with consequences for changes in ocean circulation and subduction. More detailed analysis is needed to elucidate the reasons for the differences in patterns. The lack of similarity means that our confidence in predictions of local sea level changes is low. However, we can identify a few common features on the regional and basin scale (see also Gregory *et al.*, 2001).

Seven of the nine models in Table 11.14 (also Bryan, 1996; Russell *et al.*, 2000) exhibit a maximum sea level rise in the Arctic Ocean. A possible reason for this is a freshening of the Arctic due to increased river runoff or precipitation over the ocean (Bryan, 1996; Miller and Russell, 2000). The fall in salinity leads to a reduction of density, which requires a compensating sea level rise in order to maintain the pressure gradient at depth.

Seven of the models (also Gregory, 1993; Bryan, 1996) show a minimum of sea level rise in the circumpolar Southern Ocean south of 60°S. This occurs despite the fact that the Southern Ocean is a region of pronounced heat uptake (e.g., Murphy and Mitchell, 1995; Hirst *et al.*, 1996). The low thermal expansion coefficient at the cold temperatures of the high southern latitudes, changes in wind patterns and transport of the heat taken up to lower latitudes are all possible explanations.

Bryan (1996) draws attention to a dipole pattern in sea level change in the north-west Atlantic; there is a reduced rise south of the Gulf Stream extension and enhanced rise to the north, which corresponds to a weakening of the sea surface gradient across the current. This would be consistent with a weakening of the upper

branch of the North Atlantic circulation, which is a response to greenhouse warming observed in many AOGCM experiments (e.g., Manabe and Stouffer, 1993, 1994; Hirst, 1998). This can be seen in all the models considered here except ECHAM4/OPYC3, in which the Atlantic thermohaline circulation does not weaken (Latif and Roeckner, 2000).

Local land movements, both isostatic and tectonic (Sections 11.2.4.1, 11.2.6), will continue in the 21st century at rates which are unaffected by climate change, and should be added to the regional variation described in this section. On account of the increased eustatic rate of rise in the 21st century (Section 11.5.1) it can be expected that by 2100 many regions currently experiencing relative sea level fall owing to isostatic rebound will instead have a rising relative sea level.

All the global models discussed here have a spatial resolution of 1 to 3°. To obtain information about mean sea level changes at higher resolution is currently not practical; a regional model such as that of Kauker (1998) would be needed.

11.5.3 Implications for Coastal Regions

To determine the practical consequences of projections of global sea level rise in particular coastal regions, it is necessary to understand the various components leading to relative sea level changes. These components include local land movements, global eustatic sea level rise, any spatial variability from that global average, local meteorological changes and changes in the frequency of extreme events.

11.5.3.1 Mean sea level

Titus and Narayanan (1996) propose a simple method for computing local projections of mean sea level rise given historical observations at a site and projections of global average sea level (such as Figure 11.12). To allow for local land movements and our current inability to model sea level change accurately (Section 11.4), they propose linearly extrapolating the historical record and adding to this a globally averaged projection. However, they point out that to avoid double counting, it is necessary to correct the global projection for the corresponding modelled trend of sea level rise during the period of the historical observations. Caution is required in applying this method directly to the projections of this chapter for several reasons. First, current model projections indicate substantial spatial variability in sea level rise. This variability has a standard deviation of up to 0.1 m by 2100; some locations experience a sea level rise of more than twice the global-average thermal expansion, while others may have a fall in sea level (Section 11.5.2; Table 11.15). Second, there are uncertainties in the accuracy of the trend from the historical record and in modelling of past sea level changes (Sections 11.3.2.1 and 11.4). Third, as well as changes in mean sea level there may be changes in the local meteorological regime resulting in modified storm surge statistics (Section 11.5.3.2). If the method of Titus and Narayanan is not applied, it is nonetheless important to recognise that in all models and scenarios the rate of local sea level rise in the 21st century is projected to be greater than in the 20th century at the great majority of coastal locations.

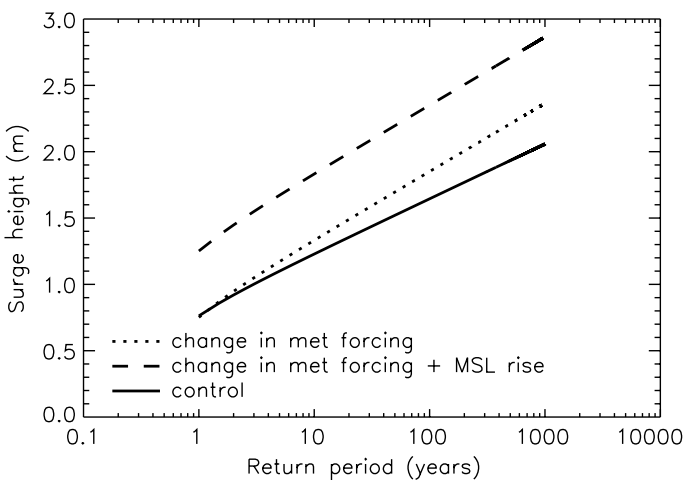


Figure 11.14: Frequency of extreme water level, expressed as return period, from a storm surge model for present day conditions (control) and the projected climate around 2100 for Immingham on the east coast of England, showing changes resulting from mean sea level rise and changes in meteorological forcing. The water level is relative to the sum of present day mean sea level and the tide at the time of the surge. (From Lowe *et al.*, 2001.)

11.5.3.2 Extremes of sea level: storm surges and waves

The probability of flood risk in coastal areas is generally expressed in terms of extreme sea level distributions. Such distributions are usually computed from observed annual maximum sea levels from several decades of tide gauge data, or from numerical models. While such distributions are readily available for many locations, a worldwide set has never been computed to common standards for studies of impacts of global sea level change.

Changes in the highest sea levels at a given locality could result mainly from two effects. First, if mean sea level rises, the present extreme levels will be attained more frequently, all else being equal. This may imply a significant increase in the area threatened with inundation (e.g., Hubbert and McInnes, 1999) and an increased risk within the existing flood plain. The effect can be estimated from a knowledge of the present day frequency of occurrence of extreme levels (e.g., Flather and Khandker, 1993; Lowe *et al.*, 2001; Figure 11.14).

Second, changes in storm surge heights would result from alterations to the occurrence of strong winds and low pressures. At low-latitude locations, such as the Bay of Bengal, northern Australia and the southern USA, tropical cyclones are the primary cause of storm surges. Changes in frequency and intensity of tropical cyclones could result from alterations to sea surface temperature, large-scale atmospheric circulation and the characteristics of ENSO (Pittock *et al.*, 1996) but no consensus has yet emerged (see Box 10.2). In other places, such as southern Australia and north-west Europe, storm surges are associated with mid-latitude low-pressure systems. For instance, Hubbert and McInnes (1999) showed that increasing the wind speeds in historical storm surge events associated with the passage of cold fronts could lead to greater flooding in Port Phillip Bay, Victoria, Australia. Changes in extratropical storms also cannot be predicted with confidence (Section 9.3.6.3).

Several studies have attempted to quantify the consequences of changes in storm climatology for the north-

west European continental shelf using regional models of the atmosphere and ocean. Using five-year integrations of the ECHAM T106 model for present and doubled CO₂, Von Storch and Reichardt (1997) and Flather and Smith (1998) did not find any significant changes in extreme events compared with the variability of the control climate (see also WASA Group, 1998). However, Langenberg *et al.* (1999) reported increases of 0.05 to 0.10 m in five-winter-mean high-water levels around all North Sea coasts, judged to be significant compared with observed natural variability. Lowe *et al.* (2001) undertook a similar study using multi-decadal integrations of the Hadley Centre regional climate model for the present climate and the end of the 21st century (Figure 11.14), finding statistically significant changes of up to 0.2 m in five-year extremes in the English Channel. Differences between these various results relate to the length of model integration and to systematic uncertainty in the modelling of both the atmospheric forcing and the ocean response.

Changes in wind forcing could result in changes to wave heights, but with the short integrations available, the WASA Group (Rider *et al.*, 1996) were not able to identify any significant changes for the North Atlantic and North Sea for a doubling of CO₂. Günther *et al.* (1998) noted that changes in future wave climate were similar to patterns of past variation.

11.5.4 Longer Term Changes

Anthropogenic emissions beyond 2100 are very uncertain, and we can only indicate a range of possibilities for sea level change. On the time-scale of centuries, thermal expansion and ice sheet changes are likely to be the most important processes.

11.5.4.1 Thermal expansion

The most important conclusion for thermal expansion is that it would continue to raise sea level for many centuries after stabilisation of greenhouse gas concentrations, so that its eventual contribution would be much larger than at the time of stabilisation.

Table 11.16: Sea level rise due to thermal expansion in 2×CO₂ and 4×CO₂ experiments. See Chapter 8, Table 8.1 for further details of models.

	Sea level rise (m) in 2×CO ₂ experiment		$\Delta h_2/\Delta h_1$	Final sea level rise (m)	
	at 2×CO ₂ (Δh_1)	500 yr later (Δh_2)		2×CO ₂ experiment	4×CO ₂ experiment
CLIMBER	0.16	0.67	4.2	0.78	1.44
ECHAM3/LSG	0.06	0.57	9.2	1.53 ^a	2.56 ^a
GFDL_R15_a	0.13	1.10	8.5	1.96	3.46
HadCM2	0.09	0.70	7.8	—	—
BERN2D GM	0.23	1.12	4.9	1.93	3.73
BERN2D HOR	0.22	0.92	4.2	1.28	4.30
UVic GM	0.11	0.44	3.9	0.53	1.24
UVic H	0.13	0.71	5.6	1.19	2.62
UVic HBL	0.10	0.44	4.3	0.65	1.78

^a Estimated from the ECHAM3/LSG experiments by fitting the time-series with exponential impulse response functions (Voss and Mikolajewicz, 2001).

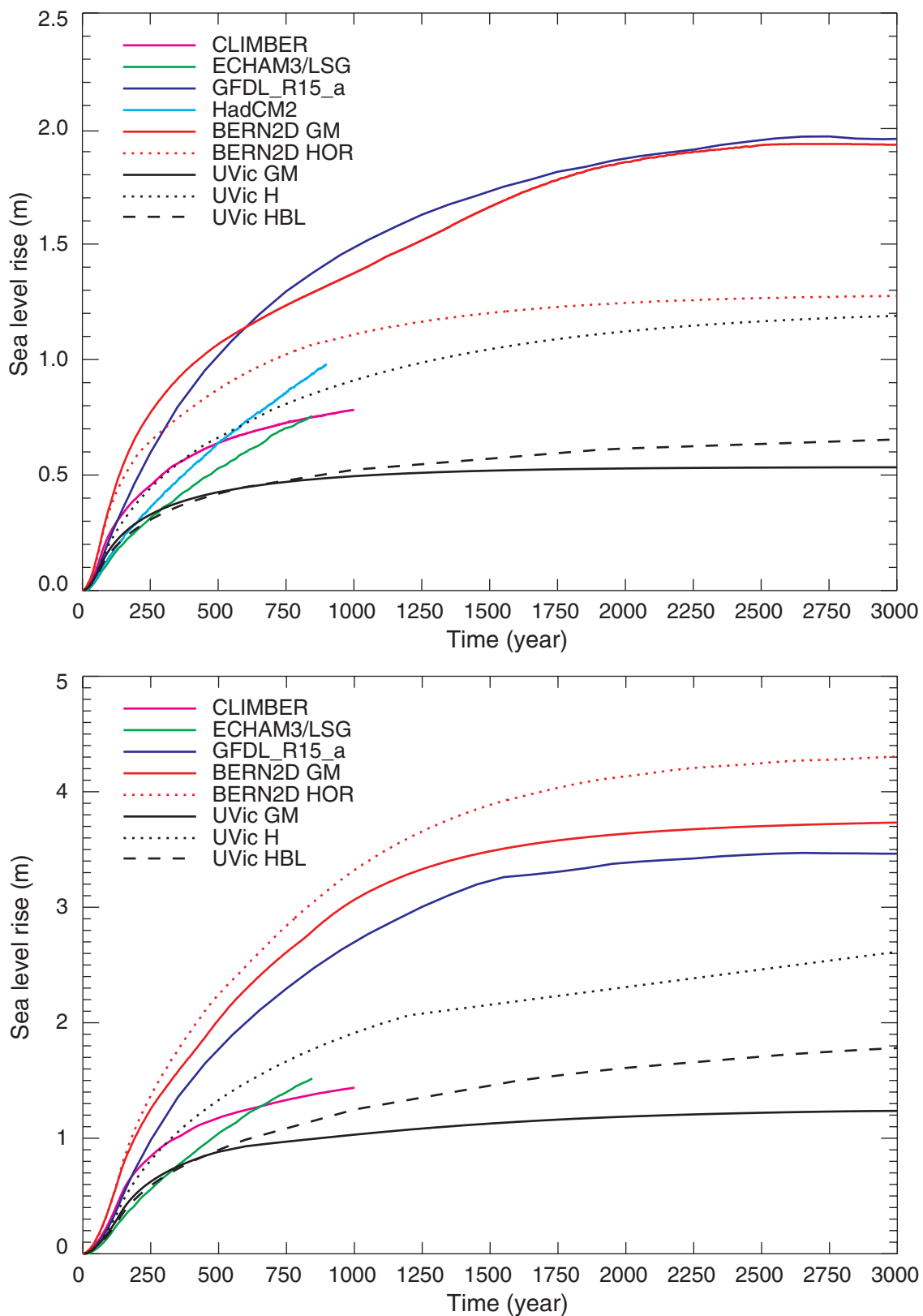


Figure 11.15: Global average sea level rise from thermal expansion in model experiments with CO₂ (a) increasing at 1%/yr for 70 years and then held constant at 2× its initial (preindustrial) concentration; (b) increasing at 1%/yr for 140 years and then held constant at 4× its initial (preindustrial) concentration.

A number of investigations have aimed to quantify this delayed but inevitable consequence of the enhanced greenhouse effect, using a simple scenario in which carbon dioxide concentration increases rapidly (at 1%/yr, not intended as a realistic historical scenario) up to double or four times its initial value (referred to as 2 \times CO₂ and 4 \times CO₂), and thereafter remains constant. (2 \times CO₂ is about 540 ppm by volume, and 4 \times CO₂ about 1080 ppm.) Long experiments of this kind have been run with three AOGCMs (Chapter 8, Table 8.1): GFDL (Manabe and Stouffer, 1994; Stouffer and Manabe, 1999), ECHAM3/LSG (Voss and Mikolajewicz, 2001) and HadCM2 (Senior and Mitchell, 2000), but owing to the computational requirement, only one of these (GFDL) has been continued until a steady state is reached. Models of intermediate complexity (Chapter 8, Table 8.1) have also been employed: CLIMBER, BERN2D and UVic. These models have a less detailed representation of some important processes, but are less expensive to run for millennia.

Thermal expansion could be greater in one model than another either because the surface warming is larger, or because the warming penetrates more deeply (Figure 11.15, Table 11.16; the suffixes to the BERN2D and UVic model names indicate versions of the models with different parametrizations of heat transport processes). For instance, UVic H and UVic GM show markedly different expansion, although they have similar surface warming (Weaver and Wiebe, 1999). The 4 \times CO₂ experiment with each model generally has around twice the expansion of the 2 \times CO₂ experiment, but the BERN2D HOR 4 \times CO₂ experiment has more than three times, because the Atlantic thermohaline circulation collapses, permitting greater warming and adding about 0.5 m to thermal expansion (Knutti and Stocker, 2000). (See also Section 9.3.4.4.) In all the models reported here, a

vertical temperature gradient is maintained, although in some cases weakened. If the whole depth of the ocean warmed to match the surface temperature, thermal expansion would be considerably larger.

The long time-scale (of the order of 1,000 years) on which thermal expansion approaches its eventual level is characteristic of the weak diffusion and slow circulation processes that transport heat to the deep ocean. On account of the time-scale, the thermal expansion in the 2 \times CO₂ experiments after 500 years of constant CO₂ is 4 to 9 times greater than at the time when the concentration stabilises. Even by this time, it may only have reached half of its eventual level, which models suggest may lie within a range of 0.5 to 2.0 m for 2 \times CO₂ and 1 to 4 m for 4 \times CO₂. For the first 1,000 years, the 4 \times CO₂ models give 1 to 3 m.

11.5.4.2 Glaciers and ice caps

Melting of all existing glaciers and ice caps would raise sea level by 0.5 m (Table 11.3). For 1990 to 2100 in IS92a, the projected loss from land-ice outside Greenland and Antarctica is 0.05 to 0.11 m (Table 11.12). Further contraction of glacier area and retreat to high altitude will restrict ablation, so we cannot use the 21st century rates to deduce that there is a time by which all glacier mass will have disappeared. However, the loss of a substantial fraction of the total glacier mass is likely. The viability of any particular glacier or ice cap will depend on whether there remains any part of it, at high altitude, where ablation does not exceed accumulation over the annual cycle. Areas which are currently marginally glaciated are most likely to become ice-free.

11.5.4.3 Greenland and Antarctic ice sheets

Several modelling studies have been conducted for time periods of several centuries to millennia (Van de Wal and Oerlemans, 1997; Warner and Budd, 1998; Huybrechts and De Wolde, 1999; Greve, 2000). A main conclusion is that the ice sheets would continue to react to the imposed climatic change during the next millennium, even if the warming stabilised early in the 22nd century. Whereas Greenland and Antarctica may largely counteract one another for most of the 21st century (Section 11.2.3.4), this situation would no longer hold after that and their combined contribution would be a rise in sea level.

Greenland ice sheet

The Greenland ice sheet is the most vulnerable to climatic warming. As the temperature rises, ablation will increase. For moderate warming, the ice sheet can be retained with reduced extent and modified shape if this results in less ablation and/or a decrease in the rate of ice discharge into the sea, each of which currently account for about half the accumulation (Section 11.2.3). The discharge can be reduced by thinning of the ice sheet near the grounding line. Ablation can be reduced by a change in the area-elevation distribution. However, once ablation has increased enough to equal accumulation, the ice sheet cannot survive, since discharge cannot be less than zero. This situation occurs for an annual-average warming of 2.7°C for the present ice-sheet topography, and for a slightly larger warming for a retreating ice sheet (Huybrechts *et al.*, 1991; see also Oerlemans,

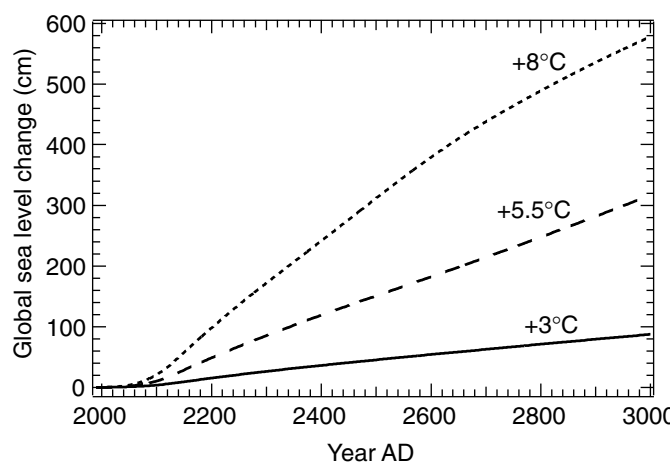


Figure 11.16: Response of the Greenland Ice Sheet to three climatic warming scenarios during the third millennium expressed in equivalent changes of global sea level. The curve labels refer to the mean annual temperature rise over Greenland by 3000 AD as predicted by a two-dimensional climate and ocean model forced by greenhouse gas concentration rises until 2130 AD and kept constant after that. (From Huybrechts and De Wolde, 1999.) Note that projected temperatures over Greenland are generally greater than globally averaged temperatures (by a factor of 1.2 to 3.1 for the range of AOGCMs used in this chapter). See Table 11.13 and Chapter 9, Fig. 9.10c.

1991; Van de Wal and Oerlemans, 1994). Models show that under these circumstances the Greenland ice sheet eventually disappears, except for residual glaciers at high altitudes. By using the AOGCM ratios of the Greenland temperature to the global average (Table 11.13) with the results of the calibrated simple model (Section 11.5.1.2 and Chapter 9, Section 9.3.3) we project increases in Greenland temperatures by 2100 of more than 2.7°C for nearly all combinations of SRES scenarios and AOGCMs. The maximum by 2100 is 9°C.

Huybrechts and De Wolde (1999) (Figure 11.16) (see also Letreguilly *et al.*, 1991) find the Greenland ice sheet contributes about 3 m of sea level rise equivalent over a thousand years under their mid-range scenario, in which the Greenland temperature change passes through 4°C in 2100 before stabilising at 5.5°C after 2130. Taking into account the high-latitude amplification of warming, this temperature change is consistent with mid-range stabilisation scenarios (Chapter 9, Section 9.3.3.1 and Figure 9.17(b)). For a warming of 8°C, they calculate a contribution of about 6 m. Their experiments take into account the effect of concomitant increases in precipitation (which reduces sensitivity) but also of the precipitation fraction falling as rain (which strongly enhances sensitivity for the larger temperature increases). Disregarding the effects of accumulation changes and rainfall, Greve (2000) reports that loss of mass would occur at a rate giving a sea level rise of between 1 mm/yr for a year-round temperature perturbation of 3°C to as much as 7 mm/yr for a sustained warming of 12°C, the latter being an extreme scenario in which the ice sheet would be largely eliminated within 1,000 years.

West Antarctic ice sheet

The WAIS contains enough ice to raise sea level by 6 m. It has received particular attention because it has been the most dynamic part of the Antarctic ice sheet in the recent geological past, and because most of it is grounded below sea level – a situation that according to models proposed in the 1970s could lead to flow instabilities and rapid ice discharge into the ocean when the surrounding ice shelves are weakened (Thomas, 1973; Weertman, 1974; Thomas *et al.*, 1979). Geological evidence suggests that WAIS may have been smaller than today at least once during the last million years (Scherer *et al.*, 1998). The potential of WAIS to collapse in response to future climate change is still a subject of debate and controversy.

The discharge of the WAIS is dominated by fast-flowing ice streams, dynamically constrained at four boundaries: the transition zone where grounded ice joins the floating ice shelf (Van der Veen, 1985; Herterich, 1987), the interface of ice with bedrock that is lubricated by sediment and water (Blankenship *et al.*, 1986; Anandakrishnan *et al.*, 1998; Bell *et al.*, 1998), the shear zone where fast-moving ice meets relatively static ice at the transverse margins of ice streams (Echelmeyer *et al.*, 1994; Jacobson and Raymond, 1998), and the ice-stream onset regions where slowly flowing inland ice accelerates into the ice streams. Mechanisms have been proposed for dynamic changes at each of these boundaries.

Early studies emphasised the role of the ice shelf boundary in ice discharge by introducing the concept of a “back-stress”

believed to buttress the grounded ice sheet and prevent it from collapsing. Recent work, however, both modelling and measurement, places greater emphasis on the other ice stream boundaries. Force balance studies on Ice Stream B show no evidence of stresses generated by the Ross ice shelf, and mechanical control emanates almost entirely from the lateral margins (Whillans and Van der Veen, 1997). If confirmed for the other Siple Coast ice streams, this suggests ice stream flow fields to be little influenced by conditions in the ice shelf, similar to the situation elsewhere at the Antarctic margin (Mayer and Huybrechts, 1999).

Nonetheless, there is a considerable body of evidence for ice stream variability, and the above analyses may not apply to dynamic situations involving large thinning or grounding line change. Ice Stream C largely stopped about a century ago (Retzlaff and Bentley, 1993) and Ice Stream B decelerated by 20% within a decade (Stephenson and Bindschadler, 1988). The mechanisms for these oscillations are not well understood and have been ascribed to processes such as basal water diversion to a neighbouring ice stream (Anandakrishnan and Alley, 1997) or thermomechanical interactions between competing catchment areas (Payne, 1998). Despite ice stream variability in the latter model on the millennial time-scale, the overall volume of the WAIS hardly changed, supporting the suggestion that ice streams may act to remove the imbalance of individual drainage basins and to stabilise rather than destabilise WAIS (Hindmarsh, 1993).

The WAIS was much larger during the LGM and has probably lost up to two thirds of its volume since then (Bindschadler, 1998). The largest losses have been from grounding line retreat below the present WAIS ice shelves (Ross and Filchner-Ronne), most likely as a gradual response to rising sea levels subsequent to melting of the Northern Hemisphere ice sheets (Ingolfsson *et al.*, 1998). Local imbalances, both positive and negative, are presently occurring (Shabtaie and Bentley, 1987; Whillans and Bindschadler, 1988; Bindschadler and Vornberger, 1998; Hamilton *et al.*, 1998; Rignot, 1998a,b; Wingham, *et al.*, 1998), but there is no conclusive observational evidence (from monitoring of surface elevation, see Section 11.2.3.2) that WAIS overall is making a significant contribution to global average sea level change (Bentley, 1997, 1998a,b; Bindschadler, 1998; Oppenheimer, 1998; Wingham *et al.* 1998). Conway *et al.* (1999) suggest that grounding line retreat since the LGM may still be ongoing, giving an average rate of recession corresponding to a rate of sea level rise of 0.9 mm/yr (Bindschadler, 1998). If projected into the future, this would imply disappearance of WAIS in 4,000 to 7,000 years (Bindschadler, 1998). However, geological estimates of ocean volume increase over the last 6,000 years place an upper limit of about half this amount on global sea level rise (Section 11.3.1).

Recent spectacular break-ups of the Larsen ice shelves in the Antarctic Peninsula (Vaughan and Doake, 1996; Doake *et al.*, 1998) demonstrate the existence of an abrupt thermal limit on ice shelf viability associated with regional atmospheric warming (Skvarca *et al.*, 1998). However, the WAIS ice shelves are not immediately threatened by this mechanism, which would require a further warming of 10°C before the -5°C mean annual isotherm reached their ice fronts (Vaughan and Doake, 1996). Although

atmospheric warming would increase the rate of deformation of the ice, causing the ice shelf to thin, response time-scales are of the order of several hundred years (Rommelaere and MacAyeal, 1997; Huybrechts and de Wolde, 1999).

In view of these considerations, it is now widely agreed that major loss of grounded ice, and accelerated sea level rise, is very unlikely during the 21st century. An interdisciplinary panel of international experts applying the techniques of risk assessment to the future evolution of WAIS concluded that there is a 98% chance that WAIS will not collapse in the next 100 years, defined as a change that contributes at least 10 mm/yr to global sea level change (Vaughan and Spouge, 2001). The probability of a contribution to sea level (exceeding 0.5 m) by the year 2100 was 5%. These results are broadly consistent with an earlier assessment by Titus and Narayanan (1996) based on a US-only panel, who found a 5% chance of a 0.16 m contribution and 1% chance of a 0.3 m contribution to sea level rise from WAIS by 2100. We note that Vaughan and Spouge also report a probability of 5% for WAIS giving a sea level fall exceeding 0.4 m within the same time frame, while Titus and Narayanan give 0.18 m.

Nonetheless, on a longer time-scale, changes in ice dynamics could result in significantly increased outflow of ice into the ice shelves and a grounding line retreat. Large-scale models show both of these phenomena to be sensitive to basal melting below the ice shelves (Warner and Budd, 1998; Huybrechts and De Wolde, 1999). Model studies do not agree on the sensitivity of the basal melting to an oceanic warming: for instance, one shows a quadrupling of the basal melting rate below the Amery ice shelf in East Antarctica for an adjacent sea warming of 1°C (Williams *et al.*, 1998), while another claims that warmer sea temperatures would reduce melting rates below the Ronne-Filchner ice shelves through alteration to sea-ice formation and the thermohaline circulation (Nicholls, 1997). Changes in open ocean circulation may also play a role. Warner and Budd (1998) suggest that even for moderate climatic warmings of a few degrees, a large increase in bottom melting of 5 m/yr becomes the dominant factor in the longer-term response of the Antarctic ice sheet. In their model, this causes the demise of WAIS ice shelves in a few hundred years and would float a large part of the WAIS (and marine portions of East Antarctica) after 1,000 years. Predicted rates of sea level rise are between 1.5 and 3.0 mm/yr depending on whether accumulation rates increase together with the warming. Allowing for runoff in addition to increased accumulation, Huybrechts and De Wolde (1999) find a maximum Antarctic contribution to global sea level rise of 2.5 mm/yr for an extreme scenario involving a warming of 8°C and a bottom melting rate of 10 m/yr. These figures are upper limits based on results currently available from numerical models, which do not resolve ice streams explicitly and which may not adequately predict the effect of ice shelf thinning on grounding line retreat owing to physical uncertainties.

Based on a wide-ranging review, Oppenheimer (1998) argues that WAIS could disintegrate within five to seven centuries following a warming of only a few degrees. Such a collapse implies a rate of sea level rise of 10 mm/yr and an average speed-up of the total outflow by at least a factor of 10 (Bentley, 1997, 1998a,b). However, the majority opinion of a recent expert panel reported by Vaughan and Spouge (2001) is that such outflow

rates are not attainable. It is, therefore, also plausible that WAIS may not make a significant contribution to sea level rise over time-scales less than a millennium. Vaughan and Spouge (2001) attribute a 50% probability to the latter scenario, but retained an equally large probability that the sea level rise will be larger than 2 mm/yr after 1,000 years, emphasising the inadequacy of our current understanding of the dynamics of WAIS, especially for predictions on the longer time-scales.

Independent of bottom melting below the ice shelves and the possibility of an ice-dynamic instability, surface melting sets an upper temperature limit on the viability of the Antarctic ice sheet, because runoff would eventually become the dominant wastage mechanism (as would be the case for Greenland in a climate several degrees warmer than today). For warmings of more than 10°C, simple runoff models predict that an ablation zone would develop around the Antarctic coast, making the mass balance at sea level sufficiently negative that the grounded ice would no longer be able to feed an ice shelf. Also the WAIS ice shelves would disintegrate to near to their inland limits as summer temperatures rise above the thermal limit of ice shelf viability believed to be responsible for the recent collapse of ice shelves at the northern tip of the Antarctic Peninsula. Disintegration of WAIS would in that case result, because the WAIS cannot retreat to higher ground once its margins are subjected to surface melting and begin to recede (Huybrechts, 1994). Depending on the strength of the warming, such a disintegration would take at least a few millennia.

East Antarctic ice sheet

Thresholds for disintegration of the East Antarctic ice sheet by surface melting involve warmings above 20°C, a situation that has not occurred for at least the last 15 million years (Barker *et al.*, 1999), and which is far more than thought possible under any scenario of climatic change currently under consideration. In that case, the ice sheet would decay over a period of at least 10,000 years. However, the recent inference of complex flow patterns in the interior of the East Antarctic ice sheet demonstrates the existence of ice-streaming features penetrating far inland, which may be indicative of a more dynamic regime than believed so far (Bamber *et al.*, 2000; Huybrechts *et al.*, 2000).

11.6 Reducing the Uncertainties in Future Estimates of Sea Level Change

It is valuable to note that the reduction in the uncertainty of estimation of the long-term ice sheet imbalance reported in Sections 11.3.1 and 11.4 came from indirect constraints and the synthesis of information of different types. Such syntheses offer promise for further progress.

11.6.1 Observations of Current Rates of Global-averaged and Regional Sea Level Change

Sections 11.3.2.1 and 11.4 reveal significant uncertainty in the analysis of 20th century sea level change. Also, we have little knowledge of the regional pattern of sea level change. Observational determination of such a pattern would be a

powerful test of the coupled models required for projections of globally averaged and regional sea level rise. Requirements for reducing uncertainties include:

- A global tide gauge network (the ‘GLOSS Core Network’) (IOC, 1997) for measuring relative change.
- A programme of measurements of vertical land movements at gauge sites by means of GPS (Global Positioning System), DORIS Beacons and/or absolute gravity meters (Neilan *et al.*, 1998).
- Improved models of postglacial rebound.
- A reanalysis of the historical record, including allowing for the impact of variable atmospheric forcing.
- A subset of mostly island tide gauge stations devoted to ongoing calibration of altimetric sea level measurements (Mitchum, 1998).
- An ongoing high-quality (TOPEX/POSEIDON class) satellite radar altimeter mission (Koblinsky *et al.*, 1992) and careful control of biases within a mission and between missions.
- Space gravity missions to estimate the absolute sea surface topography (Balmino *et al.*, 1996, 1999) and its temporal changes, to separate thermal expansion from an increase in ocean mass from melting of glaciers and ice sheets (NASA, 1996, NRC, 1997) and changes in terrestrial storage.

For assessment of possible changes to the severity of storm surges, analyses of historical storm surge data in conjunction with meteorological analyses are needed for the world’s coastlines, including especially vulnerable regions.

11.6.2 Ocean Processes

Requirements for improved projections of ocean thermal expansion include:

- Global estimates of ocean thermal expansion through analysis of the historical data archive of ocean observations and a programme of new observations, including profiling floats measuring temperature and salinity and limited sets of full-depth repeat oceanographic sections and time-series stations.
- Testing of the ability of AOGCMs to reproduce the observed three-dimensional and time-varying patterns of ocean thermal expansion.
- An active programme of ocean and atmosphere model improvement, with a particular focus on the representation of processes which transport heat into and within the interior of the ocean.

11.6.3 Glaciers and Ice Caps

Requirements for improved projections of glacier contributions include (see also Haeberli *et al.*, 1998):

- A strategy of worldwide glacier monitoring, including the application of remote sensing techniques (laser altimetry, aerial photography, high-resolution satellite visible and infrared imagery e.g. from ASTER and Landsat).
- A limited number of detailed and long-term mass balance measurements on glaciers in different climatic regions of the world, with an emphasis on winter and summer balances in order to provide a more direct link with meteorological observations.

- Development of energy balance and dynamical models for more detailed quantitative analysis of glacier geometry changes with respect to mass balance and climate change.
- Glacier inventory data to determine the distribution of glacier parameters such as area and area-altitude relations, so that mass balance, glacier dynamics and runoff/sea level rise models can be more realistically framed.

11.6.4 Greenland and Antarctic Ice Sheets

- Continued observations with satellite altimeters, including the upcoming satellite laser altimeter on ICESat and the radar interferometer on CRYOSAT. Measurements should be continued for at least 15 years (with intercalibration between missions) to establish the climate sensitivities of the mass balance and decadal-scale trends.
- Satellite radar altimetry and synthetic aperture radar interferometry (ERS-1, ERS-2 and Radarsat) for detailed topography, changes in ice sheet volume and surface velocity of the ice sheets (Mohr *et al.*, 1998; Joughin *et al.*, 1999), as well as short-term variability in their flow (Joughin *et al.*, 1996a,b) and grounding line position (Rignot, 1998a,b,c).
- Determination of the Earth’s time-variant gravity field by the Gravity Recovery and Climate Experiment (GRACE) satellite flown concurrently with ICESat to provide an additional constraint on the contemporary mass imbalances (Bentley and Wahr, 1998). This could provide estimates of sea level change to an accuracy of ± 0.35 mm/yr.
- Geological observations of sea level change during recent millennia combined with improved postglacial rebound models and palaeoclimatic and palaeoglaciological studies to learn what changes have occurred in the past.
- Further analysis of Earth rotational parameters in combination with sea level measurements.
- Improved estimates of surface mass balance (including its spatial and temporal variability) from *in situ* observations, accumulation rates inferred from atmospheric moisture budgets and improved estimates of the rate of iceberg calving and the melt-water flux.
- Improved calculation of the surface mass balance within ice sheet models or by atmospheric models, with attention to modelling of changes in sea-ice concentration because of the consequent effect on moisture transports and accumulation.
- Improved understanding and modelling of the dynamics of ice sheets, ice streams and ice shelves (requiring combined studies using glaciological, oceanographic and satellite observations), including the physics of iceberg calving.

11.6.5 Surface and Ground Water Storage

Surface and ground water storage changes are thought to be having a significant impact on sea level, but their contribution is very uncertain (Table 11.10, Figure 11.9), and could be either positive or negative. They may become more important in the future, as a result of changes related not only to climate, but also to societal decisions that are beyond the scope of this scientific assessment. There are several general issues in climate-related aspects:

- A more thorough investigative search of historical records could provide addition information on ground water mining, and storage in reservoirs.
- Accurate satellite measurements of variations in the Earth's gravity (Herring, 1998) to detect changes in land water storage due to water-table variations and impoundments.
- A better understanding of seepage losses beneath reservoirs and in irrigation is required.
- A unified systems approach is needed to trace the path of water more accurately through the atmosphere, hydrologic, and biosphere sub-systems, and to account for various feedbacks (including the use of GCMs and improved hydrologic models).
- Satellite remote sensing offers useful technology for monitoring the global hydrologic budget. A cumulative volume estimate for the many small reservoirs might be possible using high-resolution radar data, targeted ground studies and a classification of land use classes from satellite data and also of changes in deforestation and other land-use transformations (Koster *et al.*, 1999).

11.6.6 Summary

Sea level change involves many components of the climate system and thus requires a broad range of research activities. A more detailed discussion of the requirements is given in the report of the recent IGBP/GAIM Workshop on sea level changes (Sahagian and Zerbini, 1999). We recognise that it is important to assign probabilities to projections, but this requires a more critical and quantitative assessment of model uncertainties than is possible at present.

Appendix 11.1: Methods for projections of global-average sea level rise

This Appendix describes the methods used in this report to make sea level rise projections for the SRES scenarios for the 21st century. The results are discussed in Section 11.5.1.2 and shown in Figure 11.12 and Appendix II.

Global-average sea-level rise $\Delta h(t)$ is a function of time t and is expressed relative to the level in 1990. It comprises several components, which are all zero at 1990:

$$\Delta h(t) = X(t) + g(t) + G(t) + A(t) + I(t) + p(t) + s(t)$$

The components are sea-level rise due to:

X thermal expansion.

g loss of mass of glaciers and ice caps.

G loss of mass of the Greenland ice sheet due to projected and recent climate change.

A loss of mass of the Antarctic ice sheet due to projected and recent climate change.

I loss of mass of the Greenland and Antarctic ice sheets due to the ongoing adjustment to past climate change.

p runoff from thawing of permafrost.

s deposition of sediment on the ocean floor.

The components X , g , G and A are estimated for each of 35 SRES scenarios using the projections of an upwelling-diffusion energy-balance (UD/EB) model calibrated separately for each of seven AOGCMs (Appendix 9.1).

Thermal expansion X is obtained directly from the thermal expansion $X_m(t)$ projected by the UD/EB model:

$$X(t) = X_m(t) - X_m(1990)$$

No uncertainty is included in this term, because the uncertainty is sufficiently represented by the use of a range of AOGCMs.

The term g from glaciers and ice caps is estimated using the global average temperature change $T_m(t)$ projected by the UD/EB model. First, we obtain the loss of mass g_u with respect to the glacier steady state without taking contraction of glacier area into account.

$$g_u(t) = g_{1990} + \int_{1990}^t (T_{1990} + \Delta T_b + T_m(t') - T_m(1990)) \frac{\partial B_g}{\partial T_g} dt'$$

where g_{1990} is the sea-level rise from glaciers and ice caps up to 1990 calculated from AOGCM results without contraction of glacier area, T_{1990} is the AOGCM global average temperature change at 1990 with respect to the climate of the late 19th century, $\Delta T_b = 0.15$ K the difference in the global average temperature between the late 19th century and the glacier steady state (see 11.5.1.1) and $\partial B_g / \partial T_g$ is the sensitivity of global glacier mass balance for constant glacier area to global-average temperature change, expressed as sea level equivalent (from Table 11.11). Second, we estimate the loss of mass g_s with respect to the glacier steady state taking into account contraction of glacier area. This is done by using an empirical relationship between the loss of mass for changing and for constant area. The relationship was obtained by a quadratic fit to the AOGCM IS92a results of Section 11.5.1.1.

$$g_s(t) = 0.934g_u(t) - 1.165g_u^2(t)$$

for g_u and g_s in metres. Third, we calculate the change since 1990.

$$g(t) = g_s(t) - g_s(1990)$$

The uncertainty $\delta g(t)$ on this term is calculated assuming an uncertainty of $\pm 40\%$ (standard deviation) in the mass balance sensitivities, as discussed in Section 11.5.1.1.

$$\delta g(t) = 0.40g(t)$$

The term G from the Greenland ice sheet is calculated according to

$$G(t) = \int_{1990}^t (T_{1990} + T_m(t') - T_m(1990)) \frac{\partial B_G}{\partial T_g} dt'$$

where $\partial B_G / \partial T_g$ is the sensitivity of the Greenland mass balance to global-average temperature change, expressed as sea level equivalent (from Table 11.12). The uncertainty on this term comprises two components, as discussed in Section 11.5.1.1. The first uncertainty is a mass balance uncertainty

$$\delta G_1(t) = \int_{1990}^t (T_{1990} + T_m(t') - T_m(1990)) \frac{\Delta T_G}{\Delta T_g} \delta m_G dt'$$

where $\delta m_G = 0.05$ mm/yr/ $^{\circ}\text{C}$ and $\Delta T_G / \Delta T_g$ is the ratio of Greenland average temperature change to global average temperature change (from Table 11.12). The first uncertainty is the combination in quadrature of 0.03 mm/yr/ $^{\circ}\text{C}$ from ablation parametrization,

0.03 mm/yr/°C from high-resolution patterns, and 0.02 mm/yr/°C from precipitation changes, as discussed in section 11.5.1.1. The second uncertainty is an ice-dynamic uncertainty.

$$\delta G_2(t) = 0.1G(t)$$

The term A from the Antarctic ice sheet is calculated according to

$$A(t) = \int_{1990}^t (T_{1990} + T_m(t') - T_m(1990)) \frac{dB_A}{dT_g} dt'$$

where dB_A/dT_g is the sensitivity of the Antarctic mass balance to global-average temperature change, expressed as sea level equivalent (from Table 11.12). Ice-dynamical uncertainty for the Antarctic is not included and is discussed in Section 11.5.4.3. There is no uncertainty for ablation. Precipitation change uncertainty is calculated as discussed in Section 11.5.1.1 according to

$$\delta A(t) = \int_{1990}^t (T_{1990} + T_m(t') - T_m(1990)) \frac{\Delta T_A}{\Delta T_g} \delta m_A dt'$$

where $\delta m_A = 0.08$ mm/yr/°C and $\Delta T_A/\Delta T_g$ is the ratio of Antarctic average temperature change to global average temperature change (from Table 11.12).

The uncertainties on the above terms are combined in quadrature:

$$\delta h_v = \sqrt{(\delta g)^2 + (\delta G_1)^2 + (\delta G_2)^2 + (\delta A)^2}$$

The remaining terms are calculated assuming they contribute to sea-level rise at a constant rate, independent of AOGCM and scenario, thus:

$$I(t) = \int_{1990}^t \frac{dI}{dt'} dt' \quad p(t) = \int_{1990}^t \frac{dp}{dt'} dt' \quad s(t) = \int_{1990}^t \frac{ds}{dt'} dt'$$

The rates each have a range of uncertainty. For dI/dt , this is 0.0 to 0.5 mm/yr (Section 11.3.1, Table 11.9), for dp/dt 0 to 0.23 mm/yr (the upper bound is more precisely 25 mm divided by 110 years, section 11.2.5), for ds/dt 0 to 0.05 mm/yr (Section 11.2.6, Table 11.9). The central rates are 0.25, 0.11 and 0.025 mm/yr for the three terms. We denote I calculated at the minimum rate by I_{min} and at the maximum rate by I_{max} ; similarly for p and s . The minimum projected sea-level rise $\Delta h_{min}(t)$ for a given AOGCM and SRES scenario is given by

$$\Delta h_{min}(t) = X(t) + g(t) + G(t) + A(t) - 2\delta h_v(t) + I_{min}(t) + P_{min}(t) + s_{min}(t)$$

and the maximum is

$$\Delta h_{max}(t) = X(t) + g(t) + G(t) + A(t) + 2\delta h_v(t) + I_{max}(t) + P_{max}(t) + s_{max}(t)$$

In these formulae, δh_v has been doubled to convert from an uncertainty to a range, following Box 11.1.

Table 11.17: Parameters used in sea-level projections to simulate AOGCM results.

AOGCM	T_{1990} (°C)	g_{1990} (m)	$\partial B_g / \partial T_g$ (mm/yr/°C)	dB_G / dT_g (mm/yr/°C)	dB_A / dT_g (mm/yr/°C)	$\Delta T_G / \Delta T_g$	$\Delta T_A / \Delta T_g$
CSIRO Mk2	0.593	0.022	0.733	0.157	-0.373	2.042	1.120
CSM 1.3	0.567	0.021	0.608	0.146	-0.305	3.147	1.143
ECHAM4/OPYC3	0.780	0.027	0.637	0.029	-0.478	1.153	1.484
GFDL_R15_a	0.635	0.015	0.576	0.121	-0.177	1.879	0.799
HadCM2	0.603	0.027	0.613	0.096	-0.214	1.441	1.239
HadCM3	0.562	0.021	0.622	0.085	-0.354	1.443	1.288
DOE PCM	0.510	0.017	0.587	0.136	-0.484	2.165	1.618

References

- Allen, J.R.L.** and J.E. Rae, 1988: Vertical salt marsh accretion since the Roman period in the Severn Estuary, southwest Britain. *Marine Geology*, **83**, 225-235.
- Anandakrishnan, S.**, and R.B. Alley, 1997: Stagnation of ice stream C, West Antarctica by water piracy. *Geophys. Res. Lett.*, **24**, 265-268.
- Anandakrishnan, S.**, D.D. Blankenship, R.B. Alley, and P.L. Stoffa, 1998: Influence of subglacial geology on the position of a West Antarctic ice stream. *Nature*, **394**, 62-65.
- Anisimov, O.A.** and F.E. Nelson, 1997: Permafrost zonation and climate change in the northern hemisphere: results from transient general circulation models. *Clim. Change*, **35**, 241-258.
- Aniya, M.**, H. Sato, R. Naruse, P. Skvarca, G. Casassa, 1997: Recent glacier variations in the Southern Patagonian icefield, South America. *Arctic and Alpine Research*, **29** (1), 1-12.
- Antonioli, F.** and M. Oliverio, 1996: Holocene sea level rise recorded by a radiocarbon-dated mussel in a submerged speleotherm beneath the Mediterranean Sea. *Quat. Res.*, **45**, 241-244.
- Antonov, J.I.**, 1993: Linear trends of temperature at intermediate and deep layers of the North Atlantic and the Pacific Oceans: 1957-1981. *J. Climate*, **6**, 1928-42.
- Antonov, J.I.**, S. Levitus and T. P. Boyer, 2000: Ocean temperature and salinity impact on sea level rise during 1957-1994. *EOS Trans., AGU*, **81**, Fall Meet Suppl., Abstract, U61B-03-2000.
- Anzenhofer, T. G.**, 1998: Fully reprocessed ERS-1 altimeter data from 1992 to 1995: Feasibility of the detection of long term sea level change. *J. Geophys. Res.*, **103(C4)**, 8089-112.
- Arbic, B.K.** and B. Owens, 2001: Climatic Warming of Atlantic Intermediate Waters. *J. Climate*, in press.
- Arhan, M.**, H. Mercier, B. Bourles, and Y. Gouriou, 1998: Hydrographic sections across the Atlantic at 7°30N and 4°30S. *Deep-Sea Res., I*, **45**, 829-72.
- Bacon, S.** and D.J.T. Carter, 1991: Wave climate changes in the North Atlantic and North Sea. *Int. J. Climatol.*, **11**, 545-558.
- Bacon, S.** and D.J.T. Carter, 1993: A connection between mean wave height and atmospheric pressure gradient in the North Atlantic. *Int. J. Climatol.*, **13**, 423-436.
- Bahr, D.B.**, 1997: Global distributions of glacier properties: a stochastic scaling paradigm. *Water Resour. Res.*, **33**, 1669-1679.
- Bahr, D.B.**, M.F. Meier, and S.D. Peckham, 1997: The physical basis of glacier volume-area scaling. *J. Geophys. Res.*, **102(B9)**, 20355-20362.
- Bahr, D.B.**, W.T. Pfeffer, C. Sassolas, and M.F. Meier, 1998: Response time of glaciers as a function of size and mass balance: 1. Theory. *Journal of Geophysical Research*, **103**, 9777-9782.
- Balmino, G.**, R. Sabadini, C. Tscherning, and PL. Woodworth, 1996: Gravity Field and Steady-State Ocean Circulation Mission. Reports for assessment: the nine candidate Earth Explorer Missions. European Space Agency Report SP-1196(1). 77pp.
- Balmino, G.**, R. Rummel, P. Visser, and P. Woodworth, 1999. Gravity Field and Steady-State Ocean Circulation Mission. Reports for assessment: the four candidate Earth Explorer Core Missions. European Space Agency Report SP-1233(1). 217pp.
- Bamber, J.L.**, D.G. Vaughan, and I. Joughin, 2000: Widespread complex flow in the interior of the Antarctic ice sheet. *Science*, **287**, 1248-1250.
- Bard, E.**, B. Hamelin, M. Arnold, L.F. Montaggioni, G. Cabioch, G. Faure and F. Rougerie, 1996: Deglacial sea level record from Tahiti corals and the timing of global meltwater discharge. *Nature*, **382**, 241-244.
- Barker, P. F.**, P.J. Barrett, A.K. Cooper, and P. Huybrechts, 1999: Antarctic glacial history from numerical models and continental margin sediments. *Palaeogeography, Palaeoecology, Palaeoclimatology*, **150**, 247-267.
- Basnett, T.A.** and D.E. Parker, 1997: Development of the global mean sea level pressure data set GMSLP2. Climatic Research Technical Note No.79, Hadley Centre, Meteorological Office, Bracknell, 16pp. & Appendices.
- Bauer, A.**, 1968: Nouvelle estimation du bilan de masse de l'Inlandsis du Groenland. *Deep Sea Res.*, **14**, 13-17.
- Bell, R. E.**, D.D. Blankenship, C.A. Finn, D.L. Morse, T.A. Scambos, J.M. Brozena, and S.M. Hodge, 1998: Influence of subglacial geology on the onset of a West Antarctic ice stream from aerogeophysical observations. *Nature*, **394**, 58-62.
- Benson, C.S.**, 1962: Stratigraphic studies in the snow and firn of the Greenland Ice Sheet. *US Army SIPRE (now CRREL) Research Report*, **70**, 93.
- Bentley, C.R.**, 1997: Rapid sea level rise soon from West Antarctic ice sheet collapse? *Science*, **275**, 1077-1078.
- Bentley, C.R.**, 1998a: Ice on the fast track. *Nature*, **394**, 21-22.
- Bentley, C.R.**, 1998b: Rapid sea level rise from a West Antarctic ice-sheet collapse: a short-term perspective. *Journal of Glaciology*, **44** (146) 157-163.
- Bentley, C. R.**, and J. Wahr, 1998: Satellite gravimetry and the mass balance of the Antarctic ice sheet. *Journal of Glaciology*, **44** (147), 207-213.
- Bentley, M.J.**, 1999: Volume of Antarctic Ice at the Last Glacial Maximum, and its impact on global sea level change [Review]. *Quaternary Science Reviews*, **18**, 1569-1595.
- Bijl, W.**, R. Flather, J.G. de Ronde and T. Schmitt, 1999: Changing storminess? An analysis of long-term sea level data sets. *Clim. Res.*, **11**, 161-172.
- Bindoff, N.L.** and J.A. Church, 1992: Warming of the water column in the southwest Pacific Ocean. *Nature*, **357**, 59-62.
- Bindoff, N.L.**, and T.J. McDougall, 1994: Diagnosing Climate Change and Ocean Ventilation using Hydrographic Data. *Journal of Physical Oceanography*, **24**, 1137-1152.
- Bindoff, N.L.**, and T.J. McDougall, 2000: Decadal changes along an Indian Ocean section at 32S and their interpretation. *Journal of Physical Oceanography*, **30** (June), 1207-1222.
- Bindschadler, R.**, and P. Vornberger, 1998: Changes in the West Antarctic ice sheet since 1963 from declassified satellite photography. *Science*, **279**, 689-692.
- Bindschadler, R.**, 1998: Future of the West Antarctic Ice Sheet. *Science*, **282**, 428-429.
- Blankenship, D. D.**, C.R. Bentley, S.T. Rooney, and R.B. Alley, 1986: Seismic measurements reveal a saturated porous layer beneath an active Antarctic ice stream. *Nature*, **322**, 54-57.
- Braithwaite, R.J.**, 1995: Positive degree-day factors for ablation on the Greenland Ice Sheet studied by energy-balance modeling. *Journal of Glaciology*, **41(137)**, 153-160.
- Braithwaite, R.J.** and Y. Zhang, 1999: Modelling changes in glacier mass balance that may occur as a result of climate changes. *Geografiska Annaler*, **81A**, 489-496.
- Bromwich, D.**, 1995: Ice sheets and sea level. *Nature*, **373**, 18-19.
- Bromwich, D.H.**, R.I. Cullather and M.L. van Woert, 1998: Antarctic precipitation and its contribution to the global sea level budget. *Annals of Glaciology*, **27**, 220-226.
- Bryan, K.**, 1996: The steric component of sea level rise associated with enhanced greenhouse warming: a model study. *Climate Dynamics*, **12**, 545-55.
- Bryden, H.L.**, M.J. Griffiths, A.M. Lavin, R.C. Milliard, G. Parilla, and W.M. Smethie, 1996: Decadal changes in water mass characteristics at 24°N in the Subtropical North Atlantic Ocean. *Journal of Climate*, **9(12)**, 3162-86.
- Budd, W. F.**, and I.N. Smith, 1985: The state of balance of the Antarctic ice sheet, an updated assessment. In: *Glaciers, ice sheets and sea level: effects of a CO₂-induced climatic change*. National Academy Press, Washington, pp. 172-177.

- Budd**, W. F., P.A. Reid, and L.J. Minty, 1995: Antarctic moisture flux and net accumulation from global atmospheric analyses. *Annals of Glaciology*, **21**, 149-156.
- Budd**, W.F., B. Coutts, and R. Warner, 1998: Modelling the Antarctic and northern hemisphere ice-sheet changes with global climate through the glacial cycle. *Ann. Glaciol.* **27**, 153-160.
- Carmack**, E.C., K. Aagaard, J.H. Swift, R.W. MacDonald, F.A. McLaughlin, E.P. Jones, R.G. Perkin, J.N. Smith, K.M. Ellis, and L.R. Killius, 1997: Changes in temperature and tracer distributions within the Arctic Ocean: Results from the 1994 Arctic Ocean section. *Deep-Sea Research II*, **44**(8), 1487-502.
- Carter**, D.J.T. and L. Draper, 1988: Has the north-east Atlantic become rougher? *Nature*, **332**, 494.
- Casassa**, G., 1995: Glacier inventory in Chile: current status and recent glacier variations. *Annals of Glaciology*, **21**, 317-322.
- Cazenave**, A., P. Bonnefond, K. Dominh, and P. Schaeffer, 1997: Caspian sea level from Topex-Poseidon altimetry: Level now falling, *Geophysical Research Letters*, **24**, 881-884.
- Cazenave**, A., K. Dominh, M.C. Gennaro, and B. Ferret, 1998: Global mean sea level changes observed by Topex-Poseidon and ERS-1. *Physical Chemical Earth*, **23**, 1069-75.
- Cazenave**, A., K. Dominh, L. Soudarin, F. Ponchaut, and C. Le Provost, 1999: Sea level changes from TOPEX-POSEIDON altimetry and tide gauges and vertical crustal motions from DORIS. *Geophysical Research Letters*, **26**, 2077-2080.
- Chappell**, J., 1982: Evidence for smoothly falling sea level relative to north Queensland, Australia, during the past 6000 years. *Nature*, **302**, 406-408.
- Chappell**, J., A. Ohmura, T. Esat, M. McCulloch, J. Pandolfi, Y. Ota, and B. Pillans, 1996a: Reconciliation of late Quaternary sea levels derived from coral terraces at Huon Peninsula with deep sea oxygen isotope records. *Earth Planetary Science Letters*, **141**: 227-236.
- Chappell**, J., Y. Ota, and K. Berryman, 1996b: Late Quaternary coseismic uplift history of Huon Peninsula, Papua New Guinea, *Quaternary Science Review*, **15**, 7-22.
- Cheng**, M.K., C.K. Shum and B.D. Tapley, 1997: Determination of long-term changes in the Earth's gravity field from satellite laser ranging observations. *Journal Geophysical Research* **102**, 22,377-22,390.
- Chinn**, T.J., 1991: Glacier inventory of New Zealand. Institute of Geological and Nuclear Sciences, Dunedin, New Zealand.
- Chinn**, T.J., 1999: New Zealand glacier response to climate change of the past 2 decades. *Global and Planetary Change*, **22**, 155-168.
- Church**, J.A., J.S. Godfrey, D.R. Jackett, and T.J. McDougall, 1991: A model of sealevel rise caused by ocean thermal expansion. *Journal of Climate*, **4**(4), 438-56.
- Clausen**, H. B., N. S. Gundestrup, S. J. Johnsen, R. A. Bindschadler and H. J. Zwally, 1988: Glaciological investigations in the Crete area, Central Greenland. A search for a new drilling site. *Annals of Glaciology*, **10**, 10-15.
- Cogley**, J.G., W.P. Adams, 1998: Mass balance of glaciers other than ice sheets. *Journal of Glaciology*, **44**, 315-325.
- Conway**, H.W., B.L. Hall, G.H. Denton, A.M. Gades, and E.D. Waddington, 1999: Past and future grounding-line retreat of the West Antarctic ice sheet, *Science*, **286**, 280-286.
- Cubasch**, U., B.D. Santer, A. Hellbach, G. Hegerl, H. Höck, E. Meier-Reimer, U. Mikolajewicz, A. Stössel, R. Voss, 1994: Monte Carlo climate change forecasts with a global coupled ocean-atmosphere model. *Climate Dynamics*, **10**, 1-19.
- Cuffey**, K.M. and G.D. Clow, 1997: Temperature, accumulation, and ice sheet elevation in central Greenland through the last deglacial transition, *J. Geophys. Res.*, **102**, 26383-26396.
- Cuffey**, K.M. and S.J. Marshall, 2000: Substantial contribution to sea-level rise during the last interglacial from the Greenland ice sheet, *Nature*, **404**, 591-594.
- Curry**, R.G., M.S. McCartney, and T.M. Joyce, 1998: Oceanic transport of subpolar climate signals to mid-depth subtropical waters. *Nature*, **391**, 575-7.
- Dahl-Jensen**, D., S.J. Johnsen, C.U. Hammer, H.B. Clausen and J. Jouzel, 1993: Past accumulation rates derived from observed annual layers in the GRIP ice core from Summit, Central Greenland. In: *Ice in the climate system*, W.R. Peltier (ed), NATO ASI Series, **I 12**, pp. 517-532.
- Dansgaard**, W., S.J. Johnsen, H.B. Clausen, D. Dahl-Jensen, N.S. Gundestrup, C.U. Hammer, C.S. Hvidberg, J.P. Steffensen, A.E. Sveinbjörnsdóttir, J. Jouzel and G.C. Bond, 1993: Evidence for general instability of past climate from a 250-kyr ice-core record. *Nature*, **364**, 218-220.
- Davis**, J.L. and J.X. Mitrovica, 1996: Glacial isostatic adjustment and the anomalous tide gauge record of eastern North America. *Nature*, **379**, 331-333.
- Davis**, C. H., C.A. Kluever, and B.J. Haines, 1998: Elevation change of the southern Greenland Ice Sheet. *Science*, **279**, 2086-2088.
- Day**, J.W., W.H. Conner, R. Costanza, G.P. Kemp, and I.A. Mendelsohn, 1993: Impacts of sea level rise on coastal systems with special emphasis on the Mississippi River deltaic plain. In: *Climate and sea level change: observations, projections and implications*, R.A. Warrick, E.M. Barrow and T.M.L. Wigley (eds), Cambridge University Press, Cambridge, UK, pp 276-296.
- De Wolde**, J.R., R. Bintanja, and J. Oerlemans, 1995: On thermal expansion over the last hundred years. *Climate Dynamics*, **11**, 2881-2891.
- De Wolde**, J. R., P. Huybrechts, J. Oerlemans, and R.S.W. van de Wal, 1997: Projections of global mean sea level rise calculated with a 2D energy-balance climate model and dynamic ice sheet models. *Tellus*, **49A**, 486-502.
- Dickson**, R., J. Lazier, J. Meincke, P. Rhines and J. Swift, 1996: Long-term coordinated changes in the convective activity of the North Atlantic. *Progress in Oceanography*, **38**, 241-295.
- Dickson**, R., Nathan Bindoff, Annie Wong, Brian Arbic, Breck Owens, Shiro Imawaki and Jim Hurrell, 2001: The World during WOCE. In: *Ocean Circulation and Climate*, G. Siedler and J.A. Church (eds), Academic Press, London, pp 557-583.
- Doake**, C.S.M., H.F.J. Corr, H. Rott, P. Skvarca, and N.W. Young, 1998: Breakup and conditions for stability of the northern Larsen Ice Shelf, Antarctica. *Nature*, **391**, 778-780.
- Dolgushin**, L.D. and G.B. Osipova, 1989: *Glaciers*. Mysl, Moscow, 444pp.
- D'Onofrio**, E.E., M.M.E. Fiore and S.I. Romero, 1999: Return periods of extreme water levels estimated for some vulnerable areas of Buenos Aires. *Continental Shelf Research*, **19**, 1681-1693.
- Douglas**, B.C. 1991: Global sea level rise. *Journal of Geophysical Research*, **96**, 6981-6992.
- Douglas**, B.C., 1992: Global sea level acceleration. *Journal of Geophysical Research*, **97**, 12699-12706.
- Douglas**, B.C., 1995: Global sea level change: determination and interpretation. *Reviews of Geophysics*, Supplement, 1425-1432. (U.S. National Report to the International Union of Geodesy and Geophysics 1991-1994).
- Douglas**, B.C., 1997: Global sea rise: a redetermination. *Surveys in Geophysics*, **18**, 279-292.
- Dowdeswell**, J.A., J.O. Hagen, H. Björnsson, A.F. Glazovsky, W.D. Harrison, P. Holmlund, J. Jania, R.M. Koerner, B. Lefauconnier, C.S.L. Ommanney, and R.H. Thomas, 1997: The mass balance of circum-Arctic glaciers and recent climate change. *Quaternary Research*, **48**, 1-14.
- Drewry**, D.J. and E.M. Morris, 1992: The response of large ice sheets to climatic change. *Philosophical Transactions of the Royal Society of London B*, **338**, 235-242.
- Dyurgerov**, M.B., and M.F. Meier, 1997a: Mass balance of mountain and subpolar glaciers: a new assessment for 1961-1990. *Arctic and*

- Alpine Research*, **29**, 379-391.
- Dyurgerov**, M.B., and M.F. Meier, 1997b: Year-to-year fluctuations of global mass balance of small glaciers and their contribution to sea level changes. *Arctic and Alpine Research*, **29**, 392-402.
- Dyurgerov**, M.B., and M.F. Meier, 1999: Analysis of winter and summer glacier mass balances. *Geografiska Annaler*, **81A**, 541-554.
- Echelmeyer**, K. A., W.D. Harrison, C. Larsen, and J.E. Mitchell, 1994: The role of the margins in the dynamics of an active ice stream. *Journal of Glaciology*, **40**, 527-538.
- Ekman**, M., 1988: The world's longest continued series of sea level observations. *Pure and Applied Geophysics*, **127**, 73-77.
- Ekman**, M., 1999: Climate changes detected through the world's longest sea level series. *Global and Planetary Change*, **21**, 215-224.
- Eronen**, M., G. Glückert, O. van de Plassche, J. van der Plicht, and P. Rantala, 1995: Land uplift in the Olkiluoto-Pyhäjärvi area, southwestern Finland, during the last 8000 years, In: Nuclear Waste Commission of Finnish Power Companies, Helsinki, 26 pp.
- Fairbanks**, R.G., 1989: A 17,000-year glacio-eustatic sea level record: influence of glacial melting dates on the Younger Dryas event and deep ocean circulation. *Nature*, **342**, 637-642.
- Flather**, R.A. and H. Khandker, 1993: The storm surge problem and possible effects of sea level changes on coastal flooding in the Bay of Bengal, in *Climate and sea level change: observations, projections and implications*, R.A. Warrick, E.M. Barrow and T.M.L.Wigley (eds), Cambridge, Cambridge University Press, 424pp.
- Flather**, R.A., and J.A. Smith, 1998: First estimates of changes in extreme storm surge elevations due to the doubling of CO₂. *Global Atmospheric Ocean Systems*, **6**, 193-208.
- Fleming**, K., P. Johnston, D. Zwart, Y. Yokoyama, K. Lambeck, and J. Chappell, 1998: Refining the eustatic sea level curve since the Last Glacial Maximum using far- and intermediate-field sites, *Earth Planetary Science Letters*, **163**, 327-342.
- Flemming**, N.C. and C.O. Webb, 1986: Regional patterns of coastal tectonics and eustatic change of sea level in the Mediterranean during the last 10,000 years derived from archaeological data. *Zeitschrift für Geomorphologie*. December, Suppl - Bd62, p.1-29.
- Fox**, A. J., and A.P.R. Cooper, 1994: Measured properties of the Antarctic ice sheet derived from the SCAR Antarctic digital database. *Polar Record*, **30**, 201-206.
- Giovinetto**, M. B., and H.J. Zwally, 1995a: An assessment of the mass budgets of Antarctica and Greenland using accumulation derived from remotely sensed data in areas of dry snow. *Zeitschrift für Gletscherkunde und Glazialgeologie*, **31**, 25-37.
- Giovinetto**, M. B., and H.J. Zwally, 1995b: Annual changes in sea ice extent and of accumulation on ice sheets: implications for sea level variability. *Zeitschrift für Gletscherkunde und Glazialgeologie*, **31**, 39-49.
- Giovinetto**, M.B., and H.J. Zwally, 2000: Spatial distribution of net surface accumulation on the Antarctic ice sheet, *Annals of Glaciology*, **31**, 171-178.
- Glover**, R.W., 1999: Influence of spatial resolution and treatment of orography on GCM estimates of the surface mass balance of the Greenland Ice Sheet, *Journal of Climate*, **12**, 551-563.
- Gornitz**, V., 1995: A comparison of differences between recent and late Holocene sea level trends from eastern North America and other selected regions. *Journal of Coastal Research*, Special Issue 17, Holocene Cycles: Climate, Sea Levels and Sedimentation, C.W. Finkl, Jr. (ed.), pp.287-297.
- Gornitz**, V., 2000: Impoundment, groundwater mining, and other hydrologic transformations: impacts on global sea level rise. In *Sea level rise: history and consequences*, B.C. Douglas, M.S. Kearney and S.P. Leatherman (eds.), Academic Press, 97-119.
- Gornitz**, V., and S. Lebedeff, 1987: Global sea level changes during the past century. In: *sea level Fluctuation and Coastal Evolution*, D. Nummedal, O.H. Pilkey and J.D. Howard (eds.), Society for Economic Paleontologists and Mineralogists, pp. 3-16 (SEPM Special Publication No. 41).
- Gornitz**, V. and Solow, A. 1991: Observations of long-term tide-gauge records for indications of accelerated sea level rise. In, *Greenhouse-gas-induced climatic change: a critical appraisal of simulations and observations*, M.E. Schlesinger (ed.), Elsevier, Amsterdam, pp.347-367.
- Gornitz**, V., C. Rosenzweig, and D. Hillel, 1997: Effects of anthropogenic intervention in the land hydrological cycle on global sea level rise. *Global and Planetary Change*, **14**, 147-161.
- Gorshkov**, S.G. (Ed.), 1983: Arctic Ocean Vol. 3, In The World Ocean Atlas Series (in Russian), Pergamon, Oxford.
- Gregory**, J.M., 1993: Sea level changes under increasing atmospheric CO₂ in a transient coupled ocean-atmosphere GCM Experiment. *Journal of Climate*, **6**, 2247-62.
- Gregory**, J.M. and J.F.B. Mitchell, 1997: The climate response to CO₂ of the Hadley Centre coupled AOGCM with and without flux adjustment, *Geophys Res Lett*, **24**, 1943-1946.
- Gregory**, J.M. and J. Oerlemans, 1998: Simulated future sea level rise due to glacier melt based on regionally and seasonally resolved temperature changes. *Nature*, **391**, 474-6.
- Gregory**, J.M. and J.A. Lowe, 2000: Predictions of global and regional sea level rise using AOGCMs with and without flux adjustment. *Geophysical Research Letters*, **27**, 3069-3072.
- Gregory**, J.M., J.A. Church, G.J. Boer, K.W. Dixon, G.M. Flato, D. R. Jackett, J. A. Lowe, S. P. O'Farrell, E. Roeckner, G.L. Russell, R. J. Stouffer, M. Winter, 2001: Comparison of results from several AOGCMs for global and regional sea level change 1900-2100. *Clim. Dynam.*, in press.
- Greve**, R., 2000: On the response of the Greenland Ice Sheet to greenhouse climate change. *Climatic Change*, **46**, 289-283.
- Grotefendt**, K., K. Logemann, D. Quadfasel, and S. Ronki, 1998: Is the Arctic Ocean warming? *Journal of Geophysical Research*, **103**, 27,679-27,687.
- Günther**, H., W. Rosenthal, M. Stawarz, J.C. Carretero, M. Gomez, L. Lozano, O. Serrano, and M. Reistad, 1998: The wave climate of the Northeast Atlantic over the period 1955-1994: the WASA wave hindcast. *The Global Atmosphere and Ocean System*, **6**, 121-163.
- Haeberli**, W., M. Hoelzle and S. Suter (Eds.), 1998: Into the second century of worldwide glacier monitoring: prospects and strategies. A contribution to the International Hydrological Programme (IHP) and the Global Environment Monitoring System (GEMS). UNESCO - Studies and Reports in Hydrology, 56.
- Haines**, B.J., Y.E. Bar-Sever, 1998: Monitoring the TOPEX microwave radiometer with GPS: Stability of columnar water vapor measurements. *Geophysical Research Letters*, **25**, 3563-6.
- Hamilton**, G. S., I.M. Whillans, and P.J. Morgan, 1998: First point measurements of ice-sheet thickness change in Antarctica. *Annals of Glaciology*, **27**, 125-129.
- Harrison**, C.G.A., 1990: Long-term eustasy and epeirogeny in continents. pp.141-158 of *sea level Change*, National Research Council Surveys in Geophysics.
- Hastenrath**, S. and A. Ames 1995: Diagnosing the imbalance of Yanamarey Glacier in the Cordillera Blanca of Perú. *J. Geoph. Res.*, **100**, 5105-5112.
- Herring**, T.A., 1998: Appreciate the gravity. *Nature*, **391**, 434-435.
- Herterich**, K., 1987: On the flow within the transition zone between ice sheet and ice shelf. In: *Dynamics of the West Antarctic ice sheet*, C.J. van der Veen, and J. Oerlemans (eds.). D. Reidel, Dordrecht, pp. 185-202.
- Hindmarsh**, R. C. A., 1993: Qualitative dynamics of marine ice sheets. In: *Ice in the Climate System*, W.R. Peltier (eds.). NATO ASI Series I12, pp. 68-99.
- Hirst**, A.C., 1998: The Southern Ocean response to global warming in the CSIRO coupled ocean-atmosphere model. *Environmental Modeling*

- and Software*, **14**, 227-241.
- Hirst**, A.C., H.B. Gordon, and S.P. O'Farrell, 1996: Response of a coupled ocean-atmosphere model including oceanic eddy-induced advection to anthropogenic CO₂ increase. *Geophysical Research Letters*, **23**, 3361-3364.
- Hoffert**, M.I., A.J. Callegari and C.T. Hsieh, 1980: The role of deep sea heat storage in the secular response to climate forcing. *J. Geophys. Res.*, **85**, 6667-6679.
- Holbrook**, N.J., and N.L. Bindoff, 1997: Interannual and decadal temperature variability in the Southwest Pacific Ocean between 1955 and 1988. *Journal of Climate*, **10**, 1035-49.
- Hsieh**, W.W., and K. Bryan, 1996: Redistribution of sea level rise associated with enhanced greenhouse warming: a simple model study. *Climate Dynamics*, **12**, 535-544.
- Hubbert**, G.D., and K. McInnes, 1999: A storm surge inundation model for coastal planning and impact studies. *Journal of Coastal Research*, **15**, 168-185.
- Huybrechts**, P., and J. Oerlemans, 1990: Response of the Antarctic Ice Sheet to future greenhouse warming. *Climate Dynamics*, **5**, 93-102.
- Huybrechts**, P., 1994: Formation and disintegration of the Antarctic ice sheet. *Annals of Glaciology*, **20**, 336-340.
- Huybrechts**, P., A. Letreguilly, and N. Reeh, 1991: The Greenland Ice Sheet and greenhouse warming. *Paleogeography, Paleoceanography, Paleoclimatology, Paleoecology (Global and Planetary Change Section)*, **89**, 399-412.
- Huybrechts**, P., and J. De Wolde, 1999: The dynamic response of the Greenland and Antarctic ice sheets to multiple-century climatic warming. *Journal of Climate*, **12**, 2169-2188.
- Huybrechts**, P., and E. Le Meur, 1999: Predicted present-day evolution patterns of ice thickness and bedrock elevation over Greenland and Antarctica. *Polar Research*, **18**, 299-308.
- Huybrechts**, P., A. Abe-Ouchi, I. Marsiat, F. Pattyn, T. Payne, C. Ritz, and V. Rommelaaere, 1998: Report of the Third EISMINT Workshop on Model Intercomparison, European Science Foundation (Strasbourg), 140 p.
- Huybrechts**, P., C. Mayer, H. Oerter and F. Jung-Rothenhäusler, 1999: Climate change and sea level: ice-dynamics and mass-balance studies on the Greenland Ice Sheet, Report on the Contribution of the Alfred Wegener Institute to EU Contract No. ENV4-CT95-0124, European Commision, DG XII, 18 pp.
- Huybrechts**, Ph., D. Steinhage, F. Wilhelms, and J.L. Bamber, 2000: Balance velocities and measured properties of the Antarctic ice sheet from a new compilation of gridded data for modelling. *Annals of Glaciology*, **30**, 52-60.
- Hyvarinen**, H., 1999: Shore displacement and stone age dwelling sites near Helsinki, southern coast of Finland. In: *Digitall, Papers dedicated to Ari Siiriainen*. Finnish Antiquarian Society, 79-86p.
- Ingolfsson**, O., C. Hjort, P.A. Berkman, S. Björck, E. Colhoun, I.D. Goodwin, B. Hall, K. Hirakawa, M. Melles, P. Möller, and M.L. Prentice, 1998: Antarctic glacial history since the Last Glacial Maximum: an overview of the record on land. *Antarctic Science*, **10**, 326-344.
- IOC** (Intergovernmental Oceanographic Commission), 1997: Global Sea Level Observing System (GLOSS) implementation plan-1997. Intergovernmental Oceanographic Commission, Technical Series, No. 50, 91pp. & Annexes.
- IPCC**, 1996: *Climate Change 1995: The Science of Climate Change. Contribution of Working Group I to the Second Assessment Report of the Intergovernmental Panel on Climate Change*. Houghton, J.T., L.G. Meira Filho, B.A. Callander, N. Harris, A. Kattenberg, and K. Maskell (eds.). Cambridge University Press, Cambridge, United Kingdom and New York, NY, USA, 572 pp.
- IPCC**, 2001: *Climate Change 2001: Impacts, Adaptations and Vulnerability: Contribution of Working Group II to the Third Assessment Report of the Intergovernmental Panel on Climate Change*. J.J. McCarthy, O.F. Canziani, N.A. Leary, D.J. Dokken, K.S. White (eds.). Cambridge University Press, Cambridge, United Kingdom and New York, NY, USA.
- Jackett**, D.R., T.J. McDougall, M.H. England, and A.C. Hirst, 2000: Thermal expansion in ocean and coupled general circulation models. *Journal of Climate*, **13**, 1384-1405.
- Jacobs**, S.S., H.H. Hellmer, C.S.M. Doake, A. Jenkins, and R. Frolich, 1992: Melting of ice shelves and the mass balance of Antarctica. *Journal of Glaciology*, **38**, 375-387.
- Jacobs**, S.S., H.H. Hellmer, and A. Jenkins, 1996: Antarctic ice sheet melting in the Southeast Pacific. *Geophysical Research Letters*, **23**, 957-960.
- Jacobson**, H. P., and C.F. Raymond, 1998: Thermal effects on the location of ice stream margins. *Journal of Geophysical Research*, **103**, 12111-12122.
- James**, T.S., and E.R. Ivins, 1998: Predictions of Antarctic crustal motions driven by present-day ice sheet evolution and by isostatic memory of the Last Glacial Maximum. *J. Geophys. Res.*, **103**, 4993-5017.
- Janssens**, I., and P. Huybrechts, 2000: The treatment of meltwater retention in mass-balance parameterisations of the Greenland Ice Sheet, *Annals of Glaciology*, **31**, 133-140.
- Jóhannesson**, T., C. Raymond and E. Waddington, 1989: Timescale for adjustment of glaciers to changes in mass balance. *J. Glaciol.*, **35**, 355-369.
- Johnson**, G.C., A. Orsi, 1997: Southwest Pacific Ocean Water-Mass Changes between 1968/69 and 1990/91. *Journal of Climate*, **10**, 306-16.
- Johnston**, P., 1993: The effect of spatially non-uniform water loads on the prediction of sea level change. *Geophysical Journal International*, **114**, 615-634.
- Johnston**, P., K. Lambeck, and D. Wolf, 1997: Material versus isobaric internal boundaries in the Earth and their influence on postglacial rebound, *Geophysical Journal International*, **129**, 252-268.
- Johnston**, P.J. and K. Lambeck, 1999: Postglacial rebound and sea level contributions to changes in the geoid and the Earth's rotation axis. *Geophysical Journal International*, **136**, 537-558.
- Johnston**, P. and K. Lambeck, 2000: Automatic inference of ice models from postglacial sea level observations: Theory and application to the British Isles. *Journal of Geophysical Research*, **105**, 13179-13194.
- Joughin**, I., R. Kwok, M. Fahnestock, 1996a: Estimation of ice-sheet motion using satellite radar interferometry: method and error analysis with application to Humboldt Glacier, Greenland. *Journal of Glaciology*, **42**, 564-575.
- Joughin**, I., S. Tulaczyk, M. Fahnestock, R. Kwok, 1996b: A mini-surge on the Ryder Glacier, Greenland, observed by satellite radar interferometry. *Science*, **274**, 228-230.
- Joughin**, I., L. Gray, R.A. Bindschadler, S. Price, D.L. Morse, C.L. Hulbe, K. Mattar, and C. Werner, 1999: Tributaries of West Antarctic ice streams revealed by RADARSAT interferometry, *Science*, **286**, 283-286.
- Joyce**, T.M. and P. Robbins, 1996: The long-term hydrographic record at Bermuda. *Journal of Climate*, **9**, 3121-3131.
- Joyce**, T.M., R.S. Pickart, and R.C. Millard, 1999: Long-term hydrographic changes at 52 and 66W in the North Atlantic subtropical gyre and Caribbean. *Deep-Sea Research II*, **46**, 245-78.
- Jung-Rothenhäusler**, F., 1998: Remote sensing and GIS studies in North-East Greenland, Berichte zur Polarforschung (Alfred-Wegener-Institut, Bremerhaven), **280**, 161 p.
- Kapsner**, W.R., R.B. Alley, C.A. Shuman, S. Anandakrishnan and P.M. Grootes, 1995: Dominant influence of atmospheric circulation on snow accumulation in central Greenland, *Nature*, **373**, 52-54.
- Kaser**, G. 1999: A review of modern fluctuations of tropical glaciers. *Glob. and Plan. Change*, **22**, 93-104.
- Kaser**, G., Ch. Georges and A. Ames 1996: Modern glacier fluctuations in the Huascrán-Chopicalqui Massif of the Cordillera Blanca, Perú.

- Z. Gletscherkunde Glazialgeol., **32**, 91-99.
- Kass**, E., T.-S. Li, and T. Schmitt, 1996: Statistical hindcast of wind climatology in the North Atlantic and northwestern European region. *Climate Research*, **7**, 97-110.
- Kattenberg**, A., F. Giorgi, H. Grassl, G.A. Meehl, J.F.B. Mitchell, R.J. Stouffer, T. Tokioka, A.J. Weaver and T.M.L. Wigley, 1996: Climate models - projections of future climate, in Houghton, J.T., L.G. Meira Filho, B.A. Callander, N. Harris, A. Kattenberg and K. Maskell (eds), *Climate Change 1995. The Science of Climate Change*, Cambridge.
- Kaufmann**, G. and D. Wolf, 1999: Effects of lateral viscosity variations on postglacial rebound: an analytical approach. *Geophysical Journal International*, **137**, 489-500.
- Kauker**, F., 1998: Regionalization of climate model results for the North Sea. PhD thesis, University of Hamburg, 109pp.
- Kaul**, M.K., 1999: Inventory of the Himalayan glaciers. Special publication of the Geological Survey of India.
- Kearney**, M.S., 1996: sea level change during the last thousand years in Chesapeake Bay. *Journal of Coastal Research*, **12**, 977-983.
- Kearney**, M.S., and J.C. Stevenson, 1991: Island land loss and marsh vertical accretion rate evidence for historical sea level changes in Chesapeake Bay. *Journal of Coastal Resources*, **7**, no. 2, pp 403-415.
- Knutti**, R. and T.F. Stocker, 2000: Influence of the thermohaline circulation on projected sea level rise. *Journal of Climate*, **13**, 1997-2001.
- Koblinsky**, C.J., P. Gaspar and G. Lagerloef, 1992: The future of spaceborne altimetry: oceans and climate change. A long-term strategy. Joint Oceanographic Institutions Inc., Washington DC, 75pp.
- Koltermann**, K.P., A.V. Sokov, V.P. Tereschenkov, S.A. Dobroliubov, K. Lorbacher, and A. Sy, 1999: Decadal changes in the thermohaline circulation of the North Atlantic. *Deep-Sea Research II*, **46**, 109-38.
- Koster**, R.D., P.R. Houser, E.T. Engman, and W.P. Kustas, 1999: Remote sensing may provide unprecedented hydrological data. *EOS*, **80**, 156.
- Kotlyakov**, V. M., K.S. Losev, and I.A. Loseva, 1978: The ice budget of Antarctica. *Polar Geogr. Geol.*, **2**, 251-262.
- Krabill**, W., E. Frederick, S. Manizade, C. Martin, J. Sonntag, R. Swift, R. Thomas, W. Wright, and J. Yungel, 1999: Rapid thinning of parts of the southern Greenland Ice Sheet. *Science*, **283**, 1522-1524.
- Krabill**, W., W. Abdalati, E. Frederick, S. Manizade, C. Martin, J. Sonntag, R. Swift, R. Thomas, W. Wright, and J. Yungel, 2000: Greenland Ice Sheet: high-elevation balance and peripheral thinning. *Science*, **289**, 428-430.
- Kuhn**, M. 1984. Mass budget imbalances as criterion for a climatic classification of glaciers. *Geogr. Annaler*, **66A**, 229-238.
- Kuhn**, M., E. Dreiseitl, S. Hofinger, G. Markl, N. Span, G. Kaser 1999: Measurements and models of the mass balance of Hintereisferner. *Geogr. Annaler*, **81A**, 659-670.
- Kuzmichenok**, V.A., 1993: Glaciers of the Tien Shan. Computerised analysis of the Inventory. *Materialy Glyatsiologicheskikh Issledovanii*, **77**, 29-40.
- Laborel**, J., C. Morhange, R. Lafont, J. Le Campion, F. Laborel-Deguen, and S. Sartoretto, 1994: Biological evidence of sea level rise during the last 4500 years on the rocky coasts of continental southwestern France and Corsica, *Marine Geology*, **120**, 203-223.
- Lambeck**, K., 1988: *Geophysical Geodesy: The Slow Deformations of the Earth*. Oxford University Press, 718 pp.
- Lambeck**, K., 1996: Limits on the areal extent of the Barents Sea ice sheet in Late Weischelian time, *Palaeogeography Palaeoclimatology Palaeoecology*, **12**, 41-51.
- Lambeck**, K., and M. Nakada, 1990: Late Pleistocene and Holocene sea level change along the Australian coast. *Palaeogeography Palaeoclimatology Palaeoecology*, **89**, 143-176.
- Lambeck**, K. and P. Johnston, 1998: The viscosity of the mantle: Evidence from analyses of glacial rebound phenomena. In: *The Earth's mantle*, Jackson, I. (ed), Cambridge University Press, Cambridge, 461-502pp.
- Lambeck**, K., C. Smither, and M. Ekman, 1998: Tests of glacial rebound models for Fennoscandia based on instrumented sea- and lake-level records. *Geophysical Journal International*, **135**, 375-387.
- Lambeck**, K. and E. Bard, 2000: Sea level change along the French Mediterranean coast since the time of the Last Glacial Maximum. *Earth Planetary Science Letters*, **175**, 203-222.
- Lamont**, G.N., T.J. Chinn, and B.B. Fitzharris, 1999: Slopes of glacier ELAs in the Southern Alps of New Zealand in relation to atmospheric circulation patterns. *Global and Planetary Change*, **22**, 209-219.
- Langenberg**, H., A. Pfizenmayer, H. von Storch and J. Suendermann, 1999: Storm-related sea level variations along the North Sea coast: natural variability and anthropogenic change, *Continental Shelf Research*, **19**, 821-842.
- Latif**, M. and E. Roeckner, 2000: Tropical stabilisation of the thermohaline circulation in a greenhouse warming simulation, *J. Climate*, **13**, 1809-1813.
- Ledwell**, J.R., A.J. Watson and C.S. Law, 1993: Evidence for slow mixing across the pycnocline from an open-ocean tracer-release experiment. *Nature*, **364**, 701-703.
- Ledwell**, J.R., A.J. Watson and C.S. Law, 1998: Mixing of a tracer in the pycnocline. *Journal of Geophysical Research*, **103**, 21,499-21,529.
- Leggett**, J., W.J. Pepper and R.J. Swart, 1992: Emissions scenarios for the IPCC: an update. In *Climate change 1992. the supplementary report to the IPCC scientific assessment*, Houghton, J.T., B.A. Callander and S.K. Varney (eds.), Cambridge University Press, Cambridge
- Letreguilly**, A., P. Huybrechts, N. Reeh, 1991: Steady-state characteristics of the Greenland ice sheet under different climates. *J. Glaciology*, **37**, 149-157.
- Levitus**, S., 1989a: Interannual variability of temperature and salinity at intermediate depths of the North Atlantic, 1970-1974 versus 1955-1959. *Journal of Geophysical Research*, **94**, 6091-131.
- Levitus**, S., 1989b: Interannual variability of temperature and salinity in the deep North Atlantic, 1970-1974 versus 1955-1959. *Journal of Geophysical Research*, **94**, 16,125-16,131.
- Levitus**, S., 1990: Interannual variability of steric sea level and geopotential thickness of the North Atlantic, 1970-1974 versus 1955-1959. *Journal of Geophysical Research*, **95**, 5233-8.
- Levitus**, S., J.I. Antonov, T.P. Boyer, and C. Stephens, 2000: Warming of the World Ocean. *Science*, **287**, 2225-2229.
- Lingle**, C., and D.N. Covey, 1998: Elevation changes on the East Antarctic ice sheet, 1978-93, from satellite radar altimetry: a preliminary assessment. *Annals of Glaciology*, **27**, 7-18.
- Linsley**, B.K., 1996: Oxygen-isotope record of sea level and climate variations in the Sulu Sea over the past 150,000 years, *Nature*, **380**, 234-237.
- Liu**, S. Y. and Z. C. Xie, 2000: Glacier mass balance and fluctuations. In: *Glaciers and Environment in China*, Y. F. Shi (ed.), Science Press, Beijing, 101-103.
- Liu**, C.H., G.P. Song, M.X. Jin, 1992: Recent change and trend prediction of glaciers in Qilian Mountains. In *Memoirs of Lanzhou Institute of Glaciology and Geocryology*, Chinese Academy of Sciences, No. 7 (The monitoring of glacier, climate runoff changes and the research of cold region hydrology in Qilian Mountains), Beijing, Science Press.
- Lowe**, J.A., J.M. Gregory and R.A. Flather, 2001: Changes in the occurrence of storm surges around the United Kingdom under a future climate scenario using a dynamic storm surge model driven by the Hadley Centre climate model. *J. Climate*, in press.
- Manabe**, S., R.J. Stouffer, 1993: Century-scale effects of increased atmospheric CO₂ on the ocean-atmosphere system. *Nature*, **364**, 215-8.
- Manabe**, S., R. Stouffer, 1994: Multiple-century response of a coupled ocean-atmosphere model to an increase of atmospheric carbon dioxide. *Journal of Climate*, **7**, 5-23.
- Maul**, G.A. and Martin, D.M. 1993: Sea level rise at Key West, Florida, 1846-1992: America's longest instrument record? *Geophysical*

- Research Letters*, **20**, 1955-1958.
- Mayer**, C., and P. Huybrechts, 1999: Ice-dynamic conditions across the grounding zone, Ekströmisen, East Antarctica. *Journal of Glaciology*, **45**, 384-393.
- Meier**, M.F., 1984: Contribution of small glaciers to global sea level. *Science*, **226**, 1418-21.
- Meier**, M.F., 1993: Ice, climate and sea level: do we know what is happening? in: *Ice in the climate system*, Peltier, W.R. (ed.), NATO ASI Series I, Springer-Verlag, Heidelberg, 141-160.
- Meier**, M.F., and D.B. Bahr, 1996: Counting glaciers: use of scaling methods to estimate the number and size distribution of the glaciers of the world. In: *Glaciers, Ice Sheets and Volcanoes: A Tribute to Mark F. Meier*, S.C. Colbeck (ed.), CRREL Special Report 96-27, 89-94. U. S. Army Hanover, New Hampshire.
- Miller**, J.R. and G.L. Russell, 2000: Projected impact of climate change on the freshwater and salt budgets of the Arctic Ocean by a global climate model. *Geophysical Research Letters*, **27**, 1183-1186.
- Mitchell**, W., J.Chittleborough, B.Ronai and G.W.Lennon, 2000: Sea Level Rise in Australia and the Pacific. *The South Pacific Sea Level and Climate Change Newsletter, Quarterly Newsletter*, **5**, 10-19.
- Mitchum**, G.T., 1998: Monitoring the stability of satellite altimeters with tide gauges. *Journal of Atmospheric and Oceanic Technology*, **15**, 721-730.
- Mitrovica** J.X. and J.L. Davis, 1995: Present-day post-glacial sea level change far from the Late Pleistocene ice sheets: Implications for recent analyses of tide gauge records. *Geophys. Res. Lett.*, **22**, 2529-32.
- Mitrovica**, J. X. and G.A. Milne, 1998: Glaciation-induced perturbations in the Earth's rotation: a new appraisal. *Journal Geophysical Research*, **103**, 985-1005.
- Mitrovica**, J.X. and W.R. Peltier, 1991: On postglacial geoid subsidence over the equatorial oceans, *Journal of Geophysical Research*, **96**, 20053-20071.
- Mohr**, J. C., N. Reeh, and S.N. Madsen, 1998: Three-dimensional glacial flow and surface elevation measured with radar interferometry. *Nature*, **391**, 273-276.
- Morhange**, C., J. Laborel, A. Hesnard, and A. Prone, 1996: Variation of relative mean sea level during the last 4000 years on the northern shores of Lacydon, the ancient harbour of Marseille (Chantier J. Verne). *Journal of Coastal Research*, **12**, 841-849.
- Morison**, J., M. Steele, and R. Andersen, 1998: Hydrography of the upper Arctic Ocean measured from the nuclear submarine U.S.S. Pargo. *Deep-Sea Research I*, **45**, 15-38.
- Mörner**, N.A. 1973. Eustatic changes during the last 300 years. *Palaeogeography, Palaeoclimatology, Palaeoecology*, **13**, 1-14.
- Murphy**, J.M. and J.F.B. Mitchell, 1995: Transient response of the Hadley Centre coupled ocean-atmosphere model to increasing carbon dioxide. Part II: Spatial and temporal structure of response. *J. Climate*, **8**, 57-80.
- Nakada**, M. and K. Lambeck, 1988: The melting history of the Late Pleistocene Antarctic ice sheet, *Nature*, **333**, 36-40.
- Nakiboglu**, S.M. and K. Lambeck, 1991: Secular sea level change. In: *Glacial Isostasy, Sea Level and Mantle Rheology*, R. Sabadini, K. Lambeck and E. Boschi, (eds.), Kluwer Academic Publ., 237-258.
- Nakićenović**, N., J. Alcamo, G. Davis, B. de Vries, J. Fenmann, S. Gaffin, K. Gregory, A. Grubler, T. Y. Jung, T. Kram, E. L. La Rovere, L. Michaelis, S. Mori, T. Morita, W. Pepper, H. Pitcher, L. Price, K. Raihi, A. Roehrl, H-H. Rogner, A. Sankovski, M. Schlesinger, P. Shukla, S. Smith, R. Swart, S. van Rooijen, N. Victor, Z. Dadi: 2000: *IPCC Special Report on Emissions Scenarios*, Cambridge University Press, Cambridge, United Kingdom and New York, NY, USA, 599 pp.
- National Bureau of Marine Management**, 1992: *Bulletin of China's sea level*. National Bureau of Marine Management, Beijing, 26pp.
- NASA** (National Aeronautics and Space Administration), 1996: Gravity Recovery and Climate Experiment. Proposal to NASA's Earth System Science Pathfinder Program.
- Neilan**, R., P.A. Van Scoy, and P.L. Woodworth, (eds.), 1998: Proceedings of the workshop on methods for monitoring sea level: GPS and tide gauge benchmark monitoring and GPS altimeter calibration. Workshop organised by the IGS and PSMSL, Jet Propulsion Laboratory, Pasadena, California, 17-18 March 1997. 202pp.
- Nerem**, R. S. and S.M. Klosko, 1996: Secular variations of the zonal harmonics and polar motion as geophysical constraints. In: *Global gravity field and its temporal variations*, Rapp, R. H., Cazenave, A. A. and Nerem, R. S. (eds.) Springer, New York, 152-163.
- Nerem**, R.S., B.J. Haines, J. Hendricks, J.F. Minster, G.T. Mitchum, and W.B. White, 1997: Improved determination of global mean sea level variations using TOPEX/POSEIDON altimeter data. *Geophysical Research Letters*, **24**, 1331-4.
- Nerem**, R.S., 1999: Measuring very low frequency sea level variations using satellite altimeter data. *Global and Planetary Change*, **20**, 157-171.
- Nerem**, R.S., D.P. Chambers E.W. Leuliette, G.T. Mitchum, and B.S. Giese, 1999: Variations in global mean sea level associated with the 1997-98 ENSO event: implications for measuring long term sea level change. *Geophysical Research Letters*, **26**, 3005-3008.
- Nicholls**, K. W., 1997: Predicted reduction in basal melt rates of an Antarctic ice shelf in a warmer climate. *Nature*, **388**, 460-462.
- NRC** (National Research Council), 1997: *Satellite gravity and the geosphere*. National Academy Press: Washington, D.C.
- Orlemans**, J., 1981: Effect of irregular fluctuation in Antarctic precipitation on global sea level. *Nature*, **290**, 770-772.
- Orlemans**, J., 1991: The mass balance of the Greenland ice sheet: sensitivity to climate change as revealed by energy balance modelling. *Holocene*, **1**, 40-49.
- Orlemans**, J., 1999: Comments on "Mass balance of glaciers other than the ice sheets", by J. Graham Cogley and W.P. Adams. *J Glaciology*, **45**, 397-398.
- Orlemans**, J., and J.P.F. Fortuin, 1992: Sensitivity of glaciers and small ice caps to greenhouse warming. *Science*, **258**, 115-117.
- Orlemans**, J., B. Anderson, A. Hubbard, P. Huybrechts, T. Jóhannesson, W.H. Knap, M. Schmeits, A.P. Stroeve, R.S.W. van de Wal, J. Wallinga, and Z. Zuo, 1998: Modelling the response of glaciers to climate warming. *Climate Dynamics*, **14**, 267-274.
- O'Farrell**, S.P., J.L. McGregor, L.D. Rotstayn, W.F. Budd, C. Zweck, and R. Warner, 1997: Impact of transient increases in atmospheric CO₂ on the accumulation and mass balance of the Antarctic ice sheet. *Annals of Glaciology*, **25**, 137-144.
- Ohmura**, A., and N. Reeh, 1991: New precipitation and accumulation maps for Greenland. *J. Glaciol.*, **37**, 140-148.
- Ohmura**, A., M. Wild, and L. Bengtsson, 1996: A possible change in mass balance of Greenland and Antarctic ice sheets in the coming century. *Journal of Climate*, **9**, 2124-2135.
- Ohmura**, A., P. Calanca, M. Wild, and M. Anklin, 1999: Precipitation, accumulation and mass balance of the Greenland Ice Sheet. *Zeitschrift für Gletscherkunde und Glazialgeologie*, **35**, 1-20.
- Open University**, 1989. Waves, tides and shallow-water processes. Open University Oceanography Series Vol.4. Pergamon Press, Oxford, in association with the Open University, 187pp.
- Oppenheimer**, M., 1998: Global warming and the stability of the West Antarctic ice sheet. *Nature*, **393**, 325-331.
- Ota**, Y., A. Omura, and T. Miyauchi, 1992: Last interglacial shoreline map of Japan. Japanese Working Group for IGCP Project 274.
- Ota**, Y., L.J. Brown, K.R. Berryman, T. Fujimori, and T. Miyauchi, 1995: Vertical tectonic movement in northeastern Marlborough: stratigraphic, radiocarbon, and paleoecological data from Holocene estuaries, *New Zealand Journal of Geological and Geophysical*, **38**, 269-282.

- Parrilla**, G., A. Lavin, H. Bryden, M. Garcia, and R. Millard, 1994: Rising temperatures in the subtropical North Atlantic Ocean over the past 35 years. *Nature*, **369**, 48-51.
- Payne**, A.J., 1998: Dynamics of the Siple Coast ice streams, West Antarctica: results from a thermomechanical ice sheet model. *Geophysical Research Letters*, **25**, 3173-3176.
- Peltier**, W.R., 1994: Ice age paleotopography. *Science*, **265**, 195-201.
- Peltier**, W.R., 1996: Global sea level rise and glacial isostatic adjustment: an analysis of data from the east coast of North America. *Geophysical Research Letters*, **23**, 717-720.
- Peltier**, W.R., 1998: Postglacial variations in the level of the Sea: implications for climate dynamics and solid-earth geophysics. *Review of Geophysics*, **36**, 603-689.
- Peltier**, W.R., 2000: Global glacial isostatic adjustment. In *Sea level rise: history and consequences*, B.C. Douglas, M.S. Kearney and S.P. Leatherman (eds.), Academic Press, 65-95.
- Peltier**, W.R. and A.M. Tushingham, 1989: Global sea level rise and the greenhouse effect: Might they be connected? *Science*, **244**, 806-10.
- Peltier**, W.R. and A.M. Tushingham, 1991: Influence of glacial isostatic adjustment on tide gauge measurements of secular sea level change. *J Geophys Res*, **96**, 6779-6796.
- Peltier**, W.R. and X. Jiang, 1996: Mantle viscosity from the simultaneous inversion of multiple datasets pertaining to postglacial rebound. *Geophys. Res. Lett.*, **33**, 503-506.
- Peltier**, W.R., and X. Jiang, 1997: Mantle viscosity, glacial isostatic adjustment and the eustatic level of the sea. *Surveys in Geophysics*, **18**, 239-277.
- Pfeffer**, W. T., M.F. Meier, and T.H. Illangasekare, 1991: Retention of Greenland runoff by refreezing: implications for projected future sea level change. *J. Geophys. Res.*, **96**, 22117-22124.
- Pirazzoli**, P.A., 1991: *World Atlas of Holocene sea level changes*. Elsevier, Amsterdam, 300p.
- Pirazzoli**, P.A., 2000: Surges, atmospheric pressure and wind change, and flooding probability on the Atlantic coast of France. *Oceanologica Acta*, **23**, 643-661.
- Pirazzoli**, P.A., S.C. Stiros, M. Arnold, J. Laborel, F. Laborel-Deguen, and S. Papageorgiou, 1994: Episodic uplift deduced from Holocene shorelines in the Perachora Peninsula, Corinth area, Greece. *Tectonophysics*, **229**, 201-209.
- Pittock**, A.B., K. Walsh, and K. McInnes, 1996: Tropical cyclones and coastal inundation under enhanced greenhouse conditions. *Water, Air and Soil Pollution*, **92**, 159-169.
- Pugh**, D.T. and G.A. Maul, 1999: Coastal sea level prediction for climate change. In: *Coastal Ocean Prediction. Coastal and Estuarine Studies*, American Geophysical Union, Washington, D.C., **56**, 377-404.
- Quadfasel**, D., A. Sy, and D. Wells, 1991: Warming in the Arctic. *Nature*, **350**, 385.
- Qin**, D., P.A. Mayewski, C.P. Wake, S.C. Kang, J.W. Ren, S.G. Hou, T.D. Yao, Q.Z. Yang, Z.F. Jin, D.S. Mi, 2000: Evidence for recent climate change from ice cores in the central Himalaya. *Annals of Glaciology*, **31**, 153-158.
- Raper**, S.C.B., and U. Cubasch, 1996: Emulation of the results from a coupled general circulation model using a simple climate model. *Geophysical Research Letters*, **23**, 1107-1110.
- Raper**, S.C.B., T.M.L Wigley, and R.A. Warrick, 1996: Global sea level rise: Past and Future. In: *Sea Level Rise and Coastal Subsidence, Causes, Consequences and Strategies*, Kluwer Academic Publishers, Dordrecht, 369pp.
- Raper**, S.C.B., J.M. Gregory and T.J. Osborn, 2001: Use of an upwelling-diffusion energy balance climate model to simulate and diagnose AOGCM results. *Clim. Dyn.*, in press.
- Raper**, S.C.B., O. Brown and R.J. Braithwaite, 2000: A geometric glacier model suitable for sea level change calculations. *Journal of Glaciology*, **46**, 357-368.
- Read**, J.F., W.J. Gould, 1992: Cooling and freshening of the subpolar North Atlantic Ocean since the 1960s. *Nature*, **360**, 55-7.
- Reeh**, N., and W. Starzer, 1996: Spatial resolution of ice-sheet topography: influence on Greenland mass-balance modelling. *GGU rapport*, **1996/53**, 85-94.
- Reeh**, N., H.H. Thomsen, O.B. Olesen, and W. Starzer, 1997: Mass balance of north Greenland. *Science*, **278**, 207-209.
- Reeh**, N., C. Mayer, H. Miller, H.H. Thomson, and A. Weidick, 1999: Present and past climate control on fjord glaciations in Greenland: implications for IRD-deposition in the sea. *Geophysical Research Letters*, **26**, 1039-1042.
- Retzlaff**, R., and C.R. Bentley, 1993: Timing of stagnation of ice stream C, West Antarctica, from short-pulse radar studies of buried surface crevasses. *Journal of Glaciology*, **39**, 553-561.
- Rider**, K.M., G.J. Komen, and J.J. Beersma, 1996: Simulations of the response of the ocean waves in the North Atlantic and North Sea to CO₂ doubling in the atmosphere. KNMI Scientific Report WR 96-95, De Bilt, Netherlands.
- Ridgway**, K.R. and J.S. Godfrey, 1996: Long-term temperature and circulation changes off eastern Australia. *Journal of Geophysical Research*, **101**, 3615-27.
- Rignot**, E.J., 1998a: Fast recession of a West Antarctic glacier. *Science*, **281**, 549-551.
- Rignot**, E., 1998b: Radar interferometry detection of hinge-line migration on Rutford Ice Stream and Carlson Inlet, Antarctica. *Annals of Glaciology*, **27**, 25-32.
- Rignot**, E.J., 1998c: Hinge-line migration of Petermann Gletscher, north Greenland, detected using satellite-radar interferometry. *Journal of Glaciology*, **44**, 469-476.
- Rignot**, E.J., S.P. Gogineni, W.B. Krabill, and S. Ekholm, 1997: North and Northeast Greenland Ice Discharge from Satellite Radar Interferometry. *Science*, **276**, 934-937.
- Robasky**, F. M., and D.H. Bromwich, 1994: Greenland precipitation estimates from the atmospheric moisture budget. *Geophysical Research Letters*, **21**, 2485-2498.
- Roemmich**, D. and C. Wunsch, 1984: Apparent changes in the climatic state of the deep North Atlantic Ocean. *Nature*, **307**, 447-450.
- Roemmich**, D., 1990: Sea level and the thermal variability of the oceans. In: *Sea Level Change*, National Academy Press, Washington DC, 1990, 208-229.
- Roemmich**, D., 1992: Ocean warming and sea level rise along the southwest U.S. coast. *Science*, **257**, 373-5.
- Rommelaere**, V., and D.R. MacAyeal, 1997: Large-scale rheology of the Ross Ice Shelf, Antarctica, computed by a control method. *Annals of Glaciology*, **24**, 43-48.
- Rott**, H., M. Stuefer, and A. Siegel, 1998: Mass fluxes and dynamics of Moreno Glacier, Southern Patagonian Icefield. *Geoph. Res. Letters*, **25**, 1407-1410.
- Russell**, G.L., V. Gornitz and J.R. Miller, 2000: Regional sea level changes projected by the NASA/GISS atmosphere-ocean model. *Climate Dynamics*, **16**, 789-797.
- Sahagian**, D., 2000: Global physical effects of anthropogenic hydrological alterations: sea level and water redistribution. *Global and Planetary Change*, **25**, 39-48.
- Sahagian**, D.L., and S. Zerbini, 1999: Global and regional sea level changes and the hydrological cycle. IGBP/GAIM Report Series, No. 8.
- Sahagian**, D.L., F.W. Schwartz, and D.K. Jacobs, 1994: Direct anthropogenic contributions to sea level rise in the twentieth century. *Nature*, **367**, 54-7.
- SAR**, see IPCC, 1996.
- Scherer**, R. P., A. Aldahan, S. Tulaczyk, G. Possnert, H. Engelhardt, and B. Kamb, 1998: Pleistocene collapse of the West Antarctic ice sheet. *Science*, **281**, 82-85.
- Schlesinger**, M.E. and X. Jiang, 1990: Simple model representation of

- atmosphere-ocean GCMs and estimation of the timescale of CO₂-induced climate change. *J Climate*, **3**, 1297-1315.
- Schmitt**, T., E. Kaas, and T.-S. Li, 1998: Northeast Atlantic winter storminess 1875-1995 re-analysed. *Climate Dynamics*, **14**, 529-536.
- Schönwiese**, C.-D., J. Rapp, T. Fuchs and M. Denhard, 1994: Observed climate trends in Europe 1891-1990. *Meteorol. Zeitschrift*, **3**, 22-28.
- Schönwiese**, C.-D. and J. Rapp, 1997: *Climate Trend Atlas of Europe Based on Observations 1891-1990*. Kluwer Academic Publishers, Dordrecht, 228 p.
- Senior**, C.A. and J.F.B. Mitchell, 2000: The time dependence of climate sensitivity. *Geophys Res. Lett.*, **27**, 2685-2688.
- Shabtaie**, S., and C.R. Bentley, 1987: West Antarctic ice streams draining into the Ross ice shelf: configuration and mass balance. *J. Geophys. Res.*, **92**, 1311-1336.
- Shackleton**, N.J., 1987: Oxygen isotopes, ice volume and sea level. *Quaternary Science Review*, **6**, 183-190.
- Shaffer**, G., O. Leth, O. Ulloa, J. Bendtsen, G. Daneri, V. Dellarossa, S. Hormazabal, and P. Sehestedt, 2000: Warming and circulation change in the eastern South Pacific Ocean. *Geophys. Res. Lett.*, **GRL 27(9)**, 1247-1250.
- Shaw**, J. and J. Ceman, 2000: Salt-marsh aggradation in response to late-Holocene sea level rise at Amherst Point, Nova Scotia, Canada. *The Holocene*, **9**, 439-451.
- Shennan**, I. and P.L. Woodworth, 1992: A comparison of late Holocene and twentieth-century sea level trends from the UK and North Sea region. *Geophysical Journal International*, **109**, 96-105.
- Shi**, Y.F., 1996 (ed.): Sea level change in China. In: *Climatic and sea level changes and their trends and effects in China*. Shandong Science And Technology Press, Jinan, pp464.
- Shi**, Y.F. and K.J. Zhou, 1992: Characteristics and recent variation of surface water in China, and its effect on the environment. In: *Preliminary research on global change in China*, Yie, N.Z. and B.Q. Chen, (eds.), Beijing, Seismological Press, pp85-158.
- Shi**, Y. F., Z.C. Kong and S.M. Wang, L.Y. Tang, F.B. Wang, T.D. Yao, X.T. Zhao, P.Y. Zhang, S.H. Shi 1994: Climates and environments of the Holocene megathermal maximum in China. *Science in China (series B)*, **37**, 481-493.
- Skvarca**, P., H. Rott, T. Nagler, 1995: Drastic retreat of Upsala Glacier, Southern Patagonia, revealed by ESR-1/SAR images and field survey. *Revista Selper*, **11**, 51-55.
- Skvarca**, P., W. Rack, H. Rott, T. Ibarzabal y Donangelo, 1998: Evidence of recent climatic warming on the eastern Antarctic Peninsula. *Annals of Glaciology*, **27**, 628-632.
- Smith**, I. N., W.F. Budd, and P. Reid, 1998: Model estimates of Antarctic accumulation rates and their relationship to temperature changes. *Annals of Glaciology*, **27**, 246-250.
- Smith**, I., 1999: Estimating mass balance components of the Greenland Ice Sheet from a long-term GCM simulation. *Global and Planetary Change*, **20**, 19-32.
- Smith**, D., S. Raper, S. Zerbini, A. Sanchez-Arcilla, and R. Nicholls, (eds.) 2000: Sea Level Change and Coastal Processes: Implications for Europe, Office for official Publications of the European Union Community, Luxembourg, 247p.
- Spencer**, N.E. and P.L. Woodworth, 1993: Data holdings of the Permanent Service for Mean Sea Level (November 1993). Bidston, Birkenhead: Permanent Service for Mean Sea Level. 81pp.
- Stanley**, D.J., 1997: Mediterranean deltas: Subsidence as a major control of relative sea level rise, Monaco, *Bulletin de l'Institut océanographique*, **Special no. 18**, 35-62.
- Steele**, M. and T. Boyd, 1998: Retreat of the cold halocline layer in the Arctic Ocean. *Journal of Geophysical Research*, **103**, 10,419-10,435.
- Steig**, E. J., 1997: How well can we parameterize past accumulation rates in polar ice sheets? *Annals of Glaciology*, **25**, 418-422.
- Steinberger**, B. and R.J. O'Connell, 1997: Changes of the Earth's rotation axis owing to advection of mantle density heterogeneities. *Nature*, **387**, 169-173.
- Stephenson**, S. N., and R.A. Bindschadler, 1988: Observed velocity fluctuations on a major Antarctic ice stream. *Nature*, **334**, 695-697.
- Stirling**, C.H., T.M. Esat, K. Lambeck and M.T. McCulloch, 1998: Timing and duration of the Last Interglacial: evidence for a restricted interval of widespread coral reef growth, *Earth Planetary Science Letters*, **160**, 745-762.
- Stiros**, S.C., Marangou, L. and Arnold, M., 1994: Quaternary uplift and tilting of Amorgos Island (southern Aegean) and the 1956 earthquake, *Earth Planetary Science Letters*, **128**, 65-76.
- Stouffer**, R.J. and S. Manabe, 1999: Response of a coupled ocean-atmosphere model to increasing carbon dioxide: sensitivity to the rate of increase. *J. Climate*, **12**, 2224-2237.
- Stone**, J.O., D. Zwartz, M.C.G. Mabin, K. Lambeck, D. Fabel, and L.K. Fifield, 1998: Exposure dating constraints on ice volume and retreat history in East Antarctica, and prospects in West Antarctica. R. Bindschadler and H. Borns (eds.), *Chapman Conference on West Antarctic Ice Sheet*. 13-18 September 1998, American Geophysical Union, Orano, Maine, USA.
- Sturges**, W., B.D. Hong, 1995: Wind forcing of the Atlantic thermocline along 32N at low frequencies. *Journal of Physical Oceanographer*, **25(July)**, 1706-15.
- Sturges**, W., B.G. Hong, and A.J. Clarke, 1998: Decadal wind forcing of the North Atlantic subtropical gyre. *Journal of Physical Oceanographer*, **28(April)**, 659-68.
- Swift**, J.H., E.P. Jones, K. Agaard, E.C. Carmack, M. Hingston, R.W. MacDonald, F.A. McLaughlin, and R.G. Perkin, 1997: Waters of the Makarov and Canada Basins. *Deep-Sea Research II*, **44**, 1503-29.
- Thomas**, R. H., 1973: The creep of ice shelves: theory. *J. Glaciol.*, **12**, 45-53.
- Thomas**, R. H., T.J.O. Sanderson, and K.E. Rose, 1979: Effect of climatic warming on the West Antarctic ice sheet. *Nature*, **277**, 355-358.
- Thomas**, R. H., B.M. Csatho, S. Gogineni, K.C. Jezek, K. Kuivinen, 1998: Thickening of the western part of the Greenland Ice Sheet. *Journal of Glaciology*, **44**, 653-658.
- Thomas**, R., T. Akins, B. Csatho, M. Fahnestock, P. Gogineni, C. Kim, and J. Sonntag, 2000: Mass balance of the Greenland Ice Sheet at high elevations, *Science*, **289**, 426-428.
- Thompson**, S.L., and D. Pollard, 1997: Greenland and Antarctic mass balances for present and doubled atmospheric CO₂ from the GENESIS version-2 global climate model. *Journal of Climate*, **10**, 871-900.
- Thomson**, R.E. and S. Tabata, 1989: Steric sea level trends in the northeast Pacific Ocean: Possible evidence of global sea level rise. *Journal of Climate*, **2**, 542-53.
- Titus**, J.G., and V. Narayanan, 1996: The risk of sea level rise, *Climatic Change*, **33**, 151-212.
- Treshnikov**, A.F., 1977: Water masses of the Arctic Basin, in Polar Oceans, pp.17-31, edited by M. Dunbar.
- Tromp**, J. and J.X. Mitrovica, 1999: Surface loading of a viscoelastic earth - I. General theory. *Geophysical Journal International*, **137**, 847-855
- Trupin**, A. and J. Wahr, 1990: Spectroscopic analysis of global tide gauge sea level data. *Geophysical Journal International*, **100**, 441-53.
- Trupin**, A.S., M.F. Meier and J.M. Wahr, 1992: Effects of melting glaciers on the Earth's rotation and gravitational field: 1965-1984. *Geophys. J. Intern.*, **108**, 1-15.
- Tsimplis**, M.N. and Baker, T.F. 2000. Sea level drop in the Mediterranean Sea: an indicator of deep water salinity and temperature changes? *Geophysical Research Letters*, **27**, 1731-1734.
- Turner**, J., W.M. Connolley, S. Leonard, G.J. Marshall, and D.G. Vaughan, 1999: Spatial and temporal variability of net snow accumulation over the Antarctic from ECMWF re-analysis project data. *International Journal of Climatology*, **19**, 697-724.
- Tushingham**, A.M. and W.R. Peltier, 1991: Ice-3G: a new global model

- of Late Pleistocene deglaciation based upon geophysical predictions of post-glacial relative sea level change. *Journal of Geophysical Research*, **96**, 4497-4523.
- Tushingham**, A.M. and W.R. Peltier, 1992: Validation of the ICE-3G model of Würm-Wisconsin deglaciation using a global data base of relative sea level histories. *Journal of Geophysical Research*, **97**, 3285-3304.
- Tvede**, A.M. and T. Laumann, 1997: Glacial variations on a meso-scale example from glaciers in the Aurland Mountains, southern Norway. *Annals of Glaciology*, **24**, 130-134.
- Van de Plassche**, O., K. Van der Borg, and A.F.M. De Jong, 1998: Sea level-climate correlation during the past 1400 yr. *Geology*, **26**, 319-322.
- Van de Wal**, R. S. W., 1996: Mass balance modelling of the Greenland Ice Sheet: a comparison of an energy balance and a degree-day model. *Annals of Glaciology*, **23**, 36-45.
- Van de Wal**, R.S.W. and J. Oerlemans, 1994: An energy balance model for the Greenland ice sheet. *Glob. Planetary Change*, **9**, 115-131.
- Van de Wal**, R. S. W., and J. Oerlemans, 1997: Modelling the short term response of the Greenland Ice Sheet to global warming. *Climate Dynamics*, **13**, 733-744.
- Van de Wal**, R. S. W., and S. Ekholm, 1996: On elevation models as input for mass balance calculations of the Greenland Ice Sheet. *Annals of Glaciology*, **23**, 181-186.
- Van de Wal**, R.S.W. and M. Wild, 2001: Modelling the response of glaciers to climate change, applying volume area scaling in combination with a high-resolution GCM. IMAU Report R-01-06, Utrecht University, Netherlands.
- Van der Veen**, C. J., 1985: Response of a marine ice sheet to changes at the grounding line. *Quat. Res.*, **24**, 257-267.
- Van der Veen**, C. J., and J.F. Bolzan, 1999: Interannual variability in net accumulation on the Greenland Ice Sheet: observations and implications for mass balance measurements. *Journal of Geophysical Research*, **104**, 2009-2014.
- Van der Vink**, G., et al., 1998: Why the United States is becoming more vulnerable to natural disasters. *EOS, Transactions of the American Geophysical Union*, **79**, 533-537.
- Van Tatenhove**, F.G.M., J.J.M. van der Meer, and P. Huybrechts, 1995: Glacial geological/geomorphological research in West Greenland used to test an ice-sheet model. *Quaternary Research*, **44**, 317-327.
- Varekamp**, J.C. and E. Thomas, 1998: Climate change and the rise and fall of sea level over the millennium. *EOS, Transactions of the American Geophysical Union*, **79**, 69 and 74-75.
- Varekamp**, J.C., E. Thomas, and O. Van de Plassche, 1992: Relative sea level rise and climate change over the last 1500 years. *Terra Nova*, **4**, pp. 293-304. (R12689 POL library).
- Vaughan**, D. G., and C.S.M. Doake, 1996: Recent atmospheric warming and retreat of ice shelves on the Antarctic Peninsula. *Nature*, **379**, 328-331.
- Vaughan**, D. G., J.L. Bamber, M. Giovinetto, J. Russell, and A.P.R. Cooper, 1999: Reassessment of net surface mass balance in Antarctica. *Journal of Climate*, **12**, 933-946.
- Vaughan**, D.G. and J.R. Spouge, 2001: Risk estimation of collapse of the West Antarctic ice sheet, *Climatic Change*, in press.
- Von Storch**, H. and H. Reichardt, 1997: A scenario of storm surge statistics for the German Bight at the expected time of doubled atmospheric carbon dioxide concentration. *Journal of Climate*, **10**, 2653-2662.
- Vörösmarty**, C.J. and D. Sahagian, 2000: Anthropogenic disturbance of the terrestrial water cycle. *Bioscience*, **50**, 753-765.
- Voss**, R. and U. Mikolajewicz, 2001: Long-term climate changes due to increased CO₂ concentration in the coupled atmosphere-ocean general circulation model ECHAM3/LSG. *Clim. Dyn.*, **17**, 45-60.
- Wahr**, J., H. Dazhong, A. Trupin and V. Lindqvist, 1993: Secular changes in rotation and gravity: evidence of post-glacial rebound or of changes in polar ice? *Advanced Space Research*, **13**, 257-269.
- Wang**, S.H., J.M. Yang, X.L. Sun, C.S. Ceng, M.T. Yu, X.Z. Wu, 1990: Sea level changes since deglaciation in the downstream area of Min Jiang and surroundings. *Acta Oceanologica Sinica*, **12**, 64-74.
- Warner**, R. C., and W.F. Budd, 1998: Modelling the long-term response of the Antarctic ice sheet to global warming. *Annals of Glaciology*, **27**, 161-168.
- Warrick**, R.A., J. Oerlemans, 1990: Sea Level Rise. In: *Climate Change, The IPCC Scientific Assessment*. J.T. Houghton, G.J. Jenkins, J.J. Ephraums (eds.), pp 260-281.
- Warrick**, R.A., C. Le Provost, M.F. Meier, J. Oerlemans, P.L. Woodworth, 1996: Changes in Sea Level. In: *Climate Change 1995, The Science of Climate Change*, J.T. Houghton, L.G. Meira Filho, B.A. Callander, N. Harris, A. Kattenberg, K. Maskell (eds.). Cambridge University Press, 359-405.
- WASA Group**, 1998: Changing waves and storms in the northeast Atlantic. *Bulletin American Meteorological Society*, **79**, 741-760.
- Weaver**, A.J. and E.C. Wiebe, 1999: On the sensitivity of projected oceanic thermal expansion to the parameterisation of sub-grid scale ocean mixing. *Geophysical Research Letters*, **26**, 3461-3464.
- Weertman**, J., 1974: Stability of the junction of an ice sheet and an ice shelf. *Journal of Glaciology*, **13**, 3-11.
- Weidick**, A., 1984: Review of glacier changes in West Greenland. *Zeitschrift für Gletscherkunde und Glazialgeologie*, **21**, 301-309.
- Weidick**, A. and E. Morris, 1996: Local glaciers surrounding continental ice sheets. In Haeberli, W., M. Hoezle and S. Suter (eds.), *Into the second century of world glacier monitoring?prospects and strategies*. A contribution to the IHP and the GEMS. Prepared by the World Glacier Monitoring Service.
- Whillans**, I. M., and R.A. Bindschadler, 1988: Mass balance of ice stream B, West Antarctica. *Ann. Glaciol.*, **11**, 187-193.
- Whillans**, I. M., and C.J. van der Veen, 1997: The role of lateral drag in the dynamics of Ice Stream B, Antarctica. *Journal of Glaciology*, **43**, 231-237.
- Wigley**, T.M.L and S.C.B. Raper, 1987: Thermal expansion of sea water associated with global warming. *Nature*, **330**, 127-31.
- Wigley**, T.M.L and S.C.B. Raper, 1992: Implications for climate and sea level of revised IPCC emissions scenarios. *Nature*, **357** (May 28), 293-300.
- Wigley**, T.M.L and S.C.B. Raper, 1993: Future changes in global mean temperature and sea level, in Warrick, R.A., E.M. Barrow and T.M.L.Wigley (eds), *Climate and sea level change: observations, projections and implications*, Cambridge University Press, Cambridge, UK, 424pp.
- Wigley**, T.M.L and S.C.B. Raper, 1995: An heuristic model for sea level rise due to the melting of small glaciers. *Geophysical Research Letters*, **22**, 2749-2752.
- Wild**, M., and A. Ohmura, 2000: Changes in Mass balance of the polar ice sheets and sea level under greenhouse warming as projected in high resolution GCM Simulations. *Ann.Glaciol.*, **30**, 197-203.
- Williams**, M. J. M., R.C. Warner, and W.F. Budd, 1998: The effects of ocean warming on melting and ocean circulation under the Amery ice shelf, East Antarctica. *Annals of Glaciology*, **27**, 75-80.
- Wingham**, D., A.J. Ridout, R. Scharroo, R.J. Arthern, and C.K. Shum, 1998: Antarctic elevation change from 1992 to 1996. *Science*, **282**, 456-458.
- Wong**, A.P.S., 1999: Water mass changes in the North and South Pacific Oceans between the 1960s and 1985-94, PhD Thesis, University of Tasmania, 249pp.
- Wong**, A.P.S., N.L. Bindoff, and J.A. Church, 1999: Coherent large-scale freshening of intermediate waters in the Pacific and Indian Oceans. *Nature*, **400**, 440-443.
- Wong**, A.P.S., N.L. Bindoff, and J.A. Church, 2001: Freshwater and heat changes in the North and South Pacific Oceans between the 1960s and 1985-94. *J. Climate*, **14**(7), 1613-1633.
- Woodroffe**, C. and R. McLean, 1990: Microatolls and recent sea level

- change on coral atolls. *Nature*, **334**, 531-534.
- Woodworth**, P.L., 1987: Trends in U.K. mean sea level. *Marine Geodesy*, **11**, 57-87.
- Woodworth**, P.L. 1990: A search for accelerations in records of European mean sea level. *International Journal of Climatology*, **10**, 129-143.
- Woodworth**, P.L., 1999a: High waters at Liverpool since 1768: the UK's longest sea level record. *Geophysical Research Letters*, **26**, 1589-1592.
- Woodworth**, P.L. 1999b: A study of changes in high water levels and tides at Liverpool during the last two hundred and thirty years with some historical background. Proudman Oceanographic Laboratory Report No.56, 62 pp.
- Woodworth**, P.L., M.N. Tsimplis, R.A. Flather and I. Shennan, 1999: A review of the trends observed in British Isles mean sea level data measured by tide gauges. *Geophysical Journal International*, **136**, 651-670.
- Wu**, P. and Peltier W. R., 1984: Pleistocene deglaciation and the Earth's rotation: A new analysis. *Geophys. J.*, **76**, 202-242.
- Yasuda**, T. and K. Hanawa, 1997: Decadal changes in the mode waters in the midlatitude North Pacific. *Journal of Physical Oceanography*, **27**, 858-70.
- Yokoyama**, Y., K. Lambeck, P. de Dekker, P. Johnston, and K. Fifield, 2000: Timing of the last glacial maximum from observed sea level minima. *Nature*, **406**, 713-716.
- Zhang**, R.-H. and S. Levitus, 1997: Structure and cycle of decadal variability of upper-ocean temperature in the North Pacific. *Journal of Climate*, **10**, 710-27.
- Zhang**, K., B.C. Douglas, and S.P. Leatherman, 1997: East coast storm surges provide unique climate record. *EOS, Transactions of the American Geophysical Union*, **78**(37), 389-397.
- Zhang**, K., B.C. Douglas and S.P. Leatherman, 2000: Twentieth-century storm activity along the U.S. east coast. *J Climate*, **13**, 1748-1761.
- Zhang**, T., R.G. Barry, K. Knowles, J.A. Heginbottom, and J. Brown, 1999. Statistics and characteristics of permafrost and ground ice distribution in the Northern Hemisphere. *Polar Geography*, **23**, 147-169.
- Zhen**, W.Z. and R.H. Wu, 1993: Sea level changes of the World and China. *Marine Science Bulletin*, **12**, 95-99.
- Zuo**, Z., and J. Oerlemans, 1997: Contribution of glacier melt to sea level rise since AD 1865: a regionally differentiated calculation. *Climate Dynamics*, **13**, 835-845.
- Zwally**, H.J., and M.B. Giovinetto, 2000: Spatial distribution of surface mass balance on Greenland, *Annals of Glaciology*, **31**, 126-132.
- Zwart**, D., K. Lambeck, M. Bird, and J. Stone, 1997: Constraints on the former Antarctic Ice Sheet from sea level observations and geodynamics modelling. In: *The Antarctic Region: Geological Evolution and Processes*, C. Ricci (ed.), Terra Antarctica Publications, Siena, 861-868.

12

Detection of Climate Change and Attribution of Causes

Co-ordinating Lead Authors

J.F.B. Mitchell, D.J. Karoly

Lead Authors

G.C. Hegerl, F.W. Zwiers, M.R. Allen, J. Marengo

Contributing Authors

V. Barros, M. Berliner, G. Boer, T. Crowley, C. Folland, M. Free, N. Gillett, P. Groisman, J. Haigh, K. Hasselmann, P. Jones, M. Kandlikar, V. Kharin, H. Kheshgi, T. Knutson, M. MacCracken, M. Mann, G. North, J. Risbey, A. Robock, B. Santer, R. Schnur, C. Schönwiese, D. Sexton, P. Stott, S. Tett, K. Vinnikov, T. Wigley

Review Editors

F. Semazzi, J. Zillman

Contents

Executive Summary	697		
12.1 Introduction	700	12.4 Quantitative Comparison of Observed and Modelled Climate Change	716
12.1.1 The Meaning of Detection and Attribution	700	12.4.1 Simple Indices and Time-series Methods	716
12.1.2 Summary of the First and Second Assessment Reports	701	12.4.2 Pattern Correlation Methods	718
12.1.3 Developments since the Second Assessment Report	701	12.4.2.1 Horizontal patterns	718
12.2 The Elements of Detection and Attribution	701	12.4.2.2 Vertical patterns	720
12.2.1 Observed Data	701	12.4.3 Optimal Fingerprint Methods	721
12.2.2 Internal Climate Variability	702	12.4.3.1 Single pattern studies	721
12.2.3 Climate Forcings and Responses	705	12.4.3.2 Optimal detection studies that use multiple fixed signal patterns	722
12.2.3.1 Natural climate forcing	706	12.4.3.3 Space-time studies	723
12.2.3.2 Climatic response to natural forcing	708	12.4.3.4 Summary of optimal fingerprinting studies	728
12.2.3.3 Anthropogenic forcing	709		
12.2.3.4 Climatic response to anthropogenic forcing	711	12.5 Remaining Uncertainties	729
12.2.4 Some Important Statistical Considerations	712	12.6 Concluding Remarks	730
12.3 Qualitative Comparison of Observed and Modelled Climate Change	713	Appendix 12.1: Optimal Detection is Regression	732
12.3.1 Introduction	713	Appendix 12.2: Three Approaches to Optimal Detection	733
12.3.2 Thermal Indicators	714	Appendix 12.3: Pattern Correlation Methods	733
12.3.3 Hydrological Indicators	715	Appendix 12.4: Dimension Reduction	734
12.3.4 Circulation	715	Appendix 12.5: Determining the Likelihood of Outcomes (p-values)	734
12.3.5 Combined Evidence	715	References	735

Executive Summary

The IPCC WG1 Second Assessment Report (IPCC, 1996) (hereafter SAR) concluded, “the balance of evidence suggests that there is a discernible human influence on global climate”. It noted that the detection and attribution of anthropogenic climate change signals can only be accomplished through a gradual accumulation of evidence. The SAR authors also noted uncertainties in a number of factors, including the magnitude and patterns of internal climate variability, external forcing and climate system response, which prevented them from drawing a stronger conclusion. The results of the research carried out since 1995 on these uncertainties and other aspects of detection and attribution are summarised below.

A longer and more closely scrutinised observational record

Three of the five years (1995, 1996 and 1998) added to the instrumental record since the SAR are the warmest in the instrumental record of global temperatures, consistent with the expectation that increases in greenhouse gases will lead to continued long-term warming. The impact of observational sampling errors has been estimated for the global and hemispheric mean surface temperature record and found to be small relative to the warming observed over the 20th century. Some sources of error and uncertainty in both the Microwave Sounding Unit (MSU) and radiosonde observations have been identified that largely resolve discrepancies between the two data sets. However, current climate models cannot fully account for the observed difference in the trend between the surface and lower-tropospheric temperatures over the last twenty years even when all known external influences are included. New reconstructions of the surface temperature record of the last 1,000 years indicate that the temperature changes over the last 100 years are unlikely to be entirely natural in origin, even taking into account the large uncertainties in palaeo-reconstructions.

New model estimates of internal variability

Since the SAR, more models have been used to estimate the magnitude of internal climate variability. Several of the models used for detection show similar or larger variability than observed on interannual to decadal time-scales, even in the absence of external forcing. The warming over the past 100 years is very unlikely to be due to internal variability alone as estimated by current models. Estimates of variability on the longer time-scales relevant to detection and attribution studies are uncertain. Nonetheless, conclusions on the detection of an anthropogenic signal are insensitive to the model used to estimate internal variability and recent changes cannot be accounted for as pure internal variability even if the amplitude of simulated internal variations is increased by a factor of two or more. In most recent studies, the residual variability that remains in the observations after removal of the estimated anthropogenic signals is consistent with model-simulated variability on the space- and time-scales used for detection and attribution. Note, however, that the power of the consistency test is limited. Detection studies to date have shown that the observed large-scale changes in surface temperature in recent decades are unlikely (bordering on very unlikely) to be entirely the result of internal variability.

New estimates of responses to natural forcing

Fully coupled ocean-atmosphere models have used reconstructions of solar and volcanic forcings over the last one to three centuries to estimate the contribution of natural forcing to climate variability and change. Including their effects produces an increase in variance on all time-scales and brings the low-frequency variability simulated by models closer to that deduced from palaeo-reconstructions. Assessments based on physical principles and model simulations indicate that natural forcing alone is unlikely to explain the increased rate of global warming since the middle of the 20th century or changes in vertical temperature structure. The reasons are that the trend in natural forcing has likely been negative over the last two decades and natural forcing alone is unlikely to account for the observed cooling of the stratosphere. However, there is evidence for a detectable volcanic influence on climate. The available evidence also suggests a solar influence in proxy records of the last few hundred years and also in the instrumental record of the early 20th century. Statistical assessments confirm that natural variability (the combination of internal and naturally forced) is unlikely to explain the warming in the latter half of the 20th century.

Improved representation of anthropogenic forcing

Several studies since the SAR have included an explicit representation of greenhouse gases (as opposed to an equivalent increase in carbon dioxide (CO_2)). Some have also included tropospheric ozone changes, an interactive sulphur cycle, an explicit radiative treatment of the scattering of sulphate aerosols, and improved estimates of the changes in stratospheric ozone. While detection of the climate response to these other anthropogenic factors is often ambiguous, detection of the influence of greenhouse gas increases on the surface temperature changes over the past 50 years is robust.

Sensitivity to estimates of climate change signals

Since the SAR, more simulations with increases in greenhouse gases and some representation of aerosol effects have become available. In some cases, ensembles of simulations have been run to reduce noise in the estimates of the time-dependent response. Some studies have evaluated seasonal variation of the response. Uncertainties in the estimated climate change signals have made it difficult to attribute the observed climate change to one specific combination of anthropogenic and natural influences. Nevertheless, all studies since the SAR have found a significant anthropogenic contribution is required to account for surface and tropospheric trends over at least the last 30 years.

Qualitative consistencies between observed and modelled climate changes

There is a wide range of evidence of qualitative consistencies between observed climate changes and model responses to anthropogenic forcing, including global warming, increasing land-ocean temperature contrast, diminishing Arctic sea-ice extent, glacial retreat and increases in precipitation in Northern Hemisphere high latitudes. Some qualita-

tive inconsistencies remain, including the fact that models predict a faster rate of warming in the mid- to upper troposphere which is not observed in either satellite or radiosonde tropospheric temperature records.

A wider range of detection techniques

A major advance since the SAR is the increase in the range of techniques used, and the evaluation of the degree to which the results are independent of the assumptions made in applying those techniques. There have been studies using pattern correlations, optimal detection studies using one or more fixed patterns and time-varying patterns, and a number of other techniques. Evidence of a human influence on climate is obtained using all these techniques.

Results are sensitive to the range of temporal and spatial scales that are considered. Several decades of data are necessary to separate the forced response from internal variability. Idealised studies have demonstrated that surface temperature changes are detectable only on scales greater than 5,000 km. Studies also show that the level of agreement found between simulations and observations in pattern correlation studies is close to what one would expect in theory.

Attribution studies have applied multi-signal techniques to address whether or not the magnitude of the observed response to a particular forcing agent is consistent with the modelled response and separable from the influence of other forcing agents. The inclusion of time-dependent signals has helped to distinguish between natural and anthropogenic forcing agents. As more response patterns are included, the problem of degeneracy (different combinations of patterns yielding near identical fits to the observations) inevitably arises. Nevertheless, even with the responses to all the major forcing factors included in the analysis, a distinct greenhouse gas signal remains detectable. Overall, the magnitude of the model-simulated temperature response to greenhouse gases is found to be consistent with the observed greenhouse response on the scales considered. However, there remain discrepancies between the modelled and observed responses to other natural and anthropogenic factors, and estimates of signal amplitudes are model-dependent. Most studies find that, over the last 50 years, the estimated rate and magnitude of warming due to increasing concentrations of greenhouse gases alone are comparable with, or larger than, the observed warming. Furthermore, most model estimates that take into account both greenhouse gases and sulphate aerosols are consistent with observations over this period.

The increase in the number of studies, the breadth of techniques, increased rigour in the assessment of the role of anthropogenic forcing in climate, the robustness of results to the assumptions made using those techniques, and consistency of results lead to increased confidence in these results. Moreover, to be consistent with the signal observed to date, the rate of anthropogenic warming is likely to lie in the range 0.1 to 0.2°C/decade over the first half of the 21st century under the IS92a (IPCC, 1992) emission scenario.

Remaining uncertainties

A number of important uncertainties remain. These include:

- Discrepancies between the vertical profile of temperature change in the troposphere seen in observations and models. These have been reduced as more realistic forcing histories have been used in models, although not fully resolved. Also, the difference between observed surface and lower-tropospheric trends over the last two decades cannot be fully reproduced by model simulations.
- Large uncertainties in estimates of internal climate variability from models and observations, though as noted above, these are unlikely (bordering on very unlikely) to be large enough to nullify the claim that a detectable climate change has taken place.
- Considerable uncertainty in the reconstructions of solar and volcanic forcing which are based on proxy or limited observational data for all but the last two decades. Detection of the influence of greenhouse gases on climate appears to be robust to possible amplification of the solar forcing by ozone/solar or solar/cloud interactions, provided these do not alter the pattern or time dependence of the response to solar forcing. Amplification of the solar signal by these processes, which are not yet included in models, remains speculative.
- Large uncertainties in anthropogenic forcing are associated with the effects of aerosols. The effects of some anthropogenic factors, including organic carbon, black carbon, biomass aerosols, and changes in land use, have not been included in detection and attribution studies. Estimates of the size and geographic pattern of the effects of these forcings vary considerably, although individually their global effects are estimated to be relatively small.
- Large differences in the response of different models to the same forcing. These differences, which are often greater than the difference in response in the same model with and without aerosol effects, highlight the large uncertainties in climate change prediction and the need to quantify uncertainty and reduce it through better observational data sets and model improvement.

Synopsis

The SAR concluded: "The balance of evidence suggests a discernible human influence on global climate". That report also noted that the anthropogenic signal was still emerging from the background of natural climate variability. Since the SAR, progress has been made in reducing uncertainty, particularly with respect to distinguishing and quantifying the magnitude of responses to different external influences. Although many of the sources of uncertainty identified in the SAR still remain to some degree, new evidence and improved understanding support an updated conclusion.

- There is a longer and more closely scrutinised temperature record and new model estimates of variability. The warming over the past 100 years is very unlikely to be due to internal

variability alone, as estimated by current models. Reconstructions of climate data for the past 1,000 years also indicate that this warming was unusual and is unlikely to be entirely natural in origin.

- There are new estimates of the climate response to natural and anthropogenic forcing, and new detection techniques have been applied. Detection and attribution studies consistently find evidence for an anthropogenic signal in the climate record of the last 35 to 50 years.
- Simulations of the response to natural forcings alone (i.e., the response to variability in solar irradiance and volcanic eruptions) do not explain the warming in the second half of the 20th century. However, they indicate that natural forcings may have contributed to the observed warming in the first half of the 20th century.
- The warming over the last 50 years due to anthropogenic greenhouse gases can be identified despite uncertainties in forcing due to anthropogenic sulphate aerosol and natural factors (volcanoes and solar irradiance). The anthropogenic sulphate aerosol forcing, while uncertain, is negative over this period and therefore cannot explain the warming. Changes in natural forcing during most of this period are also estimated to be negative and are unlikely to explain the warming.
- Detection and attribution studies comparing model simulated changes with the observed record can now take into account

uncertainty in the magnitude of modelled response to external forcing, in particular that due to uncertainty in climate sensitivity.

- Most of these studies find that, over the last 50 years, the estimated rate and magnitude of warming due to increasing concentrations of greenhouse gases alone are comparable with, or larger than, the observed warming. Furthermore, most model estimates that take into account both greenhouse gases and sulphate aerosols are consistent with observations over this period.
- The best agreement between model simulations and observations over the last 140 years has been found when all the above anthropogenic and natural forcing factors are combined. These results show that the forcings included are sufficient to explain the observed changes, but do not exclude the possibility that other forcings may also have contributed.

In the light of new evidence and taking into account the remaining uncertainties, most of the observed warming over the last 50 years is likely to have been due to the increase in greenhouse gas concentrations.

Furthermore, it is very likely that the 20th century warming has contributed significantly to the observed sea level rise, through thermal expansion of sea water and widespread loss of land ice. Within present uncertainties, observations and models are both consistent with a lack of significant acceleration of sea level rise during the 20th century.

12.1 Introduction

12.1.1 The Meaning of Detection and Attribution

The response to anthropogenic changes in climate forcing occurs against a backdrop of natural internal and externally forced climate variability that can occur on similar temporal and spatial scales. Internal climate variability, by which we mean climate variability not forced by external agents, occurs on all time-scales from weeks to centuries and millennia. Slow climate components, such as the ocean, have particularly important roles on decadal and century time-scales because they integrate high-frequency weather variability (Hasselmann, 1976) and interact with faster components. Thus the climate is capable of producing long time-scale internal variations of considerable magnitude without any external influences. Externally forced climate variations may be due to changes in natural forcing factors, such as solar radiation or volcanic aerosols, or to changes in anthropogenic forcing factors, such as increasing concentrations of greenhouse gases or sulphate aerosols.

Definitions

The presence of this natural climate variability means that the detection and attribution of anthropogenic climate change is a statistical “signal-in-noise” problem. *Detection* is the process of demonstrating that an observed change is significantly different (in a statistical sense) than can be explained by natural internal variability. However, the detection of a change in climate does not necessarily imply that its causes are understood. As noted in the SAR, the unequivocal *attribution* of climate change to anthropogenic causes (i.e., the isolation of cause and effect) would require controlled experimentation with the climate system in which the hypothesised agents of change are systematically varied in order to determine the climate’s sensitivity to these agents. Such an approach to attribution is clearly not possible. Thus, from a practical perspective, attribution of observed climate change to a given combination of human activity and natural influences requires another approach. This involves statistical analysis and the careful assessment of multiple lines of evidence to demonstrate, within a pre-specified margin of error, that the observed changes are:

- unlikely to be due entirely to internal variability;
- consistent with the estimated responses to the given combination of anthropogenic and natural forcing; and
- not consistent with alternative, physically plausible explanations of recent climate change that exclude important elements of the given combination of forcings.

Limitations

It is impossible, even in principle, to distinguish formally between all conceivable explanations with a finite amount of data. Nevertheless, studies have now been performed that include all the main natural and anthropogenic forcing agents that are generally accepted (on physical grounds) to have had a substan-

tial impact on near-surface temperature changes over the 20th century. Any statement that a model simulation is consistent with observed changes can only apply to a subset of model-simulated variables, such as large-scale near-surface temperature trends: no numerical model will ever be perfect in every respect. To attribute all or part of recent climate change to human activity, therefore, we need to demonstrate that alternative explanations, such as pure internal variability or purely naturally forced climate change, are unlikely to account for a set of observed changes that can be accounted for by human influence. Detection (ruling out that observed changes are only an instance of internal variability) is thus one component of the more complex and demanding process of attribution. In addition to this general usage of the term detection (that some climate change has taken place), we shall also discuss the detection of the influence of individual forcings (see Section 12.4).

Detection and estimation

The basic elements of this approach to detection and attribution were recognised in the SAR. However, detection and attribution studies have advanced beyond addressing the simple question “have we detected a human influence on climate?” to such questions as “how large is the anthropogenic change?” and “is the magnitude of the response to greenhouse gas forcing as estimated in the observed record consistent with the response simulated by climate models?” The task of detection and attribution can thus be rephrased as an estimation problem, with the quantities to be estimated being the factor(s) by which we have to scale the model-simulated response(s) to external forcing to be consistent with the observed change. The estimation approach uses essentially the same tools as earlier studies that considered the problem as one of hypothesis testing, but is potentially more informative in that it allows us to quantify, with associated estimates of uncertainty, how much different factors have contributed to recent observed climate changes. This interpretation only makes sense, however, if it can be assumed that important sources of model error, such as missing or incorrectly represented atmospheric feedbacks, affect primarily the amplitude and not the structure of the response to external forcing. The majority of relevant studies suggest that this is the case for the relatively small-amplitude changes observed to date, but the possibility of model errors changing both the amplitude and structure of the response remains an important caveat. Sampling error in model-derived signals that originates from the model’s own internal variability also becomes an issue if detection and attribution is considered as an estimation problem – some investigations have begun to allow for this, and one study has estimated the contribution to uncertainty from observational sampling and instrumental error. The robustness of detection and attribution findings obtained with different climate models has been assessed.

Extensions

It is important to stress that the attribution process is inherently open-ended, since we have no way of predicting what alternative explanations for observed climate change may be proposed, and be accepted as plausible, in the future. This problem is not unique to the climate change issue, but applies to any problem of

establishing cause and effect given a limited sample of observations. The possibility of a confounding explanation can never be ruled out completely, but as successive alternatives are tested and found to be inadequate, it can be seen to become progressively more unlikely. There is growing interest in the use of Bayesian methods (Dempster, 1998; Hasselmann, 1998; Leroy, 1998; Tol and de Vos, 1998; Barnett *et al.*, 1999; Levine and Berliner, 1999; Berliner *et al.*, 2000). These provide a means of formalising the process of incorporating additional information and evaluating a range of alternative explanations in detection and attribution studies. Existing studies can be rephrased in a Bayesian formalism without any change in their conclusions, as demonstrated by Leroy (1998). However, a number of statisticians (e.g., Berliner *et al.*, 2000) argue that a more explicitly Bayesian approach would allow greater flexibility and rigour in the treatment of different sources of uncertainty.

12.1.2 Summary of the First and Second Assessment Reports

The first IPCC Scientific Assessment in 1990 (IPCC, 1990) concluded that the global mean surface temperature had increased by 0.3 to 0.6°C over the previous 100 years and that the magnitude of this warming was broadly consistent with the predictions of climate models forced by increasing concentrations of greenhouse gases. However, it remained to be established that the observed warming (or part of it) could be attributed to the enhanced greenhouse effect. Some of the reasons for this were that there was only limited agreement between model predictions and observations, because climate models were still in the early stages of development; there was inadequate knowledge of natural variability and other possible anthropogenic effects on climate and there was a scarcity of suitable observational data, particularly long, reliable time-series.

By the time of the SAR in 1995, considerable progress had been made in attempts to identify an anthropogenic effect on climate. The first area of significant advance was that climate models were beginning to incorporate the possible climatic effects of human-induced changes in sulphate aerosols and stratospheric ozone. The second area of progress was in better defining the background variability of the climate system through multi-century model experiments that assumed no changes in forcing. These provided important information about the possible characteristics of the internal component of natural climate variability. The third area of progress was in the application of pattern-based methods that attempted to attribute some part of the observed changes in climate to human activities, although these studies were still in their infancy at that time.

The SAR judged that the observed trend in global climate over the previous 100 years was unlikely to be entirely natural in origin. This led to the following, now well-known, conclusion: “Our ability to quantify the human influence on global climate is currently limited because the expected signal is still emerging from the noise of natural variability, and because there are uncertainties in key factors. Nevertheless, the balance of evidence suggests that there is a discernible human influence on global climate”. It also noted that the magnitude of the influence was uncertain.

12.1.3 Developments since the Second Assessment Report

In the following sections, we assess research developments since the SAR in areas crucial to the detection of climate change and the attribution of its causes. First, in Section 12.2, we review advances in the different elements that are needed in any detection and attribution study, including observational data, estimates of internal climate variability, natural and anthropogenic climate forcings and their simulated responses, and statistical methods for comparing observed and modelled climate change. We draw heavily on the assessments in earlier chapters of this report, particularly Chapter 2 – Observed Climate Variability and Change, Chapter 6 – Radiative Forcing of Climate Change, Chapter 8 – Model Evaluation, and Chapter 9 – Projections of Future Climate Change.

In Section 12.3, a qualitative assessment is made of observed and modelled climate change, identifying general areas of agreement and difference. This is based on the observed climate changes identified with most confidence in Chapter 2 and the model projections of climate change from Chapter 9.

Next, in Section 12.4, advances obtained with quantitative methods for climate change detection and attribution are assessed. These include results obtained with time-series methods, pattern correlation methods, and optimal fingerprint methods. The interpretation of optimal fingerprinting as an estimation problem, finding the scaling factors required to bring the amplitude of model-simulated changes into agreement with observed changes, is discussed. Some remaining uncertainties are discussed in Section 12.5 and the key findings are drawn together in Section 12.6.

12.2 The Elements of Detection and Attribution

12.2.1 Observed Data

Ideally, a detection and attribution study requires long records of observed data for climate elements that have the potential to show large climate change signals relative to natural variability. It is also necessary that the observing system has sufficient coverage so that the main features of natural variability and climate change can be identified and monitored. A thorough assessment of observed climate change, climate variability and data quality was presented in Chapter 2. Most detection and attribution studies have used near-surface air temperature, sea surface temperature or upper air temperature data, as these best fit the requirement above.

The quality of observed data is a vital factor. Homogeneous data series are required with careful adjustments to account for changes in observing system technologies and observing practices. Estimates of observed data uncertainties due to instrument errors or variations in data coverage (assessed in Chapter 2) are included in some recent detection and attribution studies.

There have been five more years of observations since the SAR. Improvements in historical data coverage and processing are described in Chapter 2. Confidence limits for observational sampling error have been estimated for the global and hemispheric mean temperature record. Applications of improved pre-instrumental proxy data reconstructions are described in the next two sections.

12.2.2 Internal Climate Variability

Detection and attribution of climate change is a statistical “signal-in-noise” problem, it requires an accurate knowledge of the properties of the “noise”. Ideally, internal climate variability would be estimated from instrumental observations, but a number of problems make this difficult. The instrumental record is short relative to the 30 to 50 year time-scales that are of interest for detection and attribution of climate change, particularly for variables in the free atmosphere. The longest records that are available are those for surface air temperature and sea surface temperature. Relatively long records are also available for precipitation and surface pressure, but coverage is incomplete and varies in time (see Chapter 2). The instrumental record also contains the influences of external anthropogenic and natural forcing. A record of natural internal variability can be reconstructed by removing estimates of the response to external forcing (for example, Jones and Hegerl, 1998; Wigley *et al.*, 1998a). However, the accuracy of this record is limited by incomplete knowledge of the forcings and by the accuracy of the climate model used to estimate the response.

Estimates using palaeoclimatic data

Palaeo-reconstructions provide an additional source of information on climate variability that strengthens our qualitative assessment of recent climate change. There has been considerable progress in the reconstruction of past temperatures. New reconstructions with annual or seasonal resolution, back to 1000 AD, and some spatial resolution have become available (Briffa *et al.*, 1998; Jones *et al.*, 1998; Mann *et al.*, 1998, 2000; Briffa *et al.*, 2000; Crowley and Lowery, 2000; see also Chapter 2, Figure 2.21). However, a number of difficulties, including limited coverage, temporal inhomogeneity, possible biases due to the palaeo-reconstruction process, uncertainty regarding the strength of the relationships between climatic and proxy indices, and the likely but unknown influence of external forcings inhibit the estimation of internal climate variability directly from palaeoclimate data. We expect, however, that the reconstructions will continue to improve and that palaeo-data will become increasingly important for assessing natural variability of the climate system. One of the most important applications of this palaeoclimate data is as a check on the estimates of internal variability from coupled climate models, to ensure that the latter are not underestimating the level of internal variability on 50 to 100 year time-scales (see below). The limitations of the instrumental and palaeo-records leave few alternatives to using long “control” simulations with coupled models (see Figure 12.1) to estimate the detailed structure of internal climate variability.

Estimates of the variability of global mean surface temperature
 Stouffer *et al.* (2000) assess variability simulated in three 1,000-year control simulations (see Figure 12.1). The models are found to simulate reasonably well the spatial distribution of variability and the spatial correlation between regional and global mean variability, although there is more disagreement between models at long time-scales (>50 years) than at short time-scales. None of the long model simulations produces a secular trend which is

comparable to that observed. Chapter 8, Section 8.6.2, assesses model-simulated variability in detail. Here we assess the aspects that are particularly relevant to climate change detection. The power spectrum of global mean temperatures simulated by the most recent coupled climate models (shown in Figure 12.2) compares reasonably well with that of detrended observations (solid black line) on interannual to decadal time-scales. However, uncertainty of the spectral estimates is large and some models are clearly underestimating variability (indicated by the asterisks). Detailed comparison on inter-decadal time-scales is difficult because observations are likely to contain a response to external forcings that will not be entirely removed by a simple linear trend. At the same time, the detrending procedure itself introduces a negative bias in the observed low-frequency spectrum.

Both of these problems can be avoided by removing an independent estimate of the externally forced response from the observations before computing the power spectrum. This independent estimate is provided by the ensemble mean of a coupled model simulation of the response to the combination of natural and anthropogenic forcing (see Figure 12.7c). The resulting spectrum of observed variability (dotted line in Figure 12.2) will not be subject to a negative bias because the observed data have not been used in estimating the forced response. It will, however, be inflated by uncertainty in the model-simulated forced response and by noise due to observation error and due to incomplete coverage (particularly the bias towards relatively noisy Northern Hemisphere land temperatures in the early part of the observed series). This estimate of the observed spectrum is therefore likely to overestimate power at all frequencies. Even so, the more variable models display similar variance on the decadal to inter-decadal time-scales important for detection and attribution.

Estimates of spatial patterns of variability

Several studies have used common empirical orthogonal function (EOF) analysis to compare the spatial modes of climate variability between different models. Stouffer *et al.* (2000) analysed the variability of 5-year means of surface temperature in 500-year or longer simulations of the three models most commonly used to estimate internal variability in formal detection studies. The distribution of the variance between the EOFs was similar between the models and the observations. HadCM2 tended to overestimate the variability in the main modes, whereas GFDL and ECHAM3 underestimated the variability of the first mode. The standard deviations of the dominant modes of variability in the three models differ from observations by less than a factor of two, and one model (HadCM2) has similar or more variability than the observations in all leading modes. In general, one would expect to obtain conservative detection and attribution results when natural variability is estimated with such a model. One should also expect control simulations to be less variable than observations because they do not contain externally forced variability. Hegerl *et al.* (2000) used common EOFs to compare 50-year June-July-August (JJA) trends of surface temperature in ECHAM3 and HadCM2. Standard deviation differences between models

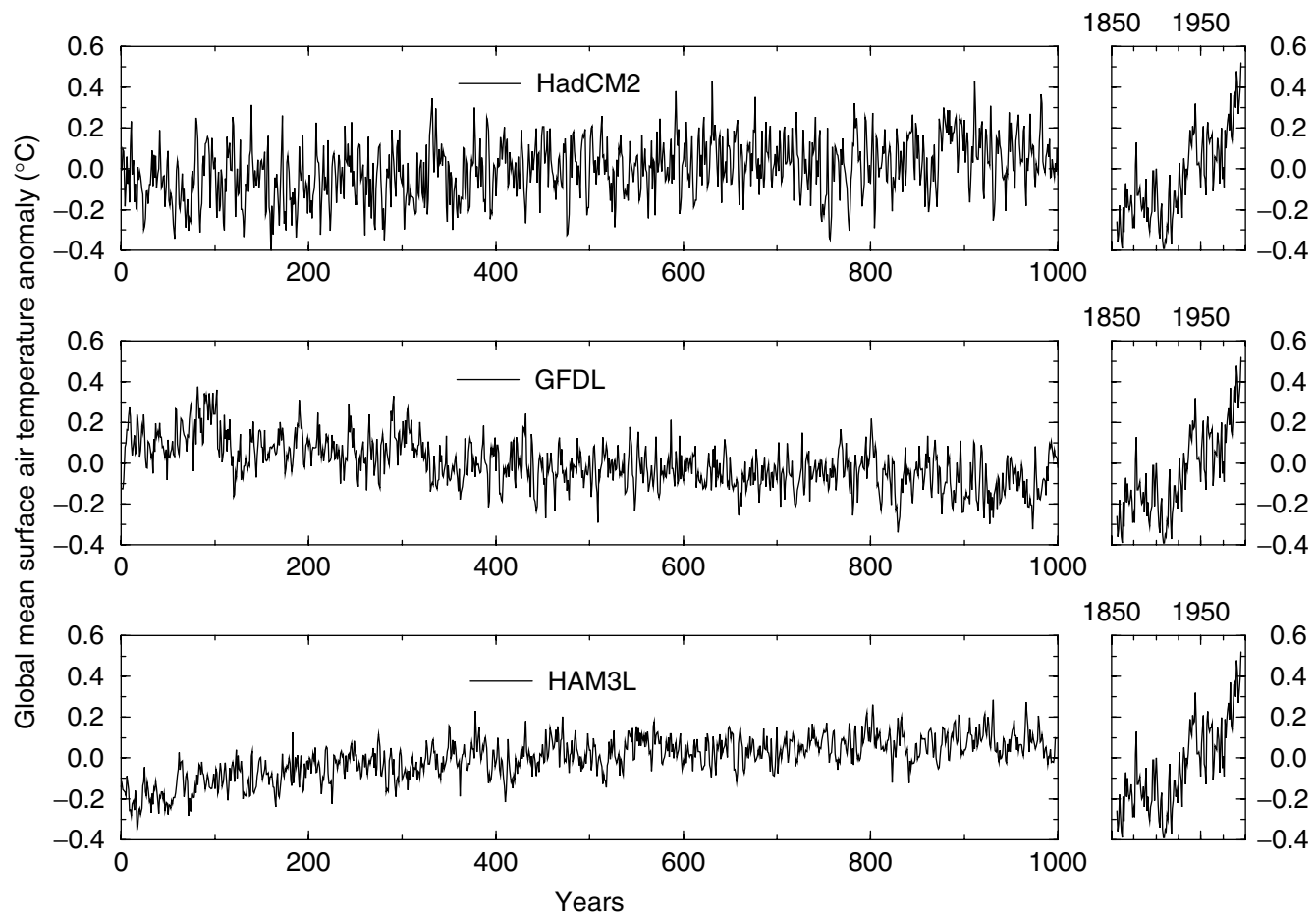


Figure 12.1: Global mean surface air temperature anomalies from 1,000-year control simulations with three different climate models, HadCM2, GFDL R15 and ECHAM3/LSG (labelled HAM3L), compared to the recent instrumental record (Stouffer *et al.*, 2000). No model control simulation shows a trend in surface air temperature as large as the observed trend. If internal variability is correct in these models, the recent warming is likely not due to variability produced within the climate system alone.

were marginally larger on the 50-year time-scale (less than a factor of 2.5). Comparison with direct observations cannot be made on this time-scale because the instrumental record is too short.

Variability of the free atmosphere

Gillett *et al.* (2000a) compared model-simulated variability in the free atmosphere with that of detrended radiosonde data. They found general agreement except in the stratosphere, where present climate models tend to underestimate variability on all time-scales and, in particular, do not reproduce modes of variability such as the quasi-biennial oscillation (QBO). On decadal time-scales, the model simulated less variability than observed in some aspects of the vertical patterns important for the detection of anthropogenic climate change. The discrepancy is partially resolved by the inclusion of anthropogenic (greenhouse gas, sulphate and stratospheric ozone) forcing in the model. However, the authors also find evidence that solar forcing plays a significant role on decadal time-scales, indicating that this should be taken into account in future detection studies based on changes in the free atmosphere (see also discussion in Chapter 6 and Section 12.2.3.1 below).

Comparison of model and palaeoclimatic estimates of variability

Comparisons between the variability in palaeo-reconstructions and climate model data have shown mixed results to date. Barnett *et al.* (1996) compared the spatial structure of climate variability of coupled climate models and proxy time-series for (mostly summer) decadal temperature (Jones *et al.*, 1998). They found that the model-simulated amplitude of the dominant proxy mode of variation is substantially less than that estimated from the proxy data. However, choosing the EOFs of the palaeo-data as the basis for comparison will maximise the variance in the palaeo-data and not the models, and so bias the model amplitudes downwards. The neglect of naturally forced climate variability in the models might also be responsible for part of the discrepancy noted in Barnett *et al.* (1996) (see also Jones *et al.*, 1998). The limitations of the temperature reconstructions (see Chapter 2, Figure 2.21), including for example the issue of how to relate site-specific palaeo-data to large-scale variations, may also contribute to this discrepancy. Collins *et al.* (2000) compared the standard deviation of large-scale Northern Hemisphere averages in a model control simulation and in tree-ring-based proxy data for the last 600 years on decadal time-scales. They found a

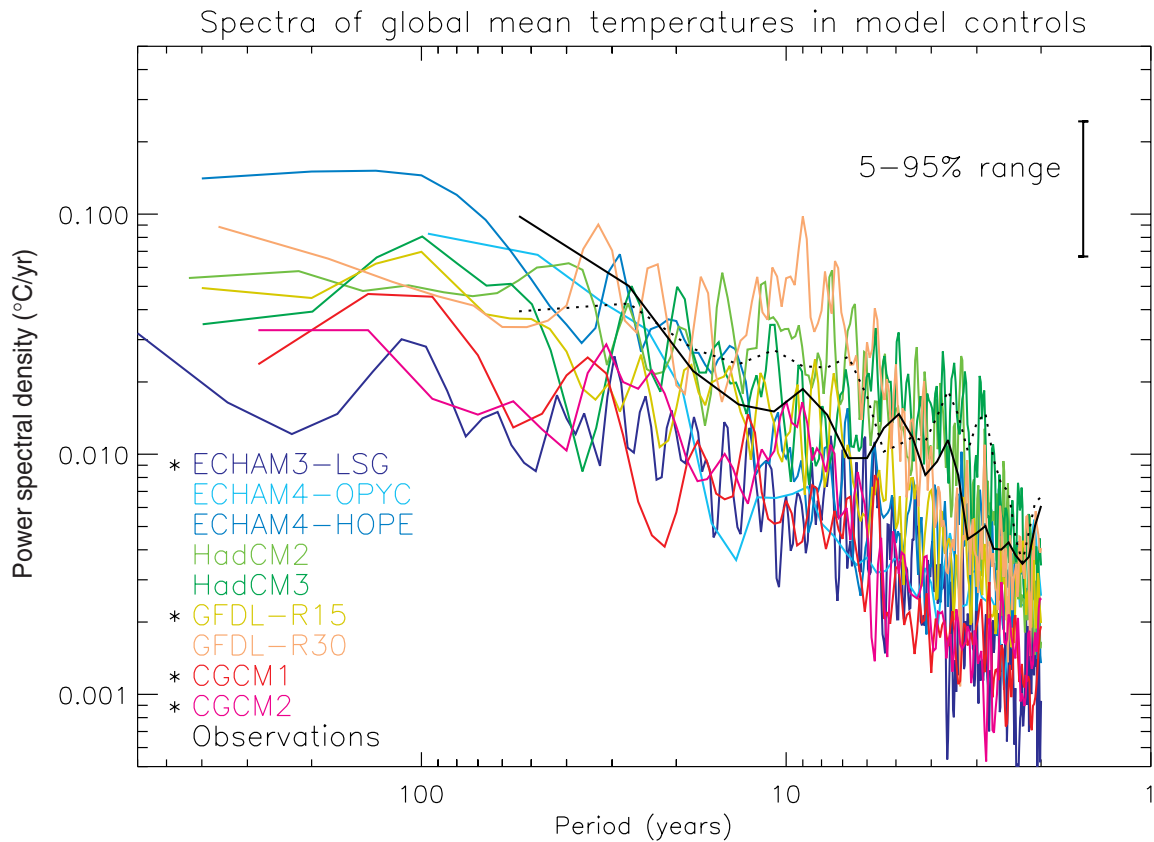


Figure 12.2: Coloured lines: power spectra of global mean temperatures in the unforced control integrations that are used to provide estimates of internal climate variability in Figure 12.12. All series were linearly detrended prior to analysis, and spectra computed using a standard Tukey window with the window width (maximum lag used in the estimate) set to one-fifth of the series length, giving each spectral estimate the same uncertainty range, as shown (see, e.g., Priestley, 1981). The first 300 years were omitted from ECHAM3-LSG, CGCM1 and CGCM2 models as potentially trend-contaminated. Solid black line: spectrum of observed global mean temperatures (Jones *et al.*, 2001) over the period 1861 to 1998 after removing a best-fit linear trend. This estimate is unreliable on inter-decadal time-scales because of the likely impact of external forcing on the observed series and the negative bias introduced by the detrending. Dotted black line: spectrum of observed global mean temperatures after removing an independent estimate of the externally forced response provided by the ensemble mean of a coupled model simulation (Stott *et al.*, 2000b, and Figure 12.7c). This estimate will be contaminated by uncertainty in the model-simulated forced response, together with observation noise and sampling error. However, unlike the detrending procedure, all of these introduce a positive (upward) bias in the resulting estimate of the observed spectrum. The dotted line therefore provides a conservative (high) estimate of observed internal variability at all frequencies. Asterisks indicate models whose variability is significantly less than observed variability on 10 to 60 year time-scales after removing either a best-fit linear trend or an independent estimate of the forced response from the observed series. Significance is based on an F-test on the ratio observed/model mean power over this frequency interval and quoted at the 5% level. Power spectral density (PSD) is defined such that unit-variance uncorrelated noise would have an expected PSD of unity (see Allen *et al.*, 2000a, for details). Note that different normalisation conventions can lead to different values, which appear as a constant offset up or down on the logarithmic vertical scale used here. Differences between the spectra shown here and the corresponding figure in Stouffer *et al.* (2000) shown in Chapter 8, Figure 8.18 are due to the use here of a longer (1861 to 2000) observational record, as opposed to 1881 to 1991 in Figure 8.18. That figure also shows 2.5 to 97.5% uncertainty ranges, while for consistency with other figures in this chapter, the 5 to 95% range is displayed here.

factor of less than two difference between model and data if the tree-ring data are calibrated such that low-frequency variability is better retained than in standard methods (Briffa *et al.*, 2000). It is likely that at least part of this discrepancy can be resolved if natural forcings are included in the model simulation. Crowley (2000) found that 41 to 69% of the variance in decadally smoothed Northern Hemisphere mean surface temperature reconstructions could be externally forced (using data from Mann *et al.* (1998) and Crowley and

Lowery (2000)). The residual variability in the reconstructions, after subtracting estimates of volcanic and solar-forced signals, showed no significant difference in variability on decadal and multi-decadal time-scales from three long coupled model control simulations. In summary, while there is substantial uncertainty in comparisons between long-term palaeo-records of surface temperature and model estimates of multi-decadal variability, there is no clear evidence of a serious discrepancy.

Summary

These findings emphasise that there is still considerable uncertainty in the magnitude of internal climate variability. Various approaches are used in detection and attribution studies to account for this uncertainty. Some studies use data from a number of coupled climate model control simulations (Santer *et al.*, 1995; Hegerl *et al.*, 1996, 1997, North and Stevens, 1998) and choose the most conservative result. In other studies, the estimate of internal variance is inflated to assess the sensitivity of detection and attribution results to the level of internal variance (Santer *et al.*, 1996a; Tett *et al.*, 1999; Stott *et al.*, 2001). Some authors also augment model-derived estimates of natural variability with estimates from observations (Hegerl *et al.*, 1996). A method for checking the consistency between the residual variability in the observations after removal of externally forced signals (see equation A12.1.1, Appendix 12.1) and the natural internal variability estimated from control simulations is also available (e.g., Allen and Tett, 1999). Results indicate that, on the scales considered, there is no evidence for a serious inconsistency between the variability in models used for optimal fingerprint studies and observations (Allen and Tett, 1999; Tett *et al.*, 1999; Hegerl *et al.*, 2000, 2001; Stott *et al.*, 2001). The use of this test and the use of internal variability from the models with the greatest variability increases confidence in conclusions derived from optimal detection studies.

12.2.3 Climate Forcings and Responses

The global mean change in radiative forcing (see Chapter 6) since the pre-industrial period may give an indication of the relative importance of the different external factors influencing climate over the last century. The temporal and spatial variation of the forcing from different sources may help to identify the effects of individual factors that have contributed to recent climate change.

The need for climate models

To detect the response to anthropogenic or natural climate forcing in observations, we require estimates of the expected space-time pattern of the response. The influences of natural and anthropogenic forcing on the observed climate can be separated only if the spatial and temporal variation of each component is known. These patterns cannot be determined from the observed instrumental record because variations due to different external forcings are superimposed on each other and on internal climate variations. Hence climate models are usually used to estimate the contribution from each factor. The models range from simpler energy balance models to the most complex coupled atmosphere-ocean general circulation models that simulate the spatial and temporal variations of many climatic parameters (Chapter 8).

The models used

Energy balance models (EBMs) simulate the effect of radiative climate forcing on surface temperature. Climate sensitivity is included as an adjustable parameter. These models are computationally inexpensive and produce noise-free estimates of the climate signal. However, EBMs cannot represent dynamical components of the climate signal, generally cannot simulate

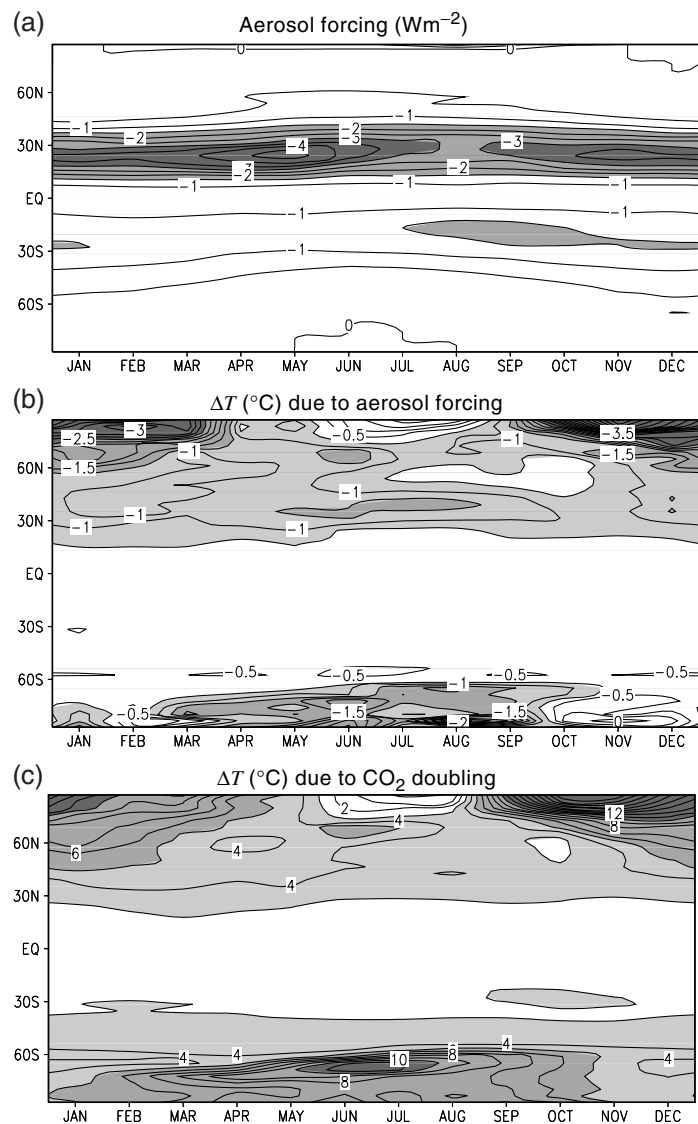


Figure 12.3: Latitude-month plot of radiative forcing and model equilibrium response for surface temperature. (a) Radiative forcing (Wm^{-2}) due to increased sulphate aerosol loading at the time of CO_2 doubling. (b) Change in temperature due to the increase in aerosol loading. (c) Change in temperature due to CO_2 doubling. Note that the patterns of radiative forcing and temperature response are quite different in (a) and (b), but that the patterns of large-scale temperature responses to different forcings are similar in (b) and (c). The experiments used to compute these fields are described by Reader and Boer (1998).

variables other than surface temperature, and may omit some of the important feedback processes that are accounted for in more complex models. Most detection and attribution approaches therefore apply signals estimated from coupled Atmosphere Ocean General Circulation Models (AOGCMs) or atmospheric General Circulation Models (GCMs) coupled to mixed-layer ocean models. Forced simulations with such models contain both the climate response to external forcing and superimposed internal climate variability. Estimates of the climate response

computed from model output will necessarily contain at least some noise from this source, although this can be reduced by the use of ensemble simulations. Note that different models can produce quite different patterns of response to a given forcing due to differences in the representation of feedbacks arising from changes in cloud (in particular), sea ice and land surface processes.

The relationship between patterns of forcing and response

There are several reasons why one should not expect a simple relationship between the patterns of radiative forcing and temperature response. First, strong feedbacks such as those due to water vapour and sea ice tend to reduce the difference in the temperature response due to different forcings. This is illustrated graphically by the response to the simplified aerosol forcing used in early studies. The magnitude of the model response is largest over the Arctic in winter even though the forcing is small, largely due to ice-albedo feedback. The large-scale patterns of change and their temporal variations are similar, but of opposite sign, to that obtained in greenhouse gas experiments (Figure 12.3, see also Mitchell *et al.*, 1995a). Second, atmospheric circulation tends to smooth out temperature gradients and reduce the differences in response patterns. Similarly, the thermal inertia of the climate system tends to reduce the amplitude of short-term fluctuations in forcing. Third, changes in radiative forcing are more effective if they act near the surface, where cooling to space is restricted, than at upper levels, and in high latitudes, where there are stronger positive feedbacks than at low latitudes (Hansen *et al.*, 1997a).

In practice, the response of a given model to different forcing patterns can be quite similar (Hegerl *et al.*, 1997; North and Stevens, 1998; Tett *et al.*, 1999). Similar signal patterns (a condition often referred to as “degeneracy”) can be difficult to distinguish from one another. Tett *et al.* (1999) find substantial degeneracy between greenhouse gas, sulphate, volcanic and solar patterns they used in their detection study using HadCM2. On the other hand, the greenhouse gas and aerosol patterns generated by ECHAM3 LSG (Hegerl *et al.*, 2000) are more clearly separable, in part because the patterns are more distinct, and in part because the aerosol response pattern correlates less well with ECHAM3 LSG’s patterns of internal variability. The vertical patterns of temperature change due to greenhouse gas and stratospheric ozone forcing are less degenerate than the horizontal patterns.

Summary

Different models may give quite different patterns of response for the same forcing, but an individual model may give a surprisingly similar response for different forcings. The first point means that attribution studies may give different results when using signals generated from different models. The second point means that it may be more difficult to distinguish between the response to different factors than one might expect, given the differences in radiative forcing.

12.2.3.1 Natural climate forcing

Since the SAR, there has been much progress in attempting to understand the climate response to fluctuations in solar

luminosity and to volcanism. These appear to be the most important among a broad range of natural external climate forcings at decadal and centennial time-scales. The mechanisms of these forcings, their reconstruction and associated uncertainties are described in Chapter 6, and further details of the simulated responses are given in Chapter 8, Section 8.6.3.

Volcanic forcing

The radiative forcing due to volcanic aerosols from the recent El Chichon and Mt. Pinatubo eruptions has been estimated from satellite and other data to be -3 Wm^{-2} (peak forcing; after Hansen *et al.*, 1998). The forcing associated with historic eruptions before the satellite era is more uncertain. Sato *et al.* (1993) estimated aerosol optical depth from ground-based observations over the last century (see also Stothers, 1996; Grieser and Schoenwiese, 1999). Prior to that, reconstructions have been based on various sources of data (ice cores, historic documents etc.; see Lamb, 1970; Simkin *et al.*, 1981; Robock and Free, 1995; Crowley and Kim, 1999; Free and Robock, 1999). There is uncertainty of about a factor of two in the peak forcing in reconstructions of historic volcanic forcing in the pre-satellite era (see Chapter 6).

Solar forcing

The variation of solar irradiance with the 11-year sunspot cycle has been assessed with some accuracy over more than 20 years, although measurements of the magnitude of modulations of solar irradiance between solar cycles are less certain (see Chapter 6). The estimation of earlier solar irradiance fluctuations, although based on physical mechanisms, is indirect. Hence our confidence in the range of solar radiation on century time-scales is low, and confidence in the details of the time-history is even lower (Harrison and Shine, 1999; Chapter 6). Several recent reconstructions estimate that variations in solar irradiance give rise to a forcing at the Earth’s surface of about 0.6 to 0.7 Wm^{-2} since the Maunder Minimum and about half this over the 20th century (see Chapter 6, Figure 6.5; Hoyt and Schatten, 1993; Lean *et al.*, 1995; Lean, 1997; Froehlich and Lean, 1998; Lockwood and Stamper, 1999). This is larger than the 0.2 Wm^{-2} modulation of the 11-year solar cycle measured from satellites. (Note that we discuss here the forcing at the Earth’s surface, which is smaller than that at the top of the atmosphere, due to the Earth’s geometry and albedo.) The reconstructions of Lean *et al.* (1995) and Hoyt and Schatten (1993), which have been used in GCM detection studies, vary in amplitude and phase. Chapter 6, Figure 6.8 shows time-series of reconstructed solar and volcanic forcing since the late 18th century. All reconstructions indicate that the direct effect of variations in solar forcing over the 20th century was about 20 to 25% of the change in forcing due to increases in the well-mixed greenhouse gases (see Chapter 6).

Reconstructions of climate forcing in the 20th century indicate that the net natural climate forcing probably increased during the first half of the 20th century, due to a period of low volcanism coinciding with a small increase in solar forcing. Recent decades show negative natural forcing due to increasing volcanism, which overwhelms the direct effect, if real, of a small increase in solar radiation (see Chapter 6, Table 6.13).

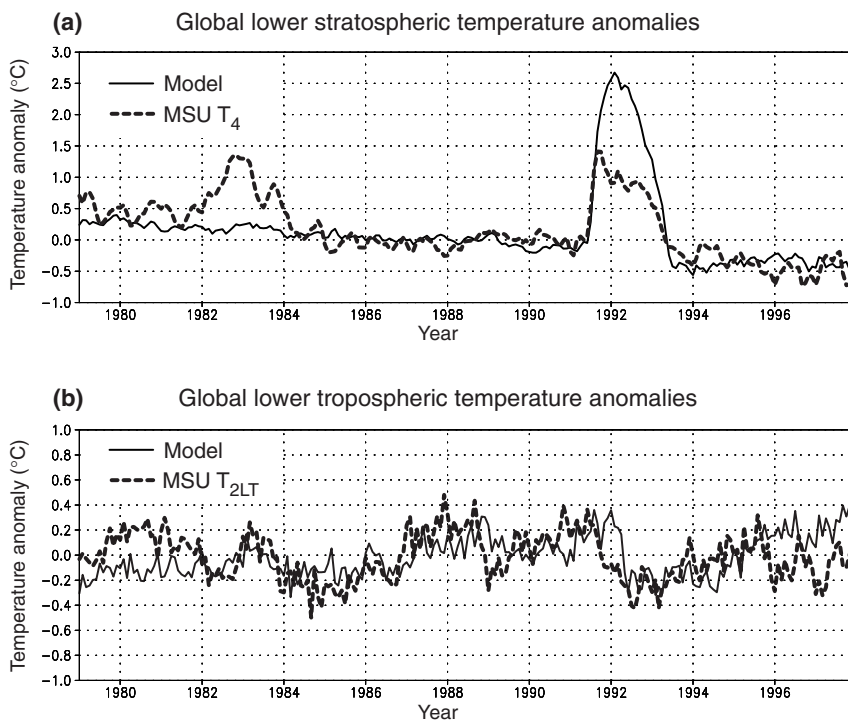


Figure 12.4: (a) Observed microwave sounding unit (MSU) global mean temperature in the lower stratosphere, shown as dashed line, for channel 4 for the period 1979 to 97 compared with the average of several atmosphere-ocean GCM simulations starting with different atmospheric conditions in 1979 (solid line). The simulations have been forced with increasing greenhouse gases, direct and indirect forcing by sulphate aerosols and tropospheric ozone forcing, and Mt. Pinatubo volcanic aerosol and stratospheric ozone variations. The model simulation does not include volcanic forcing due to El Chichon in 1982, so it does not show stratospheric warming then. (b) As for (a), except for 2LT temperature retrievals in the lower troposphere. Note the steady response in the stratosphere, apart from the volcanic warm periods, and the large variability in the lower troposphere (from Bengtsson *et al.*, 1999).

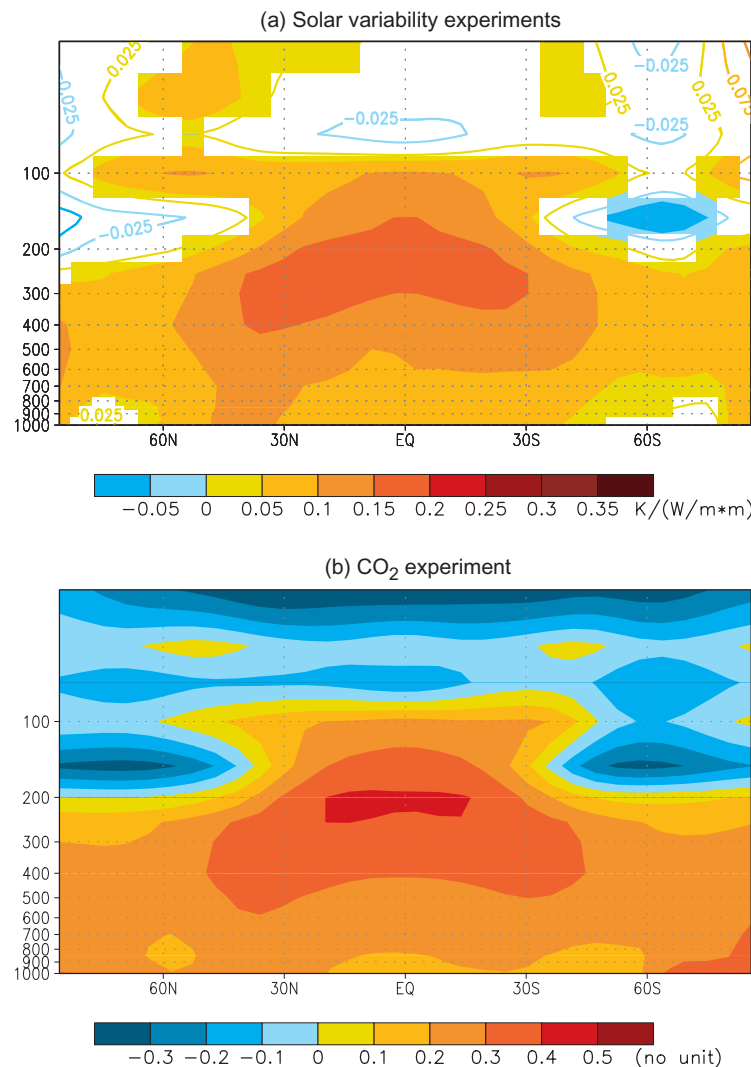


Figure 12.5: (a) Response (covariance, normalised by the variance of radiance fluctuations) of zonally averaged annual mean atmospheric temperature to solar forcing for two simulations with ECHAM3/LSG. Coloured regions indicate locally significant response to solar forcing. (b) Zonal mean of the first EOF of greenhouse gas-induced temperature change simulated with the same model (from Cubasch *et al.*, 1997). This indicates that for ECHAM3/LSG, the zonal mean temperature response to greenhouse gas and solar forcing are quite different in the stratosphere but similar in the troposphere.

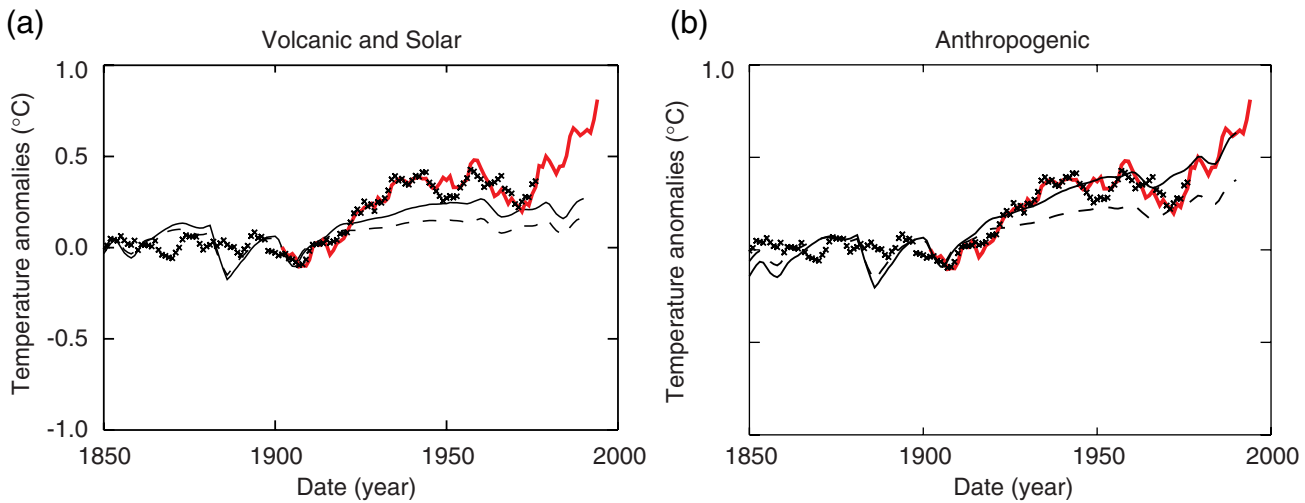


Figure 12.6: (a) Five-year running mean Northern Hemisphere temperature anomalies since 1850 (relative to the 1880 to 1920 mean) from an energy-balance model forced by Dust Veil volcanic index and Lean *et al.* (1995) solar index (see Free and Robock, 1999). Two values of climate sensitivity to doubling CO₂ were used; 3.0°C (thin solid line), and 1.5°C (dashed line). Also shown are the instrumental record (thick red line) and a reconstruction of temperatures from proxy records (crosses, from Mann *et al.*, 1998). The size of both the forcings and the proxy temperature variations are subject to large uncertainties. Note that the Mann temperatures do not include data after 1980 and do not show the large observed warming then. (b) As for (a) but for simulations with volcanic, solar and anthropogenic forcing (greenhouse gases and direct and indirect effects of tropospheric aerosols). The net anthropogenic forcing at 1990 relative to 1760 was 1.3 Wm⁻², including a net cooling of 1.3 Wm⁻² due to aerosol effects.

12.2.3.2 Climatic response to natural forcing

Response to volcanic forcing

The climate response to several recent volcanic eruptions has been studied in observations and simulations with atmospheric GCMs (e.g., Robock and Mao, 1992, 1995; Graf *et al.*, 1996; Hansen *et al.*, 1996; Kelly *et al.*, 1996; Mao and Robock, 1998; Kirchner *et al.*, 1999). The stratosphere warms and the annual mean surface and tropospheric temperature decreases during the two to three years following a major volcanic eruption. A simulation incorporating the effects of the Mt. Pinatubo eruption and observed changes in stratospheric ozone in addition to anthropogenic forcing approximately reproduces the observed stratospheric variations (Figure 12.4; Bengtsson *et al.*, 1999). It shows stratospheric warming after the volcanic eruption, superimposed on a long-term cooling trend. Although the surface temperature response in the Northern Hemisphere warm season following a volcanic eruption is dominated by global scale radiative cooling, some models simulate local warming over Eurasia and North America in the cold season due to changes in circulation (e.g., Graf *et al.*, 1996; Kirchner *et al.*, 1999). Variability from other sources makes assessment of the observed climate response difficult, particularly as the two most recent volcanic eruptions (Mt. Pinatubo and El Chichon) occurred in El Niño-Southern Oscillation (ENSO) warm years. Simulations with simple models (Bertrand *et al.*, 1999; Crowley and Kim, 1999; Grieser and Schoenwiese, 2001) and AOGCMs (Tett *et al.*, 1999; Stott *et al.*, 2001) produce a small decadal mean cooling in the 1980s and 1990s due to several volcanic eruptions in those decades. Some simulations also produce global warming in the early 20th century as a recovery from a series of strong eruptions around the turn of the 20th century. It is unclear whether such a long-term response is realistic.

Response to solar forcing

Since the SAR, there have been new modelling and observational studies on the climate effects of variations in solar irradiance. The surface temperature response to the 11-year cycle is found to be small (e.g., Cubasch *et al.*, 1997; White *et al.*, 1997; North and Stevens, 1998; Crowley and Kim, 1999; Free and Robock, 1999). Low-frequency solar variability over the last few hundred years gives a stronger surface temperature response (Cubasch *et al.*, 1997; Drijfhout *et al.*, 1999; Rind *et al.*, 1999; Tett *et al.*, 1999; Stott *et al.*, 2001). Model results show cooling circa 1800 due to the hypothesised solar forcing minimum and some warming in the 20th century, particularly in the early 20th century. Time-dependent experiments produce a global mean warming of 0.2 to 0.5°C in response to the estimated 0.7 Wm⁻² change of solar radiative forcing from the Maunder Minimum to the present (e.g., Lean and Rind, 1998; Crowley and Kim, 1999).

Ozone changes in the Earth's atmosphere caused by the 11-year solar cycle could affect the temperature response in the free atmosphere. A relation between 30 hPa geopotential and a solar index has been shown over nearly four solar cycles by Labitzke and van Loon (1997). Van Loon and Shea (1999, 2000) found a related connection between upper to middle tropospheric temperature and a solar index over the last 40 years, which is particularly strong in July and August. Variations in ozone forcing related to the solar cycle may also affect surface temperature via radiative and dynamical processes (see discussion in Chapter 6; Haigh, 1999; Shindell *et al.*, 1999, 2001), but observational evidence remains ambiguous (e.g., van Loon and Shea, 2000). The assessment of ozone-related Sun-climate interactions is uncertain as a result of the lack of long-term, reliable observations. This makes it difficult to separate effects of volcanic eruptions and solar forcing on ozone. There has also been

speculation that the solar cycle might influence cloudiness and hence surface temperature through cosmic rays (e.g., Svensmark and Friis-Christensen, 1997; Svensmark, 1998). The latter effect is difficult to assess due to limitations in observed data and the shortness of the correlated time-series.

As discussed earlier in Section 12.2.3, differences between the response to solar and greenhouse gas forcings would make it easier to distinguish the climate response to either forcing. However, the spatial response pattern of surface air temperature to an increase in solar forcing was found to be quite similar to that in response to increases in greenhouse gas forcing (e.g., Cubasch *et al.*, 1997). The vertical response to solar forcing (Figure 12.5) includes warming throughout most of the troposphere. The response in the stratosphere is small and possibly locally negative, but less so than with greenhouse gas forcing, which gives tropospheric warming and strong stratospheric cooling. The dependence of solar forcing on wavelength and the effect of solar fluctuations on ozone were generally omitted in these simulations. Hence, the conclusion that changes in solar forcing have little effect on large-scale stratospheric temperatures remains tentative.

The different time-histories of the solar and anthropogenic forcing should help to distinguish between the responses. All reconstructions suggest a rise in solar forcing during the early decades of the 20th century with little change on inter-decadal time-scales in the second half. Such a forcing history is unlikely to explain the recent acceleration in surface warming, even if amplified by some unknown feedback mechanism.

Studies linking forcing and response through correlation techniques

A number of authors have correlated solar forcing and volcanic forcing with hemispheric and global mean temperature time-series from instrumental and palaeo-data (Lean *et al.*, 1995; Briffa *et al.*, 1998; Lean and Rind, 1998; Mann *et al.*, 1998) and found statistically significant correlations. Others have compared the simulated response, rather than the forcing, with observations and found qualitative evidence for the influence of natural forcing on climate (e.g., Crowley and Kim, 1996; Overpeck *et al.*, 1997; Wigley *et al.*, 1997; Bertrand *et al.*, 1999) or significant correlations (e.g., Schönwiese *et al.*, 1997; Free and Robock, 1999; Grieser and Schönwiese, 2001). Such a comparison is preferable as the climate response may differ substantially from the forcing. The results suggest that global scale low-frequency temperature variations are influenced by variations in known natural forcings. However, these results show that the late 20th century surface warming cannot be well represented by natural forcing (solar and volcanic individually or in combination) alone (for example Figures 12.6, 12.7; Lean and Rind, 1998; Free and Robock, 1999; Crowley, 2000; Tett *et al.*, 2000; Thejll and Lassen, 2000).

Mann *et al.* (1998, 2000) used a multi-correlation technique and found significant correlations with solar and, less so, with the volcanic forcing over parts of the palaeo-record. The authors concluded that natural forcings have been important on decadal-to-century time-scales, but that the dramatic warming of the 20th century correlates best and very significantly with greenhouse gas forcing. The use of multiple correlations avoids the

possibility of spuriously high correlations due to the common trend in the solar and temperature time-series (Laut and Gunderman, 1998). Attempts to estimate the contributions of natural and anthropogenic forcing to 20th century temperature evolution simultaneously are discussed in Section 12.4.

Summary

We conclude that climate forcing by changes in solar irradiance and volcanism have likely caused fluctuations in global and hemispheric mean temperatures. Qualitative comparisons suggest that natural forcings produce too little warming to fully explain the 20th century warming (see Figure 12.7). The indication that the trend in net solar plus volcanic forcing has been negative in recent decades (see Chapter 6) makes it unlikely that natural forcing can explain the increased rate of global warming since the middle of the 20th century. This question will be revisited in a more quantitative manner in Section 12.4.

12.2.3.3 Anthropogenic forcing

In the SAR (Santer *et al.*, 1996c), pattern-based detection studies took into account changes in well-mixed greenhouse gases (often represented by an equivalent increase in CO₂), the direct effect of sulphate aerosols (usually represented by a seasonally constant change in surface albedo) and the influence of changes in stratospheric ozone. Recent studies have also included the effect of increases in tropospheric ozone and a representation of the indirect effect of sulphate aerosols on cloud albedo. Many models now include the individual greenhouse gases (as opposed to a CO₂ equivalent) and include an interactive sulphur cycle and an explicit treatment of scattering by aerosols (as opposed to using prescribed changes in surface albedo). Note that representation of the sulphur cycle in climate models is not as detailed as in the offline sulphur cycle models reported in Chapter 5. Detection and attribution studies to date have not taken into account other forcing agents discussed in Chapter 6, including biogenic aerosols, black carbon, mineral dust and changes in land use. Estimates of the spatial and temporal variation of these factors have not been available long enough to have been included in model simulations suitable for detection studies. In general, the neglected forcings are estimated to be small globally and there may be a large degree of cancellation in their global mean effect (see Chapter 6, Figure 6.8). It is less clear that the individual forcings will cancel regionally. As discussed in Section 12.4, this will add further uncertainty in the attribution of the response to individual forcing agents, although we believe it is unlikely to affect our conclusions about the effects of increases in well-mixed greenhouse gases on very large spatial scales.

Global mean anthropogenic forcing

The largest and most certain change in radiative forcing since the pre-industrial period is an increase of about 2.3 W m⁻² due to an increase in well-mixed greenhouse gases (Chapter 6, Figure 6.8 and Table 6.1). Radiative forcing here is taken to be the net downward radiative flux at the tropopause (see Chapter 6). Smaller, less certain contributions have come from increases in tropospheric ozone (about 0.3 W m⁻²), the direct effect of increases in sulphate aerosols (about -0.4 W m⁻²) and decreases in

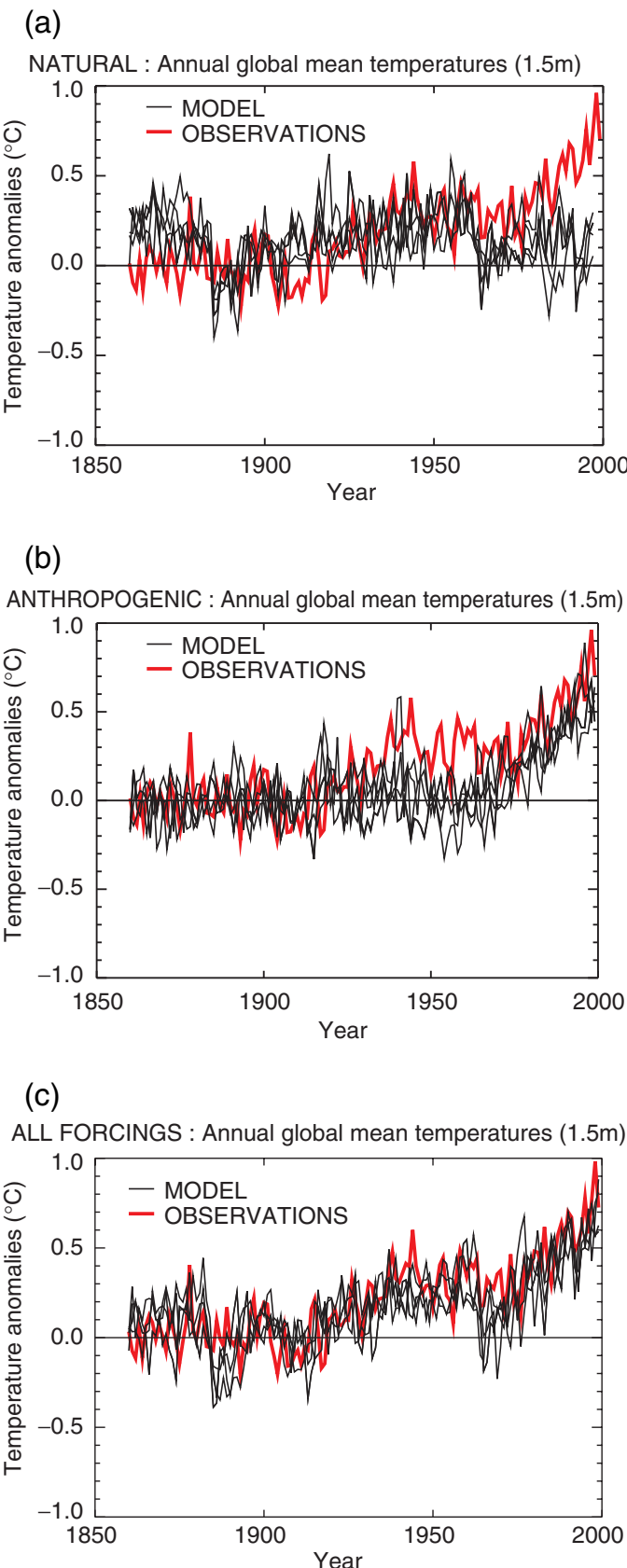


Figure 12.7: Global mean surface temperature anomalies relative to the 1880 to 1920 mean from the instrumental record compared with ensembles of four simulations with a coupled ocean-atmosphere climate model (from Stott *et al.*, 2000b; Tett *et al.*, 2000) forced (a) with solar and volcanic forcing only, (b) with anthropogenic forcing including well mixed greenhouse gases, changes in stratospheric and tropospheric ozone and the direct and indirect effects of sulphate aerosols, and (c) with all forcings, both natural and anthropogenic. The thick line shows the instrumental data while the thin lines show the individual model simulations in the ensemble of four members. Note that the data are annual mean values. The model data are only sampled at the locations where there are observations. The changes in sulphate aerosol are calculated interactively, and changes in tropospheric ozone were calculated offline using a chemical transport model. Changes in cloud brightness (the first indirect effect of sulphate aerosols) were calculated by an offline simulation (Jones *et al.*, 1999) and included in the model. The changes in stratospheric ozone were based on observations. The volcanic forcing was based on the data of Sato *et al.* (1993) and the solar forcing on Lean *et al.* (1995), updated to 1997. The net anthropogenic forcing at 1990 was 1.0 W m^{-2} including a net cooling of 1.0 W m^{-2} due to sulphate aerosols. The net natural forcing for 1990 relative to 1860 was 0.5 W m^{-2} , and for 1992 was a net cooling of 2.0 W m^{-2} due to Mt. Pinatubo. Other models forced with anthropogenic forcing give similar results to those shown in b (see Chapter 8, Section 8.6.1, Figure 8.15; Hasselmann *et al.*, 1995; Mitchell *et al.*, 1995b; Haywood *et al.*, 1997; Boer *et al.*, 2000a; Knutson *et al.*, 2000).

stratospheric ozone (about -0.2 Wm^{-2}). There is a very uncertain and possibly large negative contribution from the indirect effects of aerosols. Other factors such as that due to increases in fossil fuel organic carbon, aviation, changes in land use and mineral dust are very poorly known and not yet incorporated into simulations used in formal detection studies. Their contribution is generally believed to be small relative to well-mixed greenhouse gases, though they could be of importance on regional scales.

In order to assess temperature changes over the last two decades, Hansen *et al.* (1997b) estimated the net radiative forcing due to changes in greenhouse gases (including ozone), solar variations and stratospheric aerosols from 1979 to 1995 from the best available measurements of the forcing agents. The negative forcing due to volcanoes and decreases in stratospheric ozone compensated for a substantial fraction of the increase in greenhouse gas forcing in this period (see Chapter 6, Table 6.13).

Patterns of anthropogenic forcing

Many of the new detection studies take into account the spatial variation of climate response, which will depend to some extent on the pattern of forcing (see also Section 12.2.3). The patterns of forcing vary considerably (see Chapter 6, Figure 6.7). The magnitude of the overall forcing due to increases in well-mixed greenhouse gases varies from almost 3 Wm^{-2} in the sub-tropics to about 1 Wm^{-2} around the poles. The warming due to increases in tropospheric ozone is mainly in the tropics and northern subtropics. Decreases in stratospheric ozone observed over the last couple of decades have produced negative forcing of up to about 0.5 Wm^{-2} around Antarctica. The direct effect of sulphate aerosols predominates in the Northern Hemisphere industrial regions where the negative forcing may exceed 2 Wm^{-2} locally.

Temporal variations in forcing

Some of the new detection studies take into account the temporal as well as spatial variations in climate response (see Section 12.4.3.3). Hence the temporal variation of forcing is also important. The forcing due to well-mixed greenhouse gases (and tropospheric ozone) has increased slowly in the first half of the century, and much more rapidly in recent decades (Chapter 6, Figure 6.8). Contributions from other factors are smaller and more uncertain. Sulphur emissions increased steadily until World War I, then levelled off, and increased more rapidly in the 1950s, though not as fast as greenhouse gas emissions. This is reflected in estimates of the direct radiative effect of increases in sulphate aerosols. Given the almost monotonic increase in greenhouse gas forcing in recent decades, this means the ratio of sulphate to greenhouse gas forcing has probably been decreasing since about 1960 (see Chapter 6, Figure 6.8). This should be borne in mind when considering studies that attempt to detect a response to sulphate aerosols. The decreases in stratospheric ozone have been confined to the last two to three decades.

Uncertainties in aerosol forcing

Some recent studies have incorporated the indirect effect of increases in tropospheric aerosols. This is very poorly understood (see Chapter 6), but contributes a negative forcing which could be negligible or exceed 2 Wm^{-2} . The upper limit would imply very

little change in net global mean anthropogenic forcing over the last century although there would still be a quite strong spatial pattern of heating and cooling which may be incompatible with recent observed changes (see, for example, Mitchell *et al.*, 1995a). A negligible indirect sulphate effect would imply a large increase in anthropogenic forcing in the last few decades. There is also a large range in the inter-hemispheric asymmetry in the different estimates of forcing (see Chapter 6, Table 6.4). Given this high level of uncertainty, studies using simulations including estimates of indirect sulphate forcing should be regarded as preliminary.

Summary

Well-mixed greenhouse gases make the largest and best-known contribution to changes in radiative forcing over the last century or so. There remains a large uncertainty in the magnitude and patterns of other factors, particularly those associated with the indirect effects of sulphate aerosol.

12.2.3.4 Climatic response to anthropogenic forcing

We now consider the simulated response to anthropogenic forcing. Models run with increases in greenhouse gases alone give a warming which accelerates in the latter half of the century. When a simple representation of aerosol effects is included (Mitchell *et al.*, 1995b; Cubasch *et al.*, 1996; Haywood *et al.*, 1997; Boer *et al.*, 2000a,b) the rate of warming is reduced (see also Chapter 8, Section 8.6.1). The global mean response is similar when additional forcings due to ozone and the indirect effect of sulphates are included. GCM simulations (Tett *et al.*, 1996; Hansen *et al.*, 1997b) indicate that changes in stratospheric ozone observed over the last two decades yield a global mean surface temperature cooling of about 0.1 to 0.2°C . This may be too small to be distinguishable from the model's internal variability and is also smaller than the warming effects due to the changes in the well-mixed greenhouse gases over the same time period (about 0.2 to 0.3°C). The lack of a statistically significant surface temperature change is in contrast to the large ozone-induced cooling in the lower stratosphere (WMO, 1999; Bengtsson *et al.* 1999).

The response of the vertical distribution of temperature to anthropogenic forcing

Increases in greenhouse gases lead to a warming of the troposphere and a cooling of the stratosphere due to CO_2 (IPCC, 1996). Reductions in stratospheric ozone lead to a further cooling, particularly in the stratosphere at high latitudes. Anthropogenic sulphate aerosols cool the troposphere with little effect on the stratosphere. When these three forcings are included in a climate model (e.g., Tett *et al.*, 1996, 2000) albeit in a simplified way, the simulated changes show tropospheric warming and stratospheric cooling, as observed and as expected on physical principles (Figure 12.8). Note that this structure is distinct from that expected from natural (internal and external) influences.

The response of surface temperature to anthropogenic forcing

The spatial pattern of the simulated surface temperature response to a steady increase in greenhouse gases is well documented (e.g., Kattenberg *et al.*, 1996; Chapter 10). The warming is greater over

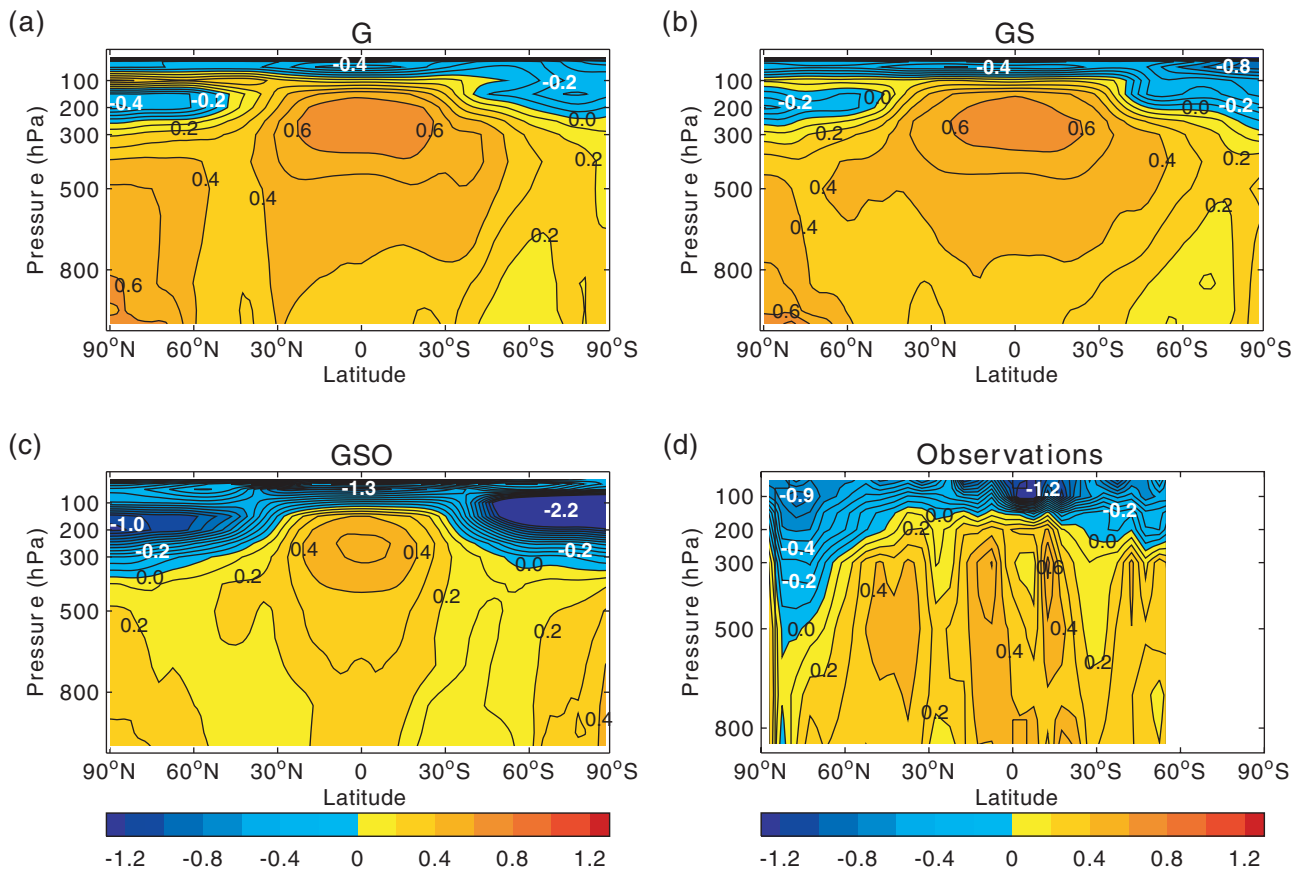


Figure 12.8: Simulated and observed zonal mean temperature change as a function of latitude and height from Tett *et al.* (1996). The contour interval is 0.1°C . All signals are defined to be the difference between the 1986 to 1995 decadal mean and the 20 year 1961 to 1980 mean. (a), increases in CO_2 only (G); (b), as (a), but with a simple representation of sulphate aerosols added (GS); (c), as (b), with observed changes in stratospheric ozone (GSO); (d), observed changes.

land than over ocean and generally small during the 20th century over the Southern Ocean and northern North Atlantic where mixing extends to considerable depth. The warming is amplified in high latitudes in winter by the recession of sea ice and snow, and is close to zero over sea ice in summer.

Despite the qualitative consistency of these general features, there is considerable variation from model to model. In Chapter 9, it was noted that the spatial correlation between the transient response to increasing CO_2 in *different* models in scenarios to the middle of the 21st century was typically 0.65. In contrast, the spatial correlation between the temperature response to greenhouse gases only, and greenhouse gases and aerosols in the *same* model was typically 0.85 (see Chapter 9, Table 9.2). Hence, attempts to detect separate greenhouse gas and aerosol patterns in different models may not give consistent results (see Section 12.4.3.2).

12.2.4 Some Important Statistical Considerations

Most recent studies (Hegerl *et al.*, 1996, 1997, 2000, 2001; North and Stevens, 1998; Allen and Tett, 1999; Tett *et al.*, 1999, 2000; Berliner *et al.*, 2000; North and Wu, 2001; Stott *et al.*, 2001) have used a regression approach in which it is assumed that observa-

tions can be represented as a linear combination of candidate signals plus noise (see Appendices 12.1 and 12.2). Other approaches, such as pattern correlation (Santer *et al.*, 1995, 1996a; see also Appendix 12.3), complement the regression approach, being particularly valuable in cases where model-simulated response patterns are particularly uncertain. In all cases, the signal patterns are obtained from climate models. In the regression approach, the unknown signal amplitudes are estimated from observations. The uncertainty of these estimates that is caused by natural variability in the observations is expressed with confidence intervals. Detection of an individual signal is achieved when the confidence interval for its amplitude does not include zero. Overall detection (that some climate change has taken place) is achieved when the joint confidence interval on the signals considered does not encompass the origin.

Attribution and consistency

Detecting that some climate change has taken place does not immediately imply that we know the cause of the detected change. The practical approach to attribution that has been taken by climatologists includes a demand for consistency between the signal amplitudes projected by climate models and estimated from observations (Hasselmann, 1997). Consequently, several

studies, including Hegerl *et al.* (1997, 2000) and Tett *et al.* (1999, 2000) have performed an “attribution” consistency test that is designed to detect inconsistency between observed and model projected signal amplitudes. This test is a useful adjunct to detection because it provides an objective means of identifying model-simulated signal amplitudes that are significantly different from those estimated from observations. However, the test does not give the final word on attribution because it is designed to identify evidence of inconsistency rather than evidence for consistency between modelled and observed estimates of signal strength. A further refinement (e.g., Stott *et al.*, 2001) is to consider the full range of signals believed, on physical grounds, to be likely to have had a significant impact on recent climate change and to identify those subsets of these signals that are consistent with recent observations. If all these subsets contain an anthropogenic component, for example, then at least part of the observed change can be attributed to anthropogenic influence. Levine and Berliner (1999) point out that a test that searches for consistency is available (Brown *et al.*, 1995), but it has not yet been used in attribution studies. Bayesian statisticians approach the problem more directly by estimating the posterior probability that the signal amplitudes projected by climate models are close to those in the observed climate. Berliner *et al.* (2000) provides a demonstration.

The use of climate models to estimate natural internal variability
 Climate models play a critical role in these studies because they provide estimates of natural internal variability as well as the signals. In most studies an estimate of natural internal variability is needed to optimise the search for the signal and this is usually obtained from a long control simulation. In addition, a separate estimate of natural variability is required to determine the uncertainty of the amplitude estimates. Unfortunately, the short instrumental record gives only uncertain estimates of variability on the 30 to 50 year time-scales that are important for detection and attribution and palaeo-data presently lacks the necessary spatial coverage (see Section 12.2.2). Thus a second control integration is generally used to estimate the uncertainty of the amplitude estimates that arises from natural climate variability (e.g., Hegerl *et al.*, 1996; Tett *et al.*, 1999).

Temporal and spatial scales used in detection studies

While a growing number of long control simulations are becoming available, there remain limitations on the spatial scales that can be included in global scale detection and attribution studies. Present day control simulations, which range from 300 to about 2,000 years in length, are not long enough to simultaneously estimate internal variability on the 30 to 50 year time-scale over a broad range of spatial scales. Consequently, detection and attribution studies are conducted in a reduced space that includes only large spatial scales. This space is selected so that it represents the signals well and allows reliable estimation of internal variability on the scales retained (see Appendix 12.4). Recently, the scale selection process has been augmented with a statistical procedure that checks for consistency between model simulated and observed variability on the scales that are retained (Allen and Tett, 1999).

Fixed and temporally-varying response patterns

Detection and attribution studies performed up to the SAR used fixed signal patterns that did not evolve with time. These studies were hampered because the mean large-scale response of climate to different types of anomalous forcing tends to be similar (e.g., Mitchell *et al.*, 1995a; Reader and Boer, 1998; see also Figure 12.3). Recent studies have been able to distinguish more clearly between signals from anthropogenic and other sources by including information from climate models about their temporal evolution. Tett *et al.* (1999, 2000) and Stott *et al.* (2001) in related studies have used a *space-time* approach in which the signal pattern evolves on the decadal time-scale over a 50-year period. North and Wu (2001) also use a space-time approach. North and Stevens (1998) used a related *space-frequency* approach (see Appendix 12.2).

Allowance for noise in signal patterns

Most studies have assumed that signal patterns are noise free. This is a reasonable assumption for fixed pattern studies (see Appendix 12.2) but space-time estimates of the 20th century climate change obtained from small ensembles of forced climate simulations are contaminated by the model’s internal variability. Allen and Tett (1999) point out that noise in the signal patterns will tend to make the standard detection algorithm (e.g., Hasselmann, 1993, 1997) somewhat conservative. Methods for accommodating this source of noise have been available for more than a century (Adcock, 1878; see also Ripley and Thompson, 1987). Allen and Stott (2000) recently applied such a method and found that, while the question of which signals could be detected was generally unaffected, the estimated amplitude of individual signals was sensitive to this modification of the procedure. Another source of uncertainty concerns differences in signal patterns between different models. Recent studies (Allen *et al.*, 2000a,b; Barnett *et al.*, 2000; Hegerl *et al.*, 2000) consider the sensitivity of detection and attribution results to these differences.

12.3 Qualitative Comparison of Observed and Modelled Climate Change

12.3.1 Introduction

This section presents a qualitative assessment of consistencies and inconsistencies between the observed climate changes identified in Chapter 2 and model projections of anthropogenic climate change described in Chapter 9.

Most formal detection and attribution studies concentrate on variables with high climate change signal-to-noise ratios, good observational data coverage, and consistent signals from different model simulations, mainly using mean surface air temperatures or zonal mean upper-air temperatures. To enhance the signal-to-noise ratio, they generally consider variations on large spatial scales and time-scales of several decades or longer.

There are many studies that have identified areas of qualitative consistency and inconsistency between observed and modelled climate change. While the evidence for an anthropogenic influence on climate from such studies is less compelling than from formal attribution studies, a broad range of evidence of

qualitative consistency between observed and modelled climate change is also required. In addition, areas of qualitative consistency may suggest the possibility for further formal detection and attribution study.

12.3.2 Thermal Indicators

Surface temperature

Global mean surface air temperature has been used in many climate change detection studies. The warming shown in the instrumental observations over the last 140 years is larger than that over a comparable period in any of the multi-century control simulations carried out to date (e.g., Figure 12.1; Stouffer *et al.*, 2000). If the real world internal variability on this time-scale is no greater than that of the models, then the temperature change over the last 140 years has been unusual and therefore likely to be externally forced. This is supported by palaeo-reconstructions of the last six centuries (Mann *et al.*, 1998) and the last 1,000 years (Briffa *et al.*, 1998; 2000; Jones *et al.*, 1998; Crowley, 2000; Crowley and Lowery, 2000; Mann *et al.*, 2000), which show that the 20th century warming is highly unusual. Three of the five years (1995, 1996 and 1998) added to the instrumental record since the SAR are the warmest globally in the instrumental record, consistent with the expectation that increases in greenhouse gases will lead to sustained long-term warming.

When anthropogenic factors are included, models provide a plausible explanation of the changes in global mean temperature over the last hundred years (Figure 12.7). It is conceivable that this agreement between models and observations is spurious. For example, if a model's response to greenhouse gas increases is too large (small) and the sulphate aerosol forcing too large (small), these errors could compensate. Differences in the spatio-temporal patterns of response to greenhouse gases and sulphate forcing nevertheless allow some discrimination between them, so this compensation is not complete. On the other hand, when forced with known natural forcings, models produce a cooling over the second half of the 20th century (see Figure 12.7) rather than the warming trend shown in the observed record. The discrepancy is too large to be explained through model estimates of internal variability and unlikely to be explained through uncertainty in forcing history (Tett *et al.*, 2000). Schneider and Held (2001) applied a technique to isolate those spatial patterns of decadal climate change in observed surface temperature data over the 20th century which are most distinct from interannual variability. They find a spatial pattern which is similar to model-simulated greenhouse gas and sulphate aerosol fingerprints in both July and December. The time evolution of this pattern shows a strong trend with little influence of interannual variability. (Note that this technique is related to optimal fingerprinting, but does not use prior information on the pattern of expected climate change.)

Other thermal indicators

While most attention in formal detection and attribution studies has been paid to mean surface air temperatures, a number of other thermal indicators of climate variations are also discussed in Chapter 2. Many of these, including warming in sub-surface land temperatures measured in bore holes, warming indicators in ice

cores and corresponding bore holes, warming in sub-surface ocean temperatures, retreat of glaciers, and reductions in Arctic sea-ice extent and in snow cover, are consistent with the recent observed warming in surface air temperatures and with model projections of the response to increasing greenhouse gases. Other observed changes in thermal indicators include a reduction in the mean annual cycle (winters warming faster than summers) and in the mean diurnal temperature range (nights warming faster than days) over land (see Chapter 2). While the changes in annual cycle are consistent with most model projections, the observed changes in diurnal temperature range are larger than simulated in most models for forcings due to increasing greenhouse gases and sulphate aerosols this century (see Chapters 2 and 8). However, the spatial and temporal coverage of data for changes in observed diurnal temperature range is less than for changes in mean temperatures, leading to greater uncertainty in the observed global changes (Karoly and Braganza, 2001; Schnur, 2001). Also, the observed reductions in diurnal temperature range are associated with increases in cloudiness (see Chapter 2), which are not simulated well by models. Few models include the indirect effects of sulphate aerosols on clouds.

Changes in sea-ice cover and snow cover in the transition seasons in the Northern Hemisphere are consistent with the observed and simulated high latitude warming. The observed trends in Northern Hemisphere sea-ice cover (Parkinson *et al.*, 1999) are consistent with those found in climate model simulations of the last century including anthropogenic forcing (Vinnikov *et al.*, 1999). Sea-ice extent in the Southern Hemisphere does not show any consistent trends.

Compatibility of surface and free atmosphere temperature trends
There is an overall consistency in the patterns of upper air temperature changes with those expected from increasing greenhouse gases and decreasing stratospheric ozone (tropospheric warming and stratospheric cooling). It is hard to explain the observed changes in the vertical in terms of natural forcings alone, as discussed in Section 12.2.3.2 (see Figure 12.8). However, there are some inconsistencies between the observed and modelled vertical patterns of temperature change. Observations indicate that, over the last three to four decades, the tropical atmosphere has warmed in the layer up to about 300 hPa and cooled above (Parker *et al.*, 1997; Gaffen *et al.*, 2000). Model simulations of the recent past produce a warming of the tropical atmosphere to about 200 hPa, with a maximum at around 300 hPa not seen in the observations. This discrepancy is less evident when co-located model and radiosonde data are used (Santer *et al.*, 2000), or if volcanic forcing is taken into account, but does not go away entirely (Bengtsson *et al.*, 1999; Brown *et al.*, 2000b). The MSU satellite temperature record is too short and too poorly resolved in the vertical to be of use here.

Comparison of upper air and surface temperature data in Chapter 2 shows that the lower to mid-troposphere has warmed less than the surface since 1979. The satellite-measured temperature over a broad layer in the lower troposphere around 750 hPa since 1979 shows no significant trend, in contrast to the warming trend measured over the same time period at the surface. This disparity has been assessed recently by a panel of experts

(National Academy of Sciences, 2000). They concluded that “the troposphere actually may have warmed much less rapidly than the surface from 1979 to the late 1990s, due both to natural causes (e.g., the sequence of volcanic eruptions that occurred within this particular 20-year period) and human activities (e.g., the cooling in the upper troposphere resulting from ozone depletion in the stratosphere)” (see also Santer *et al.*, 2000). They also concluded that “it is not currently possible to determine whether or not there exists a fundamental discrepancy between modelled and observed atmospheric temperature changes since the advent of satellite data in 1979”. Over the last 40 years, observed warming trends in the lower troposphere and at the surface are similar, indicating that the lower troposphere warmed faster than the surface for about two decades prior to 1979 (Brown *et al.*, 2000a; Gaffen *et al.*, 2000). However, in the extra-tropical Eurasian winter some additional warming of the surface relative to the lower or mid-troposphere might be expected since 1979. This is due to an overall trend towards an enhanced positive phase of the Arctic Oscillation (Thompson *et al.*, 2000) which has this signature.

Model simulations of large-scale changes in tropospheric and surface temperatures are generally statistically consistent with the observed changes (see Section 12.4). However, models generally predict an enhanced rate of warming in the mid- to upper troposphere over that at the surface (i.e., a negative lapse-rate feedback on the surface temperature change) whereas observations show mid-tropospheric temperatures warming no faster than surface temperatures. It is not clear whether this discrepancy arises because the lapse-rate feedback is consistently over-represented in climate models or because of other factors such as observational error or neglected forcings (Santer *et al.*, 2000). Note that if models do simulate too large a negative lapse-rate feedback, they will tend to underestimate the sensitivity of climate to a global radiative forcing perturbation.

Stratospheric trends

A recent assessment of temperature trends in the stratosphere (Chanin and Ramaswamy, 1999) discussed the cooling trends in the lower stratosphere described in Chapter 2. It also identified large cooling trends in the middle and upper stratosphere, which are consistent with anthropogenic forcing due to stratospheric ozone depletion and increasing greenhouse gas concentrations. An increase in water vapour, possibly due to increasing methane oxidation, is another plausible explanation for the lower stratospheric cooling (Forster and Shine, 1999) but global stratospheric water vapour trends are poorly understood.

12.3.3 Hydrological Indicators

As discussed in Chapter 2, there is less confidence in observed variations in hydrological indicators than for surface temperature, because of the difficulties in taking such measurements and the small-scale variations of precipitation. There is general consistency between the changes in mean precipitation in the tropics over the last few decades and changes in ENSO. There is no general consistency between observed changes in mean tropical precipitation and model simulations. In middle and high latitudes in the Northern Hemisphere, the observed increase in precipita-

tion is consistent with most model simulations. Observed changes in ocean salinity in the Southern Ocean appear to be consistent with increased precipitation there, as expected from model simulations (Wong *et al.*, 1999; Banks *et al.*, 2000).

The observed increases in the intensity of heavy precipitation in the tropics and in convective weather systems described in Chapter 2 are consistent with moist thermodynamics in a warmer atmosphere and model simulations. Observed increases of water vapour in the lower troposphere in regions where there is adequate data coverage are also consistent with model simulations. As discussed in Chapter 7, different theories suggest opposite variations of water vapour in the upper troposphere associated with an increased greenhouse effect and surface warming. The quality, amount and coverage of water vapour data in the upper troposphere do not appear to be sufficient to resolve this issue.

12.3.4 Circulation

In middle and high latitudes of both hemispheres, there has been a trend over the last few decades towards one phase of the North Atlantic Oscillation/Arctic Oscillation and of the Antarctic high latitude mode, sometimes also referred to as “annular modes”, (Chapter 2; Thompson *et al.*, 2000). These are approximately zonally symmetric modes of variability of the atmospheric circulation. Both trends have been associated with reduced surface pressure at high latitudes, stronger high latitude jets, a stronger polar vortex in the winter lower stratosphere and, in the Northern Hemisphere, winter warming over the western parts of the continents associated with increased warm advection from ocean regions. The trend is significant and cannot be explained by internal variability in some models (Gillett *et al.*, 2000b). These dynamical changes explain only part of the observed Northern Hemisphere warming (Gillett *et al.*, 2000b; Thompson *et al.*, 2000). Modelling studies suggest a number of possible causes of these circulation changes, including greenhouse gas increases (Fyfe *et al.*, 1999; Paeth *et al.*, 1999; Shindell *et al.*, 1999) and stratospheric ozone decreases (Graf *et al.*, 1998; Volodin and Galin, 1999). Some studies have also shown that volcanic eruptions (Graf *et al.*, 1998; Mao and Robock, 1998; Kirchner *et al.*, 1999) can induce such changes in circulation on interannual time-scales. Shindell *et al.* (2001) show that both solar and volcanic forcing are unlikely to explain the recent trends in the annular modes.

The majority of models simulate the correct sign of the observed trend in the North Atlantic or Arctic Oscillation when forced with anthropogenic increases in greenhouse gases and sulphate aerosols, but almost all underestimate the magnitude of the trend (e.g., Osborn *et al.*, 1999; Gillett *et al.*, 2000b; Shindell *et al.*, 1999). Some studies suggest that a better resolved stratosphere is necessary to simulate the correct magnitude of changes in dynamics involving the annular modes (e.g., Shindell *et al.*, 2001).

12.3.5 Combined Evidence

The combination of independent but consistent evidence should strengthen our confidence in identifying a human influence on climate. The physical and dynamical consistency of most of the

thermal and hydrological changes described above supports this conclusion. However, it is important to bear in mind that much of this evidence is associated with a global and regional pattern of warming and therefore cannot be considered to be completely independent evidence.

An elicitation of individual experts' subjective assessment of evidence for climate change detection and attribution is being carried out (Risbey *et al.*, 2000). This will help to better understand the nature of the consensus amongst experts on the subject of climate change attribution.

12.4 Quantitative Comparison of Observed and Modelled Climate Change

A major advance since the SAR has been the increase in the range of techniques used to assess the quantitative agreement between observed and modelled climate change, and the evaluation of the degree to which the results are independent of the assumptions made in applying those techniques (Table 12.1). Also, some studies have based their conclusions on estimates of the amplitude of anthropogenic signals in the observations and consideration of their consistency with model projections. Estimates of the changes in forcing up to 1990 used in these studies, where available, are given in Table 12.2. In this section we assess new studies using a number of techniques, ranging from descriptive analyses of simple indices to sophisticated optimal detection techniques that incorporate the time and space-dependence of signals over the 20th century.

We begin in Section 12.4.1 with a brief discussion of detection studies that use simple indices and time-series analyses. In Section 12.4.2 we discuss recent pattern correlation studies (see Table 12.1) that assess the similarity between observed and modelled climate changes. Pattern correlation studies were discussed extensively in the SAR, although subsequently they received some criticism. We therefore also consider the criticism and studies that have evaluated the performance of pattern correlation techniques. Optimal detection studies of various kinds are assessed in Section 12.4.3. We consider first studies that use a single fixed spatial signal pattern (Section 12.4.3.1) and then studies that simultaneously incorporate more than one fixed signal pattern (Section 12.4.3.2). Finally, optimal detection studies that take into account temporal as well as spatial variations (so-called space-time techniques) are assessed in Section 12.4.3.3.

We provide various aids to the reader to clarify the distinction between the various detection and attribution techniques that have been used. Box 12.1 in Section 12.4.3 provides a simple intuitive description of optimal detection. Appendix 12.1 provides a more technical description and relates optimal detection to general linear regression. The differences between fixed pattern, space-time and space-frequency optimal detection methods are detailed in Appendix 12.2 and the relationship between pattern correlation and optimal detection methods is discussed in Appendix 12.3. Dimension reduction, a necessary part of optimal detection studies, is discussed in Appendix 12.4.

12.4.1 Simple Indices and Time-series Methods

An index used in many climate change detection studies is global mean surface temperature, either as estimated from the instrumental record of the last 140 years, or from palaeo-reconstructions. Some studies of the characteristics of the global mean and its relationship to forcing indices are assessed in Section 12.2.3. Here we consider briefly some additional studies that examine the spatial structure of observed trends or use more sophisticated time-series analysis techniques to characterise the behaviour of global, hemispheric and zonal mean temperatures.

Spatial patterns of trends in surface temperature

An extension of the analysis of global mean temperature is to compare the spatial structure of observed trends (see Chapter 2, Section 2.2.2.4) with those simulated by models in coupled control simulations. Knutson *et al.* (2000) examined observed 1949 to 1997 surface temperature trends and found that over about half the globe they are significantly larger than expected from natural low-frequency internal variability as simulated in long control simulations with the GFDL model (Figure 12.9). A similar result was obtained by Boer *et al.* (2000a) using 1900 to 1995 trends. The level of agreement between observed and simulated trends increases substantially in both studies when observations are compared with simulations that incorporate transient greenhouse gases and sulphate aerosol forcing (compare Figure 12.9c with Figure 12.9d, see also Chapter 8, Figure 8.18). While there are areas, such as the extra-tropical Pacific and North Atlantic Ocean, where the GFDL model warms significantly more than has been observed, the anthropogenic climate change simulations do provide a plausible explanation of temperature trends over the last century over large areas of the globe. Delworth and Knutson (2000) find that one in five of their anthropogenic climate change simulations showed a similar evolution of global mean surface temperature over the 20th century to that observed, with strong warming, particularly in the high latitude North Atlantic, in the first half of the century. This would suggest that the combination of anthropogenic forcing and internal variability may be sufficient to account for the observed early-century warming (as suggested by, e.g., Hegerl *et al.*, 1996), although other recent studies have suggested that natural forcing may also have contributed to the early century warming (see Section 12.4.3).

Correlation structures in surface temperature

Another extension is to examine the lagged and cross-correlation structure of observed and simulated hemispheric mean temperature as in Wigley *et al.*, (1998a). They find large differences between the observed and model correlation structure that can be explained by accounting for the combined influences of anthropogenic and solar forcing and internal variability in the observations. Solar forcing alone is not found to be a satisfactory explanation for the discrepancy between the correlation structures of the observed and simulated temperatures. Karoly and Braganza (2001) also examined the correlation structure of surface air temperature variations. They used several simple indices, including the land-ocean contrast, the meridional

Table 12.1: Summary of the main detection and attribution studies considered.

Study	Signals	Signal source	Noise source	Method	S, V	Sources of uncertainty	Time-scale	No. of patterns	Detect
Santer <i>et al.</i> , 1996	G, GS, O etc.	Equilibrium / future LLNL, GFDL R15, HadCM2	GFDL R15, HadCM2, ECHAM1	F, Corr	V	Internal variability	25 year Annual and seasonal	1	GSO
Hegerl, 1996, 1997	G, GS	Future ECHAM3, HadCM2; observation	GFDL R15, ECHAM1, HadCM2; observation	F, Pattern	S	Internal variability	30, 50 years Annual and JJA	1, 2	G, GS, S
Tett <i>et al.</i> , 1996	G, GS, GSO	Historical HadCM2	HadCM2	F, Corr	V	Internal variability	35 years	1	GSO
Hegerl <i>et al.</i> , 2000	G, GS, Vol, Sol	Future, ECHAM3, HadCM2	ECHAM3, HadCM2	F, Pattern	S	Internal variability; model uncertainty	30, 50 years Annual and JJA	1, 2	GS, G, S (not all cases)
Allen and Tett, 1999	G, GS, GSO	Historical HadCM2	HadCM2	F, pattern	V	Internal variability	35 years Annual	1, 2	GSO and also G
Tett <i>et al.</i> , 1999 Stott <i>et al.</i> , 2001	G, GS, Sol, Vol	Historical HadCM2	HadCM2	Time-space	S	Internal variability, 2 solar signals	50 years decadal and seasonal	2 or more	G, GS, Sol (Vol)
North and Stevens, 1998 Leroy, 1998	G, GS, Sol, Vol	Historical EBM	GFDL ECHAM1, EBM	Freq-Space	S	Internal variability	Annual and hemispheric summer	4	G, S, Vol
North and Wu, 2001			Same+Had CM2	Time-space			Annual		G, Vol
Barnett <i>et al.</i> , 1999	G, GS, GSIO Sol+vol	Future ECHAM3, ECHAM4, ECHAM4, HadCM2, GFDL R15	ECHAM3, ECHAM4, HadCM2, GFDL R15	F, Pattern	S	Observed sampling error, model uncertainty, internal variability	50 years JJA trends	2	GS, G, S (S not all cases)
Hill <i>et al.</i> , 2001	G, GSO, Sol	Historical HadCM2	HadCM2	F, pattern	V	Internal variability	35 years annual	3	G
Tett <i>et al.</i> , 2000	G, GSTI, GSTIO, Nat	Historical HadCM3	HadCM3	Time-space	S	Internal variability	50, 100 years decadal	2 or more	G, SIT, GSTIO and Nat
				F, pattern	V	Internal variability	35 years, annual	2	GSTI

The columns contain the following information:

Study : the main reference to the study.

Signals : outlines the principal signals considered: G-greenhouse gases, S-sulphate aerosol direct effect, T-tropospheric ozone, I-sulphate aerosol indirect effect, O-stratospheric ozone, Sol-solar, Vol-volcanoes, Nat-solar and volcanoes.

Signal source : “historical” indicates the signal is taken from a historical hindcast simulation, “future” indicates that the pattern is taken from a prediction.

Noise source : origin of the noise estimates.

Method : “F” means fixed spatial pattern, “corr” indicates a correlation study, “pattern” an optimal detection study.

S, V : “V” indicates a vertical temperature pattern, “S” a horizontal temperature pattern.

Sources of uncertainty : any additional uncertainties allowed for are indicated. Modelled internal variability is allowed for in all studies.

Time-scale : the lengths of time interval considered. (JJA= June-July-August)

No. of patterns : the number of patterns considered simultaneously.

Detect : signals detected.

Table 12.2: Estimated forcing from pre-industrial period to 1990 in simulations used in detection studies (Wm^{-2}). GS indicates only direct sulphate forcing included, GSI indicates both direct and indirect effects included. Other details of the detection studies are given in Table 12.1. Details of the models are given in Chapter 8, Table 8.1.

Model	Aerosol	Baseline forcing	1990 aerosol forcing	1990 greenhouse gas forcing	Source of estimate
HadCM2	GS	1760	-0.6	1.9	Mitchell and Johns, 1997
HadCM3	GSI	1860	-1.0	2.0	Tett <i>et al.</i> , 2000
ECHAM3/LSG	GS	1880	-0.7	1.7	Roeckner
ECHAM4/OPYC	GSI	1760	-0.9	2.2	Roeckner <i>et al.</i> , 1999
GFDL_R30	GS	1760	-0.6	2.1	Stouffer
CGCM1,2	GS	1760	~ -1.0	~2.2	Boer <i>et al.</i> , 2000a,b

gradient, and the magnitude of the seasonal cycle, to describe global climate variations and showed that for natural variations, they contain information independent of the global mean temperature. They found that the observed trends in these indices over the last 40 years are unlikely to have occurred due to natural climate variations and that they are consistent with model simulations of anthropogenic climate change.

Statistical models of time-series

Further extensions involve the use of statistical “models” of global, hemispheric and regional temperature time-series. Note however, that the stochastic models used in these time-series studies are generally not built from physical principles and are thus not as strongly constrained by our knowledge of the physical climate system as climate models. All these studies depend on inferring the statistical properties of the time-series from an assumed noise model with parameters estimated from the residuals. As such, the conclusions depend on the appropriateness or otherwise of the noise model.

Tol and de Vos (1998), using a Bayesian approach, fit a hierarchy of time-series models to global mean near-surface temperature. They find that there is a robust statistical relationship between atmospheric CO₂ and global mean temperature and that natural variability is unlikely to be an explanation for the observed temperature change of the past century. Tol and Vellinga (1998) further conclude that solar variation is also an unlikely explanation. Zheng and Basher (1999) use similar time-series models and show that deterministic trends are detectable over a large part of the globe. Walter *et al.* (1998), using neural network models, estimate that the warming during the past century due to greenhouse gas increases is 0.9 to 1.3°C and that the counter-balancing cooling due to sulphate aerosols is 0.2 to 0.4°C. Similar results are obtained with a multiple regression model (Schönwiese *et al.*, 1997). Kaufmann and Stern (1997) examine the lagged-covariance structure of hemispheric mean temperature and find it consistent with unequal anthropogenic aerosol forcing in the two hemispheres. Smith *et al.* (2001), using similar bivariate time-series models, find that the evidence for causality becomes weak when the effects of ENSO are taken into account. Bivariate time-series models of hemispheric mean temperature that account for box-diffusion estimates of the response to anthropogenic and solar forcing are found to fit the observations

significantly better than competing statistical models. All of these studies draw conclusions that are consistent with those of earlier trend detection studies (as described in the SAR).

In summary, despite various caveats in each individual result, time-series studies suggest that natural signals and internal variability alone are unlikely to explain the instrumental record, and that an anthropogenic component is required to explain changes in the most recent four or five decades.

12.4.2 Pattern Correlation Methods

12.4.2.1 Horizontal patterns

Results from studies using pattern correlations were reported extensively in the SAR (for example, Santer *et al.*, 1995, 1996c; Mitchell *et al.*, 1995b). They found that the patterns of simulated surface temperature change due to the main anthropogenic factors in recent decades are significantly closer to those observed than expected by chance. Pattern correlations have been used because they are simple and are insensitive to errors in the amplitude of the spatial pattern of response and, if centred, to the global mean response. They are also less sensitive than regression-based optimal detection techniques to sampling error in the model-simulated response. The aim of pattern-correlation studies is to use the differences in the large-scale patterns of response, or “fingerprints”, to distinguish between different causes of climate change.

Strengths and weaknesses of correlation methods

Pattern correlation statistics come in two types – centred and uncentred (see Appendix 12.3). The centred (uncentred) statistic measures the similarity of two patterns after (without) removal of the global mean. Legates and Davis (1997) criticised the use of centred correlation in detection studies. They argued that correlations could increase while observed and simulated global means diverge. This was precisely the reason centred correlations were introduced (e.g., Santer *et al.*, 1993): to provide an indicator that was statistically independent of global mean temperature changes. If both global mean changes and centred pattern correlations point towards the same explanation of observed temperature changes, it provides more compelling evidence than either of these indicators in isolation. An explicit analysis of the role of the global mean in correlation-based studies can be provided by the

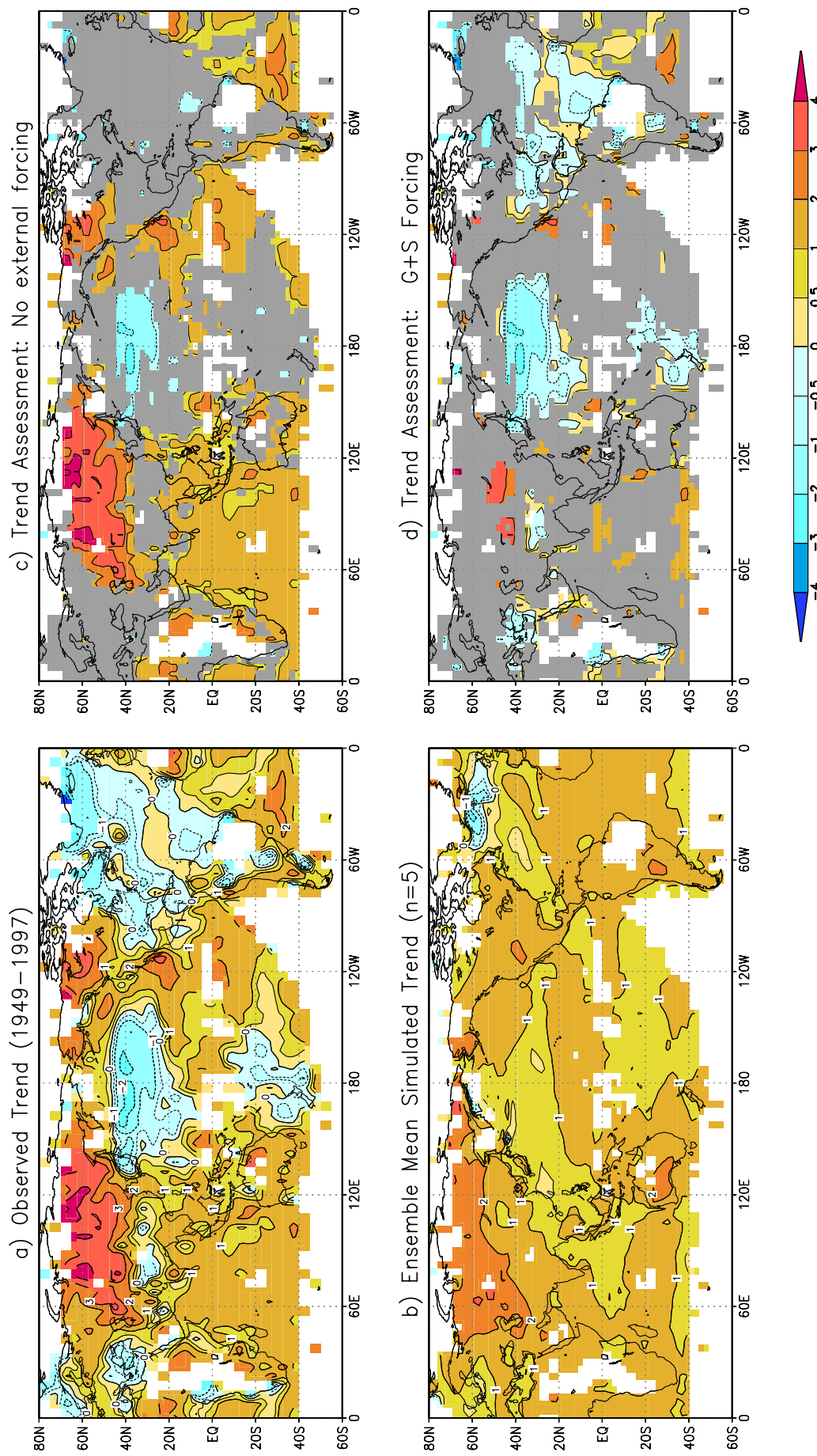


Figure 12.9: (a) Observed surface air temperature trends for 1949 to 1997. (b) Simulated surface air temperature trends for the same period as estimated from a five-member greenhouse gas plus sulphate ensemble run with the GFDL R30 model. (c) Observed trends (in colour) that lie outside the 90% natural variability confidence bounds as estimated from the GFDL R30 control run. Grey areas show regions where the observed trends are consistent with the local 49-year temperature trends in the control run. (d) As for (c) but showing observed 1949 to 1997 trends (in colour) that are significantly different (as determined with a t-test at the 10% level) from those simulated by the greenhouse gas plus aerosol simulations performed with the GFDL R30 model (from Knutson *et al.*, 2000). The larger grey areas in (d) than (c) indicate that the observed trends are consistent with the anthropogenic forced simulations over larger regions than the control simulations.

use of both centred and uncentred statistics. Pattern correlation-based detection studies account for spatial auto-correlation implicitly by comparing the observed pattern correlation with values that are realised in long control simulations (see Wigley *et al.*, 2000). These studies do not consider the amplitude of anthropogenic signals, and thus centred correlations alone are not sufficient for the attribution of climate change.

Wigley *et al.* (1998b) studied the performance of correlation statistics in an idealised study in which known spatial signal patterns were combined with realistic levels of internal variability. The statistics were found to perform well even when the signal is contaminated with noise. They found, in agreement with Johns *et al.* (2001), that using an earlier base period can enhance detectability, but that much of this advantage is lost when the reduced data coverage of earlier base periods is taken into account. They also found that reasonable combinations of greenhouse gas and aerosol patterns are more easily detected than the greenhouse gas pattern on its own. This last result indicates the importance of reducing the uncertainty in the estimate of aerosol forcing, particularly the indirect effects. In summary, we have a better understanding of the behaviour of pattern correlation statistics and reasons for the discrepancies between different studies.

12.4.2.2 Vertical patterns

As noted in Section 12.3.2, increases in greenhouse gases produce a distinctive change in the vertical profile of temperature. Santer *et al.* (1996c) assessed the significance of the observed changes in recent decades using equilibrium GCM simulations with changes in greenhouse gases, sulphate aerosols and stratospheric ozone. This study has been extended to include results from the transient AOGCM simulations, additional sensitivity studies and estimates of internal variability from three different models (Santer *et al.*, 1996a). Results from this study are consistent with the earlier results – the 25-year trend from 1963 to 1988 in the centred correlation statistic between the observed and simulated patterns for the full atmosphere was significantly different from the population of 25-year trends in the control simulations. The results were robust even if the estimates of noise levels were almost doubled, or the aerosol response (assumed linear and additive) was halved. The aerosol forcing leads to a smaller warming in the Northern Hemisphere than in the Southern Hemisphere.

Tett *et al.* (1996) refined Santer *et al.*'s (1996a) study by using ensembles of transient simulations which included increases in CO₂, and sulphate aerosols, and reductions in stratospheric ozone, as well as using an extended record of observations (see Figure 12.8). They found that the best and most significant agreement with observations was found when all three factors were included¹. Allen and Tett (1999) find that the effect of greenhouse gases can be detected with these signal patterns using optimal detection (see Appendix 12.1).

Folland *et al.* (1998) and Sexton *et al.* (2001) take a complementary approach using an atmospheric model forced with sea

surface temperatures (SST) and ice extents prescribed from observations. The correlation between the observed and simulated temperature changes in the vertical relative to the base period from 1961 to 1975 was computed. The experiments with anthropogenic forcing (including some with tropospheric ozone changes), give significantly higher correlations than when only SST changes are included.

Interpretation of results

Weber (1996) and Michaels and Knappenburger (1996) both criticised the Santer *et al.* (1996a) results, quoting upper air measurements analysed by Angell (1994). Weber argued that the increasing pattern similarity over the full atmosphere (850 to 50 hPa) resulted mainly from a Southern Hemisphere cooling associated with stratospheric ozone depletion. Santer *et al.* (1996b) pointed out that when known biases in the radiosonde data are removed (e.g., Parker *et al.*, 1997), or satellite or operationally analysed data are used, the greater stratospheric cooling in the Southern Hemisphere all but disappears. Weber (1996) is correct that stratospheric cooling due to ozone will contribute to the pattern similarity over the full atmosphere, but decreases in stratospheric ozone alone would be expected to produce a tropospheric cooling, not a warming as observed. This point should be born in mind when considering a later criticism of the pattern correlation approach. Both Weber (1996) and Michaels and Knappenburger (1996) note that the greater warming of the Southern Hemisphere relative to the Northern Hemisphere from 1963 to 1988 has since reversed. They attribute the Southern Hemisphere warming from 1963 to the recovery from the cooling following the eruption of Mount Agung. Santer *et al.* (1996b) claim that this change in asymmetry is to be expected, because the heating due to increases in greenhouse gases over the most recent years has probably been growing faster than the estimated cooling due to increases in aerosols (see Section 12.2.3.3). Calculations of the difference in the rate of warming between the Northern and Southern Hemispheres vary between different climate models and as a function of time, depending on the relative forcing due to greenhouse gases and sulphate aerosols, and on the simulated rate of oceanic heat uptake in the Southern Hemisphere (Santer *et al.*, 1996b; Karoly and Braganza, 2001).

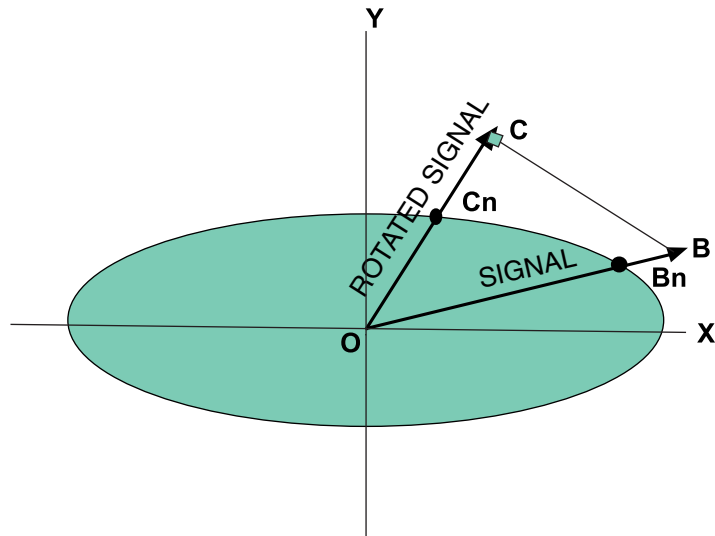
Assessing statistical significance of changes in the vertical patterns of temperature

There are some difficulties in assessing the statistical significance in detection studies based on changes in the vertical temperature profile. First, the observational record is short, and subject to error, particularly at upper levels (Chapter 2). Second, the model estimates of variability may not be realistic (Section 12.2.2), particularly in the stratosphere. Third, because of data and model limitations, the number of levels used to represent the stratosphere in detection studies to date is small, and hence may not be adequate to allow an accurate representation of the stratospheric response. Fourth, all models produce a maximum warming in the upper tropical troposphere that is not apparent in the observations and whose impact on detection results is difficult to quantify. Nevertheless, all the studies indicate that

¹ Correction of an error in a data mask (Allen and Tett, 1999) did not affect these conclusions, though the additional improvement due to adding sulphate and ozone forcing was no longer significant.

Box 12.1: Optimal detection

Optimal detection is a technique that may help to provide a clearer separation of a climate change fingerprint from natural internal climate variations. The principle is sketched in Figure 12.B1, below (after Hasselmann, 1976).



Suppose for simplicity that most of the natural variability can be described in terms of two modes (well-defined spatial patterns) of variability. In the absence of climate change, the amplitudes of these two modes, plotted on a 2D diagram along OX and OY will vary with time, and for a given fraction of occasions (usually chosen as 95 %), the amplitude of each mode will lie within the shaded ellipse. Suppose we are attempting to detect a fingerprint that can be made up of a linear combination of the two patterns such that it lies along OB. The signal to noise ratio is given by OB/OBn. Because our signal lies close to the direction of the main component of variability, the signal to noise ratio is small. On the other hand, we can choose a direction OC that overlaps less with the main component of natural variability such that the signal to noise ratio OC/OCn for the component of the signal that lies in direction OC is larger even though the projected signal OC is smaller than the full signal OB. Optimal detection techniques merely choose the direction OC that maximises the signal to noise ratio. This is equivalent to general linear regression (see Appendix 12.1). A good estimate of natural internal variability is required to optimise effectively.

anthropogenic factors account for a significant part of recent observed changes, whereas internal and naturally forced variations alone, at least as simulated by current models, cannot explain the observed changes. In addition, there are physical arguments for attributing the changes in the vertical profile of temperature to anthropogenic influence (Section 12.3.2).

12.4.3 Optimal Fingerprint Methods

The use of “optimal” techniques can increase the detectability of forced climate changes. These techniques increase the signal-to-noise ratio by looking at the component of the response away from the direction of highest internal variability (see, e.g., Hasselmann, 1979, 1997, 1993; North *et al.*, 1995; see also Box 12.1 on optimal detection and Appendix 12.1). Several new approaches to the optimal detection of anthropogenic climate change have been undertaken since the SAR. We focus on optimal detection studies that use a single pattern of climate change in the following section. Attribution (see Section 12.1.1), which requires us to consider several signals simultaneously, will be considered in Sections 12.4.3.2 and 12.4.3.3.

12.4.3.1 Single pattern studies

Since the SAR, optimal detection studies of surface temperature have been extended (Hegerl *et al.*, 1997, 2000; Barnett *et al.*, 1999) and new studies of data other than surface air temperature have been conducted (Allen and Tett, 1999; Paeth and Hense, 2001; Tett *et al.*, 2000).

Surface temperature patterns

The Hegerl *et al.* (1996) optimal detection study was extended to include more recent estimates of internal variability and simulations with a representation of sulphate aerosols (Hegerl *et al.*, 1997). As in the previous study, different control simulations were used to determine the optimal fingerprint and the significance level of recent temperature change. The authors find significant evidence for a “greenhouse gas plus sulphate aerosol” (GS) fingerprint in the most recent observed 30-year temperature trends regardless of whether internal variability is estimated from models or observations. The 30-year trend ending in the 1940s was found to be significantly larger than expected from internal variability, but less so than the more recent trends. This work has been extended to include other models (Figure 12.10a; see also Barnett *et al.*, 1999; Hegerl *et*

et al., 2000), examining whether the amplitude of the 50-year summer surface temperature trends in the GS simulations is consistent with that estimated in the observations. In eleven out of fourteen cases (seven models each evaluated using the fingerprints from the two original models), the model trends are consistent with observations. The greenhouse gas only simulations are generally not consistent with observations, as their warming trends are too large. Berliner *et al.* (2000) detect a combined greenhouse gas and sulphate signal in a fixed pattern detection study of temperature changes using Bayesian techniques.

Vertical patterns of temperature

Allen and Tett (1999) use optimal detection methods to study the change in the vertical profile of zonal mean temperature between 1961 to 1980 and 1986 to 1995. Estimated signals from ensemble AOGCM simulations with greenhouse gas alone (G), greenhouse gas plus direct sulphate (GS), and also including stratospheric ozone forcing (GSO; Tett *et al.*, 1996) are considered. The G and GSO signals are detected separately. The amplitude of the GSO fingerprint estimated from observations is found to be consistent with that simulated by the model, while the model-simulated response to greenhouse gases alone was found to be unrealistically strong. The variance of the residuals that remain after the estimated signal is removed from the observations is consistent with internal variability estimated from a control run.

Other climatic variables

Schnur (2001) applied the optimal detection technique to trends in a variety of climate diagnostics. Changes in the annual mean surface temperature were found to be highly significant (in agreement with previous results from Hegerl *et al.*, 1996, 1997). The predicted change in the annual cycle of temperature as well as winter means of diurnal temperature range can also be detected in most recent observations. The changes are most consistent with those expected from increasing greenhouse gases and aerosols. However, changes in the annual mean and annual cycle of precipitation were small and not significant.

Paeth and Hense (2001) applied a correlation method related to the optimal fingerprint method to 20-year trends of lower tropospheric mean temperature (between 500 and 1,000 hPa) in the summer half of the year in the Northern Hemisphere north of 55°N. Greenhouse gas fingerprints from two models were detected. The combined greenhouse gas plus (direct) sulphate (GS) fingerprints from the two models were not detected.

Summary

All new single-pattern studies published since the SAR detect anthropogenic fingerprints in the global temperature observations, both at the surface and aloft. The signal amplitudes estimated from observations and modelled amplitudes are consistent at the surface if greenhouse gas and sulphate aerosol forcing are taken into account, and in the free atmosphere if ozone forcing is also included. Fingerprints based on smaller areas or on other variables yield more ambiguous results at present.

12.4.3.2 Optimal detection studies that use multiple fixed signal patterns

Surface temperature patterns

Hegerl *et al.* (1997) applied a two-fingerprint approach, using a greenhouse gas fingerprint and an additional sulphate aerosol fingerprint that is made spatially independent (orthogonalised) of the greenhouse fingerprint. They analysed 50-year trends in observed northern summer temperatures. The influence of greenhouse gas and sulphate aerosol signals were both detected simultaneously in the observed pattern of 50-year temperature trends, and the amplitudes of both signals were found to be consistent between model and observations. Simulations forced with greenhouse gases alone and solar irradiance changes alone were not consistent with observations.

Hegerl *et al.* (2000) repeated this analysis using parallel simulations from a different climate model. The combined effect of greenhouse gases and aerosols was still detectable and consistent with observations, but the separate influence of sulphate aerosol forcing, as simulated by this second model, was not detectable. This was because the sulphate response was weaker in the second model, and closely resembled one of the main modes of natural variability. Hence, the detection of the net anthropogenic signal is robust, but the detection of the sulphate aerosol component is very sensitive to differences in model-simulated responses.

As in the single-pattern case, this study has been extended to include seven model GS simulations and to take into account observational sampling error (Figure 12.10b,c, see also Barnett *et al.*, 1999; Hegerl *et al.* 2001). A simple linear transformation allows results to be displayed in terms of individual greenhouse and sulphate signal amplitudes, which assists comparison with other results (see Figure 12.10; Hegerl and Allen, 2000). The amplitudes of the greenhouse gas and sulphate components are simultaneously consistent with the observed amplitudes in 10 of the fourteen GS cases (seven models for two sets of fingerprints) displayed. This contrasts with eleven out of fourteen in the combined amplitude test described in Section 12.4.3.1. If the trends to 1995 are used (Figure 12.10c), the results are similar, though in this case, the ellipse just includes the origin and six out of the fourteen GS cases are consistent with observations. The inconsistency can be seen to be mainly due to large variations in the amplitudes of the model-simulated responses to sulphate aerosols (indicated by the vertical spread of results). Model-simulated responses to greenhouse gases are generally more consistent both with each other and with observations. Two of the cases of disagreement are based on a single simulation rather than an ensemble mean and should therefore be viewed with caution (see Barnett *et al.*, 2000). Barnett *et al.* (1999) found that the degree of agreement between the five models and observations they considered was similar, whether or not the global mean response was removed from the patterns. Signal amplitudes from simulations with greenhouse gas forcing only are generally inconsistent with those estimated from observations (Figure 12.10b,c).

In most of the cases presented here, the response to natural forcings was neglected. In a similar analysis to that just described, Hegerl *et al.* (2000); see also Barnett *et al.*, 1999) also assessed simulations of the response to volcanic and solar

forcing. They find, in agreement with Tett *et al.* (1999), that there is better agreement between observations and simulations when these natural forcings are included, particularly in the early 20th century, but that natural forcings alone cannot account for the late-century warming.

In summary, the estimation of the contribution of individual factors to recent climate change is highly model dependent, primarily due to uncertainties in the forcing and response due to sulphate aerosols. However, although the estimated amplitude varies from study to study, all studies indicate a substantial contribution from anthropogenic greenhouse gases to the changes observed over the latter half of the 20th century.

Vertical patterns of temperature

Allen and Tett (1999) also used spatial fingerprints in the vertical derived from simulations with greenhouse gas forcing alone and simulations with greenhouse gas, sulphate aerosol and stratospheric ozone forcing. These authors show that, even if both greenhouse and other anthropogenic signals are estimated simultaneously in the observed record, a significant response to greenhouse gases remains detectable. Hill *et al.* (2001) extended this analysis to include model-simulated responses to both solar and volcanic forcing, and again found that the response to greenhouse gases remains detectable. Results with non-optimised fingerprints are consistent with the optimised case, but the uncertainty range is larger.

In summary, the fixed pattern studies indicate that the recent warming is unlikely (bordering on very unlikely) to be due to internal climate variability. A substantial response to anthropogenic greenhouse gases appears to be necessary to account for recent temperature trends but the majority of studies indicate that greenhouse gases alone do not appear to be able to provide a full explanation. Inclusion of the response to the direct effect of sulphate aerosols usually leads to a more satisfactory explanation of the observed changes, although the amplitude of the sulphate signal depends on the model used. These studies also provide some evidence that solar variations may have contributed to the early century warming.

12.4.3.3 Space-time studies

Here we consider studies that incorporate the time evolution of forced signals into the optimal detection formalism. These studies use evolving patterns of historical climate change in the 20th century that are obtained from climate models forced with historical anthropogenic and natural forcing. Explicit representation of the time dimension of the signals yields a more powerful approach for both detecting and attributing climate change (see Hasselmann, 1993; North *et al.*, 1995) since it helps to distinguish between responses to external forcings with similar spatial patterns (e.g., solar and greenhouse gas forcing). The time variations of the signals can be represented either directly in the time domain or transformed to the frequency domain.

Surface temperature

Tett *et al.* (1999) and Stott *et al.* (2001) describe a detection and attribution study that uses the space-time approach (see Appendix 12.2). They estimate the magnitude of modelled 20th century

greenhouse gas, aerosol, solar and volcanic signals in decadal mean data. Signals are fitted by general linear regression to moving fifty-year intervals beginning with 1906 to 1956 and ending 1946 to 1996. The signals are obtained from four ensembles of transient change simulations, each using a different historical forcing scenario. Greenhouse gas, greenhouse gas plus direct sulphate aerosol, low frequency solar, and volcanic forcing scenarios were used. Each ensemble contains four independent simulations with the same transient forcing. Two estimates of natural variability, one used for optimisation and the other for the estimation of confidence intervals, are obtained from separate segments of a long control simulation.

Signal amplitudes estimated with multiple regression become uncertain when the signals are strongly correlated ("degenerate"). Despite the problem of degeneracy, positive and significant greenhouse gas and sulphate aerosol signals are consistently detected in the most recent fifty-year period (Figure 12.11) regardless of which or how many other signals are included in the analysis (Allen *et al.*, 2000a; Stott *et al.*, 2001). The residual variation that remains after removal of the signals is consistent with the model's internal variability. In contrast, recent decadal temperature changes are not consistent with the model's internal climate variability alone, nor with any combination of internal variability and naturally forced signals, even allowing for the possibility of unknown processes amplifying the response to natural forcing.

Tett *et al.* (2000) have completed a study using a model with no flux adjustments, an interactive sulphur cycle, an explicit representation of individual greenhouse gases and an explicit treatment of scattering by aerosols. Two ensembles of four simulations for the instrumental period were run, one with natural (solar and volcanic) forcing only and the other anthropogenic (well-mixed greenhouse gases, ozone and direct and indirect sulphate aerosol) forcing only (see Figure 12.4). They find a substantial response to anthropogenic forcing is needed to explain observed changes in recent decades, and that natural forcing may have contributed significantly to early 20th century climate change. The best agreement between model simulations and observations over the last 140 years has been found when all the above anthropogenic and natural forcing factors are included (Stott *et al.*, 2000b; Figure 12.7c). These results show that the forcings included are sufficient to explain the observed changes, but do not exclude the possibility that other forcings may also have contributed.

The detection of a response to solar forcing in the early part of the century (1906 to 1956) is less robust and depends on the details of the analysis. If seasonally stratified data are used (Stott *et al.*, 2001), the detection of a significant solar influence on climate in the first half of the century becomes clearer with the solar irradiance reconstruction of Hoyt and Schatten (1993), but weaker with that from Lean *et al.* (1995). Volcanism appears to show only a small signal in recent decadal temperature trends and could only be detected using either annual mean data or specifically chosen decades (Stott *et al.*, 2001). The residual variability that remains after the naturally forced signals are removed from the observations of the most recent five decades are not consistent with model internal variability, suggesting that natural

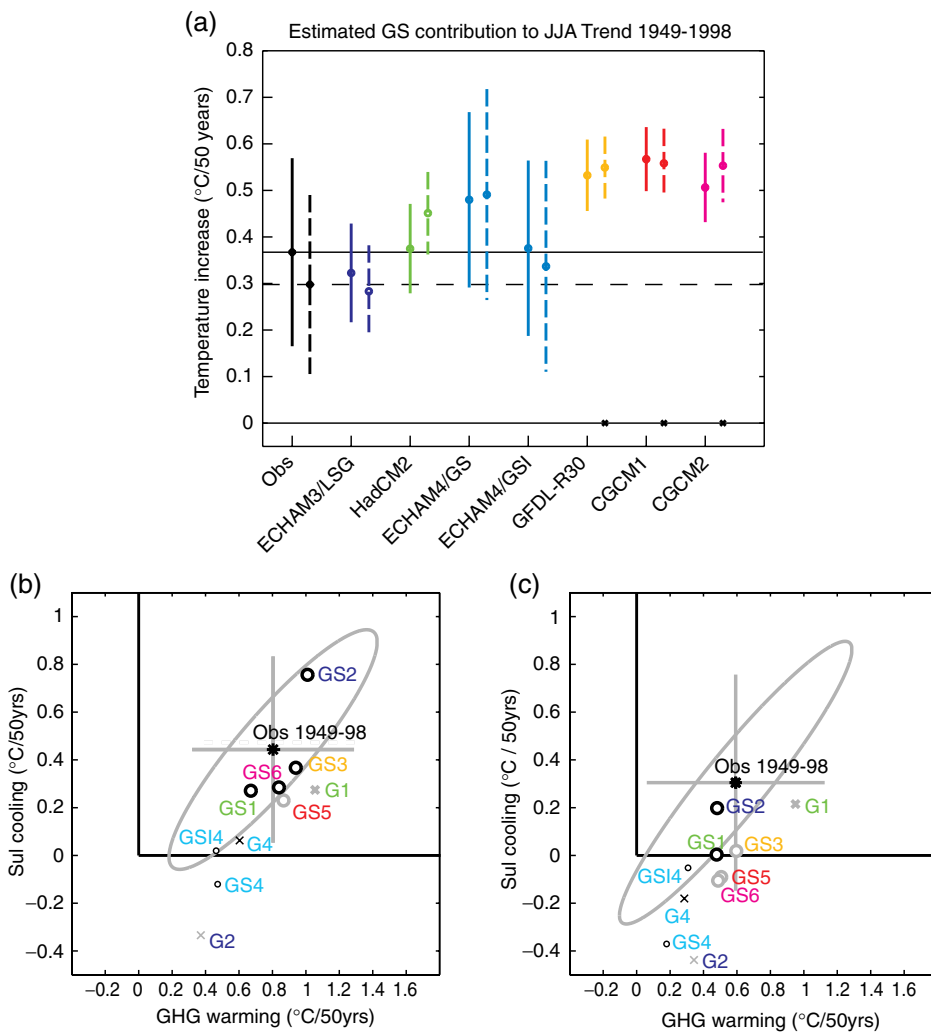


Figure 12.10: Comparison between the amplitude of anthropogenic signals from observed and modelled JJA trend patterns using fingerprints from two different climate models (ECHAM3/LSG and HadCM2) and data from five climate models. (a) Comparison of the amplitude of a single greenhouse gas + sulphate aerosol (GS) signal (expressed as change in global mean temperature [$^{\circ}\text{C}$] over 50 years). Results show that a significant GS signal can be detected in observed trend patterns 1949 to 1998 at a 5% significance level (one-sided test), independent of which pair of fingerprints was used. The observed signal amplitude is consistent with contemporaneous GS amplitudes for most models' GS simulations. 90% confidence intervals are shown by solid lines for estimates using ECHAM3/LSG fingerprints and by dashed lines for estimates based on HadCM2 fingerprints. Cases where a model's and the observed amplitude disagree are marked by a cross on the axis. (b) and (c) show an estimate of the observed amplitude of a greenhouse gas signal (horizontal axis) and a sulphate aerosol signal (vertical axis) estimated simultaneously. Both signal amplitudes can be estimated as positive from observations based on ECHAM3/LSG fingerprints shown in (b) while only the greenhouse gas signal is detected based on HadCM2 fingerprints shown in panel (c). The amplitudes of both signals from the observations are compared with those from model simulations forced with various forcing histories and using different climate models (1: HadCM2; 2: ECHAM3/LSG; 3: GFDL; 4: ECHAM4/OPYC; 5: CCCma1; 6: CCCma2). Simulations with symbols shown in black are consistent with observations relative to the uncertainty in observations (grey ellipse) and that of the model simulations (not shown). Simulations which are inconsistent are shown in grey. Model simulations where only a single ensemble member is available are illustrated by thin symbols, those based on ensembles of simulations by fat symbols.

Results from consistency tests indicate that most greenhouse gas only simulations (G, shown by “ \times ”) are inconsistent with observations. Ten of the GS simulations in both panels are in agreement with observed trend patterns, discrepancies arise mostly from the magnitude of a sulphate signal (vertical axis). The failure to detect a sulphate signal as well as a greenhouse gas signal in panel (c) is due to the two signals being very highly correlated if only spatial patterns are used- this makes separation of the signals difficult. These results show that estimates of a sulphate aerosol signal from observations are model dependent and quite uncertain, while a single anthropogenic signal can be estimated with more confidence.

All units are in $^{\circ}\text{C}/50$ year, values in the upper right quadrant refer to a physically meaningful greenhouse warming and sulphate aerosol cooling signal. The consistency test establishes whether the difference between a model's and the observed amplitude estimate is significantly larger than the combined uncertainty in the observations (internal variability + observational uncertainty) and the model simulation (internal variability). The figure is derived by updating the data used by Barnett *et al.* (1999) (for details of the analysis see Hegerl *et al.*, 2000) and then applying a simple linear transformation of the multi-regression results (Hegerl and Allen, 2000).

Results for 1946 to 1995 period used by Barnett *et al.* (1999) are similar, except fewer of the models in b and c agree with observations and the case of both signals being zero in c is not rejected. Simulations of natural forcing only ending before 1998 are also rejected in that case.

forcing alone cannot explain the observed 20th century temperature variations. Note that Delworth and Knutson (2000) find one out of five of their simulations with only anthropogenic forcing can reproduce the early century global mean warming, including the enhanced warming in Northern Hemisphere high latitudes. Hence a substantial response to anthropogenic (specifically greenhouse) forcing appears necessary to account for the warming over the past 50 years, but it remains unclear whether natural external forcings are necessary to explain the early 20th century warming.

Sensitivity of results

A variety of sensitivity tests confirm that the detection of anthropogenic signals is insensitive to differences between solar forcing reconstructions, the inclusion of additional forcing through the specification of observed stratospheric ozone concentrations, and to varying details of the analysis (including omitting the signal-to-noise optimisation). Tett *et al.* (1999, 2000) also found that detection of an anthropogenic signal continues to hold even when the standard deviation of the control simulation is inflated by a factor of two. Uncertainty in the signals is unavoidable when ensembles are small, as is the case in Tett *et al.* (1999), and biases the estimates of the signal amplitudes towards zero. Consistent results are obtained when this source of uncertainty is taken into account (Allen and Stott, 2000; Stott *et al.*, 2000a). However amplitude estimates become more uncertain, particularly if the underlying signal is small compared with internal climate variability. Accounting for sampling uncertainty in model-simulated signals indicates a greater degree of greenhouse warming and compensating aerosol cooling in the latter part of the century than shown by Tett *et al.* (1999). Gillett *et al.* (2000b) find that discounting the temperature changes associated with changes in the Arctic Oscillation (Thompson and Wallace, 1998; Thompson *et al.*, 2000), which are not simulated by the model, does not significantly alter the Tett *et al.* (1999) results.

Confidence intervals and scaling factors

Confidence intervals for the signal amplitudes that are obtained from the regression of modelled signals onto observations can be re-expressed as ranges of scaling factors that are required to make modelled signal amplitudes consistent with those estimated from observations (see, e.g., Allen and Tett, 1999). The results show that the range of scaling factors includes unity (i.e., model is consistent with observations) for both the greenhouse gas and the sulphate aerosol signal, and that the scaling factors vary only to a reasonable (and consistent) extent between 50-year intervals.

The scaling factors can also be used to estimate the contribution from anthropogenic factors other than well-mixed greenhouse gases. Using the methodology of Allen and Stott (2000) on the simulations described by Tett *et al.* (2000), the 5 to 95% uncertainty range for scaling the combined response changes in tropospheric ozone and direct and indirect sulphate forcing over the last fifty years is 0.6 to 1.6. The simulated indirect effect of aerosol forcing is by far the biggest contributor to this signal. Ignoring the possible effects of neglected forcings and assuming that the forcing can be scaled in the same way as the response, this translates to a -0.5 to -1.5 W m^{-2} change in

forcing due to the indirect effect since pre-industrial times. This range lies well within that given in Chapter 6 but the limits obtained are sensitive to the model used. Note that large values of the indirect response are consistently associated with a greater sensitivity to greenhouse gases. This would increase this model's estimate of future warming: a large indirect effect coupled with decreases in sulphate emissions would further enhance future warming (Allen *et al.*, 2000b).

Allen *et al.* (2000a) have determined scaling factors from other model simulations (Figure 12.12) and found that the modelled response to the combination of greenhouse gas and sulphate aerosol forcing is consistent with that observed. The scaling factors ranging from 0.8 to 1.2 and the corresponding 95% confidence intervals cover the range 0.5 to 1.6. Scaling factors for 50-year JJA trends are also easily derived from the results published in Hegerl *et al.* (2000). The resulting range of factors is consistent with that of Allen *et al.* (2000a), but wider because the diagnostic used in Allen *et al.* (2000b) enhances the signal-to-noise ratio. If it is assumed that the combination of greenhouse warming and sulphate cooling simulated by these AOGCMs is the only significant external contributor to inter-decadal near-surface temperature changes over the latter half of the 20th century, then Allen *et al.* (2000a) estimate that the anthropogenic warming over the last 50 years is 0.05 to $0.11^\circ\text{C}/\text{decade}$. Making a similar assumption, Hegerl *et al.* (2000) estimate 0.02 to $0.12^\circ\text{C}/\text{decade}$ with a best guess of 0.06 to $0.08^\circ\text{C}/\text{decade}$ (model dependent, Figure 12.10). The smallness of the range of uncertainty compared with the observed change indicates that natural internal variability alone is unlikely (bordering on very unlikely) to account for the observed warming.

Given the uncertainties in sulphate aerosol and natural forcings and responses, these single-pattern confidence intervals give an incomplete picture. We cannot assume that the response to sulphate forcing (relative to the greenhouse signal) is as simulated in these greenhouse-plus-sulphate simulations; nor can we assume the net response to natural forcing is negligible even though observations of surface temperature changes over the past 30 to 50 years are generally consistent with both these assumptions. Hence we need also to consider uncertainty ranges based on estimating several signals simultaneously (Figure 12.12, right hand panels). These are generally larger than the single-signal estimates because we are attempting to estimate more information from the same amount of data (Tett *et al.*, 1999; Allen and Stott, 2000; Allen *et al.*, 2000a). Nevertheless, the conclusion of a substantial greenhouse contribution to the recent observed warming trend is unchanged.

Estimation of uncertainty in predictions

The scaling factors derived from optimal detection can also be used to constrain predictions of future climate change resulting from anthropogenic emissions (Allen *et al.*, 2000b). The best guess scaling and uncertainty limits for each component can be applied to the model predictions, providing objective uncertainty limits that are based on observations. These estimates are independent of possible errors in the individual model's climate sensitivity and time-scale of oceanic adjustment, provided these

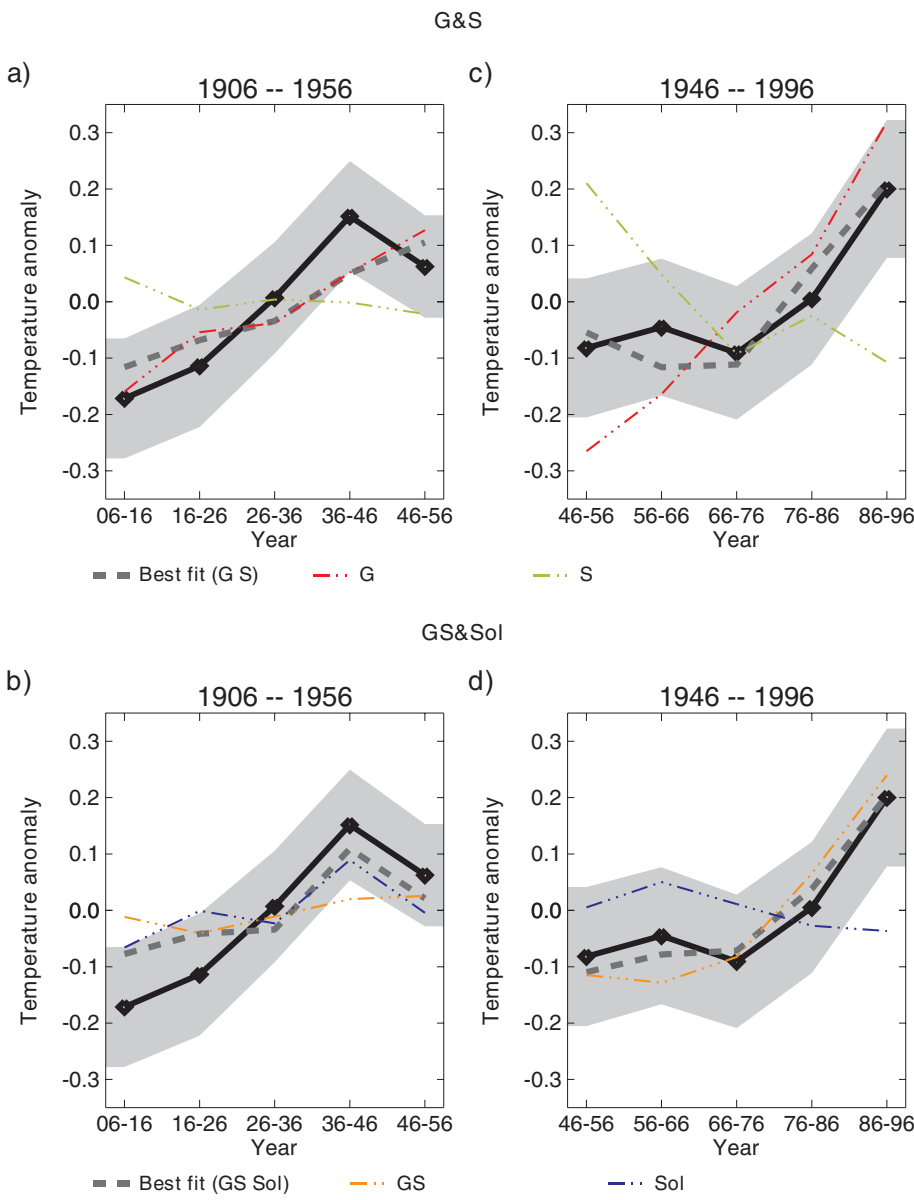


Figure 12.11: Best-estimate contributions to global mean temperature change.

Reconstruction of temperature variations for 1906 to 1956 (a and b) and 1946 to 1995 (c and d) for G and S (a and c) and GS and SOL (b and d). (G denotes the estimated greenhouse gas signal, S the estimated sulphate aerosol signal, GS the greenhouse gas / aerosol signal obtained from simulations with combined forcing, SOL the solar signal). Observed (thick black), best fit (dark grey dashed), and the uncertainty range due to internal variability (grey shading) are shown in all plots. (a) and (c) show contributions from GS (orange) and SOL (blue). (b) and (d) show contributions from G (red) and S (green). All time-series were reconstructed with data in which the 50-year mean had first been removed. (Tett *et al.*, 1999).

errors are persistent over time. An example based on the IS92a scenario (IPCC, 1992) GS scenario (whose exact forcing varies between models, see Chapter 9, Table 9.1 for details) is shown in Figure 12.13 based on a limited number of model simulations. Note that in each case, the original warming predicted by the model lies in the range consistent with the observations. A rate of warming of 0.1 to 0.2°C/decade is likely over the first few decades of the 21st century under this scenario. Allen *et al.* (2000b) quote a 5 to 95% (“very likely”) uncertainty range of 0.11 to 0.24°C/decade for the decades 1996 to 2046 under the IS92a scenario, but, given the uncertainties and assumptions behind their analysis, the more cautious “likely” qualifier is used here. For comparison, the simple model tuned to the results of seven AOGCMs used for projections in Chapter 9 gives a range of 0.12 to 0.22°C/decade under the IS92a scenario, although it should be noted that this similarity may reflect some cancellation of errors and equally good agreement between the two approaches should not be expected for all scenarios, nor for time-scales longer than the few

decades for which the Allen *et al.* (2000b) approach is valid. Figure 12.13 also shows that a similar range of uncertainty is obtained if the greenhouse gas and sulphate components are estimated separately, in which case the estimate of future warming for this particular scenario is independent of possible errors in the amplitude of the sulphate forcing and response. Most of the recent emission scenarios indicate that future sulphate emissions will decrease rather than increase in the near future. This would lead to a larger global warming since the greenhouse gas component would no longer be reduced by sulphate forcing at the same rate as in the past. The level of uncertainty also increases (see Allen *et al.*, 2000b). The final error bar in Figure 12.13 shows that including the model-simulated response to natural forcing over the 20th century into the analysis has little impact on the estimated anthropogenic warming in the 21st century.

It must be stressed that the approach illustrated in Figure 12.13 only addresses the issue of uncertainty in the large-scale climate response to a particular scenario of future greenhouse gas

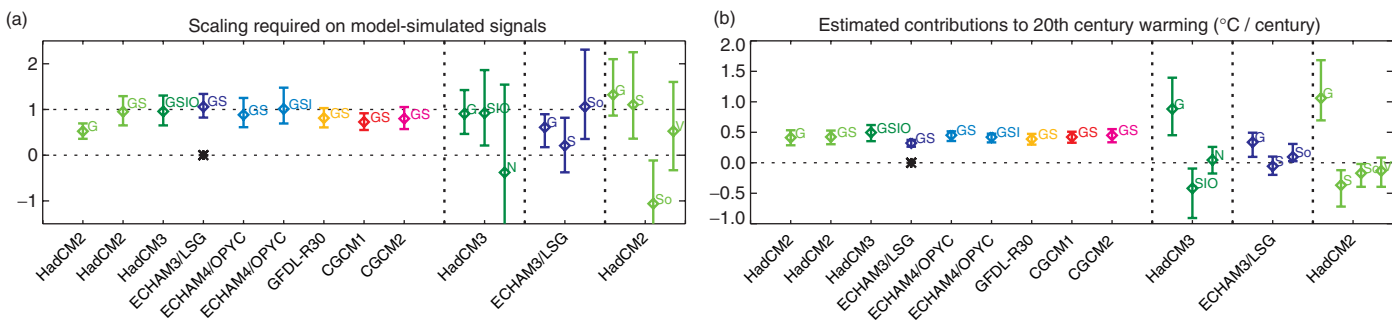


Figure 12.12: (a) Estimates of the “scaling factors” by which we have to multiply the amplitude of several model-simulated signals to reproduce the corresponding changes in the observed record. The vertical bars indicate the 5 to 95% uncertainty range due to internal variability. A range encompassing unity implies that this combination of forcing amplitude and model-simulated response is consistent with the corresponding observed change, while a range encompassing zero implies that this model-simulated signal is not detectable (Allen and Stott, 2000; Stott *et al.*, 2000a). Signals are defined as the ensemble mean response to external forcing expressed in large-scale ($>5000 \text{ km}$) near-surface temperatures over the 1946 to 1996 period relative to the 1896 to 1996 mean. The first entry (G) shows the scaling factor and 5 to 95% confidence interval obtained if we assume the observations consist only of a response to greenhouse gases plus internal variability. The range is significantly less than one (consistent with results from other models), meaning that models forced with greenhouse gases alone significantly overpredict the observed warming signal. The next eight entries show scaling factors for model-simulated responses to greenhouse and sulphate forcing (GS), with two cases including indirect sulphate and tropospheric ozone forcing, one of these also including stratospheric ozone depletion (GSI and GSIO respectively). All but one (CGCM1) of these ranges is consistent with unity. Hence there is little evidence that models are systematically over- or under-predicting the amplitude of the observed response under the assumption that model-simulated GS signals and internal variability are an adequate representation (i.e. that natural forcing has had little net impact on this diagnostic). Observed residual variability is consistent with this assumption in all but one case (ECHAM3, indicated by the asterisk). We are obliged to make this assumption to include models for which only a simulation of the anthropogenic response is available, but uncertainty estimates in these single-signal cases are incomplete since they do not account for uncertainty in the naturally forced response. These ranges indicate, however, the high level of confidence with which we can reject internal variability as simulated by these various models as an explanation of recent near-surface temperature change.

A more complete uncertainty analysis is provided by the next three entries, which show corresponding scaling factors on individual greenhouse (G), sulphate (S), solar-plus-volcanic (N), solar-only (So) and volcanic-only (V) signals for those cases in which the relevant simulations have been performed. In these cases, we estimate multiple factors simultaneously to account for uncertainty in the amplitude of the naturally forced response. The uncertainties increase but the greenhouse signal remains consistently detectable. In one case (ECHAM3) the model appears to be overestimating the greenhouse response (scaling range in the G signal inconsistent with unity), but this result is sensitive to which component of the control is used to define the detection space. It is also not known how it would respond to the inclusion of a volcanic signal. In cases where both solar and volcanic forcing is included (HadCM2 and HadCM3), G and S signals remain detectable and consistent with unity independent of whether natural signals are estimated jointly or separately (allowing for different errors in S and V responses). (b) Estimated contributions to global mean warming over the 20th century, based on the results shown in (a), with 5 to 95% confidence intervals. Although the estimates vary depending on which model’s signal and what forcing is assumed, and are less certain if more than one signal is estimated, all show a significant contribution from anthropogenic climate change to 20th century warming (from Allen *et al.*, 2000a).

concentrations. This is only one of many interlinked uncertainties in the climate projection problem, as illustrated in Chapter 13, Figure 13.2. Research efforts to attach probabilities to climate projections and scenarios are explored in Chapter 13, Section 13.5.2.3.

Forest *et al.* (2000) used simulations with an intermediate complexity climate model in a related approach. They used optimal detection results following the procedure of Allen and Tett (1999) to rule out combinations of model parameters that yield simulations that are not consistent with observations. They find that low values of the climate sensitivity ($<1^{\circ}\text{C}$) are consistently ruled out, but the upper bound on climate sensitivity and the rate of ocean heat uptake remain very uncertain.

Other space-time approaches

North and Stevens (1998) use a space-frequency method that is closely related to the space-time approach used in the studies discussed above (see Appendix 12.2). They analyse 100-year

surface temperature time-series of grid box mean surface temperatures in a global network of thirty six large ($10^{\circ} \times 10^{\circ}$) grid boxes for greenhouse gas, sulphate aerosol, volcanic and solar cycle signals in the frequency band with periods between about 8 and 17 years. The signal patterns were derived from simulations with an EBM (see Section 12.2.3). The authors found highly significant responses to greenhouse gas, sulphate aerosol, and volcanic forcing in the observations. Some uncertainty in their conclusions arises from model uncertainty (see discussion in Section 12.2.3) and from the use of control simulations from older AOGCMs, which had relatively low variability, for the estimation of internal climate variability.

A number of papers extend and analyse the North and Stevens (1998) approach. Kim and Wu (2000) extend the methodology to data with higher (monthly) time resolution and demonstrate that this may improve the detectability of climate change signals. Leroy (1998) casts the results from North and Stevens (1998) in a Bayesian framework. North and

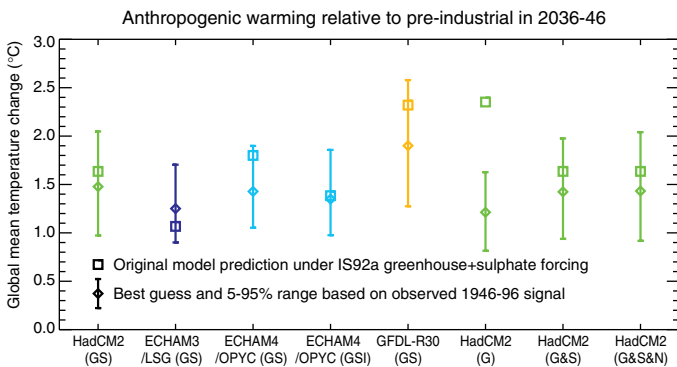


Figure 12.13: Global mean temperature in the decade 2036 to 2046 (relative to pre-industrial, in response to greenhouse gas and sulphate aerosol forcing following the IS92a (IPCC, 1992) scenario), based on original model simulations (squares) and after scaling to fit the observed signal as in Figure 12.12(a) (diamonds), with 5 to 95% confidence intervals. While the original projections vary (depending, for example, on each model's climate sensitivity), the scale should be independent of errors in both sensitivity and rate of oceanic heat uptake, provided these errors are persistent over time. GS indicates combined greenhouse and sulphate forcing. G shows the impact of setting the sulphate forcing to zero but correcting the response to be consistent with observed 20th century climate change. G&S indicates greenhouse and sulphate responses estimated separately (in which case the result is also approximately independent, under this forcing scenario, to persistent errors in the sulphate forcing and response) and G&S&N indicates greenhouse, sulphate and natural responses estimated separately (showing the small impact of natural forcing on the diagnostic used for this analysis). (From Allen *et al.*, 2000b.)

Wu (2001) modified the method to perform space-time (rather than space-frequency) detection in the 100-year record. Their results are broadly similar to those of Tett *et al.*, (1999), Stott *et al.* (2001) and North and Stevens (1998). However, their best guess includes a small sulphate aerosol signal countered by a relatively small, but highly significant, greenhouse gas signal.

All of the space-time and space-frequency optimal detection studies to date indicate a discernible human influence on global climate and yield better-constrained estimates of the magnitude of anthropogenic signals than approaches using spatial information alone. In particular, the inclusion of temporal information can reduce the degeneracy that may occur when more than one climate signal is included. Thus, results from time-space methods generally detect anthropogenic signals even if natural forcings are estimated simultaneously and show that the combination of natural signals and internal variability is inconsistent with the observed surface temperature record.

12.4.3.4 Summary of optimal fingerprinting studies

Results from optimal fingerprint methods indicate a discernible human influence on climate in temperature observations at the surface and aloft and over a range of applications. These methods can also provide a quantitative

estimate of the magnitude of this influence. The use of a number of forced climate signals, and the extensive treatment of various (but not all) sources of uncertainty increases our confidence that a considerable part of the recent warming can be attributed to anthropogenic influences. The estimated signals and scaling factors remain subject to the considerable uncertainty in our knowledge of historic climate forcing from sources other than greenhouse gases. While estimates of the amplitude of a single anthropogenic signal are quite consistent between different model signals (see Figures 12.10, 12.12) and different approaches, joint estimates of the amplitude of several signals vary between models and approaches. Thus quantitative separation of the observed warming into anthropogenic and naturally forced components requires considerable caution. Nonetheless, all recent studies reject natural forcing and internal variability alone as a possible explanation of recent climate change. Analyses based on a single anthropogenic signal focusing on continental and global scales indicate that:

- Changes over the past 30 to 50 years are very unlikely to be due to internal variability as simulated by current models.
- The combined response to greenhouse and sulphate forcing is more consistent with the observed record than the response to greenhouse gases alone.
- Inclusion of the simulated response to stratospheric ozone depletion improves the simulation of the vertical structure of the response.

Analyses based on multiple anthropogenic and natural signals indicate that:

- The combination of natural external forcing (solar and volcanic) and internal variability is unlikely to account for the spatio-temporal pattern of change over the past 30 to 50 years, even allowing for possible amplification of the amplitude of natural responses by unknown feedback processes.
- Anthropogenic greenhouse gases are likely to have made a significant and substantial contribution to the warming observed over the second half of the 20th century, possibly larger than the total observed warming.
- The contribution from anthropogenic sulphate aerosols is less clear, but appears to lie in a range broadly consistent with the spread of current model simulations. A high sulphate aerosol forcing is consistently associated with a stronger response to greenhouse forcing.
- Natural external forcing may have contributed to the warming that occurred in the early 20th century.

Results based on variables other than continental and global scale temperature are more ambiguous.

12.5 Remaining Uncertainties

The SAR identified a number of factors that limited the degree to which any human influence on climate could be quantified. It was noted that detection and attribution of anthropogenic climate change signals would be accomplished through a gradual accumulation of evidence, and that there were appreciable uncertainties in the magnitude and patterns of natural variability, and in the radiative forcing and climate response resulting from human activity.

The SAR predicted an increase in the anthropogenic contribution to global mean temperature of slightly over 0.1°C in the five years following the SAR, which is consistent with the observed change since the SAR (Chapter 2). The predicted increase in the anthropogenic signal (and the observed change) are small compared to natural variability, so it is not possible to distinguish an anthropogenic signal from natural variability on five year time-scales.

Differences in surface and free atmosphere temperature trends

There are unresolved differences between the observed and modelled temperature variations in the free atmosphere. These include apparent changes in the temperature difference between the surface and the lower atmosphere, and differences in the tropical upper troposphere. While model simulations of large-scale changes in free atmospheric and surface temperatures are generally consistent with the observed changes, simulated and observed trends in troposphere minus surface temperature differences are not consistent. It is not clear whether this is due to model or observational error, or neglected forcings in the models.

Internal climate variability

The precise magnitude of natural internal climate variability remains uncertain. The amplitude of internal variability in the models most often used in detection studies differs by up to a factor of two from that seen in the instrumental temperature record on annual to decadal time-scales, with some models showing similar or larger variability than observed (Section 12.2; Chapter 8). However, the instrumental record is only marginally useful for validating model estimates of variability on the multi-decadal time-scales that are relevant for detection. Some palaeoclimatic reconstructions of temperature suggest that multi-decadal variability in the pre-industrial era was higher than that generated internally by models (Section 12.2; Chapter 8). However, apart from the difficulties inherent in reconstructing temperature accurately from proxy data, the palaeoclimatic record also includes the climatic response to natural forcings arising, for example, from variations in solar output and volcanic activity. Including the estimated forcing due to natural factors increases the longer-term variability simulated by models, while eliminating the response to external forcing from the palaeo-record brings palaeo-variability estimates closer to model-based estimates (Crowley, 2000).

Natural forcing

Estimates of natural forcing have now been included in simulations over the period of the instrumental temperature record.

Natural climate variability (forced and/or internally generated) on its own is generally insufficient to explain the observed changes in temperature over the last few decades. However, for all but the most recent two decades, the accuracy of the estimates of forcing may be limited, being based entirely on proxy data for solar irradiance and on limited surface data for volcanoes. There are some indications that solar irradiance fluctuations have indirect effects in addition to direct radiative heating, for example due to the substantially stronger variation in the UV band and its effect on ozone, or hypothesised changes in cloud cover (see Chapter 6). These mechanisms remain particularly uncertain and currently are not incorporated in most efforts to simulate the climate effect of solar irradiance variations, as no quantitative estimates of their magnitude are currently available.

Anthropogenic forcing

The representation of greenhouse gases and the effect of sulphate aerosols has been improved in models. However, some of the smaller forcings, including those due to biomass burning and changes in land use, have not been taken into account in formal detection studies. The major uncertainty in anthropogenic forcing arises from the indirect effects of aerosols. The global mean forcing is highly uncertain (Chapter 6, Figure 6.8). The estimated forcing patterns vary from a predominantly Northern Hemisphere forcing similar to that due to direct aerosol effects (Tett *et al.*, 2000) to a more globally uniform distribution, similar but opposite in sign to that associated with changes in greenhouse gases (Roeckner *et al.*, 1999). If the response to indirect forcing has a component which can be represented as a linear combination of the response to greenhouse gases and to the direct forcing by aerosols, it will influence amplitudes of the responses to these two factors estimated through optimal detection.

Estimates of response patterns

Finally, there remains considerable uncertainty in the amplitude and pattern of the climate response to changes in radiative forcing. The large uncertainty in climate sensitivity, 1.5 to 4.5°C for a doubling of atmospheric carbon dioxide, has not been reduced since the SAR, nor is it likely to be reduced in the near future by the evidence provided by the surface temperature signal alone. In contrast, the emerging signal provides a relatively strong constraint on forecast transient climate change under some emission scenarios. Some techniques can allow for errors in the magnitude of the simulated global mean response in attribution studies. As noted in Section 12.2, there is greater pattern similarity between simulations of greenhouse gases alone, and of greenhouse gases and aerosols using the same model, than between simulations of the response to the same change in greenhouse gases using different models. This leads to some inconsistency in the estimation of the separate greenhouse gas and aerosol components using different models (see Section 12.4.3).

In summary, some progress has been made in reducing uncertainty, particularly with respect to distinguishing the responses to different external influences using multi-pattern techniques and in quantifying the magnitude of the modelled and observed responses. Nevertheless, many of the sources of uncertainty identified in the SAR still remain.

12.6 Concluding Remarks

In the previous sections, we have evaluated the different lines of evidence on the causes of recent climate change. Here, we summarise briefly the arguments that lead to our final assessment. The reader is referred to the earlier sections for more detail.

20th century climate was unusual.

Palaeoclimatic reconstructions for the last 1,000 years (e.g., Chapter 2, Figure 2.21) indicate that the 20th century warming is highly unusual, even taking into account the large uncertainties in these reconstructions.

The observed warming is inconsistent with model estimates of natural internal climate variability.

While these estimates vary substantially, on the annual to decadal time-scale they are similar, and in some cases larger, than obtained from observations. Estimates from models and observations are uncertain on the multi-decadal and longer time-scales required for detection. Nonetheless, conclusions on the detection of an anthropogenic signal are insensitive to the model used to estimate internal variability. Recent observed changes cannot be accounted for as pure internal variability even if the amplitude of simulated internal variations is increased by a factor of two or more. It is therefore unlikely (bordering on very unlikely) that natural internal variability alone can explain the changes in global climate over the 20th century (e.g., Figure 12.1).

The observed warming in the latter half of the 20th century appears to be inconsistent with natural external (solar and volcanic) forcing of the climate system.

Although there are measurements of these forcings over the last two decades, estimates prior to that are uncertain, as the volcanic forcing is based on limited measurements, and the solar forcing is based entirely on proxy data. However, the overall trend in natural forcing over the last two, and perhaps four, decades of the 20th century is likely to have been small or negative (Chapter 6, Table 6.13) and so is unlikely to explain the increased rate of global warming since the middle of the 20th century.

The observed change in patterns of atmospheric temperature in the vertical is inconsistent with natural forcing.

The increase in volcanic activity during the past two to four decades would, if anything, produce tropospheric cooling and stratospheric warming, the reverse to what has occurred over this period (e.g., Figure 12.8). Increases in solar irradiance could account for some of the observed tropospheric warming, but mechanisms by which this could cool the stratosphere (e.g., through changes in stratospheric ozone) remain speculative. Observed increases in stratospheric water vapour might also account for some of the observed stratospheric cooling. Estimated changes in solar radiative forcing over the 20th century are substantially smaller than those due to greenhouse gas forcing, unless mechanisms exist which enhance the effects of solar radiation changes at the ground. Palaeo-data show little evidence of such an enhancement at the surface in the past. Simulations based solely on the response to natural forcing (e.g.,

Figure 12.7a) are inconsistent with the observed climate record even if the model-simulated response is allowed to scale up or down to match the observations. It is therefore unlikely that natural forcing and internal variability together can explain the instrumental temperature record.

Anthropogenic factors do provide an explanation of 20th century temperature change.

All models produce a response pattern to combined greenhouse gas and sulphate aerosol forcing that is detectable in the 20th century surface temperature record (e.g., Figures 12.10, 12.12 (one model produces an estimate of internal variability which is not consistent with that observed)). Given that sulphate aerosol forcing is negative, and hence tends to reduce the response, detection of the response to the combined forcing indicates the presence of a greenhouse gas signal that is at least as large as the combined signal.

The effect of anthropogenic greenhouse gases is detected, despite uncertainties in sulphate aerosol forcing and response.

The analysis used to derive Figures 12.10a and 12.12, left box, assumes that the ratio of the greenhouse gas and sulphate aerosol responses in each model is correct. Given the uncertainty in sulphate aerosol forcing, this may not be the case. Hence one must also consider the separate responses to greenhouse gases and aerosols simultaneously. A greenhouse gas signal is consistently detected in the observations (e.g., Figure 12.10b,c, Figure 12.12 right hand boxes; North and Wu, 2001; Tett *et al.* 2000). The greenhouse gas responses are consistent with the observations in all but one case. The two component studies all indicate a substantial detectable greenhouse gas signal, despite uncertainties in aerosol forcing. The spread of estimates of the sulphate signal emphasises the uncertainty in sulphate aerosol forcing and response.

It is unlikely that detection studies have mistaken a natural signal for an anthropogenic signal.

In order to demonstrate an anthropogenic contribution to climate, it is necessary to rule out the possibility that the detection procedure has mistaken part or all of a natural signal for an anthropogenic change. On physical grounds, natural forcing is unlikely to account completely for the observed warming over the last three to five decades, given that it is likely that the overall trend in natural forcing over most of the 20th century is small or negative. Several studies have involved three or more components – the responses to greenhouse gases, sulphate aerosols and natural (solar, volcanic or volcanic and solar) forcing. These studies all detect a substantial greenhouse gas contribution over the last fifty years, though in one case the estimated greenhouse gas amplitude is inconsistent with observations. Thus it is unlikely that we have misidentified the solar signal completely as a greenhouse gas response, but uncertainty in the amplitude of the response to natural forcing continues to contribute to uncertainty in the size of the anthropogenic signal.

The detection methods used should not be sensitive to errors in the amplitude of the global mean forcing or response.

Signal estimation methods (e.g., Figures 12.10, 12.11 and 12.12)

allow for errors in the amplitude of the response, so the results should not be sensitive to errors in the magnitude of the forcing or the magnitude of the simulated model response. This would reduce the impact of uncertainty in indirect sulphate forcing on the estimated greenhouse and net sulphate signal amplitudes, to the extent that the pattern of response to indirect sulphate forcing resembles the pattern of response to direct sulphate forcing. Some models indicate this is may be the case, others do not, so this remains an important source of uncertainty. Note that if the spatio-temporal pattern of response to indirect sulphate forcing were to resemble the greenhouse response, it would lead to the amplitude of the greenhouse response being underestimated in cases where indirect sulphate forcing has not been included in the model. Detection and attribution results are also expected to be insensitive to all but the largest scale details of radiative forcing patterns. Detection is only possible at the largest spatial scales (e.g., Stott and Tett, 1998). In addition, atmospheric motions and large-scale feedbacks smooth out the response. All these arguments tend to reduce the impact of the large uncertainty in the magnitude of the forcing due to indirect sulphate aerosols. The inclusion of forcing from additional aerosols (see Chapter 6) is unlikely to alter our conclusion concerning the detection of a substantial greenhouse gas signal, though it is likely to affect estimates of the sulphate aerosol response. This is because part of the response to sulphate aerosols can be considered as surrogate for other aerosols, even though the patterns of forcing and response may differ on smaller scales. In general, the estimates of global mean forcing for other neglected factors are small (see Chapter 6, Figure 6.6).

Studies of the changes in the vertical patterns of temperature also indicate that there has been an anthropogenic influence on climate over the last 35 years.

One study finds that even when changes in stratospheric ozone and solar irradiance are taken into account, there is a detectable greenhouse gas signal in the vertical temperature record.

Observed and simulated vertical lapse rate changes are inconsistent over the last two decades, but there is an anthropogenic influence on tropospheric temperatures over a longer period.

Over the last twenty years, the observed warming trend in the lower troposphere has been smaller than at the surface. This contrasts with model simulations of the response to anthropogenic greenhouse gases and sulphate aerosols. Natural climate variability and the influence of natural external forcing, such as volcanism, can explain part of this difference. However, a discrepancy remains that cannot be accounted for with current climate models. The reduced warming in the lower troposphere does not, however, call into question the fact that the surface temperature has been warming over the satellite period (e.g., National Academy of Sciences, 2000). Over the longer period for which radiosonde data are available, an anthropogenic influence due to increasing greenhouse gases and decreasing stratospheric ozone is detected in all studies.

Natural factors may have contributed to the early century warming.

Most of the discussion in this section has been concerned with evidence relating to a human effect on late 20th century climate. The observed global mean surface temperature record shows two main periods of warming. Some studies detect a solar influence on surface temperature over the first five decades of the century, with perhaps a small additional warming due to increases in greenhouse gases. One study suggests that the early warming could be due to a combination of anthropogenic effects and a highly unusual internal variation. Thus the early century warming could be due to some combination of natural internal variability, changes in solar irradiance and some anthropogenic influence. The additional warming in the second half-century is most likely to be due to a substantial warming due to increases in greenhouse gases, partially offset by cooling due to aerosols, and perhaps by cooling due to natural factors towards the end of the period.

Appendix 12.1: Optimal Detection is Regression

The detection technique that has been used in most “optimal detection” studies performed to date has several equivalent representations (Hegerl and North, 1997; Zwiers, 1999). It has recently been recognised that it can be cast as a multiple regression problem with respect to generalised least squares (Allen and Tett, 1999; see also Hasselmann, 1993, 1997) in which a field of n “observations” \mathbf{y} is represented as a linear combination of signal patterns $\mathbf{g}_1, \dots, \mathbf{g}_m$ plus noise \mathbf{u}

$$\mathbf{y} = \sum_{i=1}^m a_i \mathbf{g}_i + \mathbf{u} = \mathbf{G}\mathbf{a} + \mathbf{u} \quad (\text{A12.1.1})$$

where $\mathbf{G}=(\mathbf{g}_1 | \dots | \mathbf{g}_m)$ is the matrix composed of the signal patterns and $\mathbf{a}=(a_1, \dots, a_m)^T$ is the vector composed of the unknown amplitudes. The field usually contains temperature observations, arrayed in space, either at the surface as grid box averages of surface temperature observations (typically 5×5 degrees; Santer *et al.*, 1995; Hegerl *et al.*, 1997; Tett *et al.*, 1999), or in the vertical as zonal averages of radiosonde observations (Karoly *et al.*, 1994; Santer *et al.*, 1996a; Allen and Tett, 1999). The fields are masked so that they represent only those regions with adequate data. The fields may also have a time dimension (Allen and Tett, 1999; North and Stevens, 1998; Stevens and North, 1996). Regardless of how the field is defined, its dimension n (the total number of observed values contained in any one single realisation of the field) is large. The signal patterns, which are obtained from climate models, and the residual noise field, have the same dimension. The procedure consists of efficiently estimating the unknown amplitudes \mathbf{a} from observations and testing the null hypotheses that they are zero. In the event of rejection, testing the hypothesis that the amplitudes are unity for some combination of signals performs the attribution consistency test. This assumes, of course, that the climate model signal patterns have been normalised. When the signal is noise-free, estimates of the amplitudes are given by

$$\tilde{\mathbf{a}} = (\mathbf{G}^T \mathbf{C}_{\mathbf{uu}}^{-1} \mathbf{G})^{-1} \mathbf{G}^T \mathbf{C}_{\mathbf{uu}}^{-1} \mathbf{y} \quad (\text{A12.1.2})$$

where $\mathbf{C}_{\mathbf{uu}}$ is the $n\times n$ covariance matrix of the noise (Hasselmann, 1997, 1998; Allen and Tett, 1999; Levine and Berliner, 1999). Generalisations allow for the incorporation of signal uncertainties (see, for example, Allen *et al.*, 2000b). A schematic two-dimensional example is given in Box 12.1. In essence, the amplitudes are estimated by giving somewhat greater weight to information in the low variance parts of the field of observations. The uncertainty of this estimate, expressed as the $m\times m$ covariance matrix of $\tilde{\mathbf{a}}$, is given by

$$\mathbf{C}_{\mathbf{aa}} = (\mathbf{G}^T \mathbf{C}_{\mathbf{uu}}^{-1} \mathbf{G})^{-1} \quad (\text{A12.1.3})$$

This leads to a $(1-\alpha)\times 100\%$ confidence ellipsoid for the unknown amplitudes when \mathbf{u} is the multivariate Gaussian that is given by

$$(\tilde{\mathbf{a}} - \mathbf{a})^T \mathbf{G}^T \mathbf{C}_{\mathbf{uu}}^{-1} \mathbf{G} (\tilde{\mathbf{a}} - \mathbf{a}) \leq \chi^2_{1-\alpha} \quad (\text{A12.1.4})$$

where $\chi^2_{1-\alpha}$ is the $(1-\alpha)$ critical value of the chi-squared distribution with m degrees of freedom. Marginal confidence ellipsoids can be constructed for subsets of signals simply by removing the appropriate rows and columns from $\mathbf{G}^T \mathbf{C}_{\mathbf{uu}}^{-1} \mathbf{G}$ and reducing the number of degrees of freedom. The marginal $(1-\alpha)\times 100\%$ confidence interval for the amplitude of signal i (i.e., the confidence interval that would be obtained in the absence of information about the other signals) is given by

$$\tilde{a}_i - z_{1-\alpha/2} (\mathbf{G}^T \mathbf{C}_{\mathbf{uu}}^{-1} \mathbf{G})_{ii} \leq a_i \leq \tilde{a}_i + z_{1-\alpha/2} (\mathbf{G}^T \mathbf{C}_{\mathbf{uu}}^{-1} \mathbf{G})_{ii} \quad (\text{A12.1.5})$$

where $Z_{1-\alpha/2}$ is the $(1-\alpha/2)$ critical value for the standard normal distribution. Signal i is said to be detected at the $\alpha/2\times 100\%$ significance level if the lower limit confidence interval (A12.1.5) is greater than zero. However, “multiplicity” is a concern when making inferences in this way. For example, two signals that are detected at the $\alpha/2\times 100\%$ significance level may not be jointly detectable at this level. The attribution consistency test is passed when the confidence ellipsoid contains the vector of units $(1, \dots, 1)^T$.

Appendix 12.2: Three Approaches to Optimal Detection

Optimal detection studies come in several variants depending upon how the time evolution of signal amplitude and structure is treated.

Fixed pattern studies (Hegerl *et al.*, 1996, 1997, 2000a; Berliner *et al.*, 2000; Schnur, 2001) assume that the spatial structure of the signals does not change during the epoch covered by the instrumental record. This type of study searches for evidence that the amplitudes of fixed anthropogenic signals are increasing with time. The observed field $\mathbf{y}=\mathbf{y}(t)$ that appears on the left hand side of equation (A12.1.1) is typically a field of 30 to 50-year moving window trends computed from annual mean observations. The regression equation (A12.1.1) is solved repeatedly with a fixed signal matrix \mathbf{G} as the moving 30 to 50-year window is stepped through the available record.

Studies with *time-varying patterns* allow the shape of the signals, as well as their amplitudes, to evolve with time. Such studies come in two flavours.

The *space-time* approach uses enlarged signal vectors that consist of a sequence of spatial patterns representing the evolution of the signal through a short epoch. For example, Tett *et al.* (1999) use signal vectors composed of five spatial patterns representing a sequence of decadal means. The enlarged signal matrix $\mathbf{G}=\mathbf{G}(t)$ evolves with time as the 5-decade window is moved one decade at a time. The observations are defined

similarly as extended vectors containing a sequence of observed decadal mean temperature patterns. As with the fixed pattern approach, a separate model is fitted for each 5-decade window so that the evolution of the signal amplitudes can be studied.

The *space-frequency* approach (North *et al.*, 1995) uses annual mean signal patterns that evolve throughout the analysis period. A Fourier transform is used to map the temporal variation of each signal into the frequency domain. Only the low-frequency Fourier coefficients representing decadal-scale variability are retained and gathered into a signal vector. The observations are similarly transformed. The selection of time-scales that is effected by retaining only certain Fourier coefficients is a form of dimension reduction (see Dimension Reduction, Appendix 12.4) in the time domain. This is coupled with spatial dimension reduction that must also be performed. The result approximates the dimension reduction that is obtained by projecting observations in space and time on low order space-time EOFs (North *et al.*, 1995). A further variation on this theme is obtained by increasing the time resolution of the signals and the data by using monthly rather than annual means. Climate statistics, including means, variances and covariances, have annual cycles at this time resolution, and thus dimension reduction must be performed with cyclo-stationary space-time EOFs (Kim and Wu, 2000).

Given the same amount of data to estimate covariance matrices, the space-time and space-frequency approaches will sacrifice spatial resolution for temporal resolution.

Appendix 12.3: Pattern Correlation Methods

The pattern correlation methods discussed in this section are closely related to optimal detection with one signal pattern. Pattern correlation studies use either a centred statistic, R , which correlates observed and signal anomalies in space relative to their respective spatial means, or an uncentred statistic, C (Barnett and Schlesinger, 1987), that correlates these fields without removing the spatial means. It has been argued that the latter is better suited for detection, because it includes the response in the global mean, while the former is more appropriate for attribution because it better measures the similarity between spatial patterns. The similarity between the statistics is emphasised by the fact that they can be given similar matrix-vector representations. In the one pattern case, the optimal (regression) estimate of signal amplitude is given by

$$\tilde{a} = \mathbf{g}_1^T \mathbf{C}_{\mathbf{uu}}^{-1} \mathbf{y} / \mathbf{g}_1^T \mathbf{C}_{\mathbf{uu}}^{-1} \mathbf{g}_1 \quad (\text{A12.3.1})$$

The uncentred statistics may be written similarly as

$$C = \mathbf{g}_1^T \mathbf{y} / \mathbf{g}_1^T \mathbf{g}_1 = \mathbf{g}_1^T \mathbf{I} \mathbf{y} / \mathbf{g}_1^T \mathbf{I} \mathbf{g}_1 \quad (\text{A12.3.2})$$

where \mathbf{I} is the $n \times n$ identity matrix. Similarly, the centred statistic can be written (albeit with an extra term in the denominator) as

$$R = \mathbf{g}_1^T (\mathbf{I} - \mathbf{U}) \mathbf{y} / [(\mathbf{g}_1^T (\mathbf{I} - \mathbf{U}) \mathbf{g}_1)^{1/2} (\mathbf{y}^T (\mathbf{I} - \mathbf{U}) \mathbf{y})^{1/2}] \quad (\text{A12.3.3})$$

where \mathbf{U} is the $n \times n$ matrix with elements $u_{i,j}=1/n$. The matrix \mathbf{U} removes the spatial means. Note that area, mass or volume weighting, as appropriate, is easily incorporated into these expressions. The main point is that each statistic is proportional to the inner product with respect to a matrix ‘kernel’ between the signal pattern and the observations (Stephenson, 1997). In contrast with the pattern correlation statistics, the optimal signal amplitude estimate, which is proportional to a correlation coefficient using the so-called Mahalonobis kernel (Stephenson, 1997), maximises the signal-to-noise ratio.

Appendix 12.4: Dimension Reduction

Estimation of the signal amplitudes, as well as the detection and attribution consistency tests on the amplitudes, requires an estimate of the covariance matrix C_{uu} of the residual noise field. However, as \mathbf{y} typically represents climate variation on time-scales similar to the length of the observed instrumental record, it is difficult to estimate the covariance matrix reliably. Thus the covariance matrix is often estimated from a long control simulation. Even so, the number of independent realisations of \mathbf{u} that are available from a typical 1,000 to 2,000-year control simulation is substantially smaller than the dimension of the field, and thus it is not possible to estimate the full covariance matrix. The solution is to replace the full fields \mathbf{y} , $\mathbf{g}_1, \dots, \mathbf{g}_m$ and \mathbf{u} with vectors of dimension k , where $m < k < n$, containing indices of their projections onto the dominant patterns of variability $\mathbf{f}_1, \dots, \mathbf{f}_k$ of \mathbf{u} . These patterns are usually taken to be the k highest variance EOFs of a control run (North and Stevens, 1998; Allen and Tett, 1999; Tett *et al.*, 1999) or a forced simulation (Hegerl *et al.*, 1996, 1997; Schnur, 2001). Stott and Tett (1998) showed with a “perfect model” study that climate change in surface air temperature can only be detected at very large spatial scales. Thus Tett *et al.* (1999) reduce the spatial resolution to a few spherical harmonics prior to EOF truncation. Kim *et al.* (1996) and Zwiers and Shen (1997) examine the sampling properties of spherical harmonic coefficients when they are estimated from sparse observing networks.

An important decision, therefore, is the choice of k . A key consideration in the choice is that the variability of the residuals should be consistent with the variability of the control simulation in the dimensions that are retained. Allen and Tett (1999) describe a simple test on the residuals that makes this consistency check. Rejection implies that the model-simulated variability is significantly different from that of the residuals. This may happen when the number of retained dimensions, k , is too large because higher order EOFs may contain unrealistically low variance due to sampling deficiencies or scales that are not well represented. In this situation, the use of a smaller value of k can still provide consistent results: there is no need to require that model-simulated variability is perfect on all spatio-temporal scales for it to be adequate on the very large scales used for detection and attribution studies. However, failing the residual check of Allen and Tett (1999) could also indicate that the model does not have the correct timing or pattern of response (in which case the residuals will contain forced variability that is not present in the control regardless of the choice of k) or that the model does not simulate the correct amount of internal variability, even at the largest scales represented by the low order EOFs. In this case, there is no satisfactory choice of k . Previous authors (e.g., Hegerl *et al.*, 1996, 1997; Stevens and North, 1996; North and Stevens, 1998) have made this choice subjectively. Nonetheless, experience in recent studies (Tett *et al.* 1999; Hegerl *et al.* 2000, 2001; Stott *et al.*, 2001) indicates that their choices were appropriate.

Appendix 12.5: Determining the Likelihood of Outcomes (p -values)

Traditional statistical hypothesis tests are performed by comparing the value of a detection statistic with an estimate of its natural internal variability in the unperturbed climate. This estimate must be obtained from control climate simulations because detection statistics typically measure change on time-scales that are a substantial fraction of the length of the available instrumental record (see Appendix 12.4). Most “optimal” detection studies use two data sets from control climate simulations, one that is used to develop the optimal detection statistic and the other to independently estimate its natural variability. This is necessary to avoid underestimating natural variability. The p -value that is used in testing the no signal null hypothesis is often computed by assuming that both the observed and simulated projections on signal patterns are

normally distributed. This is convenient, and is thought to be a reasonable assumption given the variables and the time and space scales used for detection and attribution. However, it leads to concern that very small p -values may be unreliable, because they correspond to events that have not been explored by the model in the available control integrations (Allen and Tett, 1999). They therefore recommend that p -values be limited to values that are consistent with the range visited in the available control integrations. A non-parametric approach is to estimate the p -value by comparing the value of the detection statistic with an empirical estimate of its distribution obtained from the second control simulation data set. If parametric methods are used to estimate the p -value, then very small values should be reported as being less than $1/n_p$, where n_p represents the equivalent number of independent realisations of the detection statistic that are contained in the second control integration.

References

- Adcock**, R.J., 1878: *The Analyst* (Des Moines, Iowa), **5**, 53.
- Allen**, M.R. and S.F.B.Tett, 1999: Checking for model consistency in optimal fingerprinting. *Clim. Dyn.*, **15**, 419-434.
- Allen**, M.R. and P.A. Stott, 2000: Interpreting the signal of anthropogenic climate change I: estimation theory. Tech. Report RAL-TR-2000-045, Rutherford Appleton Lab., Chilton, X11 0QX, UK.
- Allen**, M.R., N.P. Gillett, J.A. Kettleborough, R. Schnur, G.S. Jones, T. Delworth, F. Zwiers, G. Hegerl, T.P. Barnett, 2000a: Quantifying anthropogenic influence on recent near-surface temperature change”, Tech. Report RAL-TR-2000-046, Rutherford Appleton Lab., Chilton, X11 0QX, UK.
- Allen**, M.R., P.A. Stott, R. Schnur, T. Delworth and J.F.B. Mitchell, 2000b: Uncertainty in forecasts of anthropogenic climate change. *Nature*, **407**, 617-620.
- Angell**, J.K., 1994: Global, hemispheric and zonal temperature anomalies derived from radiosonde records. pp. 636-672. In “Trends '93: A compendium of data on global change” (Eds. T. A. Boden *et al.*), ORNL/CDIAC-65, Oak Ridge, TN.
- Bankes**, H.T., R.A. Wood, J.M. Gregory, T.C. Johns and G.S Jones, 2000: Are observed changes in intermediate water masses a signature of anthropogenic climate change? *Geophys. Res. Lett.*, **27**, 2961-2964.
- Barnett**, T.P. and M.E. Schlesinger, 1987: Detecting changes in global climate induced by greenhouse gases. *J. Geophys. Res.*, **92**, 14772-14780.
- Barnett**, T.P., B.D. Santer, P.D. Jones, R.S. Bradley and K.R. Briffa, 1996: Estimates of low Frequency Natural Variability in Near-Surface Air Temperature. *The Holocene*, **6**, 255-263.
- Barnett**, T.P., K. Hasselmann, M. Chelliah, T. Delworth, G. Hegerl, P. Jones, E. Rasmussen, E. Roeckner, C. Ropelewski, B. Santer and S. Tett, 1999: Detection and attribution of climate change: A Status report. *Bull. Am. Met. Soc.*, **12**, 2631-2659.
- Barnett**, T.P., G.C. Hegerl, T. Knutson and S.F.B. Tett, 2000: Uncertainty levels in predicted patterns of anthropogenic climate change. *J. Geophys. Res.*, **105**, 15525-15542.
- Bengtsson**, L., E.Roeckner, M.Stendel, 1999: Why is the global warming proceeding much slower than expected. *J. Geophys. Res.*, **104**, 3865-3876.
- Berliner**, L.M., R.A. Levine and D.J. Shea, 2000: Bayesian climate change assessment. *J.Climate*, **13**, 3805-3820.
- Bertrand**, C., J.-P. van Ypersele, A. Berger, 1999: Volcanic and solar impacts on climate since 1700. *Clim. Dyn.*, **15**, 355-367
- Boer**, G. J., G. Flato, M.C. Reader and D. Ramsden, 2000a: A transient climate change simulation with greenhouse gas and aerosol forcing: experimental design and comparison with the instrumental record for the 20th century. *Clim. Dyn.*, **16**, 405-426.
- Boer**, G.J., G. Flato, M.C. Reader and D. Ramsden, 2000b: A transient climate change simulation with greenhouse gas and aerosol forcing: projected for the 21st century. *Clim. Dyn.*, **16**, 427-450.
- Briffa**, K.R., P.D. Jones, F.H. Schweingruber and T.J. Osborn, 1998: Influence of volcanic eruptions on Northern Hemisphere summer temperature over the past 600 years. *Nature*, **393**, 450-454.
- Briffa**, K.R., T.J. Osborn, F.H. Schweingruber, I.C. Harris, P.D. Jones, S.G. Shiyatov and E.A. Vaganov, 2000: Low-frequency temperature variations from a northern tree-ring density network. *J.Geophys.Res.* **106**, 2929-2942.
- Brown**, L., G. Casella and T.G. Hwang, 1995: Optimal confidence sets, bioequivalence and the limacon of Pascal. *J. Amer. Statist. Soc.*, **90**, 880-889.
- Brown**, S.J., D.E. Parker, C.K. Folland and I. Macadam, 2000a: Decadal variability in the lower-tropospheric lapse rate. *Geophys. Res. Lett.*, **27**, 997-1000.
- Brown**, S.J., D.E. Parker and D.M.H. Sexton, 2000b: Differential changes in observed surface and atmospheric temperature since 1979. Hadley Centre Technical Note No. 12, The Met. Office Bracknell, UK, pp41.
- Chamin**, M.-L. and V. Ramaswamy, 1999: “Trends in Stratospheric Temperatures” in WMO (World Meteorological Organization), Scientific Assessment of Ozone Depletion: 1998, Global Ozone Research and Monitoring Project - Report No. 44, Geneva. 5.1-5.59
- Collins**, M., T.J. Osborn, S.F.B. Tett, K.R. Briffa and F.H. Schweingruber, 2000: A comparison of the variability of a climate model with a network of tree-ring densities. Hadley Centre Technical Note 16.
- Crowley**, T.J., 2000: Causes of climate change over the last 1000 years, *Science*, **289**, 270-277.
- Crowley**, T.J. and K.-Y. Kim, 1996: Comparison of proxy records of climate change and solar forcing. *Geophys. Res. Lett.*, **23**: 359-362.
- Crowley**, T.J. and Kim K.-Y., 1999: Modelling the temperature response to forced climate change over the last six centuries. *Geophys. Res. Lett.*, **26**, 1901-1904.
- Crowley**, T.J. and T. Lowery, 2000: How warm was the Medieval warm period? *Ambio*, **29**, 51-54.
- Cubasch**, U., G.C. Hegerl and J. Waszkewitz, 1996: Prediction, detection and regional assessment of anthropogenic climate change. *Geophysica*, **32**, 77-96.
- Cubasch**, U., G.C. Hegerl, R. Voss, J. Waszkewitz and T.J. Crowley, 1997: Simulation of the influence of solar radiation variations on the global climate with an ocean-atmosphere general circulation model. *Clim. Dyn.*, **13**, 757-767.
- Delworth**, T.L. and T.R. Knutson, 2000. Simulation of early 20th century global warming. *Science*, **287**, 2246-2250.
- Dempster**, A.P., 1998: Logistic statistics I. Models and modeling. *Statistical Science*, **13**, 248-276.
- Drijfhout**, S.S., R.J. Haarsma, J.D. Opsteegh, F.M. Selten, 1999: Solar-induced versus internal variability in a coupled climate model. *Geophys. Res. Lett.*, **26**, 205-208.
- Folland**, C.K., D.M.H. Sexton, D.J.K. Karoly, C.E. Johnston, D.P. Rowell and D.E. Parker, 1998: Influences of anthropogenic and oceanic forcing on recent climate change. *Geophys. Res. Lett.*, **25**, 353-356.
- Forest**, C.E., M.R. Allen, P.H. Stone, A.P. Sokolov, 2000: Constraining uncertainties in climate models using climate change detection techniques. *Geophys. Res. Lett.*, **27**, 569-572.
- Forster**, P.M. and K.P. Shine, 1999: Stratospheric water vapour changes as a possible contributor to observed stratospheric cooling. *Geophys. Res. Lett.*, **26**, 3309-3312.
- Free**, M. and A. Robock, 1999: Global Warming in the Context of the little Ice Age. *J.Geophys Res.*, **104**, 19057-19070.
- Froehlich**, K. and J. Lean, 1998: The Sun's Total Irradiance: Cycles, Trends and Related Climate Change Uncertainties since 1976. *Geophys. Res. Lett.*, **25**, 4377-4380.
- Fyfe**, J.C., G.J. Boer and G.M. Flato 1999: The Arctic and Antarctic Oscillations and their projected changes under global warming. *Geophys. Res. Lett.*, **26**, 1601-1604.
- Gaffen**, D.J., B.D. Santer, J.S. Boyle, J.R. Christy, N.E. Graham and R.J.Ross, 2000. Multi-decadal changes in vertical temperature structure of the tropical troposphere. *Science*, **287**, 1242-1245.
- Gillet**, N., M.R. Allen and S.F.B. Tett, 2000a: Modelled and observed variability in atmospheric vertical temperature structure. *Clim Dyn.*, **16**, 49-61.
- Gillet**, N., G.C. Hegerl, M.R. Allen, P.A. Stott, 2000b: Implications of observed changes in the Northern Hemispheric winter circulation for the detection of anthropogenic climate change. *Geophys. Res. Lett.*, **27**, 993-996..
- Graf**, H.-F., I. Kirchner, I. Schult 1996: Modelling Mt. Pinatubo Climate Effects. NATO-ASI Series, Vol 142, The Mount Pinatubo Eruption, Fiocco G and Dua D. eds., Springer, 1996: 219-231.
- Graf**, H-F., I. Kirchner and J. Perlitz, 1998: Changing lower stratospheric circulation: The role of ozone and greenhouse gases. *J.*

- Geophys. Res.*, **103**, 11251-11261.
- Grieser**, J. and C.-D. Schoenwiese, 1999: Parameterization of spatio-temporal patterns of volcanic aerosol induced stratospheric optical depth and its climate radiative forcing. *Atmosfera*, **12**, 111-133
- Grieser**, J. and C.-D. Schoenwiese, 2001: Process, forcing and signal analysis of global mean temperature variations by means of a three box energy balance model. *Clim. Change*, in press.
- Haigh**, J.D., 1999: A GCM study of climate change in response to the 11-year solar cycle. *Quart. J. R. Met. Soc.*, **125**, 871-892.
- Hansen** J., Mki.Sato, R. Ruedy, A. Lacis, K. Asamoah, S. Borenstein, E. Brown, B. Cairns, G. Caliri, M. Campbell, B. Curran, S. deCastro, L. Druyan , M. Fox, C. Johnson, J. Lerner, M.P. McCormick, R. Miller, P. Minnis, A. Morrison, L. Pandolfo, I. Ramberran, F. Zaucker, M. Robinson, P. Russell, K. Shah, P. Stone, I. Tegen, L. Thomason, J. Wilder and H. Wilson 1996: A Pinatubo climate modeling investigation. In "The Mount Pinatubo Eruption: Effects on the Atmosphere and Climate", Fiocco G and Fua Visconti G, Springer Verlag, Berlin, pp 233-272.
- Hansen**, J., M. Sato and R. Reudy, 1997a: Radiative forcing and climate response. *J. Geophys. Res.*, **102**, 6831-6864.
- Hansen**, J.E., M. Sato, A. Lacis and R. Reudy, 1997b: The missing climate forcing. *Roy. Soc. Phil. Trans. B*, **352**, 231-240.
- Hansen**, J.E., M.Sato, A. Lacis, R.Reudy, I .Tegen and E. Matthews, 1998. Climate forcings in the industrial era. *Proc. Nat. Acad. Sci. U.S.A.*, **95**, 12753-12758.
- Harrison**, R.G. and K.P. Shine, 1999: A review of recent studies of the influence of solar changes on the Earth's climate. Hadley Centre Tech. Note 6. Hadley Centre for Climate Prediction and Research, Meteorological Office, Bracknell RG12 2SY UK pp 65
- Hasselmann**, K., 1976: Stochastic climate models. Part 1. Theory. *Tellus*, **28**, 473-485.
- Hasselmann**, K., 1979. On the signal-to-noise problem in atmospheric response studies. Meteorology over the tropical oceans, D.B. Shaw ed., Roy Meteorol. Soc., 251-259
- Hasselmann**, K., 1993: Optimal fingerprints for the Detection of Time dependent Climate Change. *J. Climate*, **6**: 1957-1971.
- Hasselmann**, K. ,1997: Multi-pattern fingerprint method for detection and attribution of climate change. *Clim. Dyn.*, **13**: 601-612.
- Hasselmann**, K., 1998: Conventional and Bayesian approach to climate-change detection and attribution. *Quart. J. R. Met. Soc.*, **124**, 2541-2565.
- Hasselmann**, K., L. Bengtsson , U. Cubasch, G.C. Hegerl, H. Rodhe, E. Roeckner, H. von Storch, R.Voss and J. Waszkewitz,1995: Detection of an anthropogenic fingerprint. In:*Proceedings of Modern Meteorology" Symposium in honour of Aksle Wiin-Nielsen*, 1995. P. Ditvelson (ed) ECMWF.
- Haywood**, J.M., R. Stouffer, R. Wetherald, S. Manabe and V. Ramaswamy, 1997: Transient response of a coupled model to estimated changes in greenhouse gas and sulphate concentrations. *Geophys. Res. Lett.* , **24**, 1335- 1338.
- Hegerl**, G.C. and G.R. North 1997: Statistically optimal methods for detecting anthropogenic climate change. *J. Climate*, **10**: 1125-1133.
- Hegerl**, G.C. and M.R. Allen, 2000: Physical interpretation of optimal detection. Tech Report RAL-TR-2001-010, Rutherford Appleton Lab., Chilton, X11 0QX, U.K.
- Hegerl**, G.C., von Storch, K. Hasselmann, B.D. Santer, U. Cubasch and P.D. Jones 1996: Detecting Greenhouse Gas induced Climate Change with an Optimal Fingerprint Method. *J. Climate*, **9**, 2281-2306.
- Hegerl**, G.C., K Hasselmann, U. Cubasch, J.F.B. Mitchell, E. Roeckner, R. Voss and J. Waszkewitz 1997: Multi-fingerprint detection and attribution of greenhouse gas- and aerosol forced climate change. *Clim. Dyn.* **13**, 613-634
- Hegerl**, G.C., P. Stott, M. Allen, J.F.B.Mitchell, S.F.B.Tett and U.Cubasch, 2000: Detection and attribution of climate change: Sensitivity of results to climate model differences. *Clim. Dyn.*, **16**, 737-754
- Hegerl**, G.C., P.D. Jones and T.P. Barnett. 2001: Effect of observational sampling error on the detection of anthropogenic climate change. *J. Climate*, **14**, 198-207.
- Hill**, D.C., M.R. Allen, P.A. Stott, 2001: Allowing for solar forcing in the detection of human influence on atmospheric vertical temperature structures. *Geophys. Res. Lett.*, **28**, 1555-1558.
- Hoyt**, D.V. and K.H. Schatten,1993: A discussion of plausible solar irradiance variations, 1700-1992. *J. Geophys. Res.*, **98**, 18895-18906.
- IPCC**, 1990: Climate change: the IPCC scientific assessment [Houghton, J.T., G.J. Jenkins and J.J. Ephraums (eds.)] Cambridge University Press, Cambridge, United Kingdom, 365pp.
- IPCC**, 1992: Climate Change 1992: The Supplementary Report to the Intergovernmental Panel on Climate Change Scientific Assessment [Houghton, J.T., B.A. Callander and S.K. Varney (eds.)]. Cambridge University Press, Cambridge, United Kingdom and New York, NY, USA, 100 pp.
- IPCC**,1996: Climate Change 1995. The IPCC second scientific assessment. Houghton JT, L.G. Meira Filho, B.A. Callander, N. Harris, A. Kattenberg , K. Maskell (eds.). Cambridge University Press, Cambridge, 572 pp.
- Johns**, T.C., J.M. Gregory, P. Stott and J.F.B. Mitchell, 2001: Assessment of the similarity between modelled and observed near surface temperature changes using ensembles. *Geophys. Res. Lett.* **28**, 1007-1010.
- Jones**, A., D.L. Roberts and M.J. Woodage, 1999: The indirect effects of anthropogenic aerosol simulated using a climate model with an interactive sulphur cycle . Hadley Centre Tech. Note 14. Hadley Centre for Climate Prediction and Research, Meteorological Office, Bracknell RG12 2SY UK, pp39.
- Jones**, P.D. and G.C. Hegerl, 1998: Comparisons of two methods of removing anthropogenically related variability from the near-surface observational temperature field. *J.Geophys.Res.*, **103**, D12: 1377-13786
- Jones**, P.D., K.R. Briffa, T.P. Barnett and S.F.B. Tett, 1998: High-resolution paleoclimatic records for the last millenium. *The Holocene* **8**: 467-483.
- Jones**, P.D., T.J. Osborn, K.R. Briffa, C.K. Folland, B. Horton, L.V. Alexander, D.E. Parker and N.A. Raynor, 2001:Adjusting for sampling density in grid-box land and ocean surface temperature time series, *J. Geophys. Res.*, **106**, 3371-3380
- Karoly**, D. J. and K. Braganza, 2001: Identifying global climate change using simple indices. *Geophys. Res. Lett.*, in press.
- Karoly**, D.J., J.A. Cohen, G.A. Meehl, J.F.B. Mitchell, A.H. Oort, R.J. Stouffer, R.T. Weatherald, 1994: An example of fingerprint detection of greenhouse climate change. *Clim. Dyn.*, **10**, 97-105.
- Kattenberg**, A., F. Giorgi, H. Grassl, G.A. Meehl, J.F.B. Mitchell, R. Stouffer, T. Tokioka, A.J. Weaver and T.M.L. Wigley, 1996: Climate Models - Projections of Future Climate. Houghton *et al.* (eds.), The IPCC Second Scientific Assessment. Cambridge University Press, Cambridge, 285-357.
- Kaufmann**, R.K. and D.I. Stern, 1997: Evidence for human influence on climate from hemispheric temperature relations. *Nature*, **388**, 39-44.
- Kelly**, P.M., P.D. Jones, J. Pengqun, 1996: The spatial response of the climate system to explosive volcanic eruptions. *Int. J. Climatol.* **16**, 537-550.
- Kim**, K.-Y. and Q. Wu, 2000: Optimal detection using cyclostationary EOFs. *J. Climate*, **13**, 938-950.
- Kim**, K.-Y., G.R. North, S.S. Shen, 1996: Optimal estimation of spherical harmonic components from a sample of spatially nonuniform covariance statistics. *J. Climate*, **9**, 635-645.
- Kirchner**, I., G.L. Stenchikov, H.-F.Graf, A.Robock and J.C.Antuna, 1999: Climate model simulation of winter warming and summer cooling following the 1991 Mount Pinatubo volcanic eruption. *J. Geophys. Res.*, **104**, 19,039-19,055.
- Knutson**, T.R., T.L. Delworth, K. Dixon and R.J. Stouffer, 2000: Model

- assessment of regional surface temperature trends (1949-97), *J. Geophys. Res.*, **104**, 30981-30996.
- Labitzke**, K. and H.van Loon, 1997: The signal of the 11-year sunspot cycle in the upper troposphere-lower stratosphere. *Space Sci. Rev.*, **80**, 393-410.
- Lamb**, H. H., 1970: Volcanic dust in the atmosphere; with a chronology and assessment of its meteorological significance, *Philosophical transactions of the Royal Society of Londen*, A 266, 425-533
- Laut**, P. and J. Gunderman, 1998: Does the correlation between the solar cycle and hemispheric land temperature rule out any significant global warming from greenhouse gases? *J. Atmos. Terrest. Phys.*, **60**, 1-3.
- Lean**, J., 1997: The Sun's Variable Raditation and its relevance for earth. *Annu. Rev. Astrophys.* **35**, 33-67
- Lean**, J., J.Beer and R.Bradley, 1995: Reconstruction of solar irradiance since 1600: Implications For climate change. *Geophys. Res. Lett.*, **22**, 3195-3198.
- Lean**, J., D. Rind, 1998: Climate Forcing by Changing Solar Radiation. *J. Climate*, **11**, 3069-3094.
- Legates**, D. R. and R. E. Davis, 1997 The continuing search for an anthropogenic climate change signal: limitations of correlation based approaches. *Geophys. Res. Lett.*, **24**, 2319-2322
- Leroy**, S., 1998: Detecting Climate Signals: Some Bayesian Aspects. *J. Climate* **11**, 640-651.
- Levine**, R.A. and L.M. Berliner, 1999: Statistical principles for climate change studies. *J. Climate*, **12**, 564-574.
- Lockwood**, M. and R. Stamper 1999: Long-term drift of the coronal source magnetic flux and the total solar irradiance, *Geophys. Res. Lett.*, **26**, 2461-2464
- Mann**, M.E., R.S. Bradley, M.K. Hughes, 1998: Global scale tmperature patterns and climate forcing over the past six centuries. *Nature*, **392**, 779-787.
- Mann**, M.E., E. Gille, R.S. Bradley, M.K. Hughes, J.T. Overpeck, F.T. Keimig and W. Gross, 2000b: Global temperature patterns in past centuries: An interactive presentation. *Earth Interactions*, **4/4**, 1-29.
- Mao**, J. and A. Robock, 1998: Surface air temperature simulations by AMIP general circulation models: Volcanic and ENSO signals and systematic errors. *J. Climate*, **11**, 1538-1552.
- Michaels**, P.J. and P.C. Knappenburger, 1996: Human effect on global climate? *Nature*, **384**, 523-524.
- Mitchell**, J.F.B. and T.C. Johns, 1997: On the modification of greenhouse warming by sulphate aerosols. *J. Climate*, **10**, 245-267
- Mitchell**, J.F.B., R.A. Davis, W.J. Ingram and C.A. Senior, 1995a: On surface temperature, greenhouse Gases and aerosols, models and observations. *J. Climate*, **10**, 2364-3286.
- Mitchell**, J.F.B., T.J. Johns, J.M. Gregory and S.F.B. Tett, 1995b: Transient climate response to Increasing sulphate aerosols and greenhouse gases. *Nature*, **376**, 501-504.
- National Academy of Sciences**, 2000; Reconciling observations of global temperature change. 85pp. Nat. Acad. Press, Washington, DC.
- North**, G.R. and M. Stevens,1998: Detecting Climate Signals in the Surface Temperature Record. *J. Climate*, **11**,: 563-577.
- North**, G.R. and Q. Wu, 2001: Detecting Climate Signals Using Space Time EOFs. *J. Climate*, **14**, 1839-1863.
- North**, G.R., K-Y Kim, S. Shen and J.W. Hardin 1995: Detection of Forced Climate Signals, Part I: Filter Theory. *J. Climate*, **8**, 401-408.
- Osborn**, T.J., K.R. Briffa, S.F.B. Tett, P.D. Jones and R.M. Trigo, 1999: Evaluation of the North Atlantic Oscillation as simulated by a coupled climate model. *Clim. Dyn.* **15**, 685-702.
- Overpeck**, J., K. Hughen, D. Hardy, R. Bradley, R. Case, M. Douglas, B. Finney, K. Gajewski, G. Jacoby, A. Jennings, S. Lamoureux, A. Lasca, G. MacDonald, J. Moore, M. Retelle, S. Smith, A. Wolfe, G. Zielinski, 1997: Arctic Environmental Change of the Last Four Centuries. *Science*, **278**, 1251-1256.
- Paeth**, H. and H. Hense, 2001: Signal Analysis of the northern hemisphere atmospheric mean temperature 500/1000 hPa north of 55N between 1949 and 1994. *Clim. Dyn.*, in press.
- Paeth**, H., A. Hense, R. Glowenka-Hense, R.Voss and U.Cubasch, 1999: The North Atlantic Oscillation as an indicator for greenhouse gas induced climate change. *Clim. Dyn.*, **15**, 953-960.
- Parker**, D.E., M.Gordon, D.P.M.Cullum, D.M.H.Sexton, C.K.Folland and N.Rayner 1997: A new global gridded radiosonde temperature data base and recent temperature trends. *Geophys. Res. Lett.*, **24**, 1499-1502.
- Parkinson**, C. L., D. J. Cavalieri, P. Gloersen, H. J. Zwally and J. C.Comiso, 1999: Arctic sea ice extents, areas and trends, 1978-1996, *J. Geophys. Res.*, **104**, 20,837-20,856.
- Priestley**, M. B., "Spectral Analysis and Time-series", Volume 1, Academic Press, 1981.
- Reader**, M.C. and G.J. Boer, 1998: The modification of greenhouse gas warming by the direct effect of sulphate aerosols. *Clim. Dyn.*, **14**, 593-607.
- Rind**, D., J. Lean and R. Healy, 1999: Simulated time-depended climate response to solar radiative forcing since 1600. *J. Geophys. Res.* **104**: 1973-1990.
- Ripley**, B.D. and M. Thompson, 1987: Regression techniques for the detection of analytical bias. *Analyst*, **112**, 377-383.
- Risbey**, J., M. Kandlikar and D. Karoly, 2000: A framework to articulate and quantify uncertainty in climate change detection and attribution. *Clim. Res.*, **16**, 61-78.
- Robock**, A. and J. Mao 1992: Winter warming from large volcanic eruptions. *Geophys. Res. Lett.* **19**, 2405-2408.
- Robock**, A. and M. Free,1995: Ice cores as an index of global volcanism from 1850 to the present, *J. Geophys. Res.*, **100**, 11567-11576.
- Robock**, A. and M. Jianping, 1995: The volcanic signal in surface temperature observations. *J. Climate*, **8**, 1086-1103.
- Roeckner**, E., L. Bengtsson, J. Feichter, J. Lelieveld and H. Rodhe, 1999: Transient climate change simulations with a coupled atmosphere-ocean GCM including the tropospheric sulfur cycle. *J. Climate*, **12**, 3004-3032.
- Santer**, B.D., T.M.L. Wigley and P.D. Jones, 1993:Correlation methods in fingerprint detection studies. *Clim Dyn.*, **8**, 265-276.
- Santer**, B.D., K.E. Taylor, J.E. Penner, T.M.L. Wigley, U. Cubasch and P.D. Jones, 1995: Towards the detection and attribution of an anthropogenic effect on climate. *Clim. Dyn.*, **12**, 77-100.
- Santer**, B.D., K.E. Taylor, T.M.L. Wigley, P.D. Jones, D.J. Karoly, J.F.B. Mitchell, A.H. Oort, J.E.Penner, V. Ramaswamy, M.D. Schwarzkopf, R.S. Stouffer and S.F.B. Tett, 1996a: A search for human influences on the thermal structure in the atmosphere. *Nature*, **382**, 39-46.
- Santer**, B.D., K.E. Taylor, T.M.L. Wigley, T.C. Johns, P.D. Jones, D.J. Karoly, J.F.B. Mitchell, A.H. Oort, J.E. Penner, V. Ramaswamy, M.D. Schwartzkopf, R.J. Stouffer and S.F.B. Tett, 1996b: Human effect on global climate? *Nature*, **384**, 522-524.
- Santer**, B.D., T.M.L. Wigley, T.P. Barnett, E. Anyamba, 1996c: Detection of climate change and attribution of causes. in: J. T. Houghton *et al.* (eds.) Climate change 1995. The IPCC Second Scientific Assessment, Cambridge University Press, Cambridge, pp. 407-444.
- Santer**, B.D., T.M.L. Wigley, D.J. Gaffen, C. Doutriaux, J.S. Boyle, M. Esch, J.J. Hnilo, P.D. Jones, G.A. Meehl, E. Roeckner, K.E. Taylor and M.F. Wehner 2000: Interpreting Differential Temperature Trends at the Surface and in the lower Troposphere, *Science*, **287**, 1227-1231.
- Sato**, M., J.E. Hansen, M.P. McCormick and J. Pollack, 1993: Statospheric aerosol optical depths (1850-1990). *J. Geophys. Res.* **98**, 22987-22994
- Schönwiese**, C.-D., M. Denhard, J. Grieser and A. Walter, 1997: Assessments of the global anthropogenic greenhouse and sulphate signal using different types of simplified climate models. *Theor. Appl. Climatol.*, **57**, 119-124.
- Schneider** T and I. Held, 2001: Discriminants of twentieth-century changes in Earth surface temperatures. *J. Climate*, **14**, 249-254.

- Schnur**, R., 2001: Detection of climate change using advanced climate diagnostics: seasonal and diurnal cycle. Max-Planck-Institut fuer Meteorologie, Report No. 312, Bundesstr. 55, 20146 Hamburg, Germany.
- Sexton**, D.M.H., D.P. Rowell, C.K. Folland and D.J. Karoly, 2001: Detection of anthropogenic climate change using an atmospheric GCM. *Clim. Dyn.*, in press.
- Shindell**, D. T., R.L. Miller, G. Schmidt and L. Pandolfo, 1999: Simulation of recent northern winter climate trends by greenhouse-gas forcing. *Nature*, **399**, 452-455.
- Shindell**, D. T., G.Schmidt, R.L. Miller and D. Rind, 2001: Northern Hemispheric climate response to greenhouse gas, ozone, solar and volcanic forcing. *J. Geophys. Res. (Atmospheres)*, in press.
- Simkin**, T., L.Siebert, L.McClelland, D.Bridge, C.G.Newhall and J.H. Latter, 1981: Volcanoes of the World, 232 pp. Van Nostrand Reinhold, New York, 1981
- Smith**, R.L., T.M.L. Wigley and B.D. Santer, 2001: A bivariate time-series approach to anthropogenic trend detection in hemispheric mean temperatures. *J. Climate*, in press.
- Stephenson**, D.B., 1997: Correlation of spatial climate/weather maps and the advantages of using the Mahalonbis metric in predictions. *Tellus*, **49A**, 513-527.
- Stevens**, M.J. and G.R. North, 1996: Detection of the climate response to the solar cycle. *J. Atmos. Sci.*, **53**, 2594-2608.
- Stothers**, R.B., 1996: Major optical depth perturbations to the stratosphere from volcanic eruptions: Pyrheliometric period 1881-1960. *J.Geophys. Res.*, **101**, 3901-3920.
- Stott**, P. A. and S.F.B. Tett, 1998: Scale-dependent detection of climate change. *J. Climate*, **11**: 3282-3294.
- Stott**, P.A., M.R. Allen and G.S. Jones, 2000a: Estimating signal amplitudes in optimal fingerprinting II: Application to general circulation models. Hadley Centre Tech Note 20, Hadley Centre for Climate Prediction and Response, Meteorological Office, RG12 2SY UK.
- Stott**, P.A., S.F.B. Tett, G.S. Jones, M.R. Allen, J.F.B.Mitchell and G.J. Jenkins, 2000b: External control of twentieth century temperature variations by natural and anthropogenic forcings. *Science*, **15**, 2133-2137.
- Stott**, P.A., S.F.B. Tett, G.S. Jones, M.R. Allen, W.J. Ingram and J.F.B. Mitchell, 2001: Attribution of Twentieth Century Temperature Change to Natural and Anthropogenic Causes. *Clim. Dyn.* **17**, 1-22.
- Stouffer**, R.J., G.C. Hegerl and S.F.B. Tett, 1999: A comparison of Surface Air Temperature Variability in Three 1000-Year Coupled Ocean-Atmosphere Model Integrations. *J. Climate*, **13**, 513-537.
- Svensmark**, H. and E. Friis-Christensen, 1997: Variations of cosmic ray flux and global cloud coverage – a missing link in solar-climate relationships. *J. Atmos. Solar-Terrestrial Phys.*, **59**, 1226-1232.
- Svensmark**, H., 1998: Influence of cosmic rays on Earth's climate. *Phys. Rev. Lett.*, **81**, 5027-5030.
- Tett**, S.F.B., J.F.B. Mitchell, D.E. Parker and M.R. Allen, 1996: Human Influence on the Atmospheric Vertical Temperature Structure: Detection and Observations. *Science*, **274**, 1170-1173.
- Tett**, S.F.B., P.A. Stott, M.A. Allen, W.J. Ingram and J.F.B. Mitchell, 1999: Causes of twentieth century temperature change. *Nature*, **399**, 569-572.
- Tett**, S.F.B., G.S. Jones, P.A. Stott, D.C. Hill, J.F.B. Mitchell, M.R. Allen, W.J. Ingram, T.C. Johns, C.E. Johnson, A. Jones, D.L. Roberts, D.M.H. Sexton and M.J. Woodage, 2000: Estimation of natural and anthropogenic contributions to 20th century. Hadley Centre Tech Note 19, Hadley Centre for Climate Prediction and Response, Meteorological Office, RG12 2SY, UK pp52.
- Thejll**, P. and K. Lassen, 2000: Solar forcing of the Northern Hemisphere land air temperature: New data. *J. Atmos. Solar-Terrestrial Phys.*, **62**, 1207-1213.
- Thompson**, D.W.J. and J.M. Wallace, 1998: The Arctic oscillation signature in the wintertime geopotential height and temperature fields. *Geophys. Res. Lett.*, **25**, 1297-1300.
- Thompson**, D.W.J., J.M. Wallace and G.C. Hegerl 2000: Annular Modes in the Extratropical Circulation. Part II Trends. *J. Climate*, **13**, 1018-1036 .
- Tol**, R.S.J. and P. Vellinga, 1998: 'Climate Change, the Enhanced Greenhouse Effect and the Influence of the Sun: A Statistical Analysis', *Theoretical and Applied Climatology*, **61**, 1-7.
- Tol**, R.S.J. and A.F. de Vos, 1998: A Bayesian statistical analysis of the enhanced greenhouse effect. *Clim. Change*, **38**, 87-112.
- van Loon**, H. and D. J. Shea, 1999: A probable signal of the 11-year solar cycle in the troposphere of the Northern Hemisphere, *Geophys. Res. Lett.*, **26**, 2893-2896.
- van Loon**, H. and D. J. Shea, 2000: The global 11-year solar signal in July-August. *J. Geophys. Res.*, **27**, 2965-2968.
- Vinnikov**, K. Y., A.Robock, R. J.Stouffer, J.E.Walsh, C. L. Parkinson, D.J.Cavalieri, J.F.B Mitchell, D.Garrett and V.F. Zakharov, 1999: Global warming and Northern Hemisphere sea ice extent. *Science*, **286**, 1934-1937.
- Volodin**, E.M. and V.Y. Galin, 1999: Interpretation of winter warming on Northern Hemisphere continents 1977-94. *J. Climate*, **12**, 2947-2955.
- Walter**, A., M. Denhard, C.-D. Schoenwiese, 1998: Simulation of global and hemispheric temperature variation and signal detection studies using neural networks. *Meteor. Zeitschrift*, N.F. **7**, 171-180.
- Weber**, G.R., 1996: Human effect on global climate? *Nature*, **384**, 524-525.
- White**, W.B., J. Lean, D.R. Cayan and M.D. Dettinger, 1997: A response of global upper ocean temperature to changing solar irradiance. *J. Geophys. Res.*, **102**, 3255-3266.
- Wigley**, T.M.L., P.D. Jones and S.C.B. Raper, 1997: The observed global warming record: What does it tell us? *Proc. Natl. Acad. Sci. USA*, **94**, 8314-8320.
- Wigley**, T.M.L., R.L. Smith and B.D. Santer, 1998a: Anthropogenic influence on the autocorrelation structure of hemispheric-mean temperatures. *Science*, **282**, 1676-1679.
- Wigley**, T.M.L., P.J. Jaumann, B.D. Santer and K.E Taylor, 1998b: Relative detectability of greenhouse gas and aerosol climate change signals *Clim Dyn*, **14**, 781-790.
- Wigley**, T.M.L., B.D.Santer and K.E.Taylor, 2000: Correlation approaches to detection. *Geophys. Res. Lett.* **27**, 2973-2976.
- WMO**, 1999: Scientific assessment of ozone depletion : 1998, Global Ozone Research and Monitoring Project, World Meteorological Organisation, Report No. 44, Geneva.
- Wong**, A.P.S., N.L. Bindoff and J.A. Church, 1999: Large-scale freshening of intermediate water masses in the Pacific and Indian Oceans. *Nature*, **400**, 440-443.
- Zheng**, X. and R.E. Basher, 1999: Structural time-series models and trend detection in global and regional temperature series. *J. Climate*, **12**, 2347-2358.
- Zwiers**, F.W., 1999: The detection of climate change. In "Anthropogenic Climate Change", H. von Storch and G. Floeser, eds., Springer-Verlag, 161-206.
- Zwiers**, F.W. and S.S. Shen, 1997: Errors in estimating spherical harmonic coefficients from partially sampled GCM output. *Clim. Dyn.*, **13**, 703-716.

13

Climate Scenario Development

Co-ordinating Lead Authors

L.O. Mearns, M. Hulme

Lead Authors

T.R. Carter, R. Leemans, M. Lal, P. Whetton

Contributing Authors

L. Hay, R.N. Jones, R. Katz, T. Kittel, J. Smith, R. Wilby

Review Editors

L.J. Mata, J. Zillman

Contents

Executive Summary	741		
13.1 Introduction	743	13.4.1.3 Applications of the methods to impacts	752
13.1.1 Definition and Nature of Scenarios	743	13.4.2 Temporal Variability	752
13.1.2 Climate Scenario Needs of the Impacts Community	744	13.4.2.1 Incorporation of changes in variability: daily to interannual time-scales	752
13.4.2.2 Other techniques for incorporating extremes into climate scenarios	754		
13.2 Types of Scenarios of Future Climate	745	13.5 Representing Uncertainty in Climate Scenarios	755
13.2.1 Incremental Scenarios for Sensitivity Studies	746	13.5.1 Key Uncertainties in Climate Scenarios	755
13.2.2 Analogue Scenarios	748	13.5.1.1 Specifying alternative emissions futures	755
13.2.2.1 Spatial analogues	748	13.5.1.2 Uncertainties in converting emissions to concentrations	755
13.2.2.2 Temporal analogues	748	13.5.1.3 Uncertainties in converting concentrations to radiative forcing	755
13.2.3 Scenarios Based on Outputs from Climate Models	748	13.5.1.4 Uncertainties in modelling the climate response to a given forcing	755
13.2.3.1 Scenarios from General Circulation Models	748	13.5.1.5 Uncertainties in converting model response into inputs for impact studies	756
13.2.3.2 Scenarios from simple climate models	749	13.5.2 Approaches for Representing Uncertainties	756
13.2.4 Other Types of Scenarios	749	13.5.2.1 Scaling climate model response patterns	756
		13.5.2.2 Defining climate change signals	757
		13.5.2.3 Risk assessment approaches	759
		13.5.2.4 Annotation of climate scenarios	760
13.3 Defining the Baseline	749	13.6 Consistency of Scenario Components	760
13.3.1 The Choice of Baseline Period	749	References	761
13.3.2 The Adequacy of Baseline Climatological Data	750		
13.3.3 Combining Baseline and Modelled Data	750		
13.4 Scenarios with Enhanced Spatial and Temporal Resolution	751		
13.4.1 Spatial Scale of Scenarios	751		
13.4.1.1 Regional modelling	751		
13.4.1.2 Statistical downscaling	752		

Executive Summary

The Purpose of Climate Scenarios

A climate scenario is a plausible representation of future climate that has been constructed for explicit use in investigating the potential impacts of anthropogenic climate change. Climate scenarios often make use of climate projections (descriptions of the modelled response of the climate system to scenarios of greenhouse gas and aerosol concentrations), by manipulating model outputs and combining them with observed climate data.

This new chapter for the IPCC assesses the methods used to develop climate scenarios. Impact assessments have a very wide range of scenario requirements, ranging from global mean estimates of temperature and sea level, through continental-scale descriptions of changes in mean monthly climate, to point or catchment-level detail about future changes in daily or even sub-daily climate.

The science of climate scenario development acts as an important bridge from the climate science of Working Group I to the science of impact, adaptation and vulnerability assessment, considered by Working Group II. It also has a close dependence on emissions scenarios, which are discussed by Working Group III.

Methods for Constructing Scenarios

Useful information about possible future climates and their impacts has been obtained using various scenario construction methods. These include climate model based approaches, temporal and spatial analogues, incremental scenarios for sensitivity studies, and expert judgement. This chapter identifies advantages and disadvantages of these different methods (see Table 13.1).

All these methods can continue to serve a useful role in the provision of scenarios for impact assessment, but it is likely that the major advances in climate scenario construction will be made through the refinement and extension of climate model based approaches.

Each new advance in climate model simulations of future climate has stimulated new techniques for climate scenario construction. There are now numerous techniques available for scenario construction, the majority of which ultimately depend upon results obtained from general circulation model (GCM) experiments.

Representing the Cascade of Uncertainty

Uncertainties will remain inherent in predicting future climate change, even though some uncertainties are likely to be narrowed with time. Consequently, a range of climate scenarios should usually be considered in conducting impact assessments.

There is a cascade of uncertainties in future climate predictions which includes unknown future emissions of greenhouse gases and aerosols, the conversion of emissions to atmospheric concentrations and to radiative forcing of the climate, modelling the response of the climate system to forcing, and methods for regionalising GCM results.

Scenario construction techniques can be usefully contrasted according to the sources of uncertainty that they address and

those that they ignore. These techniques, however, do not always provide consistent results. For example, simple methods based on direct GCM changes often represent model-to-model differences in simulated climate change, but do not address the uncertainty associated with how these changes are expressed at fine spatial scales. With regionalisation approaches, the reverse is often true.

A number of methods have emerged to assist with the quantification and communication of uncertainty in climate scenarios. These include pattern-scaling techniques to interpolate/extrapolate between results of model experiments, climate scenario generators, risk assessment frameworks and the use of expert judgement. The development of new or refined scenario construction techniques that can account for multiple uncertainties merits further investigation.

Representing High Spatial and Temporal Resolution Information

The incorporation of climate changes at high spatial (e.g., tens of kilometres) and temporal (e.g., daily) resolution in climate scenarios currently remains largely within the research domain of climate scenario development. Scenarios containing such high resolution information have not yet been widely used in comprehensive policy relevant impact assessments.

Preliminary evidence suggests that coarse spatial resolution AOGCM (Atmosphere-Ocean General Circulation Model) information for impact studies needs to be used cautiously in regions characterised by pronounced sub-GCM grid scale variability in forcings. The use of suitable regionalisation techniques may be important to enhance the AOGCM results over such regions.

Incorporating higher resolution information in climate scenarios can substantially alter the assessment of impacts. The incorporation of such information in scenarios is likely to become increasingly common and further evaluation of the relevant methods and their added value in impact assessment is warranted.

Representing Extreme Events

Extreme climate/weather events are very important for most climate change impacts. Changes in the occurrence and intensity of extremes should be included in climate scenarios whenever possible.

Some extreme events are easily or implicitly incorporated in climate scenarios using conventional techniques. It is more difficult to produce scenarios of complex events, such as tropical cyclones and ice storms, which may require specialised techniques. This constitutes an important methodological gap in scenario development. The large uncertainty regarding future changes in some extreme events exacerbates the difficulty in incorporating such changes in climate scenarios.

Applying Climate Scenarios in Impact Assessments

There is no single “best” scenario construction method appropriate for all applications. In each case, the appropriate method is determined by the context and the application of the scenario.

The choice of method constrains the sources of uncertainty that can be addressed. Relatively simple techniques, such as those that rely on scaled or unscaled GCM changes, may well be the

most appropriate for applications in integrated assessment modelling or for informing policy; more sophisticated techniques, such as regional climate modelling or conditioned stochastic weather generation, are often necessary for applications involving detailed regional modelling of climate change impacts.

Improving Information Required for Scenario Development

Improvements in global climate modelling will bring a variety of benefits to most climate scenario development

methods. A more diverse set of model experiments, such as AOGCMs run under a broader range of forcings and at higher resolutions, and regional climate models run either in ensemble mode or for longer time periods, will allow a wider range of uncertainty to be represented in climate scenarios. In addition, incorporation of some of the physical, biological and socio-economic feedbacks not currently simulated in global models will improve the consistency of different scenario elements.

13.1 Introduction

13.1.1 Definition and Nature of Scenarios

For the purposes of this report, a climate scenario refers to a plausible future climate that has been constructed for explicit use in investigating the potential consequences of anthropogenic climate change. Such climate scenarios should represent future conditions that account for both human-induced climate change and natural climate variability. We distinguish a climate scenario from a climate projection (discussed in Chapters 9 and 10), which refers to a description of the response of the climate system to a scenario of greenhouse gas and aerosol emissions, as simulated by a climate model. Climate projections alone rarely provide sufficient information to estimate future impacts of climate change; model outputs commonly have to be manipulated and combined with observed climate data to be usable, for example, as inputs to impact models.

To further illustrate this point, Box 13.1 presents a simple example of climate scenario construction based on climate projections. The example also illustrates some other common considerations in performing an impact assessment that touch on issues discussed later in this chapter.

We also distinguish between a climate scenario and a climate change scenario. The latter term is sometimes used in the scientific literature to denote a plausible future climate. However, this term should strictly refer to a representation of the difference between some plausible future climate and the current or control climate (usually as represented in a climate model) (see Box 13.1, Figure 13.1a). A climate change scenario can be viewed as an interim step toward constructing a climate scenario. Usually a climate scenario requires combining the climate change scenario with a description of the current climate as represented by climate observations (Figure 13.1b). In a climate impacts context, it is the contrasting effects of these two climates – one current (the observed “baseline” climate), one

Box 13.1: Example of scenario construction.

Example of basic scenario construction for an impact study: the case of climate change and world food supply (Rosenzweig and Parry, 1994).

Aim of the study

The objective of this study was to estimate how global food supply might be affected by greenhouse gas induced climate change up to the year 2060. The method adopted involved estimating the change in yield of major crop staples under various scenarios using crop models at 112 representative sites distributed across the major agricultural regions of the world. Yield change estimates were assumed to be applicable to large regions to produce estimates of changes in total production which were then input to a global trade model. Using assumptions about future population, economic growth, trading conditions and technological progress, the trade model estimated plausible prices of food commodities on the international market given supply as defined by the production estimates. This information was then used to define the number of people at risk from hunger in developing countries.

Scenario information

Each of the stages of analysis required scenario information to be provided, including:

- scenarios of carbon dioxide (CO_2) concentration, affecting crop growth and water use, as an input to the crop models;
- climate observations and scenarios of future climate, for the crop model simulations;
- adaptation scenarios (e.g., new crop varieties, adjusted farm management) as inputs to the crop models;
- scenarios of regional population and global trading policy as an input to the trade model.

To the extent possible, the scenarios were mutually consistent, such that scenarios of population (United Nations medium range estimate) and Gross Domestic Product (GDP) (moderate growth) were broadly in line with the transient scenario of greenhouse gas emissions (based on the Goddard Institute for Space Studies (GISS) scenario A, see Hansen *et al.*, 1988), and hence CO_2 concentrations. Similarly, the climate scenarios were based on $2\times\text{CO}_2$ equilibrium GCM projections from three models, where the radiative forcing of climate was interpreted as the combined concentrations of CO_2 (555 ppm) and other greenhouse gases (contributing about 15% of the change in forcing) equivalent to a doubling of CO_2 , assumed to occur in about 2060.

Construction of the climate scenario

Since projections of current (and hence future) regional climate from the GCM simulations were not accurate enough to be used directly as an input to the crop model, modelled changes in climate were applied as adjustments to the observed climate at a location. Climate change by 2060 was computed as the difference (air temperature) or ratio (precipitation and solar radiation) of monthly mean climate between the GCM (unforced) control and $2\times\text{CO}_2$ simulations at GCM grid boxes coinciding with the crop modelling sites (Figure 13.1b). These estimates were used to adjust observed time-series of daily climate for the baseline period (usually 1961 to 1990) at each site (Figure 13.1b,c). Crop model simulations were conducted for the baseline climate and for each of the three climate scenarios, with and without CO_2 enrichment (to estimate the relative contributions of CO_2 and climate to crop yield changes), and assuming different levels of adaptation capacity.

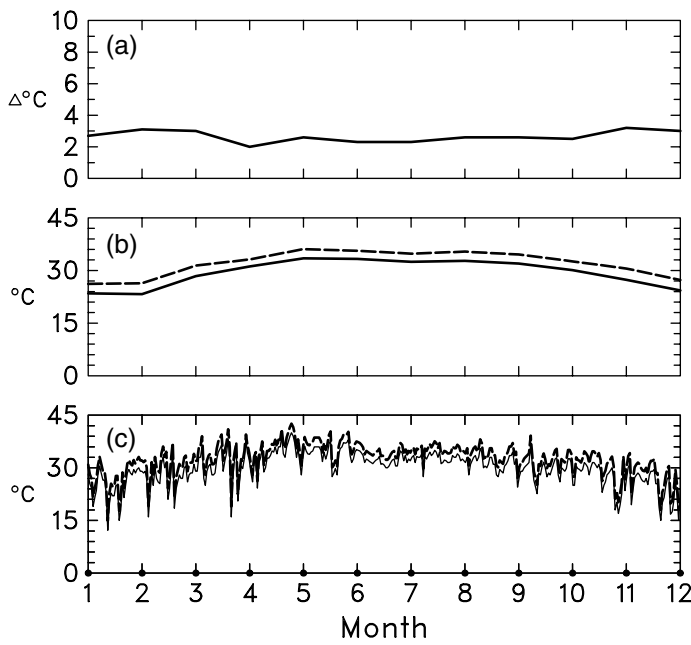


Figure 13.1: Example of the stages in the formation of a simple climate scenario for temperature using Poza Rica (20.3°N , 97.3°W) as a typical site used in the Mexican part of the Rosenzweig and Parry (1994) study.

(a) Mean monthly differences (Δ) ($2\times\text{CO}_2$ minus control) of average temperature ($^{\circ}\text{C}$) as calculated from the control and $2\times\text{CO}_2$ runs of the Geophysical Fluid Dynamics Laboratory (GFDL) GCM (Manabe and Wetherald, 1987) for the model grid box that includes the geographic location of Poza Rica. The climate model spatial resolution is 4.4° latitude by 7.5° longitude.

(b) The average 17-year (1973 to 1989) observed mean monthly maximum temperature for Poza Rica (solid line) and the $2\times\text{CO}_2$ mean monthly maximum temperature produced by adding the differences portrayed in (a) to this baseline (dashed line). The crop models, however, require daily climate data for input.

(c) A sample of one year's (1975) observed daily maximum temperature data (solid line) and the $2\times\text{CO}_2$ daily values created by adding the monthly differences in a) to the daily data (dashed line). Thus, the dashed line is the actual daily maximum temperature time-series describing future climate that was used as one of the weather inputs to the crop models for this study and for this location (see Liverman *et al.*, 1994 for further details).

future (the climate scenario) – on the exposure unit¹ that determines the impact of the climate change (Figure 13.1c).

A treatment of climate scenario development, in this specific sense, has been largely absent in the earlier IPCC Assessment Reports. The subject has been presented in independent IPCC Technical Guidelines documents (IPCC, 1992, 1994), which were briefly summarised in the Second Assessment Report of Working Group II (Carter *et al.*, 1996b). These documents, while serving a useful purpose in providing guidelines for scenario use,

did not fully address the science of climate scenario development. This may be, in part, because the field has been slow to develop and because only recently has a critical mass of important research issues coalesced and matured such that a full chapter is now warranted.

The chapter also serves as a bridge between this Report of Working Group I and the IPCC Third Assessment Report of Working Group II (IPCC, 2001) (hereafter TAR WG II) of climate change impacts, adaptation and vulnerability. As such it also embodies the maturation in the IPCC assessment process – that is, a recognition of the interconnections among the different segments of the assessment process and a desire to further integrate these segments. Chapter 3 performs a similar role in the TAR WG II (Carter and La Rovere, 2001) also discussing climate scenarios, but treating, in addition, all other scenarios (socio-economic, land use, environmental, etc.) needed for undertaking policy-relevant impact assessment. Chapter 3 serves in part as the other half of the bridge between the two Working Group Reports.

Scenarios are neither predictions nor forecasts of future conditions. Rather they describe alternative plausible futures that conform to sets of circumstances or constraints within which they occur (Hammond, 1996). The true purpose of scenarios is to illuminate uncertainty, as they help in determining the possible ramifications of an issue (in this case, climate change) along one or more plausible (but indeterminate) paths (Fisher, 1996).

Not all possible imaginable futures can be considered viable scenarios of future climate. For example, most climate scenarios include the characteristic of increased lower tropospheric temperature (except in some isolated regions and physical circumstances), since most climatologists have very high confidence in that characteristic (Schneider *et al.*, 1990; Mahlman, 1997). Given our present state of knowledge, a scenario that portrayed global tropospheric cooling for the 21st century would not be viable. We shall see in this chapter that what constitutes a viable scenario of future climate has evolved along with our understanding of the climate system and how this understanding might develop in the future.

It is worth noting that the development of climate scenarios predates the issue of global warming. In the mid-1970s, for example, when a concern emerged regarding global cooling due to the possible effect of aircraft on the stratosphere, simple incremental scenarios of climate change were formulated to evaluate what the possible effects might be worldwide (CIAP, 1975).

The purpose of this chapter is to assess the current state of climate scenario development. It discusses research issues that are addressed by researchers who develop climate scenarios and that must be considered by impacts researchers when they select scenarios for use in impact assessments. This chapter is not concerned, however, with presenting a comprehensive set of climate scenarios for the IPCC Third Assessment Report.

13.1.2 Climate Scenario Needs of the Impacts Community

The specific climate scenario needs of the impacts community vary, depending on the geographic region considered, the type of impact, and the purpose of the study. For example, distinctions

¹ An exposure unit is an activity, group, region or resource exposed to significant climatic variations (IPCC, 1994).

can be made between scenario needs for research in climate scenario development and in the methods of conducting impact assessment (e.g., Woo, 1992; Mearns *et al.*, 1997) and scenario needs for direct application in policy relevant impact and integrated assessments (e.g., Carter *et al.*, 1996a; Smith *et al.*, 1996; Hulme and Jenkins, 1998).

The types of climate variables needed for quantitative impacts studies vary widely (e.g., White, 1985). However, six “cardinal” variables can be identified as the most commonly requested: maximum and minimum temperature, precipitation, incident solar radiation, relative humidity, and wind speed. Nevertheless, this list is far from exhaustive. Other climate or climate-related variables of importance may include CO₂ concentration, sea-ice extent, mean sea level pressure, sea level, and storm surge frequencies. A central issue regarding any climate variable of importance for impact assessment is determining at what spatial and temporal scales the variable in question can sensibly be provided, in comparison to the scales most desired by the impacts community. From an impacts perspective, it is usually desirable to have a fair amount of regional detail of future climate and to have a sense of how climate variability (from short to long time-scales) may change. But the need for this sort of detail is very much a function of the scale and purpose of the particular impact assessment. Moreover, the availability of the output from climate models and the advisability of using climate model results at particular scales, from the point of view of the climate modellers, ultimately determines what scales can and should be used.

Scenarios should also provide adequate quantitative measures of uncertainty. The sources of uncertainty are many, including the

trajectory of greenhouse gas emissions in the future, their conversion into atmospheric concentrations, the range of responses of various climate models to a given radiative forcing and the method of constructing high resolution information from global climate model outputs (Pittock, 1995; see Figure 13.2). For many purposes, simply defining a single climate future is insufficient and unsatisfactory. Multiple climate scenarios that address at least one, or preferably several sources of uncertainty allow these uncertainties to be quantified and explicitly accounted for in impact assessments. Moreover, a further important requirement for impact assessments is to ensure consistency is achieved among various scenario components, such as between climate change, sea level rise and the concentration of actual (as opposed to equivalent) CO₂ implied by a particular emissions scenario.

As mentioned above, climate scenarios that are developed for impacts applications usually require that some estimate of climate change be combined with baseline observational climate data, and the demand for more complete and sophisticated observational data sets of climate has grown in recent years. The important considerations for the baseline include the time period adopted as well as the spatial and temporal resolution of the baseline data.

Much of this chapter is devoted to assessing how and how successfully these needs and requirements are currently met.

13.2 Types of Scenarios of Future Climate

Four types of climate scenario that have been applied in impact assessments are introduced in this section. The most common scenario type is based on outputs from climate models and receives most attention in this chapter. The other three types have usually been applied with reference to or in conjunction with model-based scenarios, namely: incremental scenarios for sensitivity studies, analogue scenarios, and a general category of “other scenarios”. The origins of these scenarios and their mutual linkages are depicted in Figure 13.3.

The suitability of each type of scenario for use in policy-relevant impact assessment can be assessed according to five criteria adapted from Smith and Hulme (1998):

1. *Consistency* at regional level with global projections. Scenario changes in regional climate may lie outside the range of global mean changes but should be consistent with theory and model-based results.
2. *Physical plausibility and realism*. Changes in climate should be physically plausible, such that changes in different climatic variables are mutually consistent and credible.
3. *Appropriateness* of information for impact assessments. Scenarios should present climate changes at an appropriate temporal and spatial scale, for a sufficient number of variables, and over an adequate time horizon to allow for impact assessments.
4. *Representativeness* of the potential range of future regional climate change.
5. *Accessibility*. The information required for developing climate scenarios should be readily available and easily accessible for use in impact assessments.

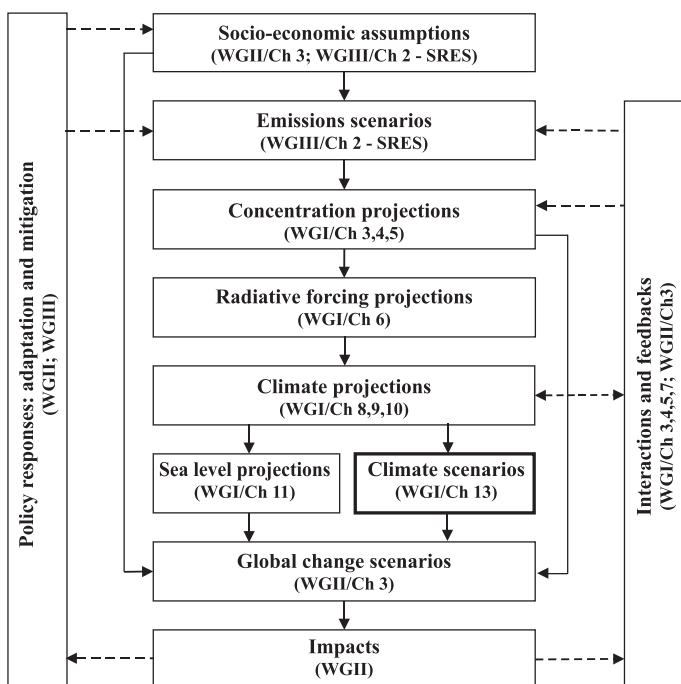


Figure 13.2: The cascade of uncertainties in projections to be considered in developing climate and related scenarios for climate change impact, adaptation and mitigation assessment.

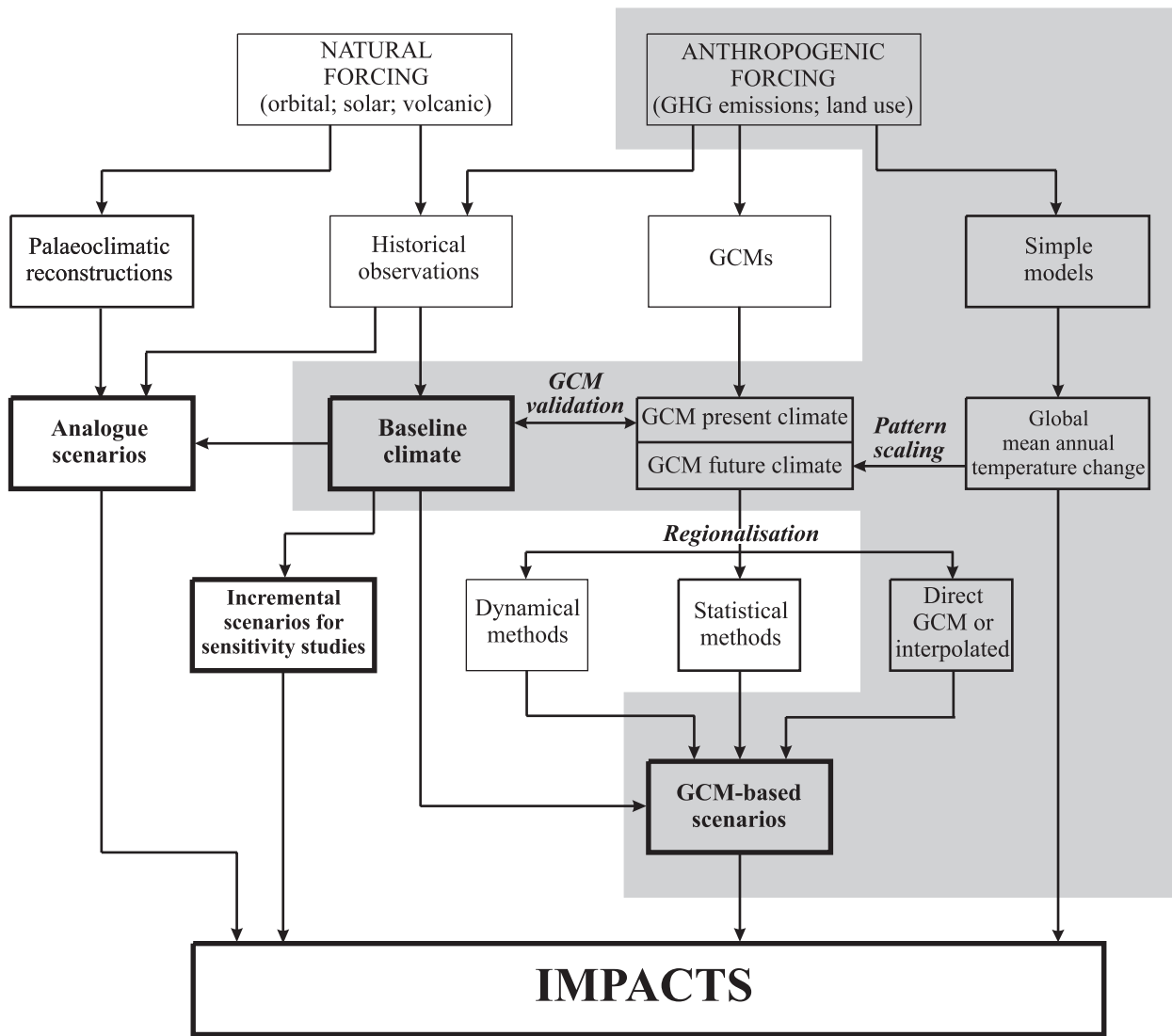


Figure 13.3: Some alternative data sources and procedures for constructing climate scenarios for use in impact assessment. Highlighted boxes indicate the baseline climate and common types of scenario (see text for details). Grey shading encloses the typical components of climate scenario generators.

A summary of the major advantages and disadvantages of different scenario development methods, based on these criteria, is presented in Table 13.1. The relative significance of the advantages and disadvantages is highly application dependent.

13.2.1 Incremental Scenarios for Sensitivity Studies

Incremental scenarios describe techniques where particular climatic (or related) elements are changed incrementally by plausible though arbitrary amounts (e.g., +1, +2, +3, +4°C change in temperature). Also referred to as synthetic scenarios (IPCC, 1994), they are commonly applied to study the sensitivity of an exposure unit to a wide range of variations in climate, often according to a qualitative interpretation of projections of future regional climate from climate model simulations (“guided sensitivity analysis”, see IPCC-TGCIA, 1999). Incremental scenarios facilitate the construction of response surfaces – graphical devices for plotting changes in climate against some

measure of impact (for example see Figure 13.9b) which can assist in identifying critical thresholds or discontinuities of response to a changing climate. Other types of scenarios (e.g., based on model outputs) can be superimposed on a response surface and the significance of their impacts readily evaluated (e.g., Fowler, 1999). Most studies have adopted incremental scenarios of constant changes throughout the year (e.g., Terjung *et al.*, 1984; Rosenzweig *et al.*, 1996), but some have introduced seasonal and spatial variations in the changes (e.g., Whetton *et al.*, 1993; Rosenthal *et al.*, 1995) and others have examined arbitrary changes in interannual, within-month and diurnal variability as well as changes in the mean (e.g., Williams *et al.*, 1988; Mearns *et al.*, 1992; Semenov and Porter, 1995; Mearns *et al.*, 1996).

Incremental scenarios provide information on an ordered range of climate changes and can readily be applied in a consistent and replicable way in different studies and regions, allowing for direct intercomparison of results. However, such scenarios do

Table 13.1: The role of various types of climate scenarios and an evaluation of their advantages and disadvantages according to the five criteria described in the text. Note that in some applications a combination of methods may be used (e.g., regional modelling and a weather generator).

Scenario type or tool	Description/Use	Advantages ^a	Disadvantages ^a
Incremental	<ul style="list-style-type: none"> • Testing system sensitivity • Identifying key climate thresholds 	<ul style="list-style-type: none"> • Easy to design and apply (5) • Allows impact response surfaces to be created (3) 	<ul style="list-style-type: none"> • Potential for creating unrealistic scenarios (1, 2) • Not directly related to greenhouse gas forcing (1)
Analogue: Palaeoclimatic	• Characterising warmer periods in past	<ul style="list-style-type: none"> • A physically plausible changed climate that really did occur in the past of a magnitude similar to that predicted for ~2100 (2) 	<ul style="list-style-type: none"> • Variables may be poorly resolved in space and time (3, 5) • Not related to greenhouse gas forcing (1)
	• Exploring vulnerabilities and some adaptive capacities	<ul style="list-style-type: none"> • Physically realistic changes (2) • Can contain a rich mixture of well-resolved, internally consistent, variables (3) • Data readily available (5) 	<ul style="list-style-type: none"> • Not necessarily related to greenhouse gas forcing (1) • Magnitude of the climate change usually quite small (1) • No appropriate analogues may be available (5)
	<ul style="list-style-type: none"> • Extrapolating climate/ecosystem relationships • Pedagogic 	<ul style="list-style-type: none"> • May contain a rich mixture of well-resolved variables (3) 	<ul style="list-style-type: none"> • Not related to greenhouse gas forcing (1, 4) • Often physically implausible (2) • No appropriate analogues may be available (5)
Climate model based: Direct AOGCM outputs	<ul style="list-style-type: none"> • Starting point for most climate scenarios • Large-scale response to anthropogenic forcing 	<ul style="list-style-type: none"> • Information derived from the most comprehensive, physically-based models (1, 2) • Long integrations (1) • Data readily available (5) • Many variables (potentially) available (3) 	<ul style="list-style-type: none"> • Spatial information is poorly resolved (3) • Daily characteristics may be unrealistic except for very large regions (3) • Computationally expensive to derive multiple scenarios (4, 5) • Large control run biases may be a concern for use in certain regions (2)
	• Providing high resolution information at global/continental scales	<ul style="list-style-type: none"> • Provides highly resolved information (3) • Information is derived from physically-based models (2) • Many variables available (3) • Globally consistent and allows for feedbacks (1,2) 	<ul style="list-style-type: none"> • Computationally expensive to derive multiple scenarios (4, 5) • Problems in maintaining viable parametrizations across scales (1,2) • High resolution is dependent on SSTs and sea ice margins from driving model (AOGCM) (2) • Dependent on (usually biased) inputs from driving AOGCM (2)
	• Providing high spatial/temporal resolution information	<ul style="list-style-type: none"> • Provides very highly resolved information (spatial and temporal) (3) • Information is derived from physically-based models (2) • Many variables available (3) • Better representation of some weather extremes than in GCMs (2, 4) 	<ul style="list-style-type: none"> • Computationally expensive, and thus few multiple scenarios (4, 5) • Lack of two-way nesting may raise concern regarding completeness (2) • Dependent on (usually biased) inputs from driving AOGCM (2)
	• Providing point/high spatial resolution information	<ul style="list-style-type: none"> • Can generate information on high resolution grids, or non-uniform regions (3) • Potential, for some techniques, to address a diverse range of variables (3) • Variables are (probably) internally consistent (2) • Computationally (relatively) inexpensive (5) • Suitable for locations with limited computational resources (5) • Rapid application to multiple GCMs (4) 	<ul style="list-style-type: none"> • Assumes constancy of empirical relationships in the future (1, 2) • Demands access to daily observational surface and/or upper air data that spans range of variability (5) • Not many variables produced for some techniques (3, 5) • Dependent on (usually biased) inputs from driving AOGCM (2)
	<ul style="list-style-type: none"> • Integrated assessments • Exploring uncertainties • Pedagogic 	<ul style="list-style-type: none"> • May allow for sequential quantification of uncertainty (4) • Provides ‘integrated’ scenarios (1) • Multiple scenarios easy to derive (4) 	<ul style="list-style-type: none"> • Usually rely on linear pattern scaling methods (1) • Poor representation of temporal variability (3) • Low spatial resolution (3)
Weather generators	<ul style="list-style-type: none"> • Generating baseline climate time-series • Altering higher order moments of climate • Statistical downscaling 	<ul style="list-style-type: none"> • Generates long sequences of daily or sub-daily climate (2, 3) • Variables are usually internally consistent (2) • Can incorporate altered frequency/intensity of ENSO events (3) 	<ul style="list-style-type: none"> • Poor representation of low frequency climate variability (2, 4) • Limited representation of extremes (2, 3, 4) • Requires access to long observational weather series (5) • In the absence of conditioning, assumes constant statistical characteristics (1, 2)
Expert judgment	<ul style="list-style-type: none"> • Exploring probability and risk • Integrating current thinking on changes in climate 	<ul style="list-style-type: none"> • May allow for a ‘consensus’ (4) • Has the potential to integrate a very broad range of relevant information (1, 3, 4) • Uncertainties can be readily represented (4) 	<ul style="list-style-type: none"> • Subjectivity may introduce bias (2) • A representative survey of experts may be difficult to implement (5)

^a Numbers in parentheses under Advantages and Disadvantages indicate that they are relevant to the criteria described. The five criteria are: (1) Consistency at regional level with global projections; (2) Physical plausibility and realism, such that changes in different climatic variables are mutually consistent and credible, and spatial and temporal patterns of change are realistic; (3) Appropriateness of information for impact assessments (i.e., resolution, time horizon, variables); (4) Representativeness of the potential range of future regional climate change; and (5) Accessibility for use in impact assessments.

not necessarily present a realistic set of changes that are physically plausible. They are usually adopted for exploring system sensitivity prior to the application of more credible, model-based scenarios (Rosenzweig and Iglesias, 1994; Smith and Hulme, 1998).

13.2.2 Analogue Scenarios

Analogue scenarios are constructed by identifying recorded climate regimes which may resemble the future climate in a given region. Both spatial and temporal analogues have been used in constructing climate scenarios.

13.2.2.1 Spatial analogues

Spatial analogues are regions which today have a climate analogous to that anticipated in the study region in the future. For example, to project future grass growth, Bergthórsson *et al.* (1988) used northern Britain as a spatial analogue for the potential future climate over Iceland. Similarly, Kalkstein and Greene (1997) used Atlanta as a spatial analogue of New York in a heat/mortality study for the future. Spatial analogues have also been exploited along altitudinal gradients to project vegetation composition, snow conditions for skiing, and avalanche risk (e.g., Beniston and Price, 1992; Holten and Carey, 1992; Gyalistras *et al.*, 1997). However, the approach is severely restricted by the frequent lack of correspondence between other important features (both climatic and non-climatic) of a study region and its spatial analogue (Arnell *et al.*, 1990). Thus, spatial analogues are seldom applied as scenarios, *per se*. Rather, they are valuable for validating the extrapolation of impact models by providing information on the response of systems to climatic conditions falling outside the range currently experienced at a study location.

13.2.2.2 Temporal analogues

Temporal analogues make use of climatic information from the past as an analogue for possible future climate (Webb and Wigley, 1985; Pittock, 1993). They are of two types: palaeoclimatic analogues and instrumentally based analogues.

Palaeoclimatic analogues are based on reconstructions of past climate from fossil evidence, such as plant or animal remains and sedimentary deposits. Two periods have received particular attention (Budyko, 1989; Shabalova and Können, 1995): the mid-Holocene (about 5 to 6 ky BP²) and the Last (Eemian) Interglacial (about 120 to 130 ky BP). During these periods, mean global temperatures were as warm as or warmer than today (see Chapter 2, Section 2.4.4), perhaps resembling temperatures anticipated during the 21st century. Palaeoclimatic analogues have been adopted extensively in the former Soviet Union (e.g., Frenzel *et al.*, 1992; Velichko *et al.*, 1995a,b; Anisimov and Nelson, 1996), as well as elsewhere (e.g., Kellogg and Schwabe, 1981; Pittock and Salinger, 1982). The major disadvantage of using palaeoclimatic analogues for climate scenarios is that the causes of past changes in climate (e.g., variations in the Earth's orbit about the Sun; continental configuration) are different from

those posited for the enhanced greenhouse effect, and the resulting regional and seasonal patterns of climate change may be quite different (Crowley, 1990; Mitchell, 1990). There are also large uncertainties about the quality of many palaeoclimatic reconstructions (Covey, 1995). However, these scenarios remain useful for providing insights about the vulnerability of systems to abrupt climate change (e.g., Severinghaus *et al.*, 1998) and to past El Niño-Southern Oscillation (ENSO) extremes (e.g., Fagan, 1999; Rodbell *et al.*, 1999). They also can provide valuable information for testing the ability of climate models to reproduce past climate fluctuations (see Chapter 8).

Periods of observed global scale warmth during the historical period have also been used as analogues of a greenhouse gas induced warmer world (Wigley *et al.*, 1980). Such scenarios are usually constructed by estimating the difference between the regional climate during the warm period and that of the long-term average or a similarly selected cold period (e.g., Lough *et al.*, 1983). An alternative approach is to select the past period on the basis not only of the observed climatic conditions but also of the recorded impacts (e.g., Warrick, 1984; Williams *et al.*, 1988; Rosenberg *et al.*, 1993; Lapin *et al.*, 1995). A further method employs observed atmospheric circulation patterns as analogues (e.g., Wilby *et al.*, 1994). The advantage of the analogue approach is that the changes in climate were actually observed and so, by definition, are internally consistent and physically plausible. Moreover, the approach can yield useful insights into past sensitivity and adaptation to climatic variations (Magalhães and Glantz, 1992). The major objection to these analogues is that climate anomalies during the past century have been fairly minor compared to anticipated future changes, and in many cases the anomalies were probably associated with naturally occurring changes in atmospheric circulation rather than changes in greenhouse gas concentrations (e.g., Glantz, 1988; Pittock, 1989).

13.2.3 Scenarios Based on Outputs from Climate Models

Climate models at different spatial scales and levels of complexity provide the major source of information for constructing scenarios. GCMs and a hierarchy of simple models produce information at the global scale. These are discussed further below and assessed in detail in Chapters 8 and 9. At the regional scale there are several methods for obtaining sub-GCM grid scale information. These are detailed in Chapter 10 and summarised in Section 13.4.

13.2.3.1 Scenarios from General Circulation Models

The most common method of developing climate scenarios for quantitative impact assessments is to use results from GCM experiments. GCMs are the most advanced tools currently available for simulating the response of the global climate system to changing atmospheric composition.

All of the earliest GCM-based scenarios developed for impact assessment in the 1980s were based on equilibrium-response experiments (e.g., Emanuel *et al.*, 1985; Rosenzweig, 1985; Gleick, 1986; Parry *et al.*, 1988). However, most of these scenarios contained no explicit information about the time of

² ky BP = thousand years before present.

realisation of changes, although time-dependency was introduced in some studies using pattern-scaling techniques (e.g., Santer *et al.*, 1990; see Section 13.5).

The evolving (transient) pattern of climate response to gradual changes in atmospheric composition was introduced into climate scenarios using outputs from coupled AOGCMs from the early 1990s onwards. Recent AOGCM simulations (see Chapter 9, Table 9.1) begin by modelling historical forcing by greenhouse gases and aerosols from the late 19th or early 20th century onwards. Climate scenarios based on these simulations are being increasingly adopted in impact studies (e.g., Neilson *et al.*, 1997; Downing *et al.*, 2000) along with scenarios based on ensemble simulations (e.g., papers in Parry and Livermore, 1999) and scenarios accounting for multi-decadal natural climatic variability from long AOGCM control simulations (e.g., Hulme *et al.*, 1999a).

There are several limitations that restrict the usefulness of AOGCM outputs for impact assessment: (i) the large resources required to undertake GCM simulations and store their outputs, which have restricted the range of experiments that can be conducted (e.g., the range of radiative forcings assumed); (ii) their coarse spatial resolution compared to the scale of many impact assessments (see Section 13.4); (iii) the difficulty of distinguishing an anthropogenic signal from the noise of natural internal model variability (see Section 13.5); and (iv) the difference in climate sensitivity between models.

13.2.3.2 Scenarios from simple climate models

Simple climate models are simplified global models that attempt to reproduce the large-scale behaviour of AOGCMs (see Chapter 9). While they are seldom able to represent the non-linearities of some processes that are captured by more complex models, they have the advantage that multiple simulations can be conducted very rapidly, enabling an exploration of the climatic effects of alternative scenarios of radiative forcing, climate sensitivity and other parametrized uncertainties (IPCC, 1997). Outputs from these models have been used in conjunction with GCM information to develop scenarios using pattern-scaling techniques (see Section 13.5). They have also been used to construct regional greenhouse gas stabilisation scenarios (e.g., Gyalistras and Fischlin, 1995). Simple climate models are used in climate scenario generators (see Section 13.5.2) and in some integrated assessment models (see Section 13.6).

13.2.4 Other Types of Scenarios

Three additional types of climate scenarios have also been adopted in impact studies. The first type involves extrapolating ongoing trends in climate that have been observed in some regions and that appear to be consistent with model-based projections of climate change (e.g., Jones *et al.*, 1999). There are obvious dangers in relying on extrapolated trends, and especially in assuming that recent trends are due to anthropogenic forcing rather than natural variability (see Chapters 2 and 12). However, if current trends in climate are pointing strongly in one direction, it may be difficult to defend the credibility of scenarios that posit a trend in the opposite direction, especially over a short projection period.

A second type of scenario, which has some resemblance to the first, uses empirical relationships between regional climate and global mean temperature from the instrumental record to extrapolate future regional climate on the basis of projected global or hemispheric mean temperature change (e.g. Vinnikov and Groisman, 1979; Anisimov and Poljakov, 1999). Again, this method relies on the assumption that past relationships between local and broad-scale climate are also applicable to future conditions.

A third type of scenario is based on expert judgement, whereby estimates of future climate change are solicited from climate scientists, and the results are sampled to obtain probability density functions of future change (NDU, 1978; Morgan and Keith, 1995; Titus and Narayanan, 1996; Kuikka and Varis, 1997; Tol and de Vos, 1998). The main criticism of expert judgement is its inherent subjectivity, including problems of the representativeness of the scientists sampled and likely biases in questionnaire design and analysis of the responses (Stewart and Glantz, 1985). Nevertheless, since uncertainties in estimates of future climate are inevitable, any moves towards expressing future climate in probabilistic terms will necessarily embrace some elements of subjective judgement (see Section 13.5).

13.3 Defining the Baseline

A baseline period is needed to define the observed climate with which climate change information is usually combined to create a climate scenario. When using climate model results for scenario construction, the baseline also serves as the reference period from which the modelled future change in climate is calculated.

13.3.1 The Choice of Baseline Period

The choice of baseline period has often been governed by availability of the required climate data. Examples of adopted baseline periods include 1931 to 1960 (Leemans and Solomon, 1993), 1951 to 1980 (Smith and Pitts, 1997), or 1961 to 1990 (Kittel *et al.*, 1995; Hulme *et al.*, 1999b).

There may be climatological reasons to favour earlier baseline periods over later ones (IPCC, 1994). For example, later periods such as 1961 to 1990 are likely to have larger anthropogenic trends embedded in the climate data, especially the effects of sulphate aerosols over regions such as Europe and eastern USA (Karl *et al.*, 1996). In this regard, the “ideal” baseline period would be in the 19th century when anthropogenic effects on global climate were negligible. Most impact assessments, however, seek to determine the effect of climate change with respect to “the present”, and therefore recent baseline periods such as 1961 to 1990 are usually favoured. A further attraction of using 1961 to 1990 is that observational climate data coverage and availability are generally better for this period compared to earlier ones.

Whatever baseline period is adopted, it is important to acknowledge that there are differences between climatological averages based on century-long data (e.g., Legates and Wilmott, 1990) and those based on sub-periods. Moreover, different 30-year periods have been shown to exhibit differences in regional annual mean baseline temperature and precipitation of up to

$\pm 0.5^{\circ}\text{C}$ and $\pm 15\%$ respectively (Hulme and New, 1997; Visser *et al.*, 2000; see also Chapter 2).

13.3.2 The Adequacy of Baseline Climatological Data

The adequacy of observed baseline climate data sets can only be evaluated in the context of particular climate scenario construction methods, since different methods have differing demands for baseline climate data.

There are an increasing number of gridded global (e.g., Leemans and Cramer, 1991; New *et al.*, 1999) and national (e.g., Kittel *et al.*, 1995, 1997; Frei and Schär, 1998) climate data sets describing mean surface climate, although few describe interannual climate variability (see Kittel *et al.*, 1997; Xie and Arkin, 1997; New *et al.*, 2000). Differences between alternative gridded regional or global baseline climate data sets may be large, and these may induce non-trivial differences in climate change impacts that use climate scenarios incorporating different baseline climate data (e.g., Arnell, 1999). These differences may be as much a function of different interpolation methods and station densities as they are of errors in observations or the result of sampling different time periods (Hulme and New, 1997; New, 1999). A common problem that some methods endeavour to correct is systematic biases in station locations (e.g., towards low elevation sites). The adequacy of different techniques (e.g., Daly *et al.*, 1994; Hutchinson, 1995; New *et al.*, 1999) to interpolate station records under conditions of varying station density and/or different topography has not been systematically evaluated.

A growing number of climate scenarios require gridded daily baseline climatological data sets at continental or global scales yet, to date, the only observed data products that meet this criterion are experimental (e.g., Piper and Stewart, 1996; Widmann and Bretherton, 2000). For this and other reasons, attempts have been made to combine monthly observed climatologies with stochastic weather generators to allow “synthetic” daily observed baseline data to be generated for national (e.g., Carter *et al.*, 1996a; Semenov and Brooks, 1999), continental (e.g., Voet *et al.*, 1996; Kittel *et al.*, 1997), or even global (e.g., Friend, 1998) scales. Weather generators are statistical models of observed sequences of weather variables, whose outputs resemble weather data at individual or multi-site locations (Wilks and Wilby, 1999). Access to long observed daily weather series for many parts of the world (e.g., oceans, polar regions and some developing countries) is a problem for climate scenario developers who wish to calibrate and use weather generators.

A number of statistical downscaling techniques (see Section 13.4 and Chapter 10, Section 10.6, for definition) used in scenario development employ Numerical Weather Prediction (NWP) reanalysis data products as a source of upper air climate data (Kalnay *et al.*, 1996). These reanalysis data sets extend over periods up to 40 years and provide spatial and temporal resolution sometimes lacking in observed climate data sets. Relatively little detailed work has compared such reanalysis data with independent observed data sets (see Santer *et al.*, 1999, and Widmann and Bretherton, 2000, for two exceptions), but it is known that certain reanalysis variables – such as precipitation and some other hydrological variables – are unreliable.

13.3.3 Combining Baseline and Modelled Data

Climate scenarios based on model estimates of future climate can be constructed either by adopting the direct model outputs or by combining model estimates of the changed climate with observational climate data. Impact studies rarely use GCM outputs directly because GCM biases are too great and because the spatial resolution is generally too coarse to satisfy the data requirements for estimating impacts. Mearns *et al.* (1997) and Mavromatis and Jones (1999) provide two of the few examples of using climate model output directly as input into an impact assessment.

Model-based estimates of climate change should be calculated with respect to the chosen baseline. For example, it would be inappropriate to combine modelled changes in climate calculated with respect to model year 1990 with an observed baseline climate representing 1951 to 1980. Such an approach would “disregard” about 0.15°C of mean global warming occurring between the mid-1970s and 1990. It would be equally misleading to apply modelled changes in climate calculated with respect to an unforced (control) climate representing “pre-industrial” conditions (e.g., “forced” t_3 minus “unforced” t_1 in Figure 13.4) to an observed baseline climate representing some period in the 20th century. Such an approach would introduce an unwarranted amount of global climate change into the scenario. This latter definition of modelled climate change was originally used in transient climate change experiments to overcome problems associated with climate “drift” in the coupled AOGCM simulations (Cubasch *et al.*, 1992), but was not designed to be used in conjunction with observed climate data. It is more appropriate to define the modelled change in climate with respect to the same baseline period that the observed climate data set is representing (e.g., “forced” t_3 minus “unforced” t_1 in Figure 13.4, added to a 1961 to 1990 baseline climate).

Whatever baseline period is selected, there are a number of ways in which changes in climate can be calculated from model results and applied to baseline data. For example, changes in

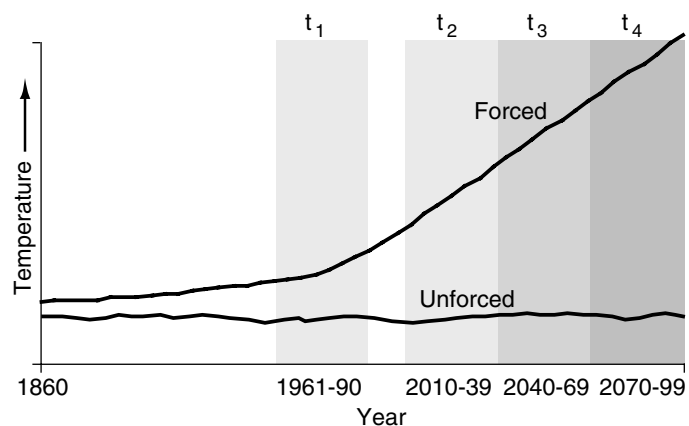


Figure 13.4: A schematic representation of different simulations and periods in a coupled AOGCM climate change experiment that may be used in the definition of modelled climate change. t_1 to t_4 define alternative 30-year periods from either forced or unforced experiments.

climate can be calculated either as the difference or as the ratio between the simulated future climate and the simulated baseline climate. These differences or ratios are then applied to the observed baseline climate – whether mean values, monthly or a daily time-series. Differences are commonly applied to temperature (as in Box 13.1), while ratios are usually used with those surface variables, such as precipitation, vapour pressure and radiation, that are either positive or zero. Climate scenarios have been constructed using both absolute and relative changes for precipitation. The effects of the two different approaches on the resulting climate change impacts depend on the types of impacts being studied and the region of application. Some studies report noticeable differences in impacts (e.g., Alcamo *et al.*, 1998), especially since applying ratio changes alters the standard deviation of the original series (Mearns *et al.*, 1996); in others, differences in impacts were negligible (e.g., Torn and Fried, 1992).

13.4 Scenarios with Enhanced Spatial and Temporal Resolution

The spatial and temporal scales of information from GCMs, from which climate scenarios have generally been produced, have not been ideal from an impacts point of view. The desire for information on climate change regarding changes in variability as well as changes in mean conditions and for information at high spatial resolutions has been consistent over a number of years (Smith and Tirpak, 1989).

The scale at which information can appropriately be taken from relatively coarse-scale GCMs has also been debated. For example, many climate scenarios constructed from GCM outputs have taken information from individual GCM grid boxes, whereas most climate modellers do not consider the outputs from their simulation experiments to be valid on a single grid box scale and usually examine the regional results from GCMs over a cluster of grid boxes (see Chapter 10, Section 10.3). Thus, the scale of information taken from coarse resolution GCMs for scenario development often exceeds the reasonable resolution of accuracy of the models themselves.

In this section we assess methods of incorporating high resolution information into climate scenarios. The issue of spatial and temporal scale embodies an important type of uncertainty in climate scenario development (see Section 13.5.1.5).

Since spatial and temporal scales in atmospheric phenomena are often related, approaches for increasing spatial resolution can also be expected to improve information at high-frequency temporal scales (e.g., Mearns *et al.*, 1997; Semenov and Barrow, 1997; Wang *et al.*, 1999; see also Chapter 10).

13.4.1 Spatial Scale of Scenarios

The climate change impacts community has long bemoaned the inadequate spatial scale of climate scenarios produced from coarse resolution GCM output (Gates, 1985; Lamb, 1987; Robinson and Finkelstein, 1989; Smith and Tirpak, 1989; Cohen, 1990). This dissatisfaction emanates from the perceived mismatch of scale between coarse resolution GCMs (hundreds of

kilometres) and the scale of interest for regional impacts (an order or two orders of magnitude finer scale) (Hostettler, 1994; IPCC, 1994). For example, many mechanistic models used to simulate the ecological effects of climate change operate at spatial resolutions varying from a single plant to a few hectares. Their results may be highly sensitive to fine-scale climate variations that may be embedded in coarse-scale climate variations, especially in regions of complex topography, along coastlines, and in regions with highly heterogeneous land-surface covers.

Conventionally, regional “detail” in climate scenarios has been incorporated by applying changes in climate from the coarse-scale GCM grid points to observation points that are distributed at varying resolutions, but often at resolutions higher than that of the GCMs (e.g., see Box 13.1; Whetton *et al.*, 1996; Arnell, 1999). Recently, high resolution gridded baseline climatologies have been developed with which coarse resolution GCM results have been combined (e.g., Saarikko and Carter, 1996; Kittel *et al.*, 1997). Such relatively simple techniques, however, cannot overcome the limitations imposed by the fundamental spatial coarseness of the simulated climate change information itself.

Three major techniques (referred to as regionalisation techniques) have been developed to produce higher resolution climate scenarios: (1) regional climate modelling (Giorgi and Mearns, 1991; McGregor, 1997; Giorgi and Mearns, 1999); (2) statistical downscaling (Wilby and Wigley, 1997; Murphy, 1999); and (3) high resolution and variable resolution Atmospheric General Circulation Model (AGCM) time-slice techniques (Cubasch *et al.*, 1995; Fox-Rabinovitz *et al.*, 1997). The two former methods are dependent on the large-scale circulation variables from GCMs, and their value as a viable means of increasing the spatial resolution of climate change information thus partially depends on the quality of the GCM simulations. The variable resolution and high resolution time-slice methods use the AGCMs directly, run at high or variable resolutions. The high resolution time-slice technique is also dependent on the sea surface temperature simulated by a coarser resolution AOGCM. There have been few completed experiments using these AGCM techniques, which essentially are still under development (see Chapter 10, Section 10.4). Moreover, they have rarely been applied to explicit scenario formation for impacts purposes (see Jendritzky and Tinz, 2000, for an exception) and are not discussed further in this chapter. See Chapter 10 for further details on all techniques.

13.4.1.1 Regional modelling

The basic strategy in regional modelling is to rely on the GCM to reproduce the large-scale circulation of the atmosphere and for the regional model to simulate sub-GCM scale regional distributions or patterns of climate, such as precipitation, temperature, and winds, over the region of interest (Giorgi and Mearns, 1991; McGregor, 1997; Giorgi and Mearns, 1999). The GCM provides the initial and lateral boundary conditions for driving the regional climate model (RCM). In general, the spatial resolution of the regional model is on the order of tens of kilometres, whereas the GCM scale is an order of magnitude coarser. Further details on the techniques of regional climate modelling are covered in Chapter 10, Section 10.5.

13.4.1.2 Statistical downscaling

In statistical downscaling, a cross-scale statistical relationship is developed between large-scale variables of observed climate such as spatially averaged 500 hPa heights, or measure of vorticity, and local variables such as site-specific temperature and precipitation (von Storch, 1995; Wilby and Wigley, 1997; Murphy, 1999). These relationships are assumed to remain constant in the climate change context. Also, it is assumed that the predictors selected (i.e., the large-scale variables) adequately represent the climate change signal for the predictand (e.g., local-scale precipitation). The statistical relationship is used in conjunction with the change in the large-scale variables to determine the future local climate. Further details of these techniques are provided in Chapter 10, Section 10.6.

13.4.1.3 Applications of the methods to impacts

While the two major techniques described above have been available for about ten years, and proponents claim use in impact assessments as one of their important applications, it is only quite recently that scenarios developed using these techniques have actually been applied in a variety of impact assessments, such as temperature extremes (Hennessy *et al.*, 1998; Mearns, 1999); water resources (Hassall and Associates, 1998; Hay *et al.*, 1999; Wang *et al.*, 1999; Wilby *et al.*, 1999; Stone *et al.*, 2001); agriculture (Mearns *et al.*, 1998, 1999, 2000a, 2001; Brown *et al.*, 2000) and forest fires (Wotton *et al.*, 1998). Prior to the past couple of years, these techniques were mainly used in pilot studies focused on increasing the temporal (and spatial) scale of scenarios (e.g., Mearns *et al.*, 1997; Semenov and Barrow, 1997).

One of the most important aspects of this work is determining whether the high resolution scenario actually leads to significantly different calculations of impacts compared to that of the coarser resolution GCM from which the high resolution scenario was partially derived. This aspect is related to the issue of uncertainty in climate scenarios (see Section 13.5). We provide examples of such studies below.

Application of high resolution scenarios produced from a regional model (Giorgi *et al.*, 1998) over the Central Plains of the USA produced changes in simulated crop yields that were significantly different from those changes calculated from a coarser resolution GCM scenario (Mearns *et al.*, 1998; 1999, 2001). For simulated corn in Iowa, for example, the large-scale (GCM) scenario resulted in a statistically significant decrease in yield, but the high resolution scenario produced an insignificant increase (Figure 13.5). Substantial differences in regional economic impacts based on GCM and RCM scenarios were also found in a recent integrated assessment of agriculture in the south-eastern USA (Mearns *et al.*, 2000a,b). Hay *et al.* (1999), using a regression-based statistical downscaling technique, developed downscaled scenarios based on the Hadley Centre Coupled AOGCM (HadCM2) transient runs and applied them to a hydrologic model in three river basins in the USA. They found that the standard scenario from the GCM produced changes in surface runoff that were quite different from those produced from the downscaled scenario (Figure 13.6).

13.4.2 Temporal Variability

The climate change information most commonly taken from climate modelling experiments comprises mean monthly, seasonal, or annual changes in variables of importance to impact assessments. However, changes in climate will involve changes in variability as well as mean conditions. As mentioned in Section 13.3 on baseline climate, the interannual variability in climate scenarios constructed from mean changes in climate is most commonly inherited from the baseline climate, not from the climate change experiment. Yet, it is known that changes in variability could be very important to most areas of impact assessment (Mearns, 1995; Semenov and Porter, 1995). The most obvious way in which variability changes affect resource systems is through the effect of variability change on the frequency of extreme events. As Katz and Brown (1992) demonstrated, changes in standard deviation have a proportionately greater effect than changes in means on changes in the frequency of extremes. However, from a climate scenario point of view, it is the relative size of the change in the mean versus standard deviation of a variable that determines the final relative contribution of these statistical moments to a change in extremes. The construction of scenarios incorporating extremes is discussed in Section 13.4.2.2.

The conventional method of constructing mean change scenarios for precipitation using the ratio method (discussed in Section 13.3) results in a change in variability of daily precipitation intensity; that is, the variance of the intensity is changed by a factor of the square of the ratio (Mearns *et al.*, 1996). However, the frequency of precipitation is not changed. Using the difference method (as is common for temperature variables) the variance of the time-series is not changed. Hence, from the perspective of variability, application of the difference approach to precipitation produces a more straightforward scenario. However, it can also result in negative values of precipitation. Essentially neither approach is realistic in its effect on the daily characteristics of the time-series. As mean (monthly) precipitation changes, both the daily intensity and frequency are usually affected.

13.4.2.1 Incorporation of changes in variability: daily to interannual time-scales

Changes in variability have not been regularly incorporated in climate scenarios because: (1) less faith has been placed in climate model simulations of changes in variability than of changes in mean climate; (2) techniques for changing variability are more complex than those for incorporating mean changes; and (3) there may have been a perception that changes in means are more important for impacts than changes in variability (Mearns, 1995). Techniques for incorporating changes in variability emerged in the early 1990s (Mearns *et al.*, 1992; Wilks, 1992; Woo, 1992; Barrow and Semenov, 1995; Mearns, 1995).

Some relatively simple techniques have been used to incorporate changes in interannual variability alone into scenarios. Such techniques are adequate in cases where the impact models use monthly climate data for input. One approach is to calculate present day and future year-by-year anomalies relative to the modelled baseline period, and to apply these anomalies (at an annual, seasonal or monthly resolution) to the long-term mean

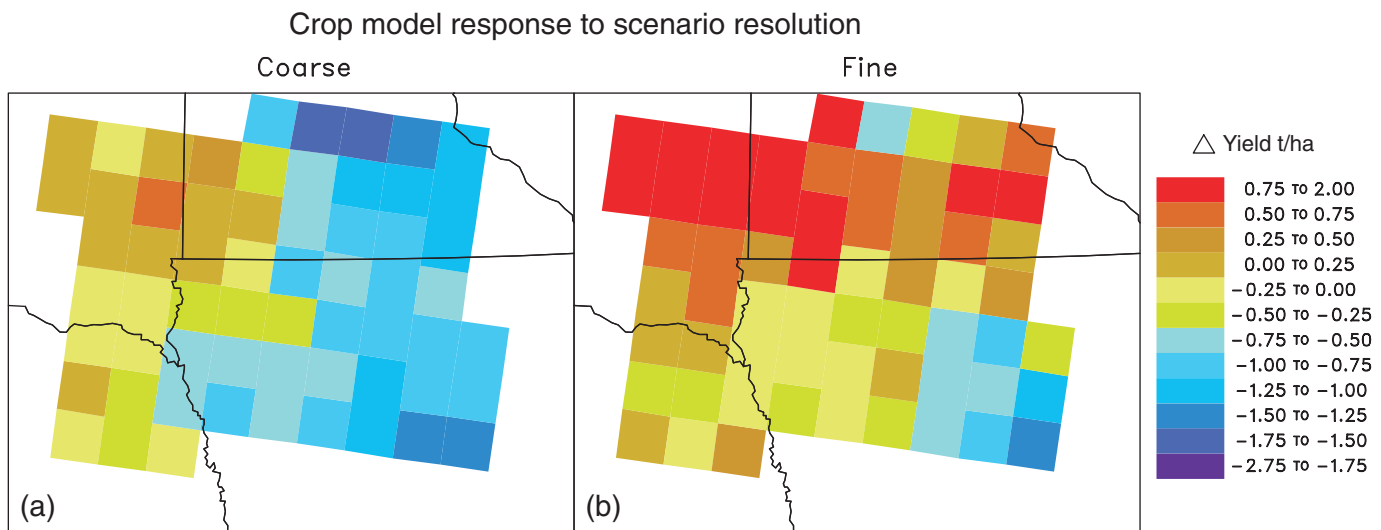


Figure 13.5: Spatial pattern of differences (future climate minus baseline) in simulated corn yields based on two different climate change scenarios for the region covering north-west Iowa and surrounding states (a) coarse spatial resolution GCM scenario (CSIRO); (b) high spatial resolution region climate model scenario (RegCM) (modified from Mearns *et al.*, 1999).

observed baseline climate. This produces climate time-series having an interannual variability equivalent to that modelled for the present day and future, both superimposed on the observed baseline climate. The approach was followed in evaluating impacts of variability change on crop yields in Finland (Carter *et al.*, 2000a), and in the formation of climate scenarios for the United States National Assessment, though in the latter case the observed variability was retained for the historical period.

Another approach is to calculate the change in modelled interannual variability between the baseline and future periods, and then to apply it as an inflator or deflator to the observed baseline interannual variability. In this way, modelled changes in interannual variability are carried forward into the climate scenario, but the observed baseline climate still provides the initial definition of variability. This approach was initially developed in Mearns *et al.* (1992) and has recently been experimented with by Arnell (1999). However, this approach can produce unrealistic features, such as negative precipitation or inaccurate autocorrelation structure of temperature, when applied to climate data on a daily time-scale (Mearns *et al.*, 1996).

The major, most complete technique for producing scenarios with changes in interannual and daily variability involves manipulation of the parameters of stochastic weather generators (defined in Section 13.3.2). These are commonly based either on a Markov chain approach (e.g., Richardson, 1981) or a spell length approach (e.g., Racksko *et al.*, 1991), and simulate changes in variability on daily to interannual time-scales (Wilks, 1992). More detailed information on weather generators is provided in Chapter 10, Section 10.6.2.

To bring about changes in variability, the parameters of the weather generator are manipulated in ways that alter the daily variance of the variable of concern (usually temperature or precipitation) (Katz, 1996). For precipitation, this usually involves changes in both the frequency and intensity of daily precipitation. By manipulating the parameters on a daily time-scale, changes in

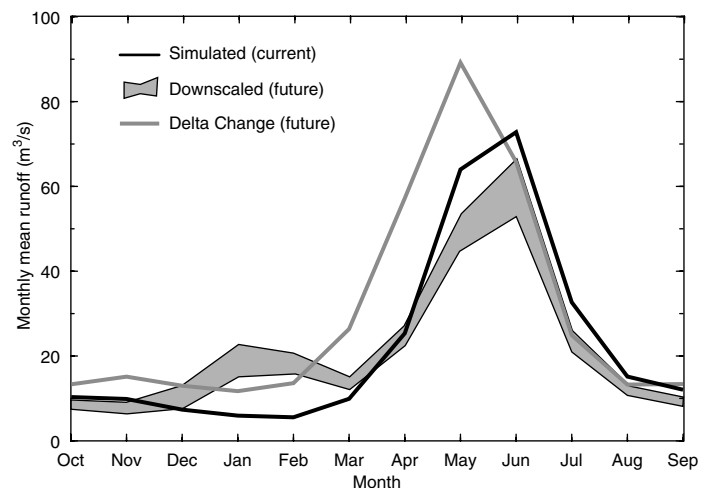


Figure 13.6: Differences in simulated runoff (m^3/s) based on a statistically downscaled climate scenario and a coarse resolution GCM scenario (labelled Delta Change) for the Animas River Basin in Colorado (modified from Hay *et al.*, 1999). The downscaled range (grey area) is based on twenty ensembles.

variability are also induced on the interannual time-scale (Wilks, 1992). Some weather generators operating at sub-daily time-scales have also been applied to climate scenario generation (e.g., Kilsby *et al.*, 1998).

A number of crop model simulations have been performed to determine the sensitivity of crop yields to incremental changes in daily and interannual variability (Barrow and Semenov, 1995; Mearns, 1995; Mearns *et al.*, 1996; Riha *et al.*, 1996; Wang and Erda, 1996; Vinocur *et al.*, 2000). In most of these studies, changes in variability resulted in significant changes in crop yield. For example, Wang and Erda (1996) combined systematic incremental changes in daily variance of temperature and precipi-

tation with mean climate scenarios in their study of climate change and corn yields in China. They found that increases in the variance of temperature and precipitation combined, further decreased crop yields compared to the effect of the mean change scenarios alone taken from several GCMs.

Studies using the variance changes in addition to mean changes from climate models to form climate scenarios also emerged in the past decade (Kaiser *et al.*, 1993; Bates *et al.* 1994). For example, Bates *et al.* (1994, 1996) adapted Wilks' (1992) method and applied it to changes in daily variability from doubled CO₂ runs of the Commonwealth Scientific and Industrial Research Organisation (CSIRO) climate model (CSIRO9). They then applied the changed time-series to a hydrological model. Combined changes in mean and variability are also evident in a broad suite of statistical downscaling methods (e.g., Katz and Parlange, 1996; Wilby *et al.*, 1998). See also Chapter 10, Section 10.6.3, for further discussion of statistical downscaling and changes in variability.

In recent years, more robust and physically meaningful changes in climatic variability on daily to interannual time scales have been found in runs of GCMs and RCMs for some regions (e.g., Gregory and Mitchell, 1995; Mearns *et al.*, 1995a,b; Whetton *et al.*, 1998a; Mearns, 1999; Boer *et al.*, 2000). For example, on both daily and interannual time-scales many models simulate temperature variability decreases in winter and increases in summer in northern mid-latitude land areas (see Chapter 9, Section 9.3). This result is likely to encourage the further application of model-derived variability changes in climate scenario construction.

The most useful studies, from the point of view of elucidating uncertainty in climate scenarios and impacts, are those that compare applying scenarios with only mean changes to those with mean and variability change. Semenov and Barrow (1997) and Mearns *et al.* (1997) used mean and variance changes from climate models, formed scenarios of climate change using weather generators and applied them to crop models. In both studies important differences in the impacts of climatic change on crop yields were calculated when including the effect of variance change, compared to only considering mean changes. They identified three key aspects of changed climate relevant to the role played by change in daily to interannual variability of climate: the marginality of the current climate for crop growth, the relative size of the mean and variance changes, and the timing of these changes.

It is difficult to generalise the importance of changes in variability to climate change impacts since significance of changes in variability is region, variable, and resource system specific. For example, based on results of equilibrium control and 2×CO₂ experiments of DARLAM (a regional model developed in Australia) nested within the CSIRO climate model over New South Wales, Whetton *et al.* (1998a) emphasised that most of the change in temperature extremes they calculated resulted from changes in the mean, not through change in the daily variance. In contrast, Mearns (1999) found large changes (e.g., decreases in winter) in daily variance of temperature in control and 2×CO₂ experiments with a regional climate model (RegCM2) over the Great Plains of the U.S. (Giorgi *et al.*, 1998). These changes were sufficient to make a significant difference in the frequency of daily

temperature extremes. Note, however, that these results are not contradictory since they concern two very different regions. More generalised statements may be made regarding the importance of change in the variability of precipitation from climate change experiments for determining changes in the frequency of droughts and floods (e.g., Gregory *et al.*, 1997; Kothavala, 1999). As noted in Chapters 9 and 10, high intensity rainfall events are expected to increase in general, and precipitation variability would be expected to increase where mean precipitation increases.

Other types of variance changes, on an interannual time-scale, based on changes in major atmospheric circulation oscillations, such as ENSO and North Atlantic Oscillation (NAO), are difficult to incorporate into impact assessments. The importance of the variability of climate associated with ENSO phases for resources systems such as agriculture and water resources have been well demonstrated (e.g., Cane *et al.*, 1994; Chiew *et al.*, 1998; Hansen *et al.*, 1998).

Where ENSO signals are strong, weather generators can be successfully conditioned on ENSO phases; and therein lies the potential for creating scenarios with changes in the frequency of ENSO events. By conditioning on the phases, either discretely (Wang and Connor, 1996) or continuously (Woolhiser *et al.*, 1993), a model can be formed for incorporating changes in the frequency and persistence of such events, which would then induce changes in the daily (and interannual) variability of the local climate sites. Weather generators can also be successfully conditioned using NAO signals (e.g., Wilby, 1998). However, it must be noted that there remains much uncertainty in how events such as ENSO might change with climate change (Knutson, *et al.*, 1997; Timmerman *et al.*, 1999; Walsh *et al.*, 1999; see also Chapter 9, Section 9.3.5, for further discussion on possible changes in ENSO events). While there is great potential for the use of conditioned stochastic models in creating scenarios of changed variability, to date, no such scenario has actually been applied to an impact model.

13.4.2.2 Other techniques for incorporating extremes into climate scenarios

While the changes in both the mean and higher order statistical moments (e.g., variance) of time-series of climate variables affect the frequency of relatively simple extremes (e.g., extreme high daily or monthly temperatures, damaging winds), changes in the frequency of more complex extremes are based on changes in the occurrence of complex atmospheric phenomena (e.g., hurricanes, tornadoes, ice storms). Given the sensitivity of many exposure units to the frequency of extreme climatic events (see Chapter 3 of TAR WG II, Table 3.10 (Carter and La Rovere, 2001)), it would be desirable to incorporate into climate scenarios the frequency and intensity of some composite atmospheric phenomena associated with impacts-relevant extremes.

More complex extremes are difficult to incorporate into scenarios for the following reasons: (1) high uncertainty on how they may change (e.g., tropical cyclones); (2) the extremes may not be represented directly in climate models (e.g., ice storms); and (3) straightforward techniques of how to incorporate changes at a particular location have not been developed (e.g., tropical cyclone intensity at Cairns, Australia).

The ability of climate models to adequately represent extremes partially depends on their spatial resolution (Skelly and Henderson-Sellers, 1996; Osborn, 1997; Mearns, 1999). This is particularly true for complex atmospheric phenomena such as hurricanes (see Chapter 10, Box 10.2). There is some very limited information on possible changes in the frequency and intensity of tropical cyclones (Bengtsson *et al.*, 1996; Henderson-Sellers *et al.*, 1998; Krishnamurti *et al.*, 1998; Knutson and Tuleya, 1999; Walsh and Ryan, 2000); and of mid-latitude cyclones (Schubert *et al.*, 1998), but these studies are far from definitive (see Chapter 9, Section 9.3.6, and Chapter 10 for discussion on changes of extremes with changes in climate).

In the case of extremes that are not represented at all in climate models, secondary variables may sometimes be used to derive them. For example, freezing rain, which results in ice storms, is not represented in climate models, but frequencies of daily minimum temperatures on wet days might serve as useful surrogate variables (Konrad, 1998).

An example of an attempt to incorporate such complex changes into climate scenarios is the study of McInnes *et al.* (2000), who developed an empirical/dynamical model that gives return period versus height for tropical cyclone-related storm surges for Cairns on the north Australian coast. To determine changes in the characteristics of cyclone intensity, they prepared a climatology of tropical cyclones based on data drawn from a much larger area than Cairns locally. They incorporated the effect of climate change by modifying the parameters of the Gumbel distribution of cyclone intensity based on increases in tropical cyclone intensity derived from climate model results over a broad region characteristic of the location in question. Estimates of sea level rise also contributed to the modelled changes in surge height. Other new techniques for incorporating such complex changes into quantitative climate scenarios are yet to be developed.

13.5 Representing Uncertainty in Climate Scenarios

13.5.1 Key Uncertainties in Climate Scenarios

Uncertainties about future climate arise from a number of different sources (see Figure 13.2) and are discussed extensively throughout this volume. Depending on the climate scenario construction method, some of these uncertainties will be explicitly represented in the resulting scenario(s), while others will be ignored (Jones, 2000a). For example, scenarios that rely on the results from GCM experiments alone may be able to represent some of the uncertainties that relate to the modelling of the climate response to a given radiative forcing, but might not embrace uncertainties caused by the modelling of atmospheric composition for a given emissions scenario, or those related to future land-use change. Section 13.5.2 therefore assesses different approaches for representing uncertainties in climate scenarios. First, however, five key sources of uncertainty, as they relate to climate scenario construction, are very briefly described. Readers are referred to the relevant IPCC chapters for a comprehensive discussion.

13.5.1.1 Specifying alternative emissions futures

In previous IPCC Assessments, a small number of future greenhouse gas and aerosol precursor emissions scenarios have been presented (e.g., Leggett *et al.*, 1992). In the current Assessment, a larger number of emissions scenarios have been constructed in the Special Report on Emissions Scenarios (SRES) (Nakićenović *et al.*, 2000), and the uncertain nature of these emissions paths have been well documented (Morita and Robinson, 2001). Climate scenarios constructed from equilibrium GCM experiments alone (e.g., Howe and Henderson-Sellers, 1997; Smith and Pitts, 1997) do not consider this uncertainty, but some assumption about the driving emissions scenario is required if climate scenarios are to describe the climate at one or more specified times in the future. This source of uncertainty is quite often represented in climate scenarios (e.g., Section 13.5.2.1).

13.5.1.2 Uncertainties in converting emissions to concentrations

It is uncertain how a given emissions path converts into atmospheric concentrations of the various radiatively active gases or aerosols. This is because of uncertainties in processes relating to the carbon cycle, to atmospheric trace gas chemistry and to aerosol physics (see Chapters 3, 4 and 5). For these uncertainties to be reflected in climate scenarios that rely solely on GCM outputs, AOGCMs that explicitly simulate the various gas cycles and aerosol physics are needed. At present, however, they are seldom, if ever, represented in climate scenarios.

13.5.1.3 Uncertainties in converting concentrations to radiative forcing

Even when presented with a given greenhouse gas concentration scenario, there are considerable uncertainties in the radiative forcing changes, especially aerosol forcing, associated with changes in atmospheric concentrations. These uncertainties are discussed in Chapters 5 and 6, but again usually remain unrepresented in climate scenarios.

13.5.1.4 Uncertainties in modelling the climate response to a given forcing

An additional set of modelling uncertainties is introduced into climate scenarios through differences in the global and regional climate responses simulated by different AOGCMs for the same forcing. Different models have different climate sensitivities (see Chapter 9, Section 9.3.4.1), and this remains a key source of uncertainty for climate scenario construction. Also important is the fact that different GCMs yield different regional climate change patterns, even for similar magnitudes of global warming (see Chapter 10). Furthermore, each AOGCM simulation includes not only the response (i.e., the “signal”) to a specified forcing, but also an unpredictable component (i.e., the “noise”) that is due to internal climate variability. This latter may itself be an imperfect replica of true climate variability (see Chapter 8). A fourth source of uncertainty concerns important processes that are missing from most model simulations. For instance AOGCM-based climate scenarios do not usually allow for the effect on climate of future land use and land cover change (which is itself, in part, climatically induced). Although the first two sources of model uncertainty – different climate sensitivities and regional climate

change patterns – are usually represented in climate scenarios, it is less common for the third and fourth sources of uncertainty – the variable signal-to-noise ratio and incomplete description of key processes and feedbacks – to be effectively treated.

13.5.1.5 Uncertainties in converting model response into inputs for impact studies

Most climate scenario construction methods combine model-based estimates of climate change with observed climate data (Section 13.3). Further uncertainties are therefore introduced into a climate scenario because observed data sets seldom capture the full range of natural decadal-scale climate variability, because of errors in gridded regional or global baseline climate data sets, and because different methods are used to combine model and observed climate data. These uncertainties relating to the use of observed climate data are usually ignored in climate scenarios. Furthermore, regionalisation techniques that make use of information from AOGCM and RCM experiments to enhance spatial and temporal scales introduce additional uncertainties into regional climate scenarios (their various advantages and disadvantages are assessed in Chapter 10 and in Section 13.4). These uncertainties could be quantified by employing a range of regionalisation techniques, but this is rarely done.

13.5.2 Approaches for Representing Uncertainties

There are different approaches for representing each of the above five generic sources of uncertainty when constructing climate scenarios. The cascade of uncertainties, and the options for representing them at each of the five stages, can result in a wide range of climate outcomes in the finally constructed scenarios (Henderson-Sellers, 1996; Wigley, 1999; Visser *et al.*, 2000). Choices are most commonly made at the stage of modelling the climate response to a given forcing, where it is common for a set of climate scenarios to include results from different GCMs. In practice, this sequential and conditional approach to representing uncertainty in climate scenarios has at least one severe limitation: at each stage of the cascade, only a limited number of the conditional outcomes have been explicitly modelled. For example, GCM experiments have used one, or only a small number, of the concentration scenarios that are plausible (for example, most transient AOGCM experiments that have been used for climate scenarios adopted by impacts assessments have been forced with a scenario of a 1% per annum growth in greenhouse gas concentration). Similarly, regionalisation techniques have been used with only a small number of the GCM experiments that have been conducted. These limitations restrict the choices that can be made in climate scenario construction and mean that climate scenarios do not fully represent the uncertainties inherent in climate prediction.

In order to overcome some of these limitations, a range of techniques has been developed to allow more flexible treatment of the entire cascade of uncertainty. These techniques manipulate or combine different modelling results in a variety of ways. If we are truly to assess the risk of climate change being dangerous, then impact and adaptation studies need scenarios that span a very substantial part of the possible range of future climates (Pittock,

1993; Parry *et al.*, 1996; Risbey, 1998; Jones, 1999; Hulme and Carter, 2000). The remainder of this section assesses four aspects of climate scenario development that originate from this concern about adequately representing uncertainty:

1. scaling climate response patterns across a range of forcing scenarios;
2. defining appropriate climate change signals;
3. risk assessment approaches;
4. annotation of climate scenarios to reflect more qualitative aspects of uncertainty.

13.5.2.1 Scaling climate model response patterns

Pattern-scaling methods allow a wider range of possible future forcings (e.g., the full range of IS92 (Leggett *et al.*, 1992) or SRES emissions scenarios) and climate sensitivities (e.g., the 1.5°C to 4.5°C IPCC range) to be represented in climate scenarios than if only the direct results from GCM experiments were used. The approach involves normalising GCM response patterns according to the global mean temperature change (although in some cases zonal mean temperature changes have been used). These normalised patterns are then rescaled using a scalar derived from simple climate models and representing the particular scenario under consideration.

This pattern-scaling method was first suggested by Santer *et al.* (1990) and was employed in the IPCC First Assessment Report to generate climate scenarios for the year 2030 (Mitchell *et al.*, 1990) using patterns from 2xCO₂ GCM experiments. It has subsequently been widely adopted in climate scenario generators (CSGs), for example in ESCAPE (Rotmans *et al.*, 1994), IMAGE-2 (Alcamo *et al.*, 1994), SCENGEN (Hulme *et al.*, 1995a,b), SILMUSCEN (Carter *et al.*, 1995, 1996a), COSMIC (Schlesinger *et al.*, 1997) and CLIMPACTS (Kenny *et al.*, 2000). A climate scenario generator is an integrated suite of simple models that takes emissions or forcing scenarios as inputs and generates geographically distributed climate scenarios combining response patterns of different greenhouse gases from GCMs with observational climate data. CSGs allow multiple sources of uncertainty to be easily represented in the calculated scenarios, usually by using pattern-scaling methods.

Two fundamental assumptions of pattern-scaling are, first, that the defined GCM response patterns adequately depict the climate “signal” under anthropogenic forcing (see Section 13.5.2.2) and, second, that these response patterns are representative across a wide range of possible anthropogenic forcings. These assumptions have been explored by Mitchell *et al.* (1999) who examined the effect of scaling decadal, ensemble mean temperature and precipitation patterns in the suite of HadCM2 experiments. Although their response patterns were defined using only 10-year means, using four-member ensemble means improved the performance of the technique when applied to reconstructing climate response patterns in AOGCM experiments forced with alternative scenarios (see Figure 13.7). This confirmed earlier work by Oglesby and Saltzman (1992), among others, who demonstrated that temperature response patterns derived from equilibrium GCMs were fairly uniform over a wide range of concentrations, scaling linearly with global mean temperature. The main exception occurred in the

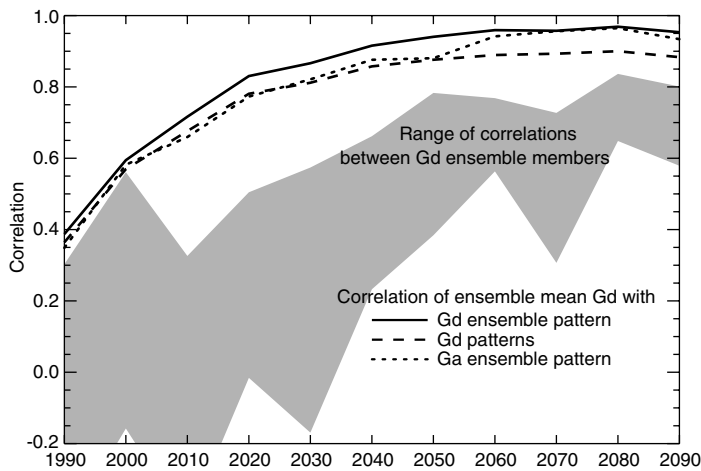


Figure 13.7: Pattern correlations between the decadal ensemble mean temperature (Northern Hemisphere only) from the HadCM2 experiment forced with a 0.5%/yr increase in greenhouse gas concentrations (Gd) and: the scaled ensemble mean pattern (solid line); the four scaled individual ensemble member patterns – average coefficient (dashed line); and the scaled ensemble mean pattern derived from the HadCM2 experiment forced with a 1%/yr increase in greenhouse gas concentrations (Ga) (dotted line). The correlations increase with time as the pattern of greenhouse gas response (the “signal”) increasingly dominates the random effects of internal climate variability (the “noise”). The shaded area shows the spread of correlations between the pairs of the individual members of the Gd ensemble; these correlations are lower than those between the realised and scaled patterns above, indicating that the scaled pattern is not due to internal climate variability. (Source: Mitchell *et al.*, 1999.)

regions of enhanced response near sea ice and snow margins. Mitchell *et al.* (1999) concluded that the uncertainties introduced by scaling ensemble decadal mean temperature patterns across different forcing scenarios are smaller than those due to the model’s internal variability, although this conclusion may not hold for variables with high spatial variability such as precipitation.

Two situations where the pattern-scaling techniques may need more cautious application are in the cases of stabilisation forcing scenarios and heterogeneous aerosol forcing. Whetton *et al.* (1998b) have shown that for parts of the Southern Hemisphere a highly non-linear regional rainfall response was demonstrated in an AOGCM forced with a stabilisation scenario, a response that could not easily be handled using a linear pattern-scaling technique. In the case of heterogeneous forcing, similar global mean warmings can be associated with quite different regional patterns, depending on the magnitude and pattern of the aerosol forcing. Pattern-scaling using single global scalars is unlikely to work in such cases. There is some evidence, however, to suggest that separate greenhouse gas and aerosol response patterns can be assumed to be additive (Ramaswamy and Chen, 1997) and pattern-scaling methods have subsequently been adapted by Schlesinger *et al.* (1997, 2000) for the case of heterogeneously forced scenarios. This is an area, however, where poor signal-to-noise ratios hamper the application of the technique and caution is advised.

The above discussion demonstrates that pattern-scaling techniques provide a low cost alternative to expensive AOGCM and RCM experiments for creating a range of climate scenarios that embrace uncertainties relating to different emissions, concentration and forcing scenarios and to different climate model responses. The technique almost certainly performs best in the case of surface air temperature and in cases where the response pattern has been constructed so as to maximise the signal-to-noise ratio. When climate scenarios are needed that include the effects of sulphate aerosol forcing, regionally differentiated response patterns and scalars must be defined and signal-to-noise ratios should be quantified. It must be remembered, however, that while these techniques are a convenient way of handling several types of uncertainty simultaneously, they introduce an uncertainty of their own into climate scenarios that is difficult to quantify. Little work has been done on exploring whether patterns of change in inter-annual or inter-daily climate variability are amenable to scaling methods.

13.5.2.2 Defining climate change signals

The question of signal-to-noise ratios in climate model simulations was alluded to above, and has also been discussed in Chapters 9 and 12. The treatment of “signal” and “noise” in constructing climate scenarios is of great importance in interpreting the results of impact assessments that make use of these scenarios. If climate scenarios contain an unspecified combination of signal plus noise, then it is important to recognise that the impact response to such scenarios will only partly be a response to anthropogenic climate change; an unspecified part of the impact response will be related to natural internal climate variability. However, if the objective is to specify the impacts of the anthropogenic climate signal alone, then there are two possible strategies for climate scenario construction:

- attempt to maximise the signal and minimise the noise;
- do not try to disentangle signal from noise, but supply impact assessments with climate scenarios containing both elements and also companion descriptions of future climate that contain only noise, thus allowing impact assessors to generate their own impact signal-to-noise ratios (Hulme *et al.*, 1999a).

The relative strength of the signal-to-noise ratio can be demonstrated in a number of ways. Where response patterns are reasonably stable over time, this ratio can be maximised in a climate change scenario by using long (30-year or more) averaging periods. Alternatively, regression or principal component techniques may be used to extract the signal from the model response (Hennessy *et al.*, 1998). A third technique is to use results from multi-member ensemble simulations, as first performed by Cubasch *et al.* (1994). Sampling theory shows that in such simulations the noise is reduced by a factor of \sqrt{n} , where n is the ensemble size. Using results from the HadCM2 four-member ensemble experiments, Giorgi and Francisco (2000), for example, suggest that uncertainty in future regional climate change associated with internal climate variability at sub-continental scales (10^7 km^2), is generally smaller than the

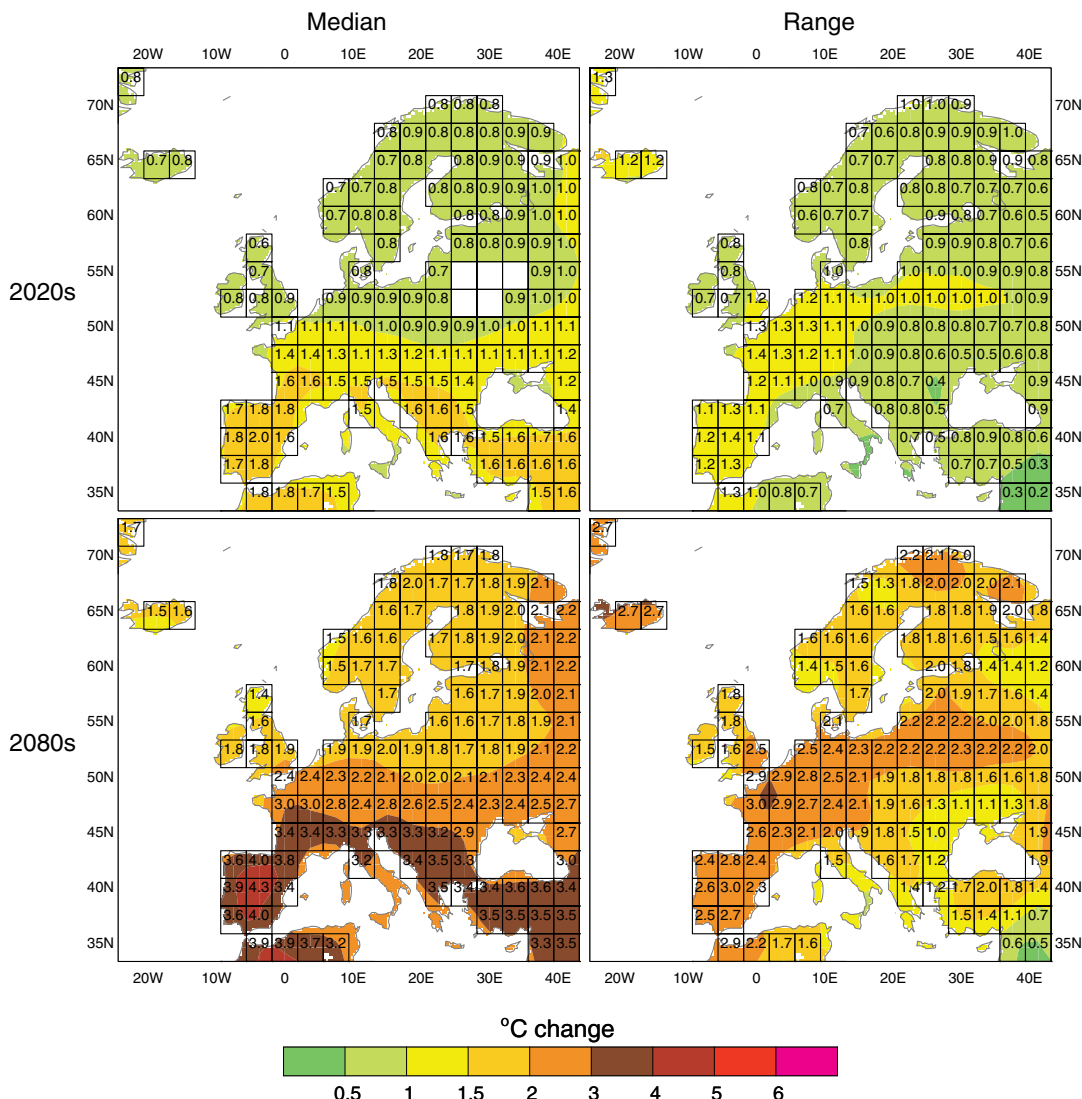


Figure 13.8: A summer (JJA) temperature change scenario for Europe for the 2020s and 2080s. Left panel is the median scaled response of five GCM experiments available on the IPCC Data Distribution Centre (<http://ipcc-ddc.cru.uea.ac.uk/>) and the right panel is the inter-model range (largest scaled response minus the smallest scaled response). (Source: Hulme and Carter, 2000.)

uncertainty associated with inter-model or forcing differences. This conclusion is scale- and variable-dependent, however (see Chapter 9, Figure 9.4; see also Räisänen, 1999), and the inverse may apply at the smaller scales (10^4 to 10^5 km^2) at which many impact assessments are conducted. Further work is needed on resolving this issue for climate scenario construction purposes.

A different way of maximising the climate change signal is to compare the responses of single realisations from experiments completed using different models. If the error for different models is random with zero mean, then sampling theory shows that this model average will yield a better estimate of the signal than any single model realisation. This approach was first suggested in the context of climate scenarios by Santer *et al.* (1990) and is illustrated further in Chapter 9, Section 9.2.2. Treating different GCM simulations in this way, i.e., as members of a multi-model ensemble, is one way of defining a more robust climate change signal, either for use in pattern-scaling techniques or directly in

constructing a climate scenario. The approach has been discussed by Räisänen (1997) and used recently by Wigley (1999), Hulme and Carter (2000; see Figure 13.8) and Carter *et al.* (2000b) in providing regional characterisations of the SRES emissions scenarios.

The second strategy requires that the noise component be defined explicitly. This can be done by relying either on observed climate data or on model-simulated natural climate variability (Hulme *et al.*, 1999a; Carter *et al.*, 2000b). Neither approach is ideal. Observed climate data may often be of short duration and therefore yield a biased estimate of the noise. Multi-decadal internal climate variability can be extracted from multi-century unforced climate simulations such as those performed by a number of modelling groups (e.g., Stouffer *et al.*, 1994; Tett *et al.*, 1997; von Storch *et al.*, 1997). In using AOGCM output in this way, it is important not only to demonstrate that these unforced simulations do not drift significantly (Osborn, 1996), but also to

evaluate the extent to which model estimates of low-frequency variability are comparable to those estimated from measured climates (Osborn *et al.*, 2000) or reconstructed palaeoclimates (Jones *et al.*, 1998). Furthermore, anthropogenic forcing may alter the character of multi-decadal climate variability and therefore the noise defined from model control simulations may not apply in the future.

13.5.2.3 Risk assessment approaches

Uncertainty analysis is required to perform quantitative risk or decision analysis (see Toth and Mwandoza (2001) for discussion of decision analysis). By itself, scenario analysis is not equivalent to uncertainty analysis because not all possible scenarios are necessarily treated and, especially, because probabilities are not attached to each scenario (see Morgan and Henrion (1990) for a general treatment of uncertainty analysis; see Katz (2000) for a more recent overview focusing on climate change). Recognising this limitation, a few recent studies (Jones, 2000b; New and Hulme, 2000) have attempted to modify climate scenario analysis, grouping a range of scenarios together and attaching a probability to the resultant classes. Such an approach can be viewed as a first step in bridging the gap between scenario and uncertainty analysis. Single climate scenarios, by definition, are limited to plausibility with no degree of likelihood attached. Since risk analysis requires that probabilities be attached to each climate scenario, subjective probabilities can be applied to the input parameters that determine the climate outcomes (e.g., emissions scenarios, the climate sensitivity, regional climate response patterns), thus allowing distributions of outcomes to be formally quantified.

In formal risk analysis, the extremes of the probability distribution should encompass the full range of possible outcomes, although in climate change studies this remains hard to achieve. The ranges for global warming and sea level rise from the IPCC WGI Second Assessment Report (IPCC, 1996) (hereafter SAR), for example, deliberately did not encompass the full range of possible outcomes and made no reference to probability distributions. As a consequence, the bulk of impact assessments have treated these IPCC ranges as having a uniform probability, i.e., acting as if no information is available about what changes are more likely than others. As pointed out by Titus and Narayanan (1996), Jones (1998, 2000a), and Parkinson and Young (1998), however, where several sources of uncertainty are combined, the resulting probability distribution is not uniform but is a function of the component probability distributions and the relationship between the component elements. For example, descriptions of regional changes in temperature and rainfall over Australia constructed from regional response patterns have been used in a number of hydrological studies where the extreme outcomes have been considered as likely as outcomes in the centre of the range (e.g., Chiew *et al.*, 1995; Schreider *et al.*, 1996; Whetton, 1998). However, when the two component ranges – global warming and normalised local temperature and rainfall change – are randomly sampled and then multiplied together, they offer a distinctly non-uniform distribution (see Figure 13.9a). Further refinements of these approaches for quantifying the risk of climate change are needed (New and Hulme, 2000).

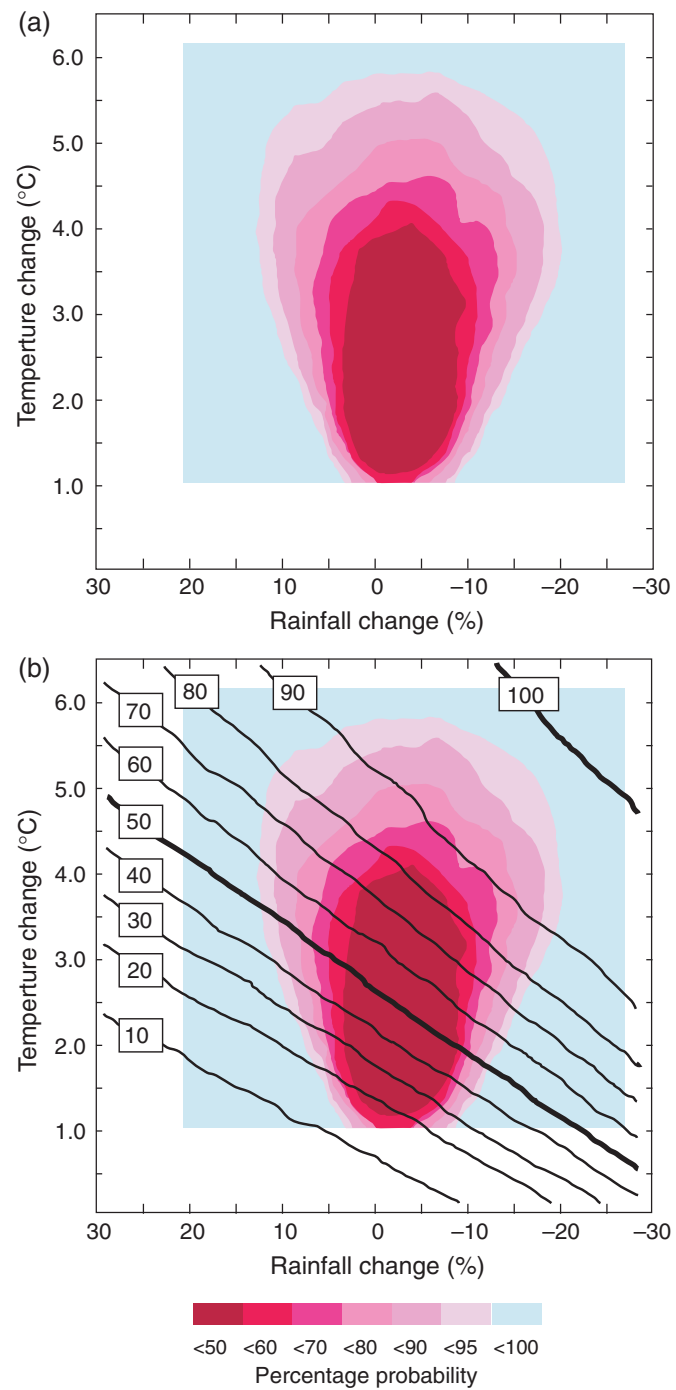


Figure 13.9: (a) Projected ranges of regional annual temperature and rainfall change for inland southern Australia in 2100 extrapolated from CSIRO (1996) with temperature sampled randomly across the projected ranges of both global and normalised regional warming and then multiplied together. Projected regional ranges for normalised seasonal rainfall change were randomly sampled, multiplied by the randomly sampled global warming as above, and then averaged. The resulting probability density surface reveals the likelihood of different climate change outcomes for this region; (b) Response surface of irrigation demand for the same region superimposed on projected climate changes as (a), showing the likelihood of exceeding an annual allocation of irrigation water supply. Risk can be calculated by summing the probabilities of all climates below a given level of annual exceedance of annual water supply; e.g., 50%, or exceedance of the annual water limit in at least one of every two years. (Source: Jones, 2000b.)

This approach to portraying uncertainty has potentially useful applications when combined with climate impact sensitivity response surfaces (see Section 13.2.1; see also Chapter 3 of TAR WG II (Carter and La Rovere, 2001)). The superimposed response surfaces allow the calculation of probabilities for exceeding particular impact thresholds (Figure 13.9b). Another method of assessing risk using quantified probability distributions is through a series of linked models such as those used for calculating sea level rise (Titus and Narayanan, 1996) and economic damage due to sea level rise (Yohe and Schlesinger, 1998), for quantifying climate uncertainty (Visser *et al.*, 2000), and in integrated assessments (Morgan and Dowlatabadi, 1996). Efforts to make explicit probabilistic forecasts of the climate response to a given emissions scenario for the near future have been made using the current observed climate trajectory to constrain the “forecasts” from several GCMs (Allen *et al.*, 2000). More details on this technique are given in Section 12.4.3.3.

13.5.2.4 Annotation of climate scenarios

Even if quantifiable uncertainties are represented, further uncertainties in climate scenarios may still need to be documented or explicitly treated. These include the possible impact on scenarios of errors in the unforced model simulation, the possibility that current models cannot adequately simulate the enhanced greenhouse response of a climatic feature of interest, or inconsistencies between results of model simulations and emerging observed climatic trends. For these reasons climate scenarios are often annotated with a list of caveats, along with some assessment as to their importance for the scenario user.

When choosing which GCM(s) to use as the basis for climate scenario construction, one of the criteria that has often been used is the ability of the GCM to simulate present day climate. Many climate scenarios have used this criterion to assist in their choice of GCM, arguing that GCMs that simulate present climate more faithfully are likely to simulate more plausible future climates (e.g., Whetton and Pittock, 1991; Robock *et al.*, 1993; Risbey and Stone, 1996; Gyalistras *et al.*, 1997; Smith and Pitts, 1997; Smith and Hulme, 1998; Lal and Harasawa, 2000). A good simulation of present day climate, however, is neither a necessary nor a sufficient condition for accurate simulation of climate change (see Chapter 8). It is possible, for example, that a model with a poor simulation of present day climate could provide a more accurate simulation of climate change than one which has a good simulation of present climate, if it contains a better representation of the dominant feedback processes that will be initiated by radiative forcing. While such uncertainties are difficult to test, useful insights into the ability of models to simulate long-term climate change can also be obtained by comparing model simulations of the climate response to past changes in radiative forcing against reconstructed paleoclimates.

This approach to GCM selection, however, raises a number of questions. Over which geographic domain should the GCM be evaluated – the global domain or only over the region of study? Which climate variables should be evaluated – upper air synoptic features that largely control the surface climate, or only those climate variables, mostly surface, that are used in impact studies? Recent AOGCMs simulate observed 1961 to 1990 mean climate

more faithfully than earlier GCMs (Kittel *et al.*, 1998; see also Chapter 8), but they still show large errors in simulating inter-annual climate variability in some regions (Giorgi and Francisco, 2000; Lal *et al.*, 2000) and in replicating ENSO-like behaviour in the tropics (Knutson *et al.*, 1997). These questions demonstrate that there is no easy formula to apply when choosing GCMs for climate scenario construction; there will always be a role for informed but, ultimately, individual judgement. This judgement, however, should be made not just on empirical grounds (for example, which model’s present climate correlates best with observations) but also on the basis of understanding the reasons for good or bad model performance, particularly if those reasons are important for the particular scenario application.

Several examples of such annotations can be given. Lal and Giorgi (1997) suggested that GCMs that cannot simulate the observed interannual variability of the Indian monsoon correctly should not be used as the basis for climate scenarios. Giorgi *et al.* (1998) commented that model-simulated spring temperatures over the USA Central Plains were too cold in both the CSIRO GCM and in the CSIRO-driven RegCM2 control simulations and affected the credibility of the ensuing temperature climate scenarios. Finally, scenarios prepared for the Australian region have often been accompanied by the note that ENSO is an important component of Australian climate that may change in the future, but that is not yet adequately simulated in climate models (e.g., Hennessy *et al.*, 1998). Expert judgment can also be used to place confidence estimates on scenario ranges (Morgan and Keith, 1995). For example, Jones *et al.* (2000) placed “high confidence” on the temperature scenarios (incorporating quantifiable uncertainty) prepared for the South Pacific, but only “moderate to low confidence” in the corresponding rainfall scenarios.

13.6 Consistency of Scenario Components

This section discusses some of the caveats of climate scenario development and focuses on the need for consistency in representing different physical aspects of the climate system. It does not discuss the many possible inconsistencies with respect to socio-economic issues in scenario development. Chapter 3 of the TAR WG II (Carter and La Rovere, 2001) and Chapter 2 of the TAR WG III (Morita and Robinson, 2001) provide a detailed treatment of these issues. Three common inconsistencies in applying climate scenarios are discussed, concerning the representation of ambient versus equivalent CO₂ concentrations, biosphere-ocean-atmosphere interactions and time lags between sea level rise and temperature change.

The climate system consists of several components that interact with and influence each other at many different temporal and spatial scales (see Chapter 7). This complexity adds further constraints to the development of climate scenarios, though their relevance is strongly dependent on the objectives and scope of the studies that require scenarios. Most climate scenarios are based on readily available climate variables (e.g., from AOGCMs) and, where these are used in impact assessments, studies are often restricted to an analysis of the effects of changes in climate alone. However, other related environmental aspects may also change, and these are often neglected or inadequately represented, thus

potentially reducing the comprehensiveness of the impact assessment. Furthermore, some feedback processes that are seldom considered in AOGCM simulations, may modify regional changes in climate (e.g., the effect of climate-induced shifts in vegetation on albedo and surface roughness).

Concurrent changes in atmospheric concentrations of gases such as CO₂, sulphur dioxide (SO₂) and ozone (O₃) can have important effects on biological systems. Studies of the response of biotic systems require climate scenarios that include consistent information on future levels of these species. For example, most published AOGCM simulations have used CO₂-equivalent concentrations to represent the combined effect of the various gases. Typically, only an annual 1% increase in CO₂-equivalent concentrations, which approximates changes in radiative forcing of the IS92a emission scenario (Leggett *et al.*, 1992), has been used. However, between 10 and 40% of this increase results from non-CO₂ greenhouse gases (Alcamo *et al.*, 1995). The assumption that CO₂ concentrations equal CO₂-equivalent concentrations (e.g., Schimel *et al.*, 1997; Walker *et al.*, 1999) has led to an exaggeration of direct CO₂ effects. If impacts are to be assessed more consistently, proper CO₂ concentration levels and CO₂-equivalent climate forcing must be used. Many recent impact assessments that recognise these important requirements (e.g., Leemans *et al.*, 1998; Prinn *et al.*, 1999; Downing *et al.*, 2000) make use of tools such as scenario generators (see Section 13.5.2.1) that explicitly treat atmospheric trace gas concentrations. Moreover, some recent AOGCM simulations now discriminate between the individual forcings of different greenhouse gases (see Chapter 9, Table 9.1)

The biosphere is an important control in defining changes in greenhouse gas concentrations. Its surface characteristics, such as albedo and surface roughness, further influence climate patterns. Biospheric processes, such as CO₂-sequestration and release, evapotranspiration and land-cover change, are in turn affected by climate. For example, warming is expected to result in a poleward expansion of forests (IPCC, 1996b). This would increase biospheric carbon storage, which lowers future CO₂ concentrations and change the surface albedo which would directly affect climate. A detailed discussion of the role of the biosphere on climate can be found elsewhere (Chapters 3 and 7), but there is a clear need for an improved treatment of biospheric responses in scenarios that are designed for regional impact assessment. Some integrated assessment models, which include simplifications of many key biospheric responses, are beginning to provide consistent information of this kind (e.g., Alcamo *et al.*, 1996, 1998; Harvey *et al.*, 1997; Xiao *et al.*, 1997; Goudriaan *et al.*, 1999).

Another important input to impact assessments is sea level rise. AOGCMs usually calculate the thermal expansion of the oceans directly, but this is only one component of sea level rise (see Chapter 11). Complete calculations of sea level rise, including changes in the mass balance of ice sheets and glaciers, can be made with simpler models (e.g., Raper *et al.*, 1996), and the transient dynamics of sea level rise should be explicitly calculated because the responses are delayed (Warrick *et al.*, 1996). However, the current decoupling of important dynamic processes in most simple models could generate undesirable inaccuracies in the resulting scenarios.

Climate scenario generators can comprehensively address some of these inconsistencies. Full consistency, however, can only be attained through the use of fully coupled global models (earth system models) that systematically account for all major processes and their interactions, but these are still under development.

References

- Alcamo**, J., G.J. van denBorn, A.F. Bouwman, B.J. deHaan, K. Klein Goldewijk, O. Klepper, J. Krabec, R. Leemans, J.G.J. Olivier, A.M.C. Toet, H.J.M. deVries, and H.J. van der Word, 1994: Modeling the global society-biosphere-climate system. *Water Air Soil Pollut.*, **76**, 1-78.
- Alcamo**, J., A. Bouwman, J. Edmonds, A. Grübler, T. Morita and A. Sugandhy, 1995: An evaluation of the IPCC IS92 emission scenarios. In: *Climate Change 1994: Radiative forcing of climate change and an evaluation of the IPCC IS92 emission scenarios. Reports of Working Groups I and III of the Intergovernmental Panel on Climate Change* [Houghton, J.T., L.G. Meira Filho, J. Bruce, H. Lee, B.A. Callander, E. Haites, N. Harris and K. Maskell (eds.)]. Cambridge University Press, Cambridge, United Kingdom and New York, NY, USA, pp. 247-304.
- Alcamo**, J., G.J.J. Kreileman, J.C. Bollen, G.J. van den Born, R. Gerlagh, M.S. Krol, A.M.C. Toet and H.J.M. de Vries, 1996: Baseline scenarios of global environmental change. *Global Environ. Change*, **6**, 261-303.
- Alcamo**, J., R. Leemans, and E. Kreileman (eds.), 1998: *Global Change Scenarios of the 21st Century*. Pergamon & Elsevier Science, London, UK, 296 pp.
- Allen**, M. R., P. A. Stott, R. Schnur, T. Delworth, and J. F. B. Mitchell, 2000: Uncertainty in forecasts of anthropogenic climate change. *Nature*, **407**, 617-620.
- Anisimov**, O.A. and F.E. Nelson, 1996: Permafrost distribution in the northern hemisphere under scenarios of climatic change. *Global Planet. Change*, **14**, 59-72.
- Anisimov**, O.A. and V.Yu. Poljakov, 1999: On the prediction of the air temperature in the first quarter of the XXI century. *Meteorology and Hydrology*, **2**, 25-31 (in Russian).
- Arnell**, N.W., 1999: A simple water balance model for the simulation of streamflow over a large geographic domain. *J. Hydrol.*, **217**, 314-335.
- Arnell**, N.W., R.P.C. Brown, and N.S. Reynard, 1990: *Impact of Climatic Variability and Change on River Flow Regimes in the UK*. IH Report No. 107, Institute of Hydrology, Wallingford, UK, 154 pp.
- Barrow**, E. M., and M. A. Semenov, 1995: Climate change scenarios with high resolution and temporal resolution and agricultural applications. *Forestry*, **68**, 349-360.
- Bates**, B.C., S.P. Charles, N.R. Sumner, and P.M. Fleming, 1994: Climate change and its hydrological implications for South Australia. *T. Roy. Soc. South. Aust.*, **118(1)**, 35-43.
- Bates**, B.C., A.J. Jakeman, S.P. Charles, N.R. Sumner, and P.M. Fleming, 1996: Impact of climate change on Australia's surface water resources. In: *Greenhouse: Coping with Climate Change* [Bouma, W.J., G.I. Pearman, and M.R. Manning (eds.)]. CSIRO, Melbourne, pp. 248-262.
- Bengtsson**, L., M. Botzet, and M. Esch, 1996: Will greenhouse gas induced warming over the next 50 years lead to higher frequency and greater intensity of hurricanes? *Tellus*, **48A**, 57-73.
- Beniston**, M. and M. Price, 1992: Climate scenarios for the Alpine regions: a collaborative effort between the Swiss National Climate Program and the International Center for Alpine Environments. *Env. Conserv.*, **19**, 360-363.
- Berghórsson**, P., H. Björnsson, O. Dórmundsson, B. Gudmundsson, A. Helgadóttir, and J.V. Jónmundsson, 1988: The effects of climatic variations on agriculture in Iceland. In: *The Impact of Climatic*

- Variations on Agriculture, Volume 1, Assessments in Cool Temperate and Cold Regions* [Parry, M.L., T.R. Carter, and N.T. Konijn (eds.)]. Kluwer, Dordrecht, The Netherlands, pp. 381-509.
- Boer**, G.J., G.M. Flato, and D. Ramsden, 2000: A transient climate change simulation with greenhouse gas and aerosol forcing: projected climate to the twenty-first century. *Clim. Dyn.*, **16(6)**, 427-450.
- Brown**, R.A., N. J. Rosenberg, W.E. Easterling, C. Hays, and L. O. Mearns, 2000: Potential production and environmental effects of switchgrass and traditional crops under current and greenhouse-altered climate in the MINK region of the central United States. *Ecol. Agric. Environ.*, **78**, 31-47.
- Budyko**, M.I., 1989: Empirical estimates of imminent climatic changes. *Soviet Meteorology and Hydrology*, **10**, 1-8.
- Cane**, M.A., G. Eshel, and R.W. Buckland, 1994: Forecasting Zimbabwean maize yield using eastern equatorial Pacific sea surface temperature. *Nature*, **370**, 204-205.
- Carter**, T., M. Posch, and H. Tuomenvirta, 1995: SILMUSCEN and CLIGEN user's guide. Guidelines for the construction of climatic scenarios and use of a stochastic weather generator in the Finnish Research Programme on Climate Change (SILMU). *Publications of the Academy of Finland*, **1/95**, 62 pp.
- Carter**, T.R., M. Posch, and H. Tuomenvirta, 1996a: The SILMU scenarios: specifying Finland's future climate for use in impact assessment. *Geophysica*, **32**, 235-260.
- Carter**, T.R., M. Parry, S. Nishioka, and H. Harasawa, 1996b: Technical Guidelines for assessing climate change impacts and adaptations. In: *Climate Change 1995. Impacts, Adaptations and Mitigation of Climate Change: Scientific-Technical Analysis. Contribution of Working Group II to the Second Assessment Report of the Intergovernmental Panel on Climate Change* [Watson, R.T., M.C. Zinyowere and R.H. Moss (eds.)]. Cambridge University Press, Cambridge, United Kingdom and New York, NY, USA, pp. 823-833.
- Carter**, T.R., R.A. Saarikko, and S.K.H. Joukainen, 2000a: Modelling climate change impacts on wheat and potatoes in Finland. In: *Climate Change, Climate Variability and Agriculture in Europe: An Integrated Assessment* [Downing, T.E., P.E. Harrison, R.E. Butterfield and K.G. Lonsdale (eds.)]. Research Report No. 21, ECU, University of Oxford, Oxford, UK, pp. 289-312.
- Carter**, T.R., M. Hulme, J.F. Crossley, S. Malyshev, M.G. New, M.E. Schlesinger and H. Tuomenvirta, 2000b: *Climate change in the 21st century: interim characterizations based on the new IPCC SRES Emissions Scenarios*. Finnish Environment Institute Report, No. 433, Helsinki, Finland, 148pp.
- Carter**, T.R. and E.L. La Rovere, 2001: Developing and Applying Scenarios. In *Climate Change: Impacts, Adaptation and Vulnerability. Contribution of Working Group II to the IPCC Third Assessment Report*.
- Chiew**, F.H.S., P.H. Whetton, T.A. McMahon, and A.B. Pittock, 1995: Simulation of the impacts of climate change on runoff and soil moisture in Australian catchments. *J. Hydrol.*, **167**, 121-147.
- Chiew**, F.H.S., T.C. Piechota, J.A. Dracup, and T.A. McMahon, 1998: El Niño Southern Oscillation and Australian rainfall, streamflow and drought—links and potential for forecasting. *J. Hydrol.*, **204**, 138-149.
- Climate Impact Assessment Program** (CIAP), 1975: *Impacts of Climatic Change on the Biosphere*. CIAP Monograph 5, Part 2 - Climate Effects. Department of Transportation, CIAP, Washington, D.C.
- Cohen**, S. J., 1990: Bringing the global warming issue closer to home: the challenge of regional impact studies. *Bull. Am. Met. Soc.*, **71**, 520-526.
- Covey**, C., 1995: Using paleoclimates to predict future climate: how far can analogy go? *Clim. Change*, **29**, 403-407.
- Crowley**, T.J., 1990: Are there any satisfactory geologic analogs for a future greenhouse warming? *J. Climate*, **3**, 1282-1292.
- CSIRO**, 1996: OzClim: A climate scenario generator and impacts package for Australia. CSIRO, Canberra, November 1996, 4pp. [Available on line from <http://www.dar.csiro.au/publications/ozclim.htm>]
- Cubasch**, U., K. Hasselmann, H. Hock, E. Maier-Reimer, U. Mikolajewicz, B.D. Santer, and R. Sausen, 1992: Time-dependent greenhouse warming computations with a coupled ocean-atmosphere model. *Clim. Dyn.*, **8**, 55-69.
- Cubasch**, U., B.D. Santer, A. Hellbach, G. Hegerl, H. Höck, E. Maier-Reimer, U. Mikolajewicz, A. Stössel, and R. Voss, 1994: Monte Carlo climate change forecasts with a global coupled ocean-atmosphere model. *Clim. Dyn.*, **10**, 1-19.
- Cubasch**, U., J. Waszkewitz, G. Hegerl, and J. Perlitz, 1995: Regional climate changes as simulated in time-slice experiments. *Clim. Change*, **31**, 273-304.
- Daly**, C., R.P. Neilson, and D.L. Phillips, 1994: A statistical-topographic model for mapping climatological precipitation over mountainous terrain. *J. Appl. Met.*, **33**, 140-158.
- Downing**, T.E., P.A. Harrison, R.E. Butterfield, and K.G. Lonsdale (eds.), 2000: *Climate Change, Climatic Variability and Agriculture in Europe: An Integrated Assessment*. Research Report No. 21, Environmental Change Unit, University of Oxford, Oxford, UK, 445 pp.
- Emanuel**, W.R., H.H. Shugart, and M.P. Stevenson, 1985: Climatic change and the broad-scale distribution of terrestrial ecosystem complexes. *Clim. Change*, **7**, 29-43.
- Fagan**, B. 1999: *Floods, Famines and Emperors; El Niño and the Fate of Civilizations*. Basic Books, NY, 284 pp.
- Fisher**, R. W., 1996: Future Energy Use. *Future Research Quarterly*, **31**, 43-47.
- Fowler**, A., 1999: Potential climate change impacts on water resources in the Auckland Region (New Zealand). *Clim. Res.*, **11**, 221-245.
- Fox-Rabinovitz**, M. S., G. Stenchikov, and L.L. Takacs, 1997: A finite-difference GCM dynamical core with a variable resolution stretched grid. *Mon. Wea. Rev.*, **125**, 2943-2961.
- Frei**, C. and C. Schär, 1998: A precipitation climatology of the Alps from high-resolution rain-gauge observations. *Int. J. Climatol.*, **18**, 873-900.
- Frenzel**, B., B. Pecsi, and A.A. Velichko (eds.), 1992: *Atlas of Palaeoclimates and Palaeoenvironments of the Northern Hemisphere*. INQUA/Hungarian Academy of Sciences, Budapest.
- Friend**, A.D., 1998: Parameterisation of a global daily weather generator for terrestrial ecosystem modelling. *Ecol. Modelling*, **109**, 121-140.
- Gates**, W. L., 1985: The use of general circulation models in the analysis of the ecosystem impacts of climatic change. *Clim. Change*, **7**, 267-284.
- Giorgi**, F. and L.O. Mearns, 1991: Approaches to regional climate change simulation: A review. *Rev. Geophys.*, **29**, 191-216.
- Giorgi**, F. and L.O. Mearns, 1999: Regional climate modeling revisited: an introduction to the special issue. *J. Geophys. Res.*, **104(D6)**, 6335-6352.
- Giorgi**, F. and R. Francisco, 2000: Uncertainties in regional climate change prediction: a regional analysis of ensemble simulations with HadCM2 coupled AOGCM. *Clim. Dyn.*, **16**, 169-182.
- Giorgi**, F., L. Mearns, S. Shields, and L. McDaniel, 1998: Regional nested model simulations of present day and 2xCO₂ climate over the Central Great Plains of the United States. *Clim. Change*, **40**, 457-493.
- Glantz**, M., 1988: *Societal Responses to Regional Climatic Change: Forecasting by Analogy*. Westview Press, Boulder, Colorado, 77 pp.
- Gleick**, P.H., 1986: Methods for evaluating the regional hydrologic impacts of global climatic changes. *J. Hydrol.*, **88**, 97-116.
- Goudriaan**, J., H.H. Shugart, H. Bugmann, W. Cramer, A. Bondeau, R.H. Gardner, L.A. Hunt, W.K. Lauwenroth, J.J. Landberg, S. Linder, I.R. Noble, W. J. Parton, L.F. Pitelka, M. Stafford Smith, R.W.

- Sutherst, C. Valentin and F.I. Woodward, 1999: Use of models in global change studies. In: *The Terrestrial Biosphere and Global Change: Implications for Natural and Managed Ecosystems* [Walker, B., W. Steffen, J. Canadell and J. Ingram (eds.)]. Cambridge University Press, Cambridge, pp. 106-140.
- Gregory**, J.M. and J.F.B. Mitchell, 1995: Simulation of daily variability of surface temperature and precipitation over Europe in the current and 2xCO₂ climates using the UKMO climate model. *Quart. J. R. Met. Soc.*, **121**, 1451-1476.
- Gregory**, J.M., J.F.B. Mitchell, and A.J. Brady, 1997: Summer drought in northern midlatitudes in a time-dependent CO₂ climate experiment. *J. Climate*, **10**, 662-686.
- Gyalistras**, D. and A. Fischlin, 1995: Downscaling: applications to ecosystems modelling. In: *Proceedings of the 6th International Meeting on Statistical Climatology, Galway, Ireland, June 19-23, 1995* [Muirterchaigh, I. (ed.)]. University College, Galway, pp. 189-192.
- Gyalistras**, D., C. Schär, H.C. Davies, and H. Wanner, 1997: Future alpine climate. In: *Views from the Alps: Regional Perspectives on Climate Change* [Cebon, P., U. Dahinden, H. Davies, D.M. Imboden, and C.C. Jaeger (eds.)]. The MIT Press, Cambridge, MA, pp. 171-223.
- Hammond**, A., 1996: *Which World?* Island Press, Washington, D.C., 306 pp.
- Hansen**, J., II Fung, A. Lacis, D. Rind, G. Russell, S. Lebedeff, R. Ruedy, and P. Stone, 1988: Global climate changes as forecast by the GISS 3-D model. *J. Geophys. Res.*, **93(D8)**, 9341-9364.
- Hansen**, J.W., A.W. Hedges, and J.W. Jones, 1998: ENSO influences on agriculture in the southeastern US. *J. Climate*, **11**, 404-411.
- Harvey**, D., J. Gregory, M. Hoffert, A. Jain, M. Lal, R. Leemans, S. Raper, T. Wigley and J. de Wolde, 1997: *An Introduction to Simple Climate Models Used in the IPCC Second Assessment Report*. Intergovernmental Panel on Climate Change, Geneva, February 1997, IPCC Technical Paper II, 50 pp.
- Hassall and Associates**, 1998: *Climate Change Scenarios and Managing the Scarce Water Resources of the Macquarie River*. Australian Greenhouse Office, Canberra, 113 pp.
- Hay**, E.L., R. B. Wilby, and G.H. Leavesy, 1999: A comparison of delta change and downscaled GCM scenarios: implications for climate change scenarios in three mountainous basins in the United States. In: *Proceedings of the AWRA Specialty conference on Potential Consequences of Climatic Variability and Change to Water Resources of the United States, May, 1999, Atlanta, GA* [Adams, D.B. (ed.)]. AWRA, Middleburg, VA, 424 pp.
- Henderson-Sellers**, A., 1996: Can we integrate climatic modelling and assessment? *Environ. Modeling & Assessment*, **1**, 59-70.
- Henderson-Sellers**, A., H. Zhang, G. Berz, K. Emanuel, W. Gray, C. Landsea, G. Holland, J. Lighthill, S.L. Shieh, P. Webster, and K. McGuffie, 1998: Tropical cyclones and global climate change: A post-IPCC assessment. *Bull. Am. Met. Soc.*, **79**, 19-38.
- Hennessy**, K.J., P.H. Whetton, J.J. Katzfey, J.L. McGregor, R.N. Jones, C.M. Page, and K.C. Nguyen, 1998: *Fine Resolution Climate Change Scenarios for New South Wales*. Annual Report, 1997/98, CSIRO, Australia, 48 pp.
- Holten**, J.I. and P.D. Carey, 1992: *Responses of Climate Change on Natural Terrestrial Ecosystems in Norway*. NINA Forskningsrapport 29, Norwegian Institute for Nature Research, Trondheim, Norway, 59 pp.
- Hostetler**, S., 1994: Hydrologic and atmospheric models: the problem of discordant scales: an editorial comment. *Clim. Change*, **27**, 345-350.
- Howe**, W. and A. Henderson-Sellers (eds.), 1997: *Assessing Climate Change*. Results from the Model Evaluation Consortium for Climate Assessment. Gordon Breach Science Publishers, Amsterdam, 418 pp.
- Hulme**, M. and M. New, 1997: The dependence of large-scale precipitation climatologies on temporal and spatial gauge sampling. *J. Climate*, **10**, 1099-1113.
- Hulme**, M. and G.J. Jenkins, 1998: *Climate change scenarios for the United Kingdom*. UKCIP Technical Note No.1, Climatic Research Unit, Norwich, UK, 80 pp.
- Hulme**, M. and T.R. Carter, 2000: The changing climate of Europe. Chapter 3 in: *Assessment of the Potential Effects of Climate Change in Europe* [Parry, M.L. (ed.)]. Report of the ACACIA Concerted Action, November 2000, UEA, Norwich, UK, 350 pp.
- Hulme**, M., T. Jiang, and T.M.L. Wigley, 1995a: *SCENGEN: A Climate Change SCENARIO GENERATOR, Software User Manual, Version 1.0*. Climatic Research Unit, University of East Anglia, Norwich, 38 pp.
- Hulme**, M., S.C.B. Raper, and T.M.L. Wigley, 1995b: An integrated framework to address climate change (ESCAPE) and further developments of the global and regional climate modules (MAGICC). *Energy Policy*, **23**, 347-355.
- Hulme**, M., E.M. Barrow, N. Arnell, P.A. Harrison, T.E. Downing, and T.C. Johns, 1999a: Relative impacts of human-induced climate change and natural climate variability. *Nature*, **397**, 688-691.
- Hulme**, M., J.F.B. Mitchell, W. Ingram, T.C. Johns, J.A. Lowe, M.G. New and D. Viner, 1999b: Climate change scenarios for global impacts studies. *Global Environ. Change*, **9**, S3-S19.
- Hutchinson**, M.F., 1995: Interpolating mean rainfall using thin-plate smoothing splines. *Int. J. Geogr. Inf. Systems*, **9**, 385-403.
- IPCC**, 1992: *Preliminary Guidelines for Assessing Impacts of Climate Change*. Prepared by Intergovernmental Panel on Climate Change, Working Group II for WMO and UNEP [Carter, T.R., M.L. Parry, S. Nishioka, and H. Harasawa (eds.)]. Cambridge University Press, Cambridge, United Kingdom.
- IPCC**, 1994: *IPCC Technical Guidelines for Assessing Climate Change Impacts and Adaptations*. Prepared by Working Group II [Carter, T.R., M.L. Parry, H. Harasawa, and S. Nishioka] and WMO/UNEP. CGER-IO15-'94. University College London, UK and Center for Global Environmental Research, National Institute for Environmental Studies, Tsukuba, Japan, 59 pp.
- IPCC**, 1996a: *Climate Change 1995: The Science of Climate Change*. Contribution of Working Group I to the Second Assessment Report of the Intergovernmental Panel on Climate Change [Houghton, J.T., L.G. Meira Filho, B.A. Callander, N. Harris, A. Kattenberg, and K. Maskell (eds.)]. Cambridge University Press, Cambridge, United Kingdom and New York, NY, USA, 572 pp.
- IPCC**, 1996b: *Climate Change 1995: Impacts, Adaptations and Mitigation of Climate Change: Scientific-Technical Analyses*. Contribution of Working Group II to the Second Assessment Report of the Intergovernmental Panel on Climate Change [Watson, R.T., M.C. Zinyowera, and R.H. Moss (eds.)]. Cambridge University Press, Cambridge, United Kingdom and New York, NY, USA, 880 pp.
- IPCC**, 1997: *An introduction to simple climate models used in the IPCC Second Assessment Report* [Harvey, L.D., J. Gregory, M. Hoffert, A. Jain, M. Lal, R. Leemans, S. Raper, T. Wigley and J. de Wolde]. IPCC Technical Paper 2, Intergovernmental Panel on Climate Change, Geneva, Switzerland, 50 pp.
- IPCC**, 2001: Climate Change: Impacts, Adaptation and Vulnerability. Contribution of Working Group II to the Third Assessment Report of the Intergovernmental Panel on Climate Change.
- IPCC-TGCIA**, 1999: *Guidelines on the Use of Scenario Data for Climate Impact and Adaptation Assessment*. Version 1. Prepared by Carter, T.R., M. Hulme, and M. Lal, Intergovernmental Panel on Climate Change, Task Group on Scenarios for Climate Impact Assessment. Cambridge University Press, Cambridge, United Kingdom, 69 pp.
- Jendritzky**, G. and B. Tinz, 2000: Human bioclimate maps for climate impact research. In: *Proceedings of Int. Conf. Biomet and Int. Conf. Urban Climate*. ICB-ICUC '99, Sidney, 8-12 November 1999 (in press).

- Jones**, R.N., 1998: Climate change scenarios, impact thresholds and risk. In: *Proceedings of the Workshop on Impacts of Global Change on Australian Temperate Forests* [Gorman, J. and S.M. Howden (eds.)]. February 1998, CSIRO Wildlife and Ecology, Canberra, Australia, pp. 14-28.
- Jones**, R.N., 1999: Climate change scenarios, impact thresholds and risk. In: *Impacts of Global Change on Australian Temperate Forests* [Howden, S.M. and J. Gorman (eds.)]. Working Paper Series 99/08, Resource Future Program, CSIRO Wildlife and Ecology, Canberra, Australia, pp. 40-52.
- Jones**, R.N., 2000a: Managing uncertainty in climate change projections-issues for impact assessment. *Clim. Change*, **45**(3/4), 403-419.
- Jones**, R.N., 2000b: Analyzing the risk of climate change using an irrigation demand model. *Clim. Res.*, **14**, 89-100.
- Jones**, P.D., K.R. Briffa, T.P. Barnett, and S.F.B. Tett, 1998: High-resolution palaeoclimatic records for the last millennium: interpretation, integration and comparison with GCM control-run temperatures. *The Holocene*, **8**, 455-471.
- Jones**, R.N., K.J. Hennessy, and D.J. Abbs, 1999: *Climate Change Analysis Relevant to Jabiluka*, Attachment C. Assessment of the Jabiluka Project, Report of the Supervising Scientist to the World Heritage Committee. Environment Australia, Canberra.
- Jones**, R.N., K.J. Hennessy, C.M. Page, A.B. Pittock, R. Suppiah, K.J.E. Walsh, and P.H. Whetton, 2000: *An analysis of the effects of the Kyoto Protocol on Pacific Island countries. Part 2: regional climate change scenarios and risk assessment methods*. South Pacific Regional Environment Programme, Apia, Western Samoa (in press).
- Kaiser**, H.M., S.J. Riha, D.S. Wilks, D.G. Rossiter, and R. Sampath, 1993: A farm-level analysis of economic and agronomic impacts of gradual climate warming. *Am. J. Ag. Econ.*, **75**, 387-398.
- Kalkstein**, L.S. and J.S. Greene, 1997: An evaluation of climate/mortality relationships in large U.S. cities and possible impacts of a climate change. *Environmental Health Perspectives*, **105**, 84-93.
- Kalnay**, E., M. Kanamitsu, R. Kistler, W. Collins, D. Deaven, L. Gandin, M. Iredell, S. Saha, G. White, J. Woollen, Y. Zhu, A. Leetmaa, R. Reynolds, M. Chelliah, W. Ebisuzaki, W. Higgins, J. Janowiak, K. Mo, C. Ropelewski, J. Wang, R. Jenne, and D. Joseph, 1996: The NCEP/NCAR 40-year reanalysis project. *Bull. Am. Met. Soc.*, **77**, 437-472.
- Karl**, T.R., R.W. Knight, D.R. Easterling, and R.G. Quayle, 1996: Indices of climate change for the United States. *Bull. Am. Met. Soc.*, **77**, 279-292.
- Katz**, R.W., 1996: The use of stochastic models to generate climate change scenarios. *Clim. Change*, **32**, 237-255.
- Katz**, R.W., 2000: Techniques for estimating uncertainty in climate change scenarios and impact studies. *Clim. Res.* (accepted).
- Katz**, R.W. and B.G. Brown, 1992: Extreme events in a changing climate: variability is more important than averages. *Clim. Change*, **21**, 289-302.
- Katz**, R.W., and M.B. Parlange, 1996: Mixtures of stochastic processes: Application to statistical downscaling. *Clim. Res.*, **7**, 185-193.
- Kellogg**, W.W. and R. Schware, 1981: *Climate Change and Society: Consequences of Increasing Atmospheric Carbon Dioxide*. Westview Press, Boulder, Colorado, 178 pp.
- Kenny**, G.J., R.A. Warrick, B.D. Campbell, G.C. Sims, M. Camilleri, P.D. Jamieson, N.D. Mitchell, H.G. McPherson, and M.J. Salinger, 2000: Investigating climate change impacts and thresholds: an application of the CLIMACTS integrated assessment model for New Zealand agriculture. *Clim. Change*, **46**(1/2), 91-113.
- Kilsby**, C.G., P.E. O'Connell, and C.S. Fallows, 1998: Producing rainfall scenarios for hydrological impact modelling. In: *Hydrology in a Changing Environment* [Wheater, H. and C. Kirby (eds.)]. Wiley, Chichester, volume 1, pp. 33-42.
- Kittel**, T.G.F., N.A. Rosenbloom, T.H. Painter, D.S. Schimel, and VEMAP Modeling Participants, 1995: The VEMAP integrated database for modeling United States ecosystem/vegetation sensitivity to climate change. *J. Biogeography*, **22**, 857-862.
- Kittel**, T.G.F., J.A. Royle, C. Daly, N.A. Rosenbloom, W.P. Gibson, H.H. Fisher, D.S. Schimel, L.M. Berliner, and VEMAP2 Participants, 1997: A gridded historical (1895-1993) bioclimate dataset for the conterminous United States. In: *Proceedings of the 10th Conference on Applied Climatology*, 20-24 October 1997, Reno, NV, American Meteorological Society, Boston, pp. 219-222.
- Kittel**, T.G.F., F. Giorgi, and G.A. Meehl, 1998: Intercomparison of regional biases and doubled CO₂-sensitivity of coupled atmosphere-ocean general circulation model experiments. *Clim. Dyn.*, **14**, 1-15.
- Knutson**, T.R. and R.E. Tuleya, 1999: Increased hurricane intensities with CO₂-induced warming as simulated using the GFDL hurricane prediction system. *Clim. Dyn.*, **15**(7), 503-519.
- Knutson**, T.R., S. Manabe, and D. Gu, 1997: Simulated ENSO in a global coupled ocean-atmosphere model: Multidecadal amplitude modulation and CO₂ sensitivity. *J. Climate*, **10**, 138-161.
- Konrad**, C.E., 1998: An empirical approach for delineating fine scaled spatial patterns of freezing rain in the Appalachian region of the USA. *Clim. Res.*, **10**, 217-227.
- Kothavala**, Z., 1999: Extreme precipitation events and the applicability of global climate models to study floods and droughts. *Math. and Comp. in Simulation*, **43**, 261-268.
- Krishnamurti**, T.N., R. Correa-Torres, M. Latif, and G. Daughenbaugh, 1998: The impact of current and possibly future sea surface temperature anomalies on the frequency of Atlantic hurricanes. *Tellus*, **50A**, 186-210.
- Kuikka**, S. and O. Varis, 1997: Uncertainties of climatic change impacts in Finnish watersheds: a Bayesian network analysis of expert knowledge. *Boreal Environment Research*, **2**, 109-128.
- Lal**, M. and F. Giorgi, 1997: *Regional Climate Modelling and Applications*. Paper presented at the World Climate Research Programme: achievements, benefits and challenges, Geneva, Switzerland, 26-28 August, 1997, WMO, Geneva.
- Lal**, M. and H. Harasawa, 2000: Comparison of the present-day climate simulation over Asia in selected coupled atmosphere-ocean global climate models. *J. Met. Soc. Japan* (in press).
- Lal**, M., G.A. Meehl and J.M. Arblaster, 2000: Simulation of Indian summer monsoon rainfall and its intraseasonal variability. *Regional Environmental Change* (in press).
- Lamb**, P., 1987: On the development of regional climatic scenarios for policy oriented climatic impact assessment. *Bull. Am. Met. Soc.*, **68**, 1116-1123.
- Lapin**, M., E. Nieplová, and P. Fa?ko, 1995: Regional scenarios of temperature and precipitation changes for Slovakia (In Slovak with English abstract). *Monographs of the Slovak National Climate Program*, **3**, 17-57.
- Leemans**, R. and W. Cramer, 1991: *The IIASA Database for Mean Monthly Values of Temperature, Precipitation and Cloudiness on a Global Terrestrial Grid*. IIASA Report RR-91-18, Laxenburg, 63 pp.
- Leemans**, R. and A.M. Solomon, 1993: Modeling the potential change in yield and distribution of the earth's crops under a warmed climate. *Clim. Res.*, **3**, 79-96.
- Leemans**, R., E. Kreileman, G. Zuidema, J. Alcamo, M. Berk, G.J. van den Born, M. den Elzen, R. Hootsmans, M. Janssen, M. Schaeffer, A.M.C. Toet and H.J.M. de Vries, 1998: *The IMAGE User Support System: Global Change Scenarios from IMAGE 2.1*. National Institute of Public Health and the Environment, Bilthoven. October 1998. RIVM Publication, CD-rom.
- Legates**, D.R. and C.J. Willmott, 1990: Mean seasonal and spatial variability in gauge-corrected, global precipitation. *Int. J. Climatol.*, **10**, 111-128.
- Leggett**, J., W.J. Pepper and R.J. Swart, 1992: Emissions Scenarios for the IPCC: an Update. In: *Climate Change 1992. The Supplementary Report to the IPCC Scientific Assessment* [Houghton, J.T., B.A.

- Callander and S.K. Varney (eds.)]. Cambridge University Press, Cambridge, UK and New York, NY, USA, pp. 71-95.
- Liverman**, D., M. Dilley, and K. O'Brien, 1994: Possible impacts of climate change on maize yields in Mexico. In: *Implications of Climate Change for International Agriculture: Crop Modeling Study*. EPA Report 230-B-94-003, United States Environmental Protection Agency, Policy, Planning and Evaluation, Climate Change Division, Washington, DC.
- Lough**, J.M., T.M.L. Wigley, and J.P. Palutikof, 1983: Climate and climate impact scenarios for Europe in a warmer world. *J. Clim. Appl. Met.*, **22**, 1673-1684.
- Magalhães**, A.R. and M.H. Glantz, 1992: *Socioeconomic Impacts of Climate Variations and Policy Responses in Brazil*. United Nations Environment Programme/SEPLAN-CE/Esquel Foundation, Brasilia, Brazil.
- Mahlman**, J.D., 1997: Uncertainties in projections of human-caused climate warming. *Science*, **278**, 1416-1417 (in Policy Forum).
- Manabe**, W. and R.T. Wetherald, 1987: Large-scale changes of soil wetness induced by an increase in atmospheric carbon dioxide. *J. Atmos. Sci.*, **44**, 1211-1235.
- Mavromatis**, T. and P.D. Jones, 1999: Evaluation of HadCM2 and direct use of daily GCM data in impact assessment studies. *Clim. Change*, **41**, 583-614.
- McGregor**, J.J., 1997: Regional climate modeling. *Meteorological Atmospheric Physics*, **63**, 105-117.
- McInnes**, K.L., K.J.E. Walsh, and A.B. Pittock, 2000: *Impact of sea level rise and storm surges on coastal resorts*. A report for CSIRO Tourism Research: final report. CSIRO Atmospheric Research, Aspendale, Vic., 13 pp.
- Mearns**, L. O., 1995: Research issues in determining the effects of changing climatic variability on crop yields. In: *Climate Change and Agriculture: Analysis of Potential International Impacts* [Rosenzweig, C. (ed.)]. American Society of Agronomy Special Publication No. 58, Madison, ASA, Chapter 6, pp. 123-146.
- Mearns**, L. O., 1999: The effect of spatial and temporal resolution of climate change scenarios on changes in frequencies of temperature and precipitation extremes. In: *Elements of Change 1998* [Hassol, S.J. and J. Katzenberger (eds.)]. Aspen Global Change Institute, Aspen, CO, pp. 316-323.
- Mearns**, L.O., C. Rosenzweig, and R. Goldberg, 1992: Effect of changes in interannual climatic variability on CERES-Wheat yields: sensitivity and 2 \times CO₂ general circulation model studies. *Agric. For. Meteorol.*, **62**, 159-189.
- Mearns**, L.O., F. Giorgi, C. Shields, and L. McDaniel, 1995a: Analysis of the variability of daily precipitation in a nested modeling experiment: comparison with observations and 2 \times CO₂ results. *Global Planet. Change*, **10**, 55-78.
- Mearns**, L.O., F. Giorgi, C. Shields, and L. McDaniel, 1995b: Analysis of the diurnal range and variability of daily temperature in a nested model experiment: comparison with observations and 2 \times CO₂ results. *Clim. Dyn.*, **11**, 193-209.
- Mearns**, L. O., C. Rosenzweig, and R. Goldberg, 1996: The effect of changes in daily and interannual climatic variability on CERES-wheat: a sensitivity study. *Clim. Change*, **32**, 257-292.
- Mearns**, L. O., C. Rosenzweig, and R. Goldberg, 1997: Mean and variance change in climate scenarios: methods, agricultural applications, and measures of uncertainty. *Clim. Change*, **35**, 367-396.
- Mearns**, L. O., W. Easterling, and C. Hays 1998: *The Effect of Spatial Scale of Climate Change Scenarios on the Determination of Impacts: An Example of Agricultural Impacts on the Great Plains*. Proceedings of the International Workshop on Regional Modeling of the General Monsoon System in Asia, Beijing, October 20—23, START Regional Center for Temperate East Asia, TEACOM Report No. 4, pp. 70-73.
- Mearns**, L.O., T. Mavromatis, E. Tsvetsinskaya, C. Hays, and W. Easterling, 1999: Comparative responses of EPIC and CERES crop models to high and low resolution climate change scenario. *J. Geophys. Res.*, **104(D6)**, 6623-6646.
- Mearns**, L.O., G. Carbone, W. Gao, L. McDaniel, E. Tsvetsinskaya, B. McCarl, and R. Adams, 2000a: The issue of spatial scale in integrated assessments: An example of agriculture in the Southeastern U.S. In: *Preprints of the American Meteorological Society of America Annual Meeting*, 9-14 January, Long Beach, CA. AMS, Boston, MA, pp. 38-41.
- Mearns**, L.O., G. Carbone, L. McDaniel, W. Gao, B. McCarl, R. Adams, and W. Easterling, 2000b: The importance of spatial scale of climate scenarios for regional climate change impacts analysis: implications for regional climate modeling activities. In: *Preprints of the Tenth PSU/NCAR Mesoscale Model Users' Workshop*, June 21-22 2000, National Center for Atmospheric Research, Mesoscale and Microscale Meteorology Division, Boulder, Colorado, pp. 127-130.
- Mearns**, L. O., W. Easterling, and C. Hays, 2001: Comparison of agricultural impacts of climate change calculated from high and low resolution climate model scenarios: part I: the uncertainty due to spatial scale. *Clim. Change* (in press).
- Mitchell**, J.F.B., 1990: Greenhouse warming: is the mid-Holocene a good analogue? *J. Climate*, **3**, 1177-1192.
- Mitchell**, J.F.B., S. Manabe, V. Meleshko, and T. Tokioka, 1990: Equilibrium climate change - and its implications for the future. In: *Climate Change: The IPCC Scientific Assessment. Report prepared by Working Group I* [Houghton, J.T., G.J. Jenkins, and J.J. Ephraums (eds.)]. Cambridge University Press, Cambridge, United Kingdom, and New York, NY, USA, pp. 131-164.
- Mitchell**, J.F.B., T.C. Johns, M. Eagles, W.J. Ingram, and R.A. Davis, 1999: Towards the construction of climate change scenarios. *Clim. Change*, **41**, 547-581.
- Morgan**, M.G. and M. Henrion, 1990: *Uncertainty: A Guide to Dealing with Uncertainty in Quantitative Risk and Policy Analysis*. Cambridge University Press, Cambridge, UK.
- Morgan**, M.G. and D. Keith, 1995: Subjective judgements by climate experts. *Envir. Sci. Tech.*, **29**, 468-476.
- Morgan**, M.G. and H. Dowlatabadi, 1996: Learning from integrated assessment of climate change. *Clim. Change*, **34**, 337-368.
- Morita**, T. and J. Robinson, 2001: Greenhouse Gas Emission Mitigation Scenarios and Implications. In *Climate Change 2001: Mitigation*. Contribution of Working Group III to the IPCC Third Assessment Report.
- Murphy**, J.M., 1999: An evaluation of statistical and dynamical techniques for downscaling local climate. *J. Climate*, **12(8)**, 2256-2284.
- Nakićenović**, N., J. Alcamo, G. Davis, B. de Vries, J. Fenner, S. Gaffin, K. Gregory, A. Grübler, T. Y. Jung, T. Kram, E. L. La Rovere, L. Michaelis, S. Mori, T. Morita, W. Pepper, H. Pitcher, L. Price, K. Raihi, A. Roehrl, H-H. Rogner, A. Sankovski, M. Schlesinger, P. Shukla, S. Smith, R. Swart, S. van Rooijen, N. Victor, Z. Dadi, 2000: *IPCC Special Report on Emissions Scenarios*, Cambridge University Press, Cambridge, United Kingdom and New York, NY, USA, 599 pp.
- NDU**, 1978: *Climate Change to the Year 2000*. Dept. of Defense, National Defense University, US Government Printing Office, Washington, D.C., 109 pp.
- Neilson**, R.P., I.C. Prentice, B. Smith, 1997: Simulated changes in vegetation distribution under global warming. In: *The Regional Impacts of Climate Change: An Assessment of Vulnerability. A Special Report of IPCC Working Group II* [Watson, R.T., M.C. Zinyowera, and R.H. Moss (eds.)]. Cambridge University Press, Cambridge, United Kingdom and New York, NY, USA, pp. 439-456.
- New**, M., 1999: Uncertainty in representing the observed climate. In: *Proceedings of the ECLAT-2 Helsinki Workshop, 14-16 April, 1999* [Carter, T.R., M. Hulme, and D. Viner (eds.)]. Climatic Research

- Unit, Norwich, UK, pp. 59-66.
- New**, M. and M.Hulme, 2000: Representing uncertainties in climate change scenarios: a Monte Carlo approach. *Integrated Assessment*, **1**, 203-213.
- New**, M., M. Hulme, M. and P.D. Jones, 1999: Representing twentieth century space-time climate variability. Part 1: development of a 1961-90 mean monthly terrestrial climatology. *J. Climate*, **12**, 829-856.
- New**, M., M. Hulme, and P.D. Jones, 2000: Representing twentieth century space-time climate variability. Part 2: development of 1901-96 monthly grids of terrestrial surface climate. *J. Climate*, **13(13)**, 2217-2238.
- Oglesby**, R.J. and B. Saltzman, 1992: Equilibrium climate statistics of a general circulation model as a function of atmospheric carbon dioxide, part I. *J. Climate*, **5**, 66-92.
- Osborn**, T.J., 1996: Comment on Climate drift in a global ocean general circulation model. *J. Phys. Oceanogr.*, **26**, 166a-1663.
- Osborn**, T.J., 1997: Areal and point precipitation intensity changes: Implications for the application of climate models. *Geophys. Res. Lett.*, **24**, 2829-2832.
- Osborn**, T.J., K.R. Briffa, S.F.B. Tett, P.D. Jones, and R.M. Trigo, 2000: Evaluation of the North Atlantic Oscillation as simulated by a coupled climate model. *Clim. Dyn.*, **15(9)**, 685-702.
- Parkinson**, S.D. and P.C. Young, 1998: Uncertainty and sensitivity in global carbon cycle monitoring. *Clim. Res.*, **9**, 157-174.
- Parry**, M.L. and M. Livermore (eds.), 1999: A new assessment of the global effects of climate change. *Global Environ. Change*, **9**, S1-S107, Supplementary Issue.
- Parry**, M.L., T.R. Carter, and M. Hulme, 1996: What is a dangerous climate change? *Global Environ. Change*, **6**, 1-6.
- Parry**, M.L., T.R. Carter, and N.T. Konijn (eds.), 1988: *The Impact of Climatic Variations on Agriculture. Volume 1. Assessments in Cool Temperate and Cold Regions*. Kluwer, Dordrecht, The Netherlands, 876 pp.
- Piper**, S.C. and E.F. Stewart, 1996: A gridded global data set of daily temperature and precipitation for terrestrial biospheric modelling. *Global Biogeochem. Cycles*, **10**, 757-782.
- Pittock**, A.B., 1989: Book review: Societal Responses to Regional Climatic Change [Glantz, M.] *Bull. Am. Met. Soc.*, **70**, 1150-1152.
- Pittock**, A.B., 1993: Climate scenario development. In: *Modelling Change in Environmental Systems* [Jakeman, A.J., M.B. Beck, and M.J. McAleer (eds.)]. John Wiley, Chichester, New York, pp. 481-503.
- Pittock**, A.B., 1995: Comments on climate change scenario development. *Math. Comput. Modelling*, **21**, 1-4.
- Pittock**, A.B. and M.J. Salinger, 1982: Toward regional scenarios for a CO₂-warmed earth. *Clim. Change*, **4**, 23-40.
- Prinn**, R. H. Jacoby, A. Sokolov, C. Wang, X. Xiao, Z. Yang, R. Eckaus, P. Stone, D. Ellerman, J. Melillo, J. Fitzmaurice, D. Kicklighter, Y. Liu, and G. Holian, 1999: Integrated global system model for climate policy analysis: Feedbacks and sensitivity studies. *Clim. Change*, **41**, 469-546.
- Racksko**, P., L. Szeidl, and M. Semenov, 1991: A serial approach to local stochastic weather models. *Ecological Modeling*, **57**, 27-41.
- Räisänen**, J., 1997: Objective comparison of patterns of CO₂ induced climate change in coupled GCM experiments. *Clim. Dyn.*, **13**, 197-212.
- Räisänen**, J., 1999: Internal variability as a cause of qualitative inter-model disagreement on anthropogenic climate changes *Theor. Appl. Climatol.*, **64**, 1-13.
- Ramaswamy**, V. and T.C. Chen, 1997: Linear additivity of climate response for combined albedo and greenhouse perturbations. *Geophys. Res. Lett.*, **24**, 567-570.
- Raper**, S.C.B., T.M.L. Wigley, and R.A. Warrick, 1996: Global sea level rise: Past and future. In: *Sea-Level Rise and Coastal Subsidence: Causes, Consequences and Strategies* [Milliman, J. and B.U. Haq (eds.)]. Kluwer Academic Publishers, Dordrecht, The Netherlands, pp. 11-45.
- Richardson**, C.W., 1981: Stochastic simulation of daily precipitation, temperature, and solar radiation. *Water Resour. Res.*, **17**, 182-190.
- Riha**, S. J., D. W. Wilks, and P. Simoens, 1996: Impact of temperature and precipitation variability on crop model predictions. *Clim. Change*, **32(3)**, 293-311.
- Risbey**, J.S., 1998: Sensitivities of water supply planning decisions to streamflow and climate scenario uncertainties. *Water Policy*, **1**, 321-340.
- Risbey**, J.S. and P.H. Stone, 1996: A case study of the adequacy of GCM simulations for input to regional climate change assessments. *J. Climate*, **9**, 1441-1467.
- Robinson**, P. J., and P. L. Finkelstein, 1989: *Strategies for Development of Climate Scenarios*. Final Report to the U. S. Environmental Protection Agency. Atmosphere Research and Exposure Assessment Laboratory, Office of Research and Development, USEPA, Research Triangle Park, NC, 73 pp.
- Robock**, A., R.P. Turco, M.A. Harwell, T.P. Ackerman, R. Andressen, H.S. Chang, and M.V.K. Sivakumar, 1993: Use of general circulation model output in the creation of climate change scenarios for impact analysis. *Clim. Change*, **23**, 293-355.
- Rodbell**, D., G. O. Seltzer, D. M. Anderson, D. B. Enfield, M. B. Abbott, and J. H. Newman, 1999: A high-resolution 15000 year record of El Niño driven alluviation in southwestern Ecuador. *Science*, **283**, 516-520.
- Rosenberg**, N.J., P.R. Crosson, K.D. Frederick, W.E. Easterling, M.S. McKenney, M.D. Bowes, R.A. Sedjo, J. Darmstadter, L.A. Katz, and K.M. Lemon, 1993: Paper 1. The MINK methodology: background and baseline. *Clim. Change*, **24**, 7-22.
- Rosenthal**, D.H., H.K. Gruenspecht, and E.A. Moran, 1995: Effects of global warming on energy use for space heating and cooling in the United States. *Energy J.*, **16**, 41-54.
- Rosenzweig**, C. 1985: Potential CO₂-induced climate effects on North American wheat-producing regions. *Clim. Change*, **4**, 239-254.
- Rosenzweig**, C. and A. Iglesias (eds.), 1994: *Implications of Climate Change for International Agriculture: Crop Modeling Study*. EPA Report 230-B-94-003, United States Environmental Protection Agency, Policy, Planning and Evaluation, Climate Change Division, Washington, DC.
- Rosenzweig**, C. and M. L. Parry, 1994: Potential impact of climate change on world food supply. *Nature*, **367**, 133-137.
- Rosenzweig**, C., J. Phillips, R. Goldberg, J. Carroll, and T. Hodges, 1996: Potential impacts of climate change on citrus and potato production in the US. *Agricultural Systems*, **52**, 455-479.
- Rotmans**, J., M. Hulme, and T.E. Downing, 1994: Climate change implications for Europe: an application of the ESCAPE model. *Global Env. Change*, **4**, 97-124.
- Saarikko**, R.A., and T.R. Carter, 1996: Estimating regional spring wheat development and suitability in Finland under climatic warming. *Clim. Res.*, **7**, 243-252.
- Santer**, B.D., T.M.L. Wigley, M.E. Schlesinger, and J.F.B. Mitchell, 1990: *Developing Climate Scenarios from Equilibrium GCM results*. Report No. 47, Max-Planck-Institut-für-Meteorologie, Hamburg, 29 pp.
- Santer**, B.D., J.J. Hnilo, T.M.L. Wigley, J.S. Boyle, C. Doutriaux, M. Fiorino, D.E. Parker, and K.E. Taylor, 1999: Uncertainties in observationally based estimates of temperature change in the free atmosphere. *J. Geophys. Res.*, **104**, 6305-6333.
- Schimel**, D.S., W. Emanuel, B. Rizzo, T. Smith, F.I. Woodward, H. Fisher, T.G.F. Kittel, R. McKeown, T. Painter, N. Rosenbloom, D.S. Ojima, W.J. Parton, D.W. Kicklighter, A.D. McGuire, J.M. Melillo, Y. Pan, A. Haxeltine, C. Prentice, S. Sitch, K. Hibbard, R. Nemani, L. Pierce, S. Running, J. Borchers, J. Chaney, R. Neilson, and B.H. Braswell, 1997: Continental scale variability in ecosystem processes:

- models, data, and the role of disturbance. *Ecological Monographs*, **67**(2), 251-271.
- Schlesinger**, M.E., N. Andronova, A. Ghanem, S. Malyshev, T. Reichler, E. Rozanov, W. Wang, and F. Yang, 1997: *Geographical Scenarios of Greenhouse Gas and Anthropogenic-Sulfate-Aerosol Induced Climate Changes*. CRG manuscript, July 1997, University of Illinois, Department of Atmospheric Sciences, Urbana, IL, 85 pp.
- Schlesinger**, M.E., S. Malyshev, E.V. Rozanov, F. Yang, N.G. Andronova, B. de Vries, A. Grüber, K. Jiang, T. Masui, T. Morita, J. Penner, W. Pepper, A. Sankovski and Y. Zhang, 2000: Geographical distributions of temperature change for scenarios of greenhouse gas and sulfur dioxide emissions. *Tech. Forecast. Soc. Change*, **65**, 167-193.
- Schneider**, S. H., P. H. Gleick and L. O. Mearns, 1990: Prospects for Climate Change. In: *Climate and Water: Climate Change, Climatic Variability, and the Planning and Management of U. S. Water Resources*. Wiley Press, New York, Chapter 3, pp. 41-73.
- Schreider**, S. Yu, A.J. Jakeman, A.B. Pittock, and P.H. Whetton, 1996: Estimation of possible climate change impacts on water availability, extreme flow events and soil moisture in the Goulburn and Ovens Basins, Victoria. *Clim. Change*, **34**, 513-546.
- Schubert**, M., J. Perlitz, R. Blender, K. Fraedrich, and F. Lunkeit, 1998: North Atlantic cyclones in CO₂-induced warm climate simulations: Frequency, intensity, and tracks. *Clim. Dyn.*, **14**, 827-837.
- Semenov**, M.A. and J.R. Porter, 1995: Climatic variability and the modelling of crop yields. *Agric. For. Meteorol.*, **73**, 265-283.
- Semenov**, M. A. and E. Barrow, 1997: Use of a stochastic weather generator in the development of climate change scenarios. *Clim. Change*, **35**, 397-414.
- Semenov**, M.A. and R.J. Brooks, 1999: Spatial interpolation of the LARS-WG stochastic weather generator in Great Britain. *Clim. Res.*, **11**, 137-148.
- Severinghaus**, J.P., T. Sowers, E. Brook, R.B. Alley, and M.L. Bender, 1998: Timing of abrupt climate change at the end of the Younger Dryas interval from thermally fractionated gases in polar ice. *Nature*, **391**, 141-146.
- Shabalova**, M.V., and G.P. Können, 1995: Climate change scenarios: comparisons of paleo-reconstructions with recent temperature changes. *Clim. Change*, **29**, 409-428.
- Skelly**, W.C. and A. Henderson-Sellers, 1996: Grid box or grid point: what type of data do GCMs deliver to climate impacts researchers? *Int. J. Climatol.*, **16**, 1079-1086.
- Smith**, J.B. and G.J. Pitts, 1997: Regional climate change scenarios for vulnerability and adaptation assessments. *Clim. Change*, **36**, 3-21.
- Smith**, J.B. and M. Hulme, 1998: Climate change scenarios. In: *Handbook on Methods of Climate Change Impacts Assessment and Adaptation Strategies* [Feenstra, J., I. Burton, J.B. Smith, and R.S.J. Tol (eds.)]. UNEP/IES, Version 2.0, October, Amsterdam, Chapter 3.
- Smith**, J.B. and D.A. Tirpak (eds.) 1989: *The Potential Effects of Global Climate Change on the United States*. Report to Congress, United States Environmental Protection Agency, EPA-230-05-89-050, Washington, D.C., 409 pp.
- Smith**, J.B., S. Huq, S. Lenhart, L.J. Mata, I. Neme?ová, and S. Toure (eds.), 1996: *Vulnerability and Adaptation to Climate Change: Interim Results from the U.S. Country Studies Program*. Kluwer, Dordrecht, The Netherlands, 366 pp.
- Stewart**, T.R. and M.H. Glantz, 1985: Expert judgment and climate forecasting: a methodological critique of Climate Change to the Year 2000. *Clim. Change*, **7**, 159-183.
- Stone**, M.C., R.H. Hotchkiss, C.M. Hubbard, T.A. Fontaine, L.O. Mearns, and J.G. Arnold, 2001: Impacts of climate change on the water yield of the Missouri River. *J. Am. Water Resour. As.* (accepted).
- Stouffer**, R.J., S. Manabe, and K.Ya. Vinnikov, 1994: Model assessment of the role of natural variability in recent global warming. *Nature*, **367**, 634-636.
- Terjung**, W.H., D.M. Liverman, J.T. Hayes, and collaborators, 1984: Climatic change and water requirements for grain corn in the North American Great Plains. *Clim. Change*, **6**, 193-220.
- Tett**, S.F.B., T.C. Johns, and J.F.B. Mitchell, 1997: Global and regional variability in a coupled AOGCM. *Clim. Dyn.*, **13**, 303-323.
- Timmermann**, A., J. Oberhuber, A. Bacher, M. Esch, M. Latif, and E. Roeckner, 1999: Increased El Niño frequency in a climate model forced by future greenhouse warming. *Nature*, **398**, 694-696.
- Titus**, J.G. and V. Narayanan, 1996: The risk of sea level rise. *Clim. Change*, **33**, 151-212.
- Tol**, R.S.J. and A.F. de Vos, 1998: A Bayesian statistical analysis of the enhanced greenhouse effect. *Clim. Change*, **38**, 87-112.
- Torn**, M.S and J.S. Fried, 1992: Predicting the impacts of global warming on wildland fire. *Clim. Change*, **21**, 257-274.
- Toth**, L. and M. Mwandoisa, 2001: Decision-making Frameworks. In *Climate Change 2001: Mitigation*. Contribution of Working Group III to the IPCC Third Assessment Report, Cambridge University Press.
- Velichko**, A. A., O. K. Borisova, E. M. Zelikson, and V. P Nechaev, 1995a: Permafrost and vegetation response to global warming in North Eurasia. In: *Biotic Feedbacks in the Global Climatic System*. New York, Oxford, Oxford University Press, pp. 134-156.
- Velichko**, A.A., L.O. Karpachevsky, and T.D. Morozova, 1995b: Water reserves in soils under global climate warming: an approach to forecasting for Eastern Europe as an example. *Pochvovedenie*, **8**, 933-942 (in Russian).
- Vinnikov**, K. Ya. and P. Ya. Groisman, 1979: An empirical model of present-day climatic changes. *Meteor. Gidrol.*, **3**, 25-28 (in Russian).
- Vinocur**, M.G., R.A. Seiler, and L.O. Mearns, 2000: Forecasting the impact of climate variability on peanut crop production in Argentina. In: *Proceedings of the International Forum on Climate Prediction, Agriculture and Development*. International Research Institute for Climate Prediction (IRI), Palisades, NY (in press).
- Visser**, H., R.J.M. Folkert, J. Hoekstra, and J.J. deWolff, 2000: Identifying key sources of uncertainty in climate change projections. *Clim. Change*, **45(3/4)**, 421-457.
- Voet**, P. van der, K. Kramer, and C.A. van Diepen, 1996: *Parametrization of the Richardson Weather Generator within the European Union*. DLO Winand Staring Centre Report 92, Wageningen, The Netherlands, 73 pp.
- von Storch**, H., 1995: Inconsistencies at the interface of climate impact studies and global climate research. *Meteor. Z.*, **4 NF**, 72-80.
- von Storch**, J.S., V. Kharin, U. Cubasch, G.C. Hergel, D. Schriever, H. von Storch, and E. Zorita, 1997: A description of a 1260-year control integration with the coupled ECHAM1/LSG general circulation model. *J. Climate*, **10**, 1525-1543.
- Walker**, B., W. Steffen, J. Canadell and J. Ingram (eds.), 1999: *The Terrestrial Biosphere and Global Change: Implications for Natural and Managed Ecosystems*. Cambridge University Press, Cambridge, 439 pp.
- Walsh**, K.J.E. and B.F. Ryan, 2000: Tropical cyclone intensity increase near Australia as a result of climate change. *J. Climate*, **13**, 3029-3036.
- Walsh**, K., R. Allan, R. Jones, B. Pittock, R. Suppiah, and P. Whetton, 1999: *Climate Change in Queensland under Enhanced Greenhouse Conditions*. First Annual Report, CSIRO Atmospheric Branch, Aspendale, Victoria, Australia, 84 pp.
- Wang**, Y. P., and D. J. Connor, 1996: Simulation of optimal development for spring wheat at two locations in southern Australia under present and changed climate conditions. *Agric. For. Meteorol.*, **79**, 9-28.
- Wang**, J. and L. Erda, 1996: The Impacts of potential climate change and climate variability on simulated maize production in China. *Water Air Soil Pollut.*, **92**, 75-85.
- Wang**, Q. J., R. J. Nathan, R. J. Moran, and B. James, 1999: *Impact of climate Changes on the Security of the Water Supply of the Campaspe System*. Proceedings of 25th Hydrology and Water Resources

- Symposium, Vol. 1, 6-8 July 1999, Brisbane, Institution of Engineers, Australia, Water 99 Joint Congress, pp. 135-140.
- Warrick, R.A.**, 1984: The possible impacts on wheat production of a recurrence of the 1930s drought in the U.S. Great Plains. *Clim. Change*, **6**, 5-26.
- Warrick, R.A.**, C. Leprovost, M.F. Meier, J. Oerlemans, P.L. Woodworth, R.B. Alley, R.A. Bindschadler, C.R. Bentley, R.J. Braithwaite, J.R. de Wolde, B.C. Douglas, M. Dyurgerov, N.C. Flemming, C. Genton, V. Gornitz, J. Gregory, W. Haeberli, P. Huybrechts, T. Jóhannesson, U. Mikolajewicz, S.C.B. Raper, D.L. Sahagian, R.S.W. van de Wal and T.M.L. Wigley, 1996: Changes in sea level. In: *Climate Change 1995: The Science of Climate Change. Contribution of Working Group I to the Second Assessment Report of the Intergovernmental Panel on Climate Change* [Houghton, J.T., L.G.M. Filho, B.A. Callander, N. Harris, A. Kattenberg and K. Maskell (eds.)]. Cambridge University Press, Cambridge, United Kingdom and New York, NY, USA, pp. 359-405.
- Webb, T., III**, and T.M.L. Wigley, 1985: What past climates can indicate about a warmer world. In: *Projecting the Climatic Effects of Increasing Carbon Dioxide* [MacCracken, M.C. and F.M. Luther (eds.)]. United States Department of Energy, Office of Energy Research, DOE/ER-0237, Washington, D.C., pp. 237-257.
- Whetton, P. H.**, 1998: Climate change impacts on the spatial extent of snow-cover in the Australian Alps. In: *Snow: A Natural History, An Uncertain Future* [K. Green (ed.)]. Australian Alps Liaison Committee, Canberra, pp. 195-206.
- Whetton, P.H.** and A.B. Pittock, 1991: *Australian Region Intercomparison of the Results of some Greenhouse General Circulation Modelling Experiments*. Tech. Paper No. 21, CSIRO Div. of Atmospheric Research, Melbourne, Australia, 73 pp.
- Whetton, P.H.**, A.M. Fowler, M.R. Haylock, and A.B. Pittock, 1993: Implications of climate change due to the enhanced greenhouse effect on floods and droughts in Australia. *Climatic Change*, **25(3-4)**, 289-317.
- Whetton, P.H.**, M.R. Haylock, and R. Galloway, 1996: Climate change and snow-cover duration in the Australian Alps. *Clim. Change*, **32(4)**, 447-479.
- Whetton, P.H.**, J.J. Katzfey, K.C. Nguyen, J.L. McGregor, C.M. Page, T.I. Elliott, and K.J. Hennessy, 1998a: *Fine Resolution Climate Change Scenarios for New South Wales. Part 2: Climatic Variability*. Annual Report, 1996/7, CSIRO, Australia, 51 pp.
- Whetton, P. H.**, Z. Long, and I.N. Smith, 1998b: Comparison of simulated climate change under transient and stabilised increased CO₂ conditions. In: *Coupled Climate Modelling: Abstracts of Presentations at the Tenth Annual BMRC Modelling Workshop, BMRC, Melbourne* [P. J. Meighen (ed.)]. BMRC Research Report, 69, Melbourne, Bureau of Meteorology Research Centre, pp. 93-96.
- White, M.R.**, 1985: *Characterization of Information Requirements for Studies of CO₂ Effects: Water Resources, Agriculture, Fisheries, Forests, and Human Health*. US Dept. of Energy, Office of Energy Research, DOE/ER-0236, Washington, DC.
- Widmann, M.** and C.S. Bretherton, 2000: Validation of mesoscale precipitation in the NCEP reanalysis using a new grid-cell data set for the northwestern United States. *J.Climate*, **13(11)**, 936-950.
- Wigley, T.M.L.**, 1999: *The Science of Climate Change: Global and US Perspectives*. Pew Center on Global Climate Change, Arlington, VA, 48 pp.
- Wigley, T.M.L.**, P.D. Jones, and P.M. Kelly, 1980: Scenarios for a warm, high-CO₂ world. *Nature*, **288**, 17-21.
- Wilby, R.L.**, 1998: Statistical downscaling of daily precipitation using daily airflow and seasonal teleconnection indices. *Clim. Res.*, **10**, 163-178.
- Wilby, R.L.** and T.M.L. Wigley, 1997: Downscaling general circulation model output: a review of methods and limitations. *Progress in Physical Geography*, **21**, 530-548.
- Wilby, R.L.**, B. Greenfield, and C. Glenny, 1994: A coupled synoptic-hydrological model for climate change impact assessment. *Journal of Hydrology*, **153**, 265-290.
- Wilby, R.L.**, T.M.L. Wigley, D. Conway, P.D. Jones, B.C. Hewitson, J. Main, and D.S. Wilks, 1998: Statistical downscaling of General Circulation Model output: a comparison of methods. *Water Resources Research*, **34**, 2995-3008.
- Wilby, R.L.**, L.E. Hay, and G.H. Leavesley, 1999: A comparison of downscaled and raw GCM output: implications for climate change scenarios in the San Juan River Basin, Colorado. *J. Hydrol.* **225**, 67-91.
- Wilks, D. S.**, 1992: Adapting stochastic weather generation algorithms for climate change studies. *Clim.Change*, **22**, 67-84.
- Wilks, D. S.** and R.L. Wilby, 1999: The weather generation game: A review of stochastic weather models. *Progress in Physical Geography*, **23**, 329-358.
- Williams, G.D.V.**, R.A. Fautley, K.H. Jones, R.B. Stewart, and E.E. Wheaton, 1988: Estimating effects of climatic change on agriculture in Saskatchewan, Canada. In: *The Impact of Climatic Variations on Agriculture, Volume 1, Assessments in Cool Temperate and Cold Regions* [Parry, M.L., T.R. Carter, and N.T. Konijn (eds.)]. Kluwer, Dordrecht, The Netherlands, pp. 219-379.
- Woo, M.K.**, 1992: Application of stochastic simulation to climatic change studies. *Clim.Change*, **20**, 313-330.
- Woolhiser, D.A.**, T.O. Keefer, and K.T. Redmond, 1993: Southern Oscillation effects on daily precipitation in the southwestern United States. *Water Resour. Res.*, **29**, 1287-1295.
- Wotton, B.M.**, B. J. Stocks, M.D. Flannigan, R. LaPrise, and J-P Blanchet, 1998: Estimating future 2xCO₂ fire climates in the boreal forest of Canada using a regional climate model. In: *Proceedings of Third International Conference on Forest Fire Research and the 14th Conference in Fire and Forest Meteorology*. University of Coimbra, Portugal, pp. 1207-1221.
- Xiao, X.**, D.W. Kicklighter, J.M. Melillo, A.D. McGuire, P.H. Stone and A. P. Sokolov, 1997: Linking a global terrestrial biogeochemical model with a 2-dimensional climate model: Implications for global carbon budget. *Tellus*, **49B**, 18-37.
- Xie, P.** and P.A. Arkin, 1997: Global precipitation: a 17-year monthly analysis based on gauge observations, satellite estimates, and numerical model outputs. *Bull. Am. Met. Soc.*, **78**, 2539-2558.
- Yohe, G.W.** and M.E. Schlesinger, 1998: Sea-level change: the expected economic cost of protection or abandonment in the United States. *Clim. Change*, **38**, 447-472.

14

Advancing Our Understanding

Co-ordinating Lead Author

B. Moore III

Lead Authors

W.L. Gates, L.J. Mata, A. Underdal

Contributing Author

R.J. Stouffer

Review Editors

B. Bolin, A. Ramirez Rojas

Contents

Executive Summary	771		
14.1 Introduction	772	14.2.4 The Global Carbon Cycle	777
		14.2.4.1 The marine carbon system	778
		14.2.4.2 The terrestrial system	779
14.2 The Climate System	772	14.2.5 Precipitation, Soil Moisture, and River Flow: Elements of the Hydrological Cycle	779
14.2.1 Overview	772	14.2.6 Trace Gases, Aerosols, and the Climate System	781
14.2.2 Predictability in a Chaotic System	773		
14.2.2.1 Initialisation and flux adjustments	773		
14.2.2.2 Balancing the need for finer scales and the need for ensembles	774	14.3 The Human System	782
14.2.2.3 Extreme events	774	14.3.1 Overview	782
14.2.2.4 Organised variability	775	14.3.2 Humans: Drivers of Global Change: Recipients of Global Change	783
14.2.3 Key Sub-systems and Phenomena in the Physical-Climate System	775		
14.2.3.1 Clouds	775	14.4 Outlook	784
14.2.3.2 Thermohaline circulation	776		
14.2.3.3 Arctic sea ice	777	References	785

Executive Summary

Further work is required to improve the ability to detect, attribute, and understand climate change, to reduce uncertainties, and to project future climate changes. In particular, there is a need for additional systematic observations, modelling and process studies. A serious concern is the decline of observational networks. Further work is needed in eight broad areas:

- *Reverse the decline of observational networks in many parts of the world.* Unless networks are significantly improved, it may be difficult or impossible to detect climate change over large parts of the globe.
- *Sustain and expand the observational foundation for climate studies by providing accurate, long-term, consistent data including implementation of a strategy for integrated global observations.* Given the complexity of the climate system and the inherent multi-decadal time-scale, there is a need for long-term consistent data to support climate and environmental change investigations and projections. Data from the present and recent past, climate-relevant data for the last few centuries, and for the last several millennia are all needed. There is a particular shortage of data in polar regions and data for the quantitative assessment of extremes on the global scale.
- *Understand better the mechanisms and factors leading to changes in radiative forcing; in particular, improve the observations of the spatial distribution of greenhouse gases and aerosols.* It is particularly important that improvements are realised in deriving concentrations from emissions of gases and particularly aerosols, and in addressing biogeochemical sequestration and cycling, and specifically, in determining the spatial-temporal distribution of carbon dioxide (CO_2) sources and sinks, currently and in the future. Observations are needed that would decisively improve our ability to model the carbon cycle; in addition, a dense and well-calibrated network of stations for monitoring CO_2 and oxygen (O_2) concentrations will also be required for international verification of carbon sinks. Improvements in deriving concentrations from emissions of gases and in the prediction and assessment of direct and indirect aerosol forcing will require an integrated effort involving *in situ* observations, satellite remote sensing, field campaigns and modelling.
- *Understand and characterise the important unresolved processes and feedbacks, both physical and biogeochemical, in the climate system.* Increased understanding is needed to improve prognostic capabilities generally. The interplay of observation and models will be the key for progress. The rapid forcing of a non-linear system has a high prospect of producing surprises.
- *Address more completely patterns of long-term climate variability including the occurrence of extreme events.* This topic arises both in model calculations and in the climate system. In simulations, the issue of climate drift within model calculations needs to be clarified better in part because it compounds the difficulty of distinguishing signal and noise. With respect to the long-term natural variability in the climate system *per se*, it is important to understand this variability and to expand the emerging capability of predicting patterns of organised variability such as El Niño-Southern Oscillation (ENSO). This predictive capability is both a valuable test of model performance and a useful contribution in natural resource and economic management.
- *Improve methods to quantify uncertainties of climate projections and scenarios, including development and exploration of long-term ensemble simulations using complex models.* The climate system is a coupled non-linear chaotic system, and therefore the long-term prediction of future climate states is not possible. Rather the focus must be upon the prediction of the probability distribution of the system's future possible states by the generation of ensembles of model solutions. Addressing adequately the statistical nature of climate is computationally intensive and requires the application of new methods of model diagnosis, but such statistical information is essential.
- *Improve the integrated hierarchy of global and regional climate models with a focus on the simulation of climate variability, regional climate changes, and extreme events.* There is the potential for increased understanding of extremes events by employing regional climate models; however, there are also challenges in realising this potential. It will require improvements in the understanding of the coupling between the major atmospheric, oceanic, and terrestrial systems, and extensive diagnostic modelling and observational studies that evaluate and improve simulation performance. A particularly important issue is the adequacy of data needed to attack the question of changes in extreme events.
- *Link models of the physical climate and the biogeochemical system more effectively, and in turn improve coupling with descriptions of human activities.* At present, human influences generally are treated only through emission scenarios that provide external forcings to the climate system. In future more comprehensive models, human activities need to begin to interact with the dynamics of physical, chemical, and biological sub-systems through a diverse set of contributing activities, feedbacks, and responses.

Cutting across these foci are crucial needs associated with strengthening international co-operation and co-ordination in order to utilise better scientific, computational, and observational resources. This should also promote the free exchange of data among scientists. A special need is to increase the observational and research capacities in many regions, particularly in developing countries. Finally, as is the goal of this assessment, there is a continuing imperative to communicate research advances in terms that are relevant to decision making.

The challenges to understanding the Earth system, including the human component, are daunting, but these challenges simply must be met.

14.1 Introduction

There has been encouraging progress over this first decade of the IPCC process. We understand better the coupling of the atmosphere and ocean. Significant steps have been taken in linking the atmosphere and the terrestrial systems although the focus tends to be on water-energy and the biosphere with fixed vegetation patterns. Even so, revealing and unexpected teleconnections are being discovered; moreover, progress is being made towards model structures and data sets that will allow implementation of coupled atmosphere-ocean-terrestrial models that include key biological-biogeochemical feedbacks. There is also encouraging progress in developing integrated assessment models that couple economic activity, with associated emissions and impacts, with models of the biogeochemical and climate systems. This work has yielded preliminary insights into system behaviour and key policy-relevant uncertainties.

The challenges are significant, but the record of progress suggests that within the next decade the scientific community will develop fully coupled dynamical (prognostic) models of the full Earth system (e.g., the coupled physical climate, biogeochemical, human sub-systems) that can be employed on multi-decadal time-scales and at spatial scales relevant to strategic impact assessment. Future models should certainly advance in completeness and sophistication; however, the key will be to demonstrate some degree of prognostic skill. The strategy will be to couple the biogeochemical-physical climate system to representations of key aspects of the human system, and then to develop more coherent scenarios of human actions in the context of feedbacks from the biogeochemical-physical climate system.

Developing these coupled models is an important step. From the perspective of understanding the Earth system, determining the nature of the link between the biogeochemical system and the physical climate system represents a fundamental scientific goal. Present understanding is incomplete, and a successful attack will require extensive interdisciplinary collaboration. It will also require global data that clearly document the state of the system and how that state is changing as well as observations to illuminate important processes more clearly.

14.2 The Climate System

14.2.1 Overview

Models of physical processes in the ocean and atmosphere provide much of our current understanding of future climate change. They incorporate the contributions of atmospheric dynamics and thermodynamics through the methods of computational fluid dynamics. This approach was initially developed in the 1950s to provide an objective numerical approach to weather prediction. It is sometimes forgotten that the early development of “supercomputers” at that time was motivated in large part by the need to solve this problem. In the 1960s, versions of these weather prediction models were developed to study the “general circulation” of the atmosphere, i.e., the physical statistics of weather systems satisfying requirements of conservation of mass, momentum, and energy. To obtain realistic simulations, it was

found necessary to include additional energy sources and sinks: in particular, energy exchanges with the surface and moist atmospheric processes with the attendant latent heat release and radiative heat inputs.

Development of models for the general circulation of the ocean started later, but has proceeded in a similar manner. Models that deal with the physics of the oceans have been developed and linked to models of the atmospheric system. Within ocean models, the inclusion of geochemical and biological interactions has begun, with a focus upon the carbon cycle. Since the late 1960s, the geochemical aspects of the carbon cycle have been included in low-dimensional box models. More recently, including the carbon chemistry system in general circulation models has simply been a question of allocation of computing resources. Modelling of the biological system, however, has been more challenging, and it has only been recently that primitive ecosystem models have been incorporated in global general circulation ocean models. Even though progress has been significant, much remains to be done. Eddy-resolving ocean models with chemistry and biology need to be tested and validated in a transient mode, and the prognostic aspects of marine ecosystems including nutrient dynamics need greater attention at basin and global scales.

Model development for the ocean and atmosphere has had a fundamental theoretical advantage: it is based on firmly established hydrodynamic equations. At present there is less theoretical basis for a “first principles” development of the dynamical behaviour of the terrestrial system. There is a need to develop a fundamental methodology to describe this very heterogeneous and complex system. For the moment, it is necessary to rely heavily upon parametrizations and empirical relationships. Such reliance is data intensive and hence independent validation of terrestrial system models is problematical. In spite of these difficulties, a co-ordinated strategy has been developed to improve estimates of terrestrial primary productivity and respiration by means of measurement and modelling. The strategy has begun to yield dividends. Techniques from statistical mechanics have been wedged to biogeochemistry and population ecology, yielding new vegetation dynamic models. Global terrestrial models at meso-spatial scales (roughly 50 km grids) now exist which capture complex ecophysiological processes and ecosystem dynamics.

Expanded efforts are needed in these domain-specific models. In the ocean, we need to consider better the controls on thermohaline circulation, on potential changes in biological productivity, and on the overall stability of the ocean circulation system. Within terrestrial systems the question of the carbon sink-source pattern is central: what is it and how might it change? Connected to this question is the continued development of dynamic vegetation models, which treat competitive processes within terrestrial ecosystems and their response to multiple stresses. And for the atmosphere, a central question has been, is, and likely will be the role of clouds. Also, there is a corresponding non-linearity associated with change in the distribution and extent of sea ice. Further increased efforts will be needed in linking terrestrial ecosystems with the atmosphere, the land with the ocean, the ocean (and its ecosystems) with the atmosphere, the chemistry of the atmosphere with the physics of the

atmosphere, and finally linking the human system to them all. Such models will also need to be able to highlight different regions with increased spatial and temporal detail.

Models, however, depend upon high quality data. Data allow hypotheses about processes and their linkages to be rejected or to be given increased consideration. Giving formal (e.g., quantitative) expression to processes is at the heart of the scientific enterprise. Such expressions reflect our knowledge and form the basis for models. Models are simply formal expressions of processes and how they fit together. And all rest upon data. Models are of limited use without observations; the value of observations increases by interaction with models. Systematic global observations are an essential underpinning of research to improve understanding of the climate system. For numerous applications in climate-impact research, information about the complex nature of the system is needed. Unfortunately, there continue to be justifiable concerns about the loss of some monitoring of climate parameters and deterioration of coverage. There is a basic need for more observations with better coverage, higher accuracy, and with increased availability. This overriding importance of data has been recognised repeatedly in the past and in this volume (e.g., Chapter 2, Section 2.8; Chapter 3, Section 3.5; Chapter 4, Section 4.2; Chapter 6, Section 6.14; Chapter 11, Section 11.6.1 and Chapter 12, Section 12.4), and there are reasons for guarded optimism on the issue of data even though there are also significant reasons for concern. One such reason for tempered optimism is the plan for and beginning implementation of global observing systems such as the Global Climate Observing System (GCOS), Global Ocean Observing System (GOOS), and Global Terrestrial Observing System (GTOS). However plans in themselves do not produce data, and data that are not accessible are of limited value. The issue of data remains central for progress.

14.2.2 Predictability in a Chaotic System

The climate system is particularly challenging since it is known that components in the system are inherently chaotic; there are feedbacks that could potentially switch sign, and there are central processes that affect the system in a complicated, non-linear manner. These complex, chaotic, non-linear dynamics are an inherent aspect of the climate system. As the IPCC WGI Second Assessment Report (IPCC, 1996) (hereafter SAR) has previously noted, “future unexpected, large and rapid climate system changes (as have occurred in the past) are, by their nature, difficult to predict. This implies that future climate changes may also involve ‘surprises’. In particular, these arise from the non-linear, chaotic nature of the climate system ... Progress can be made by investigating non-linear processes and sub-components of the climatic system.” These thoughts are expanded upon in this report: “Reducing uncertainty in climate projections also requires a better understanding of these non-linear processes which give rise to thresholds that are present in the climate system. Observations, palaeoclimatic data, and models suggest that such thresholds exist and that transitions have occurred in the past ... Comprehensive climate models in conjunction with sustained observational systems, both *in situ* and remote, are the only tool to decide whether the evolving climate system is approaching such thresholds. Our

knowledge about the processes, and feedback mechanisms determining them, must be significantly improved in order to extract early signs of such changes from model simulations and observations.” (See Chapter 7, Section 7.7).

14.2.2.1 Initialisation and flux adjustments

Integrations of models over long time-spans are prone to error as small discrepancies from reality compound. Models, by definition, are reduced descriptions of reality and hence incomplete and with error. Missing pieces and small errors can pose difficulties when models of sub-systems such as the ocean and the atmosphere are coupled. As noted in Chapter 8, Section 8.4.2, at the time of the SAR most coupled models had difficulty in reproducing a stable climate with current atmospheric concentrations of greenhouse gases, and therefore non-physical “flux adjustment terms” were added. In the past few years significant progress has been achieved, but difficulties posed by the problem of flux adjustment, while reduced, remain problematic and continued investigations are needed to reach the objective of avoiding dependence on flux adjustment (see Chapter 8, Section 8.4.2; see also Section 8.5.1.1).

Another important (and related) challenge is the initialisation of the models so that the entire system is in balance, i.e., in statistical equilibrium with respect to the fluxes of heat, water, and momentum between the various components of the system. The problem of determining appropriate initial conditions in which fluxes are dynamically and thermodynamically balanced throughout a coupled stiff system, such as the ocean-atmosphere system, is particularly difficult because of the wide range of adjustment times ranging from days to thousands of years. This can lead to a “climate drift”, making interpretation of transient climate calculations difficult (see Chapter 8, Section 8.4.1).

The initialisation of coupled models is important because it produces the climate base state or “starting point” for climate change experiments. Climate model initialisation continues to be an area of active research and refinement of techniques (see Chapter 8, Section 8.4). Most groups use long integrations of the sub-component models to provide a dynamically and thermodynamically balanced initial state for the coupled model integration. However, there are at least as many different methods used to initialise coupled models as there are modelling groups. See Stouffer and Dixon (1998) for a more complete discussion of the various issues and methods used to initialise coupled models.

Since the SAR, improvements in developing better initialisation techniques for coupled models have been realised. For instance, starting with observed oceanic conditions has yielded improved simulations with reduced climate drift (Gordon *et al.*, 1999). Earlier attempts with this technique usually resulted in relatively large trends in the surface variables (Meehl and Washington, 1995; Washington and Meehl, 1996). Successfully starting long coupled integrations from observations is important for a number of reasons: it simplifies the initialisation procedure, saves time and effort, and reduces the overhead for starting new coupled model integrations.

Such progress is important, but again further work is needed. We simply do not fully understand the causes of climate drift in coupled models (see Chapter 8, Section 8.4.2).

14.2.2.2 Balancing the need for finer scales and the need for ensembles

There is a natural tendency to produce models at finer spatial scales that include both a wider array of processes and more refined descriptions. Higher resolution can lead to better simulations of atmospheric dynamics and hydrology (Chapter 8, Section 8.9.1), less diffusive oceanic simulations, and improved representation of topography. In the atmosphere, fine-scale topography is particularly important for resolving small-scale precipitation patterns (see Chapter 8, Section 8.9.1). In the ocean, bottom topography is very important for the various boundary flows (see Chapter 7, Section 7.3.4). The use of higher oceanic resolution also improves the simulation of internal variability such as ENSO (see Chapter 8, Section 8.7.1). However, in spite of the use of higher resolution, important climatic processes are still not resolved by the model's grid, necessitating the continued use of sub-grid scale parametrizations.

It is anticipated that the grids used in the ocean sub-components of the coupled climate models will begin to resolve eddies by the next report. As the oceanic eddies become resolved by the grid, the need for large diffusion coefficients and various mixing schemes should be reduced (see Chapter 8, Section 8.9.3; see also, however, the discussion in Section 8.9.2). In addition, the amount of diapycnal mixing, which is used for numerical stability in this class of ocean models, will also be reduced as the grid spacing becomes smaller. This reduction in the sub-grid scale oceanic mixing should reduce the uncertainty associated with the mixing schemes and coefficients currently being used.

Underlying this issue of scale and detail is an important tension. As the spatial and process detail in a model is increased, the required computing resources increase, often significantly; models with less detail may miss important non-linear dynamics and feedbacks that affect model results significantly, and yet simpler models may be more appropriate to generating the needed statistics. The issue of spatial detail is intertwined with the representation of the physical (and other) processes, and hence the need for a balance between level of process detail and spatial detail. These tensions must be recognised forthrightly, and strategies must be devised to use the available computing resources wisely. Analyses to determine the benefits of finer scale and increased resolution need to be carefully considered. These considerations must also recognise that the potential predictive capability will be unavoidably statistical, and hence it must be produced with statistically relevant information. This implies that a variety of integrations (and models) must be used to produce an ensemble of climate states. Climate states are defined in terms of averages and statistical quantities applying over a period typically of decades (see Chapter 7, Section 7.1.3 and Chapter 9, Section 9.2.2).

Fortunately, many groups have performed ensemble integrations, that is, multiple integrations with a single model using identical radiative forcing scenarios but different initial conditions. Ensemble integrations yield estimates of the variability of the response for a given model. They are also useful in determining to what extent the initial conditions affect the magnitude and pattern of the response. Furthermore, many groups have now performed model integrations using similar

radiative forcings. This allows ensembles of model results to be constructed (see Chapter 9, Section 9.3; see also the end of Chapter 7, Section 7.1.3 for an interesting question about ensemble formation).

In sum, a strategy must recognise what is possible. In climate research and modelling, we should recognise that we are dealing with a coupled non-linear chaotic system, and therefore that the long-term prediction of future climate states is not possible. The most we can expect to achieve is the prediction of the probability distribution of the system's future possible states by the generation of ensembles of model solutions. This reduces climate change to the discernment of significant differences in the statistics of such ensembles. The generation of such model ensembles will require the dedication of greatly increased computer resources and the application of new methods of model diagnosis. Addressing adequately the statistical nature of climate is computationally intensive, but such statistical information is essential.

14.2.2.3 Extreme events

Extreme events are, almost by definition, of particular importance to human society. Consequently, the importance of understanding potential extreme events is first order. The evidence is mixed, and data continue to be lacking to make conclusive cases. Chapter 9, Sections 9.3.5 and 9.3.6 consider projections of changes in patterns of variability (discussed in the next section) and changes in extreme events (see also Chapters 2 and 10). Though the conclusions are mixed in both of these topical areas, certain results begin to appear robust. There appear to be some consistent patterns with increased CO₂ with respect to changes in variability: (a) the Pacific climate base state could be a more El Niño-like state and (b) an enhanced variability in the daily precipitation in the Asian summer monsoon with increased precipitation intensity (Chapter 9, Section 9.3.5). More generally, the intensification of the hydrological cycle with increased CO₂ is a robust conclusion. For possible changes in extreme weather and climate events, the most robust conclusions appear to be: (a) an increased probability of extreme warm days and decreased probability of extreme cold days and (b) an increased chance of drought for mid-continental areas during summer with increasing CO₂ (see Chapter 9, Section 9.3.6).

The evaluation of many types of extreme events is made difficult because of issues of scale. Damaging extreme events are often at small temporal and spatial scales. Intense, short-duration events are not well-represented (or not represented at all) in model-simulated climates. In addition, there is often a basic mismatch between the scales resolved in models and those of the validating data. A promising approach is to use multi-fractal models of rainfall events in that they naturally generate extreme events. Reanalysis has also helped in this regard, but reanalysis *per se* is not the sole answer because the models used for reanalysis rely on sub-grid scale parametrizations almost as heavily as climate models do.

One area that is possibly ripe for a direct attack on improving the modelling of extreme events is tropical cyclones (see Section Chapter 2, 2.7.3.1; Chapter 8, Section 8.8.4; Chapter 9, Section 9.3.6.4, and Chapter 10, Box 10.2). Also, there is the potential for

increased understanding of extreme events by employing regional climate models (RCMs); however, there are also challenges to realising this potential (see Chapter 10). It must be established that RCMs produce more realistic extremes than general circulation models (GCMs). Most RCM simulations to date are not long enough (typically 5 or 10 years for nested climate change simulations) to evaluate extremes well (see Chapter 10, Section 10.5.2).

Another area in which developments are needed is that of extremes associated with the land surface (flood and drought). There is still a mismatch between the scale of climate models and the finer scales appropriate for surface hydrology. This is particularly problematical for impact studies. For droughts there is a basic issue of predictability; drought prediction is difficult regardless of scale.

A particularly important issue is the adequacy of data needed to attack the question of changes in extreme events. There have been recent advances in our understanding of extremes in simulated climates (see, for example, Meehl *et al.*, 2000), but thus far the approach has not been very systematic. Atmospheric Model Intercomparison Project 2 (AMIP2) provides an opportunity for a more systematic approach: AMIP2 will be collecting and organising some of the high-frequency data that are needed to study extremes. However, it must be recognised that we are still unfortunately short of data for the quantitative assessment of extremes on the global scale in the observed climate.

Finally, it is often stated that the impacts of climate change will be felt through changes in extremes because they stress our present day adaptations to climate variability. What does this imply for the research agenda for the human dimension side of climate studies?

14.2.2.4 Organised variability

An overriding challenge to modelling and to the IPCC is prediction. This challenge is particularly acute when predictive capability is sought for a system that is chaotic, that has significant non-linearities, and that is inherently stiff (i.e., widely varying time constants). And within prognostic investigations of such a complex system, the issue of predicting extreme events presents a particularly vexing yet important problem. However, there appear to be coherent modes of behaviour that not only support a sense of optimism in attacking the prediction problem, but also these modes may offer measurable prediction targets that can be used as benchmarks for evaluating our understanding of the climate system. In addition, predictions of these modes represent valuable contributions in themselves.

Evaluating the prognostic skill of a model and understanding the characteristics of this skill are clearly important objectives. In the case of weather prediction, one can estimate the range of predictability by evaluating the change of the system from groups of initial states that are close to each other. The differences in these time-evolving states give a measure of the predictive utility of the model. In addition, one has the near-term reality of the evolving weather as a constant source of performance metrics. For the climate issue, the question of predictability is wrapped up with understanding the physics behind the low-frequency variability of climate and distinguishing the signal of climate

change (see Chapter 9, Section 9.2.2.1). In other words, there are the paired challenges of capturing (predicting) “natural” variability of climate as well as the emerging anthropogenically forced climate signal. This dual challenge is distinctively climatic in nature, and whereas the longer-term character of climate projections is unavoidable and problematic, the intra-seasonal to inter-decadal modes of climate variability (e.g., ENSO, Pacific Decadal Oscillation (PDO), and North Atlantic Oscillation (NAO) – see also Chapter 7, Box 7.2) offer opportunities to test prognostic climate skill. Here, some predictive skill for the climate system appears to exist on longer time-scales. One example is the ocean-atmosphere phenomenon of ENSO. This skill has been advanced and more clearly demonstrated since the SAR, and this progress and demonstration are important (see Chapter 7, Section 7.6; Chapter 8, Section 8.7 and Chapter 9, Section 9.3.5). Such demonstrations and the insights gained in developing and making prognostic statements on climate modes frame an important area for further work.

This opportunity is well summarised in Chapter 8 (in particular, Section 8.7), “The atmosphere-ocean coupled system shows various modes of variability that range widely from intra-seasonal to inter-decadal time-scales (see Chapters 2 and 7). Since the SAR, considerable progress has been achieved in characterising the decadal to inter-decadal variability of the ocean-atmosphere system. Successful evaluation of models over a wide range of phenomena increases our confidence.”

14.2.3 Key Sub-systems and Phenomena in the Physical Climate System

Central to the climate system are the coupled dynamics of the atmosphere-ocean-terrestrial system, the physical processes associated with the energy and water cycles and the associated biological and chemical processes controlling the biogeochemical cycles, particularly carbon, nitrogen, phosphorus, sulphur, iron, and silicon. The atmosphere plays a unique role in the climate system since on a zeroth order basis it sets the radiative forcing. Specific sub-systems that are important and yet still poorly understood are clouds and sea ice; the thermohaline ocean circulation is a fundamentally important phenomenon that needs to be known better, and underlying these sub-systems and phenomena are the still ill-understood non-linear processes of advection (large-scale) and convection (small-scale) of dynamical and thermodynamical oceanic and atmospheric quantities. These sub-systems, phenomena, and processes are important and merit increased attention to improve prognostic capabilities generally.

14.2.3.1 Clouds

The role of clouds in the climate system continues to challenge the modelling of climate (e.g., Chapter 7, Section 7.2.2). It is generally accepted that the net effect of clouds on the radiative balance of the planet is negative and has an average magnitude of about 10 to 20 W m^{-2} . This balance consists of a short-wave cooling (the albedo effect) of about 40 to 50 W m^{-2} and a long-wave warming of about 30 W m^{-2} . Unfortunately, the size of the uncertainties in this budget is large when compared to the

expected anthropogenic greenhouse forcing. Although we know that the overall net effect of clouds on the radiative balance is slightly negative, we do not know the sign of cloud feedback with respect to the increase of greenhouse gases, and it may vary with the region. In fact, the basic issue of the nature of the future cloud feedback is not clear. Will it remain negative? If the planet warms, then it is plausible that evaporation will increase, which probably implies that liquid water content will increase but the volume of clouds may not. What will be the effect and how will the effects be distributed in time and space? Finally, the issue of cloud feedbacks is also coupled to the very difficult issue of indirect aerosol forcing (see Chapter 5, Section 5.3).

The importance of clouds was summarised in the SAR: “The single largest uncertainty in determining the climate sensitivity to either natural or anthropogenic changes are clouds and their effects on radiation and their role in the hydrological cycle” (Kattenberg *et al.*, 1996, p.345). And yet, the single greatest source of uncertainty in the estimates of the climate sensitivity continues to be clouds (see also Chapter 7, Section 7.2). Since the SAR, there have been a number of improvements in the simulation of both the cloud distribution and in the radiative properties of clouds (Chapter 7, Section 7.2.2). The simulation of cloud distribution has improved as the overall simulation of the atmospheric models has improved. In addition, the cloud sub-component models used in the coupled models have become more realistic. Also, our understanding of the radiative properties of clouds and their effects on climate sensitivity have improved. And yet in Chapter 7, Section 7.2.2 we find that, “In spite of these improvements, there has been no apparent narrowing of the uncertainty range associated with cloud feedbacks in current climate change simulations.”

Handling the physics and/or the parametrization of clouds in climate models remains a central difficulty. There is a need for increased observations. J. Mitchell highlighted the challenge in a recent paper at the World Climate Research Programme (WCRP) Workshop on Cloud Properties and Cloud Feedbacks in Large-scale Models where he stated that “Reducing the uncertainty in cloud-climate feedbacks is one of the toughest challenges facing atmospheric physicists” (Mitchell, 2000).

Cloud modelling is a particularly challenging scientific problem because it involves processes covering a very wide range of space- and time-scales. For example, cloud systems extending over thousands of kilometres to cloud droplets and aerosols of microscopic size are all important components of the climate system. The time-scales of interest can range from hundreds of years (e.g., future equilibrium climates) to fractions of a second (e.g., droplet collisions). This is not to say that all cloud micro-physics must be included in modelling cloud formation and cloud properties, but the demarcation between what must be included and what can be parametrized remains unclear. Clarifying this demarcation and improving both the resulting phenomenological characterisations and parametrizations will depend critically on improved global observations of clouds (see Chapter 2, Section 2.5.5; see also Senior, 1999). Of particular importance are observations of cloud structure and distribution against natural patterns of climate variability (e.g., ENSO). Complementing the broad climatologies will be important observations of cloud ice-

water and liquid-water content, radiative heating and optical depth profiles, and precipitation occurrence and cloud geometry.

The recently approved CloudSat and PICASSO missions, which will fly in formation with the National Aeronautics and Space Administration (USA) (NASA) Earth Observing System (EOS) PM (the Aqua Mission), will provide valuable profiles of cloud ice and liquid content, optical depth, cloud type, and aerosol properties. These observations, combined with wider swath radiometric data from EOS PM sensors, will provide a rich new source of information about the properties of clouds (Stephens *et al.*, 2000).

And yet, this question of cloud feedback remains open, and it is not clear how it will be answered. Given that the current generation of global climate models represents the Earth in terms of grid-points spaced roughly 200 km apart, many features observed on smaller scales, such as individual cloud systems and cloud geometry, are not explicitly resolved. Without question, the strategy for attacking the feedback question will involve comparison of model simulations with appropriate observations on global or local scales. The interplay of observation and models, again, will be the key for progress. Mitchell (Mitchell, 2000) states this clearly, “Unless there are stronger links between those making observations and those using climate models, then there is little chance of a reduction in the uncertainty in cloud feedback in the next twenty years.” This is echoed in this report (see Chapter 7, Section 7.2.2), “A straightforward approach of model validation is not sufficient to constrain efficiently the models and a more dedicated approach is needed. It should be favoured by a larger availability of satellite measurements.”

14.2.3.2 Thermohaline circulation

In the oceanic component of climate models, ocean current patterns are represented significantly better in models of higher resolution in large part because ocean current systems (including mesoscale eddies), ocean variability (including ENSO events), and the thermohaline circulation (and other vertical mixing processes) and topography which greatly influence the ocean circulation, can be better represented. Improved resolution and understanding of the important facets of coupling in both atmosphere and ocean components of global climate models have also been proven to reduce flux imbalance problems arising in the coupling of the oceanic and the atmospheric components. However, it must still be noted that uncertainties associated with clouds still cause problems in the computation of surface fluxes. With the availability of computer power, a central impediment to the gain in model accuracy is being reduced; however, there is still a long way to go before many of the important processes are explicitly resolved by the numerical grid. In addition there continues to be a necessary “concomitant” increase in resources for process studies and for diagnosis as computer power increases. It must still be remembered that the system presents chaotic characteristics that can only be evaluated through an analysis of ensembles statistics, and these ensembles must be generated by running suites of models under varied initial and forcing conditions.

In a few model calculations, a large rate of increase in the radiative forcing of the planet is enough to cause the ocean’s

global thermohaline circulation almost to disappear, though in some experiments it reappears given sufficiently long integration times (see Chapter 7, Section 7.3.7 and Chapter 9, 9.3.4.3). This circulation is important because in the present climate it is responsible for a large portion of the heat transport from the tropics to higher latitudes, and it plays an important role in the oceanic uptake of CO₂. Palaeo-oceanographic investigations suggest that aspects of longer-term climate change are associated with changes in the ocean's thermohaline circulation. We need appropriate observations of the thermohaline circulation, and its natural variations, to compare with model simulations (see Chapter 9, Section 9.3.4.3; see also Chapter 7, Section 7.6 and Chapter 8, Section 8.5.2.2).

The coming decade will be important for ocean circulation in the context of climate. A particularly exciting development is the potential for assimilating synoptic ocean observations (e.g., the US/French ocean TOPOgraphy satellite altimeter EXperiment (TOPEX-POSEIDON) and Argo) into ocean general circulation models. Key questions, such as how well do the ocean models capture the inferred heat flux or tracer distributions, are central to the use of these models in climate studies. The effort of comparing models with data, as the direct path for model rejection and model improvement, is central to increasing our understanding of the system.

14.2.3.3 Arctic sea ice

There is increasing evidence that there is a decline in the extent and thickness of Arctic sea ice in the summer that appears to be connected with the observed recent Arctic warming (see Chapter 2, Section 2.2.5.2; Chapter 7, Box 7.1, and Chapter 8, Section 8.5.3; see also Chapter 7, Section 7.5.2 for a general discussion on the role of sea ice in the climate system as well as recent advances in modelling sea ice).

It is not known whether these changes reflect anthropogenic warming transmitted either from the atmosphere or the ocean or whether they mostly reflect a major mode of multi-decadal variability. Some of this pattern of warming has been attributed to recent trends in the Arctic Oscillation (see Section 2.6); however, how the anthropogenic signal is imprinted on the natural patterns of climate variability remains a central question. What does seem clear is that the changes in Arctic sea ice are significant, and there is a positive feedback that could be triggered by declines in sea-ice extent through changes in the planetary albedo. If the Arctic shifted from being a bright summer object to a less bright summer object, then this would be an important positive feedback on a warming pattern (see the "left loop" in Chapter 7, Figure 7.6).

In addition to these recently available observations, there have been several models (Commonwealth Scientific and Industrial Research Organisation (Australia) (CSIRO) – Gordon and O'Farrell, 1997; Department of Energy (USA) Parallel Climate Model (DOE PCM) – Washington *et al.*, 2000; National Center for Atmospheric Research (USA) Climate System Model (NCAR CSM) – Weatherly *et al.*, 1998; see also Chapter 7, Section 7.5.2 and Chapter 8, Section 8.5.3) that have improved their sea ice representation since the SAR. These improvements include simulation of open water within the ice pack, snow cover

upon the ice, and sea ice dynamics. The incorporation of sophisticated sea ice components in climate models provides a framework for testing and calibrating these models with observations. Further, as the formulation of sea ice dynamics becomes more realistic, the validity of spatial patterns of the simulated wind stress over the polar oceans is becoming an issue in Atmosphere-Ocean General Circulation Model (AOGCM) simulations. Hence, improvements, such as the above-mentioned data, in the observational database will become increasingly relevant to climate model development. In addition, satellite observations have recently been used to determine sea-ice velocity (Emery *et al.*, 1997) and melt season (Smith, 1998).

New field programmes are under way with the explicit goal of improving the accuracy of model simulations of sea ice and polar climate (see Randall *et al.*, 1998, for a review). In order to improve model representations and validation, it will be essential to enhance the observations over the Arctic including ocean, atmosphere, and sea ice state variables. This will help provide more reliable projections for a region of the world where significant changes are expected.

The refinement of sea-ice models along with enhanced observations reduces the uncertainty associated with ice processes. (See Chapter 7, Section 7.5 and Chapter 8, Section 8.5.3 for more discussion and evaluation of model performance; for some open issues see Chapter 9, Section 9.4.) This progress is important, and efforts are needed to expand upon it and, as stated, to improve the observational basis significantly.

14.2.4 The Global Carbon Cycle

From measurements of air trapped in ice cores and from direct measurements of the atmosphere, we know that in the past 200 years the abundance of CO₂ in the atmosphere has increased by over 30% (i.e., from a concentration of 280 ppm by volume (ppmv) in 1700 to nearly 370 ppmv in 2000). We also know that the concentration was relatively constant (roughly within ±10 ppmv of 275) for more than 1,000 years prior to the human-induced rapid increase in atmospheric CO₂ (see Chapter 3, Figures 3.2a and 3.2b).

Looking further back in time, we find an extraordinarily regular record of change. The Vostok core (Figure 3.2d) captures a remarkable and intriguing signal of the periodicity of interglacial and glacial climate periods in step with the transfer of significant pools of carbon from the land (most likely through the atmosphere) to the ocean and then the recovery of terrestrial carbon back from the ocean. The repeated pattern of a 100 to 120 ppmv decline in atmospheric CO₂ from an inter-glacial value of 280 to 300 ppmv to a 180 ppmv floor and then the rapid recovery as the planet exits glaciation suggests a tightly governed control system. There is a similar methane (CH₄) cycle between 320 to 350 ppbv (parts per billion by volume) and 650 to 770 ppbv. What begs explanation is not just the linked periodicity of carbon and glaciation, but also the apparent consistent limits on the cycles over the period. See Chapter 3, Box 3.4.

Today's atmosphere, imprinted with the fossil fuel CO₂ signal, stands at nearly 90 to 70 ppmv above the previous interglacial maximum of 280 to 300 ppmv. The current methane value

is even further (percentage-wise) from its previous inter-glacial high values. In essence, carbon has been moved from a relatively immobile pool (in fossil fuel reserves) in the slow carbon cycle to the relatively mobile pool (the atmosphere) in the fast carbon cycle, and the ocean, terrestrial vegetation and soils have yet to equilibrate with this “rapidly” changing concentration of CO₂ in the atmosphere.

Given this remarkable and unprecedented history one cannot help but wonder about the characteristics of the carbon cycle in the future (Chapter 3). To understand better the global carbon cycle, two themes are clear: (1) there is a need for global observations that can contribute significantly to determining the sources and sinks of carbon and (2) there is a need for fundamental work on critical biological processes and their interaction with the physical system. Two observational needs must be highlighted:

- Observations that would decisively improve our ability to model the carbon cycle. For example, a dense and well-calibrated network for monitoring CO₂ and O₂ concentrations that will also be required for international verification of carbon sources and sinks is central.
- “Benchmarks” data sets that allow model intercomparison activities to move in the direction of becoming data-model comparisons and not just model-model comparisons.

We note that the Subsidiary Body for Scientific and Technological Advice (SBSTA) of the United Nations Framework Convention on Climate Change (UNFCCC) recognised the importance of an Integrated Global Observing Strategy Partnership in developing observing systems for the oceans and terrestrial carbon sources and sinks in the global carbon cycle and in promoting systematic observations.

There is also a range of areas where present day biogeochemistry modelling is not only in need of additional data, but is also crucially limited by insufficient understanding at the level of physical or biological processes. Clarifying these processes and their controls is central to a better understanding of the global carbon cycle.

14.2.4.1 The marine carbon system

The marine carbon cycle plays an important role in the partitioning of CO₂ between the atmosphere and the ocean (Chapter 3, Section 3.2.3). The primary controls are the circulation of the ocean (a function of the climate system), and two important biogeochemical processes: the solubility pump and the biological pump, both of which act to create a global mean increase of dissolved inorganic carbon with depth.

The physical circulation and the interplay of the circulation and the biogeochemical processes are central to understanding the ocean carbon system and future concentrations of CO₂ in the atmosphere. In the ocean, the prevailing focus on surface conditions and heat transport has led to a comparative neglect of transport processes below about 800 m depth. For carbon cycle modelling, however, vertical transports and deep horizontal transports assume fundamental importance. The importance of the thermohaline circulation is obviously

important (and insufficiently well understood; see Section 14.2.3.2) in moving carbon from the surface to deeper layers. Similarly, the regional distribution of upwelling, which brings carbon- and nutrient-rich water to surface layers, is poorly known and inconsistently simulated in models. The ventilation of the Southern Ocean provides an extreme, though not unique, example.

It has been pointed out by a number of modelling studies that if there were no marine biological system, then the pre-industrial atmospheric CO₂ concentration would have been 450 ppmv instead of 280 ppmv (Sarmiento and Toggweiler 1984; Maier-Raimer *et al.*, 1996). Any complete model of the natural ocean carbon cycle should therefore include the biological system; however, most recent assessments of the oceanic uptake of anthropogenic CO₂ have assumed that the biological system would not be affected by climate change and have therefore only modelled the chemical solubility in addition to the physical circulation. This was based on the understanding that nitrate or other nutrients limit marine phytoplankton growth. There would therefore be no CO₂ fertilisation effect as has been suggested for terrestrial plants and that, unless there was a large change in the nutrient supply to the upper ocean because of a climate-induced shift in circulation, then no extra anthropogenic CO₂ could be sequestered to the deep ocean by the organic matter pump. More recently, a number of studies have suggested possible ways in which the organic matter pump might be affected by climate change over a 200-year time-scale (see Chapter 3, Sections 3.2.3.2 and 3.2.3.3). The main conclusion was that, because of the complexity of biological systems, it was not yet possible to say whether some of the likely feedbacks would be positive or negative. However, it is clear that our understanding of these issues needs to be improved.

Simulating the calcium carbonate system with a process-oriented model presents another level of complexity beyond simulating the organic matter formation-decomposition: the distribution of particular phytoplankton species (mainly coccolithophorids) must be simulated. The calcium carbonate pump, however, contributes relatively little to the vertical dissolved inorganic carbon (DIC) gradient compared to the organic matter and solubility pumps. The importance of this pump needs careful evaluation and its past (palaeo) role in the carbon cycle needs to be considered (see end of Chapter 3, Section 3.2.3.3).

In the ocean, models incorporating biology are relatively underdeveloped and incorporate empirical assumptions (such as fixed Redfield (nutrient) ratios) rather than explicitly modelling the underlying processes. As a result, present models may be unduly constrained in the range of responses they can show to changes in climate and ocean dynamics. A better understanding is required concerning the workings of nutrient constraints on productivity, the controls of nitrogen fixation, and the controls on the geographical distribution of biogeochemically important species and functional types in the ocean. To develop this understanding it will be necessary to combine remotely sensed information with a greatly expanded network of continuous biogeochemical monitoring sites, and to gather data on the space-time patterns of variability in species composition of marine ecosystems in relation to climate variability phenomena such as ENSO and NAO. (See Chapter 3, Sections 3.6.3 and 3.7).

14.2.4.2 The terrestrial system

The metabolic processes that are responsible for plant growth and maintenance and the microbial turnover, which is associated with dead organic matter decomposition, control the cycle of carbon, nutrients, and water through plants and soil on both rapid and intermediate time-scales. Moreover, these cycles affect the energy balance and provide key controls over biogenic trace gas production. Looking at the carbon fixation-organic material decomposition as a linked process, one sees that some of the carbon fixed by photosynthesis and incorporated into plant tissue is perhaps delayed from returning to the atmosphere until it is oxidised by decomposition or fire. This slower carbon loop through the terrestrial component of the carbon cycle affects the rate of growth of atmospheric CO₂ concentration and, in its shorter term expression, imposes a seasonal cycle on that trend (Chapter 3, Figure 3.2a). The structure of terrestrial ecosystems, which respond on even longer time-scales, is determined by the integrated response to changes in climate and to the intermediate time-scale carbon-nutrient machinery. The loop is closed back to the climate system, since it is the structure of ecosystems, including species composition, that largely sets the terrestrial boundary condition of the climate in terms of surface roughness, albedo, and latent heat exchange (see Chapter 3, Section 3.2.2).

Modelling interactions between terrestrial and atmospheric systems requires coupling successional models to biogeochemical models and physiological models that describe the exchange of water and energy between vegetation and the atmosphere at fine time-scales. At each step toward longer time-scales, the climate system integrates the more fine-scaled processes and applies feedbacks onto the terrestrial biome. At the finest time-scales, the influence of temperature, radiation, humidity and winds has a dramatic effect on the ability of plants to transpire. On longer time-scales, integrated weather patterns regulate biological processes such as the timing of leaf emergence or excision, uptake of nitrogen by autotrophs, and rates of organic soil decay and turnover of inorganic nitrogen. The effect of climate at the annual or interannual scale defines the net gain or loss of carbon by the biota, its water status for the subsequent growing season, and even its ability to survive.

As the temporal scale is extended, the development of dynamic vegetation models, which respond to climate and human land use as well as other changes, is a central issue. These models must not only treat successional dynamics, but also ecosystem redistribution. The recovery of natural vegetation in abandoned areas depends upon the intensity and length of the agricultural activity and the amount of soil organic matter on the site at the time of abandonment. To simulate the biogeochemistry of secondary vegetation, models must capture patterns of plant growth during secondary succession. These patterns depend substantially on the nutrient pools inherited from the previous stage. The changes in hydrology need also to be considered, since plants that experience water stress will alter the allocation of carbon to allocate more carbon to roots. Processes such as reproduction, establishment, and light competition have been added to such models, interactively with the carbon, nitrogen, and water cycles. Disturbance regimes such as fire are also incorporated into the models, and these disturbances are essential

in order to treat successfully competitive dynamics and hence future patterns of ecosystem. It should be noted also that these forcing terms themselves might be altered by the changes that result from changes in the terrestrial system.

This coupling across time-scales represents a significant challenge. Immediate challenges that confront models of the terrestrial-atmosphere system include exchanges of carbon and water between the atmosphere and land, and the terrestrial sources and sinks of trace gases.

Prognostic models of terrestrial carbon cycle and terrestrial ecosystem processes are central for any consideration of the effects of environmental change and analysis of mitigation strategies; moreover, these demands will become even more significant as countries begin to adopt carbon emission targets. At present, several rather complex models are being developed to account for the ecophysiological and biophysical processes, which determine the spatial and temporal features of primary production and respiration (see Chapter 3, Sections 3.6.2 and 3.7.1). Despite recent progress in developing and evaluating terrestrial biosphere models, several crucial questions remain open. For example, current models are highly inconsistent in the way they treat the response of Net Primary Production (NPP) to climate variability and climate change – even though this response is fundamental to predictions of the total terrestrial carbon balance in a changing climate. Models also differ significantly in the degree of CO₂ fertilisation they allow, and the extent to which CO₂ responses are constrained by nutrient availability; the extent to which CO₂ concentrations affect the global distribution of C₃ and C₄ photosynthetic pathways; and the impacts of climate, CO₂ and land management on the tree-grass balance. These are all areas where modelling capability is limited by lack of knowledge, thus making it crucially important to expand observational and experimental research. Important areas are interannual variability in terrestrial fluxes and the interplay of warming, management, and CO₂ enrichment responses at the ecosystem scale. Moreover, these issues must be far better resolved if there is to be an adequate verification scheme to confirm national performance in meeting targets for CO₂ emissions. (See Chapter 3, Sections 3.6.2 and 3.7.1.)

Finally, while progress will be made on modelling terrestrial processes, more integrative studies are also needed wherein terrestrial systems are coupled with models of the physical atmosphere and eventually with the chemical atmosphere as well.

14.2.5 Precipitation, Soil Moisture, and River Flow: Elements of the Hydrological Cycle

Changes in precipitation could have significant impacts on society. Precipitation is an essential element in determining the availability of drinking water and the level of soil moisture. Improved treatment of precipitation (see Section Chapter 7, 7.2.3) is an essential step.

Soil moisture is a key component in the land surface schemes in climate models, since it is closely related to evapotranspiration and thus to the apportioning of sensible and latent heat fluxes. It is primary in the formation of runoff and hence river-flow. Further, soil moisture is an important determinant of ecosystem

structure and therein a primary means by which climate regulates (and is partially regulated by) ecosystem distribution. Soil moisture is an important regulator of plant productivity and sustainability of natural ecosystems. In turn terrestrial ecosystems recycle water vapour at the land-surface/atmosphere boundary, exchange numerous important trace gases with the atmosphere, and transfer water and biogeochemical compounds to river systems (see also the discussion in Chapter 7, Section 7.4.3 and Chapter 8, Section 8.5.4). New efforts are needed in the development of models, which successfully represent the space-time dynamics interaction between soil, climate and vegetation. If water is a central controlling aspect, then the interaction necessarily passes all the way through the space-time dynamics of soil moisture. Finally, adequate soil moisture is an essential resource for human activity. Consequently, accurate prediction of soil moisture is crucial for simulation of the hydrological cycle, of soil and vegetation biochemistry, including the cycling of carbon and nutrients, and of ecosystem structure and distribution as well as climate.

River systems are linked to regional and continental-scale hydrology through interactions among precipitation, evapotranspiration, soil water, and runoff in terrestrial ecosystems. River systems, and more generally the entire global water cycle, control the movement of constituents over vast distances, from the continental land-masses to the world's oceans and to the atmosphere. Rivers are also central features of human settlement and development.

It appears, however, that a significant level of variance exists among land models, associated with unresolved differences among parametrization details (particularly difficulties in the modelling of soil hydrology) and parameter sets. In fact, many of the changes in land-surface models since the SAR fall within this range of model diversity. It is not known to what extent these differences in land-surface response translate into differences in global climate sensitivity (see Chapter 8, Section 8.5.4.3) although the uncertainty associated with the land-surface response must be smaller than the uncertainty associated with clouds (Lofgren, 1995). There is model-based evidence indicating that these differences in the land-surface response may be significant for the simulation of the local land-surface climate and regional atmospheric climate changes (see Chapter 7, Section 7.4).

Much attention in the land-surface modelling community has been directed toward the diversity of parametrizations of water and energy fluxes (see Chapter 7, Sections 7.4, 7.5, and Chapter 8, Section 8.5). Intercomparison experiments (see Chapter 8, Section 8.5.4) have quantified the inter-model differences in response to prescribed atmospheric forcing, and have demonstrated that the most significant outliers can be understood in terms of unrealistic physical approximations in their formulation, particularly the neglect of stomatal resistance. Some coupled models now employ some form of stomatal resistance to evaporation.

Climate-induced changes in vegetation have potentially large climatic implications, but are still generally neglected in the coupled-model experiments used to estimate future changes in climate (see Chapter 8).

There is, obviously, a direct coupling between predicted soil moisture and predicted river flows and the availability of water for human use. Complex patterns of locally generated runoff are transformed into horizontal transport as rivers through the drainage basin. Moreover, any global perspective on surface hydrology must explicitly recognise the impact of human intervention in the water cycle, not only through climate and land-use change, but also through the operation of impoundments, inter-basin transfers, and consumptive use.

Recognition of the importance of land hydrology for the salinity distribution of the oceans is one reason for seeking improvements in models for routing runoff to the oceans (see more precise cites here and in Chapter 7). Most coupled models now return land runoff to the ocean as fresh water (see Chapter 8). Runoff is collected over geographically realistic river basins and mixed into the ocean at the appropriate river mouths. Although this routing is performed instantaneously in some models, the trend is toward model representation of the significant time-lag (order of a month) in runoff production to river-ocean discharge. What is needed for a variety of reasons, however, is for river flow itself to be treated in models of the climate system. (See Chapter 7, Section 7.4.3.)

On land, surface processes have until very recently been treated summarily in Atmospheric General Circulation Models (AGCMs). The focus of evaluating AGCMs has been on large-scale dynamics and certain meteorological variables; far less so on the partitioning of sensible and latent heat flux, or the moisture content of the planetary boundary layer. When the goals of climate modelling are expanded to include terrestrial biosphere function, such aspects become of central importance as regulators of the interaction between the carbon and water cycles. Terrestrial flux and boundary-layer measurements represent a new, expanding and potentially hugely important resource for improving our understanding of these processes and their representation in models of the climate system. (See Chapter 7, Section 7.4.1.)

The spatial resolution of current global climate models, roughly 200 km, is too coarse to simulate the impact of global change on most individual river basins. To verify the transport models will require budgets of water and other biogeochemical constituents for large basins of the world. This requires ground-based meteorology in tandem with remotely sensed data for a series of variables, including information on precipitation, soils, land cover, surface radiation, status of the vegetative canopy, topography, floodplain extent, and inundation. Model results can be constrained by using a database of observed discharge and constituent fluxes at key locations within the drainage basins analysed. Climate time-series and monthly discharge data for the past several decades at selected locations provide the opportunity for important tests of models, including appraisal of the impact of episodic events, such as El Niño, on surface water balance and river discharge. It will be necessary to inventory, document, and make available such data sets to identify gaps in our knowledge, and where it is necessary to collect additional data. Even in the best-represented regions of the globe coherent time-series are available for only the last 30 years or less. This lack of data constrains our ability to construct

and test riverine flux models. Standardised protocols, in terms of sampling frequency, spatial distribution of sampling networks, and chemical analyses are needed to ensure the production of comparable data sets in disparate parts of the globe. Upgrades of the basic monitoring system for discharge and riverborne constituents at the large scale are therefore required.

In sum, hydrological processes and energy exchange, especially those involving clouds, surface exchanges, and interactions of these with radiation are crucial for further progress in modelling the atmosphere. Feedbacks with land require careful attention to the treatments of evapotranspiration, soil moisture storage, and runoff. All of these occur on spatial scales which are fine compared with the model meshes, so the question of scaling must be addressed. These improvements must be paralleled by the acquisition of global data sets for validation of these treatments. Validation of models against global and regional requirements for conservation of energy is especially important in this regard. As noted in Chapter 8 (Section 8.5.4.3), “Uncertainty in land surface processes, coupled with uncertainty in parameter data combines, at this time, to limit the confidence we have in the simulated regional impacts of increasing CO₂.”

14.2.6 Trace Gases, Aerosols, and the Climate System

The goal is a completely interactive simulation of the dynamical, radiative, and chemical processes in the atmosphere-ocean-land system with a central theme of characterising adequately the radiative forcing in the past, in the present, and into the future (See Chapter 6, Sections 6.1 and 6.2; see also Chapter 9, Section 9.1). Such a model will be essential in future studies of the broad question on the role of the oceans, terrestrial ecosystems, and human activities in the regulation of atmospheric concentrations of CO₂ and other radiatively active atmospheric constituents. It will be required for understanding tropospheric trace constituents such as nitrogen oxides, ozone, and sulphate aerosols. Nitrogen oxides are believed to control the production and destruction of tropospheric ozone, which controls the chemical reactivity of the lower atmosphere and is itself a significant greenhouse gas. Tropospheric sulphate aerosols, carbonaceous aerosols from both natural and anthropogenic processes, dust, and sea salt, on the other hand, are believed to affect the Earth’s radiation budget significantly, by scattering solar radiation and through their effects on clouds. Systematic observations of different terrestrial ecosystems and surface marine systems under variable meteorological conditions are needed along with the development of ecosystem and surface models that will provide parametrizations of these exchanges.

Models that incorporate atmospheric chemical processes provide the basis for much of our current understanding in such critical problem areas as acid rain, photochemical smog production in the troposphere, and depletion of the ozone layer in the stratosphere. These formidable problems require models that include chemical, dynamical, and radiative processes, which through their mutual interactions determine the circulation, thermal structure, and distribution of constituents in the

atmosphere. That is, the problems require a coupling of the physics and chemistry of the atmosphere. Furthermore, the models must be applicable on a variety of spatial (regional-to-global) and temporal (days-to-decades) scales (see Chapter 6). A particularly important and challenging issue is the need to reduce the uncertainty on the size and spatial pattern of the indirect aerosol effects (see Chapter 6, Section 6.8).

Most of the effort in three-dimensional atmospheric chemistry models over the last decade has been in the use of transport models in the analysis of certain chemically active species, e.g., long-lived gases such as nitrous oxide (N₂O) or the chlorofluorocarbons (CFCs). In part, the purpose of these studies was not to improve our understanding of the chemistry of the atmosphere, but rather to improve the transport formulation associated with general circulation models and, in association with this improvement, to understand sources and sinks of CO₂. The additional burden imposed by incorporating detailed chemistry into a comprehensive general circulation model has made long-term simulations and transient experiments with existing computing resources challenging. Current three-dimensional atmospheric chemistry models which focus on the stratosphere seek a compromise solution by employing coarse resolution (both vertical and horizontal dimensions); incorporating constituents by families (similar to the practice used in most two-dimensional models); omitting or simplifying parametrizations for tropospheric physical processes; or conducting “off line” transport simulations in which previously calculated wind and temperature fields are used as known input to continuity equations including chemical source/sink terms. This last approach renders the problem tractable and has produced much progress towards understanding the transport of chemically reacting species in the atmosphere. The corresponding disadvantage is the lack of the interactive feedback between the evolving species distributions and the atmospheric circulation. Better descriptions of the complex relationship between hydrogen, nitrogen, and oxygen species as well as hydrocarbons and other organic species are needed in order to establish simplified chemical schemes that will be implemented in chemical/transport models. In parallel, better descriptions of how advection, turbulence, and convection affect the chemical composition of the atmosphere are needed. (See Chapter 4, Section 4.5.2.)

We also need improved understanding of the processes involving clouds, surface exchanges, and their interactions with radiation. The coupling of aerosols with both the energy and water cycles as well as with the chemistry components of the system is of increasing importance. Determining feedbacks between the land surface and other elements of the climate system will require careful attention to the treatments of evapotranspiration, soil moisture storage and runoff. All of these occur on spatial scales that are small compared with the model meshes, so the question of scaling must be addressed. These improvements must be paralleled by the acquisition of global data sets for validation of these treatments. Validation of models against global and regional requirements for conservation of energy is especially important in this regard. (See Chapter 4, Section 4.5.1.)

The problems associated with how to treat clouds within the climate system are linked to problems associated with aerosols. Current model treatments of climate forcing from aerosols predict effects that are not easily consistent with the past climate record. A major challenge is to develop and validate the treatments of the microphysics of clouds and their interactions with aerosols on the scale of a general circulation model grid. A second major challenge is to develop an understanding of the carbon components of the aerosol system. Meeting this challenge requires that we develop data for a mechanistic understanding of carbonaceous aerosol effects on clouds as well as developing an understanding of the magnitude of the anthropogenic and natural components of the carbonaceous aerosol system. (See Chapter 6, Sections 6.7 and 6.8; see also Chapter 4, Section 4.5.1.2.)

As attention is turned toward the troposphere, the experimental strategy simply cannot adopt the stratospheric simplifications. The uneven distribution of emission sources at the surface of the Earth and the role of meteorological processes at various scales must be addressed directly. Fine-scaled, three-dimensional models of chemically active trace gases in the troposphere are needed to resolve transport processes at the highest possible resolution. These models should be designed to simulate the chemistry and transport of atmospheric tracers on global and regional scales, with accurate parametrizations of sub-scale processes that affect the chemical composition of the troposphere. It is therefore necessary to pursue an ambitious long-term programme to develop comprehensive models of the troposphere system, including chemical, dynamical, radiative, and eventually biological components. (See Chapter 4, Sections 4.4 to 4.6.)

The short-lived radiatively important species pose an observational challenge. The fact that they are short-lived implies that observations of the concentrations are needed over wide spatial regions and over long periods of time. This is particularly important for aerosols. The current uncertainties are non-trivial (see again Chapter 6, Figure 6.7) and need to be reduced.

In sum, there needs to be an expanded attack on the key contributors to uncertainty about the behaviour of the climate system today and in the future. As stated in Chapter 13, Section 13.1.2, “Scenarios should also provide adequate quantitative measures of uncertainty. The sources of uncertainty are many, including the trajectory of greenhouse gas emissions in the future, their conversion into atmospheric concentrations, the range of responses of various climate models to a given radiative forcing and the method of constructing high resolution information from global climate model outputs (see Chapter 13, Figure 13.2). For many purposes, simply defining a single climate future is insufficient and unsatisfactory. Multiple climate scenarios that address at least one, or preferably several, sources of uncertainty allow these uncertainties to be quantified and explicitly accounted for in impact assessments.”

In addition to this needed expansion in the attack on uncertainties in the climate system, there is an important new challenge that should now be addressed more aggressively. It is time to link more formally physical climate-biogeochemical

models with models of the human system. At present, human influences generally are treated only through emission scenarios that provide external forcings to the climate system. In future comprehensive models, human activities will interact with the dynamics of physical, chemical, and biological subsystems through a diverse set of contributing activities, feedbacks, and responses. This does not mean that it is necessary or even logical to attempt to develop prognostic models of human actions since much will remain inherently unpredictable; however, the scenarios analysis could and should be more fully coupled to the coupled physical climate-biogeochemical system.

As part of the foundation-building to meet this challenge, we turn attention now to the human system.

14.3 The Human System

14.3.1 Overview

Human processes are critically linked to the climate system as contributing causes of global change, as determinants of impacts, and through responses. Representing these linkages poses perhaps the greatest challenge to modelling the total Earth system. But understanding them is essential to understanding the behaviour of the whole system and to providing useful advice to inform policy and response. Significant progress has been made, but formidable challenges remain.

Human activities have altered the Earth system, and many such influences are accelerating with population growth and technological development. The use of fossil fuels and chemical fertilisers are major influences, as is the human transformation of much of the Earth’s surface in the past 300 years.

Land-use change illustrates the potential complexity of linkages between human activity and major non-human components of the Earth system. The terrestrial biosphere is fundamentally modified by land clearing for agriculture, industrialisation, urbanisation, and by forest and rangeland management practices. These changes affect the atmosphere through an altered energy balance over the more intensively managed parts of the land surface, as well as through changed fluxes of water vapour, CO₂, CH₄ and other trace gases between soils, vegetation, and the atmosphere. Changed land use also greatly alters the fluxes of carbon, nutrients, and inorganic sediments into river systems, and consequently into oceanic coastal zones.

The response of the total Earth system to these changes in anthropogenic forcing is currently not known. Sensitivity studies with altered land cover distributions in general circulation models have shown that drastic changes, such as total deforestation of all tropical or boreal forests, may lead to feedbacks in atmospheric circulation and a changed climate that would not support the original vegetation (e.g., Claussen, 1996). Regional climate simulations, on the other hand, have shown that at the continental scale, important teleconnections may exist through which more modest tropical forest clearing may cause a change in climate in undisturbed areas. Coupling the global to the local is a key challenge; regional studies may prove to be uniquely valuable.

Human land-use change will continue and probably accelerate due to increasing demands for food and fibre, changes in forest and water management practices, and possibly large-scale projects to sequester carbon in forests or to produce biomass fuels. In addition, anthropogenic changes in material and energy fluxes, resulting from such activities as fossil fuel combustion and chemical fertiliser use, are expected to increase in the coming decades. Predictions of changes in the carbon and nitrogen cycles are sensitive to estimates of human activity and predictions of the impacts of these global changes must take into account human vulnerability, adaptation, and response. Predicting the future response of the Earth system to changes in climate and in parallel to changes in land use and land cover will require projections of trends in the human contributions to these global changes; this sort of modelling presents difficult challenges because of the multiple factors operating at local, regional, continental, and global levels to influence local land-use decisions.

In sum, the human element probably represents the most important aspect both of the causes and effects of climate change and environmental impacts. Any policy intervention will have human activities as its immediate target.

14.3.2 Humans: Drivers of Global Change: Recipients of Global Change

The provision of useful guidance to inform policy requires observation and description of human contributions to global change, as well as theoretical studies of the underlying social processes that shape them. We also need to understand how global change affects human welfare. This requires not merely studies of direct exposure but also of the capacity to respond.

Causal models of social processes have large uncertainties, and pose problems that are of a qualitatively different character than those encountered in modelling non-human components of the Earth system. This is due, first and foremost, to the inherent reflexivity of human behaviour; i.e., the fact that human beings have intellectual capabilities and emotional endowments enabling them to invent new solutions and transcend established “laws” in ways that no other species can do. As a consequence, predictive models may well alter the behaviour that they seek to predict and explain – indeed, such models are sometimes deliberately used exactly for that purpose. Moreover, the diversity of societies, cultures, and political and economic systems often frustrates attempts to generalise findings and propositions from one setting to another. Representation of human behaviour at the micro (individual) and macro (collective) scale may require fundamentally different approaches (see Gibson *et al.*, 1998).

These kinds of difficulties intrinsically limit the predictive power that can be ascribed to models of social processes. As a consequence, research on human drivers and responses to climate change cannot be expected to produce conventional predictions beyond a very short time horizon. This does not imply, however, that research on human behaviour and social processes cannot provide knowledge and insight that can inform policy deliberations. A considerable amount of basic knowledge and insight exist, and this knowledge can be used, *inter alia*, for constructing

scenarios showing plausible trajectories and identifying the critical factors that will have to be targeted in order to switch from one trajectory to another. From the perspective of policy-makers, this can indeed be an important contribution.

To make the most of this potential, further progress is required along two main frontiers. One challenge is to develop a more integrated understanding of social systems and human behaviour. With some exceptions, the first generation of models in this area represented “the human system” by a few key variables. For example, resource use was often conceived of as a function of population size and income level. The performance of such simplistic models was by-and-large poor. It is abundantly clear that the impact of human activities as drivers of climate change depends upon a complex set of interrelated factors, including also technologies in use, social institutions, and individual beliefs, attitudes, and values. At present, it seems fair to say that we have a reasonably good theoretical grasp of important types of institutions, such as markets and hierarchies, in ideal-type form. What we need to understand better is how their impure real-world counterparts work, and to improve our understanding of the intricate interplay of institutional complexes, i.e., how markets, governments and other social institutions interact to shape human behaviour. Research in political economy clearly indicates that phenomena such as economic growth are to a significant extent affected by the functioning of interlocking networks of institutional arrangements.

Similarly, we have a fairly good grasp on particular kinds of intellectual processes – in particular, the logic of rational choice – but we are doing less well when it comes to understanding how beliefs, attitudes and values change and how change in these factors in turn affects manifest human behaviour, such as consumption patterns. To address these challenges we need more interdisciplinary research designed to integrate knowledge from different fields and sub-fields into a more holistic understanding of “the human system”. The intellectual and organisational problems involved should not be underestimated, but we are confident that the prospects for making progress along this frontier are better now than ever before.

The other main challenge is to find better ways of integrating models of the biogeophysical Earth system with models of social systems and human behaviour. Some encouraging progress has been made at this interface, particularly over the last decade. For example, there has been a rapid increase in attempts to integrate representations of human activities in models with explicit formal linkages to other components of the Earth system. Such integrated assessment models have offered preliminary characterisations of human-climate linkages, particularly through models of multiple linked human and climate stresses on land cover. Moreover, they have provided preliminary characterisation of broad classes of policy responses, and have been employed to characterise and prioritise policy-relevant uncertainties.

Yet, effective integration is frustrated by at least two main obstacles. One is incongruity of temporal and spatial scales. Social science research cannot match the long time horizons of much natural science research. On the other hand, in studying consequences for human welfare and responses to these consequences, social scientists need estimates of biophysical

impacts of climate change differentiated by political units or even smaller social systems. Aggregate global-scale estimates are of limited use in this context; human sensitivity to climate change varies significantly across regions and social groups, and so does response capacity. We can expect to see some progress in alleviating the spatial resolution problem, as regional-scale models of climate change are further developed, but we have to recognise that the scale problems are fundamental and that no quick fixes are in sight. The other problem pertains to the interface between different methodological approaches. In particular, concerted efforts are required to develop better tools for coupling approaches relying on numerical modelling with “softer” approaches using interpretative frameworks and qualitative methods. Some of these differences are too profound to be eliminated, but that does not imply that bridges cannot be built. Learning how to work more effectively across these methodological divides is essential to the further development of integrated global change research. Again, some encouraging progress is being made.

14.4 Outlook

There is a growing recognition in the scientific community and more broadly that:

- The Earth functions as a system, with properties and behaviour that are characteristic of the system as a whole. These include critical thresholds, “switch” or “control” points, strong non-linearities, teleconnections, chaotic elements, and unresolvable uncertainties. Understanding the components of the Earth system is critically important, but is insufficient on its own to understand the functioning of the Earth system as a whole.
- Humans are now a significant force in the Earth system, altering key process rates and absorbing the impacts of global environmental changes. The environmental significance of human activities is now so profound that the current geological era can be called the “Anthropocene” (Crutzen and Stoermer, 2000).

A scientific understanding of the Earth system is required to help human societies develop in ways that sustain the global life support system. The clear challenge of understanding climate variability and change and the associated consequences and feedbacks is a specific and important example of the need for a scientific understanding of the Earth as a system. It is also clear that the scientific study of the whole Earth system, taking account of its full functional and geographical complexity over time, requires an unprecedented effort of international collaboration. It is well beyond the scope of individual countries and regions.

The world’s scientific community, working in part through the three global environmental change programmes (the International Geosphere-Biosphere Programme (IGBP), the International Human Dimensions Programme on Global Environmental Change (IHDP), and the World Climate Research Programme (WCRP)), has built a solid base for understanding the Earth system. The IGBP, IHDP and WCRP have also developed effective and efficient strategies for implementing global environmental change research at the international level. The challenge to

IGBP, IHDP and WCRP is to build an international programme of Earth system science, driven by a common mission and common questions, employing visionary and creative scientific approaches, and based on an ever closer collaboration across disciplines, research themes, programmes, nations and regions.

We need to build on our existing understanding of the Earth system and its interactive human and non-human processes through time in order to:

- improve evaluation and understanding of current and future global change; and
- place on an increasingly firm scientific basis the challenge of sustaining the global environment for future human societies.

The climate system is particularly challenging since it is known that components in the system are inherently chaotic, and there are central components which affect the system in a non-linear manner and potentially could switch the sign of critical feedbacks. The non-linear processes include the basic dynamical response of the climate system and the interactions between the different components. These complex, non-linear dynamics are an inherent aspect of the climate system. Amongst the important non-linear processes are the role of clouds, the thermohaline circulation, and sea ice. There are other broad non-linear components, the biogeochemical system and, in particular, the carbon system, the hydrological cycle, and the chemistry of the atmosphere.

Given the complexity of the climate system and the inherent multi-decadal time-scale, there is a central and unavoidable need for long-term consistent data to support climate and environmental change investigations. Data from the present and recent past, credible global climate-relevant data for the last few centuries, along with lower frequency data for the last several millennia, are all needed. Research observational data sets that span significant temporal and spatial scales are needed so that models can be refined, validated, or perhaps, most importantly, rejected. The elimination of models because they are in conflict with climate-relevant data is particularly important. Running unrealistic models will consume scarce computing resources, and the results may add unrealistic information to the needed distribution functions. Such data must be adequate in temporal and spatial coverage, in parameters measured, and in precision, to permit meaningful validation. We are still unfortunately short of data for the quantitative assessment of extremes on the global scale in the observed climate.

In sum, there is a need for:

- more comprehensive data, contemporary, historical, and palaeological, relevant to the climate system;
- expanded process studies that more clearly elucidate the structure of fundamental components of the Earth system and the potential for changes in these central components;
- greater effort in testing and developing increasingly comprehensive and sophisticated Earth system models;

- increased emphasis upon producing ensemble calculations of Earth system models that yield descriptions of the likelihood of a broad range of different possibilities, and finally;
- new efforts in understanding the fundamental behaviour of large-scale non-linear systems.

These are significant challenges, but they are not insurmountable. The challenges to understanding the Earth system including the human component are daunting, and the pressing needs are significant. However, the opportunity for progress exists, and, in fact, this opportunity simply must be realised. The issues are too important, and they will not vanish. The challenges simply must be met.

References

- Claussen, M.**, 1996: Variability of global biome patterns as a function of initial and boundary conditions in a climate model. *Clim. Dyn.*, **12**, 371-379.
- Crutzen, P.**, and E. Stoermer, 2000: *International Geosphere Biosphere Programme (IGBP) Newsletter*, **41**.
- Emery, W. J.**, C. W. Fowler, and J. A. Maslanik, 1997: Satellite-derived maps of Arctic and Antarctic sea-ice motion: 1988-1994. *Geophys. Res. Lett.*, **24**, 897-900.
- Gibson, C.**, E. Ostrom, and Toh-Kyeong Ahn. 1998: Scaling Issues in the Social Sciences. IHDP Working Paper No. 1. International Human dimensions Programme on Global Environmental Change. Bonn, Germany. See also <http://www.uni-bonn.de/ihdp>.
- Gordon, H. B.**, and S. P. O'Farrell, 1997: Transient climate change in the CSIRO coupled model with dynamic sea ice. *Mont. Weath. Rev.*, **125**(5), 875-907.
- Gordon, C.**, C. Cooper, C.A. Senior, H. Banks, J.M. Gregory, T.C. Johns, J.F.B. Mitchell, and R.A. Wood, 1999: The simulation of SST, sea-ice extents and ocean heat transport in a version of the Hadley Centre coupled model without flux adjustments. Accepted, *Clim. Dyn.*
- IPCC**, 1996: Climate Change 1995: The Science of Climate Change. Contribution of Working Group 1 to the Second Assessment Report of the Intergovernmental Panel on Climate Change. Houghton, J.T., L.G.M. Filho, B.A. Callendar, N. Harris, A. Kattenberg, and K. Maskell (eds). Cambridge University Press, New York, 572 pp.
- Kattenberg, A.**, F. Giorgi, H. Grassl, G.A. Meehl, J.F.B. Mitchell, R.J. Stouffer, T. Tokioka, A.J. Weaver, and T.M.L. Wigley. 1996: Climate Models - Projections of Future Climate. In: Houghton, J.T., L.G.M. Filho, B.A. Callendar, N. Harris, A. Kattenberg, and K. Maskell (eds). 1996. Climate Change 1995: The Science of Climate Change. Contribution of Working Group 1 to the Second Assessment Report of the Intergovernmental Panel on Climate Change. p. 285-357. Cambridge University Press, New York, 572 pp.
- Lofgren, B.M.** 1995: Sensitivity of the land-ocean circulations, precipitation and soil moisture to perturbed land surface albedo. *J. Climate*, **8**, 2521-2542.
- Maier-Reimer, E.**, U. Mikolajewicz, and A. Winguth, 1996: Future ocean uptake of CO₂ - Interaction between ocean circulation and biology. *Clim. Dyn.*, **12**, 711-721.
- Meehl, G.A** and W.M. Washington, 1995: Cloud albedo feedback and the super greenhouse effect in a global coupled GCM. *Clim. Dyn.*, **11**, 399-411.
- Meehl, G. A.**, G.J. Boer, C. Covey, M. Latif, and R.J. Stouffer, 2000: The Coupled Model Intercomparison Project (CMIP). *Bull. Am. Met. Soc.*, **81**(2), 313-318.
- Mitchell, J.** 2000. Modelling cloud-climate feedbacks in predictions of human-induced climate change. In: Workshop on Cloud Processes and Cloud Feedbacks in Large-scale Models. World Climate Research Programme. WCRP-110; WMO/TD-No.993. Geneva.
- Randall, S.D.**, J. Curry, D. Battisti, G. Flato, R. Grumbine, S. Hakkinen, D. Martinson, R. Preller, J. Walsh, J. Weatherly, 1998: Status of and outlook for large-scale modelling of atmosphere-ice-ocean interactions in the Arctic. *Bull. Am. Met. Soc.*, **79**, 197-219.
- SAR**, see IPCC, 1996.
- Sarmiento, J.L.** and J.R. Toggweiler, 1984: A new model for the role of the oceans in determining atmospheric CO₂. *Nature*, **308**, 621-624.
- Senior, C.A.**, 1999: Comparison of mechanisms of cloud-climate feedbacks in a GCM. *J. Climate*, **12**, 1480-1489.
- Smith, D. M.**, 1998: Recent increase in the length of the melt season of perennial Arctic sea ice. *Geophys. Res. Lett.*, **25**, 655-658.
- Stephens, G.**, D. Varne, S. Walker. 2000: The CLOUDSAT mission: A new dimension to space-based observations of cloud in the coming millennium. In: Workshop on Cloud Processes and Cloud Feedbacks in Large-scale Models. World Climate Research Programme. WCRP-110; WMO/TD-No.993. Geneva.
- Stouffer, R. J.**, and K. W. Dixon, 1998: Initialization of coupled models for use in climate studies: A review. In: *Research Activities in Atmospheric and Oceanic Modelling*, Report No. **27**, WMO/TD-No. 865, World Meteorological Organization, Geneva, Switzerland, I.1-I.8.
- Washington, W.M.**, and G.A. Meehl, 1996: High-latitude climate change in a global coupled ocean-atmosphere-sea ice model with increased atmospheric CO₂. *J. Geophys. Res.*, **101**, 12795-12801.
- Washington, W.M.**, J.W. Weatherly, G.A. Meehl, A.J. Semtner Jr., T.W. Bettge, A.P. Craig, W.G. Strand Jr., J.M. Arblaster, V.B. Wayland, R. James, Y. Zhang, 2000: Parallel climate model (PCM) control and 1% per year CO₂ simulations with a 2/3 degree ocean model and a 27 km dynamical sea ice model. *Clim. Dyn.*, **16** (10,11), 755-774.
- Weatherly, J. W.**, B. P. Briegleb, W. G. Large, J. A. Maslanik, 1998: Sea ice and polar climate in the NCAR CSM. *J. Climate*, **11**, 1472-1486.

Appendix I

Glossary

Editor: A.P.M. Baede

A → indicates that the following term is also contained in this Glossary.

Adjustment time

See: →Lifetime; see also: →Response time.

Aerosols

A collection of airborne solid or liquid particles, with a typical size between 0.01 and 10 µm and residing in the atmosphere for at least several hours. Aerosols may be of either natural or anthropogenic origin. Aerosols may influence climate in two ways: directly through scattering and absorbing radiation, and indirectly through acting as condensation nuclei for cloud formation or modifying the optical properties and lifetime of clouds. See: →Indirect aerosol effect.

The term has also come to be associated, erroneously, with the propellant used in “aerosol sprays”.

Afforestation

Planting of new forests on lands that historically have not contained forests. For a discussion of the term →forest and related terms such as afforestation, →reforestation, and →deforestation: see the IPCC Report on Land Use, Land-Use Change and Forestry (IPCC, 2000).

Albedo

The fraction of solar radiation reflected by a surface or object, often expressed as a percentage. Snow covered surfaces have a high albedo; the albedo of soils ranges from high to low; vegetation covered surfaces and oceans have a low albedo. The Earth's albedo varies mainly through varying cloudiness, snow, ice, leaf area and land cover changes.

Altimetry

A technique for the measurement of the elevation of the sea, land or ice surface. For example, the height of the sea surface (with respect to the centre of the Earth or, more conventionally, with respect to a standard “ellipsoid of revolution”) can be measured from space by current state-of-the-art radar altimetry with

centrimetric precision. Altimetry has the advantage of being a measurement relative to a geocentric reference frame, rather than relative to land level as for a →tide gauge, and of affording quasi-global coverage.

Anthropogenic

Resulting from or produced by human beings.

Atmosphere

The gaseous envelope surrounding the Earth. The dry atmosphere consists almost entirely of nitrogen (78.1% volume mixing ratio) and oxygen (20.9% volume mixing ratio), together with a number of trace gases, such as argon (0.93% volume mixing ratio), helium, and radiatively active →greenhouse gases such as →carbon dioxide (0.035% volume mixing ratio), and ozone. In addition the atmosphere contains water vapour, whose amount is highly variable but typically 1% volume mixing ratio. The atmosphere also contains clouds and →aerosols.

Attribution

See: →Detection and attribution.

Autotrophic respiration

→Respiration by photosynthetic organisms (plants).

Biomass

The total mass of living organisms in a given area or volume; recently dead plant material is often included as dead biomass.

Biosphere (terrestrial and marine)

The part of the Earth system comprising all →ecosystems and living organisms, in the atmosphere, on land (terrestrial biosphere) or in the oceans (marine biosphere), including derived dead organic matter, such as litter, soil organic matter and oceanic detritus.

Black carbon

Operationally defined species based on measurement of light absorption and chemical reactivity and/or thermal stability; consists of soot, charcoal, and/or possible light-absorbing refractory organic matter. (Source: Charlson and Heintzenberg, 1995, p. 401.)

Burden

The total mass of a gaseous substance of concern in the atmosphere.

Carbonaceous aerosol

Aerosol consisting predominantly of organic substances and various forms of →black carbon. (Source: Charlson and Heintzenberg, 1995, p. 401.)

Carbon cycle

The term used to describe the flow of carbon (in various forms, e.g. as carbon dioxide) through the atmosphere, ocean, terrestrial →biosphere and lithosphere.

Carbon dioxide (CO₂)

A naturally occurring gas, also a by-product of burning fossil fuels and →biomass, as well as →land-use changes and other industrial processes. It is the principal anthropogenic →greenhouse gas that affects the earth's radiative balance. It is the reference gas against which other greenhouse gases are measured and therefore has a →Global Warming Potential of 1.

Carbon dioxide (CO₂) fertilisation

The enhancement of the growth of plants as a result of increased atmospheric CO₂ concentration. Depending on their mechanism of →photosynthesis, certain types of plants are more sensitive to changes in atmospheric CO₂ concentration. In particular, →C₃ plants generally show a larger response to CO₂ than →C₄ plants.

Charcoal

Material resulting from charring of biomass, usually retaining some of the microscopic texture typical of plant tissues; chemically it consists mainly of carbon with a disturbed graphitic structure, with lesser amounts of oxygen and hydrogen. See: →Black carbon; Soot particles. (Source: Charlson and Heintzenberg, 1995, p. 402.)

Climate

Climate in a narrow sense is usually defined as the "average weather", or more rigorously, as the statistical description in terms of the mean and variability of relevant quantities over a period of time ranging from months to thousands or millions of years. The classical period is 30 years, as defined by the World Meteorological Organization (WMO). These quantities are most often surface variables such as temperature, precipitation, and wind. Climate in a wider sense is the state, including a statistical description, of the →climate system.

Climate change

Climate change refers to a statistically significant variation in

either the mean state of the climate or in its variability, persisting for an extended period (typically decades or longer). Climate change may be due to natural internal processes or external forcings, or to persistent anthropogenic changes in the composition of the atmosphere or in land use.

Note that the →Framework Convention on Climate Change (UNFCCC), in its Article 1, defines "climate change" as: "a change of climate which is attributed directly or indirectly to human activity that alters the composition of the global atmosphere and which is in addition to natural climate variability observed over comparable time periods". The UNFCCC thus makes a distinction between "climate change" attributable to human activities altering the atmospheric composition, and "climate variability" attributable to natural causes.

See also: →Climate variability.

Climate feedback

An interaction mechanism between processes in the →climate system is called a climate feedback, when the result of an initial process triggers changes in a second process that in turn influences the initial one. A positive feedback intensifies the original process, and a negative feedback reduces it.

Climate model (hierarchy)

A numerical representation of the →climate system based on the physical, chemical and biological properties of its components, their interactions and feedback processes, and accounting for all or some of its known properties. The climate system can be represented by models of varying complexity, i.e. for any one component or combination of components a *hierarchy* of models can be identified, differing in such aspects as the number of spatial dimensions, the extent to which physical, chemical or biological processes are explicitly represented, or the level at which empirical →parametrizations are involved. Coupled atmosphere/ocean/sea-ice General Circulation Models (AOGCMs) provide a comprehensive representation of the climate system. There is an evolution towards more complex models with active chemistry and biology.

Climate models are applied, as a research tool, to study and simulate the climate, but also for operational purposes, including monthly, seasonal and interannual →climate predictions.

Climate prediction

A climate prediction or climate forecast is the result of an attempt to produce a most likely description or estimate of the actual evolution of the climate in the future, e.g. at seasonal, interannual or long-term time scales. See also: →Climate projection and →Climate (change) scenario.

Climate projection

A →projection of the response of the climate system to →emission or concentration scenarios of greenhouse gases and aerosols, or →radiative forcing scenarios, often based upon simulations by →climate models. Climate projections are distinguished from →climate predictions in order to emphasise that climate projections depend upon the emission/concentration/

radiative forcing scenario used, which are based on assumptions, concerning, e.g., future socio-economic and technological developments, that may or may not be realised, and are therefore subject to substantial uncertainty.

Climate scenario

A plausible and often simplified representation of the future climate, based on an internally consistent set of climatological relationships, that has been constructed for explicit use in investigating the potential consequences of anthropogenic →climate change, often serving as input to impact models. →Climate projections often serve as the raw material for constructing climate scenarios, but climate scenarios usually require additional information such as about the observed current climate. A *climate change scenario* is the difference between a climate scenario and the current climate.

Climate sensitivity

In IPCC Reports, *equilibrium climate sensitivity* refers to the equilibrium change in global mean surface temperature following a doubling of the atmospheric (→equivalent) CO₂ concentration. More generally, equilibrium climate sensitivity refers to the equilibrium change in surface air temperature following a unit change in →radiative forcing (°C/Wm⁻²). In practice, the evaluation of the equilibrium climate sensitivity requires very long simulations with Coupled General Circulation Models (→Climate model).

The *effective climate sensitivity* is a related measure that circumvents this requirement. It is evaluated from model output for evolving non-equilibrium conditions. It is a measure of the strengths of the →feedbacks at a particular time and may vary with forcing history and climate state. Details are discussed in Section 9.2.1 of Chapter 9 in this Report.

Climate system

The climate system is the highly complex system consisting of five major components: the →atmosphere, the →hydrosphere, the →cryosphere, the land surface and the →biosphere, and the interactions between them. The climate system evolves in time under the influence of its own internal dynamics and because of external forcings such as volcanic eruptions, solar variations and human-induced forcings such as the changing composition of the atmosphere and →land-use change.

Climate variability

Climate variability refers to variations in the mean state and other statistics (such as standard deviations, the occurrence of extremes, etc.) of the climate on all temporal and spatial scales beyond that of individual weather events. Variability may be due to natural internal processes within the climate system (*internal variability*), or to variations in natural or anthropogenic external forcing (*external variability*). See also: →Climate change.

Cloud condensation nuclei

Airborne particles that serve as an initial site for the condensation of liquid water and which can lead to the formation of cloud droplets. See also: →Aerosols.

CO₂ fertilisation

See →Carbon dioxide (CO₂) fertilisation

Cooling degree days

The integral over a day of the temperature above 18°C (e.g. a day with an average temperature of 20°C counts as 2 cooling degree days). See also: →Heating degree days.

Cryosphere

The component of the →climate system consisting of all snow, ice and permafrost on and beneath the surface of the earth and ocean. See: →Glacier; →Ice sheet.

C₃ plants

Plants that produce a three-carbon compound during photosynthesis; including most trees and agricultural crops such as rice, wheat, soybeans, potatoes and vegetables.

C₄ plants

Plants that produce a four-carbon compound during photosynthesis; mainly of tropical origin, including grasses and the agriculturally important crops maize, sugar cane, millet and sorghum.

Deforestation

Conversion of forest to non-forest. For a discussion of the term →forest and related terms such as →afforestation, →reforestation, and deforestation: see the IPCC Report on Land Use, Land-Use Change and Forestry (IPCC, 2000).

Desertification

Land degradation in arid, semi-arid, and dry sub-humid areas resulting from various factors, including climatic variations and human activities. Further, the UNCCD (The United Nations Convention to Combat Desertification) defines land degradation as a reduction or loss, in arid, semi-arid, and dry sub-humid areas, of the biological or economic productivity and complexity of rain-fed cropland, irrigated cropland, or range, pasture, forest, and woodlands resulting from land uses or from a process or combination of processes, including processes arising from human activities and habitation patterns, such as: (i) soil erosion caused by wind and/or water; (ii) deterioration of the physical, chemical and biological or economic properties of soil; and (iii) long-term loss of natural vegetation.

Detection and attribution

Climate varies continually on all time scales. **Detection** of →climate change is the process of demonstrating that climate has changed in some defined statistical sense, without providing a reason for that change. **Attribution** of causes of climate change is the process of establishing the most likely causes for the detected change with some defined level of confidence.

Diurnal temperature range

The difference between the maximum and minimum temperature during a day.

Dobson Unit (DU)

A unit to measure the total amount of ozone in a vertical column above the Earth's surface. The number of Dobson Units is the thickness in units of 10^{-5} m, that the ozone column would occupy if compressed into a layer of uniform density at a pressure of 1013 hPa, and a temperature of 0°C. One DU corresponds to a column of ozone containing 2.69×10^{20} molecules per square meter. A typical value for the amount of ozone in a column of the Earth's atmosphere, although very variable, is 300 DU.

Ecosystem

A system of interacting living organisms together with their physical environment. The boundaries of what could be called an ecosystem are somewhat arbitrary, depending on the focus of interest or study. Thus the extent of an ecosystem may range from very small spatial scales to, ultimately, the entire Earth.

El Niño-Southern Oscillation (ENSO)

El Niño, in its original sense, is a warm water current which periodically flows along the coast of Ecuador and Peru, disrupting the local fishery. This oceanic event is associated with a fluctuation of the intertropical surface pressure pattern and circulation in the Indian and Pacific oceans, called the Southern Oscillation. This coupled atmosphere-ocean phenomenon is collectively known as El Niño-Southern Oscillation, or ENSO. During an El Niño event, the prevailing trade winds weaken and the equatorial countercurrent strengthens, causing warm surface waters in the Indonesian area to flow eastward to overlie the cold waters of the Peru current. This event has great impact on the wind, sea surface temperature and precipitation patterns in the tropical Pacific. It has climatic effects throughout the Pacific region and in many other parts of the world. The opposite of an El Niño event is called *La Niña*.

Emission scenario

A plausible representation of the future development of emissions of substances that are potentially radiatively active (e.g. →greenhouse gases, →aerosols), based on a coherent and internally consistent set of assumptions about driving forces (such as demographic and socio-economic development, technological change) and their key relationships.

Concentration scenarios, derived from emission scenarios, are used as input into a climate model to compute →climate projections.

In IPCC (1992) a set of emission scenarios was presented which were used as a basis for the →climate projections in IPCC (1996). These emission scenarios are referred to as the IS92 scenarios. In the IPCC Special Report on Emission Scenarios (Nakićenović *et al.*, 2000) new emission scenarios, the so called →SRES scenarios, were published some of which were used, among others, as a basis for the climate projections presented in Chapter 9 of this Report. For the meaning of some terms related to these scenarios, see →SRES scenarios.

Energy balance

Averaged over the globe and over longer time periods, the energy budget of the →climate system must be in balance. Because the

climate system derives all its energy from the Sun, this balance implies that, globally, the amount of incoming →solar radiation must on average be equal to the sum of the outgoing reflected solar radiation and the outgoing →infrared radiation emitted by the climate system. A perturbation of this global radiation balance, be it human induced or natural, is called →radiative forcing.

Equilibrium and transient climate experiment

An *equilibrium climate experiment* is an experiment in which a →climate model is allowed to fully adjust to a change in →radiative forcing. Such experiments provide information on the difference between the initial and final states of the model, but not on the time-dependent response. If the forcing is allowed to evolve gradually according to a prescribed →emission scenario, the time dependent response of a climate model may be analysed. Such experiment is called a *transient climate experiment*. See: →Climate projection.

Equivalent CO₂ (carbon dioxide)

The concentration of →CO₂ that would cause the same amount of →radiative forcing as a given mixture of CO₂ and other →greenhouse gases.

Eustatic sea-level change

A change in global average sea level brought about by an alteration to the volume of the world ocean. This may be caused by changes in water density or in the total mass of water. In discussions of changes on geological time-scales, this term sometimes also includes changes in global average sea level caused by an alteration to the shape of the ocean basins. In this Report the term is not used with that sense.

Evapotranspiration

The combined process of evaporation from the Earth's surface and transpiration from vegetation.

External forcing

See: →Climate system.

Extreme weather event

An extreme weather event is an event that is rare within its statistical reference distribution at a particular place. Definitions of "rare" vary, but an extreme weather event would normally be as rare as or rarer than the 10th or 90th percentile. By definition, the characteristics of what is called *extreme weather* may vary from place to place.

An *extreme climate event* is an average of a number of weather events over a certain period of time, an average which is itself extreme (e.g. rainfall over a season).

Faculae

Bright patches on the Sun. The area covered by faculae is greater during periods of high →solar activity.

Feedback

See: →Climate feedback.

Flux adjustment

To avoid the problem of coupled atmosphere-ocean general circulation models drifting into some unrealistic climate state, adjustment terms can be applied to the atmosphere-ocean fluxes of heat and moisture (and sometimes the surface stresses resulting from the effect of the wind on the ocean surface) before these fluxes are imposed on the model ocean and atmosphere. Because these adjustments are precomputed and therefore independent of the coupled model integration, they are uncorrelated to the anomalies which develop during the integration. In Chapter 8 of this Report it is concluded that present models have a reduced need for flux adjustment.

Forest

A vegetation type dominated by trees. Many definitions of the term forest are in use throughout the world, reflecting wide differences in bio-geophysical conditions, social structure, and economics. For a discussion of the term forest and related terms such as →afforestation, →reforestation, and →deforestation: see the IPCC Report on Land Use, Land-Use Change and Forestry (IPCC, 2000).

Fossil CO₂ (carbon dioxide) emissions

Emissions of CO₂ resulting from the combustion of fuels from fossil carbon deposits such as oil, gas and coal.

Framework Convention on Climate Change

See: →United Nations Framework Convention on Climate Change (UNFCCC).

General Circulation

The large scale motions of the atmosphere and the ocean as a consequence of differential heating on a rotating Earth, aiming to restore the →energy balance of the system through transport of heat and momentum.

General Circulation Model (GCM)

See: →Climate model.

Geoid

The surface which an ocean of uniform density would assume if it were in steady state and at rest (i.e. no ocean circulation and no applied forces other than the gravity of the Earth). This implies that the geoid will be a surface of constant gravitational potential, which can serve as a reference surface to which all surfaces (e.g., the Mean Sea Surface) can be referred. The geoid (and surfaces parallel to the geoid) are what we refer to in common experience as “level surfaces”.

Glacier

A mass of land ice flowing downhill (by internal deformation and sliding at the base) and constrained by the surrounding topography e.g. the sides of a valley or surrounding peaks; the bedrock topography is the major influence on the dynamics and surface slope of a glacier. A glacier is maintained by accumulation of snow at high altitudes, balanced by melting at low altitudes or discharge into the sea.

Global surface temperature

The global surface temperature is the area-weighted global average of (i) the sea-surface temperature over the oceans (i.e. the subsurface bulk temperature in the first few meters of the ocean), and (ii) the surface-air temperature over land at 1.5 m above the ground.

Global Warming Potential (GWP)

An index, describing the radiative characteristics of well mixed →greenhouse gases, that represents the combined effect of the differing times these gases remain in the atmosphere and their relative effectiveness in absorbing outgoing →infrared radiation. This index approximates the time-integrated warming effect of a unit mass of a given greenhouse gas in today’s atmosphere, relative to that of →carbon dioxide.

Greenhouse effect

→Greenhouse gases effectively absorb →infrared radiation, emitted by the Earth’s surface, by the atmosphere itself due to the same gases, and by clouds. Atmospheric radiation is emitted to all sides, including downward to the Earth’s surface. Thus greenhouse gases trap heat within the surface-troposphere system. This is called the *natural greenhouse effect*.

Atmospheric radiation is strongly coupled to the temperature of the level at which it is emitted. In the →troposphere the temperature generally decreases with height. Effectively, infrared radiation emitted to space originates from an altitude with a temperature of, on average, -19°C, in balance with the net incoming solar radiation, whereas the Earth’s surface is kept at a much higher temperature of, on average, +14°C.

An increase in the concentration of greenhouse gases leads to an increased infrared opacity of the atmosphere, and therefore to an effective radiation into space from a higher altitude at a lower temperature. This causes a →radiative forcing, an imbalance that can only be compensated for by an increase of the temperature of the surface-troposphere system. This is the *enhanced greenhouse effect*.

Greenhouse gas

Greenhouse gases are those gaseous constituents of the atmosphere, both natural and anthropogenic, that absorb and emit radiation at specific wavelengths within the spectrum of infrared radiation emitted by the Earth’s surface, the atmosphere and clouds. This property causes the →greenhouse effect. Water vapour (H₂O), carbon dioxide (CO₂), nitrous oxide (N₂O), methane (CH₄) and ozone (O₃) are the primary greenhouse gases in the Earth’s atmosphere. Moreover there are a number of entirely human-made greenhouse gases in the atmosphere, such as the →halocarbons and other chlorine and bromine containing substances, dealt with under the →Montreal Protocol. Beside CO₂, N₂O and CH₄, the →Kyoto Protocol deals with the greenhouse gases sulphur hexafluoride (SF₆), hydrofluorocarbons (HFCs) and perfluorocarbons (PFCs).

Gross Primary Production (GPP)

The amount of carbon fixed from the atmosphere through →photosynthesis.

Grounding line/zone

The junction between →ice sheet and →ice shelf or the place where the ice starts to float.

Halocarbons

Compounds containing either chlorine, bromine or fluorine and carbon. Such compounds can act as powerful →greenhouse gases in the atmosphere. The chlorine and bromine containing halocarbons are also involved in the depletion of the →ozone layer.

Heating degree days

The integral over a day of the temperature below 18°C (e.g. a day with an average temperature of 16°C counts as 2 heating degree days). See also: →Cooling degree days.

Heterotrophic respiration

The conversion of organic matter to CO₂ by organisms other than plants.

Hydrosphere

The component of the climate system comprising liquid surface and subterranean water, such as: oceans, seas, rivers, fresh water lakes, underground water etc.

Ice cap

A dome shaped ice mass covering a highland area that is considerably smaller in extent than an→ice sheet.

Ice sheet

A mass of land ice which is sufficiently deep to cover most of the underlying bedrock topography, so that its shape is mainly determined by its internal dynamics (the flow of the ice as it deforms internally and slides at its base). An ice sheet flows outwards from a high central plateau with a small average surface slope. The margins slope steeply, and the ice is discharged through fast-flowing ice streams or outlet glaciers, in some cases into the sea or into ice-shelves floating on the sea. There are only two large ice sheets in the modern world, on Greenland and Antarctica, the Antarctic ice sheet being divided into East and West by the Transantarctic Mountains; during glacial periods there were others.

Ice shelf

A floating →ice sheet of considerable thickness attached to a coast (usually of great horizontal extent with a level or gently undulating surface); often a seaward extension of ice sheets.

Indirect aerosol effect

→Aerosols may lead to an indirect →radiative forcing of the →climate system through acting as condensation nuclei or modifying the optical properties and lifetime of clouds. Two indirect effects are distinguished:

First indirect effect

A radiative forcing induced by an increase in anthropogenic aerosols which cause an initial increase in droplet concentration and a decrease in droplet size for fixed liquid water content,

leading to an increase of cloud →albedo. This effect is also known as the *Twomey effect*. This is sometimes referred to as the *cloud albedo effect*. However this is highly misleading since the second indirect effect also alters cloud albedo.

Second indirect effect

A radiative forcing induced by an increase in anthropogenic aerosols which cause a decrease in droplet size, reducing the precipitation efficiency, thereby modifying the liquid water content, cloud thickness, and cloud life time. This effect is also known as the *cloud life time effect* or *Albrecht effect*.

Industrial revolution

A period of rapid industrial growth with far-reaching social and economic consequences, beginning in England during the second half of the eighteenth century and spreading to Europe and later to other countries including the United States. The invention of the steam engine was an important trigger of this development. The industrial revolution marks the beginning of a strong increase in the use of fossil fuels and emission of, in particular, fossil carbon dioxide. In this Report the terms *pre-industrial* and *industrial* refer, somewhat arbitrarily, to the periods before and after 1750, respectively.

Infrared radiation

Radiation emitted by the earth's surface, the atmosphere and the clouds. It is also known as terrestrial or long-wave radiation. Infrared radiation has a distinctive range of wavelengths ("spectrum") longer than the wavelength of the red colour in the visible part of the spectrum. The spectrum of infrared radiation is practically distinct from that of →solar or short-wave radiation because of the difference in temperature between the Sun and the Earth-atmosphere system.

Integrated assessment

A method of analysis that combines results and models from the physical, biological, economic and social sciences, and the interactions between these components, in a consistent framework, to evaluate the status and the consequences of environmental change and the policy responses to it.

Internal variability

See: →Climate variability.

Inverse modelling

A mathematical procedure by which the input to a model is estimated from the observed outcome, rather than *vice versa*. It is, for instance, used to estimate the location and strength of sources and sinks of CO₂ from measurements of the distribution of the CO₂ concentration in the atmosphere, given models of the global →carbon cycle and for computing atmospheric transport.

Isostatic land movements

Isostasy refers to the way in which the →lithosphere and mantle respond to changes in surface loads. When the loading of the lithosphere is changed by alterations in land ice mass, ocean mass, sedimentation, erosion or mountain building, vertical isostatic adjustment results, in order to balance the new load.

Kyoto Protocol

The Kyoto Protocol to the United Nations →Framework Convention on Climate Change (UNFCCC) was adopted at the Third Session of the Conference of the Parties (COP) to the United Nations →Framework Convention on Climate Change, in 1997 in Kyoto, Japan. It contains legally binding commitments, in addition to those included in the UNFCCC. Countries included in Annex B of the Protocol (most OECD countries and countries with economies in transition) agreed to reduce their anthropogenic →greenhouse gas emissions (CO_2 , CH_4 , N_2O , HFCs, PFCs, and SF_6) by at least 5% below 1990 levels in the commitment period 2008 to 2012. The Kyoto Protocol has not yet entered into force (April 2001).

Land use

The total of arrangements, activities and inputs undertaken in a certain land cover type (a set of human actions). The social and economic purposes for which land is managed (e.g., grazing, timber extraction, and conservation).

Land-use change

A change in the use or management of land by humans, which may lead to a change in land cover. Land cover and land-use change may have an impact on the →albedo, →evapotranspiration, →sources and →sinks of →greenhouse gases, or other properties of the →climate system and may thus have an impact on climate, locally or globally. See also: the IPCC Report on Land Use, Land-Use Change, and Forestry (IPCC, 2000).

La Niña

See: →El Niño-Southern Oscillation.

Lifetime

Lifetime is a general term used for various time-scales characterising the rate of processes affecting the concentration of trace gases. The following lifetimes may be distinguished:

Turnover time (T) is the ratio of the mass M of a reservoir (e.g., a gaseous compound in the atmosphere) and the total rate of removal S from the reservoir: $T = M/S$. For each removal process separate turnover times can be defined. In soil carbon biology this is referred to as *Mean Residence Time (MRT)*.

Adjustment time or *response time* (T_a) is the time-scale characterising the decay of an instantaneous pulse input into the reservoir. The term *adjustment time* is also used to characterise the adjustment of the mass of a reservoir following a step change in the source strength. *Half-life* or *decay constant* is used to quantify a first-order exponential decay process. See: →Response time, for a different definition pertinent to climate variations. The term *lifetime* is sometimes used, for simplicity, as a surrogate for *adjustment time*.

In simple cases, where the global removal of the compound is directly proportional to the total mass of the reservoir, the adjustment time equals the turnover time: $T = T_a$. An example is CFC-11 which is removed from the atmosphere only by photochemical processes in the stratosphere. In more complicated cases, where several reservoirs are involved or where the removal is not proportional to the total mass, the equality $T = T_a$ no longer holds.

→Carbon dioxide (CO_2) is an extreme example. Its turnover time is only about 4 years because of the rapid exchange between atmosphere and the ocean and terrestrial biota. However, a large part of that CO_2 is returned to the atmosphere within a few years. Thus, the adjustment time of CO_2 in the atmosphere is actually determined by the rate of removal of carbon from the surface layer of the oceans into its deeper layers. Although an approximate value of 100 years may be given for the adjustment time of CO_2 in the atmosphere, the actual adjustment is faster initially and slower later on. In the case of methane (CH_4) the adjustment time is different from the turnover time, because the removal is mainly through a chemical reaction with the hydroxyl radical OH , the concentration of which itself depends on the CH_4 concentration. Therefore the CH_4 removal S is not proportional to its total mass M .

Lithosphere

The upper layer of the solid Earth, both continental and oceanic, which comprises all crustal rocks and the cold, mainly elastic, part of the uppermost mantle. Volcanic activity, although part of the lithosphere, is not considered as part of the →climate system, but acts as an external forcing factor. See: →Isostatic land movements.

LOSU (Level of Scientific Understanding)

This is an index on a 4-step scale (High, Medium, Low and Very Low) designed to characterise the degree of scientific understanding of the radiative forcing agents that affect climate change. For each agent, the index represents a subjective judgement about the reliability of the estimate of its forcing, involving such factors as the assumptions necessary to evaluate the forcing, the degree of knowledge of the physical/ chemical mechanisms determining the forcing and the uncertainties surrounding the quantitative estimate.

Mean Sea Level

See: →Relative Sea Level.

Mitigation

A human intervention to reduce the →sources or enhance the →sinks of →greenhouse gases.

Mixing ratio

See: →Mole fraction.

Model hierarchy

See: →Climate model.

Mole fraction

Mole fraction, or *mixing ratio*, is the ratio of the number of moles of a constituent in a given volume to the total number of moles of all constituents in that volume. It is usually reported for dry air. Typical values for long-lived →greenhouse gases are in the order of $\mu\text{mol/mol}$ (parts per million: ppm), nmol/mol (parts per billion: ppb), and fmol/mol (parts per trillion: ppt). Mole fraction differs from *volume mixing ratio*, often expressed in ppmv etc., by the corrections for non-ideality of gases. This correction is

significant relative to measurement precision for many greenhouse gases. (Source: Schwartz and Warneck, 1995).

Montreal Protocol

The Montreal Protocol on Substances that Deplete the Ozone Layer was adopted in Montreal in 1987, and subsequently adjusted and amended in London (1990), Copenhagen (1992), Vienna (1995), Montreal (1997) and Beijing (1999). It controls the consumption and production of chlorine- and bromine-containing chemicals that destroy stratospheric ozone, such as CFCs, methyl chloroform, carbon tetrachloride, and many others.

Net Biome Production (NBP)

Net gain or loss of carbon from a region. NBP is equal to the →Net Ecosystem Production minus the carbon lost due to a disturbance, e.g. a forest fire or a forest harvest.

Net Ecosystem Production (NEP)

Net gain or loss of carbon from an →ecosystem. NEP is equal to the →Net Primary Production minus the carbon lost through →heterotrophic respiration.

Net Primary Production (NPP)

The increase in plant →biomass or carbon of a unit of a landscape. NPP is equal to the →Gross Primary Production minus carbon lost through →autotrophic respiration.

Nitrogen fertilisation

Enhancement of plant growth through the addition of nitrogen compounds. In IPCC Reports, this typically refers to fertilisation from anthropogenic sources of nitrogen such as human-made fertilisers and nitrogen oxides released from burning fossil fuels.

Non-linearity

A process is called “non-linear” when there is no simple proportional relation between cause and effect. The →climate system contains many such non-linear processes, resulting in a system with a potentially very complex behaviour. Such complexity may lead to →rapid climate change.

North Atlantic Oscillation (NAO)

The North Atlantic Oscillation consists of opposing variations of barometric pressure near Iceland and near the Azores. On average, a westerly current, between the Icelandic low pressure area and the Azores high pressure area, carries cyclones with their associated frontal systems towards Europe. However, the pressure difference between Iceland and the Azores fluctuates on time-scales of days to decades, and can be reversed at times.

Organic aerosol

→Aerosol particles consisting predominantly of organic compounds, mainly C, H, O, and lesser amounts of other elements. (Source: Charlson and Heintzenberg, 1995, p. 405.) See: →Carbonaceous aerosol.

Ozone

Ozone, the triatomic form of oxygen (O_3), is a gaseous atmospheric constituent. In the →troposphere it is created both naturally and by photochemical reactions involving gases resulting from human activities (“smog”). Tropospheric ozone acts as a →greenhouse gas. In the →stratosphere it is created by the interaction between solar ultraviolet radiation and molecular oxygen (O_2). Stratospheric ozone plays a decisive role in the stratospheric radiative balance. Its concentration is highest in the →ozone layer.

Ozone hole

See: →Ozone layer.

Ozone layer

The →stratosphere contains a layer in which the concentration of ozone is greatest, the so called ozone layer. The layer extends from about 12 to 40 km. The ozone concentration reaches a maximum between about 20 and 25 km. This layer is being depleted by human emissions of chlorine and bromine compounds. Every year, during the Southern Hemisphere spring, a very strong depletion of the ozone layer takes place over the Antarctic region, also caused by human-made chlorine and bromine compounds in combination with the specific meteorological conditions of that region. This phenomenon is called the **ozone hole**.

Parametrization

In →climate models, this term refers to the technique of representing processes, that cannot be explicitly resolved at the spatial or temporal resolution of the model (sub-grid scale processes), by relationships between the area or time averaged effect of such sub-grid scale processes and the larger scale flow.

Patterns of climate variability

Natural variability of the →climate system, in particular on seasonal and longer time-scales, predominantly occurs in preferred spatial patterns, through the dynamical non-linear characteristics of the atmospheric circulation and through interactions with the land and ocean surfaces. Such spatial patterns are also called “regimes” or “modes”. Examples are the →North Atlantic Oscillation (NAO), the Pacific-North American pattern (PNA), the →El Niño-Southern Oscillation (ENSO), and the Antarctic Oscillation (AO).

Photosynthesis

The process by which plants take CO_2 from the air (or bicarbonate in water) to build carbohydrates, releasing O_2 in the process. There are several pathways of photosynthesis with different responses to atmospheric CO_2 concentrations. See: →Carbon dioxide fertilisation.

Pool

See: →Reservoir.

Post-glacial rebound

The vertical movement of the continents and sea floor following

the disappearance and shrinking of →ice sheets, e.g. since the Last Glacial Maximum (21 ky BP). The rebound is an →isostatic land movement.

Ppm, ppb, ppt

See: →Mole fraction.

Precursors

Atmospheric compounds which themselves are not →greenhouse gases or →aerosols, but which have an effect on greenhouse gas or aerosol concentrations by taking part in physical or chemical processes regulating their production or destruction rates.

Pre-industrial

See: →Industrial revolution.

Projection (generic)

A projection is a potential future evolution of a quantity or set of quantities, often computed with the aid of a model. Projections are distinguished from *predictions* in order to emphasise that projections involve assumptions concerning, e.g., future socio-economic and technological developments that may or may not be realised, and are therefore subject to substantial uncertainty. See also →Climate projection; →Climate prediction.

Proxy

A proxy climate indicator is a local record that is interpreted, using physical and biophysical principles, to represent some combination of climate-related variations back in time. Climate related data derived in this way are referred to as proxy data. Examples of proxies are: tree ring records, characteristics of corals, and various data derived from ice cores.

Radiative forcing

Radiative forcing is the change in the net vertical irradiance (expressed in Watts per square metre: W m^{-2}) at the →tropopause due to an internal change or a change in the external forcing of the →climate system, such as, for example, a change in the concentration of →carbon dioxide or the output of the Sun. Usually radiative forcing is computed after allowing for stratospheric temperatures to readjust to radiative equilibrium, but with all tropospheric properties held fixed at their unperturbed values. Radiative forcing is called *instantaneous* if no change in stratospheric temperature is accounted for. Practical problems with this definition, in particular with respect to radiative forcing associated with changes, by aerosols, of the precipitation formation by clouds, are discussed in Chapter 6 of this Report.

Radiative forcing scenario

A plausible representation of the future development of →radiative forcing associated, for example, with changes in atmospheric composition or land-use change, or with external factors such as variations in →solar activity. Radiative forcing scenarios can be used as input into simplified →climate models to compute →climate projections.

Radio-echosounding

The surface and bedrock, and hence the thickness, of a glacier can be mapped by radar; signals penetrating the ice are reflected at the lower boundary with rock (or water, for a floating glacier tongue).

Rapid climate change

The →non-linearity of the →climate system may lead to rapid climate change, sometimes called *abrupt events* or even *surprises*. Some such abrupt events may be imaginable, such as a dramatic reorganisation of the →thermohaline circulation, rapid deglaciation, or massive melting of permafrost leading to fast changes in the →carbon cycle. Others may be truly unexpected, as a consequence of a strong, rapidly changing, forcing of a non-linear system.

Reforestation

Planting of forests on lands that have previously contained forests but that have been converted to some other use. For a discussion of the term →forest and related terms such as →afforestation, reforestation, and →deforestation: see the IPCC Report on Land Use, Land-Use Change and Forestry (IPCC, 2000).

Regimes

Preferred →patterns of climate variability.

Relative Sea Level

Sea level measured by a →tide gauge with respect to the land upon which it is situated. Mean Sea Level (MSL) is normally defined as the average Relative Sea Level over a period, such as a month or a year, long enough to average out transients such as waves.

(Relative) Sea Level Secular Change

Long term changes in relative sea level caused by either →eustatic changes, e.g. brought about by →thermal expansion, or changes in vertical land movements.

Reservoir

A component of the →climate system, other than the atmosphere, which has the capacity to store, accumulate or release a substance of concern, e.g. carbon, a →greenhouse gas or a →precursor. Oceans, soils, and →forests are examples of reservoirs of carbon. *Pool* is an equivalent term (note that the definition of pool often includes the atmosphere). The absolute quantity of substance of concerns, held within a reservoir at a specified time, is called the *stock*.

Respiration

The process whereby living organisms convert organic matter to CO_2 , releasing energy and consuming O_2 .

Response time

The response time or *adjustment time* is the time needed for the →climate system or its components to re-equilibrate to a new state, following a forcing resulting from external and internal processes or →feedbacks. It is very different for various

components of the climate system. The response time of the →troposphere is relatively short, from days to weeks, whereas the →stratosphere comes into equilibrium on a time-scale of typically a few months. Due to their large heat capacity, the oceans have a much longer response time, typically decades, but up to centuries or millennia. The response time of the strongly coupled surface-troposphere system is, therefore, slow compared to that of the stratosphere, and mainly determined by the oceans. The →biosphere may respond fast, e.g. to droughts, but also very slowly to imposed changes.

See: →Lifetime, for a different definition of response time pertinent to the rate of processes affecting the concentration of trace gases.

Scenario (generic)

A plausible and often simplified description of how the future may develop, based on a coherent and internally consistent set of assumptions about driving forces and key relationships. Scenarios may be derived from →projections, but are often based on additional information from other sources, sometimes combined with a “narrative storyline”. See also: →SRES scenarios; →Climate scenario; →Emission scenarios.

Sea level rise

See: →Relative Sea Level Secular Change; →Thermal expansion.

Sequestration

See: →Uptake.

Significant wave height

The average height of the highest one-third of all sea waves occurring in a particular time period. This serves as an indicator of the characteristic size of the highest waves.

Sink

Any process, activity or mechanism which removes a →greenhouse gas, an →aerosol or a precursor of a greenhouse gas or aerosol from the atmosphere.

Soil moisture

Water stored in or at the land surface and available for evaporation.

Solar activity

The Sun exhibits periods of high activity observed in numbers of →sunspots, as well as radiative output, magnetic activity, and emission of high energy particles. These variations take place on a range of time-scales from millions of years to minutes. See: →Solar cycle.

Solar (“11 year”) cycle

A quasi-regular modulation of →solar activity with varying amplitude and a period of between 9 and 13 years.

Solar radiation

Radiation emitted by the Sun. It is also referred to as short-wave radiation. Solar radiation has a distinctive range of wavelengths

(spectrum) determined by the temperature of the Sun. See also: →Infrared radiation.

Soot particles

Particles formed during the quenching of gases at the outer edge of flames of organic vapours, consisting predominantly of carbon, with lesser amounts of oxygen and hydrogen present as carboxyl and phenolic groups and exhibiting an imperfect graphitic structure. See: →Black carbon; Charcoal. (Source: Charlson and Heintzenberg, 1995, p. 406.)

Source

Any process, activity or mechanism which releases a greenhouse gas, an aerosol or a precursor of a greenhouse gas or aerosol into the atmosphere.

Spatial and temporal scales

Climate may vary on a large range of spatial and temporal scales. Spatial scales may range from local (less than 100,000 km²), through regional (100,000 to 10 million km²) to continental (10 to 100 million km²). Temporal scales may range from seasonal to geological (up to hundreds of millions of years).

SRES scenarios

SRES scenarios are →emission scenarios developed by Nakićenović *et al.* (2000) and used, among others, as a basis for the climate projections in Chapter 9 of this Report. The following terms are relevant for a better understanding of the structure and use of the set of SRES scenarios:

(Scenario) Family

Scenarios that have a similar demographic, societal, economic and technical-change storyline. Four scenario families comprise the SRES scenario set: A1, A2, B1 and B2.

(Scenario) Group

Scenarios within a family that reflect a consistent variation of the storyline. The A1 scenario family includes four groups designated as A1T, A1C, A1G and A1B that explore alternative structures of future energy systems. In the Summary for Policymakers of Nakićenović *et al.* (2000), the A1C and A1G groups have been combined into one ‘Fossil Intensive’ A1FI scenario group. The other three scenario families consist of one group each. The SRES scenario set reflected in the Summary for Policymakers of Nakićenović *et al.* (2000) thus consist of six distinct scenario groups, all of which are equally sound and together capture the range of uncertainties associated with driving forces and emissions.

Illustrative Scenario

A scenario that is illustrative for each of the six scenario groups reflected in the Summary for Policymakers of Nakićenović *et al.* (2000). They include four revised ‘scenario markers’ for the scenario groups A1B, A2, B1, B2, and two additional scenarios for the A1FI and A1T groups. All scenario groups are equally sound.

(Scenario) Marker

A scenario that was originally posted in draft form on the SRES website to represent a given scenario family. The choice of markers was based on which of the initial quantifications best

reflected the storyline, and the features of specific models. Markers are no more likely than other scenarios, but are considered by the SRES writing team as illustrative of a particular storyline. They are included in revised form in Nakićenović *et al.* (2000). These scenarios have received the closest scrutiny of the entire writing team and via the SRES open process. Scenarios have also been selected to illustrate the other two scenario groups (see also ‘Scenario Group’ and ‘Illustrative Scenario’).

(Scenario) Storyline

A narrative description of a scenario (or family of scenarios) highlighting the main scenario characteristics, relationships between key driving forces and the dynamics of their evolution.

Stock

See: →Reservoir.

Storm surge

The temporary increase, at a particular locality, in the height of the sea due to extreme meteorological conditions (low atmospheric pressure and/or strong winds). The storm surge is defined as being the excess above the level expected from the tidal variation alone at that time and place.

Stratosphere

The highly stratified region of the atmosphere above the →troposphere extending from about 10 km (ranging from 9 km in high latitudes to 16 km in the tropics on average) to about 50 km.

Sunspots

Small dark areas on the Sun. The number of sunspots is higher during periods of high →solar activity, and varies in particular with the →solar cycle.

Thermal expansion

In connection with sea level, this refers to the increase in volume (and decrease in density) that results from warming water. A warming of the ocean leads to an expansion of the ocean volume and hence an increase in sea level.

Thermohaline circulation

Large-scale density-driven circulation in the ocean, caused by differences in temperature and salinity. In the North Atlantic the thermohaline circulation consists of warm surface water flowing northward and cold deep water flowing southward, resulting in a net poleward transport of heat. The surface water sinks in highly restricted sinking regions located in high latitudes.

Tide gauge

A device at a coastal location (and some deep sea locations) which continuously measures the level of the sea with respect to the adjacent land. Time-averaging of the sea level so recorded gives the observed →Relative Sea Level Secular Changes.

Transient climate response

The globally averaged surface air temperature increase, averaged over a 20 year period, centred at the time of CO₂ doubling, i.e., at

year 70 in a 1% per year compound CO₂ increase experiment with a global coupled →climate model.

Tropopause

The boundary between the →troposphere and the →stratosphere.

Troposphere

The lowest part of the atmosphere from the surface to about 10 km in altitude in mid-latitudes (ranging from 9 km in high latitudes to 16 km in the tropics on average) where clouds and “weather” phenomena occur. In the troposphere temperatures generally decrease with height.

Turnover time

See: →Lifetime.

Uncertainty

An expression of the degree to which a value (e.g. the future state of the climate system) is unknown. Uncertainty can result from lack of information or from disagreement about what is known or even knowable. It may have many types of sources, from quantifiable errors in the data to ambiguously defined concepts or terminology, or uncertain projections of human behaviour. Uncertainty can therefore be represented by quantitative measures (e.g. a range of values calculated by various models) or by qualitative statements (e.g., reflecting the judgement of a team of experts). See Moss and Schneider (2000).

United Nations Framework Convention on Climate Change (UNFCCC)

The Convention was adopted on 9 May 1992 in New York and signed at the 1992 Earth Summit in Rio de Janeiro by more than 150 countries and the European Community. Its ultimate objective is the “stabilisation of greenhouse gas concentrations in the atmosphere at a level that would prevent dangerous anthropogenic interference with the climate system”. It contains commitments for all Parties. Under the Convention, Parties included in Annex I aim to return greenhouse gas emissions not controlled by the Montreal Protocol to 1990 levels by the year 2000. The convention entered into force in March 1994. See: →Kyoto Protocol.

Uptake

The addition of a substance of concern to a →reservoir. The uptake of carbon containing substances, in particular carbon dioxide, is often called (carbon) *sequestration*.

Volume mixing ratio

See: →Mole fraction.

Sources:

Charlson, R. J., and J. Heintzenberg (Eds.): *Aerosol Forcing of Climate*, pp. 91-108, copyright 1995 ©John Wiley and Sons Limited. Reproduced with permission.

- IPCC**, 1992: *Climate Change 1992: The Supplementary Report to the IPCC Scientific Assessment* [J. T. Houghton, B. A. Callander and S. K. Varney (eds.)]. Cambridge University Press, Cambridge, UK, xi + 116 pp.
- IPCC**, 1994: *Climate Change 1994: Radiative Forcing of Climate Change and an Evaluation of the IPCC IS92 Emission Scenarios*, [J. T. Houghton, L. G. Meira Filho, J. Bruce, Hoesung Lee, B. A. Callander, E. Haites, N. Harris and K. Maskell (eds.)]. Cambridge University Press, Cambridge, UK and New York, NY, USA, 339 pp.
- IPCC**, 1996: *Climate Change 1995: The Science of Climate Change. Contribution of Working Group I to the Second Assessment Report of the Intergovernmental Panel on Climate Change* [J. T. Houghton., L.G. Meira Filho, B. A. Callander, N. Harris, A. Kattenberg, and K. Maskell (eds.)]. Cambridge University Press, Cambridge, United Kingdom and New York, NY, USA, 572 pp.
- IPCC**, 1997a: *IPCC Technical Paper 2: An introduction to simple climate models used in the IPCC Second Assessment Report*, [J. T. Houghton, L.G. Meira Filho, D. J. Griggs and K. Maskell (eds.)]. 51 pp.
- IPCC**, 1997b: *Revised 1996 IPCC Guidelines for National Greenhouse Gas Inventories* (3 volumes) [J. T. Houghton, L. G. Meira Filho, B. Lim, K. Tréanton, I. Mamaty, Y. Bonduki, D. J. Griggs and B. A. Callander (eds.)].
- IPCC**, 1997c: *IPCC technical Paper 4: Implications of proposed CO₂ emissions limitations*. [J. T. Houghton, L.G. Meira Filho, D. J. Griggs and M Noguer (eds.)]. 41 pp.
- IPCC**, 2000: *Land Use, Land-Use Change, and Forestry. Special Report of the IPCC*. [R.T. Watson, I.R. Noble, B. Bolin, N.H. Ravindranath and D. J. Verardo, D. J. Dokken, , (eds.)] Cambridge University Press, Cambridge, United Kingdom and New York, NY, USA, 377 pp.
- Maunder, W. John** , 1992: *Dictionary of Global Climate Change*, UCL Press Ltd.
- Moss, R. and S. Schneider**, 2000: *IPCC Supporting Material, pp. 33-51: Uncertainties in the IPCC TAR: Recommendations to Lead Authors for more consistent Assessment and Reporting*, [R. Pachauri, T. Taniguchi and K. Tanaka (eds.)]
- Nakićenović**, N., J. Alcamo, G. Davis, B. de Vries, J. Fenhann, S. Gaffin, K. Gregory, A. Grübler, T. Y. Jung, T. Kram, E. L. La Rovere, L. Michaelis, S. Mori, T. Morita, W. Pepper, H. Pitcher, L. Price, K. Raihi, A. Roehrl, H-H. Rogner, A. Sankovski, M. Schlesinger, P. Shukla, S. Smith, R. Swart, S. van Rooijen, N. Victor, Z. Dadi, 2000: *Emissions Scenarios, A Special Report of Working Group III of the Intergovernmental Panel on Climate Change*. Cambridge University Press, Cambridge, United Kingdom and New York, NY, USA, 599 pp.
- Schwartz, S. E. and P. Warneck**, 1995: *Units for use in atmospheric chemistry*, Pure & Appl. Chem., 67, pp. 1377-1406.

Appendix II

SRES Tables

Contents

Introduction	800		
II.1: Anthropogenic Emissions	801		
II.1.1 CO ₂ emissions (PgC/yr)	801	II.3.2 CH ₄ radiative forcing (Wm ⁻²)	818
II.1.2 CH ₄ emissions (Tg(CH ₄)/yr)	801	II.3.3 N ₂ O radiative forcing (Wm ⁻²)	818
II.1.3 N ₂ O emissions (TgN/yr)	802	II.3.4 PFCs, SF ₆ and HFCs radiative forcing (Wm ⁻²)	819
II.1.4 PFCs, SF ₆ and HFCs emissions (Gg/yr)	802	II.3.5 Tropospheric O ₃ radiative forcing (Wm ⁻²)	822
II.1.5 NO _x emissions (TgN/yr)	805	II.3.6 SO ₄ ²⁻ aerosols (direct effect) radiative forcing (Wm ⁻²)	822
II.1.6 CO emissions (Tg(CO)/yr)	806	II.3.7 BC aerosols radiative forcing (Wm ⁻²)	822
II.1.7 VOC emissions (Tg/yr)	806	II.3.8 OC aerosols radiative forcing (Wm ⁻²)	822
II.1.8 SO ₂ emissions (TgS/yr)	806	II.3.9 CFCs and HFCs following the Montreal (1997) Amendments – radiative forcing (Wm ⁻²)	823
II.1.9 BC aerosols emissions (Tg/yr)	807	II.3.10 Radiative Forcing (Wm ⁻²) from fossil fuel plus biomass Organic and Black Carbon as used in the Chapter 9 Simple Model SRES Projections	823
II.1.10 OC aerosols emissions (Tg/yr)	807	II.3.11 Total Radiative Forcing (Wm ⁻²) from GHG plus direct and indirect aerosol effects	823
II.2: Abundances and Burdens	807	II.4: Surface Air Temperature Change (°C)	824
II.2.1 CO ₂ abundances (ppm)	807		
II.2.2 CH ₄ abundance (ppb)	809	II.5: Sea Level Change (mm)	824
II.2.3 N ₂ O abundance (ppb)	809	II.5.1 Total sea level change (mm)	824
II.2.4 PFCs, SF ₆ and HFCs abundances (ppt)	809	II.5.2 Sea level change due to thermal expansion (mm)	825
II.2.5 Tropospheric O ₃ burden (global mean column in DU)	814	II.5.3 Sea level change due to glaciers and ice caps (mm)	825
II.2.6 Tropospheric OH (as a factor relative to year 2000)	814	II.5.4 Sea level change due to Greenland (mm)	826
II.2.7 SO ₄ ²⁻ aerosols burden (TgS)	814	II.5.5 Sea level change due to Antarctica (mm)	826
II.2.8 BC aerosol burden (Tg)	815		
II.2.9 OC aerosol burden (Tg)	815		
II.2.10 CFCs and HFCs abundances from WMO98 Scenario A1 (baseline) following the Montreal (1997) Amendments (ppt)	816		
II.3: Radiative Forcing (Wm⁻²)	817	References	826
II.3.1 CO ₂ radiative forcing (Wm ⁻²)	817		

Introduction

Appendix II gives, in tabulated form, the values for emissions, abundances and burdens, and, radiative forcing of major greenhouse gases and aerosols based on the SRES¹ scenarios (Nakićenović *et. al.*, 2000). The Appendix also presents global projections of changes in surface air temperature and sea level using these SRES emission scenarios.

The emission values are only anthropogenic emissions and are the ones published in Appendix VII of the SRES Report. Apart from the CO₂ emissions, for which deforestation and land use values are given in the SRES Report, the SRES scenarios for the rest of the gases define only the changes in direct anthropogenic emissions and do not specify the current magnitude of the natural emissions nor the concurrent changes in natural emissions due either to direct human activities such as land-use change or to the indirect impacts of climate change. Emissions for black carbon (BC) aerosols and organic matter carbonaceous (OC) aerosols species not covered in the SRES Report, are calculated by scaling to the SRES anthropogenic CO emissions.

The abundances and burdens for each of the species are calculated with the latest climate chemistry and climate carbon models (see Chapters 3, 4 and 5 for details).

The radiative forcings due to well-mixed greenhouse gases are computed using each of the simplified expressions given in

Chapter 6, Table 6.2. The radiative forcings associated with future tropospheric O₃ increase are calculated on the basis of the O₃ changes presented in Chapter 4 for the various SRES scenarios. The mean forcing per DU estimated from the various models, and given in Chapter 6, Table 6.3 (i.e., 0.042 Wm⁻²/DU), is used to derive these future forcings. For each aerosol species, the ratio of the column burdens for the particular scenario to that of the year 2000 is multiplied by the “best estimate” of the present day radiative forcing (see Chapter 6 for more details). The radiative forcings for all the species have been calculated since pre-industrial time.

The global mean surface air temperature and sea level projections, based on the SRES scenarios, have been calculated using Simple Climate models which have been “tuned” to get similar responses to the AOGCMs in the global mean (see Chapters 9 and 11 for details).

The results presented are global mean values, every ten years from 2000 to 2100, for a range of scenarios. These scenarios are the final approved Illustrative Marker Scenarios (A1B, A1T, A1FI, A2, B1, and B2); the preliminary marker scenarios (A1p, A2p, B1p, B2p, approved by the IPCC Bureau in June 1998) and, for comparison and for some species, results based on a previous scenario used by IPCC (IS92a) have also been added. For some gases, the values tabulated in the IPCC Second Assessment Report (IPCC, 1996; hereafter SAR), for that IS92a scenario using the previous generation of chemistry and climate models, are also given.

¹ IPCC Special Report on Emission Scenarios (Nakićenović *et. al.*, 2000), hereafter SRES.

Main Chemical Symbols used in this Appendix:

CO ₂	carbon dioxide	O ₃	ozone
CH ₄	methane	OH	hydroxyl
CFC	chlorofluorocarbon	PFC	perfluorocarbon
CO	carbon monoxide	SO ₂	sulphur dioxide
HFC	hydrofluorocarbon	SO ₄ ²⁻	sulphate ion
N ₂ O	nitrous oxide	SF ₆	sulphur hexafluoride
NO _x	the sum of NO (nitric oxide) and NO ₂ (nitrogen dioxide)	VOC	volatile organic compound

II.1: Anthropogenic Emissions

II.1.1: CO₂ emissions (PgC/yr)

CO₂ emissions from fossil fuel and industrial processes (PgC/yr)

Year	A1B	A1T	A1FI	A2	B1	B2	A1p	A2p	B1p	B2p	IS92a
2000	6.90	6.90	6.90	6.90	6.90	6.90	6.8	6.8	6.8	6.8	7.1
2010	9.68	8.33	8.65	8.46	8.50	7.99	9.7	8.4	7.7	7.9	8.68
2020	12.12	10.00	11.19	11.01	10.00	9.02	12.2	10.9	8.3	8.9	10.26
2030	14.01	12.26	14.61	13.53	11.20	10.15	14.2	13.3	8.4	10.0	11.62
2040	14.95	12.60	18.66	15.01	12.20	10.93	15.2	14.7	9.1	10.8	12.66
2050	16.01	12.29	23.10	16.49	11.70	11.23	16.2	16.4	9.8	11.1	13.7
2060	15.70	11.41	25.14	18.49	10.20	11.74	15.9	18.2	10.4	11.6	14.68
2070	15.43	9.91	27.12	20.49	8.60	11.87	15.6	20.2	10.1	11.8	15.66
2080	14.83	8.05	29.04	22.97	7.30	12.46	15.0	22.7	8.7	12.4	17.0
2090	13.94	6.27	29.64	25.94	6.10	13.20	14.1	25.6	7.5	13.1	18.7
2100	13.10	4.31	30.32	28.91	5.20	13.82	13.2	28.8	6.5	13.7	20.4

CO₂ emissions from deforestation and land use (PgC/yr)

Year	A1B	A1T	A1FI	A2	B1	B2	A1p	A2p	B1p	B2p	IS92a
2000	1.07	1.07	1.07	1.07	1.07	1.07	1.6	1.6	1.6	1.6	1.3
2010	1.20	1.04	1.08	1.12	0.78	0.80	1.5	1.6	0.8	1.8	1.22
2020	0.52	0.26	1.55	1.25	0.63	0.03	1.6	1.7	1.3	1.6	1.14
2030	0.47	0.12	1.57	1.19	-0.09	-0.25	0.7	1.5	0.7	0.3	1.04
2040	0.40	0.05	1.31	1.06	-0.48	-0.24	0.3	1.3	0.6	0.0	0.92
2050	0.37	-0.02	0.80	0.93	-0.41	-0.23	-0.2	1.2	0.5	-0.3	0.8
2060	0.30	-0.03	0.55	0.67	-0.46	-0.24	-0.3	0.7	0.7	-0.2	0.54
2070	0.30	-0.03	0.16	0.40	-0.42	-0.25	-0.3	0.4	0.8	-0.2	0.28
2080	0.35	-0.03	-0.36	0.25	-0.60	-0.31	-0.4	0.3	1.0	-0.2	0.12
2090	0.36	-0.01	-1.22	0.21	-0.78	-0.41	-0.5	0.2	1.2	-0.2	0.06
2100	0.39	0.00	-2.08	0.18	-0.97	-0.50	-0.6	0.2	1.4	-0.2	-0.1

CO₂ emissions – total (PgC/yr)

Year	A1B	A1T	A1FI	A2	B1	B2	A1p	A2p	B1p	B2p	IS92a
2000	7.97	7.97	7.97	7.97	7.97	7.97	8.4	8.4	8.4	8.4	8.4
2010	10.88	9.38	9.73	9.58	9.28	8.78	11.2	10.0	8.5	9.7	9.9
2020	12.64	10.26	12.73	12.25	10.63	9.05	13.8	12.6	9.6	10.5	11.4
2030	14.48	12.38	16.19	14.72	11.11	9.90	14.9	14.8	9.1	10.3	12.66
2040	15.35	12.65	19.97	16.07	11.72	10.69	15.5	16.0	9.7	10.8	13.58
2050	16.38	12.26	23.90	17.43	11.29	11.01	16.0	17.6	10.3	10.8	14.5
2060	16.00	11.38	25.69	19.16	9.74	11.49	15.6	18.9	11.1	11.4	15.22
2070	15.73	9.87	27.28	20.89	8.18	11.62	15.3	20.6	10.9	11.6	15.94
2080	15.18	8.02	28.68	23.22	6.70	12.15	14.6	23.0	9.7	12.2	17.12
2090	14.30	6.26	28.42	26.15	5.32	12.79	13.6	25.8	8.7	12.9	18.76
2100	13.49	4.32	28.24	29.09	4.23	13.32	12.6	29.0	7.9	13.5	20.3

II.1.2: CH₄ emissions (Tg(CH₄)/yr)

Year	A1B	A1T	A1FI	A2	B1	B2	A1p	A2p	B1p	B2p	IS92a
2000	323	323	323	323	323	323	347	347	347	347	390
2010	373	362	359	370	349	349	417	394	367	389	433
2020	421	415	416	424	377	384	484	448	396	448	477
2030	466	483	489	486	385	426	547	506	403	501	529
2040	458	495	567	542	381	466	531	560	423	528	580
2050	452	500	630	598	359	504	514	621	444	538	630
2060	410	459	655	654	342	522	464	674	445	544	654
2070	373	404	677	711	324	544	413	732	446	542	678
2080	341	359	695	770	293	566	370	790	447	529	704
2090	314	317	715	829	266	579	336	848	413	508	733
2100	289	274	735	889	236	597	301	913	379	508	762

II.1.3: N₂O emissions (TgN/yr)

Year	A1B	A1T	A1FI	A2	B1	B2	A1p	A2p	B1p	B2p	IS92a
2000	7.0	7.0	7.0	7.0	7.0	7.0	6.9	6.9	6.9	6.9	5.5
2010	7.0	6.1	8.0	8.1	7.5	6.2	7.3	7.9	7.4	7.1	6.2
2020	7.2	6.1	9.3	9.6	8.1	6.1	7.7	9.4	8.1	7.1	7.1
2030	7.3	6.2	10.9	10.7	8.2	6.1	7.5	10.5	8.3	6.7	7.7
2040	7.4	6.2	12.8	11.3	8.3	6.2	7.1	11.1	8.6	6.4	8.0
2050	7.4	6.1	14.5	12.0	8.3	6.3	6.8	11.8	8.9	6.0	8.3
2060	7.3	6.0	15.0	12.9	7.7	6.4	6.3	12.7	8.8	5.8	8.3
2070	7.2	5.7	15.4	13.9	7.4	6.6	5.9	13.7	8.7	5.5	8.4
2080	7.1	5.6	15.7	14.8	7.0	6.7	5.5	14.6	8.6	5.4	8.5
2090	7.1	5.5	16.1	15.7	6.4	6.8	5.2	15.5	8.3	5.2	8.6
2100	7.0	5.4	16.6	16.5	5.7	6.9	4.9	16.4	8.0	5.1	8.7

II.1.4: PFCs, SF₆ and HFCs emissions (Gg/yr)**CF₄ emissions (Gg/yr)**

Year	A1B	A1T	A1FI	A2	B1	B2	A1p	A2p	B1p	B2p
2000	12.6	12.6	12.6	12.6	12.6	12.6	26.7	26.7	26.7	26.7
2010	15.3	15.3	15.3	20.3	14.5	21.0	28.4	28.9	27.0	29.9
2020	21.1	21.1	21.1	25.2	15.7	27.1	41.0	35.2	29.6	37.7
2030	30.1	30.1	30.1	31.4	16.6	34.6	59.4	43.0	31.4	47.4
2040	38.2	38.2	38.2	37.9	18.5	43.6	71.7	50.9	33.1	58.9
2050	43.8	43.8	43.8	45.6	20.9	52.7	77.3	60.0	35.5	70.5
2060	48.1	48.1	48.1	56.0	23.1	59.2	76.7	72.6	36.1	78.5
2070	52.1	52.1	52.1	63.6	22.5	63.1	64.2	84.7	29.6	85.1
2080	56.1	56.1	56.1	73.2	21.3	64.2	40.6	97.9	19.7	86.6
2090	58.9	58.9	58.9	82.8	22.5	62.9	46.8	110.9	20.8	84.7
2100	57.0	57.0	57.0	88.2	22.2	59.9	53.0	117.9	20.5	80.6

C₂F₆ emissions (Gg/yr)

Year	A1B	A1T	A1FI	A2	B1	B2	A1p	A2p	B1p	B2p
2000	1.3	1.3	1.3	1.3	1.3	1.3	2.7	2.7	2.7	2.7
2010	1.5	1.5	1.5	2.0	1.5	2.1	2.8	2.9	2.7	3.0
2020	2.1	2.1	2.1	2.5	1.6	2.7	4.1	3.5	3.0	3.8
2030	3.0	3.0	3.0	3.1	1.7	3.5	5.9	4.3	3.1	4.7
2040	3.8	3.8	3.8	3.8	1.8	4.4	7.2	5.1	3.3	5.9
2050	4.4	4.4	4.4	4.6	2.1	5.3	7.7	6.0	3.6	7.1
2060	4.8	4.8	4.8	5.6	2.3	5.9	7.7	7.3	3.6	7.9
2070	5.2	5.2	5.2	6.4	2.2	6.3	6.4	8.5	3.0	8.5
2080	5.6	5.6	5.6	7.3	2.1	6.4	4.1	9.8	2.0	8.7
2090	5.9	5.9	5.9	8.3	2.2	6.3	4.7	11.1	2.1	8.5
2100	5.7	5.7	5.7	8.8	2.2	6.0	5.3	11.8	2.1	8.1

SF₆ emissions (Gg/yr)

Year	A1B	A1T	A1FI	A2	B1	B2	A1p	A2p	B1p	B2p
2000	6.2	6.2	6.2	6.2	6.2	6.2	6.2	6.2	6.2	6.2
2010	6.7	6.7	6.7	7.6	5.6	7.4	7.2	8.0	6.4	7.7
2020	7.3	7.3	7.3	9.7	5.7	8.4	7.9	10.2	6.5	9.9
2030	10.2	10.2	10.2	11.6	7.2	9.2	10.7	12.0	8.0	12.5
2040	15.2	15.2	15.2	13.7	8.9	11.7	15.8	14.0	9.7	15.8
2050	18.3	18.3	18.3	16.0	10.4	12.1	18.8	16.8	11.2	18.6
2060	19.5	19.5	19.5	18.8	10.9	12.2	20.0	18.7	11.6	20.4
2070	17.3	17.3	17.3	19.8	9.5	11.4	17.8	19.7	10.2	22.0
2080	13.5	13.5	13.5	20.7	7.1	9.6	12.0	20.6	6.8	22.8
2090	13.0	13.0	13.0	23.4	6.5	10.0	13.5	23.3	7.2	23.9
2100	14.5	14.5	14.5	25.2	6.5	10.6	15.0	25.1	7.2	24.4

HFC-23 emissions (Gg/yr)

Year	A1B	A1T	A1FI	A2	B1	B2	A1p	A2p	B1p	B2p
2000	13	13	13	13	13	13	13	13	13	13
2010	15	15	15	15	15	15	15	15	15	15
2020	5	5	5	5	5	5	5	5	5	5
2030	2	2	2	2	2	2	2	2	2	2
2040	2	2	2	2	2	2	2	2	2	2
2050	1	1	1	1	1	1	0	0	0	0
2060	1	1	1	1	1	1	0	0	0	0
2070	1	1	1	1	1	1	0	0	0	0
2080	1	1	1	1	1	1	0	0	0	0
2090	1	1	1	1	1	1	0	0	0	0
2100	1	1	1	1	1	1	0	0	0	0

HFC-32 emissions (Gg/yr)

Year	A1B	A1T	A1FI	A2	B1	B2	A1p	A2p	B1p	B2p
2000	0	0	0	0	0	0	2	2	2	2
2010	4	4	4	4	3	3	3	3	3	3
2020	8	8	8	6	6	6	8	6	6	7
2030	14	14	14	9	8	9	14	9	8	10
2040	19	19	19	11	10	11	19	10	10	12
2050	24	24	24	14	14	14	24	13	14	16
2060	28	28	28	17	14	17	26	16	14	19
2070	29	29	29	20	14	20	27	19	14	21
2080	30	30	30	24	14	22	28	23	14	23
2090	30	30	30	29	14	24	28	28	13	24
2100	30	30	30	33	13	26	28	33	13	25

HFC-125 emissions (Gg/yr)

Year	A1B	A1T	A1FI	A2	B1	B2	A1p	A2p	B1p	B2p	IS92a
2000	0	0	0	0	0	0	7	7	7	7	0
2010	12	12	12	11	11	11	11	10	10	10	1
2020	27	27	27	21	21	22	26	19	20	22	9
2030	45	45	45	29	29	30	44	27	28	32	46
2040	62	62	62	35	36	38	62	33	35	40	111
2050	80	80	80	46	48	49	78	43	47	52	175
2060	94	94	94	56	48	58	84	53	48	62	185
2070	98	98	98	66	48	67	88	62	47	70	194
2080	100	100	100	79	48	76	91	74	46	75	199
2090	101	101	101	94	46	83	92	89	45	79	199
2100	101	101	101	106	44	89	93	104	43	83	199

HFC-134a emissions (Gg/yr)

Year	A1B	A1T	A1FI	A2	B1	B2	A1p	A2p	B1p	B2p	IS92a
2000	80	80	80	80	80	80	147	147	147	147	148
2010	176	176	176	166	163	166	220	204	206	216	290
2020	326	326	326	252	249	262	427	315	319	359	396
2030	515	515	515	330	326	352	693	412	422	496	557
2040	725	725	725	405	414	443	997	508	545	638	738
2050	931	931	931	506	547	561	1215	635	734	816	918
2060	1076	1076	1076	633	550	679	1264	800	732	991	969
2070	1078	1078	1078	758	544	799	1272	962	718	1133	1020
2080	1061	1061	1061	915	533	910	1247	1169	698	1202	1047
2090	1029	1029	1029	1107	513	1002	1204	1422	667	1261	1051
2100	980	980	980	1260	486	1079	1142	1671	627	1317	1055

HFC-143a emissions (Gg/yr)

Year	A1B	A1T	A1FI	A2	B1	B2	A1p	A2p	B1p	B2p
2000	0	0	0	0	0	0	6	6	6	6
2010	9	9	9	9	8	8	8	8	8	8
2020	21	21	21	16	15	16	20	15	15	17
2030	34	34	34	22	21	22	34	21	21	24
2040	47	47	47	27	26	27	48	26	26	30
2050	61	61	61	35	35	35	60	33	35	39
2060	70	70	70	43	35	42	64	41	35	47
2070	74	74	74	51	35	49	67	48	35	53
2080	75	75	75	61	35	55	69	58	35	57
2090	76	76	76	73	34	60	70	70	33	60
2100	76	76	76	82	32	65	70	81	32	63

HFC-152a emissions (Gg/yr)

Year	A1B	A1T	A1FI	A2	B1	B2	A1p	A2p	B1p	B2p	IS92a
2000	0	0	0	0	0	0	0	0	0	0	0
2010	0	0	0	0	0	0	0	0	0	0	0
2020	0	0	0	0	0	0	0	0	0	0	18
2030	0	0	0	0	0	0	0	0	0	0	114
2040	0	0	0	0	0	0	0	0	0	0	281
2050	0	0	0	0	0	0	0	0	0	0	448
2060	0	0	0	0	0	0	0	0	0	0	495
2070	0	0	0	0	0	0	0	0	0	0	542
2080	0	0	0	0	0	0	0	0	0	0	567
2090	0	0	0	0	0	0	0	0	0	0	568
2100	0	0	0	0	0	0	0	0	0	0	570

HFC-227ea emissions (Gg/yr)

Year	A1B	A1T	A1FI	A2	B1	B2	A1p	A2p	B1p	B2p
2000	0	0	0	0	0	0	8	8	8	8
2010	13	13	13	12	13	14	12	11	11	12
2020	22	22	22	17	18	20	21	16	17	18
2030	34	34	34	21	24	26	33	19	22	25
2040	48	48	48	26	30	33	48	24	28	32
2050	62	62	62	32	39	41	57	29	38	41
2060	72	72	72	40	40	50	60	37	37	49
2070	71	71	71	48	39	59	60	44	37	57
2080	68	68	68	58	38	67	59	53	36	60
2090	65	65	65	70	36	74	56	64	34	63
2100	61	61	61	80	34	80	53	76	32	66

HFC-245ca emissions (Gg/yr)

Year	A1B	A1T	A1FI	A2	B1	B2	A1p	A2p	B1p	B2p
2000	0	0	0	0	0	0	38	38	38	38
2010	62	62	62	59	60	61	56	52	53	55
2020	100	100	100	79	80	85	98	73	75	84
2030	158	158	158	98	102	112	159	92	97	114
2040	222	222	222	121	131	144	229	113	128	149
2050	292	292	292	149	173	178	281	140	173	188
2060	350	350	350	190	173	216	298	179	172	229
2070	343	343	343	228	170	255	299	216	168	266
2080	330	330	330	276	166	290	287	262	163	280
2090	312	312	312	334	159	323	271	319	155	291
2100	288	288	288	388	150	353	251	376	145	302

HFC43-10mee emissions (Gg/yr)

Year	A1B	A1T	A1FI	A2	B1	B2	A1p	A2p	B1p	B2p
2000	0	0	0	0	0	0	5	5	5	5
2010	7	7	7	7	6	6	6	6	6	6
2020	9	9	9	8	7	7	8	7	7	7
2030	12	12	12	8	8	8	10	7	7	8
2040	15	15	15	9	9	10	13	8	9	9
2050	18	18	18	11	11	11	15	9	10	11
2060	22	22	22	12	11	12	17	11	10	12
2070	24	24	24	14	11	14	20	12	10	13
2080	27	27	27	16	11	15	22	14	10	14
2090	29	29	29	19	11	17	24	17	10	15
2100	30	30	30	22	10	18	26	19	10	15

Note: Table II.1.4 contains supplementary data to the SRES Report (Nakićenović *et. al.*, 2000): The data contained in the SRES Report was insufficient to break down the individual contributions to HFCs, PFCs and SF₆, these emissions were supplied by Lead Authors of the SRES Report and are also available at the CIESIN (Center for International Earth Science Information Network) Website (<http://sres.ciesin.org>). The sample scenario IS92a is only included for HFC-125, HFC-134a, and HFC-152a.
All PFCs, SF₆ and HFCs emissions are the same for family A1 (A1B, A1T and A1FI).

II.1.5: NO_x emissions (TgN/yr)

Year	A1B	A1T	A1FI	A2	B1	B2	A1p	A2p	B1p	B2p	IS92a
2000	32.0	32.0	32.0	32.0	32.0	32.0	32.5	32.5	32.5	32.5	37.0
2010	39.3	38.8	39.7	39.2	36.1	36.7	41.0	39.6	34.8	37.6	43.4
2020	46.1	46.4	50.4	50.3	39.9	42.7	48.9	50.7	39.3	43.4	49.8
2030	50.2	55.9	62.8	60.7	42.0	48.9	52.5	60.8	40.7	48.4	55.2
2040	48.9	59.7	77.1	65.9	42.6	53.4	50.9	65.8	44.8	52.8	59.6
2050	47.9	61.0	94.9	71.1	38.8	54.5	49.3	71.5	48.9	53.7	64.0
2060	46.0	59.6	102.1	75.5	34.3	56.1	47.2	75.6	48.9	55.4	67.8
2070	44.2	51.7	108.5	79.8	29.6	56.3	45.1	80.1	48.9	55.6	71.6
2080	42.7	42.8	115.4	87.5	25.7	59.2	43.3	87.3	48.9	58.5	75.4
2090	41.4	34.8	111.5	98.3	22.2	60.9	41.8	97.9	41.2	60.1	79.2
2100	40.2	28.1	109.6	109.2	18.7	61.2	40.3	109.7	33.6	60.4	83.0

Note: NO_x is the sum of NO and NO₂

II.1.6: CO emissions (Tg(CO)/yr)

Year	A1B	A1T	A1FI	A2	B1	B2	A1p	A2p	B1p	B2p	IS92a
2000	877	877	877	877	877	877	1036	1036	1036	1036	1048
2010	1002	1003	1020	977	789	935	1273	1136	849	1138	1096
2020	1032	1147	1204	1075	751	1022	1531	1234	985	1211	1145
2030	1109	1362	1436	1259	603	1111	1641	1413	864	1175	1207
2040	1160	1555	1726	1344	531	1220	1815	1494	903	1268	1282
2050	1214	1770	2159	1428	471	1319	1990	1586	942	1351	1358
2060	1245	1944	2270	1545	459	1423	2174	1696	984	1466	1431
2070	1276	2078	2483	1662	456	1570	2359	1816	1026	1625	1504
2080	1357	2164	2776	1842	426	1742	2455	1985	1068	1803	1576
2090	1499	2156	2685	2084	399	1886	2463	2218	1009	1948	1649
2100	1663	2077	2570	2326	363	2002	2471	2484	950	2067	1722

II.1.7: Total VOC emissions (Tg/yr)

Year	A1B	A1T	A1FI	A2	B1	B2	A1p	A2p	B1p	B2p	IS92a
2000	141	141	141	141	141	141	151	151	151	151	126
2010	178	164	166	155	141	159	178	164	143	172	142
2020	222	190	192	179	140	180	207	188	151	192	158
2030	266	212	214	202	131	199	229	210	144	202	173
2040	272	229	256	214	123	214	255	221	147	215	188
2050	279	241	322	225	116	217	285	235	150	217	202
2060	284	242	361	238	111	214	324	246	155	214	218
2070	289	229	405	251	103	202	301	260	160	202	234
2080	269	199	449	275	99	192	263	282	165	192	251
2090	228	167	435	309	96	178	223	315	159	178	267
2100	193	128	420	342	87	170	174	352	154	170	283

Note: Volatile Organic Compounds (VOC) include non-methane hydrocarbons (NMHC) and oxygenated NMHC (e.g., alcohols, aldehydes and organic acids).

II.1.8: SO₂ emissions (TgS/yr)

Year	A1B	A1T	A1FI	A2	B1	B2	A1p	A2p	B1p	B2p	IS92a
2000	69.0	69.0	69.0	69.0	69.0	69.0	69.0	69.0	69.0	69.0	79.0
2010	87.1	64.7	80.8	74.7	73.9	65.9	87.4	74.7	59.8	68.2	95.0
2020	100.2	59.9	86.9	99.5	74.6	61.3	100.8	99.5	56.2	65.0	111.0
2030	91.0	59.6	96.1	112.5	78.2	60.3	91.4	111.9	53.5	59.9	125.8
2040	68.9	45.9	94.0	109.0	78.5	59.0	77.9	108.1	53.3	58.8	139.4
2050	64.1	40.2	80.5	105.4	68.9	55.7	64.3	105.4	51.4	57.2	153.0
2060	46.9	34.4	56.3	89.6	55.8	53.8	51.2	86.3	51.2	53.7	151.8
2070	35.7	30.1	42.6	73.7	44.3	50.9	44.9	71.7	49.2	51.9	150.6
2080	30.7	25.2	39.4	64.7	36.1	50.0	30.7	64.2	42.2	49.1	149.4
2090	29.1	23.3	39.8	62.5	29.8	49.0	29.1	61.9	33.9	48.0	148.2
2100	27.6	20.2	40.1	60.3	24.9	47.9	27.4	60.3	28.6	47.3	147.0

Note: The SRES emissions for SO₂ are used with a linear offset in all scenarios to 69.0 TgS/yr in year 2000.

II.1.9: BC aerosol emissions (Tg/yr)

Year	A1B	A1T	A1FI	A2	B1	B2	A1p	A2p	B1p	B2p	IS92a
2000	12.4	12.4	12.4	12.4	12.4	12.4	12.4	12.4	12.4	12.4	12.4
2010	13.9	13.9	14.1	13.6	11.3	13.1	15.2	13.6	10.2	13.6	13.0
2020	14.3	15.6	16.3	14.8	10.9	14.1	18.3	14.8	11.8	14.5	13.6
2030	15.2	18.2	19.1	17.0	9.1	15.2	19.6	16.9	10.3	14.1	14.3
2040	15.8	20.5	22.6	18.0	8.3	16.5	21.7	17.9	10.8	15.2	15.2
2050	16.4	23.1	27.7	19.0	7.5	17.7	23.8	19.0	11.3	16.2	16.1
2060	16.8	25.2	29.1	20.4	7.4	18.9	26.0	20.3	11.8	17.5	17.0
2070	17.2	26.8	31.6	21.8	7.4	20.7	28.2	21.7	12.3	19.4	17.9
2080	18.1	27.8	35.1	24.0	7.0	22.8	29.4	23.8	12.8	21.6	18.7
2090	19.8	27.7	34.0	26.8	6.7	24.5	29.5	26.5	12.1	23.3	19.6
2100	21.8	26.8	32.7	29.7	6.2	25.9	29.6	29.7	11.4	24.7	20.5

Note: Emissions for BC are scaled to SRES anthropogenic CO emissions offset to year 2000.

II.1.10: OC aerosol emissions (Tg/yr)

Year	A1B	A1T	A1FI	A2	B1	B2	A1p	A2p	B1p	B2p	IS92a
2000	81.4	81.4	81.4	81.4	81.4	81.4	81.4	81.4	81.4	81.4	81.4
2010	91.2	91.3	92.6	89.3	74.5	86.0	100.0	89.3	66.7	89.4	85.2
2020	93.6	102.6	107.1	97.0	71.5	92.8	120.3	97.0	77.4	95.2	89.0
2030	99.6	119.5	125.3	111.4	59.9	99.8	128.9	111.0	67.9	92.3	93.9
2040	103.6	134.7	148.1	118.1	54.2	108.3	142.6	117.4	71.0	99.6	99.8
2050	107.9	151.6	182.1	124.7	49.5	116.1	156.4	124.6	74.0	106.2	105.8
2060	110.3	165.2	190.9	133.9	48.6	124.3	170.8	133.3	77.3	115.2	111.5
2070	112.8	175.8	207.6	143.1	48.3	135.9	185.4	142.7	80.6	127.7	117.2
2080	119.1	182.5	230.6	157.2	46.0	149.4	192.9	156.0	83.9	141.7	122.9
2090	130.3	181.9	223.5	176.2	43.8	160.7	193.5	174.3	79.3	153.1	128.6
2100	143.2	175.7	214.4	195.2	41.0	169.8	194.2	195.2	74.6	162.4	134.4

Note: Emissions for OC are scaled to SRES anthropogenic CO emissions offset to year 2000.

II.2: Abundances and burdens**II.2.1: CO₂ abundances (ppm)**

ISAM model (reference) – CO ₂ abundances (ppm)										IS92a/ SAR	
Year	A1B	A1T	A1FI	A2	B1	B2	A1p	A2p	B1p	B2p	IS92a
1970	325	325	325	325	325	325	325	325	325	325	325
1980	337	337	337	337	337	337	337	337	337	337	338
1990	353	353	353	353	353	353	353	353	353	353	354
2000	369	369	369	369	369	369	369	369	369	369	372
2010	391	389	389	390	388	388	393	391	388	390	393
2020	420	412	417	417	412	408	425	419	409	414	415
2030	454	440	455	451	437	429	461	453	429	438	444
2040	491	471	504	490	463	453	499	492	450	462	475
2050	532	501	567	532	488	478	538	535	472	486	509
2060	572	528	638	580	509	504	577	583	497	512	543
2070	611	550	716	635	525	531	615	637	522	539	582
2080	649	567	799	698	537	559	652	699	544	567	623
2090	685	577	885	771	545	589	685	771	563	597	670
2100	717	582	970	856	549	621	715	856	578	630	723

ISAM model (low) – CO₂ abundances (ppm)

Year	A1B	A1T	A1FI	A2	B1	B2	A1p	A2p	B1p	B2p	IS92a
2000	368	368	368	368	368	368	368	368	368	368	368
2010	383	381	381	382	380	380	385	383	380	382	382
2020	405	398	403	402	398	394	409	404	395	400	401
2030	432	419	433	429	416	410	438	431	410	417	423
2040	461	443	473	460	436	427	467	461	425	435	446
2050	493	466	525	493	455	446	498	495	442	454	472
2060	524	486	584	532	470	466	528	534	460	473	499
2070	554	501	647	576	480	486	557	577	479	492	529
2080	582	511	715	626	486	507	583	627	495	513	561
2090	607	516	783	686	490	530	607	686	507	536	598
2100	630	516	851	755	490	554	627	755	517	561	640

ISAM model (high) – CO₂ abundances (ppm)

Year	A1B	A1T	A1FI	A2	B1	B2	A1p	A2p	B1p	B2p	IS92a
2000	369	369	369	369	369	369	369	369	369	369	369
2010	397	394	394	395	394	393	398	396	393	396	396
2020	431	422	427	427	422	417	435	429	418	424	426
2030	470	455	471	466	452	443	477	469	444	453	460
2040	513	491	527	511	483	472	521	514	469	482	498
2050	560	527	597	561	514	502	568	564	496	512	539
2060	609	560	678	617	541	534	615	620	527	543	583
2070	656	590	767	681	563	567	661	682	558	577	631
2080	703	613	863	754	581	602	706	755	586	612	682
2090	748	631	962	838	594	640	749	838	611	650	739
2100	790	642	1062	936	603	680	789	936	634	691	804

Note: A “reference” case was defined with climate sensitivity 2.5°C, ocean uptake corresponding to the mean of the ocean model results in Chapter 3, Figure 3.10, and terrestrial uptake corresponding to the mean of the responses of mid–range models, LPJ, IBIS and SDGM (Chapter 3, Figure 3.10). A “low CO₂” parametrization was chosen with climate sensitivity 1.5°C and maximal CO₂ uptake by oceans and land. A “high CO₂” parametrization was defined with climate sensitivity 4.5°C and minimal CO₂ uptake by oceans and land. See Chapter 3, Box 3.7, and Jain *et al.* (1994) for more details on the ISAM model.

The IS92a column values are calculated using the ISAM parametrization noted above with IS92a emissions starting in the year 2000; whereas the IS92a/SAR column refers to values as reported in the SAR using IS92a emissions starting in 1990, using the SAR parametrization of ISAM.

Bern–CC model (reference) – CO₂ abundances (ppm)

Year	A1B	A1T	A1FI	A2	B1	B2	A1p	A2p	B1p	B2p	IS92a	SAR
1970	325	325	325	325	325	325	325	325	325	325	325	325
1980	337	337	337	337	337	337	337	337	337	337	337	337
1990	352	352	352	352	352	352	352	352	352	352	352	353
2000	367	367	367	367	367	367	367	367	367	367	367	370
2010	388	386	386	386	386	385	390	388	385	387	387	391
2020	418	410	415	414	410	406	421	416	407	412	413	416
2030	447	435	449	444	432	425	454	447	425	433	439	444
2040	483	466	495	481	457	448	490	484	445	457	468	475
2050	522	496	555	522	482	473	529	525	467	481	499	507
2060	563	523	625	568	503	499	569	571	492	506	533	541
2070	601	545	702	620	518	524	606	622	515	532	568	577
2080	639	563	786	682	530	552	642	683	537	559	607	616
2090	674	572	872	754	538	581	674	754	555	588	653	660
2100	703	575	958	836	540	611	702	836	569	618	703	709

Bern–CC model (low) – CO₂ abundances (ppm)

Year	A1B	A1T	A1FI	A2	B1	B2	A1p	A2p	B1p	B2p	IS92a
2000	367	367	367	367	367	367	367	367	367	367	367
2010	383	381	381	381	381	380	384	383	380	382	383
2020	407	400	405	404	400	396	411	406	397	402	403
2030	432	419	432	428	417	410	437	431	410	417	424
2040	460	442	472	459	436	427	466	461	425	434	448
2050	491	464	521	492	455	445	496	495	440	452	473
2060	522	483	577	529	470	464	524	531	458	470	500
2070	548	496	636	569	479	482	550	569	475	487	527
2080	575	505	700	617	485	502	575	616	490	507	559
2090	598	508	763	671	487	522	596	670	501	528	593
2100	617	506	824	735	486	544	613	734	509	550	632

Bern–CC model (high) – CO₂ abundances (ppm)

Year	A1B	A1T	A1FI	A2	B1	B2	A1p	A2p	B1p	B2p	IS92a
2000	367	367	367	367	367	367	367	367	367	367	367
2010	395	393	393	393	392	392	397	395	392	394	395
2020	436	427	433	431	426	422	441	434	424	430	431
2030	483	467	484	477	463	454	491	482	455	465	471
2040	538	514	552	533	503	491	548	538	488	504	517
2050	599	562	638	597	544	531	609	602	524	544	568
2060	666	610	743	670	584	575	675	675	566	588	624
2070	732	653	859	753	617	620	738	757	608	632	684
2080	797	689	985	848	645	668	802	851	648	680	750
2090	860	717	1118	957	666	718	863	959	682	730	822
2100	918	735	1248	1080	681	769	918	1082	713	782	902

Note: A “reference” case was defined with an average ocean uptake for the 1980s of 2.0 PgC/yr. A “low CO₂” parameterisation was obtained by combining a “fast ocean” (ocean uptake of 2.54 PgC/yr for the 1980s) and no response of heterotrophic respiration to temperature. A “high CO₂” parameterisation was obtained by combining a “slow ocean” (ocean uptake of 1.46 PgC/yr for the 1980s) and capping CO₂ fertilisation. Climate sensitivity was set to 2.5°C for a doubling of CO₂. See Chapter 3, Box 3.7 for more details on the Bern–CC model.

The IS92a/SAR column refers to values as reported in the SAR using IS92a emissions; whereas the IS92a column is calculated using IS92a emissions but with year 2000 starting values and the BERN-CC model as described in Chapter 3.

The Bern-CC model was initialised for observed atmospheric CO₂ which was prescribed for the period 1765 to 1999. The CO₂ data were smoothed by a spline. Scenario calculations started at the beginning of the year 2000. This explains the difference in the values given for the years upto 2000. Values shown are for the beginning of each year. Annual-mean values are generally higher (up to 7ppm) depending on the scenario and the year.

II.2.2: CH₄ abundances (ppb)

Year	A1B	A1T	A1FI	A2	B1	B2	A1p	A2p	B1p	B2p	IS92a	SAR
1970	1420	1420	1420	1420	1420	1420	1420	1420	1420	1420	1420	1420
1980	1570	1570	1570	1570	1570	1570	1570	1570	1570	1570	1570	1570
1990	1700	1700	1700	1700	1700	1700	1700	1700	1700	1700	1700	1700
2000	1760	1760	1760	1760	1760	1760	1760	1760	1760	1760	1760	1810
2010	1871	1856	1851	1861	1827	1839	1899	1861	1816	1862	1855	1964
2020	2026	1998	1986	1997	1891	1936	2126	1997	1878	2020	1979	2145
2030	2202	2194	2175	2163	1927	2058	2392	2159	1931	2201	2129	2343
2040	2337	2377	2413	2357	1919	2201	2598	2344	1963	2358	2306	2561
2050	2400	2503	2668	2562	1881	2363	2709	2549	2009	2473	2497	2793
2060	2386	2552	2875	2779	1836	2510	2736	2768	2049	2552	2663	3003
2070	2301	2507	3030	3011	1797	2639	2669	2998	2077	2606	2791	3175
2080	2191	2420	3175	3252	1741	2765	2533	3238	2100	2625	2905	3328
2090	2078	2310	3307	3493	1663	2872	2367	3475	2091	2597	3019	3474
2100	1974	2169	3413	3731	1574	2973	2187	3717	2039	2569	3136	3616

Note: The IS92a/SAR column refers to values as reported in the SAR using IS92a emissions; whereas the IS92a column is calculated using IS92a emissions but with year 2000 starting values and the new feedbacks on the lifetime. See Chapter 4 for details.

II.2.3: N₂O abundances (ppb)

Year	A1B	A1T	A1FI	A2	B1	B2	A1p	A2p	B1p	B2p	IS92a	SAR
1970	295	295	295	295	295	295	295	295	295	295	295	295
1980	301	301	301	301	301	301	301	301	301	301	301	301
1990	308	308	308	308	308	308	308	308	308	308	308	308
2000	316	316	316	316	316	316	316	316	316	316	316	319
2010	324	323	325	325	324	323	324	325	324	324	324	328
2020	331	328	335	335	333	328	332	335	333	331	333	339
2030	338	333	347	347	341	333	340	347	341	338	343	350
2040	344	338	361	360	349	338	346	360	350	343	353	361
2050	350	342	378	373	357	342	351	373	358	347	363	371
2060	356	345	396	387	363	346	355	386	366	350	372	382
2070	360	348	413	401	368	350	358	400	373	352	381	391
2080	365	350	429	416	371	354	360	415	380	354	389	400
2090	368	352	445	432	374	358	361	430	385	355	396	409
2100	372	354	460	447	375	362	361	446	389	356	403	417

Note: The IS92a/SAR column refers to values as reported in the SAR using IS92a emissions; whereas the IS92a column is calculated using IS92a emissions but with year 2000 starting values and the new feedbacks on the lifetime. See Chapter 4 for details.

II.2.4: PFCs, SF₆ and HFCs abundances (ppt)**CF₄ abundances (ppt)**

Year	A1B	A1T	A1FI	A2	B1	B2	A1p	A2p	B1p	B2p
1990	70	70	70	70	70	70	70	70	70	70
2000	82	82	82	82	82	82	82	82	82	82
2010	91	91	91	92	91	93	100	100	100	100
2020	103	103	103	107	101	108	122	121	118	122
2030	119	119	119	125	111	128	154	146	138	150
2040	141	141	141	148	122	153	197	176	159	184
2050	168	168	168	175	135	184	245	212	181	226
2060	198	198	198	208	150	221	296	255	204	274
2070	230	230	230	246	164	261	342	306	226	327
2080	265	265	265	291	179	302	377	365	242	383
2090	303	303	303	341	193	344	405	433	256	439
2100	341	341	341	397	208	384	437	508	269	493

C₂F₆ abundances (ppt)

Year	A1B	A1T	A1FI	A2	B1	B2	A1p	A2p	B1p	B2p
1990	2	2	2	2	2	2	2	2	2	2
2000	3	3	3	3	3	3	3	3	3	3
2010	4	4	4	4	4	4	4	4	4	4
2020	5	5	5	5	4	5	6	6	6	6
2030	6	6	6	6	5	6	8	7	7	8
2040	7	7	7	7	6	8	11	9	8	10
2050	9	9	9	9	7	10	14	12	10	12
2060	11	11	11	11	8	12	17	14	11	16
2070	13	13	13	14	8	15	20	18	12	19
2080	15	15	15	17	9	17	22	21	13	22
2090	17	17	17	20	10	20	24	26	14	26
2100	20	20	20	23	11	22	26	30	15	30

SF₆ abundances (ppt)

Year	A1B	A1T	A1FI	A2	B1	B2	A1p	A2p	B1p	B2p
1990	3	3	3	3	3	3	3	3	3	3
2000	5	5	5	5	5	5	5	5	5	5
2010	7	7	7	7	7	7	7	7	7	7
2020	10	10	10	11	9	10	10	11	10	11
2030	13	13	13	15	12	14	14	15	12	15
2040	18	18	18	20	15	18	19	20	16	21
2050	25	25	25	26	19	23	26	26	20	27
2060	32	32	32	32	23	27	33	33	24	35
2070	39	39	39	40	27	32	41	41	29	43
2080	45	45	45	48	30	36	46	48	32	52
2090	50	50	50	56	33	40	51	57	35	61
2100	56	56	56	65	35	44	57	66	37	70

HFC-23 abundances (ppt)

Year	A1B	A1T	A1FI	A2	B1	B2	A1p	A2p	B1p	B2p
1990	8	8	8	8	8	8	8	8	8	8
2000	15	15	15	15	15	15	15	15	15	15
2010	26	26	26	26	26	26	26	26	26	26
2020	33	33	33	33	33	33	33	33	33	33
2030	35	35	35	35	35	35	35	35	35	35
2040	35	35	35	35	35	35	36	35	35	35
2050	35	35	35	35	35	35	35	35	35	35
2060	35	35	35	35	34	35	34	34	33	34
2070	35	35	34	34	34	34	33	32	32	33
2080	34	34	34	34	33	34	32	31	31	31
2090	34	34	34	34	33	34	31	30	30	30
2100	34	34	34	33	32	34	30	29	29	29

HFC-32 abundance (ppt)

Year	A1B	A1T	A1FI	A2	B1	B2	A1p	A2p	B1p	B2p
1990	0	0	0	0	0	0	0	0	0	0
2000	0	0	0	0	0	0	0	0	0	0
2010	1	1	1	1	1	1	1	1	1	1
2020	3	3	3	3	3	3	3	3	3	3
2030	7	7	6	4	4	4	7	4	4	5
2040	10	10	10	6	5	6	11	5	5	7
2050	14	14	13	7	7	8	15	7	7	9
2060	17	17	16	9	8	10	18	9	8	11
2070	19	19	18	11	8	12	20	11	8	13
2080	19	21	19	14	8	14	21	13	8	14
2090	20	22	20	17	8	15	21	16	8	15
2100	19	22	20	20	8	17	20	20	8	16

HFC-125 abundance (ppt)

Year	A1B	A1T	A1FI	A2	B1	B2	A1p	A2p	B1p	B2p	IS92a
1990	0	0	0	0	0	0	0	0	0	0	0
2000	0	0	0	0	0	0	0	0	0	0	0
2010	2	2	2	2	2	4	3	3	3	3	0
2020	9	9	9	8	8	10	8	8	9	9	2
2030	21	21	21	16	16	22	15	16	17	17	12
2040	37	37	37	24	24	26	38	23	24	27	40
2050	57	56	55	34	33	36	57	32	33	38	87
2060	77	78	76	45	43	48	78	43	42	51	137
2070	97	98	95	58	49	61	96	54	49	65	177
2080	112	115	111	72	54	75	111	68	54	77	210
2090	124	129	124	89	57	88	123	83	57	89	236
2100	133	140	134	107	58	102	132	101	58	99	255

HFC-134a abundance (ppt)

Year	A1B	A1T	A1FI	A2	B1	B2	A1p	A2p	B1p	B2p	IS92a
1990	0	0	0	0	0	0	0	0	0	0	0
2000	12	12	12	12	12	12	12	12	12	12	12
2010	58	58	58	55	55	56	80	76	76	79	94
2020	130	130	129	111	108	113	172	141	142	155	183
2030	236	235	233	170	165	179	319	214	215	250	281
2040	375	373	366	231	223	250	522	290	294	356	401
2050	537	535	521	299	293	330	754	375	393	477	537
2060	698	701	675	382	352	424	954	480	476	615	657
2070	814	832	791	480	380	526	1092	606	515	756	743
2080	871	912	859	594	391	633	1167	753	530	878	807
2090	887	952	893	729	390	737	1185	930	531	968	850
2100	875	956	899	877	379	835	1157	1132	522	1041	878

HFC-143a abundance (ppt)

Year	A1B	A1T	A1FI	A2	B1	B2	A1p	A2p	B1p	B2p
1990	0	0	0	0	0	0	0	0	0	0
2000	0	0	0	0	0	0	0	0	0	0
2010	3	3	3	3	2	2	4	4	4	4
2020	11	11	11	10	9	9	12	11	11	11
2030	26	26	26	20	18	19	27	20	20	22
2040	47	47	47	32	29	31	48	31	31	35
2050	73	73	72	45	43	45	75	44	44	51
2060	103	103	101	62	57	62	104	60	58	69
2070	132	133	130	81	68	81	131	78	69	89
2080	158	161	157	103	77	101	156	98	79	110
2090	181	185	180	129	85	121	179	123	86	129
2100	200	207	201	157	90	142	197	151	92	147

HFC-152a abundance (ppt)

HFC–227ea abundance (ppt)

Year	A1B	A1T	A1FI	A2	B1	B2	A1p	A2p	B1p	B2p
1990	0	0	0	0	0	0	0	0	0	0
2000	0	0	0	0	0	0	0	0	0	0
2010	2	2	2	2	2	3	3	3	3	3
2020	6	6	6	5	6	6	7	6	6	7
2030	13	13	13	10	10	11	13	9	10	11
2040	22	22	22	14	15	17	22	13	15	17
2050	33	33	32	19	21	24	33	18	20	23
2060	45	45	44	25	27	31	43	23	26	31
2070	56	56	55	32	31	40	52	29	30	39
2080	63	65	62	40	34	49	60	36	33	47
2090	68	71	68	49	35	59	64	45	34	54
2100	70	74	71	60	36	68	67	55	35	60

HFC–245ca abundance (ppt)

Year	A1B	A1T	A1FI	A2	B1	B2	A1p	A2p	B1p	B2p
1990	0	0	0	0	0	0	0	0	0	0
2000	0	0	0	0	0	0	0	0	0	0
2010	8	8	8	8	8	8	11	10	10	10
2020	20	20	20	17	17	18	20	16	16	18
2030	34	34	33	23	23	26	35	21	22	26
2040	52	51	50	29	29	34	55	27	28	35
2050	72	72	69	36	38	44	76	34	38	46
2060	92	93	88	46	43	55	92	43	44	58
2070	102	105	99	58	44	67	101	55	44	70
2080	101	108	101	72	43	80	101	68	44	79
2090	97	107	99	88	42	92	96	84	43	84
2100	90	101	94	105	40	103	88	101	41	88

HFC–43–10mee abundance (ppt)

Year	A1B	A1T	A1FI	A2	B1	B2	A1p	A2p	B1p	B2p
1990	0	0	0	0	0	0	0	0	0	0
2000	0	0	0	0	0	0	0	0	0	0
2010	1	1	1	1	1	1	1	1	1	1
2020	2	2	2	2	1	1	2	2	2	2
2030	3	3	3	2	2	2	3	2	2	2
2040	4	4	4	3	2	3	4	2	2	3
2050	5	5	5	3	3	3	5	3	3	3
2060	7	7	6	4	3	4	6	3	3	4
2070	8	8	8	4	4	5	7	4	3	4
2080	9	9	9	5	4	5	8	4	4	5
2090	10	11	10	6	4	6	9	5	4	5
2100	11	12	11	7	4	7	10	6	4	6

Note: Even though all PFCs, SF6 and HFCs emissions are the same for family A1 (A1B, A1T and A1FI), the OH changes due to CH₄, NO_x, CO and VOC (affecting only HFCs burdens). Hence the burden for HFCs can diverge for each of these scenarios within family A1. See Chapter 4 for details.

II.2.5: Tropospheric O₃ burden (global mean column in DU)

Year	A1B	A1T	A1FI	A2	B1	B2	A1p	A2p	B1p	B2p	IS92a/SAR	
											IS92a	SAR
1990	34.0	34.0	34.0	34.0	34.0	34.0	34.0	34.0	34.0	34.0	34.0	34.0
2000	34.0	34.0	34.0	34.0	34.0	34.0	34.0	34.0	34.0	34.0	34.0	34.3
2010	35.8	35.6	35.8	35.7	34.8	35.2	36.2	35.6	34.3	35.4	35.5	34.8
2020	37.8	37.7	38.4	38.2	35.6	36.7	38.8	38.2	35.4	37.1	37.1	35.3
2030	39.3	40.3	41.5	40.8	35.9	38.4	40.5	40.7	35.7	38.5	38.7	35.8
2040	39.7	41.9	45.1	42.6	35.8	39.8	41.3	42.4	36.5	39.9	40.1	36.5
2050	39.8	42.9	49.6	44.2	35.0	40.7	41.6	44.1	37.5	40.6	41.6	37.1
2060	39.6	43.1	51.9	45.7	34.0	41.5	41.8	45.6	37.7	41.2	42.9	37.7
2070	39.1	41.9	53.8	47.2	33.1	42.1	41.4	47.1	37.9	41.6	44.0	38.2
2080	38.5	40.2	55.9	49.3	32.1	43.0	40.8	49.1	38.1	42.3	45.1	38.7
2090	38.0	38.4	55.6	52.0	31.2	43.7	39.9	51.8	36.8	42.6	46.1	39.1
2100	37.5	36.5	55.2	54.8	30.1	44.2	38.9	54.7	35.2	42.8	47.2	39.5

Note: IS92a/SAR column refers to IS92a emissions as reported in the SAR which estimated this O₃ change only as an indirect feedback effect from CH₄ increases; whereas IS92a column uses the latest models (see Chapter 4) which include also changes in emissions of NO_x, CO and VOC. A mean tropospheric O₃ content of 34 DU in 1990 is adopted; and 1 ppb of tropospheric O₃ = 0.65 DU.

These projected increases in tropospheric O₃ are likely to be 25% too large, see note to Table 4.11 of Chapter 4 describing corrections made after government review.

II.2.6: Tropospheric OH (as a factor relative to year 2000)

Year	A1B	A1T	A1FI	A2	B1	B2	A1p	A2p	B1p	B2p	IS92a
2000	1.00	1.00	1.00	1.00	1.00	1.00	1.00	1.00	1.00	1.00	1.00
2010	0.99	0.99	0.99	1.00	1.01	0.99	0.98	1.00	1.02	0.99	1.00
2020	0.97	0.98	0.99	1.00	1.02	0.99	0.94	1.00	1.01	0.97	0.99
2030	0.94	0.96	0.98	0.99	1.04	0.98	0.90	0.99	1.02	0.96	0.98
2040	0.91	0.93	0.96	0.98	1.06	0.96	0.85	0.98	1.03	0.95	0.96
2050	0.90	0.89	0.94	0.96	1.06	0.93	0.81	0.96	1.04	0.93	0.95
2060	0.89	0.87	0.92	0.94	1.05	0.91	0.78	0.94	1.03	0.92	0.93
2070	0.89	0.84	0.90	0.92	1.04	0.89	0.77	0.92	1.01	0.90	0.92
2080	0.89	0.81	0.88	0.90	1.04	0.87	0.77	0.90	1.01	0.89	0.91
2090	0.90	0.81	0.86	0.89	1.04	0.86	0.80	0.89	0.98	0.89	0.90
2100	0.90	0.82	0.86	0.88	1.05	0.84	0.82	0.88	0.97	0.89	0.89

II.2.7: SO₄²⁻ aerosol burden (TgS)

Year	A1B	A1T	A1FI	A2	B1	B2	A1p	A2p	B1p	B2p	IS92a
2000	0.52	0.52	0.52	0.52	0.52	0.52	0.52	0.52	0.52	0.52	0.52
2010	0.66	0.49	0.61	0.56	0.56	0.50	0.66	0.56	0.45	0.51	0.64
2020	0.76	0.45	0.65	0.75	0.56	0.46	0.76	0.75	0.42	0.49	0.76
2030	0.69	0.45	0.72	0.85	0.59	0.45	0.69	0.84	0.40	0.45	0.87
2040	0.52	0.35	0.71	0.82	0.59	0.44	0.59	0.81	0.40	0.44	0.98
2050	0.48	0.30	0.61	0.79	0.52	0.42	0.48	0.79	0.39	0.43	1.08
2060	0.35	0.26	0.42	0.68	0.42	0.41	0.39	0.65	0.39	0.40	1.07
2070	0.27	0.23	0.32	0.56	0.33	0.38	0.34	0.54	0.37	0.39	1.06
2080	0.23	0.19	0.30	0.49	0.27	0.38	0.23	0.48	0.32	0.37	1.05
2090	0.22	0.18	0.30	0.47	0.22	0.37	0.22	0.47	0.26	0.36	1.04
2100	0.21	0.15	0.30	0.45	0.19	0.36	0.21	0.45	0.22	0.36	1.03

Note: Global burden is scaled to emissions: 0.52 Tg burden for 69.0 TgS/yr emissions.

II.2.8: BC aerosol burden (Tg)

Year	A1B	A1T	A1FI	A2	B1	B2	A1p	A2p	B1p	B2p	IS92a
2000	0.26	0.26	0.26	0.26	0.26	0.26	0.26	0.26	0.26	0.26	0.26
2010	0.29	0.29	0.30	0.29	0.24	0.27	0.32	0.29	0.21	0.29	0.27
2020	0.30	0.33	0.34	0.31	0.23	0.30	0.38	0.31	0.25	0.30	0.28
2030	0.32	0.38	0.40	0.36	0.19	0.32	0.41	0.35	0.22	0.29	0.30
2040	0.33	0.43	0.47	0.38	0.17	0.35	0.46	0.37	0.23	0.32	0.32
2050	0.34	0.48	0.58	0.40	0.16	0.37	0.50	0.40	0.24	0.34	0.34
2060	0.35	0.53	0.61	0.43	0.16	0.40	0.55	0.43	0.25	0.37	0.36
2070	0.36	0.56	0.66	0.46	0.15	0.43	0.59	0.46	0.26	0.41	0.37
2080	0.38	0.58	0.74	0.50	0.15	0.48	0.62	0.50	0.27	0.45	0.39
2090	0.42	0.58	0.71	0.56	0.14	0.51	0.62	0.56	0.25	0.49	0.41
2100	0.46	0.56	0.68	0.62	0.13	0.54	0.62	0.62	0.24	0.52	0.43

Note: Global burden is scaled to emissions: 0.26 Tg burden for 12.4 Tg/yr emissions.

II.2.9: OC aerosol burden (Tg)

Year	A1B	A1T	A1FI	A2	B1	B2	A1p	A2p	B1p	B2p	IS92a
2000	1.52	1.52	1.52	1.52	1.52	1.52	1.52	1.52	1.52	1.52	1.52
2010	1.70	1.70	1.73	1.67	1.39	1.61	1.87	1.67	1.25	1.67	1.59
2020	1.75	1.92	2.00	1.81	1.34	1.73	2.25	1.81	1.45	1.78	1.66
2030	1.86	2.23	2.34	2.08	1.12	1.86	2.41	2.07	1.27	1.72	1.75
2040	1.94	2.51	2.77	2.21	1.01	2.02	2.66	2.19	1.32	1.86	1.86
2050	2.01	2.83	3.40	2.33	0.92	2.17	2.92	2.33	1.38	1.98	1.97
2060	2.06	3.09	3.56	2.50	0.91	2.32	3.19	2.49	1.44	2.15	2.08
2070	2.11	3.28	3.88	2.67	0.90	2.54	3.46	2.66	1.51	2.38	2.19
2080	2.22	3.41	4.31	2.94	0.86	2.79	3.60	2.91	1.57	2.65	2.29
2090	2.43	3.40	4.17	3.29	0.82	3.00	3.61	3.25	1.48	2.86	2.40
2100	2.67	3.28	4.00	3.65	0.77	3.17	3.63	3.64	1.39	3.03	2.51

Note: Global burden is scaled to emissions: 1.52 Tg burden for 81.4 Tg/yr emissions.

II.2.10: CFCs and HFCs abundances from WMO98 Scenario A1(baseline) following the Montreal (1997) Amendments (ppt)

Year	CFC-11	CFC-12	CFC-113	CFC-114	CFC-115	CCl ₄	CH ₃ CCl ₃	HCFC-22	HCFC-141b	HCFC-142b	HCFC-123	CF ₂ BrCl	CF ₃ Br	EESCI
1970	50	109	4	6	0	56	13	13	0	0	0	0	0	1.25
1975	106	199	9	8	1	77	36	25	0	0	0	0	0	1.54
1980	164	290	18	10	1	92	75	41	0	0	0	1	0	1.99
1985	207	373	34	12	3	100	102	64	0	0	0	2	1	2.44
1990	258	467	67	15	5	102	125	90	0	1	0	3	2	2.87
1995	271	520	86	16	7	100	110	112	3	7	0	4	2	3.30
2000	267	535	85	16	9	92	44	145	13	15	0	4	3	3.28
2010	246	527	81	16	9	75	6	257	22	33	2	4	3	3.03
2020	214	486	72	15	9	59	1	229	16	32	3	3	3	2.74
2030	180	441	64	15	9	47	0	137	9	23	2	2	3	2.42
2040	149	400	57	14	9	37	0	88	6	17	2	1	3	2.16
2050	123	362	51	14	9	29	0	46	2	11	1	1	3	1.94
2060	101	328	45	13	9	23	0	20	1	6	1	0	2	1.76
2070	83	298	40	13	9	18	0	9	0	4	0	0	2	1.62
2080	68	270	36	12	8	14	0	4	0	2	0	0	2	1.51
2090	56	245	32	12	8	11	0	2	0	1	0	0	2	1.41
2100	45	222	28	12	8	9	0	1	0	1	0	0	1	1.33

Notes: Only significant greenhouse halocarbons shown (ppt).

EESCI = Equivalent Effective Stratospheric Chlorine in ppb (includes Br).

[Source: UNEP/WMO Scientific Assessment of Ozone Depletion: 1998 (Chapter 11), Version 5, June 3, 1998, Calculations by John Daniel and Guus Velders – guus.velders@rivm.nl & jdaniel@al.noaa.gov]

II.3: Radiative Forcing (Wm⁻²) (relative to pre-industrial period, 1750)

The concentrations of CO₂ and CH₄ considered here correspond to the year 2000 and differ slightly from those considered in Chapter 6 which used the values corresponding to the year 1998 (as appropriate for the time frame when Chapter 6 began its preparation). The resulting difference in the computed present day forcings is about 3% in the case of CO₂ and about 2% in the case of CH₄. For N₂O, the difference in the computed forcings is negligible. In the case of tropospheric ozone, the forcing for the year 2000 given here and that in Chapter 6 are the results of slightly different scenarios employed which leads to about a 9% difference in the forcings. For the halogen containing compounds, the absolute differences in concentrations between here and Chapter 6 lead to a difference in present day forcing of less than 0.002 Wm⁻² for any species.

II.3.1: CO₂ radiative forcing (Wm⁻²)

ISAM model (reference) – CO ₂ radiative forcing (Wm ⁻²)										IS92a/ SAR	
Year	A1B	A1T	A1FI	A2	B1	B2	A1p	A2p	B1p	B2p	IS92a
2000	1.51	1.51	1.51	1.51	1.51	1.51	1.51	1.51	1.51	1.51	1.56
2010	1.82	1.80	1.80	1.81	1.78	1.78	1.85	1.82	1.78	1.81	1.85
2020	2.21	2.10	2.17	2.17	2.10	2.05	2.27	2.19	2.07	2.13	2.14
2030	2.62	2.46	2.64	2.59	2.42	2.32	2.71	2.61	2.32	2.43	2.50
2040	3.04	2.82	3.18	3.03	2.73	2.61	3.13	3.05	2.58	2.72	2.87
2050	3.47	3.15	3.81	3.47	3.01	2.90	3.53	3.50	2.83	2.99	3.23
2060	3.86	3.43	4.44	3.93	3.24	3.18	3.91	3.96	3.11	3.27	3.58
2070	4.21	3.65	5.06	4.42	3.40	3.46	4.25	4.44	3.37	3.54	3.95
2080	4.54	3.81	5.65	4.93	3.52	3.74	4.56	4.93	3.59	3.81	4.32
2090	4.82	3.91	6.20	5.46	3.60	4.02	4.82	5.46	3.78	4.09	4.71
2100	5.07	3.95	6.69	6.02	3.64	4.30	5.05	6.02	3.92	4.38	5.11
ISAM model (low) – CO ₂ radiative forcing (Wm ⁻²)										IS92a	
Year	A1B	A1T	A1FI	A2	B1	B2	A1p	A2p	B1p	B2p	IS92a
2000	1.50	1.50	1.50	1.50	1.50	1.50	1.50	1.50	1.50	1.50	1.50
2010	1.71	1.69	1.69	1.70	1.67	1.67	1.74	1.71	1.67	1.70	1.70
2020	2.01	1.92	1.99	1.97	1.92	1.87	2.07	2.00	1.88	1.95	1.96
2030	2.36	2.19	2.37	2.32	2.16	2.08	2.43	2.35	2.08	2.17	2.25
2040	2.71	2.49	2.84	2.69	2.41	2.30	2.78	2.71	2.27	2.40	2.53
2050	3.06	2.76	3.40	3.06	2.64	2.53	3.12	3.09	2.48	2.62	2.83
2060	3.39	2.99	3.97	3.47	2.81	2.76	3.43	3.49	2.69	2.84	3.13
2070	3.69	3.15	4.52	3.90	2.92	2.99	3.72	3.91	2.91	3.05	3.44
2080	3.95	3.26	5.05	4.34	2.99	3.21	3.96	4.35	3.09	3.28	3.76
2090	4.18	3.31	5.54	4.83	3.03	3.45	4.18	4.83	3.21	3.51	4.10
2100	4.38	3.31	5.99	5.35	3.03	3.69	4.35	5.35	3.32	3.76	4.46
ISAM model (high) – CO ₂ radiative forcing (Wm ⁻²)										IS92a	
Year	A1B	A1T	A1FI	A2	B1	B2	A1p	A2p	B1p	B2p	IS92a
2000	1.51	1.51	1.51	1.51	1.51	1.51	1.51	1.51	1.51	1.51	1.51
2010	1.91	1.87	1.87	1.88	1.87	1.85	1.92	1.89	1.85	1.89	1.89
2020	2.35	2.23	2.30	2.30	2.23	2.17	2.40	2.32	2.18	2.26	2.28
2030	2.81	2.64	2.82	2.76	2.60	2.49	2.89	2.80	2.50	2.61	2.69
2040	3.28	3.04	3.42	3.26	2.96	2.83	3.36	3.29	2.80	2.94	3.12
2050	3.75	3.42	4.09	3.76	3.29	3.16	3.82	3.78	3.10	3.27	3.54
2060	4.20	3.75	4.77	4.27	3.56	3.49	4.25	4.29	3.42	3.58	3.96
2070	4.59	4.03	5.43	4.79	3.78	3.81	4.63	4.80	3.73	3.91	4.39
2080	4.96	4.23	6.06	5.34	3.94	4.13	4.99	5.35	3.99	4.22	4.80
2090	5.30	4.39	6.64	5.90	4.06	4.46	5.30	5.90	4.21	4.54	5.23
2100	5.59	4.48	7.17	6.49	4.14	4.79	5.58	6.49	4.41	4.87	5.68
Bern–CC model (reference) – CO ₂ radiative forcing (Wm ⁻²)										IS92a/ SAR	
Year	A1B	A1T	A1FI	A2	B1	B2	A1p	A2p	B1p	B2p	IS92a
2000	1.49	1.49	1.49	1.49	1.49	1.49	1.49	1.49	1.49	1.49	1.53
2010	1.78	1.76	1.76	1.76	1.76	1.74	1.81	1.78	1.74	1.77	1.77
2020	2.18	2.08	2.14	2.13	2.08	2.03	2.22	2.16	2.04	2.10	2.12
2030	2.54	2.40	2.56	2.50	2.36	2.27	2.62	2.54	2.27	2.37	2.44
2040	2.96	2.76	3.09	2.93	2.66	2.55	3.03	2.97	2.52	2.66	2.79
2050	3.37	3.10	3.70	3.37	2.94	2.84	3.44	3.40	2.78	2.93	3.13
2060	3.78	3.38	4.33	3.82	3.17	3.13	3.83	3.85	3.05	3.20	3.48
2070	4.12	3.60	4.96	4.29	3.33	3.39	4.17	4.31	3.30	3.47	3.82
2080	4.45	3.78	5.56	4.80	3.45	3.67	4.48	4.81	3.52	3.74	4.18
2090	4.74	3.86	6.12	5.34	3.53	3.94	4.74	5.34	3.70	4.01	4.57
2100	4.96	3.89	6.62	5.89	3.55	4.21	4.96	5.89	3.83	4.27	4.96

Bern–CC model (low) – CO₂ radiative forcing (Wm⁻²)

Year	A1B	A1T	A1FI	A2	B1	B2	A1p	A2p	B1p	B2p	IS92a
2000	1.49	1.49	1.49	1.49	1.49	1.49	1.49	1.49	1.49	1.49	1.49
2010	1.71	1.69	1.69	1.69	1.69	1.67	1.73	1.71	1.67	1.70	1.71
2020	2.04	1.95	2.01	2.00	1.95	1.89	2.09	2.03	1.91	1.97	1.99
2030	2.36	2.19	2.36	2.31	2.17	2.08	2.42	2.35	2.08	2.17	2.26
2040	2.69	2.48	2.83	2.68	2.41	2.30	2.76	2.71	2.27	2.38	2.55
2050	3.04	2.74	3.36	3.05	2.64	2.52	3.10	3.09	2.46	2.60	2.84
2060	3.37	2.96	3.91	3.44	2.81	2.74	3.39	3.46	2.67	2.81	3.14
2070	3.63	3.10	4.43	3.83	2.91	2.94	3.65	3.83	2.87	3.00	3.42
2080	3.89	3.19	4.94	4.27	2.98	3.16	3.89	4.26	3.03	3.21	3.74
2090	4.10	3.23	5.40	4.71	3.00	3.37	4.08	4.71	3.15	3.43	4.05
2100	4.27	3.20	5.81	5.20	2.99	3.59	4.23	5.19	3.24	3.65	4.39

Bern–CC model (high) – CO₂ radiative forcing (Wm⁻²)

Year	A1B	A1T	A1FI	A2	B1	B2	A1p	A2p	B1p	B2p	IS92a
2000	1.49	1.49	1.49	1.49	1.49	1.49	1.49	1.49	1.49	1.49	1.49
2010	1.88	1.85	1.85	1.85	1.84	1.84	1.91	1.88	1.84	1.87	1.88
2020	2.41	2.30	2.37	2.35	2.28	2.23	2.47	2.38	2.26	2.33	2.35
2030	2.96	2.78	2.97	2.89	2.73	2.62	3.04	2.94	2.64	2.75	2.82
2040	3.53	3.29	3.67	3.48	3.17	3.04	3.63	3.53	3.01	3.18	3.32
2050	4.11	3.77	4.44	4.09	3.59	3.46	4.20	4.13	3.39	3.59	3.82
2060	4.67	4.20	5.26	4.71	3.97	3.89	4.75	4.75	3.80	4.01	4.33
2070	5.18	4.57	6.04	5.33	4.27	4.29	5.23	5.36	4.19	4.39	4.82
2080	5.63	4.86	6.77	5.97	4.50	4.69	5.67	5.99	4.53	4.79	5.31
2090	6.04	5.07	7.45	6.61	4.67	5.08	6.06	6.62	4.80	5.17	5.80
2100	6.39	5.20	8.03	7.26	4.79	5.44	6.39	7.27	5.04	5.53	6.30

II.3.2: CH₄ radiative forcing (Wm⁻²)

Year	A1B	A1T	A1FI	A2	B1	B2	A1p	A2p	B1p	B2p	IS92a/
											SAR
2000	0.49	0.49	0.49	0.49	0.49	0.49	0.49	0.49	0.49	0.49	0.51
2010	0.53	0.52	0.52	0.53	0.51	0.52	0.54	0.53	0.51	0.53	0.56
2020	0.59	0.58	0.57	0.58	0.54	0.55	0.62	0.58	0.53	0.58	0.57
2030	0.65	0.64	0.64	0.63	0.55	0.60	0.71	0.63	0.55	0.64	0.62
2040	0.69	0.70	0.71	0.70	0.55	0.64	0.77	0.69	0.56	0.70	0.68
2050	0.71	0.74	0.79	0.76	0.53	0.70	0.80	0.76	0.58	0.73	0.74
2060	0.71	0.76	0.85	0.83	0.52	0.74	0.81	0.82	0.59	0.76	0.79
2070	0.68	0.74	0.90	0.89	0.50	0.78	0.79	0.89	0.60	0.77	0.83
2080	0.64	0.72	0.94	0.96	0.48	0.82	0.75	0.96	0.61	0.78	0.86
2090	0.60	0.68	0.97	1.02	0.45	0.85	0.70	1.02	0.61	0.77	0.90
2100	0.57	0.63	1.00	1.09	0.42	0.88	0.64	1.08	0.59	0.76	0.93

II.3.3: N₂O radiative forcing (Wm⁻²)

Year	A1B	A1T	A1FI	A2	B1	B2	A1p	A2p	B1p	B2p	IS92a/
											SAR
2000	0.15	0.15	0.15	0.15	0.15	0.15	0.15	0.15	0.15	0.15	0.16
2010	0.18	0.17	0.18	0.18	0.18	0.17	0.18	0.18	0.18	0.18	0.19
2020	0.20	0.19	0.21	0.21	0.21	0.19	0.20	0.21	0.21	0.20	0.22
2030	0.22	0.21	0.25	0.25	0.23	0.21	0.23	0.25	0.23	0.22	0.24
2040	0.24	0.22	0.29	0.29	0.25	0.22	0.25	0.29	0.26	0.24	0.27
2050	0.26	0.23	0.34	0.33	0.28	0.23	0.26	0.33	0.28	0.25	0.30
2060	0.28	0.24	0.39	0.37	0.30	0.25	0.27	0.36	0.31	0.26	0.32
2070	0.29	0.25	0.44	0.41	0.31	0.26	0.28	0.40	0.33	0.26	0.35
2080	0.30	0.26	0.48	0.45	0.32	0.27	0.29	0.45	0.35	0.27	0.37
2090	0.31	0.26	0.53	0.49	0.33	0.28	0.29	0.49	0.36	0.27	0.39
2100	0.32	0.27	0.57	0.53	0.33	0.29	0.29	0.53	0.37	0.28	0.41

II.3.4: PFCs, SF₆ and HFCs radiative forcing (Wm⁻²)

CF₄ radiative forcing (Wm⁻²)

Year	A1B	A1T	A1FI	A2	B1	B2	A1p	A2p	B1p	B2p
2000	0.003	0.003	0.003	0.003	0.003	0.003	0.003	0.003	0.003	0.003
2010	0.004	0.004	0.004	0.004	0.004	0.004	0.005	0.005	0.005	0.005
2020	0.005	0.005	0.005	0.005	0.005	0.005	0.007	0.006	0.006	0.007
2030	0.006	0.006	0.006	0.007	0.006	0.007	0.009	0.008	0.008	0.009
2040	0.008	0.008	0.008	0.009	0.007	0.009	0.013	0.011	0.010	0.012
2050	0.010	0.010	0.010	0.011	0.008	0.012	0.016	0.014	0.011	0.015
2060	0.013	0.013	0.013	0.013	0.009	0.014	0.020	0.017	0.013	0.019
2070	0.015	0.015	0.015	0.016	0.010	0.018	0.024	0.021	0.015	0.023
2080	0.018	0.018	0.018	0.020	0.011	0.021	0.027	0.026	0.016	0.027
2090	0.021	0.021	0.021	0.024	0.012	0.024	0.029	0.031	0.017	0.032
2100	0.024	0.024	0.024	0.029	0.013	0.028	0.032	0.037	0.018	0.036

C₂F₆ radiative forcing (Wm⁻²)

Year	A1B	A1T	A1FI	A2	B1	B2	A1p	A2p	B1p	B2p
2000	0.001	0.001	0.001	0.001	0.001	0.001	0.001	0.001	0.001	0.001
2010	0.001	0.001	0.001	0.001	0.001	0.001	0.001	0.001	0.001	0.001
2020	0.001	0.001	0.001	0.001	0.001	0.001	0.002	0.002	0.002	0.002
2030	0.002	0.002	0.002	0.002	0.001	0.002	0.002	0.002	0.002	0.002
2040	0.002	0.002	0.002	0.002	0.002	0.002	0.003	0.002	0.002	0.003
2050	0.002	0.002	0.002	0.002	0.002	0.003	0.004	0.003	0.003	0.003
2060	0.003	0.003	0.003	0.003	0.002	0.003	0.004	0.004	0.003	0.004
2070	0.003	0.003	0.003	0.004	0.002	0.004	0.005	0.005	0.003	0.005
2080	0.004	0.004	0.004	0.004	0.002	0.004	0.006	0.005	0.003	0.006
2090	0.004	0.004	0.004	0.005	0.003	0.005	0.006	0.007	0.004	0.007
2100	0.005	0.005	0.005	0.006	0.003	0.006	0.007	0.008	0.004	0.008

SF₆ radiative forcing (Wm⁻²)

Year	A1B	A1T	A1FI	A2	B1	B2	A1p	A2p	B1p	B2p
2000	0.003	0.003	0.003	0.003	0.003	0.003	0.003	0.003	0.003	0.003
2010	0.004	0.004	0.004	0.004	0.004	0.004	0.004	0.004	0.004	0.004
2020	0.005	0.005	0.005	0.006	0.005	0.005	0.005	0.006	0.005	0.006
2030	0.007	0.007	0.007	0.008	0.006	0.007	0.007	0.008	0.006	0.008
2040	0.009	0.009	0.009	0.010	0.008	0.009	0.010	0.010	0.008	0.011
2050	0.013	0.013	0.013	0.014	0.010	0.012	0.014	0.014	0.010	0.014
2060	0.017	0.017	0.017	0.017	0.012	0.014	0.017	0.017	0.012	0.018
2070	0.020	0.020	0.020	0.021	0.014	0.017	0.021	0.021	0.015	0.022
2080	0.023	0.023	0.023	0.025	0.016	0.019	0.024	0.025	0.017	0.027
2090	0.026	0.026	0.026	0.029	0.017	0.021	0.027	0.030	0.018	0.032
2100	0.029	0.029	0.029	0.034	0.018	0.023	0.030	0.034	0.019	0.036

HFC–23 radiative forcing (Wm^{-2})

HFC-32 radiative forcing (Wm⁻²)

Year	A1B	A1T	A1FI	A2	B1	B2	A1p	A2p	B1p	B2p
2000	0.000	0.000	0.000	0.000	0.000	0.000	0.000	0.000	0.000	0.000
2010	0.000	0.000	0.000	0.000	0.000	0.000	0.000	0.000	0.000	0.000
2020	0.000	0.000	0.000	0.000	0.000	0.000	0.000	0.000	0.000	0.000
2030	0.001	0.001	0.001	0.000	0.000	0.000	0.001	0.000	0.000	0.000
2040	0.001	0.001	0.001	0.001	0.000	0.001	0.001	0.000	0.000	0.001
2050	0.001	0.001	0.001	0.001	0.001	0.001	0.001	0.001	0.001	0.001
2060	0.002	0.002	0.001	0.001	0.001	0.001	0.002	0.001	0.001	0.001
2070	0.002	0.002	0.002	0.001	0.001	0.001	0.002	0.001	0.001	0.001
2080	0.002	0.002	0.002	0.001	0.001	0.001	0.002	0.001	0.001	0.001
2090	0.002	0.002	0.002	0.002	0.001	0.001	0.002	0.001	0.001	0.001
2100	0.002	0.002	0.002	0.002	0.001	0.002	0.002	0.002	0.001	0.001

HFC-125 radiative forcing (Wm⁻²)

Year	A1B	A1T	A1FI	A2	B1	B2	A1p	A2p	B1p	B2p	IS92a
2000	0.000	0.000	0.000	0.000	0.000	0.000	0.000	0.000	0.000	0.000	0.000
2010	0.000	0.000	0.000	0.000	0.000	0.000	0.001	0.001	0.001	0.001	0.000
2020	0.002	0.002	0.002	0.002	0.002	0.002	0.002	0.002	0.002	0.002	0.000
2030	0.005	0.005	0.005	0.004	0.004	0.004	0.005	0.003	0.004	0.004	0.003
2040	0.009	0.009	0.009	0.006	0.006	0.006	0.009	0.005	0.006	0.006	0.009
2050	0.013	0.013	0.013	0.008	0.008	0.008	0.013	0.007	0.008	0.009	0.020
2060	0.018	0.018	0.017	0.010	0.010	0.011	0.018	0.010	0.010	0.012	0.032
2070	0.022	0.023	0.022	0.013	0.011	0.014	0.022	0.012	0.011	0.015	0.041
2080	0.026	0.026	0.026	0.017	0.012	0.017	0.026	0.016	0.012	0.018	0.048
2090	0.029	0.030	0.029	0.020	0.013	0.020	0.028	0.019	0.013	0.020	0.054
2100	0.031	0.032	0.031	0.025	0.013	0.023	0.030	0.023	0.013	0.023	0.059

HFC-134a radiative forcing (Wm⁻²)

Year	A1B	A1T	A1FI	A2	B1	B2	A1p	A2p	B1p	B2p	IS92a
2000	0.002	0.002	0.002	0.002	0.002	0.002	0.002	0.002	0.002	0.002	0.002
2010	0.009	0.009	0.009	0.008	0.008	0.008	0.012	0.011	0.011	0.012	0.014
2020	0.020	0.020	0.019	0.017	0.016	0.017	0.026	0.021	0.021	0.023	0.027
2030	0.035	0.035	0.035	0.026	0.025	0.027	0.048	0.032	0.032	0.038	0.042
2040	0.056	0.056	0.055	0.035	0.033	0.038	0.078	0.043	0.044	0.053	0.060
2050	0.081	0.080	0.078	0.045	0.044	0.050	0.113	0.056	0.059	0.072	0.081
2060	0.105	0.105	0.101	0.057	0.053	0.064	0.143	0.072	0.071	0.092	0.099
2070	0.122	0.125	0.119	0.072	0.057	0.079	0.164	0.091	0.077	0.113	0.111
2080	0.131	0.137	0.129	0.089	0.059	0.095	0.175	0.113	0.079	0.132	0.121
2090	0.133	0.143	0.134	0.109	0.059	0.111	0.178	0.140	0.080	0.145	0.128
2100	0.131	0.143	0.135	0.132	0.057	0.125	0.174	0.170	0.078	0.156	0.132

HFC-143a radiative forcing (Wm⁻²)

Year	A1B	A1T	A1FI	A2	B1	B2	A1p	A2p	B1p	B2p
2000	0.000	0.000	0.000	0.000	0.000	0.000	0.000	0.000	0.000	0.000
2010	0.000	0.000	0.000	0.000	0.000	0.000	0.001	0.001	0.001	0.001
2020	0.001	0.001	0.001	0.001	0.001	0.001	0.002	0.001	0.001	0.001
2030	0.003	0.003	0.003	0.003	0.002	0.002	0.004	0.003	0.003	0.003
2040	0.006	0.006	0.006	0.004	0.004	0.004	0.006	0.004	0.004	0.005
2050	0.009	0.009	0.009	0.006	0.006	0.006	0.010	0.006	0.006	0.007
2060	0.013	0.013	0.013	0.008	0.007	0.008	0.014	0.008	0.008	0.009
2070	0.017	0.017	0.017	0.011	0.009	0.011	0.017	0.010	0.009	0.012
2080	0.021	0.021	0.020	0.013	0.010	0.013	0.020	0.013	0.010	0.014
2090	0.024	0.024	0.023	0.017	0.011	0.016	0.023	0.016	0.011	0.017
2100	0.026	0.027	0.026	0.020	0.012	0.018	0.026	0.020	0.012	0.019

HFC–152a radiative forcing (Wm⁻²)

Year	A1B	A1T	A1FI	A2	B1	B2	A1p	A2p	B1p	B2p	IS92a
2000	0.000	0.000	0.000	0.000	0.000	0.000	0.000	0.000	0.000	0.000	0.000
2010	0.000	0.000	0.000	0.000	0.000	0.000	0.000	0.000	0.000	0.000	0.000
2020	0.000	0.000	0.000	0.000	0.000	0.000	0.000	0.000	0.000	0.000	0.000
2030	0.000	0.000	0.000	0.000	0.000	0.000	0.000	0.000	0.000	0.000	0.001
2040	0.000	0.000	0.000	0.000	0.000	0.000	0.000	0.000	0.000	0.000	0.003
2050	0.000	0.000	0.000	0.000	0.000	0.000	0.000	0.000	0.000	0.000	0.005
2060	0.000	0.000	0.000	0.000	0.000	0.000	0.000	0.000	0.000	0.000	0.006
2070	0.000	0.000	0.000	0.000	0.000	0.000	0.000	0.000	0.000	0.000	0.007
2080	0.000	0.000	0.000	0.000	0.000	0.000	0.000	0.000	0.000	0.000	0.007
2090	0.000	0.000	0.000	0.000	0.000	0.000	0.000	0.000	0.000	0.000	0.007
2100	0.000	0.000	0.000	0.000	0.000	0.000	0.000	0.000	0.000	0.000	0.007

HFC–227ea radiative forcing (Wm⁻²)

Year	A1B	A1T	A1FI	A2	B1	B2	A1p	A2p	B1p	B2p
2000	0.000	0.000	0.000	0.000	0.000	0.000	0.000	0.000	0.000	0.000
2010	0.001	0.001	0.001	0.001	0.001	0.001	0.001	0.001	0.001	0.001
2020	0.002	0.002	0.002	0.002	0.002	0.002	0.002	0.002	0.002	0.002
2030	0.004	0.004	0.004	0.003	0.003	0.003	0.004	0.003	0.003	0.003
2040	0.007	0.007	0.007	0.004	0.004	0.005	0.007	0.004	0.004	0.005
2050	0.010	0.010	0.010	0.006	0.006	0.007	0.010	0.005	0.006	0.007
2060	0.014	0.014	0.013	0.008	0.008	0.009	0.013	0.007	0.008	0.009
2070	0.017	0.017	0.016	0.010	0.009	0.012	0.016	0.009	0.009	0.012
2080	0.019	0.020	0.019	0.012	0.010	0.015	0.018	0.011	0.010	0.014
2090	0.020	0.021	0.020	0.015	0.010	0.018	0.019	0.014	0.010	0.016
2100	0.021	0.022	0.021	0.018	0.011	0.020	0.020	0.016	0.010	0.018

HFC–245ca radiative forcing (Wm⁻²)

Year	A1B	A1T	A1FI	A2	B1	B2	A1p	A2p	B1p	B2p
2000	0.000	0.000	0.000	0.000	0.000	0.000	0.000	0.000	0.000	0.000
2010	0.002	0.002	0.002	0.002	0.002	0.002	0.003	0.002	0.002	0.002
2020	0.005	0.005	0.005	0.004	0.004	0.004	0.005	0.004	0.004	0.004
2030	0.008	0.008	0.008	0.005	0.005	0.006	0.008	0.005	0.005	0.006
2040	0.012	0.012	0.012	0.007	0.007	0.008	0.013	0.006	0.006	0.008
2050	0.017	0.017	0.016	0.008	0.009	0.010	0.017	0.008	0.009	0.011
2060	0.021	0.021	0.020	0.011	0.010	0.013	0.021	0.010	0.010	0.013
2070	0.023	0.024	0.023	0.013	0.010	0.015	0.023	0.013	0.010	0.016
2080	0.023	0.025	0.023	0.017	0.010	0.018	0.023	0.016	0.010	0.018
2090	0.022	0.025	0.023	0.020	0.010	0.021	0.022	0.019	0.010	0.019
2100	0.021	0.023	0.022	0.024	0.009	0.024	0.020	0.023	0.009	0.020

HFC–43–10mee radiative forcing (Wm⁻²)

Year	A1B	A1T	A1FI	A2	B1	B2	A1p	A2p	B1p	B2p
2000	0.000	0.000	0.000	0.000	0.000	0.000	0.000	0.000	0.000	0.000
2010	0.000	0.000	0.000	0.000	0.000	0.000	0.000	0.000	0.000	0.000
2020	0.001	0.001	0.001	0.001	0.000	0.000	0.001	0.001	0.001	0.001
2030	0.001	0.001	0.001	0.001	0.001	0.001	0.001	0.001	0.001	0.001
2040	0.002	0.002	0.002	0.001	0.001	0.001	0.002	0.001	0.001	0.001
2050	0.002	0.002	0.002	0.001	0.001	0.001	0.002	0.001	0.001	0.001
2060	0.003	0.003	0.002	0.002	0.001	0.002	0.002	0.001	0.001	0.002
2070	0.003	0.003	0.003	0.002	0.002	0.002	0.003	0.002	0.001	0.002
2080	0.004	0.004	0.004	0.002	0.002	0.002	0.003	0.002	0.002	0.002
2090	0.004	0.004	0.004	0.002	0.002	0.002	0.004	0.002	0.002	0.002
2100	0.004	0.005	0.004	0.003	0.002	0.003	0.004	0.002	0.002	0.002

II.3.5: Tropospheric O₃ radiative forcing (Wm⁻²)

Year	A1B	A1T	A1FI	A2	B1	B2	A1p	A2p	B1p	B2p	IS92a	SAR
2000	0.38	0.38	0.38	0.38	0.38	0.38	0.38	0.38	0.38	0.38	0.38	0.39
2010	0.45	0.45	0.45	0.45	0.41	0.43	0.47	0.45	0.39	0.44	0.44	0.41
2020	0.54	0.53	0.56	0.55	0.45	0.49	0.58	0.55	0.44	0.51	0.51	0.43
2030	0.60	0.64	0.69	0.66	0.46	0.56	0.65	0.66	0.45	0.57	0.58	0.45
2040	0.62	0.71	0.84	0.74	0.45	0.62	0.68	0.73	0.48	0.63	0.63	0.48
2050	0.62	0.75	1.03	0.81	0.42	0.66	0.70	0.80	0.52	0.66	0.70	0.51
2060	0.61	0.76	1.13	0.87	0.38	0.69	0.71	0.87	0.53	0.68	0.75	0.53
2070	0.59	0.71	1.21	0.93	0.34	0.72	0.69	0.93	0.54	0.70	0.80	0.55
2080	0.57	0.64	1.30	1.02	0.30	0.76	0.66	1.01	0.55	0.73	0.84	0.58
2090	0.55	0.56	1.29	1.13	0.26	0.79	0.63	1.13	0.50	0.74	0.89	0.59
2100	0.52	0.48	1.27	1.25	0.21	0.81	0.58	1.25	0.43	0.75	0.93	0.61

II.3.6: SO₄²⁻ aerosols (direct effect) radiative forcing (Wm⁻²)

Year	A1B	A1T	A1FI	A2	B1	B2	A1p	A2p	B1p	B2p	IS92a
2000	-0.40	-0.40	-0.40	-0.40	-0.40	-0.40	-0.40	-0.40	-0.40	-0.40	-0.40
2010	-0.51	-0.38	-0.47	-0.43	-0.43	-0.38	-0.51	-0.43	-0.35	-0.39	-0.49
2020	-0.58	-0.35	-0.50	-0.58	-0.43	-0.35	-0.58	-0.58	-0.32	-0.38	-0.58
2030	-0.53	-0.35	-0.55	-0.65	-0.45	-0.35	-0.53	-0.65	-0.31	-0.35	-0.67
2040	-0.40	-0.27	-0.55	-0.63	-0.45	-0.34	-0.45	-0.62	-0.31	-0.34	-0.75
2050	-0.37	-0.23	-0.47	-0.61	-0.40	-0.32	-0.37	-0.61	-0.30	-0.33	-0.83
2060	-0.27	-0.20	-0.32	-0.52	-0.32	-0.32	-0.30	-0.50	-0.30	-0.31	-0.82
2070	-0.21	-0.18	-0.25	-0.43	-0.25	-0.29	-0.26	-0.42	-0.28	-0.30	-0.82
2080	-0.18	-0.15	-0.23	-0.38	-0.21	-0.29	-0.18	-0.37	-0.25	-0.28	-0.81
2090	-0.17	-0.14	-0.23	-0.36	-0.17	-0.28	-0.17	-0.36	-0.20	-0.28	-0.80
2100	-0.16	-0.12	-0.23	-0.35	-0.15	-0.28	-0.16	-0.35	-0.17	-0.28	-0.79

II.3.7: BC aerosols radiative forcing (Wm⁻²)

Year	A1B	A1T	A1FI	A2	B1	B2	A1p	A2p	B1p	B2p	IS92a
2000	0.40	0.40	0.40	0.40	0.40	0.40	0.40	0.40	0.40	0.40	0.40
2010	0.45	0.45	0.46	0.45	0.37	0.42	0.49	0.45	0.32	0.45	0.42
2020	0.46	0.51	0.52	0.48	0.35	0.46	0.58	0.48	0.38	0.46	0.43
2030	0.49	0.58	0.62	0.55	0.29	0.49	0.63	0.54	0.34	0.45	0.46
2040	0.51	0.66	0.72	0.58	0.26	0.54	0.71	0.57	0.35	0.49	0.49
2050	0.52	0.74	0.89	0.62	0.25	0.57	0.77	0.62	0.37	0.52	0.52
2060	0.54	0.82	0.94	0.66	0.25	0.62	0.85	0.66	0.38	0.57	0.55
2070	0.55	0.86	1.02	0.71	0.23	0.66	0.91	0.71	0.40	0.63	0.57
2080	0.58	0.89	1.14	0.77	0.23	0.74	0.95	0.77	0.42	0.69	0.60
2090	0.65	0.89	1.09	0.86	0.22	0.78	0.95	0.86	0.38	0.75	0.63
2100	0.71	0.86	1.05	0.95	0.20	0.83	0.95	0.95	0.37	0.80	0.66

II.3.8: OC aerosols radiative forcing (Wm⁻²)

Year	A1B	A1T	A1FI	A2	B1	B2	A1p	A2p	B1p	B2p	IS92a
2000	-0.50	-0.50	-0.50	-0.50	-0.50	-0.50	-0.50	-0.50	-0.50	-0.50	-0.50
2010	-0.56	-0.56	-0.57	-0.55	-0.46	-0.53	-0.62	-0.55	-0.41	-0.55	-0.52
2020	-0.58	-0.63	-0.66	-0.60	-0.44	-0.57	-0.74	-0.60	-0.48	-0.59	-0.55
2030	-0.61	-0.73	-0.77	-0.68	-0.37	-0.61	-0.79	-0.68	-0.42	-0.57	-0.58
2040	-0.64	-0.83	-0.91	-0.73	-0.33	-0.66	-0.88	-0.72	-0.43	-0.61	-0.61
2050	-0.66	-0.93	-1.12	-0.77	-0.30	-0.71	-0.96	-0.77	-0.45	-0.65	-0.65
2060	-0.68	-1.02	-1.17	-0.82	-0.30	-0.76	-1.05	-0.82	-0.47	-0.71	-0.68
2070	-0.69	-1.08	-1.28	-0.88	-0.30	-0.84	-1.14	-0.88	-0.50	-0.78	-0.72
2080	-0.73	-1.12	-1.42	-0.97	-0.28	-0.92	-1.18	-0.96	-0.52	-0.87	-0.75
2090	-0.80	-1.12	-1.37	-1.08	-0.27	-0.99	-1.19	-1.07	-0.49	-0.94	-0.79
2100	-0.88	-1.08	-1.32	-1.20	-0.25	-1.04	-1.19	-1.20	-0.46	-1.00	-0.83

II.3.9: Radiative forcing (Wm⁻²) from CFCs and HCFCs following the Montreal (1997) Amendments

Year	CFC-11	CFC-12	CFC-113	CFC-114	CFC-115	CCL ₄	CH ₃ CCl ₃	HCFC-22	HCFC-141b	HCFC-142b	HCFC-123	CF ₂ BrCl	CF ₃ Br	SUM
2000	0.0668	0.1712	0.0255	0.0050	0.0016	0.0120	0.0026	0.0290	0.0018	0.0030	0.0000	0.0012	0.0010	0.3206
2010	0.0615	0.1686	0.0243	0.0050	0.0016	0.0098	0.0004	0.0514	0.0031	0.0066	0.0004	0.0012	0.0010	0.3348
2020	0.0535	0.1555	0.0216	0.0047	0.0016	0.0077	0.0001	0.0458	0.0022	0.0064	0.0006	0.0009	0.0010	0.3015
2030	0.0450	0.1411	0.0192	0.0047	0.0016	0.0061	0.0000	0.0274	0.0013	0.0046	0.0004	0.0006	0.0010	0.2529
2040	0.0373	0.1280	0.0171	0.0043	0.0016	0.0048	0.0000	0.0176	0.0008	0.0034	0.0004	0.0003	0.0010	0.2166
2050	0.0308	0.1158	0.0153	0.0043	0.0016	0.0038	0.0000	0.0092	0.0003	0.0022	0.0002	0.0003	0.0010	0.1848
2060	0.0253	0.1050	0.0135	0.0040	0.0016	0.0030	0.0000	0.0040	0.0001	0.0012	0.0002	0.0000	0.0006	0.1585
2070	0.0208	0.0954	0.0120	0.0040	0.0016	0.0023	0.0000	0.0018	0.0000	0.0008	0.0000	0.0000	0.0006	0.1393
2080	0.0170	0.0864	0.0108	0.0037	0.0014	0.0018	0.0000	0.0008	0.0000	0.0004	0.0000	0.0000	0.0006	0.1230
2090	0.0140	0.0784	0.0096	0.0037	0.0014	0.0014	0.0000	0.0004	0.0000	0.0002	0.0000	0.0000	0.0006	0.1098
2100	0.0113	0.0710	0.0084	0.0037	0.0014	0.0012	0.0000	0.0002	0.0000	0.0002	0.0000	0.0000	0.0003	0.0977

II.3.10: Radiative Forcing (Wm⁻²) from fossil fuel plus biomass Organic and Black Carbon as used in the Chapter 9 Simple Model SRES Projections

Year	A1B	A1T	A1FI	A2	B1	B2	IS92a
1990	-0.0997	-0.0997	-0.0997	-0.0997	-0.0997	-0.0997	-0.0998
2000	-0.1361	-0.1361	-0.1361	-0.1361	-0.1361	-0.1361	-0.1586
2010	-0.1308	-0.1468	-0.1280	-0.1392	-0.1081	-0.1203	-0.1357
2020	-0.0524	-0.0799	-0.1714	-0.1248	-0.0926	-0.0516	-0.1103
2030	-0.0562	-0.0598	-0.1745	-0.1088	-0.0154	-0.0148	-0.0872
2040	-0.0780	-0.0644	-0.1614	-0.1064	0.0349	-0.0075	-0.0610
2050	-0.0804	-0.0603	-0.1351	-0.1029	0.0280	-0.0049	-0.0339
2060	-0.0948	-0.0615	-0.1417	-0.1002	0.0241	0.0015	-0.0190
2070	-0.1071	-0.0613	-0.1193	-0.0939	0.0147	0.0064	-0.0026
2080	-0.1161	-0.0629	-0.0644	-0.0871	0.0300	0.0180	0.0166
2090	-0.1178	-0.0619	0.0365	-0.0816	0.0421	0.0341	0.0390
2100	-0.1208	-0.0629	0.0565	-0.0762	0.0351	0.0510	0.0635

II.3.11: Total Radiative Forcing (Wm⁻²) from GHG plus direct and indirect aerosol effects as used in the Chapter 9 Simple Model SRES Projections

Year	A1B	A1T	A1FI	A2	B1	B2	IS92a
1990	1.03	1.03	1.03	1.03	1.03	1.03	1.03
2000	1.33	1.33	1.33	1.33	1.33	1.33	1.31
2010	1.65	1.85	1.69	1.74	1.73	1.82	1.63
2020	2.16	2.48	2.17	2.04	2.15	2.36	2.00
2030	2.84	3.07	2.78	2.56	2.56	2.81	2.40
2040	3.61	3.76	3.67	3.22	2.93	3.26	2.82
2050	4.16	4.31	4.83	3.89	3.30	3.70	3.25
2060	4.79	4.73	5.99	4.71	3.65	4.11	3.76
2070	5.28	4.97	7.02	5.56	3.92	4.52	4.24
2080	5.62	5.11	7.89	6.40	4.09	4.92	4.74
2090	5.86	5.12	8.59	7.22	4.18	5.32	5.26
2100	6.05	5.07	9.14	8.07	4.19	5.71	5.79

II.4: Model Average Surface Air Temperature Change (°C)

Year	A1B	A1T	A1FI	A2	B1	B2	IS92a
1750 to 1990	0.33	0.33	0.33	0.33	0.33	0.33	0.34
1990	0.00	0.00	0.00	0.00	0.00	0.00	0.00
2000	0.16	0.16	0.16	0.16	0.16	0.16	0.15
2010	0.30	0.40	0.32	0.35	0.34	0.39	0.27
2020	0.52	0.71	0.55	0.50	0.55	0.66	0.43
2030	0.85	1.03	0.85	0.73	0.77	0.93	0.61
2040	1.26	1.41	1.27	1.06	0.98	1.18	0.80
2050	1.59	1.75	1.86	1.42	1.21	1.44	1.00
2060	1.97	2.04	2.50	1.85	1.44	1.69	1.26
2070	2.30	2.25	3.10	2.33	1.63	1.94	1.52
2080	2.56	2.41	3.64	2.81	1.79	2.20	1.79
2090	2.77	2.49	4.09	3.29	1.91	2.44	2.08
2100	2.95	2.54	4.49	3.79	1.98	2.69	2.38

Note: See Chapter 9 for details.

II.5: Sea Level Change (mm)

Note: Values are for the middle of the year..

II.5.1: Total sea level change (mm)

Models average – Total sea level change (mm)					
Year	A1B	A1T	A1FI	A2	B1
1990	0	0	0	0	0
2000	17	17	17	17	17
2010	37	39	37	38	38
2020	61	66	61	61	64
2030	91	97	90	88	89
2040	127	134	126	120	118
2050	167	175	172	157	150
2060	210	217	228	201	183
2070	256	258	290	250	216
2080	301	298	356	304	249
2090	345	334	424	362	281
2100	387	367	491	424	310
					358

Note: The sum of the components listed in Appendix II.5.2 to II.5.5 does not equal the values shown above owing to the addition of other terms. See Chapter 11, Section 11.5.1 for details.

Models minimum – Total sea level change (mm)

Year	A1B	A1T	A1FI	A2	B1	B2
1990	0	0	0	0	0	0
2000	6	6	6	6	6	6
2010	13	13	13	13	13	13
2020	22	22	24	21	22	23
2030	34	33	36	31	32	34
2040	48	47	49	44	42	45
2050	63	66	64	58	52	56
2060	78	89	77	75	63	68
2070	93	113	89	93	72	79
2080	107	137	99	113	80	91
2090	119	160	106	133	87	103
2100	129	182	111	155	92	114

Note: The final values of these timeseries correspond to the lower limit of the coloured bars on the right-hand side of Chapter 11, Figure 11.12.

Model maximum – Total sea level change (mm)

Year	A1B	A1T	A1FI	A2	B1	B2
1990	0	0	0	0	0	0
2000	29	29	29	29	29	29
2010	63	63	65	64	64	65
2020	103	104	110	104	105	109
2030	153	153	164	149	151	159
2040	214	214	228	204	203	216
2050	284	291	299	269	259	277
2060	360	386	375	343	319	344
2070	442	494	453	430	381	414
2080	527	612	529	526	444	488
2090	611	735	602	631	507	566
2100	694	859	671	743	567	646

Note: The final values of these timeseries correspond to the upper limit of the coloured bars on the right-hand side of Chapter 11, Figure 11.12.

II.5.2: Sea level change due to thermal expansion (mm)

Year	A1B	A1T	A1FI	A2	B1	B2
1990	0	0	0	0	0	0
2000	10	10	10	10	10	10
2010	23	24	23	23	23	24
2020	39	43	39	39	39	42
2030	60	66	60	57	58	62
2040	87	93	86	81	79	85
2050	117	123	122	109	101	110
2060	150	155	166	142	125	137
2070	185	186	217	180	149	165
2080	220	216	272	224	173	196
2090	255	243	329	272	195	227
2100	288	267	388	325	216	260

II.5.3: Sea level change due to glaciers and ice caps (mm)

Year	A1B	A1T	A1FI	A2	B1	B2
1990	0	0	0	0	0	0
2000	4	4	4	4	4	4
2010	9	10	9	10	10	10
2020	16	17	16	16	16	16
2030	23	25	23	23	23	24
2040	32	35	32	31	31	34
2050	43	46	44	41	41	44
2060	55	58	57	52	50	54
2070	67	71	72	65	61	66
2080	80	83	89	79	71	77
2090	93	95	105	93	82	89
2100	106	106	120	108	92	101

II.5.4: Sea level change due to Greenland (mm)

Year	A1B	A1T	A1FI	A2	B1	B2
1990	0	0	0	0	0	0
2000	0	0	0	0	0	0
2010	1	1	1	1	1	1
2020	2	2	2	2	2	2
2030	4	4	4	4	4	4
2040	5	6	5	5	5	6
2050	8	8	8	7	7	8
2060	10	11	11	10	9	10
2070	13	14	15	13	12	13
2080	17	17	19	16	14	16
2090	20	21	24	20	17	19
2100	24	24	29	25	20	22

II.5.5: Sea level change due to Antarctica (mm)

Year	A1B	A1T	A1FI	A2	B1	B2
1990	0	0	0	0	0	0
2000	-2	-2	-2	-2	-2	-2
2010	-5	-5	-5	-5	-5	-5
2020	-8	-9	-8	-8	-8	-9
2030	-12	-14	-13	-12	-13	-13
2040	-18	-20	-18	-17	-17	-19
2050	-25	-27	-25	-23	-23	-25
2060	-33	-35	-35	-31	-30	-32
2070	-42	-45	-46	-40	-37	-41
2080	-52	-54	-59	-50	-44	-49
2090	-63	-64	-74	-62	-53	-59
2100	-74	-75	-90	-76	-61	-70

References

- IPCC**, 1996: *Climate Change 1995: The Science of Climate Change. Contribution of Working Group I to the Second Assessment Report of the Intergovernmental Panel on Climate Change* [Houghton, J.T., L.G. Meira Filho, B.A. Callander, N. Harris, A. Kattenberg, and K. Maskell (eds.)]. Cambridge University Press, Cambridge, United Kingdom and New York, NY, USA, 572 pp.
- Jain**, A.K., H.S. Kheshgi, and D.J. Wuebbles, 1994: Integrated Science Model for Assessment of Climate Change. Lawrence Livermore National Laboratory, UCRL-JC-116526.
- Nakićenović**, N., J. Alcamo, G. Davis, B. de Vries, J. Fenner, S. Gaffin, K. Gregory, A. Grübler, T. Y. Jung, T. Kram, E. L. La Rovere, L. Michaelis, S. Mori, T. Morita, W. Pepper, H. Pitcher, L. Price, K. Raihi, A. Roehrl, H-H. Rogner, A. Sankovski, M. Schlesinger, P. Shukla, S. Smith, R. Swart, S. van Rooijen, N. Victor, Z. Dadi, 2000: *IPCC Special Report on Emissions Scenarios*, Cambridge University Press, Cambridge, United Kingdom and New York, NY, USA, 599 pp.
- WMO**, 1999: Scientific Assessment of Ozone Depletion: 1998. Global Ozone Research and Monitoring Project - Report No. 44, World Meteorological Organization, Geneva, Switzerland, 732 pp.

Appendix III

Contributors

to the IPCC WGI Third Assessment Report

Technical Summary

Co-ordinating Lead Authors

D.L. Albritton
L.G. Meira Filho
NOAA Aeronomy Laboratory, USA
Agência Espacial Brasileira, Brazil

Lead Authors

U. Cubasch
X. Dai
Y. Ding
D.J. Griggs
B. Hewitson
J.T. Houghton
I. Isaksen
T. Karl
M. McFarland
V.P. Meleshko
J.F.B. Mitchell
M. Noguer
B.S. Nyenzi
M. Oppenheimer
J.E. Penner
S. Pollonais
T. Stocker
K.E. Trenberth
Max-Planck Institute for Meteorology, Germany
IPCC WGI Technical Support Unit, UK/National Climate Center, China
IPCC WGI Co-Chairman, National Climate Center, China
IPCC WGI Technical Support Unit, UK
University of Capetown, South Africa
IPCC WGI Co-Chairman, UK
University of Oslo, Norway
NOAA National Climatic Data Centre, USA
Dupont Fluoroproducts, USA
Voeikov Main Geophysical Observatory, Russia
Hadley Centre for Climate Prediction and Research, Met Office, UK
IPCC WGI Technical Support Unit, UK
Zimbabwe Drought Monitoring Centre, Tanzania
Environmental Defense, USA
University of Michigan, USA
Environment Management Authority, Trinidad and Tobago
University of Bern, Switzerland
National Center for Atmospheric Research, USA

Contributing Authors

M.R. Allen
A.P.M. Baede
J.A. Church
D.H. Ehhalt
C.K. Folland
F. Giorgi
J.M. Gregory
J.M. Haywood
J.I. House
M. Hulme
V.J. Jaramillo
Rutherford Appleton Laboratory, UK
Koninklijk Nederlands Meteorologisch Instituut, Netherlands
CSIRO Division of Marine Research, Australia
Institut für Chemie der KFA Jülich GmbH, Germany
Hadley Centre for Climate Prediction and Research, Met Office, UK
Abdus Salam International Centre for Theoretical Physics, Italy
Hadley Centre for Climate Prediction and Research, Met Office, UK
Hadley Centre for Climate Prediction and Research, Met Office, UK
Max-Plank Institute for Biogeochemistry, Germany
University of East Anglia, UK
Instituto de Ecología, UNAM, Mexico

A. Jayaraman	Physical Research Laboratory, India
C.A. Johnson	IPCC WGI Technical Support Unit, UK
S. Joussaume	Institut Pierre Simon Laplace, Laboratoire des Sciences du Climat et de l'Environnement, France
D.J. Karoly	Monash University, Australia
H. Kheshgi	Exxon Mobil Research and Engineering Company, USA
C. Le Quéré	Max Plank Institute for Biogeochemistry, France
K. Maskell	IPCC WGI Technical Support Unit, UK
L.J. Mata	Universitaet Bonn, Germany
B.J. McAvaney	Bureau of Meteorology Research Centre, Australia
L.O. Mearns	National Center for Atmospheric Research, USA
G.A. Meehl	National Center for Atmospheric Research, USA
B. Moore III	University of New Hampshire, USA
R.K. Mugara	Zambia Meteorological Department, Zambia
M. Prather	University of California, USA
C. Prentice	Max-Planck Institute for Biogeochemistry, Germany
V. Ramaswamy	NOAA Geophysical Fluid Dynamics Laboratory, USA
S.C.B. Raper	University of East Anglia, UK
M.J. Salinger	National Institute of Water & Atmospheric Research, New Zealand
R. Scholes	Division of Water, Environment and Forest Technology, South Africa
S. Solomon	NOAA Aeronomy Laboratory, USA
R. Stouffer	NOAA Geophysical Fluid Dynamics Laboratory, USA
M.-X. Wang	Institute of Atmospheric Physics, Chinese Academy of Sciences, China
R.T. Watson	Chairman IPCC, The World Bank, USA
K.-S. Yap	Malaysian Meteorological Service, Malaysia

Review Editors

F. Joos	University of Bern, Switzerland
A. Ramirez-Rojas	Universidad Central Venezuela, Venezuela
J.M.R. Stone	Environment Canada, Canada
J. Zillman	Bureau of Meteorology, Australia

Chapter 1. The Climate System: an Overview**Co-ordinating Lead Author**

A.P.M. Baede	Koninklijk Nederlands Meteorologisch Instituut, Netherlands
--------------	---

Lead Authors

E. Ahlonsou	National Meteorological Service, Benin
Y. Ding	IPCC WG1 Co-Chairman, National Climate Center, China
D. Schimel	Max-Planck Institute for Biogeochemistry, Germany/NCAR, USA

Review Editors

B. Bolin	Retired, Sweden
S. Pollonais	Environment Management Authority, Trinidad and Tobago

Chapter 2. Observed Climate Variability and Change**Co-ordinating Lead Authors**

C.K. Folland	Hadley Centre for Climate Prediction and Research, Met Office, UK
T.R. Karl	NOAA National Climatic Data Center, USA

Lead Authors

J.R. Christy	University of Alabama, USA
R.A. Clarke	Bedford Institute of Oceanography, Canada
G.V. Gruza	Institute for Global Climate and Ecology, Russia

J. Jouzel	Institut Pierre Simon Laplace, Laboratoire des Sciences du Climat et de l'Environnement, France
M.E. Mann	University of Virginia, USA
J. Oerlemans	University of Utrecht, Netherlands
M.J. Salinger	National Institute of Water & Atmospheric Research, New Zealand
S.-W. Wang	Peking University, China

Contributing Authors

J. Bates	NOAA Environmental Research Laboratories, USA
M. Crowe	NOAA National Climatic Data Center, USA
P. Frich	Hadley Centre for Climate Prediction and Research, Met Office, UK
P. Groissman	NOAA National Climatic Data Center, USA
J. Hurrell	National Center for Atmospheric Research, USA
P. Jones	University of East Anglia, UK
D. Parker	Hadley Centre for Climate Prediction and Research, Met Office, UK
T. Peterson	NOAA National Climatic Data Center, USA
D. Robinson	Rutgers University, USA
J. Walsh	University of Illinois at Urbana-Champaign, USA
M. Abbott	Oregon State University, USA
L. Alexander	Hadley Centre for Climate Prediction and Research, Met Office, UK
H. Alexanderson	Swedish Meteorological and Hydrological Institute, Sweden
R. Allan	CSIRO Division of Atmospheric Research, Australia
R. Alley	Pennsylvania State University, USA
P. Ambenje	Department of Meteorology, Kenya
P. Arkin	Lamont-Doherty Earth Observatory of Columbia University, USA
L. Bajuk	Mathsoft Data Analysis Products Division, USA
R. Balling	Arizona State University, USA
M.Y. Bardin	Institute for Global Climate and Ecology, Russia
R. Bradley	University of Massachusetts, USA
R. Brázdil	Masaryk University, Czech Republic
K.R. Briffa	University of East Anglia, UK
H. Brooks	NOAA National Severe Storms Laboratory, USA
R.D. Brown	Atmospheric Environment Service, Canada
S. Brown	Hadley Centre for Climate Prediction and Research, Met Office, UK
M. Brunet-India	University Rovira I Virgili, Spain
M. Cane	Lamont-Doherty Earth Observatory of Columbia University, USA
D. Changnon	Northern Illinois University, USA
S. Changnon	University of Illinois at Urbana-Champaign, USA
J. Cole	University of Colorado, USA
D. Collins	Bureau of Meteorology, Australia
E. Cook	Lamont-Doherty Earth Observatory of Columbia University, USA
A. Dai	National Center for Atmospheric Research, USA
A. Douglas	Creighton University, USA
B. Douglas	University of Maryland, USA
J.C. Duplessy	Institut Pierre Simon Laplace, Laboratoire des Sciences du Climat et de l'Environnement, France
D. Easterling	NOAA National Climatic Data Center, USA
P. Englehart	USA
R.E. Eskridge	NOAA National Climatic Data Center, USA
D. Etheridge	CSIRO Division of Atmospheric Research, Australia
D. Fisher	Geological Survey of Canada, Canada
D. Gaffen	NOAA Air Resources Laboratory, USA
K. Gallo	National Environmental Satellite, Data and Information Service, USA
E. Genikhovich	Main Geophysical Observatory, Russia
D. Gong	Peking University, China
G. Gutman	National Environmental Satellite, Data and Information Service, USA
W. Haeberli	University of Zurich, Switzerland
J. Haigh	Imperial College, UK
J. Hansen	Goddard Institute for Space Studies, USA

D. Hardy	University of Massachusetts, USA
S. Harrison	Max-Planck Institute for Biogeochemistry, Germany
R. Heino	Finnish Meteorological Institute, Finland
K. Hennessy	CSIRO Division of Atmospheric Research, Australia
W. Hogg	Atmospheric Environment Service, Canada
S. Huang	University of Michigan, USA
K. Hughen	Woods Hole Oceanographic Institute, USA
M.K. Hughes	University of Arizona, USA
M. Hulme	University of East Anglia, UK
H. Iskenderian	Atmospheric and Environmental Research, Inc., USA
O.M. Johannessen	Nasen Environmental and Remote Sensing Center, Norway
D. Kaiser	Oak Ridge National Laboratory, USA
D. Karoly	Monash University, Australia
D. Kley	Institut fuer Chemie und Dynamik der Geosphaere, Germany
R. Knight	NOAA National Climatic Data Center, USA
K.R. Kumar	Indian Institute of Tropical Meteorology, India
K. Kunkel	Illinois State Water Survey, USA
M. Lal	Indian Institute of Technology, India
C. Landsea	NOAA Atlantic Oceanographic & Meteorological Laboratory, USA
J. Lawrimore	NOAA National Climatic Data Center, USA
J. Lean	Naval Research Laboratory, USA
C. Leovy	University of Washington, USA
H. Lins	US Geological Survey, USA
R. Livezey	NOAA National Weather Service, USA
K.M. Lugina	St Petersburg University, Russia
I. Macadam	Hadley Centre for Climate Prediction and Research, Met Office, UK
J.A. Majorowicz	Northern Geothermal, Canada
B. Manighetti	National Institute of Water & Atmospheric Research, New Zealand
J. Marengo	Instituto Nacional de Pesquisas Espaciais, Brazil
E. Mekis	Environment Canada, Canada
M.W. Miles	Nasen Environmental and Remote Sensing Center, Norway
A. Moberg	Stockholm University, Sweden
I. Mokhov	Institute of Atmospheric Physics, Russia
V. Morgan	University of Tasmania, Australia
L. Mysak	McGill University, Canada
M. New	Oxford University, UK
J. Norris	NOAA Geophysical Fluid Dynamics Laboratory, USA
L. Ogallo	University of Nairobi, Kenya
J. Overpeck	NOAA National Geophysical Data Center, USA
T. Owen	NOAA National Climatic Data Center, USA
D. Paillard	Institut Pierre Simon Laplace, Laboratoire des Sciences du Climat et de l'Environnement, France
T. Palmer	European Centre for Medium-range Weather Forecasting, UK
C. Parkinson	NASA Goddard Space Flight Center, USA
C.R. Pfister	Unitobler, Switzerland
N. Plummer	Bureau of Meteorology, Australia
H. Pollack	University of Michigan, USA
C. Prentice	Max-Planck Institute for Biogeochemistry, Germany
R. Quayle	NOAA National Climatic Data Center, USA
E.Ya. Rankova	Institute for Global Climate and Ecology, Russia
N. Rayner	Hadley Centre for Climate Prediction and Research, Met Office, UK
V.N. Razuvaev	Chief Climatology Department, Russia
G. Ren	National Climate Center, China
J. Renwick	National Institute of Water & Atmospheric Research, New Zealand
R. Reynolds	NOAA National Centers for Environmental Prediction, USA
D. Rind	Goddard Institute of Space Studies, USA
A. Robock	Rutgers University, USA
R. Rosen	Atmospheric and Environmental Research, Inc., USA

S. Rösner	Department Climate and Environment, Deutscher Wetterdienst, Germany
R. Ross	NOAA Air Resources Laboratory, USA
D. Rothrock	Applied Physics Laboratory, USA
J.M. Russell	Hampton University, USA
M. Serreze	University of Colorado, USA
W.R. Skinner	Environment Canada, Canada
J. Slack	US Geological Survey, USA
D.M. Smith	Hadley Centre for Climate Prediction and Research, Met Office, UK
D. Stahle	University of Arkansas, USA
M. Stendel	Danish Meteorological Institute, Denmark
A. Sterin	RIHMI-WDCB, Russia
T. Stocker	University of Bern, Switzerland
B. Sun	University of Massachusetts, USA
V. Swail	Environment Canada, Canada
V. Thapliyal	India Meteorological Department, India
L. Thompson	Ohio State University, USA
W.J. Thompson	University of Washington, USA
A. Timmermann	Koninklijk Nederlands Meteorologisch Instituut, Netherlands
R. Toumi	Imperial College, UK
K. Trenberth	National Center for Atmospheric Research, USA
H. Tuomenvirta	Finnish Meteorological Institute, Finland
T. van Ommen	University of Tasmania, Australia
D. Vaughan	British Antarctic Survey, UK
K.Y. Vinnikov	University of Maryland, USA
U. von Grafenstein	Institut Pierre Simon Laplace, Laboratoire des Sciences du Climat et de l'Environnement, France
H. von Storch	GKSS Research Center, Germany
M. Vuille	University of Massachusetts, USA
P. Wadhams	Scott Polar Research Institute, UK
J.M. Wallace	University of Washington, USA
S. Warren	University of Washington, USA
W. White	Scripps Institution of Oceanography, USA
P. Xie	NOAA National Centers for Environmental Prediction, USA
P. Zhai	National Climate Center, China

Review Editors

R. Hallgren	American Meteorological Society, USA
B. Nyenzi	Zimbabwe Drought Monitoring Centre, Tanzania

Chapter 3. The Carbon Cycle and Atmospheric Carbon Dioxide**Co-ordinating Lead Author**

I.C. Prentice	Max-Planck Institute for Biogeochemistry, Germany
---------------	---

Lead Authors

G.D. Farquhar	Australian National University, Australia
M.J.R. Fasham	Southampton Oceanography Centre, UK
M.L. Goulden	University of California, USA
M. Heimann	Max-Planck Institute for Biogeochemistry, Germany
V.J. Jaramillo	Instituto de Ecología, UNAM, Mexico
H.S. Kheshgi	Exxon Mobil Research and Engineering Company, USA
C. Le Quéré	Max-Planck Institute for Biogeochemistry, Germany
R.J. Scholes	Division of Water, Environment and Forest Technology, South Africa
D.W.R. Wallace	Universitat Kiel, Germany

Contributing Authors

D. Archer	University of Chicago, USA
-----------	----------------------------

M.R. Ashmore	University of Bradford, UK
O. Aumont	Institut Pierre Simon Laplace, Laboratoire des Sciences du Climat et de l'Environnement, France
D. Baker	Princeton University, USA
M. Battle	Bowdoin College, USA
M. Bender	Princeton University, USA
L.P. Bopp	Institut Pierre Simon Laplace, Laboratoire des Sciences du Climat et de l'Environnement, France
P. Bousquet	Institut Pierre Simon Laplace, Laboratoire des Sciences du Climat et de l'Environnement, France
K. Caldeira	Lawrence Livermore National Laboratory, USA
P. Ciais	CEA, LMCE/DSM, France
P.M. Cox	Hadley Centre for Climate Prediction and Research, Met Office, UK
W. Cramer	Potsdam Institute for Climate Impact Research, Germany
F. Dentener	Environment Institute, Italy
I.G. Enting	CSIRO Division of Atmospheric Research, Australia
C.B. Field	Carnegie Institute of Washington, USA
P. Friedlingstein	Institut Pierre Simon Laplace, Laboratoire des Sciences du Climat et de l'Environnement, France
E.A. Holland	Max-Planck Institute for Biochemistry, Germany
R.A. Houghton	Woods Hole Research Center, USA
J.I. House	Max-Planck Institute for Biogeochemistry, Germany
A. Ishida	Institute for Global Change Research, Japan
A.K. Jain	University of Illinois, USA
I.A. Janssens	Universiteit Antwerpen, Belgium
F. Joos	University of Bern, Switzerland
T. Kaminski	Max-Planck Institute for Meteorology, Germany
C.D. Keeling	University of California at San Diego, USA
R.F. Keeling	University of California at San Diego, USA
D.W. Kicklighter	Marine Biological Laboratory, USA
K.E. Kohfeld	Max-Planck Institute for Biogeochemistry, Germany
W. Knorr	Max-Planck Institute for Biogeochemistry, Germany
R. Law	Monash University, Australia
T. Lenton	Institute of Terrestrial Ecology, UK
K. Lindsay	National Center for Atmospheric Research, USA
E. Maier-Reimer	Max-Planck Institute for Meteorology, Germany
A.C. Manning	University of California at San Diego, USA
R.J. Matear	CSIRO Division of Marine Research, Australia
A.D. McGuire	University of Alaska at Fairbanks, USA
J.M. Melillo	Woods Hole Oceanographic Institution, USA
R. Meyer	University of Bern, Switzerland
M. Mund	Max-Planck Institute for Biogeochemistry, Germany
J.C. Orr	Institut Pierre Simon Laplace, Laboratoire des Sciences du Climat et de l'Environnement, France
S. Piper	Scripps Institution of Oceanography, USA
K. Plattner	University of Bern, Switzerland
P.J. Rayner	CSIRO Division of Atmospheric Research, Australia
S. Sitch	Institut für Klimafolgenforschung, Germany
R. Slater	Princeton University Atmospheric and Oceanic Sciences Program, USA
S. Taguchi	National Institute for Research & Environment, Japan
P.P. Tans	NOAA Climate Monitoring & Diagnostics Laboratory, USA
H.Q. Tian	Marine Biological Laboratory, USA
M.F. Weirig	Alfred Wegener Institute for Polar and Marine Research, Germany
T. Whorf	University of California at San Diego, USA
A. Yool	Southampton Oceanography Centre, UK

Review Editors

L. Pitelka
A. Ramirez Rojas

University of Maryland, USA
Universidad Central Venezuela, Venezuela

Chapter 4. Atmospheric Chemistry and Greenhouse Gases

Co-ordinating Lead Authors

D. Ehhalt
Institut für Chemie der KFA Jülich GmbH, Germany
M. Prather
University of California, USA

Lead Authors

F. Dentener	Institute for Marine and Atmospheric Research, Netherlands
R. Derwent	Met Office, UK
E. Dlugokencky	NOAA Climate Monitoring & Diagnostics Laboratory, USA
E. Holland	Max-Planck Institute for Biogeochemistry, Germany
I. Isaksen	University of Oslo, Norway
J. Katima	University of Dar-Es-Salaam, Tanzania
V. Kirchhoff	Instituto Nacional de Pesquisas Espaciais, Brazil
P. Matson	Stanford University, USA
P. Midgley	M&D Consulting, Germany
M. Wang	Institute of Atmospheric Physics, China

Contributing Authors

T. Berntsen	Centre for International Climate and Environmental Research, Norway
I. Bey	Harvard University, USA/France
G. Brasseur	Max-Planck Institute for Meteorology, Germany
L. Buja	National Center for Atmospheric Research, USA
W.J. Collins	Hadley Centre for Climate Prediction and Research, Met Office, UK
J. Daniel	NOAA Aeronomy Laboratory, USA
W.B. DeMore	Jet Propulsion Laboratory, USA
N. Derek	CSIRO Division of Atmospheric Research, Australia
R. Dickerson	University of Maryland, USA
D. Etheridge	CSIRO Division of Atmospheric Research, Australia
J. Feichter	Max-Planck Institute for Meteorology, Germany
P. Fraser	CSIRO Division of Atmospheric Research, Australia
R. Friedl	Jet Propulsion Laboratory, USA
J. Fuglestvedt	University of Oslo, Norway
M. Gauss	University of Oslo, Norway
L. Grenfell	NASA Goddard Institute for Space Studies, USA
A. Grubler	International Institute for Applied Systems Analysis, Austria
N. Harris	European Ozone Research Coordinating Unit, UK
D. Hauglustaine	Center National de la Recherche Scientifique, Service Aeronomie, France
L. Horowitz	National Center for Atmospheric Research, USA
C. Jackman	NASA Goddard Space Flight Center, USA
D. Jacob	Harvard University, USA
L. Jaeglé	Harvard University, USA
A. Jain	University of Illinois, USA
M. Kanakidou	Environmental Chemical Processes Laboratory, Greece
S. Karlsson	University of Oslo, Norway
M. Ko	Atmospheric & Environmental Research Inc., USA
M. Kurylo	NASA Headquarters, USA
M. Lawrence	Max-Planck Institute for Chemistry, Germany
J.A. Logan	Harvard University, USA
M. Manning	National Institute of Water & Atmospheric Research, New Zealand
D. Mauzerall	Princeton University, USA
J. McConnell	York University, Canada
L. Mickley	Harvard University, USA
S. Montzka	NOAA Climate Monitoring & Diagnostics Laboratory, USA
J.F. Muller	Belgian Institute for Space Aeronomy, Belgium
J. Olivier	National Institute of Public Health and the Environment, Netherlands
K. Pickering	University of Maryland, USA

G. Pitari	Università Degli Studi dell'Aquila, Italy
G.J. Roelofs	University of Utrecht, Netherlands
H. Rogers	University of Cambridge, UK
B. Rognerud	University of Oslo, Norway
S. Smith	Pacific Northwest National Laboratory, USA
S. Solomon	NOAA Aeronomy Laboratory, USA
J. Staehelin	Federal Institute of Technology, Switzerland
P. Steele	CSIRO Division of Atmospheric Research, Australia
D. S. Stevenson	Met Office, UK
J. Sundet	University of Oslo, Norway
A. Thompson	NASA Goddard Space Flight Center, USA
M. van Weele	Koninklijk Nederlands Meteorologisch Instituut, Netherlands
R. von Kuhlmann	Max-Planck Institute for Chemistry, Germany
Y. Wang	Georgia Institute of Technology, USA
D. Weisenstein	Atmospheric & Environmental Research Inc., USA
T. Wigley	National Center for Atmospheric Research, USA
O. Wild	Frontier Research System for Global Change, Japan
D. Wuebbles	University of Illinois, USA
R. Yantosca	Harvard University, USA

Review Editors

F. Joos	University of Bern, Switzerland
M. McFarland	Dupont Fluoroproducts, USA

Chapter 5. Aerosols, their Direct and Indirect Effects**Co-ordinating Lead Author**

J.E. Penner	University of Michigan, USA
-------------	-----------------------------

Lead Authors

M. Andreae	Max-Planck Institute for Chemistry, Germany
H. Annegarn	University of the Witwatersrand, South Africa
L. Barrie	Atmospheric Environment Service, Canada
J. Feichter	Max-Planck Institute for Meteorology, Germany
D. Hegg	University of Washington, USA
A. Jayaraman	Physical Research Laboratory, India
R. Leaitch	Atmospheric Environment Service, Canada
D. Murphy	NOAA Aeronomy Laboratory, USA
J. Nganga	University of Nairobi, Kenya
G. Pitari	Università Degli Studi dell'Aquila, Italy

Contributing Authors

A. Ackerman	NASA Ames Research Center, USA
P. Adams	Caltech, USA
P. Austin	University of British Columbia, Canada
R. Boers	CSIRO Division of Atmospheric Research, Australia
O. Boucher	Laboratoire d'Optique Atmosphérique, France
M. Chin	Goddard Space Flight Center, USA
C. Chuang	Lawrence Livermore National Laboratory, USA
W. Collins	Met Office, UK
W. Cooke	NOAA Geophysical Fluid Dynamics Laboratory, USA
P. DeMott	Colorado State University, USA
Y. Feng	University of Michigan, USA
H. Fischer	Scripps Institution of Oceanography, Germany
I. Fung	University of California, USA
S. Ghan	Pacific Northwest National Laboratory, USA

P. Ginoux	NASA Goddard Space Flight Center, USA
S.-L. Gong	Atmospheric Environment Service, Canada
A. Guenther	National Center for Atmospheric Research, USA
M. Herzog	University of Michigan, USA
A. Higurashi	National Institute for Environmental Studies, Japan
Y. Kaufman	NASA Goddard Space Flight Center, USA
A. Kettle	Max-Planck Institute for Chemistry, Germany
J. Kiehl	National Center for Atmospheric Research, USA
D. Koch	National Center for Atmospheric Research, USA
G. Lammel	Max-Planck Institute for Meteorology, Germany
C. Land	Max-Planck Institute for Meteorology, Germany
U. Lohmann	Dalhousie University, Canada
S. Madronich	National Center for Atmospheric Research, USA
E. Mancini	Università Degli Studi dell' Aquila, Italy
M. Mishchenko	NASA Goddard Institute for Space Studies, USA
T. Nakajima	University of Tokyo, Japan
P. Quinn	National Oceanographic and Atmospheric Administration, USA
P. Rasch	National Center for Atmospheric Research, USA
D.L. Roberts	Hadley Centre for Climate Prediction and Research, Met Office, UK
D. Savoie	University of Miami, USA
S. Schwartz	Brookhaven National Laboratory, USA
J. Seinfeld	California Institute of Technology, USA
B. Soden	Princeton University, USA
D. Tanré	Laboratoire d'Optique Atmosphérique, France
K. Taylor	Lawrence Livermore National Laboratory, USA
I. Tegen	Max-Planck Institute for Biogeochemistry, Germany
X. Tie	National Center for Atmospheric Research, USA
G. Vali	University of Wyoming, USA
R. Van Dingenen	Environment Institute of European Commission, Italy
M. van Weele	Koninklijk Nederlands Meteorologisch Instituut, The Netherlands
Y. Zhang	University of Michigan, USA

Review Editors

B. Nyenzi	Zimbabwe Drought Monitoring Centre, Tanzania
J. Prospero	University of Miami, USA

Chapter 6. Radiative Forcing of Climate Change**Co-ordinating Lead Author**

V. Ramaswamy NOAA Geophysical Fluid Dynamics Laboratory, USA

Lead Authors

O. Boucher	Max-Planck Institute for Chemistry, Germany/Laboratoire d'Optique Atmosphérique, France
J. Haigh	Imperial College, UK
D. Hauglustaine	Center National de la Recherche Scientifique, France
J. Haywood	Meteorological Research Flight, Met Office, UK
G. Myhre	University of Oslo, Norway
T. Nakajima	University of Tokyo, Japan
G.Y. Shi	Institute of Atmospheric Physics, China
S. Solomon	NOAA Aeronomy Laboratory, USA

Contributing Authors

R. Betts	Hadley Centre for Climate Prediction and Research, Met Office, UK
R. Charlson	Stockholm University, Sweden
C. Chuang	Lawrence Livermore National Laboratory, USA
J.S. Daniel	NOAA Aeronomy Laboratory, USA

A. Del Genio	NASA Goddard Institute for Space Studies, USA
J. Feichter	Max-Planck Institute for Meteorology, Germany
J. Fuglestvedt	University of Oslo, Norway
P.M. Forster	Monash University, Australia
S.J. Ghan	Pacific Northwest National Laboratory, USA
A. Jones	Hadley Centre for Climate Prediction and Research, Met Office, UK
J.T. Kiehl	National Center for Atmospheric Research, USA
D. Koch	Yale University, USA
C. Land	Max-Planck Institute for Meteorology, Germany
J. Lean	Naval Research Laboratory, USA
U. Lohmann	Dalhousie University, Canada
K. Minschwaner	New Mexico Institute of Mining and Technology, USA
J.E. Penner	University of Michigan, USA
D.L. Roberts	Hadley Centre for Climate Prediction and Research, Met Office, UK
H. Rodhe	University of Stockholm, Sweden
G.J. Roelofs	University of Utrecht, Netherlands
L.D. Rotstayn	CSIRO, Australia
T.L. Schneider	Institute for World Forestry and Ecology, Germany
U. Schumann	Institut für Physik der Atmosphäre, Germany
S.E. Schwartz	Brookhaven National Laboratory, USA
M.D. Schwartzkopf	NOAA Geophysical Fluid Dynamics Laboratory, USA
K.P. Shine	University of Reading, UK
S. Smith	Pacific Northwest National Laboratory, USA
D.S. Stevenson	Met Office, UK
F. Stordal	Norwegian Institute for Air Research, Norway
I. Tegen	Max-Planck Institute for Biogeochemistry, Germany
R. van Dorland	Knoinklij Nederlands Meteorologisch Instituut, The Netherlands
Y. Zhang	University of Michigan, USA

Review Editors

J. Srinivasan	Indian Institute of Science, India
F. Joos	University of Bern, Switzerland

Chapter 7. Physical Climate Processes and Feedbacks**Co-ordinating Lead Author**

T.F. Stocker	University of Bern, Switzerland
--------------	---------------------------------

Lead Authors

G.K.C. Clarke	University of British Columbia, Canada
H. Le Treut	Laboratoire de Météorologie Dynamique du Center National de la Recherche Scientifique, France
R.S. Lindzen	Massachusetts Institute of Technology, USA
V.P. Meleshko	Voeikov Main Geophysical Observatory, Russia
R.K. Mugara	Zambia Meteorological Department, Zambia
T.N. Palmer	European Centre for Medium-range Weather Forecasting, UK
R.T. Pierrehumbert	University of Chicago, USA
P.J. Sellers	NASA Johnson Space Centre, USA
K.E. Trenberth	National Center for Atmospheric Research, USA
J. Willebrand	Institut für Meereskunde an der Universität Kiel, Germany

Contributing Authors

R.B. Alley	Pennsylvania State University, USA
O.E. Anisimov	State Hydrological Institute, Russia
C. Appenzeller	University of Bern, Switzerland
R.G. Barry	University of Colorado, USA

J.J. Bates	NOAA Environmental Research Laboratories, USA
R. Bindschadler	NASA Goddard Space Flight Centre, USA
G.B. Bonan	National Center for Atmospheric Research, USA
C.W. Böning	Universtat Kiel, Germany
S. Bony	Laboratoire de Météorologie Dynamique du Center National de la Recherche Scientifique, France
H. Bryden	Southampton Oceanography Centre, UK
M.A. Cane	Lamont-Doherty Earth Observatory of Columbia University, USA
J.A. Curry	Aerospace Engineering, USA
T. Delworth	NOAA Geophysical Fluid Dynamics Laboratory, USA
A.S. Denning	Colorado State University, USA
R.E. Dickinson	University of Arizona, USA
K. Echelmeyer	University of Alaska, USA
K. Emanuel	Massachusetts Institute of Technology, USA
G. Flato	Canadian Centre for Climate Modelling & Analysis, Canada
I. Fung	University of California, USA
M. Geller	New York State University, USA
P.R. Gent	National Center for Atmospheric Research, USA
S.M. Griffies	NOAA Princeton University, USA
I. Held	NOAA Geophysical Fluid Dynamics Laboratory, USA
A. Henderson-Sellers	Australian Nuclear Science and Technology Organisation, Australia
A.A.M. Holtslag	Royal Netherlands Meteorological Institute, Netherlands
F. Hourdin	Center National de la Recherche Scientifique, Laboratoire de Météorologie Dynamique, France
J.W. Hurrell	National Center for Atmospheric Research, USA
V.M. Kattsov	Voeikov Main Geophysical Observatory, Russia
P.D. Killworth	Southampton Oceanography Centre, UK
Y. Kushnir	Lamont-Doherty Earth Observatory of Columbia University, USA
W.G. Large	National Center for Atmospheric Research, USA
M. Latif	Max-Planck Institute for Meteorology, Germany
P. Lemke	Alfred-Wegener Institute for Polar & Marine Research, Germany
M.E. Mann	University of Virginia, USA
G. Meehl	National Centre for Atmospheric Research, USA
U. Mikolajewicz	Max-Planck Institute for Meteorology, Germany
W. O'Hirok	Institute for Computational Earth System Science, USA
C.L. Parkinson	NASA Goddard Space Flight Center, USA
A. Payne	University of Southampton, UK
A. Pitman	Macquarie University, Australia
J. Polcher	Center National de la Recherche Scientifique, Laboratoire de Météorologie Dynamique, France
I. Polyakov	Princeton University, USA
V. Ramaswamy	NOAA Geophysical Fluid Dynamics Laboratory, USA
P.J. Rasch	National Center for Atmospheric Research, USA
E.P. Salathe	University of Washington, USA
C. Schär	Institut fur Klimaforschung ETH, Switzerland
R.W. Schmitt	Woods Hole Oceanographic Institution, USA
T.G. Shepherd	University of Toronto, Canada
B.J. Soden	Princeton University, USA
R.W. Spencer	Marshall Space Flight Center, USA
P. Taylor	Southampton Oceanography Centre, UK
A. Timmermann	Koninklijk Nederlands Meteorologisch Instituut, Netherlands
K.Y. Vinnikov	University of Maryland, USA
M. Visbeck	Lamont Doherty Earth Observatory of Columbia University, USA
S.E. Wijffels	CSIRO Division of Marine Research, Australia
M. Wild	Swiss Federal Institute of Technology, Switzerland

Review Editors

S. Manabe	Institute for Global Change, Japan
P. Mason	Met Office, UK

Chapter 8. Model Evaluation

Co-ordinating Lead Author

B.J. McAvaney

Bureau of Meteorology Research Centre, Australia

Lead Authors

C. Covey	Lawrence Livermore National Laboratory, USA
S. Joussaume	Institut Pierre Simon Laplace, Laboratoire des Sciences du Climat et de l'Environnement, France
V. Kattsov	Voeikov Main Geophysical Observatory, Russia
A. Kitoh	Meteorological Research Institute, Japan
W. Ogana	University of Nairobi, Kenya
A.J. Pitman	Macquarie University, Australia
A.J. Weaver	University of Victoria, Canada
R.A. Wood	Hadley Centre for Climate Prediction and Research, Met Office, UK
Z.-C. Zhao	National Climate Center, China

Contributing Authors

K. AchutaRao	Lawrence Livermore National Laboratory, USA
A. Arking	NASA Goddard Space Flight Centre, USA
A. Barnston	NOAA Climate Prediction Center, USA
R. Betts	Hadley Centre for Climate Prediction and Research, Met Office, UK
C. Bitz	Quaternary Research, USA
G. Boer	Canadian Center for Climate Modelling & Analysis, Canada
P. Braconnot	Institut Pierre Simon Laplace, Laboratoire des Sciences du Climat et de l'Environnement, France
A. Broccoli	NOAA Geophysical Fluid Dynamics Laboratory, USA
F. Bryan	Programe in Atmospheric and Oceanic Sciences, USA
M. Claussen	Potsdam Institute for Climate Impact Research, Germany
R. Colman	Bureau of Meteorology Research Centre, Australia
P. Delecluse	Institut Pierre Simon Laplace, Laboratoire d'Oceanographie Dynamique et Climatologie, France
A. Del Genio	NASA Goddard Institute for Space Studies, USA
K. Dixon	NOAA Geophysical Fluid Dynamics Laboratory, USA
P. Duffy	Lawrence Livermore National Laboratory, USA
L. Dümenil	Max-Planck Institute for Meteorology, Germany
M. England	University of New South Wales, Australia
T. Fichefet	Universite Catholique de Louvain, Belgium
G. Flato	Canadian Centre for Climate Modelling & Analysis, Canada
J.C. Fyfe	Canadian Centre for Climate Modelling & Analysis, Canada
N. Gedney	Hadley Centre for Climate Prediction and Research, Met Office, UK
P. Gent	National Center for Atmospheric Research, USA
C. Genthon	Laboratoire de Glaciologie et Geophysique de l'Environnement, France
J. Gregory	Hadley Centre for Climate Prediction and Research, Met Office, UK
E. Guilyardi	Institut Pierre Simon Laplace, Laboratoire d'Oceanographie Dynamique et Climatologie, France
S. Harrison	Max-Planck Institute for Biogeochemistry, Germany
N. Hasegawa	Japan Environment Agency, Japan
G. Holland	Bureau of Meteorology Research Centre, Australia
M. Holland	National Center for Atmospheric Research, USA
Y. Jia	Southampton Oceanography Centre, UK
P.D. Jones	University of East Anglia, UK
M. Kageyama	Institut Pierre Simon Laplace, Laboratoire Sciences du Climat et de l'Environnement, France
D. Keith	Harvard University, USA
K. Kodera	Meteorological Research Institute, Japan
J. Kutzbach	University of Wisconsin at Madison, USA
S. Lambert	University of Victoria, Canada
S. Legutke	Deutsches Klimarechenzentrum GmbH, Germany
G. Madec	Institut Pierre Simon Laplace, Laboratoire d'Oceanographie Dynamique et Climatologie, France
S. Maeda	Meteorological Research Institute, Japan

M.E. Mann	University of Virginia, USA
G. Meehl	National Centre for Atmospheric Research, USA
I. Mokhov	Institute of Atmospheric Physics, Russia
T. Motoi	Frontier Research System for Global Change, Japan
T. Phillips	Lawrence Livermore National Laboratory, USA
J. Polcher	Center National de la Recherche Scientifique, Laboratoire de Météorologie Dynamique, France
G.L. Potter	Lawrence Livermore National Laboratory, USA
V. Pope	Hadley Centre for Climate Prediction and Research, Met Office, UK
C. Prentice	Max-Planck Institute for Biogeochemistry, Germany
G. Roff	Bureau of Meteorology Research Centre, Australia
P. Sellers	NASA Johnson Space Centre, USA
F. Semazzi	Southampton Oceanography Centre, UK
D.J. Stensrud	NOAA National Severe Storms Laboratory, USA
T. Stockdale	European Centre for Medium-range Weather Forecasting, UK
R. Stouffer	NOAA Geophysical Fluid Dynamics Laboratory, USA
K.E. Taylor	Lawrence Livermore National Laboratory, USA
R. Tol	Vrije Universiteit, Netherlands
K. Trenberth	National Center for Atmospheric Research, USA
J. Walsh	University of Illinois at Urbana-Champaign, USA
M. Wild	Swiss Federal Institute of Technology, Switzerland
D. Williamson	National Center for Atmospheric Research, USA
S.-P. Xie	University of Hawaii at Manoa, USA
X.-H. Zhang	Chinese Academy of Sciences, China
F. Zwiers	Canadian Centre for Climate Modelling and Analysis, Canada

Review Editors

Y. Qian	Nanjing University, China
J. Stone	Environment Canada, Canada

Chapter 9. Projections of Future Climate Change**Co-ordinating Lead Authors**

U. Cubasch	Max-Planck Institute for Meteorology, Germany
G.A. Meehl	National Center for Atmospheric Research, USA

Lead Authors

G.J. Boer	University of Victoria, Canada
R.J. Stouffer	NOAA Geophysical Fluid Dynamics Laboratory, USA
M. Dix	CSIRO Division of Atmospheric Research, Australia
A. Noda	Meteorological Research Institute, Japan
C.A. Senior	Hadley Centre for Climate Prediction and Research, Met Office, UK
S. Raper	University of East Anglia, UK
K.S. Yap	Malaysian Meteorological Service, Malaysia

Contributing Authors

A. Abe-Ouchi	University of Tokyo, Japan
S. Brinkop	Institute für Physik der Atmosphäre, Germany
M. Claussen	Potsdam Institute for Climate Impact Research, Germany
M. Collins	Hadley Centre for Climate Prediction and Research, Met Office, UK
J. Evans	Pennsylvania State University, USA
I. Fischer-Bruns	Max-Planck Institute for Meteorology, Germany
G. Flato	Canadian Centre for Climate Modelling & Analysis, Canada
J.C. Fyfe	Canadian Centre for Climate Modelling & Analysis, Canada
A. Ganopolski	Potsdam Institute for Climate Impact Research, Germany
J.M. Gregory	Hadley Centre for Climate Prediction and Research, Met Office, UK
Z.-Z. Hu	Center for Ocean-Land-Atmosphere Studies, USA

F. Joos	University of Bern, Switzerland
T. Knutson	NOAA Geophysical Fluid Dynamics Laboratory, USA
C. Landsea	NOAA Atlantic Oceanographic & Meteorological Laboratory, USA
L. Mearns	National Center for Atmospheric Research, USA
C. Milly	US Geological Survey, USA
J.F.B. Mitchell	Hadley Centre for Climate Prediction and Research, Met Office, UK
T. Nozawa	National Institute for Environmental Studies, Japan
H. Paeth	Universität Bonn, Germany
J. Räisänen	Swedish Meteorological and Hydrological Institute, Sweden
R. Sausen	Institute für Physik der Atmosphäre, Germany
S. Smith	Pacific Northwest National Laboratory, USA
T. Stocker	University of Bern, Switzerland
A. Timmermann	Royal Netherlands Meteorological Institute, Netherlands
U. Ulbrich	Institut fuer Geophysik und Meteorologie, Germany
A. Weaver	University of Victoria, Canada
J. Wegner	Deutsches Klimarechenzentrum, Germany
P. Whetton	CSIRO Division of Atmospheric Research, Australia
T. Wigley	National Center for Atmospheric Research, USA
M. Winton	NOAA Geophysical Fluid Dynamics Laboratory, USA
F. Zwiers	Canadian Centre for Climate Modelling and Analysis, Canada

Review Editors

J. Stone	Environment Canada, Canada
J.-W. Kim	Yonsei University, South Korea

Chapter 10. Regional Climate Information - Evaluation and Projections**Co-ordinating Lead Authors**

F. Giorgi	Abdus Salam International Centre for Theoretical Physics, Italy
B. Hewitson	University of Capetown, South Africa

Lead Authors

J. Christensen	Danish Meteorological Institute, Denmark
M. Hulme	University of East Anglia, UK
H. Von Storch	GKSS, Germany
P. Whetton	CSIRO Division of Atmospheric Research, Australia
R. Jones	Hadley Centre for Climate Prediction and Research, Met Office, UK
L. Mearns	National Center for Atmospheric Research, USA
C. Fu	Institute of Atmospheric Physics, China

Contributing Authors

R. Arritt	Iowa State University, USA
B. Bates	CSIRO Land and Water, Australia
R. Benestad	Det Norske Meteorologiske Institutt, Norway
G. Boer	Canadian Centre for Climate Modelling & Analysis, Canada
A. Buishand	Koninklijk Nederlands Meteorologisch Instituut, Netherlands
M. Castro	Universidad Complutense de Madrid, Spain
D. Chen	Göteborg University, Sweden
W. Cramer	Potsdam Institute for Climate Impact Research, Germany
R. Crane	The Pennsylvania State University, USA
J.F. Crossley	University of East Anglia, UK
M. Dehn	University of Bonn, Germany
K. Dethloff	Alfred Wegener Institute for Polar and Marine Research, Germany
J. Dippner	Institute for Baltic Research, Germany
S. Emori	National Institute for Environmental Studies, Japan
R. Francisco	Weather Bureau, Philippines

J. Fyfe	Canadian Centre for climate modelling and analysis, Canada
F.W. Gerstengarbe	Potsdam Institute for Climate Impact Research, Germany
W. Gutowski	Iowa State University, USA
D. Gyalistras	University of Berne, Switzerland
I. Hanssen-Bauer	The Norwegian Meteorological Institute, Norway
M. Hantel	University of Vienna, Austria
D.C. Hassell	Hadley Centre for Climate Prediction and Research, Met Office, UK
D. Heimann	Institute of Atmospheric Physics, Germany
C. Jack	University of Cape Town, South Africa
J. Jacobbeit	Universitaet Wuerzburg, Germany
H. Kato	Central Research Institute of Electric Power Industry, Japan
R. Katz	National Center for Atmospheric Research, USA
F. Kauker	Alfred Wegener Institute for Polar and Marine Research, Germany
T. Knutson	NOAA Geophysical Fluid Dynamics Laboratory, USA
M. Lal	Indian Institute of Technology, India
C. Landsea	NOAA Atlantic Oceanographic & Meteorological Laboratory, USA
R. Laprise	University of Quebec at Montreal, Canada
L.R. Leung	Pacific Northwest National Laboratory, USA
A.H. Lynch	University of Colorado, USA
W. May	Danish Meteorological Institute, Denmark
J.L. McGregor	CSIRO Division of Atmospheric Research, Australia
N.L. Miller	Lawrence Berkeley National Laboratory, USA
J. Murphy	Hadley Centre for Climate Prediction and Research, Met Office, UK
J. Ribalaygua	Fundación para la Investigación del Clima, Spain
A. Rinke	Alfred Wegener Institute for Polar and Marine Research, Germany
M. Rummukainen	Swedish Meteorological and Hydrological Institute, Sweden
F. Semazzi	Southampton Oceanography Centre, UK
K. Walsh	CSIRO Division of Atmospheric Research, Australia
P. Werner	Potsdam Institute for Climate Impact Research, Germany
M. Widmann	GKSS Research Centre, Germany
R. Wilby	University of Derby, UK
M. Wild	Swiss Federal Institute of Technology, Switzerland
Y. Xue	University of California at Los Angeles, USA

Review Editors

M. Mietus	Institute of Meteorology & Water Management, Poland
J. Zillman	Bureau of Meteorology, Australia

Chapter 11. Changes in Sea Level**Co-ordinating Lead Authors**

J.A. Church	CSIRO Division of Marine Research, Australia
J.M. Gregory	Hadley Centre for Climate Prediction and Research, Met Office, UK

Lead Authors

P. Huybrechts	Vrije Universiteit Brussel, Belgium
M. Kuhn	Innsbruck University, Austria
K. Lambeck	Australian National University, Australia
M.T. Nhuan	Hanoi University of Sciences, Vietnam
D. Qin	Chinese Academy of Sciences, China
P.L. Woodworth	Bidston Observatory, UK

Contributing Authors

O.A. Anisimov	State Hydrological Institute, Russia
F.O. Bryan	Programe in Atmospheric and Oceanic Sciences, USA
A. Cazenave	Groupe de Recherche de Geodesie Spatiale CNES, France

K.W. Dixon	NOAA Geophysical Fluid Dynamics Laboratory, USA
B.B. Fitzharris	University of Otago, New Zealand
G.M. Flato	Canadian Centre for Climate Modelling & Analysis, Canada
A. Ganopolski	Potsdam Institute for Climate Impact Research, Germany
V. Gornitz	Goddard Institute for Space Studies, USA
J.A. Lowe	Hadley Centre for Climate Prediction and Research, Met Office, UK
A. Noda	Japan Meteorological Agency, Japan
J.M. Oberhuber	German Climate Computing Centre, Germany
S.P. O'Farrell	CSIRO Division of Atmospheric Research, Australia
A. Ohmura	Geographisches Institute ETH, Switzerland
M. Oppenheimer	Environmental Defense, USA
W.R. Peltier	University of Toronto, Canada
S.C.B. Raper	University of East Anglia, UK
C. Ritz	Laboratoire de Glaciologie et Geophysique de l'Environnement, France
G.L. Russell	NASA Goddard Institute for Space Studies, USA
E. Schlosser	Innsbruck University, Austria
C.K. Shum	Ohio State University, USA
T.F. Stocker	University of Bern, Switzerland
R.J. Stouffer	NOAA Geophysical Fluid Dynamics Laboratory, USA
R.S.W. van de Wal	Institute for Marine and Atmospheric Research, Netherlands
R. Voss	Deutsches Klimarechenzentrum, Germany
E.C. Wiebe	University of Victoria, Canada
M. Wild	Swiss Federal Institute of Technology, Switzerland
D.J. Wingham	University College London, UK
H.J. Zwally	NASA Goddard Space Flight Center, USA

Review Editors

B.C. Douglas	University of Maryland, USA
A. Ramirez	Universidad Central Venezuela, Venezuela

Chapter 12. Detection of Climate Change and Attribution of Causes**Co-ordinating Lead Authors**

J.F.B. Mitchell	Hadley Centre for Climate Prediction and Research, Met Office, UK
D.J. Karoly	Monash University, Australia

Lead Authors

G.C. Hegerl	Texas A&M University, USA/Germany
F.W. Zwiers	University of Victoria, Canada
M.R. Allen	Rutherford Appleton Laboratory, UK
J. Marengo	Instituto Nacional de Pesquisas Espaciais, Brazil

Contributing Authors

V. Barros	Ciudad Universitaria, Argentina
M. Berliner	Ohio State University, USA
G. Boer	Canadian Centre for Climate Modelling & Analysis, Canada
T. Crowley	Texas A&M University, USA
C. Folland	Hadley Centre for Climate Prediction and Research, Met Office, UK
M. Free	NOAA Air Resources Laboratory, USA
N. Gillett	University of Oxford, UK
P. Groissman	NOAA National Climatic Data Center, USA
J. Haigh	Imperial College, UK
K. Hasselmann	Max-Planck Institute for Meteorology, Germany
P. Jones	University of East Anglia, UK
M. Kandlikar	Carnegie-Mellon University, USA
V. Kharin	Canadian Centre for Climate Modelling and Analysis, Canada

H. Khesghi	Exxon Mobil Research & Engineering Company, USA
T. Knutson	NOAA Geophysical Fluid Dynamics Laboratory, USA
M. MacCracken	Office of the US Global Change Research Program, USA
M. Mann	University of Virginia, USA
G. North	Texas A&M University, USA
J. Risbey	Carnegie-Mellon University, USA
A. Robock	Rutgers University, USA
B. Santer	Lawrence Livermore National Laboratory, USA
R. Schnur	Max-Planck Institute for Meteorology, Germany
C. Schönwiese	J.W. Goethe University, Germany
D. Sexton	Hadley Centre for Climate Prediction and Research, Met Office, UK
P. Stott	Hadley Centre for Climate Prediction and Research, Met Office, UK
S. Tett	Hadley Centre for Climate Prediction and Research, Met Office, UK
K. Vinnikov	University of Maryland, USA
T. Wigley	National Center for Atmospheric Research, USA

Review Editors

F. Semazzi	Southampton Oceanography Centre, UK
J. Zillman	Bureau of Meteorology, Australia

Chapter 13. Climate Scenario Development**Co-ordinating Lead Authors**

L.O. Mearns	National Center for Atmospheric Research, USA
M. Hulme	University of East Anglia, UK

Lead Authors

T.R. Carter	Finnish Environment Institute, Finland
R. Leemans	Rijksinstituut voor Volksgezondheid en Milieu, Netherlands
M. Lal	Indian Institute of Technology, India
P. Whetton	CSIRO Division of Atmospheric Research, Australia

Contributing Authors

L. Hay	US Geological Survey, USA
R.N. Jones	CSIRO Division of Atmospheric Research, Australia
R. Katz	National Center for Atmospheric Research, USA
T. Kittel	National Center for Atmospheric Research, USA
J. Smith	Stratus Consulting Inc., USA
R. Wilby	University of Derby, UK

Review Editors

L.J. Mata	Universidad Central Venezuela, Venezuela
J. Zillman	Bureau of Meteorology, Australia

Chapter 14. Advancing our Understanding**Co-ordinating Lead Author**

B. Moore III	University of New Hampshire, USA
--------------	----------------------------------

Lead Authors

W.L. Gates	Lawrence Livermore National Laboratory, USA
L.J. Mata	Universidad Central Venezuela, Venezuela
A. Underdal	University of Oslo, Norway

Contributing Author

R.J. Stouffer

NOAA Geophysical Fluid Dynamics Laboratory, USA

Review Editors

B. Bolin

Retired, Sweden

A. Ramirez Rojas

Universidad Central Venezuela, Venezuela

Appendix IV

Reviewers

of the IPCC WGI Third Assessment Report

Argentina

M. Nuñez Ciudad Universitaria

Australia

K. Abel	Australian Greenhouse Office
G. Ayers	CSIRO Division of Atmospheric Research
S. Barrell	Bureau of Meteorology
P. Bate	Bureau of Meteorology
B. Bates	CSIRO Division of Land and Water
T. Beer	CSIRO Division of Atmospheric Research
R. Boers	CSIRO Division of Atmospheric Research
W. Budd	University of Tasmania
I. Carruthers	Australian Greenhouse Office
S. Charles	CSIRO Division of Atmospheric Research
J. Church	CSIRO Division of Marine Research
D. Collins	Bureau of Meteorology
R. Colman	Bureau of Meteorology Research Centre
D. Cosgrove	Bureau of Transport Economics
S. Crimp	Department of Natural Resources
B. Curran	Bureau of Meteorology
M. Davison	Australian Industry Greenhouse Network
M. Dix	CSIRO Division of Atmospheric Research
B. Dixon	Bureau of Meteorology
M. England	University of New South Wales
I. Enting	CSIRO Division of Atmospheric Research
D. Etheridge	CSIRO Division of Atmospheric Research
G. Farquhar	Australian National University
P. Forster	Monash University
R. Francey	CSIRO Division of Atmospheric Research
P. Fraser	CSIRO Division of Atmospheric Research
R. Gifford	CSIRO Division of Plant Industry
I. Goodwin	University of Tasmania
J. Gras	CSIRO Division of Atmospheric Research
G. Hassall	Australian Greenhouse Office
A. Henderson-Sellers	Australian Nuclear Science and Technology Organisation

K. Hennessy	CSIRO Division of Atmospheric Research
A. Ivanovici	Australian Greenhouse Office
J. Jacka	Australian Antarctic Division
I. Jones	University of Sydney
R. Jones	CSIRO Division of Atmospheric Research
D. Karoly	Monash University
J. Katzfey	CSIRO Division of Atmospheric Research
B. Kininmonth	Australasian Climate Research
J. Lough	Australian Institute of Marine Science
G. Love	Bureau of Meteorology
M. Manton	Bureau of Meteorology Research Centre
B. McAvaney	Bureau of Meteorology Research Centre
T. McDougall	CSIRO Division of Marine Research
A. McEwan	Bureau of Meteorology
J. McGregor	CSIRO Division of Atmospheric Research
L. Minty	Bureau of Meteorology
B. Mitchell	Flinders University of South Australia
N. Plummer	Bureau of Meteorology
L. Powell	Australian Greenhouse Office
L. Quick	Australian Greenhouse Office
P. Rayner	CSIRO Division of Atmospheric Research
L. Rikus	Bureau of Meteorology Research Centre
L. Rotstayn	CSIRO Division of Atmospheric Research
W. Scherer	Flinders University of South Australia
I. Smith	CSIRO Division of Atmospheric Research
P. Steele	CSIRO Division of Atmospheric Research
K. Walsh	CSIRO Division of Atmospheric Research
I. Watterson	CSIRO Division of Atmospheric Research
P. Whetton	CSIRO Division of Atmospheric Research
J. Zillman	Bureau of Meteorology

Austria

M. Hantel	University of Vienna
K. Radunsky	Federal Environment Agency

Belgium

T. Fichefet	Université Catholique de Louvain
J. Franklin	Solvay Research and Technology
A. Mouchet	Astrophysics and Geophysics Institute
J. van Ypersele	Université Catholique de Louvain
R. Zander	University of Liege

Benin

E. Ahlonsou	National Meteorological Service
-------------	---------------------------------

Brazil

P. Fearnside	National Institute for Research in the Amazon
J. Marengo	Instituto Nacional de Pesquisas Espaciais

Canada

P. Austin	University of British Columbia
E. Barrow	Atmospheric and Hydrologic Science Division
J. Bourgeois	Geological Survey of Canada
R. Brown	Atmospheric Environment Service
E. Bush	Environment Canada
M. Demuth	Geological Survey of Canada
K Denman	Department of Fisheries and Oceans
P. Edwards	Environment Canada
W. Evans	Trent University
D. Fisher	Geological Survey of Canada
G. Flato	University of Victoria
W. Gough	University of Toronto at Scarborough
D. Harvey	University of Toronto
H. Hengeveld	Environment Canada
W. Hogg	Atmospheric Environment Service
P. Kertland	Natural Resources Canada
R. Koerner	Geological Survey of Canada
R. Laprise	University of Quebec at Montreal
Z. Li	Natural Resources Canada
U. Lohmann	Dalhousie University
J. Majorowicz	Northern Geothermal
L. Malone	Environment Canada
N. McFarlane	University of Victoria
L. Mysak	McGill University
W. Peltier	University of Toronto
I. Perry	Fisheries and Oceans Canada
J. Rudolph	York University
P. Samson	Natural Resources Canada
J. Sargent	Finance Canada
J. Shaw	Geological Survey of Canada
S. Smith	Natural Resources Canada
J. Stone	Environment Canada
R. Street	Environment Canada
D. Whelpdale	Environment Canada
R. Wong	Government of Alberta
F. Zwiers	University of Victoria

China

D. Gong	Peking University
W. Li	Institute of Atmospheric Physics
G. Ren	National Climate Center
S. Sun	Institute of Atmospheric Physics
R. Yu	Institute of Atmospheric Physics
P. Zhai	National Climate Center
X. Zhang	Institute of Atmospheric Physics
G. Zhou	Institute of Atmospheric Physics
T. Zhou	Institute of Atmospheric Physics

Czech Republic

R. Brazdil	Masaryk University
------------	--------------------

Denmark

J. Bates	University of Copenhagen
B. Christiansen	Danish Meteorological Institute
P. Frich	Danmarks Miljøundersøgelser (DMU)
A. Hansen	University of Copenhagen
A. Jørgensen	Danish Meteorological Institute
T. Jørgensen	Danish Meteorological Institute
E. Kaas	Danish Meteorological Institute
P. Laut	Technical University of Denmark
B. Machenhauer	Danish Meteorological Institute
L. Prahm	Danish Meteorological Institute
M. Stendel	Danish Meteorological Institute
P. Thejll	Danish Meteorological Institute

Finland

T. Carter	Finnish Environment Institute
E. Holopainen	University of Helsinki
R. Korhonen	Technical Research Centre of Finland (VTT)
M. Kulmala	University of Helsinki
J. Launiainen	Finnish Institute of Marine Research
H. Tuomenvirta	Finnish Meteorological Institute

France

A. Alexiou	Intergovernmental Oceanographic Commission
P. Braconnot	Institut Pierre Simon Laplace, Laboratoire des Sciences du Climat et de l'Environnement
J. Brenguier	Meteo France
N. Chaumerliac	Université Blaise Pascal
M. Deque	Meteo France
Y. Fouquart	Université des Sciences & Technologie de Lille
C. Genton	Laboratoire de Glaciologie et Géophysique de l'Environnement du CNRS
M. Gillet	Mission Interministérielle de l'Effet de Serre
S. Joussaume	Institut Pierre Simon Laplace, Laboratoire des Sciences du Climat et de l'Environnement
J. Jouzel	Institut Pierre Simon Laplace, Laboratoire des Sciences du Climat et de l'Environnement
R. Juvanon du Vachat	Mission Interministérielle de l'Effet de Serre
H. Le Treut	Centre National de la Recherche Scientifique, Laboratoire de Météorologie Dynamique
M. Petit	Ecole Polytechnique
P. Pirazzoli	Centre National de la Recherche Scientifique, Laboratoire de Géographie Physique
S. Planton	Meteo France
J. Polcher	Centre National de la Recherche Scientifique, Laboratoire de Météorologie Dynamique
A. Riedacker	INRA
J. Salmon	Ministère de l'Aménagement du Territoire et de l'Environnement
D. Tanré	Laboratoire d'Optique Atmosphérique

Germany

H. Ahlgrimm	Federal Agricultural Research Center
M. Andreae	Max-Planck Institut für Biochemistry
R. Benndorf	Federal Environmental Agency
U. Boehm	Universität Potsdam
O. Boucher	Max-Planck Institut für Chemie
S. Brinkop	Institut für Physik der Atmosphäre

M. Claussen	Potsdam Institute for Climate Impact Research
M. Dehn	Universität Bonn
P. Dietze	Private
E. Holland	Max-Planck Institut für Biochemistry
J. Jacobbeit	Universität Wuerzburg
K. Kartschall	Federal Environmental Agency
B. Kärcher	Institut für Physik der Atmosphäre
K. Lange	Federal Ministry for Environment, Nature Conservation and Nuclear Safety
P. Mahrenholz	Federal Environmental Agency
J. Oberhuber	German Climate Computing Centre
R. Sartorius	Federal Environmental Agency
C. Schoenwiese	J.W. Goethe University
U. Schumann	Institut für Physik der Atmosphäre
U. Ulbrich	Institut für Geophysik und Meteorologie
T. Voigt	Federal Environment Agency
A. Volz-Thomas	Forschungszentrum Juelich
G. Weber	Gesamtverband Steinkohlenbergbau (GVST)
G. Wefer	Universität Bremen
M. Widmann	GKSS-Forschungszentrum

Hungary

G. Koppány	University of Szeged
------------	----------------------

Iceland

T. Johannesson	Icelandic Meteorological Office
----------------	---------------------------------

Israel

P. Alpert	Tel Aviv University
S. Krichark	Tel Aviv University
C. Price	Tel Aviv University
Z. Levin	Tel Aviv University

Italy

W. Dragoni	Perugia Universita
A. Mariotti	National Agency for New Technology, Energy and Environment (ENEA)
T. Nanni	ISAO National Research Council
P. Ruti	National Agency for New Technology, Energy and Environment (ENEA)
R. van Dingenen	Environment Institute of European Commission
G. Visconti	Università Degli Studi dell' Aquila

Japan

M. Amino	Japan Meteorological Agency
T. Asoh	Japan Meteorological Agency
H. Isobe	Japan Meteorological Agency
H. Kanzawa	Environment Agency
H. Kato	Central Research Institute of Electric Power Industry
M. Kimoto	University of Tokyo

K. Kurihara	Japan Meteorological Agency
S. Kusunoki	Meteorological Research Institute
S. Manabe	Institute for Global Change
S. Nagata	Environment Agency
Y. Nikaidou	Japan Meteorological Agency
J. Ohyama	Japan Meteorological Agency
Y. Sato	Meteorological Research Institute
A. Sekiya	National Institute of Materials and Chemical Research
M. Shinoda	Tokyo Metropolitan University
S. Taguchi	National Institute for Research & Environment
T. Tokioka	Japan Meteorological Agency
Y. Tsutsumi	Japan Meteorological Agency
O. Wild	Frontier Research System for Global Change
R. Yamamoto	Kyoto University

Kenya

J. Ng'ang'a	University of Nairobi
N. Sabogal	United Nations Environment Programme

Malaysia

A. Chan	Malaysian Meteorological Service
---------	----------------------------------

Morocco

A. Allali	Ministry of Agriculture & Moroccan Association for Environment Protection
S. Khatri	Meteorological Office of Morocco
A. Mokssit	Meteorological Office of Morocco
A. Sbaibi	Universite Hassan II - Mohammedia

Netherlands

A.P.M. Baede	Koninklijk Nederlands Meteorologisch Instituut
J. Beersma	Koninklijk Nederlands Meteorologisch Instituut
L. Bijlsma	Rijksinstituut voor Kust en Zee
T. Buishand	Koninklijk Nederlands Meteorologisch Instituut
G. Burgers	Koninklijk Nederlands Meteorologisch Instituut
H. Dijkstra	Koninklijk Nederlands Meteorologisch Instituut
S. Drijfhout	University of Utrecht
W. Hazeleger	Koninklijk Nederlands Meteorologisch Instituut
B. Holtslag	Koninklijk Nederlands Meteorologisch Instituut
C. Jacobs	Wageningen University
A. Jeuken	Koninklijk Nederlands Meteorologisch Instituut
H. Kelder	Koninklijk Nederlands Meteorologisch Instituut
G. Komen	Koninklijk Nederlands Meteorologisch Instituut
N. Maat	Koninklijk Nederlands Meteorologisch Instituut and University of Utrecht
L. Meyer	Koninklijk Nederlands Meteorologisch Instituut
J. Olivier	Ministry of Housing, Spatial Planning & the Environment
J. Opsteegh	Rijksinstituut voor Volksgezondheid en Milieu
A. Petersen	Koninklijk Nederlands Meteorologisch Instituut
H. Radder	Vrije Universiteit
H. Renssen	Vrije Universiteit
	Vrije Universiteit

J. Ronde	Rijksinstituut voor Kust en Zee
M. Scheffers	Rijksinstituut voor Kust en Zee
C. Schuurmans	University of Utrecht
P. Siegmund	Koninklijk Nederlands Meteorologisch Instituut
A. Sterl	Koninklijk Nederlands Meteorologisch Instituut
H. ten Brink	Energieonderzoek Centrum Nederland
R. Tol	Vrije Universiteit
S. van de Geijn	Plant Research International
R. van Dorland	Koninklijk Nederlands Meteorologisch Instituut
G. van Tol	Expertisecentrum LNV
A. van Ulden	Koninklijk Nederlands Meteorologisch Instituut
M. van Weele	Koninklijk Nederlands Meteorologisch Instituut
P. Veefkind	Koninklijk Nederlands Meteorologisch Instituut
G. Velders	Rijksinstituut voor Volksgezondheid en Milieu
J. Verbeek	Koninklijk Nederlands Meteorologisch Instituut
H. Visser	KEMA

New Zealand

C. de Freitas	University of Auckland
B. Fitzharris	University of Otago
V. Gray	Climate Consultant, New Zealand
J. Kidson	National Institute of Water & Atmospheric Research
H. Larsen	National Institute of Water & Atmospheric Research
P. Maclarens	University of Canterbury
M. Manning	National Institute of Water & Atmospheric Research
J. Renwick	National Institute of Water & Atmospheric Research

Norway

T. Asphjell	Norwegian State Pollution Control Authority
R. Benestad	Norwegian Meteorological Institute
O. Christoffersen	Ministry of Environment
E. Forland	Norwegian Meteorological Institute
J. Fuglestvedt	University of Oslo
O. Godal	University of Oslo
S. Grønås	University of Bergen
I. Hanssen-Bauer	Norwegian Meteorological Institute
E. Jansen	University of Bergen
N. Koc	Norsk Polarinstitutt
H. Loeng	Institute of Marine Research
S. Mylona	Norwegian State Pollution Control Authority
M. Pettersen	Norwegian State Pollution Control Authority
A. Rosland	Norwegian State Pollution Control Authority
T. Segalstad	University of Oslo
J. Winther	Norwegian Polar Institute

Peru

N. Gamboa	Pontificia Universidad Catolica del Peru
-----------	--

Poland

M. Mietus Institute of Meteorology & Water Management

Portugal

C. Borrego Universidade de Aveiro

Russian Federation

O. E. Anisimov	State Hydrological Institute
R. Burlutsky	Hydrometeorological Research Centre of Russia
N. Datsenko	Hydrometeorological Research Centre of Russia
G. Golitsyn	Institute of Atmospheric Physics
N. Ivachtchenko	Hydrometeorological Research Centre of Russia
I. Karol	Main Geophysical Observatory
K. Kondratyev	Research Centre for Ecological Safety
V. P. Meleshko	Main Geophysical Observatory
I. Mokhov	Institute of Atmospheric Physics
D. Sonechkin	Hydrometeorological Research Centre of Russia

Saudi Arabia

M. Al-Sabban Ministry of Petroleum

Slovak Republic

M. Lapin Comenius University
K. Mareckova Slovak Hydrometeorological Institute

Slovenia

A. Kranjc Hydrometeorological Institute of Slovenia

Spain

S. Alonso	Universitat de les Illes Balears
L. Balairon	National Institute of Meteorology
Y. Castro-Diez	Universidad de Granada
J. Cortina	Universitat d'Alacant
M. de Luis	Universitat d'Alacant
E. Fanjul	Clima Maritimo - Puertos del Estado
B. Gomez	Clima Maritimo - Puertos del Estado
M. Gomez-Lahoz	Puertos del Estado
J. Gonzalez-Hidalgo	University of Zaragoza
A. Lavin	Instituto Español de Oceanografía
J. Peñuelas	Universitat Autònoma de Barcelona
J. Raventos	Universitat d'Alacant
J. Sanchez	Universitat d'Alacant
I. Sanchez-Arevalo	Clima Maritimo - Puertos del Estado
M. Vazquez	Instituto de Astrofísica de Canarias

Sudan

N. Awad	Higher Council for Environment & Natural Resources
I. Elgizouli	Higher Council for Environment & Natural Resources
N. Goutbi	Higher Council for Environment & Natural Resources

Sweden

R. Charlson	Stockholm University
E. Källén	Stockholm University
A. Moberg	Stockholm University
N. Morner	Stockholm University
J. Raisanen	Swedish Meteorological and Hydrological Institute
H. Rodhe	Stockholm University
M. Rummukainen	Swedish Meteorological and Hydrological Institute

Switzerland

U. Baltensperger	Paul Scherrer Institute
D. Gyalistras	University of Bern
W. Haeberli	University of Zurich
F. Joos	University of Bern
H. Lang	Swiss Federal Institute of Technology
C. Pfister	Unitobler
J. Romero	Federal Office of Environment, Forests and Landscape
C. Schaer	Swiss Federal Institute of Technology
J. Staehelin	Swiss Federal Institute of Technology
H. Wanner	University of Bern
M. Wild	Swiss Federal Institute of Technology

Thailand

J. Boonjawat	Chulalongkorn University
--------------	--------------------------

Togo

A. Ajavon	Universite du Benin
-----------	---------------------

Turkey

A. Danchev	Fatih University
M. Turkes	Turkish State Meteorological Service

United Kingdom

M. Allen	Rutherford Appleton Laboratory
S. Allison	Southampton Oceanography Centre
R. Betts	Hadley Centre for Climate Prediction and Research, Met Office
S. Boehmer-Christiansen	Sussex University
R. Braithwaite	University of Manchester
K. Briffa	University of East Anglia

S. Brown	Hadley Centre for Climate Prediction and Research, Met Office
I. Colbeck	University of Essex
R. Courtney	European Science and Environment Forum
M. Crompton	Department of the Environment, Transport and the Regions
X. Dai	IPCC WGI Technical Support Unit
C. Doake	British Antarctic Survey
C. Folland	Hadley Centre for Climate Prediction and Research, Met Office
N. Gedney	Hadley Centre for Climate Prediction and Research, Met Office
N. Gillett	University of Oxford
W. Gould	Southampton Oceanography Centre
J. Gregory	Hadley Centre for Climate Prediction and Research, Met Office
S. Gregory	University of Sheffield
D. J Griggs	IPCC WGI Technical Support Unit
J. Grove	University of Cambridge
J. Haigh	Imperial College
R. Harding	Centre for Ecology and Hydrology
M. Harley	English Nature
J. Haywood	Meteorological Research Flight, Met Office
J. Houghton	IPCC WGI Co-Chairman
W. Ingram	Hadley Centre for Climate Prediction and Research, Met Office
T. Iversen	European Centre for Medium-range Weather Forecasting
J. Lovelock	Retired, United Kingdom
K. Maskell	IPCC WGI Technical Support Unit
A. McCulloch	Marbury Technical Consulting, United Kingdom
G. McFadyen	Department of the Environment, Transport and the Regions
J. Mitchell	Hadley Centre for Climate Prediction and Research, Met Office
J. Murphy	Hadley Centre for Climate Prediction and Research, Met Office
C. Newton	Environment Agency
M. Noguer	IPCC WGI Technical Support Unit
T. Osborn	University of East Anglia
D. Parker	Hadley Centre for Climate Prediction and Research, Met Office
D. Pugh	Southampton Oceanography Centre
S. Raper	University of East Anglia
D. Roberts	Hadley Centre for Climate Prediction and Research, Met Office
D. Sexton	Hadley Centre for Climate Prediction and Research, Met Office
K. Shine	University of Reading
K. Smith	University of Edinburgh
P. Smithson	University of Sheffield
P. Stott	Hadley Centre for Climate Prediction and Research, Met Office
S. Tett	Hadley Centre for Climate Prediction and Research, Met Office
P. Thorne	University of East Anglia
R. Toumi	Imperial College
P. Viterbo	European Centre for Medium-range Weather Forecasting
D. Warrilow	Department of the Environment, Transport and the Regions
R. Wilby	University of Derby
P. Williamson	Plymouth Marine Laboratory
P. Woodworth	Bidston Observatory

United States of America

M. Abbott	Oregon State University
W. Abdalati	NASA Goddard Space Flight Centre
D. Adamec	NASA Goddard Space Flight Centre
R. B. Alley	Pennsylvania State University
R. Andres	University of Alaska at Fairbanks
J. Angel	Illinois State Water Survey

P. Arkin	Columbia University
R. Arritt	Iowa State University
E. Atlas	National Centre for Atmospheric Research
D. Bader	Department of Energy
T. Baerwald	National Science Foundation
R. Bales	University of Arizona
R. Barber	Duke University
T. Barnett	Scripps Institute of Oceanography
P. Bartlein	University of Oregon
J. J. Bates	NOAA Environmental Technology Laboratory
T. Bates	NOAA Pacific Marine Environmental Laboratory
M. Bender	Princeton University
C. Bentley	University of Wisconsin at Madison
K. Bergman	NASA Global Modeling and Analysis Program
C. Berkowitz	Pacific Northwest National Laboratory
M. Berliner	Ohio State University
J. Berry	Carnegie Institution of Washington
R. Bindschadler	NASA Goddard Space Flight Centre
D. Blake	University of California at Irvine
T. Bond	University of Washington
A. Broccoli	Princeton University
W. Broecker	Lamont Doherty Earth Observatory of Columbia University
L. Bruhwiler	NOAA Climate Monitoring and Diagnostics Laboratory
K. Bryan	Princeton University
K. Caldeira	Lawrence Livermore National Laboratory
M. A. Cane	Lamont Doherty Earth Observatory of Columbia University
A. Carleton	Pennsylvania State University
R. Cess	State University of New York
W. Chameides	Georgia Institute of Technology
T. Charlock	NASA Langley Research Center
M. Chin	NASA Goddard Space Flight Center
K. Cook	Cornell University
W. Cooke	Princeton University
C. Covey	Lawrence Livermore National Laboratory
T. Crowley	Texas A&M University
D. Cunnold	Georgia Institute of Technology
J. A. Curry	University of Colorado
R. Dahlman	Department of Energy
A. Dai	National Center for Atmospheric Research
B. DeAngelo	Environmental Protection Agency
P. DeCola	NASA
P. DeMott	Colorado State University
A. S. Denning	Colorado State University
W. Dewar	Florida State University
R. E. Dickerson	University of Maryland
R. Dickinson	Georgia Institute of Technology
L. Dilling	NOAA Office of Global Programs
E. Dlugokencky	NOAA Climate Monitoring & Diagnostics Laboratory
S. Doney	National Centre for Atmospheric Research
S. Drobot	University of Nebraska
H. Ducklow	Virginia Institute of Marine Sciences
W. Easterling	Pennsylvania State University
J. Elkins	NOAA Climate Monitoring & Diagnostics Laboratory
E. Elliott	National Science Foundation
W. Elliott	NOAA Air Resources Laboratory
H. Ellsaesser	Atmospheric Consultant
S. Esbensen	Oregon State University

C. Fairall	NOAA Environmental Technology Laboratory
Y. Fan	Centre for Ocean-Land-Atmosphere Studies
P. Farrar	Naval Oceanographic Office
R. Feely	NOAA Pacific Marine Environmental Laboratory
F. Fehsenfeld	NOAA Environmental Research Laboratories
G. Feingold	NOAA Environmental Technology Laboratory
R. Fleagle	University of Washington
R. Forte	Environmental Protection Agency
M. Fox-Rabinovitz	University of Maryland
J. Francis	Rutgers University
M. Free	NOAA Air Resources Laboratory
R. Friedl	Jet Propulsion laboratory
I. Fung	University of California
D. Gaffen	NOAA Air Resources Laboratory
W. Gates	Lawrence Livermore National Laboratory
C. Gautier	University of California at Santa Barbara
P. Geckler	Lawrence Livermore National Laboratory
L. Gerhard	University of Kansas
S. Ghan	Pacific Northwest National Laboratory
M. Ghil	University of California at Los Angeles
P. Gleckler	Lawrence Livermore National Laboratory
V. Gornitz	NASA Goddard Institute for Space Studies
V. Grewe	NASA Goddard Institute for Space Studies
W. Gutowski	Iowa State University
P. Guttorm	University of Washington
R. Hallgren	American Meteorological Society
D. Hardy	University of Massachusetts
E. Harrison	NOAA Pacific Marine Environmental Laboratory
G. Hegerl	Texas A&M University
B. Hicks	NOAA Air Resources Laboratory
W. Higgins	NOAA Climate Protection Center
D. Houghton	University of Wisconsin at Madison
R. Houghton	Woods Hole Research Center
Z. Hu	Center for Ocean-Land-Atmosphere Studies
B. Huang	Centre for Ocean-Land-Atmosphere Studies
J. Hudson	Desert Research Institute
M. Hughes	University of Arizona
C. Hulbe	NASA Goddard Space Flight Center
D. Jacob	Harvard University
S. Jacobs	Columbia University
M. Jacobson	Stanford University
A. Jain	University of Illinois
D. James	National Science Foundation
G. Johnson	NOAA Pacific Marine Environmental Laboratory
R. Johnson	Colorado State University
T. Joyce	Woods Hole Oceanographic Institution
R. Katz	National Center for Atmospheric Research
R. Keeling	Scripps Institute of Oceanography
J. Kiehl	National Center for Atmospheric Research
J. Kim	Lawrence Berkeley National Laboratory
J. Kinter	Centre for Ocean-Land-Atmosphere Studies
B. Kirtman	Centre for Ocean-Land-Atmosphere Studies
T. Knutson	NOAA Geophysical Fluid Dynamics Laboratory
D. Koch	National Center for Atmospheric Research
S. Kreidenweis	Colorado State University
V. Krishnamurthy	Centre for Ocean-Land-Atmosphere Studies
D. Kruger	Environmental Protection Agency

J. Kutzbach	University of Wisconsin at Madison
C. Landsea	NOAA Atlantic Oceanographic & Meteorological Laboratory
N. Lauainen	Pacific Northwest National Laboratory
J. Lean	Naval Research Laboratory
M. Ledbetter	National Science Foundation
T. Ledley	TERC
A. Leetmaa	NOAA National Weather Service
C. Leith	Lawrence Livermore National Laboratory
S. Levitus	NOAA National Oceanographic Data Center
J. Levy	NOAA Office of Global Programs
L. Leung	Pacific Northwest National Laboratory
R. Lindzen	Massachusetts Institute of Technology
C. Lingle	University of Alaska at Fairbanks
J. Logan	Harvard University
A. Lupo	University of Missouri
M. MacCracken	Office of the US Global Change Research Program
G. Magnusdottir	University of California
J. Mahlman	Princeton University
T. Malone	Connecticut Academy of Science and Engineering
M. E. Mann	University of Virginia
P. Matrai	Bigelow Laboratory for Ocean Sciences
D. Mauzerall	Princeton University
M. McFarland	Dupont Fluoroproducts
A. McGuire	University of Alaska at Fairbanks
S. Meacham	National Science Foundation
M. Meier	Institute of Arctic & Alpine Research
P. Michaels	University of Virginia
N. Miller	Lawrence Berkeley National Laboratory
M. Mishchenko	NASA Goddard Institute for Space Studies
V. Misra	Centre for Ocean-Land-Atmosphere Studies
R. Molinari	NOAA Atlantic Oceanographic and Meteorological Laboratory
S. Montzka	NOAA Climate Monitoring & Diagnostics Laboratory
K. Mooney	NOAA Office of Global Programs
A. Mosier	Department of Agriculture
D. Neelin	University of California at Los Angeles
R. Neilson	Oregon State University
J. Norris	Princeton University
G. North	Texas A & M University
T. Novakov	Lawrence Berkeley National Laboratory
W. O'Hirok	Institute for Computational Earth System Science
M. Palecki	Illinois State Water Survey
S. Pandis	Carnegie Mellon University
C. L. Parkinson	NASA Goddard Space Flight Center
J. Penner	University of Michigan
K. Pickering	University of Maryland
R. Pielke	Colorado State University
S. Piper	Scripps Institution of Oceanography
H. Pollack	University of Michigan
G. Potter	Lawrence Livermore National Laboratory
M. Prather	University of California at Irvine
R. Prinn	Massachusetts Institute of Technology
N. Psuty	State University of New Jersey
V. Ramanathan	Scripps Institute of Oceanography
V. Ramaswamy	Princeton University
R. Randall	The Rainforest Regeneration Institution
J. Randerson	California Institute of Technology
C. Raymond	University of Washington

P. Rhines	University of Washington
C. Rinsland	NASA Langley Research Centre
D. Ritson	Stanford University
A. Robock	Rutgers University
B. Rock	University of New Hampshire
J. Rodriguez	University of Miami
R. Ross	NOAA Air Resources Laboratory
D. Rotman	Lawrence Livermore National Laboratory
C. Sabine	University of Washington
D. Sahagian	University of New Hampshire
E. Saltzman	National Science Foundation
S. Sander	NASA Jet Propulsion Laboratory
E. Sarachik	University of Washington
V. Saxena	North Carolina State University
S. Schauffler	National Centre for Atmospheric Research
E. Scheehle	Environmental Protection Agency
W. Schlesinger	Duke University
C. Schlosser	Centre for Ocean-Land-Atmosphere Studies
R. W. Schmitt	Woods Hole Oceanographic Institution
E. Schneider	Centre for Ocean-Land-Atmosphere Studies
S. Schneider	Stanford University
S. Schwartz	Brookhaven National Laboratory
M. Schwartzkopf	Princeton University
J. Seinfeld	California Institute of Technology
A. Semtner	Naval Postgraduate School
J. Severinghaus	University of California
D. Shindell	NASA Goddard Institute for Space Studies
H. Sievering	University of Colorado
J. Simpson	University of California
H. Singh	NASA Ames Research Centre
D. Skole	Michigan State University
S. Smith	Pacific Northwest National Laboratory
B. J. Soden	Princeton University
R. Somerville	University of California
M. Spector	Lehigh University
T. Spence	National Science Foundation
P. Stephens	National Science Foundation
P. Stone	Massachusetts Institute of Technology
R. Stouffer	Princeton University
D. Straus	Centre for Ocean-Land-Atmosphere Studies
C. Sucher	NOAA Office of Global Programs
Y. Sud	NASA Goddard Space Flight Center
B. Sun	University of Massachusetts
P. Tans	NOAA Climate Monitoring & Diagnostics Laboratory
R. Thomas	NASA Wallops Flight Facility
D. Thompson	University of Washington
J. Titus	Environmental Protection Agency
K. E. Trenberth	National Center for Atmospheric Research
S. Trumbore	University of California at Irvine
G. Tselioudis	NASA Goddard Institute for Space Studies
C. van der Veen	Ohio State University
M. Visbeck	Lamont Doherty Earth Observatory of Columbia University
M. Vuille	University of Massachusetts
M. Wahlen	University of California
J. Wallace	University of Washington
J. Walsh	University of Illinois at Urbana-Champaign
J. Wang	NOAA Air Resources Laboratory

W. Wang	State University of New York at Albany
Y. Wang	Georgia Institute of Technology
M. Ward	Lamont Doherty Earth Observatory of Columbia University
S. Warren	University of Washington
W. Washington	National Center for Atmospheric Research
B. Weare	University of California at Davis
T. Webb	Brown University
M. Wehner	Lawrence Livermore National Laboratory
R. Weller	Woods Hole Oceanographic Institution
P. Wennberg	California Institute of Technology
H. Weosky	Federal Aviation Administration
D. Williamson	National Center for Atmospheric Research
D. Winstanley	Illinois State Water Survey
S. Wofsy	Harvard University
J. Wong	NOAA Air Resources Laboratory
C. Woodhouse	NOAA National Geophysical Data Center
Z. Wu	Centre for Ocean-Land-Atmosphere Studies
X. Xiao	University of New Hampshire
Z. Yang	University of Arizona
S. Yvon-Lewis	NOAA Atlantic Oceanographic & Meteorological Laboratory
C. Zender	University of California at Irvine

United Nations Organisations and Specialised Agencies

N. Harris	European Ozone Research Coordinating Unit, United Kingdom
F. Raes	Environment Institute of European Commission, Italy

Non-Governmental Organisations

J. Owens	3M Company
C. Kolb	Aerodyne Research Inc.
H. Feldman	American Petroleum Institute
J. Martín-Vide	Asociación Española de Climatología, Spain
M. Ko	Atmospheric & Environmental Research Inc.
S. Baughcum	Boeing Company
C. Field	Carnegie Institute of Washington
K. Gregory	Centre for Business and the Environment, United Kingdom
W. Hennessy	CRL Energy Ltd., New Zealand
E. Olaguer	The Dow Chemical Company
D. Fisher	DuPont Company
A. Salamanca	ECO Justicia, Spain
C. Hakkilainen	Electric Power Research Institute, USA
M. Oppenheimer	Environmental Defense, USA
H. Kheshgi	Exxon Mobil Research & Engineering Company, USA
S. Japar	Ford Motor Company
W. Hare	Greenpeace International, Netherlands
L. Bishop	Honeywell International Inc.
J. Neumann	Industrial Economics, Incorporated
I. Smith	International Energy Agency Coal Research, United Kingdom
L. Bernstein	International Petroleum Industry Environmental Conservation Association
J. Grant	International Petroleum Industry Environmental Conservation Association
D. Hoyt	Raytheon
K. Green	Reason Public Policy Institute
S. Singer	Science & Environmental Policy Project, USA
J. Le Cornu	SHELL Australia Ltd.

Appendix V

Acronyms and Abbreviations

AABW	Antarctic Bottom Water
AAO	Antarctic Oscillation
ABL	Atmospheric Boundary Layer
ACC	Antarctic Circumpolar Current
ACE	Aerosol Characterisation Experiment
ACRIM	Active Cavity Radiometer Irradiance Monitor
ACSYS	Arctic Climate System Study
ACW	Antarctic Circumpolar Wave
AEROCE	Atmosphere Ocean Chemistry Experiment
AGAGE	Advanced Global Atmospheric Gases Experiment
AGCM	Atmospheric General Circulation Model
AGWP	Absolute Global Warming Potential
AMIP	Atmospheric Model Intercomparison Project
ANN	Artificial Neural Networks
AO	Arctic Oscillation
AOGCM	Atmosphere-Ocean General Circulation Model
ARESE	Atmospheric Radiation Measurement Enhanced Shortwave Experiment
ARGO	Part of the Integrated Global Observation Strategy
ARM	Atmospheric Radiation Measurement
ARPEGE/OPA	Action de Recherche Petite Echelle Grande Echelle/Océan Paralléléisé
ASHOE/MAESA	Airborne Southern Hemisphere Ozone Experiment/Measurement for Assessing the Effects of Stratospheric Aircraft
AVHRR	Advanced Very High Resolution Radiometer
AWI	Alfred Wegener Institute (Germany)
BAHC	Biospheric Aspects of the Hydrological Cycle
BC	Black Carbon
BERN2D	Two-dimensional Climate Model of University of Bern
BIOME 6000	Global Palaeo-vegetation Mapping Project
BMRC	Bureau of Meteorology Research Centre (Australia)
CART	Classification and Tree Analysis
CCA	Canonical Correlation Analysis
CCC(ma)	Canadian Centre for Climate (Modelling and Analysis) (Canada)
CCM	Community Climate Model
CCMLP	Carbon Cycle Model Linkage Project
CCN	Cloud Condensation Nuclei
CCSR	Centre for Climate System Research (Japan)
CERFACS	European Centre for Research and Advanced Training in Scientific Computation (France)
CIAP	Climate Impact Assessment Program

CLIMAP	Climate: Long-range Investigation, Mapping and Prediction
CLIMBER	Climate-Biosphere Model
CLIMACTS	Integrated Model for Assessment of the Effects of Climate Change on the New Zealand Environment
CMAP	CPC Merged Analysis of Precipitation
CMDL	Climate Monitoring and Diagnostics Laboratory of NOAA (USA)
CMIP	Coupled Model Intercomparison Project
CNRM	Centre National de Recherches Météorologiques (France)
CNRS	Centre National de la Recherche Scientifique (France)
COADS	Comprehensive Ocean Atmosphere Data Set
COHMAP	Co-operative Holocene Mapping Project
COLA	Centre for Ocean-Land-Atmosphere Studies (USA)
COSAM	Comparison of Large-scale Atmospheric Sulphate Aerosol Model
COSMIC	Country Specific Model for Intertemporal Climate
COWL	Cold Ocean Warm Land
CPC	Climate Prediction Center of NOAA (USA)
CRF	Cloud Radiative Forcing
CRU	Climatic Research Unit of UEA (UK)
CRYOSat	Cryosphere Satellite
CSG	Climate Scenario Generator
CSIRO	Commonwealth Scientific and Industrial Research Organisation (Australia)
CSM	Climate System Model
CTM	Chemistry Transport Model
DARLAM	CSIRO Division of Atmospheric Research Limited Area Model
DDC	Data Distribution Centre of IPCC
DGVM	Dynamic Global Vegetation Model
DERF	Dynamical Extended Range Forecasting group of GFDL (USA)
DIC	Dissolved Inorganic Carbon
DJF	December, January, February
DKRZ	Deutsche KlimaRechenZentrum (Germany)
DMS	Dimethylsulfide
DMSP	Defense Meteorological Satellite Program
DNM	Department of Numerical Mathematics (Russia)
DOC	Dissolved Organic Carbon
DOE	Department of Energy (USA)
DORIS	Determination d'Orbite et Radiopositionnement Intégrés par Satellite
DRF	Direct Radiative Forcing
DTR	Diurnal Temperature Range
DYNAMO	Dynamics of North Atlantic Models
EBM	Energy Balance Model
ECHAM	ECMWF/MPI AGCM
ECMWF	European Centre for Medium-range Weather Forecasting
ECS	Effective Climate Sensitivity
EDGAR	Emission Database for Global Atmospheric Research
EISMINT	European Ice Sheet Modelling initiative
EMDI	Ecosystem Model/Data Intercomparison
EMIC	Earth system Models of Intermediate Complexity
ENSO	El Niño-Southern Oscillation
EOF	Empirical Orthogonal Function
EOS	Earth Observing System
ERA	ECMWF Reanalysis
ERB	Earth Radiation Budget
ERBE	Earth Radiation Budget Experiment
ERBS	Earth Radiation Budget Satellite
ESCAPE	Evaluation of Strategies to Address Climate Change by Adapting to and Preventing Emissions
ESMR	Electrically Scanning Microwave Radiometer
EURECA	European Retrievable Carrier
FACE	Free Air Carbon-dioxide Enrichment

FAO	Food and Agriculture Organisation (UN)
FCCC	Framework Convention on Climate Change
FDH	Fixed Dynamical Heating
FF	Fossil Fuel
FPAR	Plant-absorbed Fraction of Incoming Photosynthetically Active Radiation
FSU	Former Soviet Union
GASP	Global Assimilation and Prediction
GCIP	GEWEX Continental-scale International Program
GCM	General Circulation Model
GCOS	Global Climate Observing System
GCR	Galactic Cosmic Ray
GDP	Gross Domestic Product
GEBA	Global Energy Balance Archive
GEIA	Global Emissions Inventory Activity
GEISA	Gestion et Etude des Informations Spectroscopiques Atmosphériques
GEWEX	Global Energy and Water cycle Experiment
GFDL	Geophysical Fluid Dynamics Laboratory (USA)
GHCN	Global Historical Climate Network
GHG	Greenhouse Gas
GIM	Global Integration and Modelling
GISP	Greenland Ice Sheet Project
GISS	Goddard Institute for Space Studies (USA)
GISST	Global Sea Ice and Sea Surface Temperature
GLOSS	Global Sea Level Observing System
GOALS	Global Ocean-Atmosphere-Land System
GPCP	Global Precipitation Climatology Project
GPP	Gross Primary Production
GPS	Global Positioning System
GRACE	Gravity Recovery and Climate Experiment
GRIP	Greenland Ice Core Project
GSFC	Goddard Space Flight Centre (USA)
GSWP	Global Soil Wetness Project
GUAN	GCOS Upper Air Network
GWP	Global Warming Potential
HadCM	Hadley Centre Coupled Model
HIRETYCS	High Resolution Ten-Year Climate Simulations
HITRAN	High Resolution Transmission Molecular Absorption Database
HLM	High Latitude Mode
HNLC	High Nutrient-Low Chlorophyll
HRBM	High Resolution Biosphere Model
IAHS	International Association of Hydrological Science
IAP	Institute of Atmospheric Physics (China)
IASB	Institut d'Aéronomie Spatiale de Belgique (Belgium)
IBIS	Integrated Biosphere Simulator
ICESat	Ice, Cloud and Land Elevation Satellite
ICSI	International Commission on Snow and Ice
ICSU	International Council of Scientific Unions
IGAC	International Global Atmospheric Chemistry
IGBP	International Geosphere Biosphere Programme
IGCR	Institute for Global Change Research (Japan)
IHDP	International Human Dimensions Programme on Global Environmental Change
IMAGE	Integrated Model to Assess the Global Environment
IN	Ice Nuclei
INDOEX	Indian Ocean Experiment
IOC	Intergovernmental Oceanographic Commission
IPCC	Intergovernmental Panel on Climate Change
IPO	Interdecadal Pacific Oscillation

IPSL-CM	Institut Pierre Simon Laplace/Coupled Atmosphere-Ocean-Vegetation Model
ISAM	Integrated Science Assessment Model
ISCCP	International Satellite Cloud Climatology Project
ISLSCP	International Satellite Land Surface Climatology Project
ITCZ	Inter-Tropical Convergence Zone
IUPAC	International Union of Pure and Applied Chemistry
JGOFS	Joint Global Ocean Flux Study
JJA	June, July, August
JMA	Japan Meteorological Agency (Japan)
JPL	Jet Propulsion Laboratory of NASA (USA)
KNMI	Koninklijk Nederlands Meteorologisch Instituut (Netherlands)
LAI	Leaf Area Index
LASG	State Key Laboratory of Numerical Modelling for Atmospheric Sciences and Geophysical Fluid Dynamics (China)
LBA	Large-scale Biosphere-atmosphere Experiment in Amazonia
LGGE	Laboratoire de Glaciologie et Géophysique de l'Environnement (France)
LGM	Last Glacial Maximum
LLNL	Lawrence Livermore National Laboratory (USA)
LMD	Laboratoire de Météorologie Dynamique (France)
LOSU	Level of Scientific Understanding
LPJ	Land-Potsdam-Jena Terrestrial Carbon Model
LSAT	Land Surface Air Temperature
LSG	Large-Scale Geostrophic Ocean Model
LSP	Land Surface Parameterisation
LT	Lifetime
LWP	Liquid Water Path
MAGICC	Model for the Assessment of Greenhouse-gas Induced Climate Change
MAM	March, April, May
MARS	Multivariate Adaptive Regression Splines
MGO	Main Geophysical Observatory (Russia)
MJO	Madden-Julian Oscillation
ML	Mixed Layer
MLOPEX	Mauna Loa Observatory Photochemistry Experiment
MODIS	Moderate Resolving Imaging Spectroradiometer
MOGUNTIA	Model of the General Universal Tracer Transport in the Atmosphere
MOM	Modular Ocean Model
MOZART	Model for Ozone and Related Chemical Tracers
MPI	Max-Plank Institute for Meteorology (Germany)
MRI	Meteorological Research Institute (Japan)
MSLP	Mean Sea Level Pressure
MSU	Microwave Sounding Unit
NADW	North Atlantic Deep Water
NAO	North Atlantic Oscillation
NARE	North Atlantic Regional Experiment
NASA	National Aeronautics and Space Administration (USA)
NBP	Net Biome Production
NCAR	National Center for Atmospheric Research (USA)
NCC	National Climate Centre (China)
NCDC	National Climatic Data Center of NOAA (USA)
NCEP	National Centers for Environmental Prediction of NOAA (USA)
NDVI	Normalised Difference Vegetation Index
NEP	Net Ecosystem Production
NESDIS	National Environmental Satellite, Data and Information Service of NOAA (USA)
NIC	National Ice Centre of NOAA (USA)
NIED	National Research Institute for Earth Science and Disaster Prevention (Japan)
NIES	National Institute for Environmental Studies (Japan)
NMAT	Night Marine Air Temperature

NMHC	Non-Methane Hydrocarbon
NOAA	National Oceanic and Atmospheric Administration (USA)
NPP	Net Primary Production
NPZD	Nutrients, Phytoplankton, Zooplankton and Detritus
NRC	National Research Council (USA)
NRL	Naval Research Laboratory (USA)
NWP	Numerical Weather Prediction
OC	Organic Carbon
OCMIP	Ocean Carbon-cycle Model Intercomparison Project
OCS	Organic Carbonyl Sulphide
OGCM	Ocean General Circulation Model
OLR	Outgoing Long-wave Radiation
OPYC	Ocean Isopycnal GCM
OxComp	Tropospheric Oxidant Model Comparison
PC	Principal Component
PCM	Parallel Climate Model
PDF	Probability Density Function
PDO	Pacific Decadal Oscillation
PEM	Pacific Exploratory Missions
PFT	Plant Functional Type
PGR	Post-Glacial Rebound
PhotoComp	Ozone Photochemistry Model Comparison
PICASSO	Pathfinder Instruments for Cloud and Aerosol Spaceborne Observations
PIK	Potsdam Institute for Climate Impact Research (Germany)
PILPS	Project for the Intercomparison of Land-surface Parameterisation Schemes
PIUB	Physics Institute University of Bern (Switzerland)
PMIP	Palaeoclimate Model Intercomparison Project
PNA	Pacific-North American
PNNL	Pacific Northwest National Laboratory (USA)
POC	Particulate Organic Carbon
POLDER	Polarisation and Directionality of the Earth's Reflectances
POPCORN	Photo-Oxidant Formation by Plant Emitted Compounds and OH Radicals in North-eastern Germany
PSMSL	Permanent Service for Mean Sea Level
PT	Perturbation Lifetime
QBO	Quasi-Biennial Oscillation
RAMS	Regional Atmospheric Modelling System
RCM	Regional Climate Model
RIHMI	Research Institute for Hydrometeorological Information
SAGE	Stratospheric Aerosol & Gas Experiment
SAR	IPCC Second Assessment Report
SAT	Surface Air Temperature
SBUV	Solar Backscatter Ultra Violet
SCAR-B	Smoke Cloud and Radiation-Brazil
SCE	Snow Cover Extent
SCENGEN	Scenario Generator
SCSWP	Small-scale Severe Weather Phenomena
SDD	Statistical-Dynamical Downscaling
SDGVM	Sheffield Dynamic Global Vegetation Model
SEFDH	Seasonally Evolving Fixed Dynamical Heating
SHEBA	Surface Heat Balance of the Arctic Ocean
SHI	State Hydrological Institute (Russia)
SIMIP	Sea Ice Model Intercomparison Project
SIO	Scripps Institution of Oceanography (USA)
SLP	Sea Level Pressure
SMMR	Scanning Multichannel Microwave Radiometer
SOA	Secondary Organic Aerosol
SOC	Southampton Oceanography Centre (UK)

SOHO	Solar Heliospheric Observatory
SOI	Southern Oscillation Index
SOLSTICE	Solar Stellar Irradiance Comparison Experiment
SON	September, October, November
SONEX	Subsonic Assessment Program Ozone and Nitrogen Oxide Experiment
SOS	Southern Oxidant Study
SPADE	Stratospheric Photochemistry, Aerosols, and Dynamics Expedition
SPARC	Stratospheric Processes and Their Role in Climate
SPCZ	South Pacific Convergence Zone
SRES	IPCC Special Report on Emission Scenarios
SSM/T-2	Special Sensor Microwave Water Vapour Sounder
SSM/I	Special Sensor Microwave/Imager
SST	Sea Surface Temperature
SSU	Stratospheric Sounding Unit
STRAT	Stratospheric Tracers of Atmospheric Transport
SUCCESS	Subsonic Aircraft Contrail and Cloud Effects Special Study
SUNGEN	State University of New York at Albany/NCAR Global Environmental and Ecological Simulation of Interactive Systems
SUSIM	Solar Ultraviolet Spectral Irradiance Monitor
TAR	IPCC Third Assessment Report
TARFOX	Tropospheric Aerosol Radiative Forcing Observational Experiment
TBFRA	Temperate and Boreal Forest Resource Assessment
TBO	Tropospheric Biennial Oscillation
TCR	Transient Climate Response
TEM	Terrestrial Ecosystem Model
TEMPUS	Sea Surface Temperature Evolution Mapping Project based on Alkenone Stratigraphy
THC	Thermohaline Circulation
TMR	TOPEX Microwave Radiometer
TOA	Top of the Atmosphere
TOMS	Total Ozone Mapping Spectrometer
TOPEX/POSEIDON	US/French Ocean Topography Satellite Altimeter Experiment
TOVS	Television Infrared Observation Satellite Operational Vertical Sounder
TPI	Trans Polar Index
TRIFFID	Top-down Representation of Interactive Foliage and Flora Including Dynamics
TSI	Total Solar Irradiance
UARS	Upper Atmosphere Research Satellite
UCAM	University of Cambridge (UK)
UCI	University of California at Irvine (USA)
UD/EB	Upwelling Diffusion-Energy Balance
UEA	University of East Anglia (UK)
UGAMP	University Global Atmospheric Modelling Project
UIO	Universitetet I Oslo (Norway)
UIUC	University of Illinois at Urbana-Champaign (USA)
UKHI	United Kingdom High-resolution climate model
UKMO	United Kingdom Met Office (UK)
UKTR	United Kingdom Transient climate experiment
ULAQ	Università degli studi dell'Aquila (Italy)
UM	Unified Model
UNEP	United Nations Environment Programme
UNESCO	United Nations Education, Scientific and Cultural Organisation
UNFCCC	United Nations Framework Convention on Climate Change
USSR	Union of Soviet Socialist Republics
UTH	Upper Tropospheric Humidity
UV	Ultraviolet radiation
UVic	University of Victoria (Canada)
VIRGO	Variability of Solar Irradiance and Gravity Oscillations
VLM	Vertical Land Movement

VOC	Volatile Organic Compounds
WAIS	West Antarctic Ice Sheet
WASA	Waves and Storms in the North Atlantic
WAVAS	Water Vapour Assessment
WBCs	Western Boundary Currents
WCRP	World Climate Research Programme
WMGGs	Well-Mixed Greenhouse Gases
WMO	World Meteorological Organization
WOCE	World Ocean Circulation Experiment
WP	Western Pacific
WRE	Wigley, Richels and Edmonds
YONU	Yonsei University (Korea)

Appendix VI

Units

SI (Système Internationale) Units:

Physical Quantity	Name of Unit	Symbol
length	metre	m
mass	kilogram	kg
time	second	s
thermodynamic temperature	kelvin	K
amount of substance	mole	mol

Fraction	Prefix	Symbol	Multiple	Prefix	Symbol
10^{-1}	deci	d	10	deca	da
10^{-2}	centi	c	10^2	hecto	h
10^{-3}	milli	m	10^3	kilo	k
10^{-6}	micro	μ	10^6	mega	M
10^{-9}	nano	n	10^9	giga	G
10^{-12}	pico	p	10^{12}	tera	T
10^{-15}	femto	f	10^{15}	peta	P

Special Names and Symbols for Certain SI-Derived Units:

Physical Quantity	Name of SI Unit	Symbol for SI Unit	Definition of Unit
force	newton	N	kg m s^{-2}
pressure	pascal	Pa	$\text{kg m}^{-1} \text{s}^{-2}$ ($=\text{N m}^{-2}$)
energy	joule	J	$\text{kg m}^2 \text{s}^{-2}$
power	watt	W	$\text{kg m}^2 \text{s}^{-3}$ ($=\text{J s}^{-1}$)
frequency	hertz	Hz	s^{-1} (cycles per second)

Decimal Fractions and Multiples of SI Units Having Special Names:

Physical Quantity	Name of Unit	Symbol for Unit	Definition of Unit
length	Ångstrom	Å	$10^{-10} \text{ m} = 10^{-8} \text{ cm}$
length	micron	μm	10^{-6} m
area	hectare	ha	10^4 m^2
force	dyne	dyn	10^{-5} N
pressure	bar	bar	$10^5 \text{ N m}^{-2} = 10^5 \text{ Pa}$
pressure	millibar	mb	$10^2 \text{ N m}^{-2} = 1 \text{ hPa}$
mass	tonne	t	10^3 kg
mass	gram	g	10^{-3} kg
column density	Dobson units	DU	$2.687 \times 10^{16} \text{ molecules cm}^{-2}$
streamfunction	Sverdrup	Sv	$10^6 \text{ m}^3 \text{ s}^{-1}$

Non-SI Units:

°C	degree Celsius ($0 \text{ }^\circ\text{C} = 273 \text{ K}$ approximately) Temperature differences are also given in °C (=K) rather than the more correct form of “Celsius degrees”.
ppmv	parts per million (10^6) by volume
ppbv	parts per billion (10^9) by volume
pptv	parts per trillion (10^{12}) by volume
yr	year
ky	thousands of years
bp	before present

The units of mass adopted in this report are generally those which have come into common usage and have deliberately not been harmonised, e.g.,

GtC	gigatonnes of carbon (1 GtC = 3.7 Gt carbon dioxide)
PgC	petagrams of carbon (1 PgC = 1 GtC)
MtN	megatonnes of nitrogen
TgC	teragrams of carbon (1 TgC = 1 MtC)
Tg(CH ₄)	teragrams of methane
TgN	teragrams of nitrogen
TgS	teragrams of sulphur

Appendix VII

Some chemical symbols used in this report

C	carbon (there are three isotopes: ^{12}C , ^{13}C , ^{14}C)	DOC	dissolved organic carbon
Ca	calcium	H₂	hydrogen
CaCO₃	calcium carbonate	halon-1211	CF ₂ ClBr
CCl₄	carbon tetrachloride	halon-1301	CF ₃ Br
CF₄	perfluoromethane	halon-2402	CF ₂ BrCF ₂ Br
C₂F₆	perfluoroethane	HCFC	hydrochlorofluorocarbon
C₃F₈	perfluoropropane	HCFC-21	CHCl ₂ F
C₄F₈	perfluorocyclobutane	HCFC-22	CHF ₂ Cl
C₄F₁₀	perfluorobutane	HCFC-123	C ₂ F ₃ HCl ₂
C₅F₁₂	perfluoropentane	HCFC-124	CF ₃ CHClF
C₆F₁₄	perfluorohexane	HCFC-141b	CH ₃ CFCl ₂
CFC	chlorofluorocarbon	HCFC-142b	CH ₃ CF ₂ Cl
CFC-11	CFCl ₃ (trichlorofluoromethane)	HCFC-225ca	CF ₃ CF ₂ CHCl ₂
CFC-12	CF ₂ Cl ₂ (dichlorodifluoromethane)	HCFC-225cb	CClF ₂ CF ₂ CHClF
CFC-13	CF ₃ Cl (chlorotrifluoromethane)	HCFE-235da2	CF ₃ CHClOCHF ₂
CFC-113	CF ₂ ClCFCl ₂ (trichlorotrifluoroethane)	HCO₃⁻	bicarbonate ion
CFC-114	CF ₂ ClCF ₂ Cl (dichlorotetrafluoroethane)	HFC	hydrofluorocarbon
CFC-115	CF ₃ CF ₂ Cl (chloropentafluoroethane)	HFC-23	CHF ₃
CF₃I	trifluoroiodomethane	HFC-32	CH ₂ F ₂
CH₄	methane	HFC-41	CH ₃ F
C₂H₆	ethane	HFC-125	CHF ₂ CF ₃
C₅H₈	isoprene	HFC-134	CHF ₂ CHF ₂
C₆H₆	benzene	HFC-134a	CF ₃ CH ₂ F
C₇H₈	toluene	HFC-143	CH ₂ F CHF ₂
C₁₀H₁₆	terpene	HFC-143a	CH ₃ CF ₃
CH₃Br	methylbromide	HFC-152	CH ₂ FCH ₂ F
CH₃CCl₃	methyl chloroform	HFC-152a	CH ₃ CHF ₂
CHCl₃	chloroform/trichloromethane	HFC-161	CH ₃ CH ₂ F
CH₂Cl₂	dichloromethane/methylene chloride	HFC-227ea	CF ₃ CHFCF ₃
CH₃Cl	methylchloride	HFC-236cb	CF ₃ CF ₂ CH ₂ F
CH₃OCH₃	dimethyl ether	HFC-236ea	CF ₃ CHFCHF ₂
CO	carbon monoxide	HFC-236fa	CF ₃ CH ₂ CF ₃
CO₂	carbon dioxide	HFC-245ca	CH ₂ FCF ₂ CHF ₂
CO₃²⁻	carbonate ion	HFC-245ea	CHF ₂ CHFCHF ₂
DIC	dissolved inorganic carbon	HFC-245eb	CF ₃ CHFCH ₂ F

HFC-245fa	CHF ₂ CH ₂ CF ₃	HFOC-134	CF ₂ HOCH ₂ F
HFC-263fb	CF ₃ CH ₂ CH ₃	HFOC-143a	CF ₃ OCH ₃
HFC-338pcc	CHF ₂ CF ₂ CF ₂ CF ₂ H	HFOC-152a	CH ₃ OCHF ₂
HFC-356mcf	CF ₃ CF ₂ CH ₂ CH ₂ F	HFOC-245fa	CHF ₂ OCH ₂ CF ₃
HFC-356mff	CF ₃ CH ₂ CH ₂ CF ₃	HFOC-356mmf	CF ₃ CH ₂ OCH ₂ CF ₃
HFC-365mfc	CF ₃ CH ₂ CF ₂ CH ₃	HG-01	CHF ₂ OCH ₂ CF ₂ OCHF ₂
HFC-43-10mee	CF ₃ CHFC ₂ CF ₂ CF ₃	HG-10	CHF ₂ OCH ₂ OCHF ₂
HFC-458mfcf	CF ₃ CH ₂ CF ₂ CH ₂ CF ₃	H-Galden 1040x	CHF ₂ OCF ₂ OC ₂ F ₄ OCHF ₂
HFC-55-10mcff	CF ₃ CF ₂ CH ₂ CH ₂ CF ₂ CF ₃	HNO₃	nitric acid
HFE-125	CF ₃ OCHF ₂	HO₂	hydroperoxyl
HFE-134	CF ₂ HOCH ₂ H	HO_x	the sum of OH and HO ₂
HFE-143a	CF ₃ OCH ₃	H₂O	water vapour
HFE-152a	CH ₃ OCHF ₂	H₂SO₄	sulphuric acid
HFE-227ea	CF ₃ CHFOCF ₃	N₂	molecular nitrogen
HFE-236ea2	CF ₃ CHFOCHF ₂	NF₃	nitrogen trifluoride
HFE-236fa	CF ₃ CH ₂ OCF ₃	NH₃	ammonia
HFE-245cb2	CF ₃ CF ₂ OCH ₃	NH₄⁺	ammonium ion
HFE-245fa1	CHF ₂ CH ₂ OCF ₃	NMHC	non-methane hydrocarbon
HFE-245fa2	CHF ₂ OCH ₂ CF ₃	NO	nitric oxide
HFE-254cb2	CHF ₂ CF ₂ OCH ₃	NO₂	nitrogen dioxide
HFE-263fb2	CF ₃ CH ₂ OCH ₃	NO_x	nitrogen oxides (the sum of NO and NO ₂)
HFE-329mcc2	CF ₃ CF ₂ OCF ₂ CHF ₂	NO₃	nitrate radical
HFE-338mcf2	CF ₃ CF ₂ OCH ₂ CF ₃	NO₃⁻	nitrate ion
HFE-347mcc3	CF ₃ CF ₂ CF ₂ OCH ₃	N₂O	nitrous oxide
HFE-347mcf2	CF ₃ CF ₂ OCH ₂ CHF ₂	O₂	molecular oxygen
HFE-356mec3	CF ₃ CHFC ₂ OCH ₃	O₃	ozone
HFE-356mff2	CF ₃ CH ₂ OCH ₂ CF ₃	OCS	organic carbonyl sulphide
HFE-356pcc3	CHF ₂ CF ₂ CF ₂ OCH ₃	OH	hydroxyl radical
HFE-356pcf2	CHF ₂ CF ₂ OCH ₂ CHF ₂	PAN	peroxyacetyl nitrate
HFE-356pcf3	CHF ₂ CF ₂ CH ₂ OCHF ₂	PFC	perfluorocarbon
HFE-365mcf3	CF ₃ CF ₂ CH ₂ OCH ₃	SF₆	sulphur hexafluoride
HFE-374pc2	CHF ₂ CF ₂ OCH ₂ CH ₃	SF₅CF₃	trifluoromethyl sulphur pentafluoride
HFE-7100	C ₄ F ₉ OCH ₃	SO₂	sulphur dioxide
HFE-7200	C ₄ F ₉ OC ₂ H ₅	SO₄²⁻	sulphate ion
HFOC-125	CF ₃ OCHF ₂	VOC	volatile organic compounds

Appendix VIII

Index

† Term also appears in Appendix I: Glossary.

Numbers in italics indicate a reference to a table or diagram.

Numbers in bold indicate a reference to an entire chapter.

A

Absorption

anomalous 433

Aerosol(s)[†]

biogenic 299, 300-303, 312, 331

black carbon[†] 294, 299-300, 306, 314, 332-334, 369-372, 395, 397, 400-402

carbonaceous[†] 299-300, 314, 369-372, 377-378, 395, 397, 400-402

cloud condensation nuclei (CCN) 308-310

concentration(s) past and current 306

direct effect 293-295, 304, 322-324, 367-374, 400-404

effect on clouds 307-312, 324-325, 328-330, 379, 395, 397-399, 404

from biomass burning 299-300, 309, 322, 323, 324, 395, 397, 400-402

from fossil fuel burning 299-300, 301, 322, 323, 369-372

future concentration(s) 330-335

ice nuclei (IN) 311-312

indirect effect(s)[†] 293-295, 307-312, 324-330, 375-379, 395

industrial dust 299

interactions with tropospheric ozone and OH 277

lifetimes 293, 295

mineral dust 296-297, 314, 320, 331-332, 372-373, 378, 395, 397

modelling 313-330, 781-782

nitrates 303, 332-334, 373

observations 304-306, 314-318, 374, 378-379

optical properties 293-295, 295, 318-322, 367-373

organic 299-300, 306, 314, 320, 370-372

precursors 295, 300-303

radiative forcing from 322-324, 328-330, 367-380, 391-399,

400-404

scenarios of future emissions – see also IS92 and

SRES scenarios 330-335

sea salt

297-299, 314, 320, 332, 374

size distribution

294, 369

soil dust – see Aerosols, mineral dust

295-307, 330-335

sources and sinks

304, 379-380, 395

stratospheric

304, 379-380, 395

sulphates 314, 320, 324, 367-369, 375-377, 378, 395, 397,

400-402, 548, 593-596

trends – see Aerosol(s), concentration(s) past and current

uncertainties 322-324, 328-330, 334-335, 374, 395, 404

volatile organic compounds (VOC)

300, 331

volcanic

303-304, 379-380

Afforestation[†] – see Forests

Agriculture

CH₄ sources and sinks

248

CO₂ sources and sinks

194

N₂O sources and sinks

251

Aircraft

259-260, 262, 263, 296, 312, 366-367, 391, 395, 399

Albedo[†]

380, 425, 429, 434, 443-446, 448

single scattering

293, 306

Ammonia

246, 267, 260, 278, 296, 303, 330, 332

Antarctic ice sheet – see Ice sheets

Antarctic Oscillation

92, 154, 568-570

Anthropogenic climate forcing – see Radiative forcing

Arctic Oscillation

153, 568-570

Artificial Neural Network

591, 618

Atmosphere

definition

87-88

Atmosphere ocean general circulation models (AOGCMs)

– see Climate modelling

Atmosphere/ocean interaction – see also El Niño-Southern

Oscillation 436, 449-451

Atmospheric Boundary Layer – see Boundary Layer

Atmospheric chemistry

239-287

feedbacks – see Feedbacks, chemical		Terrestrial Biogeochemical Models (TBMs)	213																																																																							
impacts of climate change	278	terrestrial carbon processes	191-197, 779																																																																							
modelling	264-266, 267-271, 277-278, 781	Carbon dioxide (CO₂)[†]	183-237																																																																							
possible future changes	267-277	and land-use change	193-194, 204-205, 212-213, 215, 224																																																																							
Atmospheric circulation	97, 715	concentration(s) past and current	185, 187, 201-203, 205-208																																																																							
observed changes	103, 150-154	during ice age cycles	202-203																																																																							
projections of future changes	565-570, 602	enhancing ocean uptake by iron fertilisation	198, 200, 202																																																																							
regimes	435	equivalent – see Equivalent carbon dioxide (CO ₂)																																																																								
Atmospheric composition	87-88, 92-93	fertilisation [†]	195-196, 219																																																																							
Attribution of climate change – see Detection and attribution of climate change		from fossil-fuel burning	204, 205, 224																																																																							
Aviation induced cirrus	395	future concentration	186, 219-224																																																																							
B		geological history	201-202																																																																							
Baseline climatological data	749-750	Global Warming Potential (GWP)	388																																																																							
Biogenic aerosol(s) – see Aerosol(s)		interannual variability of concentrations	208-210																																																																							
Biological pump – see Carbon cycle		missing sink	208																																																																							
Biomass burning – see also Aerosols, from biomass burning	257-258, 262, 296, 299, 300, 322, 323, 361, 372, 377	radiative forcing from scenarios of future emissions	356-357, 358-359, 391-396																																																																							
Biosphere[†]		sources and sinks	192, 193-194, 195-197, 199, 204-208, 210-213, 215, 216-218, 224																																																																							
marine	89, 197-198, 200	spatial distribution	210-212																																																																							
terrestrial	89, 191-197, 456	stabilisation of concentration	224																																																																							
Black carbon aerosol(s) – see Aerosol(s)		trends – see Carbon dioxide, concentration(s) past and current																																																																								
Blocking	154, 506, 566-567	Carbon isotopes	207, 216-218, 248																																																																							
Bölling-Allerød warm period	137	Carbon monoxide (CO)	256, 365-366, 387-390																																																																							
Borehole measurements (of temperature)	130, 132	Carbonaceous aerosol(s) – see Aerosol(s)																																																																								
Boundary-layer	428-429, 441	CFCs	255, 357-359																																																																							
Budget of greenhouse gases – see Greenhouse gases		Chemical transport models – see Atmospheric chemistry, modelling																																																																								
C		Climate[†]																																																																								
Calcium carbonate (CO₃²⁻)	198, 199, 200, 202, 203, 216, 224	Climate change [†]		definition	87	Canonical Correlation Analysis	617	definition	87	Carbon budget	185, 205-208	detection and attribution – see Detection and attribution of climate change		Carbon cycle[†]	183-237, 777-779	Climate change commitment	531-536, 675-679	biological pump	197-198, 778	Climate change signals – see also Detection and attribution of climate change	532-536, 538-540, 543-554, 565-570, 593-603, 607, 613-615, 622-623, 664-666, 757-759	carbon management	224	Climate extremes	92, 432	description	191-193, 197-199	modelling – see Climate modelling		Dynamic global vegetation models (DGVMs)	213, 219	observed changes	97, 103-104, 155-163, 575, 774-775	effects of nitrogen deposition	196-197, 215	projections of future changes	570-576, 602-603, 606, 615, 774-775	feedbacks	91, 186, 194-195, 200, 208-210, 219-220, 224	representation in climate scenarios – see Climate scenarios		inverse modelling	210-212	Climate forcing – see Radiative forcing		model evaluation	213-218	Climate modelling		modelling	213-218, 219-224, 443	atmospheric circulation	435	ocean carbon processes	197-200, 216, 778	boundary layer	428-429	ocean models	216-218	cloud processes and feedbacks	427-431, 484, 775-776	response to climate change	186, 194, 200, 215, 219-220	confidence in models	511-512, 531-532, 567-568, 570-576, 587, 591, 664-666, 772-782	response to increasing CO ₂	185-186, 195-196, 199, 219-220		simplified fast carbon cycle models	221		soil carbon	191	
Climate change [†]		definition	87																																																																							
Canonical Correlation Analysis	617	definition	87																																																																							
Carbon budget	185, 205-208	detection and attribution – see Detection and attribution of climate change																																																																								
Carbon cycle[†]	183-237, 777-779	Climate change commitment	531-536, 675-679																																																																							
biological pump	197-198, 778	Climate change signals – see also Detection and attribution of climate change	532-536, 538-540, 543-554, 565-570, 593-603, 607, 613-615, 622-623, 664-666, 757-759																																																																							
carbon management	224	Climate extremes	92, 432																																																																							
description	191-193, 197-199	modelling – see Climate modelling																																																																								
Dynamic global vegetation models (DGVMs)	213, 219	observed changes	97, 103-104, 155-163, 575, 774-775																																																																							
effects of nitrogen deposition	196-197, 215	projections of future changes	570-576, 602-603, 606, 615, 774-775																																																																							
feedbacks	91, 186, 194-195, 200, 208-210, 219-220, 224	representation in climate scenarios – see Climate scenarios																																																																								
inverse modelling	210-212	Climate forcing – see Radiative forcing																																																																								
model evaluation	213-218	Climate modelling																																																																								
modelling	213-218, 219-224, 443	atmospheric circulation	435																																																																							
ocean carbon processes	197-200, 216, 778	boundary layer	428-429																																																																							
ocean models	216-218	cloud processes and feedbacks	427-431, 484, 775-776																																																																							
response to climate change	186, 194, 200, 215, 219-220	confidence in models	511-512, 531-532, 567-568, 570-576, 587, 591, 664-666, 772-782																																																																							
response to increasing CO ₂	185-186, 195-196, 199, 219-220																																																																									
simplified fast carbon cycle models	221																																																																									
soil carbon	191																																																																									

dependence on resolution	509-511, 603-607, 774	Climate models [†] – see also Climate modelling	94-95
Earth System models	476	high resolution	587, 589-590, 603-607
Energy Balance Models	577, 670-673	intercomparison	479-512
ENSO	503-504, 567-568	nested	587, 590, 607
evaluation	471-523 , 591-593, 603-607, 760	types	475-476
extra-tropical storms	508, 573	variable resolution	587, 589-590, 603-607
extreme events	432, 499-500, 503-509, 570-576, 592-593, 604, 610-613, 774-775	Climate projection [†] – see Climate modelling	
flux adjustment	94, 449-450, 476-479, 530-532, 773	Climate response	94, 532-534, 559-565, 705-712
General Circulation Models (GCMs), description	94-95, 475, 476-479	time-scales	563-565
initialisation	476, 773	to anthropogenic forcing – see Detection and attribution of climate change	
land ice	448-449, 615, 652-653	to natural forcing – see Detection and attribution of climate change	
land surface	440-443, 490-493, 493-496, 570-572, 779-781	transient	533, 538-540, 561-562, 593-596, 600
Madden-Julian Oscillation (MJO)	505-506	Climate scenarios [†]	739-768
mean sea level pressure	479-484, 548, 592	analogue	748
mixed layer models	530-531	application to impact assessment	743-745, 752
monsoons	484, 505, 568, 572-573, 612-613	baseline climate	749-751
North Atlantic Oscillation	506, 568-570, 573, 715	definition	743-744
ocean processes, circulation and feedbacks	421, 435-440, 486-489, 493, 561-565, 646-647	derived from climate models	748-759, 750-751
orographic processes	435	expert judgement	749
Pacific North American (PNA) pattern	506	inconsistencies	760-761
parametrisation	94, 427-432, 436-438, 440-443	incremental	746-748
precipitation processes	431-432, 479-484, 572-573, 591-592, 604, 610	pattern scaling	756-757
projections of future climate: description		representing uncertainty	745, 755-760
of methods	94-96, 476-479, 532-536, 588-591, 593-603, 617-618, 622-623, 666-679	risk assessment	759-760
projections of future climate: results (see also entries		variability and extremes	752-755
for individual variables and phenomena)	525-582 , 607, 613-615, 666-679	weather generators	617, 619-620, 750, 753
radiative processes	432-434	Climate sensitivity [†]	353-355, 596, 755-756
sea ice	445-446, 489, 543, 548	effective	534, 559-562, 577
simple climate models	94-95, 475-476, 531-532, 533, 554-558, 577, 646-647, 670-673, 749	equilibrium	93, 530-531, 532-536, 559-561, 577
simulation of 20th century climate	496-498, 502-503, 592	Climate system [†]	85-98
simulation of past climates	493-496	components	87-89
snow	543, 548	description	87-89
stratospheric climate	434-435, 484-486	Climate variability [†]	452-453
temperature	479-484, 591-592, 604, 610	human-induced	92-97
thermohaline circulation	439, 439-440, 486-488, 562-563, 565, 577, 776-777	modelling – see Climate modelling	
tropical cyclones	508-509, 574, 606, 774-775	natural	89-92, 702-705
uncertainties	492-493, 511-512, 531-532, 536, 554-558, 567-568, 577, 591, 601-602, 755-756, 772-782	observed changes	155-163
variability	432, 499-500, 503-509, 534-536, 538-540, 565-570, 592-593, 604, 610-613	projections of future changes	565-570, 602-603, 615
water vapour and water vapour feedback	424, 425-426, 484	representation in climate scenarios – see Climate scenarios	
		Cloud condensation nuclei (CCN) [†] – see Aerosol(s), cloud condensation nuclei	
		Cloud/radiative feedback(s) – see Clouds, processes and feedbacks	
		Clouds	
		influence of aerosol(s) on – see Aerosol(s)	
		modelling – see Climate modelling	
		observed changes	103, 148-149
		processes and feedbacks	90, 91, 421, 423-431

radiative forcing – see also Aerosol(s), indirect forcing and effect on clouds	429-431, 430	El Niño – see El Niño-Southern Oscillation
Contrails	379, 395, 399	El Niño-Southern Oscillation (ENSO)[†] 92, 454-455, 456 and behaviour of carbon cycle 208-210 influence on climate 109, 121, 123, 130, 143-145, 148, 151, 152-153, 453-455, 567-568, 588 modelling – see Climate modelling
Convection		observed changes 97, 103, 139-140, 141, 150, 154 projections of future changes 567-568 representation in climate scenarios 754
Corals	130, 131	
Cosmic rays (effect on clouds)	384-385	
Coupled ocean/atmosphere models – see Climate modelling		
Cryosphere[†]	456	Emission scenarios[†] – see IS92 and SRES scenarios
definition	88, 444-449	Energy Balance Model – see Climate modelling
processes and feedbacks	444-449	Ensembles of climate integrations 534-536, 543-554, 593-596, 602, 774
D		
Dansgaard-Oeschger events	137, 140-141, 203	Equilibrium climate change[†] 530, 533
Deforestation[†]	192, 193, 194, 204-205, 212-213 CO ₂ released from – see Carbon dioxide	Equivalent carbon dioxide (CO₂)[†] 533, 761
Detection and attribution of climate change[†]	97, 695-738	Eustasy[†] 643, 654-656, 661
circulation patterns	715	Evaporation 148 observed changes
conclusions	730-731	External variability (of climate system) 91
definition(s)	700-701	Extra-tropical cyclones
estimates of internal variability	702-705, 713, 729	modelling – see Climate modelling
hydrological indicators	715	observed changes 161, 664
observed data	701	projections of future changes 573, 602-607, 675
optimal methods – see Optimal detection of climate change		
pattern correlation methods	718-721	Extreme events[†] – see Climate extremes
qualitative comparison of observation with models	713-716	
response to anthropogenic forcing	711-712, 729	
response to natural forcing	708-709, 729	
uncertainties	725-727, 729	
using horizontal temperature patterns	711-712, 714, 718-720	
using temperature time-series	709, 714, 716-718	
using vertical temperature patterns	711, 714-715, 720-721	
Dimethylsulphide (DMS)[†]	301, 331	
Diurnal temperature range (DTR) – see Temperature		
Downscaling	619-621	
empirical/statistical	587, 591, 616-621	Feedback(s)[†] 91, 93, 275, 417-470 carbon cycle – see Carbon cycle, feedbacks
issues	619-620	chemical 245-246, 247, 278
predictors and predictands	616-617, 619-620	cloud – see Clouds, processes and feedbacks
statistical/dynamical	587, 591, 616-621, 751-752	ice albedo 445-446
Drought	572-573, 603, 615	land ice – see Land ice, processes and feedbacks
observed changes	143-145, 161-162	land surface – see Land surface, feedbacks
Dust – see Aerosol(s)		ocean – see Ocean processes and feedbacks
		sea ice – see Sea ice, processes and feedbacks
		temperature/moisture – see Temperature/moisture feedback
		water vapour – see Water vapour, feedback
E		
Earth System Models – see Climate modelling		Fingerprint methods – see Optimal detection of climate change
Eemian	137, 141	Flux adjustment[†] – see Climate modelling
El Chichon	107, 121	Forcing – see Radiative forcing
		Forests[†] 192, 193, 204-205, 212-213
		Fossil fuel burning 204, 205, 248, 251-252, 257-258, 259-260, 296, 299-301, 322, 323
		Framework Convention on Climate Change[†] – see United Nations Framework Convention on Climate Change
		Future climate – see Climate modelling and entries under individual variables and phenomena

Little Ice Age	102, 127, 133-136	radiative forcing from scenarios of future emissions sources and sinks trends – see Nitrous oxide, concentration(s) past and current	357, 358-359 266-267 251, 252
M			
Madden-Julian Oscillation	505-506	Non-linear climate processes[†]	91, 96, 455-456
Markov chain	617	Non-methane hydrocarbons (NMHC)	257-258, 365-366, 391
Maximum temperature(s) – see Temperature, maximum		North Atlantic Oscillation (NAO)[†]	92, 451-452, 456, 588, 715
Medieval Climate Optimum – see Medieval Warm Period		modelling – see Climate modelling observed changes projection of future changes	103, 117, 152-153 568-570, 573
Medieval Warm Period	102, 133-136		
Mesoscale eddies (in ocean) – see Ocean processes and feedbacks			
Methane (CH₄)	248-251	O	
adjustment time	247, 250-251	Observations of climate and climate change – see also Detection and attribution of climate change and entries for individual variables	96, 99-181
atmospheric chemistry	248, 365		
concentration(s) past and current	248-250	Ocean circulation – see also Ocean processes and feedbacks modelling – see Climate modelling observed changes	103
future concentration	275		
Global Warming Potential (GWP)	244-245, 387, 388	Ocean heat transport – see Ocean processes and feedbacks	
indirect forcing	247, 365-366	Ocean processes and feedbacks	435-440, 493, 588, 609, 644-647, 680
interannual variability of concentrations	248-250	circulation	438-439
lifetime	248, 250-251	heat transport	449-450
radiative forcing from	357, 358-359, 391-396	mesoscale eddies	437-438
scenarios of future emissions	266-267	mixed layer	436
sources and sinks	248	mixing	437
trends – see Methane, concentration(s) past and current		modelling – see Climate modelling	
Mid-Holocene – see Holocene		Ocean/atmosphere interaction – see atmosphere/ocean interaction	
Mid-latitude storms – see Extra-tropical cyclones			
Minimum temperature(s) – see Temperature, minimum		Optimal detection of climate change	721-729
Model – see Climate model		multiple fixed pattern studies	722-723
Monsoons	451-452	single pattern studies	721-722
modelling – see Climate modelling		using spatially and temporally varying patterns	723-728
observed changes	152		
projections of future changes	568, 600, 602, 613-615	Organic aerosol(s)[†] – see Aerosol(s)	
Montreal Protocol[†]	243, 255-256	Organic carbon – see also Aerosol(s)	
MSU (Microwave Sounder Unit) – see also Temperature, upper air	119, 122, 145	Organic carbon aerosol(s) – see Aerosol(s)	
Mt. Pinatubo (eruption of)	107	Orography	435
N		OxComp	267-268
Natural climate forcing – see Radiative forcing		Ozone (O₃)[†]; stratospheric	255-256
Net Ecosystem Production (NEP)[†]	191	depletion of	256, 277-278, 359-361
Net Primary Production (NPP)[†]	191, 197-198	future concentration	361
Nitrate (NO₃) aerosol(s) – see Aerosol(s)		radiative forcing from	359-361, 393, 400-402
Nitrogen fertilisation[†] – see Carbon cycle, effects of nitrogen deposition		Ozone (O₃)[†]; tropospheric	260-263, 278
Nitrogen oxides (NO_x)	259-260, 366, 391	chemical processes	262
Nitrous oxide (N₂O)	251-253, 391-396	concentration past and current	262
concentration(s) past and current	252-253	future concentration	272, 275, 364-365
future concentration	275	radiative forcing from	361-365, 393-395, 400-402
Global Warming Potential (GWP)	244, 388	sources and sinks	262
interannual variability of concentrations	252-253		
lifetime	252	Ozone hole[†] – see Ozone, stratospheric	
		Ozone layer[†] – see Ozone, stratospheric	

P		
Pacific Decadal Oscillation (PDO)	150, 504-505	
Pacific oscillation(s)	150, 151-152	
Pacific-North American (PNA)	152-153, 451-452	
Palaeoclimate	101, 130-133, 137, 143-145, 748	
Palaeo-drought	143-145	
Parametrisation[†] – see Climate modelling		
Perfluorocarbons (PFCs)	254	
Permafrost	127, 444-445, 657-658, 665	
Photochemistry	263-266	
Photosynthesis[†]	191, 195, 442	
Precipitation		
extremes – see Climate extremes		
modelling – see Climate modelling		
observed changes	101, 103-104, 142-145, 157-160, 163, 164, 575	
processes	431-432	
projections of future changes	538-540, 541-554, 566, 572-573, 575, 593-602, 607, 613-615, 653-654, 668-670	
Predictability (of climate)	91, 95-96, 422-423	
Projection of future climate – see Climate modelling and entries		
under individual variables and phenomena		
Q		
Quasi-biennial Oscillation (QBO)	434	
R		
Radiative balance	89	
Radiative forcing[†] – see also the entries for individual greenhouse gases and aerosols	349-416	
and climate response relationship	353-355, 361, 396, 400, 532-534, 706-712	
anthropogenic	353, 356-359, 379, 391-396, 397-399, 400-404, 532-534, 554-558, 577, 709-711, 729	
definition of	90-91, 353	
description	405-406	
from land-use change – see Land-use change		
from volcanoes – see Volcanoes		
geographic distribution	396-400, 711	
global mean estimates	391-396	
indirect	365-367, 375-379, 395, 397-399, 404	
natural	89-91, 353, 379-380, 391-396, 400-402, 706-709, 729	
solar – see Solar variability		
strengths/limitations of concept	355, 396	
time evolution	400-404	
Radiative processes		
modelling – see Climate modelling		
stratosphere	433-434	
troposphere	432-433	
Radiosondes – see Weather balloons		
Rapid climate change[†] – see also Non-linear climate processes		96, 136, 455-456
Reanalyses data		96, 120-121
Reforestation[†] – see Forests		
Regional climate change		97, 583-638
climate variability and extremes		602-603, 607, 615
mean climate		593-602, 607, 613-615
Regional climate change information		
methods of deriving		587-591, 622-623
Regional climate models (RCMs)		589-590, 607-616
derivation of climate scenarios – see also Climate scenarios		751
projection of future climate using		613-615
simulation of current climate		609-613
Regionalisation		587-588, 621-623
Resolution (of models) – see Climate modelling and Climate models		
Respiration[†]		191, 442
River flow		143, 159-160
River ice		129, 163
Runoff		444
S		
S Stabilisation profiles		224, 557-559
Salinity (of oceans)		118, 138
Satellite altimeter observations of sea level		663-664
Satellites		120, 123-125, 145, 147, 148-149, 163, 380-381
Scenarios[†] – see Climate scenarios and SRES and IS92 scenarios		
Sea ice		445-448
Antarctic		124-127, 129, 448
Arctic		124-127, 129, 153, 445, 447-448, 777
modelling – see Climate modelling		
observed changes		124-127, 129, 446
processes and feedbacks		445, 446, 596
Sea level		639-693
acceleration in sea level rise		663, 665-666
changes since last glacial period		654-656, 659-661
extremes		664, 675
observed changes over last 100 to 200 years		661-666
processes contributing to change		644-659
projections of future changes		666-679
regional changes		659, 673-674
scenarios		761
uncertainties		679-682
Sea salt – see Aerosol(s)		
Severe weather		162-163
Simple climate models – see Climate modelling		
Sink strength of greenhouse gases – see Greenhouse gases		
Snow cover		444-445
extent (SCE)		102, 123-124, 129, 142, 159-160
modelling – see Climate modelling		

observed changes	102, 123-124	
Soil carbon – see Carbon cycle		
Soil dust – see Aerosol(s)		
Soil moisture [†]	444, 570-573	
Solar cycle [†] – see Solar variability		
Solar (or short-wave) radiation [†]	89, 293, 297, 380-385	
Solar forcing of climate – see Solar variability		
Solar variability		
influence on climate	91, 120, 136, 380-385, 500-502, 708-709	
radiative forcing from	380-385, 395, 400, 706	
Soot [†] – see Aerosol(s), black carbon		
Source strength of greenhouse gases – see Greenhouse gases		
Southern Oscillation Index (SOI)	455	
SRES scenarios [†]	95	
emissions	266-267, 755	
implications for future climate	541-543, 554-558, 600-601, 670-673	
implications for future concentrations	223, 224, 274-275, 330, 332-334	
implications for future radiative forcing	402-404	
markers	266, 531-532, 541-543, 554-558, 600-601	
Stabilisation of climate – see also WRE and S		
stabilisation profiles	557-558, 675-677	
Stabilisation of concentrations – see entries under		
individual gases and aerosols	557-558	
Statistical downscaling – see Downscaling		
Storm surges [†]	664, 675	
Storms – see Tropical Storms, Tropical Cyclones and Extra-tropical cyclones		
Stratosphere [†]		
aerosol(s) – see Aerosol(s)		
cooling – see Temperature, stratospheric		
dynamics	434-435	
influence on surface climate	435	
modelling – see Climate modelling, stratospheric climate		
temperatures – see Temperature, stratospheric		
water vapour – see Water vapour, stratospheric		
Stratospheric ozone – see Ozone		
Stratospheric/tropospheric coupling	434	
Sulphate aerosol(s) – see Aerosol(s)		
Sulphur dioxide (SO₂) – see also Aerosol(s)	301, 303	
Sulphur hexafluoride (SF₆)	254	
Sunspots [†]	381-382	
Surface Boundary Layer – see Boundary layer		
T		
Taiga	194-195	
Tectonic land movements	658-659	
Teleconnections	139, 151, 451-452	
Temperature		
20th century trends	101, 108, 115	
consistency of surface and upper air measurements	121-123	
diurnal range (DTR)	101, 108, 129, 570-572, 575	
during Holocene	138-140	
during last glacial	140-141	
during previous inter-glacials	141-142	
extreme(s)	156-157	
instrumental record	105-119	
land surface	105-110	
maximum	108-110, 570-572, 575	
minimum	108-110, 570-572, 575	
night marine air (NMAT)	108, 110	
observed changes	101-103, 105-130	
ocean	110-112, 118-119, 644-646	
over past 1,000 years	130-133	
projections of future changes	538-540, 541-554, 570-572, 593-602, 607, 613-615, 649, 653-654, 669	
satellite record	120, 121-123	
sea surface	108, 110-112	
stratospheric	122	
sub-surface land	132, 136	
upper air	119-121, 122	
Temperature/moisture feedback	432	
Terrestrial (or long-wave) radiation	89-90	
Terrestrial storage (of water)	657-658, 680-681	
Thermal expansion (of ocean) [†]	644-647, 665, 666-667, 675-677	
Thermohaline circulation [†]	138, 141, 436, 439-440, 456, 565	
modelling – see Climate modelling		
projection of future changes	562-563, 677	
Tide gauge observations of sea level [†]	661-664	
Time-slice AGCM experiment	589-590, 603-607	
Tornadoes	162-163, 573	
Transfer function	617, 620	
Transient climate change [†]		
definition	533	
Transient climate response [†] – see Climate response, transient		
Tree rings	130, 131, 133	
Tropical cyclones	455	
modelling – see Climate modelling		
observed changes	160-161, 575	
projections of future changes	574, 575, 606, 675	
Tropical monsoons – see monsoons		
Tropical storms	160, 455, 574, 606	
Tropospheric aerosol(s) – see Aerosol(s)		
Tropospheric OH – see Hydroxyl radical (OH)		
Tropospheric ozone – see Ozone		
Tropospheric/stratospheric coupling – see Stratospheric/ tropospheric coupling		

Tundra	194-195	observed changes	103, 146-148
Typhoons – see Tropical cyclones		representation in climate models – see Climate modelling	
U		stratospheric	146-148, 263, 366-367
United Nations Framework Convention on Climate Change		surface	146-147
(UNFCCC) Article 2	557-558	tropospheric	146-148
Upwelling-diffusion model	646-647, 670-673		
Urban heat island – see Urban influence on temperature			
Urban influence on temperature	94, 106, 163		
UV radiation	88, 89		
V			
Volatile organic compounds (VOCs)	257-259		
Volcanoes – see also Mt. Pinatubo and El Chichon			
as source of aerosol(s) – see Aerosol(s)			
influence on climate	91, 136, 500-502, 708		
radiative forcing from	379-380, 395, 400-402, 706		
W			
Warming commitment – see Climate change, commitment			
Water vapour (H_2O)			
feedback	93, 421, 423-427		
		X	
		Y	
		Younger-Dryas	137, 140
		Z	

